

Advanced Burner Test Reactor Preconceptual Design Report

Nuclear Engineering Division

About Argonne National Laboratory

Argonne is a U.S. Department of Energy laboratory managed by The University of Chicago under contract W-31-109-Eng-38. The Laboratory's main facility is outside Chicago, at 9700 South Cass Avenue, Argonne, Illinois 60439. For information about Argonne, see www.anl.gov.

Disclaimer

This report was prepared as an account of work sponsored by an agency of the United States Government. Neither the United States Government nor any agency thereof, nor The University of Chicago, nor any of their employees or officers, makes any warranty, express or implied, or assumes any legal liability or responsibility for the accuracy, completeness, or usefulness of any information, apparatus, product, or process disclosed, or represents that its use would not infringe privately owned rights. Reference herein to any specific commercial product, process, or service by trade name, trademark, manufacturer, or otherwise, does not necessarily constitute or imply its endorsement, recommendation, or favoring by the United States Government or any agency thereof. The views and opinions of document authors expressed herein do not necessarily state or reflect those of the United States Government or any agency thereof, Argonne National Laboratory, or The University of Chicago.

September 5, 2006

ANL-ABR-1
(ANL-AFCI-173)

Advanced Burner Test Reactor Preconceptual Design Report

Project Leaders

Y. I. Chang, P. J. Finck, and C. Grandy

Technical Contributors

J. Cahalan, L. Deitrich, F. Dunn, D. Fallin, M. Farmer, T. Fanning,
T. Kim, L. Krajl, S. Lomperski, A. Moisseytsev, Y. Momozaki,
J. Sienicki, Y. Park, Y. Tang, C. Reed, C. Tzanos, S. Wiedmeyer,
W. Yang, and Y. Chikazawa (JAEA Visiting Scientist)

TABLE OF CONTENTS

EXECUTIVE SUMMARY	1
PART I INTRODUCTION.....	10
I.1 Overall Objectives	10
I.2 Plant Design Approach.....	11
I.3 Safety Design Approach.....	14
PART II PLANT DESIGN DESCRIPTION	19
II.1 Reactor System.....	19
II.1.1 Reactor Core.....	19
II.1.1.1 Core and Assembly Design Description	20
II.1.1.2 Fuel Cycle Performance Characteristics	25
II.1.1.3 Kinetics Parameters and Reactivity Coefficients	29
II.1.1.4 Spent Fuel Characteristics	30
II.1.2 Upper Internals Structure	32
II.1.3 Lower Internals Structure.....	35
II.1.4 Core Restraint System.....	36
II.1.5 Reactivity Control and Shutdown System	38
References.....	42
II.2 Reactor Enclosure System.....	43
II.2.1 Reactor Vessel.....	43
II.2.2 Reactor Vessel Enclosure.....	46
II.2.3 Rotatable Plug	47
II.2.4 Guard Vessel	48
II.2.5 Redan.....	49
II.2.6 Core Support Structure.....	50
II.2.7 Reactor Containment Boundary	51
II.2.8 Integrity of Primary Coolant Boundary	51
II.3 Primary Heat Transport System	54
II.3.1 System Requirements and Description	54
II.3.2 Primary Sodium Pump	55
II.3.2.1 Mechanical pump	55
II.3.2.2 Electromagnetic Pump	60
II.3.3 Intermediate Heat Exchanger	64
II.3.4 Internal Piping.....	70
References.....	71
II.4 Intermediate Heat Transport System.....	73
II.4.1 System Requirements and Description	73
II.4.2 Intermediate Sodium Pump.....	75
II.4.3 IHTS Piping	75
II.4.4 IHTS Sodium Storage Tank, Expansion Tank, and Cleanup System	77
II.5 Power Conversion System	78
II.5.1 Supercritical CO ₂ Brayton Cycle	78
II.5.1.1 Supercritical CO ₂ Brayton Cycle Arrangement	78
II.5.1.2 Turbine Generator	87
II.5.1.3 Compressor.....	88

TABLE OF CONTENTS (contd)

II.5.1.4 Sodium-to-CO ₂ Heat Exchanger	91
II.5.1.5 Recuperator	95
II.5.1.6 Control System.....	98
II.5.1.7 Cooler and Heat Rejection System.....	99
II.5.1.8 Carbon Dioxide Release Mitigation System	102
II.5.2 Steam Rankine Cycle	102
II.5.2.1 Steam Generator.....	103
II.5.2.2 Steam Cycle.....	106
II.5.2.3 Auxiliary Systems	107
II.6 Shutdown Heat Removal System.....	113
II.7 Fuel Handling System	118
II.7.1 Rotatable Plug Assembly	118
II.7.2 Pantograph Fuel Handling Machine.....	122
II.7.3 Fuel Storage Rack	128
II.7.4 Fuel Unloading Machine and Transfer Port.....	128
II.7.5 Intra-Building Cask.....	130
II.7.6 Intra-Building Transfer Tunnel	132
II.7.7 Fuel Handling Operation.....	133
II.7.8 Refueling Time.....	134
II.7.9 Spent Fuel Cooling During Transfer Operations	136
II.7.10 New Fuel Cooling During Transfer Operations.....	138
Reference	138
II.8 Instrumentation and Control Systems	139
II.8.1 Flux Monitoring System	139
II.8.2 Heat Transport Instrumentation System.....	140
II.8.3 Radiation Monitoring System	142
II.8.4 Impurity Monitoring and Analysis System.....	143
II.8.5 Leak Detection System	144
II.8.6 Data Handling and Signal Transmission System	146
II.8.7 Plant Control System.....	146
II.8.8 Plant Protection System	147
II.8.9 Communications System.....	148
II.8.10 Industrial Security and Safeguards System.....	148
II.8.11 Auxiliary Sodium Systems.....	149
II.9 Buildings and Structures	150
II.9.1 Reactor Building	150
II.9.2 Balance of Plant Building System.....	154
II.9.3 Control Room and Personnel Building	154
II.9.4 Radwaste/Maintenance Building	154
II.9.5 Security Building	155
II.9.6. Emergency Generator Building.....	155
II.9.8 Lift Station and Waste Treatment Plant Building	156
II.9.9 Seismic Isolation System	156
References.....	159

TABLE OF CONTENTS (contd)

II.10 Balance of Plant Systems	163
II.10.1 Compressed Gas System	163
II.10.2 Chilled Water System	164
II.10.3 Essential Chilled Water System	164
II.10.4 Radioactive Waste System	165
II.10.5 Nuclear Island Heating, Ventilating, and Air Conditioning System.....	166
II.10.6 Balance of Plant Heating, Ventilating, and Air Conditioning System.....	167
II.10.7 Fire Protection System	167
II.10.8 Recirculating Gas Cooling System	168
II.10.9 Fuel Receiving, Storage, and Shipping System	169
II.10.10 Feedwater and Condensate System	169
II.10.11 Main and Auxiliary Steam System	170
II.10.12 Circulating Water System	171
II.10.13 Service Water System	171
II.10.14 Treated Water System	172
II.10.15 Industrial Waste Water Treatment System	172
II.10.16 Liquid Metal Auxiliaries System	172
II.10.17 Inert Gas Receiving and Processing System	173
II.10.18 Other Auxiliary Systems	174
II.10.18.1 Reactor Vessel Heating System	174
II.10.18.2 Shield and Thimble Cooling System.....	174
II.10.18.3 Emergency and Backup Systems	175
II.11 Electrical Power Systems	176
II.11.1 Power Transmission System	176
II.11.2 Station Power System	176
II.11.3 Sodium Piping and Equipment Heating and Insulation System	179
II.12 In-Service Inspection.....	181
II.12.1 In-Service Inspection Requirements	181
II.12.1.1 Components Subject to Inspection.....	181
II.12.1.2 Accessibility	181
II.12.1.3 Examination Methods	182
II.12.1.4 Inspection Plans and Schedules.....	183
II.12.2 Examination Techniques	186
II.12.2.1 Description of Examination Techniques	186
II.12.2.2 Evaluation of Examination Techniques	187
II.12.3 In-service Inspection Approach for ABTR	188
II.12.3.1 Approaches for Accessibility	189
II.12.3.2 Proposed Inspection Methods and Procedures.....	189
PART III DETAILED DESIGN ANALYSES AND TRADE-OFF STUDIES	200
III.1 Primary Pump Design Analyses	200
III.1.1 Mechanical Pump Design	200
III.1.2 Electromagnetic Pump	205
References.....	212
III.2 IHX and DRACS Sizing Calculations	213

TABLE OF CONTENTS (contd)

References.....	215
III.3 Supercritical CO ₂ Brayton Cycle	220
III.3.1 Turbine Generator	220
III.3.2 Compressor	221
III.3.3 Sodium-to-CO ₂ Heat Exchanger.....	221
III.3.4 Recuperator	227
III.3.5 Cooler.....	232
III.4 Core Design Trade-off Studies	237
III.4.1 Trade-off Study for ABTR Power Level Determination	237
III.4.2 Design Studies of Range of Conversion Ratios.....	244
III.4.3 Alternative Core Design for Oxide Fuel.....	253
III.4.3.1 Oxide Fuel Assembly Design	253
III.4.3.2 Fuel Cycle Performance Characteristics	254
III.4.3.3 Kinetics Parameters and Reactivity Coefficients.....	255
III.4.3.4 Reactivity Control Requirements and Shutdown Margins	258
III.4.4 Performances with LWR Spent Fuel TRU	264
III.4.5 Low Conversion Ratio Core Designs	266
References.....	269
III.5 In-Vessel Shielding Analysis.....	270
References.....	274
III.6 Thermal-Hydraulic Analysis.....	275
Reference	276
III.7 Safety Analysis	282
III.7.1 Introduction and Summary	282
III.7.2 Analysis Scope.....	284
III.7.3 Analysis Methods and Input Data.....	286
III.7.4 Analysis Results.....	297
References.....	304
III.8 System Response during LOF/LOHS Events.....	305
III.9 Spent Fuel Cooling Requirements for Transfer Operations	311
III.9.1 Spent Fuel Assembly Transfer.....	311
III.9.2 Fresh Fuel Assembly Transfer	317
III.9.3 Intra-Building Cask Transient Analysis	317
References.....	321
LIST OF ACRONYMS	322
<i>APPENDIX A Evaluation Of Safety Design Criteria</i>	<i>324</i>
A.1 Safety Design Criteria Comparison	325
A.2 Evaluation of Safety Design Criteria	330
<i>APPENDIX B Overall ABTR Design Requirements</i>	<i>335</i>
B.1 Base Requirements.....	335
B.2 Technical Requirements.....	337

EXECUTIVE SUMMARY

The goals of the Global Nuclear Energy Partnership (GNEP) are to expand the use of nuclear energy to meet increasing global energy demand, to address nuclear waste management concerns and to promote non-proliferation. Implementation of the GNEP requires development and demonstration of three major technologies:

- Light water reactor (LWR) spent fuel separations technologies that will recover transuranics to be recycled for fuel but not separate plutonium from other transuranics, thereby providing proliferation-resistance;
- Advanced Burner Reactors (ABRs) based on a fast spectrum that transmute the recycled transuranics to produce energy while also reducing the long term radiotoxicity and decay heat loading in the repository; and
- Fast reactor fuel recycling technologies to recover and refabricate the transuranics for repeated recycling in the fast reactor system.

The primary mission of the ABR Program is to demonstrate the transmutation of transuranics recovered from the LWR spent fuel, and hence the benefits of the fuel cycle closure to nuclear waste management. The transmutation, or burning of the transuranics is accomplished by fissioning and this is most effectively done in a fast spectrum. In the thermal spectrum of commercial LWRs, some transuranics capture neutrons and become even heavier transuranics rather than being fissioned. Only in a fast spectrum can all transuranics be effectively fissioned to eliminate their long-term radiotoxicity and decay heat.

The Advanced Burner Test Reactor (ABTR) is the first step in demonstrating the transmutation technologies. It directly supports development of a prototype full-scale Advanced Burner Reactor, which would be followed by commercial deployment of ABRs.

The primary objectives of the ABTR are:

- To demonstrate reactor-based transmutation of transuranics as part of an advanced fuel cycle;
- To qualify the transuranics-containing fuels and advanced structural materials needed for a full-scale ABR;
- To support the research, development and demonstration required for certification of an ABR standard design by the U.S. Nuclear Regulatory Commission.

The ABTR should also address the following additional objectives:

- To incorporate and demonstrate innovative design concepts and features that may lead to significant improvements in cost, safety, efficiency, reliability, or other favorable characteristics that could promote public acceptance and future private sector investment in ABRs;

- To demonstrate improved technologies for safeguards and security;
- To support development of the U.S. infrastructure for design, fabrication and construction, testing and deployment of systems, structures and components for the ABRs.

Based on these objectives, a pre-conceptual design of a 250 MWt ABTR has been developed; it is documented in this report. In addition to meeting the primary and additional objectives listed above, the lessons learned from fast reactor programs in the U.S. and worldwide and the operating experience of more than a dozen fast reactors around the world, in particular the Experimental Breeder Reactor-II have been incorporated into the design of the ABTR to the extent possible.

In order to demonstrate the transmutation of transuranics, the ABTR is required to provide a test environment prototypic of future commercial reactors, which implies that the reactor size should be large enough. On the other hand, a high power level means more complexity in engineering and higher project construction costs. Therefore, trade studies have been conducted which concluded that ~250 MWt is a reasonable compromise balancing the prototypic irradiation environment and the project cost.

The reactor core design parameters have been selected to be representative of commercial-scale reactors, which results in a moderate conversion ratio of ~0.6 and a plutonium or transuranics enrichment in the range where extensive irradiation databases exist. However, the core has flexibility to accommodate a wide range of conversion ratios by changing the assembly design parameters appropriately.

Based on the past trade studies and lessons learned from operating reactors, the pool-type arrangement was selected as the basis for the ABTR pre-conceptual design due to its potential for design simplicity, inherent passive safety and economics.

The key plant design parameters for the ABTR are summarized in Table 1. The overall plant site arrangement is shown in Figure 1. The major systems – the reactor vessel containing the reactor core and the primary heat transport system, the intermediate heat transport system with the sodium-to-CO₂ heat exchangers, and the Brayton cycle power conversion system – are shown in an elevation view in Figure 2.

The reactor and the primary and secondary heat transport systems are located below grade. Note that all of the nuclear components of the plant are located on a nuclear island, which is seismically isolated from its foundations, which is also illustrated in Figure 2.

Table 1 ABTR Plant Design Parameters

Reactor Power	250 MWt, 95 MWe
Coolant	Sodium
Coolant Temperature, Inlet/Outlet	355°C/510°C
Driver Fuel	Reference: Metal (~20% TRU, 80% U) Backup: Oxide
Cladding and Duct Material	HT-9
Cycle Length	4 months
Plant Life	30 years with the expectation of life extension
Reactor Vessel Size	5.8 m diameter, 16 m height
Structural and Piping Material	Austenitic Stainless Steel
Primary Pump	Reference: Electromagnetic Backup: Mechanical (centrifugal)
Power Conversion Cycle	Reference: Supercritical CO ₂ Brayton Backup: Steam Rankine
Thermal Efficiency	38 %

The reactor core consists of 24 assemblies in an inner enrichment zone and 30 assemblies in an outer zone. Reactivity control and neutronic shutdown are provided by 7 primary and 3 secondary control rod assemblies. A total of nine test locations are provided -- six for fuel tests and three for material tests. This core design is the product of extensive trade studies involving power rating, conversion ratio, fuel type (metal, oxide), fissile material (weapons Pu, TRU from LWR spent fuel), control requirements and shutdown margin. The reference design uses weapons-grade plutonium-based ternary metal driver fuel as the initial core and envisions a gradual transition to transuranics-containing driver fuel as it is qualified. It has a TRU conversion ratio of 0.65.

The primary system is configured in a pool-type arrangement (similar to that used successfully in EBR-II), with the reactor core, primary pumps, intermediate heat exchangers, and direct reactor auxiliary cooling system (DRACS) heat exchangers all immersed in a pool of sodium coolant within the reactor vessel. A schematic view of the primary system is shown in Figure 3 and some specific dimensions are given in Figure 4. The pool-type arrangement was selected because of its inherent simplicity and safety. All primary coolant piping is within the sodium pool, which greatly reduces the possibility of loss of coolant, and the sodium pool provides a large thermal inertia in the system. In addition, the reactor vessel is a simple structure having no penetrations. The hot sodium at core outlet temperature is separated from the cold sodium at core inlet temperature by a structure called the redan. The reactor vessel is exposed only to cold sodium, so it is not subjected to severe thermal transients. A guard vessel is provided as an additional passive safety feature.

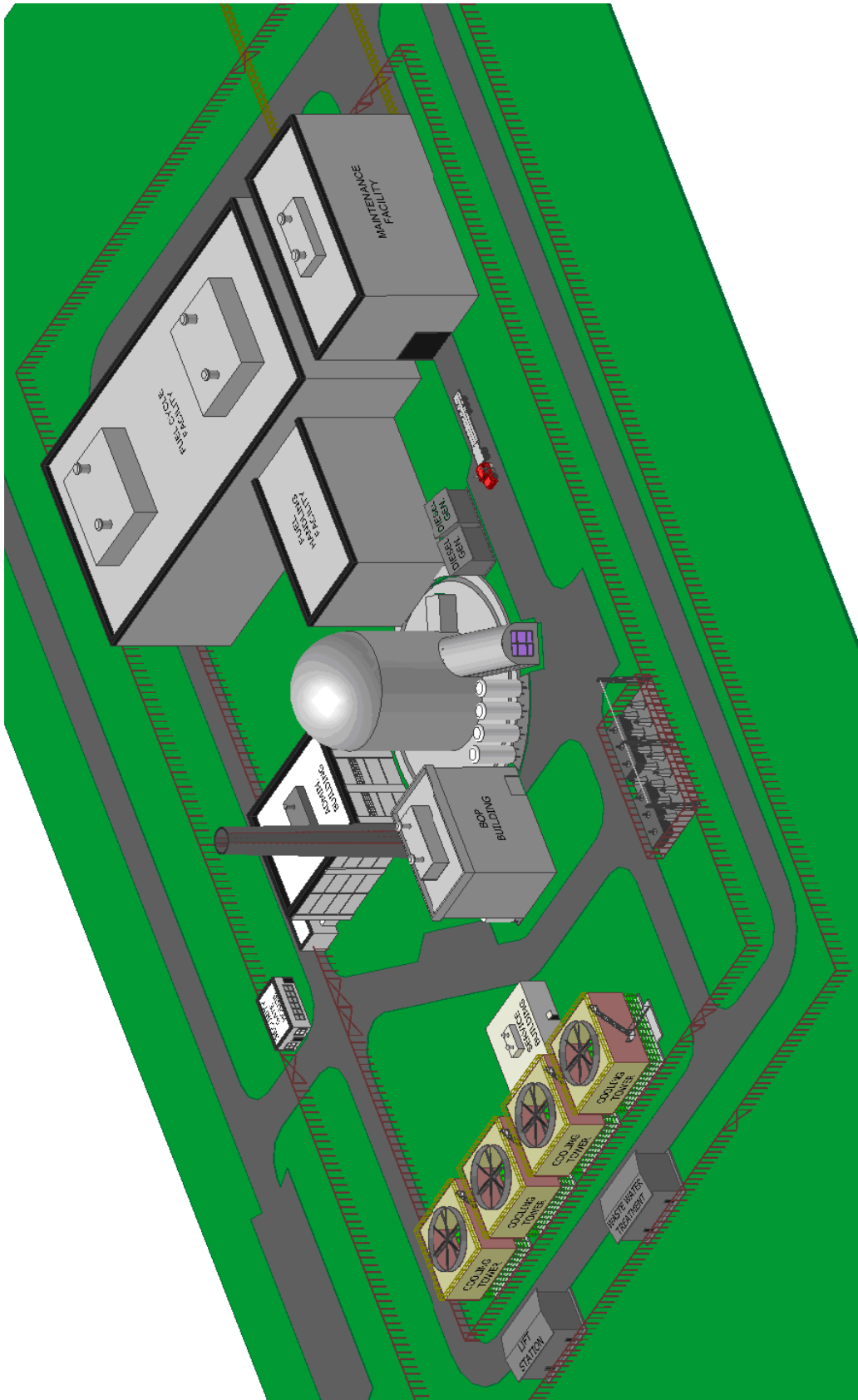


Figure 1 Overall Site View of the ABTR Plant

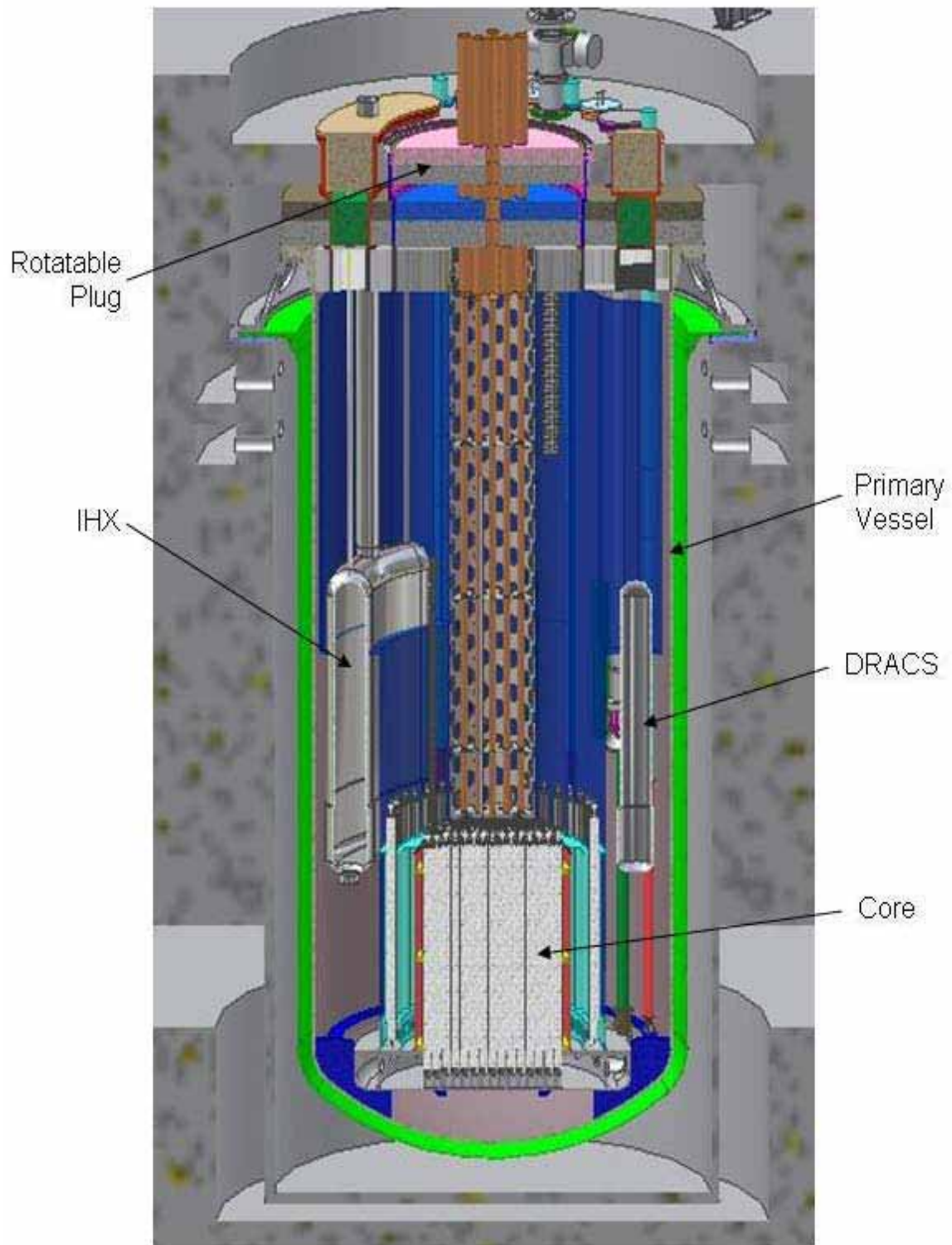


Figure 3 Schematic View of Primary System

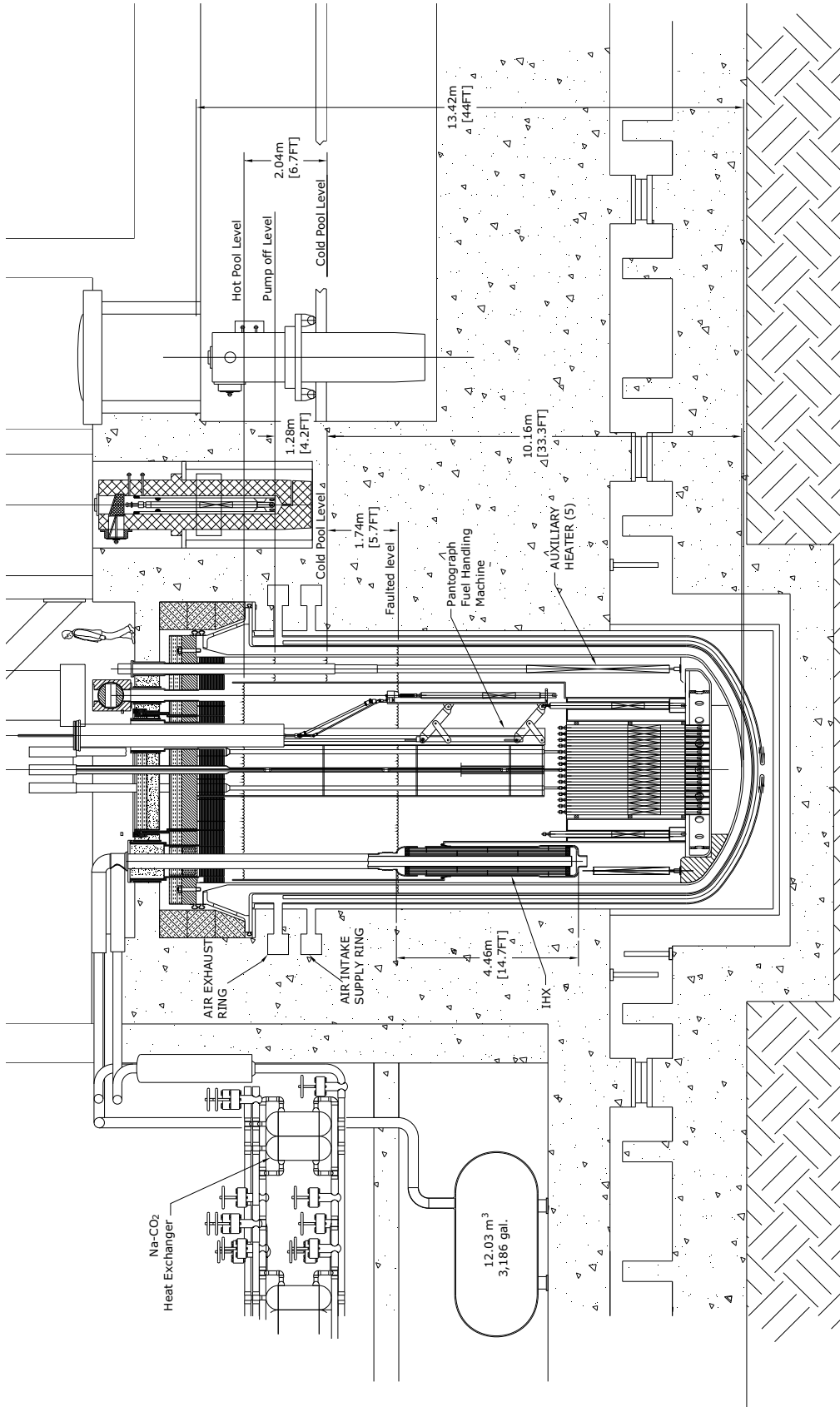


Figure 4 Elevation View of Primary System

Within the reactor vessel, two primary electromagnetic pumps take suction from the lower regions of the cold pool and discharge the sodium into a header that distributes the sodium into 3 feeder pipes, which distribute sodium evenly into the inlet plenum. The inlet plenum distributes the primary sodium to the inlet of the core assemblies, which are individually orificed for proper flow distribution. The sodium is heated as it flows through the core and exits the core assemblies into the outlet plenum. The hot sodium then rises into the redan and then enters the inlet of the intermediate heat exchanger (IHX). After the primary sodium transfers its heat to the intermediate sodium, it exits the IHX into the lower regions of the cold pool. The IHX is contoured to the shape of the annular gap between the redan and the reactor vessel to minimize the overall diameter of the reactor vessel. The guard vessel that surrounds the reactor vessel will capture and contain any reactor vessel leakage and prevent the IHX inlet, DRACS heat exchangers, and core assemblies from being uncovered.

An innovative power conversion system using a Brayton cycle with supercritical CO₂ was selected for the reference design because of its simple layout with relatively few components, small turbo-machinery components and the potential for higher cycle efficiencies at higher sodium outlet temperatures. It also offers improved inherent safety because the potential for sodium-water chemical reaction is eliminated.

The intermediate sodium exits the IHX and flows to the Na-to-CO₂ heat exchanger located below grade on the nuclear island. This heat exchanger is part of the Brayton cycle power conversion system. The intermediate sodium heats the supercritical CO₂ which then flows into the turbine-generator performing work and generating electricity. The CO₂ then goes through a series of recuperator heat exchangers, coolers, and compressors before it re-enters the Na-to-CO₂ heat exchanger. The CO₂ rejects about 60% of its heat to a forced draft cooling tower which provides the ultimate heat sink. A schematic diagram of the reference power conversion system is shown in Figure 5.

Removal of decay heat from the reactor core is a fundamental safety function. In the reference ABTR design, normal decay heat removal is through the normal power conversion systems. However, a direct reactor auxiliary cooling system (DRACS) is provided, having both forced flow and natural convection capability. This system removes decay heat from the pool to the atmosphere using heat exchangers located in the cold part of the sodium pool and in the atmosphere above grade. If electrical power is available, forced flow can be used; in an emergency, natural convection flow can remove the decay heat.

The ABTR will have a short refueling interval so efficient and reliable fuel handling is essential. The reference design provides in-vessel fuel storage cooled by natural convection. Movement of fuel into and out of the core is done using a simple and reliable pantograph-type fuel handling machine. This machine operates with a single rotating plug in the vessel head, which simplifies the design of the head and allows a smaller reactor vessel diameter, both of which afford cost savings. Movement of fuel from the reactor vessel to the fuel handling building is done using a fuel unloading machine and inter-building transfer cask similar to the system used for many years at EBR-II.

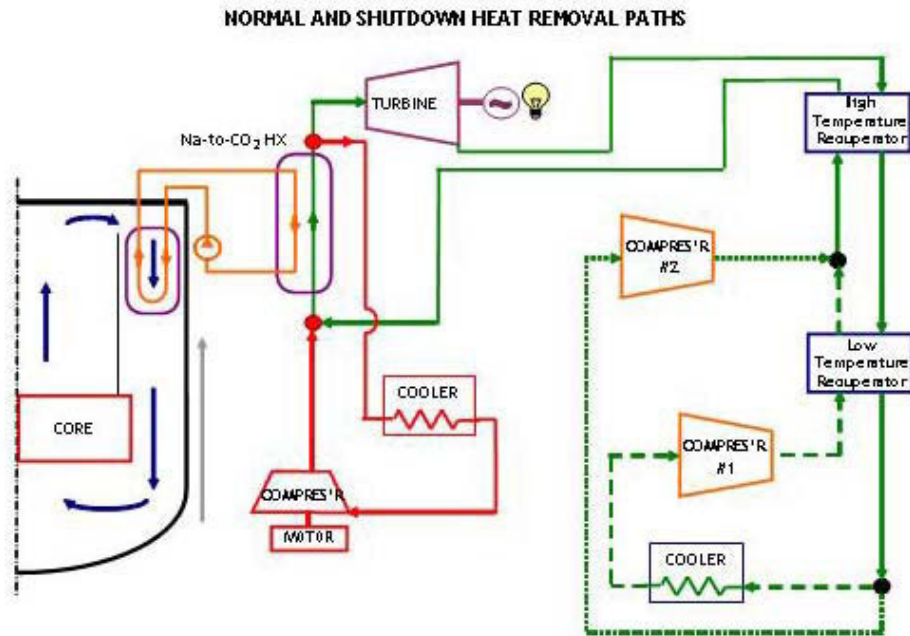


Figure 5 Overall Thermodynamic Cycle

The pre-conceptual design presented in this report reflects the results of extensive and detailed design analyses and trade-off studies. Areas that were the subject of special attention in the design analyses include the core design and in-vessel shielding analysis, the thermal-hydraulics of the vessel and the in-vessel structures and the various components in the heat transport systems. The performance of the reactor and heat transport systems during natural circulation transients and several design basis events was considered. These analyses are documented in Part III of this report.

PART I INTRODUCTION

1.1 Overall Objectives

The goals of the Global Nuclear Energy Partnership (GNEP) are to expand the use of nuclear energy to meet increasing global energy demand, to address nuclear waste management concerns and to promote non-proliferation. Implementation of the GNEP requires development and demonstration of three major technologies:

- Light water reactor (LWR) spent fuel separations technologies that will recover transuranics to be recycled for fuel but not separate plutonium from other transuranics, thereby providing proliferation-resistance;
- Advanced Burner Reactors (ABRs) based on a fast spectrum that transmute the recycled transuranics to produce energy while also reducing the long term radiotoxicity and decay heat loading in the repository; and
- Fast reactor fuel recycling technologies to recover and refabricate the transuranics for repeated recycling in the fast reactor system.

The primary mission of the ABR Program is to demonstrate the transmutation of transuranics recovered from the LWR spent fuel, and hence the benefits of the fuel cycle closure to nuclear waste management. The transmutation, or burning of the transuranics is accomplished by fissioning and this is most effectively done in a fast spectrum. In the thermal spectrum of commercial LWRs, some transuranics capture neutrons and become even heavier transuranics rather than being fissioned. Even with repeated recycling, only about 30% can be transmuted, which is an intrinsic limitation of all thermal spectrum reactors. Only in a fast spectrum can all transuranics be effectively fissioned to eliminate their long-term radiotoxicity and decay heat.

The Advanced Burner Test Reactor (ABTR) is the first step in demonstrating the transmutation technologies. It directly supports development of a prototype full-scale Advanced Burner Reactor, which would be followed by commercial deployment of ABRs.

The primary objectives of the ABTR are:

- To demonstrate reactor-based transmutation of transuranics as part of an advanced fuel cycle;
- To qualify the transuranics-containing fuels and advanced structural materials needed for a full-scale ABR;
- To support the research, development and demonstration required for certification of an ABR standard design by the U.S. Nuclear Regulatory Commission.

The ABTR should also address the following additional objectives:

- To incorporate and demonstrate innovative design concepts and features that may lead to significant improvements in cost, safety, efficiency, reliability, or other favorable characteristics that could promote public acceptance and future private sector investment in ABRs;
- To demonstrate improved technologies for safeguards and security;
- To support development of the U.S. infrastructure for design, fabrication and construction, testing and deployment of systems, structures and components for the ABRs.

Based on these objectives, a pre-conceptual design of a 250 MWt ABTR has been developed; it is documented in this report. In addition to meeting the primary and additional objectives listed above, the lessons learned from fast reactor programs in the U.S. and worldwide and the operating experience of more than a dozen fast reactors around the world, in particular the Experimental Breeder Reactor-II have been incorporated into the design of the ABTR to the extent possible.

1.2 Plant Design Approach

In order to address the ABTR objectives, the following major design goals governed the pre-conceptual design of the ABTR:

- *Demonstrate Transmutation of Transuranics:* The reactor core will be designed to demonstrate actinide transmutation in a fast spectrum using the plutonium containing fuel as its initial core driver fuel, gradually transitioning into transuranics containing fuel, recovered from LWR spent fuel. It will accommodate test positions for irradiation testing of transuranic fuels and non-fuel materials within the core.
- *Demonstrate Fast Reactor Safety:* The reactor and system design will incorporate inherent safety features and shall utilize passive safety systems to the maximum extent possible. The design will incorporate the major features that would be expected in a commercial-scale ABR so that safety demonstrations and operating experience is applicable to the future ABRs.
- *Demonstrate Cost Reduction Design Features:* The design will emphasize simplicity, reliability and long life of its systems, structures and components, and will seek innovative design options that reduce cost without compromise of the mission or safety. The design will emphasize ease of operation, inspection and maintenance. The design will be suitable for location on a wide variety of sites.

In order to demonstrate the transmutation of transuranics, the ABTR is required to provide a test environment prototypic of future commercial reactors, which implies that the reactor size should be large enough. For a smaller plant size, much higher fissile enrichment is required due to high neutron leakage, distorting the irradiation environment compared to that expected in commercial reactors. On the other hand, a high power level means more complexity in engineering and higher project construction costs. Therefore, trade studies have been conducted which

concluded that ~250 MWt is a reasonable compromise balancing the prototypic irradiation environment and the project cost.

The reactor core design parameters have been selected to be representative of commercial-scale reactors, which results in a moderate conversion ratio of ~0.6 and a plutonium or transuranics enrichment in the range where extensive irradiation databases exist. However, the core has flexibility to accommodate a wide range of conversion ratios by changing the assembly design parameters appropriately.

Once the core envelope has been defined, the next key design decision is selection of the overall plant layout option, namely loop-type or pool-type arrangement. Based on the past trade studies and lessons learned from operating reactors, the pool-type arrangement was selected as the basis for the ABTR pre-conceptual design. The reasons for this selection are summarized below.

Simplicity

Assurance of primary system integrity and leak tightness is a major design objective. In the pool concept, the primary system coolant boundary is simple and regular, resulting in low stresses and high structural reliability. There are no penetrations in the reactor vessel wall. Because of the submerged primary piping and other major components, small leakages internal to the primary boundary are permissible. By contrast, in the loop concept, the primary pumps and intermediate heat exchangers are housed external to the reactor vessel in steel-lined, nitrogen-inerted cells. The piping normally penetrates the reactor vessel below the top head closure and runs in inerted pipeways to and from the steel-lined cells. Elimination of these inerted steel-lined primary heat transport system cells and the complex network of piping, supports and restraints results in a major simplification of the plant design and reduction of containment building size and associated commodities.

Inherent Passive Safety

There is a significant difference between the responses of the pool and loop designs to various system transients. The pool system generally is less sensitive than the loop system to plant upsets associated with loss of heat sink or loss of forced cooling. This reduced sensitivity allows greater opportunity for inherent passive safety features such as natural convective flow and negative reactivity feedback to protect the core. The major design considerations relate to the thermal inertia, the rate of pump coastdown, and the reactivity feedback characteristics of the system. An extended coastdown time, combined with the large thermal inertia of the pool system, may well allow reactivity feedback mechanisms to accommodate the unprotected transients. Such mechanisms are inherently provided by the thermal expansion of the support grid and thermal elongation of the control rod drivelines. With these factors properly combined, it may be feasible to design a pool system to survive loss of all electric power (and forced coolant flow) without

scram and thus significantly further reduce the probability of a serious accident. This is much more difficult to achieve in a loop system because following a scram the primary pumps must coast down rapidly to avoid serious thermal shock to the reactor nozzles, primary piping and downstream components.

Diverse and redundant decay heat removal capacity can be supplied in either a loop or pool system. However, because of the large reactor vessel that contains both primary pumps and intermediate heat exchangers, diversity and redundancy can be achieved more easily and reliably in the pool system. Also, passive protective systems, including decay heat removal, can be provided with simpler engineering solutions. For example, the normal primary heat transport system in a pool design can also be used for in-vessel passive decay heat removal with proper location of dedicated heat removal systems, whereas the loop concept requires an alternative flow path with either check valves or changes in direction of coolant circulation.

Economics

Past design studies based on use of standard stainless steel materials of construction have concluded that the pool arrangement costs less than the loop arrangement, both in capital cost and in operating costs over the life of the plant. The primary reasons for reduced capital cost lie in the smaller reactor containment building and all of the associated reductions in plant size. Furthermore, the simplicity of the primary system and elimination of the additional inerted steel-lined cells housing various sodium heat transport system components contribute significantly to cost savings. The simplicity of the pool system translates into a shortened construction schedule, which also contributes to capital cost savings. The operating and maintenance costs can be reduced because of reduced plant outage times and less radiation exposure to personnel performing inspection, testing, and maintenance work. Also, there appears to be greater potential for design improvements to reduce cost in the pool system than for the loop system.

Even though the pre-conceptual pool design described in this report is still preliminary and incomplete, the attractiveness of the design is apparent. In essence, it maximizes the advantages of the pool concept identified in previous design studies by unique design innovations. Specific examples of features unique to the design include:

- A vertical redan which reduces the load on the support structure, eliminates complex pump and IHX penetrations, increases the volume of cold sodium in the primary vessel, and decreases heat losses to the top closure;
- A passive cooling system to keep the reactor vessel wall at a low and uniform temperature thus reducing costs, enhancing integrity of the primary coolant boundary and simplifying the design;
- Elimination of valves from the primary sodium piping system to improve reliability and reduce cost;
- A reactor support grid incorporating individual inlet modules for reactor assemblies and simple hydraulic hold-down providing flexibility and reducing vertical space requirements;

- Shutdown heat removal system within the reactor vessel which enhances safety and reduces the cost of the secondary system;
- Electromagnetic pump that is expected to simplify the overall plant design and improve reliability by eliminating moving parts.

The ABTR design project also focused on incorporating innovative design features with the goal of reducing the overall plant costs. Some of the innovative design features incorporated into the ABTR plant design include:

- A compact fuel handling system that aids in reducing the reactor vessel size, which should translate into an overall primary plant cost reduction;
- An innovative balance-of-plant option using a supercritical carbon dioxide Brayton cycle system that may simplify the power conversion system, reduce the commodities associated with balance of plant systems and reduce its overall costs; and eliminate the possibility of water-sodium interactions.
- Seismic isolation of the ‘nuclear island’ so that the need for expensive design features to accommodate large earthquakes is reduced and limitations on the seismicity of candidate sites can be relaxed. The pre-conceptual design incorporates an innovative multiple friction pendulum system.

1.3 Safety Design Approach

The safety goals in nuclear power reactor design and operation are to assure the health and safety of the public, to protect the plant operating staff from harm, and to prevent plant damage. Traditionally, these goals have been fulfilled by an approach that 1) minimizes risk by maximizing safety margins in design and operation, 2) reduces the likelihood of potentially harmful events by providing safety systems to deal with anticipated events, and 3) provides additional design features to mitigate the harmful consequences of low probability events. This approach is usually identified as “defense in depth.”

The basic principle of “defense in depth” is to provide multiple levels of protection against release of radioactive material. One part of defense-in-depth is physical barriers, like the multiple barriers to release of radioactivity provided by the fuel cladding, the primary coolant system boundary and the reactor containment building. Generally, active or passive safety systems are provided to protect the physical barriers. These include the reactor shutdown systems and the reactor cooling systems. Inherent characteristics of the design, such as negative reactivity feedback and long flow coastdown, may provide an additional level of protection. Emergency planning provides an additional layer of defense-in-depth, should the other barriers be threatened. However, in all instances, the “defense in depth” strategy depends on the independence of the protective measures, so that no single event can breach more than one protective level.

The ABTR safety design approach implements the “defense in depth” strategy by adopting the traditional three levels of safety. In addition, the ABTR design features

have been selected to provide significant safety margin enhancements by inherent passive safety responses to upset conditions and equipment failures.

At the first level, the ABTR is designed to operate with a high level of reliability, so that accident initiators are prevented from occurring. The first level of safety is assured in part by selection of fuel, cladding, coolant, and structural materials that are stable and compatible, and provide large margins between normal operating conditions and limiting failure conditions. Next, the first level of safety is assured by adopting an arrangement of components that allows monitoring, inspection, and testing for performance changes or degradation. Finally, the ABTR design provides for repair and replacement of components necessary to assure that safety margins are not degraded.

The selection of liquid sodium coolant and metallic fuel with a pool-type primary system arrangement provides a highly reliable reactor system with large operational safety margins. The coolant thermo-physical properties provide superior heat removal and transport characteristics at low operating pressure with a large temperature margin to boiling. The metallic fuel operates at a relatively low temperature, below the coolant boiling point, due to its high thermal conductivity. The pool-type primary system confines all significantly radioactive materials within a single vessel, allows for easy removal and replacement of components as well as shutdown heat removal by natural circulation.

At the second level of safety, the ABTR is designed to provide protection in the event of equipment failure or operating error. This level of protection is provided by engineered safety systems for reactor shutdown, reactor heat removal, and emergency power. Each of these safety-grade back-up systems functions in the event of failure in the corresponding operating system, and are subjected to continuous monitoring and periodic testing and inspection.

The ABTR design provides an independently powered and instrumented secondary reactor shutdown system that operates automatically to reduce reactor power rapidly in the event that the primary shutdown system fails. For shutdown cooling, the ABTR design includes a safety-grade emergency heat removal system, independent from the normal heat removal system and capable of removing residual decay heat by natural circulation. In addition to the normal off-site power supply, the ABTR is equipped with a second independent off-site power connection. The two off-site power connections are supplemented by a safety-grade on-site emergency power supply.

The third level of safety provides additional protection of the public health and safety in an extremely unlikely event that is not expected to occur in the life of the plant, or which was not foreseen at the time the plant was designed and constructed.

In the ABTR design, the level 3 protections for cooling assurance and containment of radioactivity are provided by the reactor guard vessel and the reactor containment building. The reactor guard vessel is designed to hold primary coolant in the event of a leak in the primary coolant system. The reactor guard vessel assures that the reactor core

remains covered with sodium and cooled by the emergency heat removal system, even if the primary reactor vessel fails. If primary coolant leaks and oxidizes in the reactor building air atmosphere, or if failures of the cladding and the primary system barriers lead to release of gaseous fission products, the reactor containment building provides a final low-leakage barrier to release of radioactivity to the environment.

The three levels of safety together are the safety design basis for ABTR. For the purposes of subsequent safety design development, qualification, and documentation, it is customary during the pre-conceptual design phase to identify general design criteria that collectively serve as the basis for safety assessment of the design. A preliminary cross reference and evaluation of existing general design criteria from 10CFR Part 50 Appendix A, from ANSI/ANS Standard 54.1, and from DOE Order 5480.30 are included in Appendix A.

The normal process of safety assessment of a design considers a spectrum of design basis accidents (DBAs) as tests of the various safety systems. These DBAs generally assume single failures. Accidents within the design basis must be accommodated by the design and shown to present risks to the public that are within regulatory standards. Beyond the design basis, there exists a class of accidents of such low probability that they have been termed “hypothetical.” These events involve multiple failures of safety grade systems, and usually are considered to have a frequency of less than 10^{-6} per reactor year. Because of the potentially severe consequences of accidents in this class, they have received significant regulatory scrutiny in prior sodium-cooled fast reactor licensing reviews for the purpose of characterizing thermal and structural safety margins beyond the design basis.

Three beyond-design-basis accident (BDBA) sequences, each involving failure of both reactor scram systems, have received attention in past licensing safety assessments. In the unprotected loss-of-flow (ULOF) sequence, it is assumed that power is lost to all primary and secondary coolant pumps and the reactor scram systems fail to activate. In the unprotected transient overpower (UTOP) sequence, it is assumed that one or more inserted control rods are withdrawn, and the reactor scram systems fail to operate. In the unprotected loss-of-heat-sink (LOHS) accident, it is assumed that heat removal through the power conversion system is lost, and the reactor scram systems do not activate. Taken collectively, these three accident initiators encompass all the ways that an operating reactor can be perturbed, i.e. by a change in coolant flow, by a change in reactivity, or by a change in coolant inlet temperature.

The proposed ABTR design is capable of accommodating these beyond design basis accident initiators without producing high temperatures and conditions that might lead to a severe accident, such as coolant boiling, cladding failures, or fuel melting. The inherent neutronic, hydraulic, and thermal performance characteristics of the ABTR design provide self-protection in beyond-design-basis sequences to limit accident consequences without activation of engineered systems or operator actions. This characteristic has been termed ‘inherent passive safety.’

The efficacy of such passive safety was demonstrated through two landmark tests conducted on the Experimental Breeder Reactor-II (EBR-II), namely loss-of-flow without scram and loss-of-heat-sink without scram tests. With the automated safety systems disabled, the two most demanding accident initiating events were deliberately induced with the reactor at full power, first one then the other. Each time the reactor simply coasted to a safe low power state without any damage at all to the fuel or any reactor component. These tests proved conclusively that passive safety design is achievable for metallic fueled fast reactors with sodium cooling.

Within the overall safety framework for ABTR, passive safety serves to provide additional margins for public protection in the event of very low probability events whose frequency of occurrence is lower than the normal threshold for deterministic assessment. The ABTR passive safety performance characteristic assures that no abnormal radioactivity releases will occur in the event of beyond-design-basis accidents, and that all of the multiple defense-in-depth barriers (fuel cladding, reactor vessel, containment building) for public protection will remain intact, just as for design basis accidents. The passive safety performance of ABTR eliminates the potential for severe accident consequences in very low frequency, beyond-design-basis sequences. Consequently, for ABTR, beyond-design-basis accidents need to be considered only in the context of probabilistic risk assessments.

Security must now be considered as an integral part of the design. The inherent and passive safety features of the ABTR offer a high level of protection against malevolent events, as well as against accidents. Since the inherent and passive features do not rely on operator action, external power or functioning of active components, they remove these potential vulnerabilities. In addition, the location of the reactor vessel, the core, and the primary heat transport system below grade within a strong containment structure provides protection against external threats.

Implications on Licensing Approach

Historically, safety assessment of reactor designs has been based on a deterministic approach, in which a set of postulated initiating events are defined and the consequences of these events are determined by analysis. The events to be considered are selected to represent challenges to the reactor's control and safety systems, based on judgment, experience and regulatory requirements. The probability of an initiating event occurring is evaluated only qualitatively. USNRC licensing practice using the deterministic approach is highly developed for light-water power reactors and is codified in 10CFR Part 50. The general design criteria found in Appendix A of Part 50 and the related body of regulatory guidance have been applied successfully to licensing of the current fleet of LWRs. They were used with modification in licensing of the Fast Flux Test Facility and the Clinch River Breeder Reactor Project. However, it is recognized that use of criteria designed for LWR technology for new, innovative reactor designs is not efficient, nor does it lead to a stable and predictable regulatory process. In addition, recent trends in safety assessment and licensing have led to an increased emphasis on risk informed

decision-making, with a consequent emphasis on the use of probabilistic risk assessment throughout design, safety assessment, licensing and operation. All operating nuclear power plants are now required to have a probabilistic risk analysis (PRA) including both internal and external events, and probabilistic insights are now used in some aspects of operation and regulation.

The USNRC is now developing a risk-informed, performance based alternative to 10CFR Part 50 to be used in licensing of future nuclear power plants [1]. The framework for this alternative approach is based on the NRC's Safety Goals Policy and fundamental safety principles such as defense-in-depth and safety margins. It combines probabilistic and deterministic elements. It is technology-independent, with technology-specific requirements for particular designs.

Under the new regulatory framework, a probabilistic risk assessment would be an integral part of the design process and safety assessment, as well as having a fundamental role in the licensing process. Deterministic criteria and multiple lines of defense against undue radioactive release would continue to be required. Under this approach, a probabilistic analysis would be used to establish the event sequences to be considered in the licensing process and to classify equipment as to its safety significance. The selected events, called Licensing Basis Events (LBEs) would be analyzed deterministically to demonstrate the conservatism of the probabilistic analysis. The allowable consequences of an event would be matched to its frequency quantitatively.

As design work proceeds beyond the pre-conceptual stage, use of probabilistic analysis will be central to the design, especially to demonstrating the effectiveness of the inherent and passive safety features of the ABTR. It will also allow a quantitative selection of LBEs for deterministic analysis to show compliance with the NRC's Safety Goal Policy. In previous licensing of sodium-cooled fast reactors, a great deal of attention was focused on beyond-design-basis events leading to severe accidents. Probabilistic analysis affords the opportunity to show quantitatively that such events have a frequency below the lower limit for consideration as LBEs (the current proposal is a frequency less than 10^{-7} per reactor-year); nevertheless, defense-in-depth considerations will likely require mitigation features such as low-leakage containment.

At the present time, the approach to be used for licensing of the ABTR is not clear, given the project schedule and the likely time frame for introduction of the risk-informed, performance-based alternative. However, it is clear that an approach to design and safety assessment using both probabilistic and deterministic methods will be needed. In the longer term, such an approach will surely be needed for ABR licensing, and the ABTR licensing offers the opportunity to develop the methods and data needed to support the ABR in the future.

Reference

1. NUREG-1860, Framework for Development of a Risk-Informed, Performance-Based Alternative to 10 CFR Part 50, Working Draft, July 2006.

PART II PLANT DESIGN DESCRIPTION

II.1 Reactor System

II.1.1 Reactor Core

The primary goals of the Advanced Burner Test Reactor (ABTR) are to demonstrate the benefits of a closed nuclear fuel cycle and provide a suitable irradiation facility for development and qualification of transuranic (TRU) fuels of the Advanced Burner Reactor (ABR). Core design studies were performed to develop a reference core design that meets these ABTR goals [1]. Various design trade-off studies were performed to determine the appropriate power level and conversion ratio. Both metallic and oxide fuel forms were considered with TRU feeds from weapons-grade plutonium (WG-Pu) and TRU recovered from light water reactor spent fuel (LWR-SF).

The trade-off study on power level suggested that ~250 MWt is a reasonable compromise to allow a low project cost, at the same time providing a reasonable prototypic irradiation environment for demonstrating TRU-based fuels. Preliminary design studies showed that it is feasible to design the ABTR to accommodate a wide range of conversion ratio (CR) by employing different assembly designs. The TRU enrichments required for various conversion ratios and the irradiation database suggested a phased approach with initial startup using conventional enrichment plutonium-based fuel and gradual transitioning to full core loading of transmutation fuel after its qualification phase (resulting in ~0.6 CR). The low CR transmutation fuel tests can be accommodated in the designated test assemblies, and if fully developed, core conversion to low CR fuel can be envisioned. The details of these trade-off studies are discussed in Sections III.4.1 and III.4.2.

Based on the results of these trade-off studies, a reference core design with a rated power of 250 MWt was developed for ternary metal alloy (U-TRU-Zr) fuel with WG-Pu feed. An alternative design was developed for mixed oxide (UO₂-TRUO₂) fuel. Since it is expected that the ABTR core will be converted gradually into LWR-SF TRU drivers, the performance characteristics of the metal and oxide core designs loaded with LWR-SF TRU drivers were also evaluated.

The design descriptions and performance characteristics of the reference metal core design are presented in this section. The alternative oxide core design is discussed in Section III.4.3. The performances of the LWR-SF TRU fuel and the low CR assembly designs are provided in Sections III.4.4 and III.4.5, respectively.

II.1.1.1 Core and Assembly Design Description

Using WG-Pu drivers, a 250 MWt reference core design was developed for ternary metal alloy fuel. It is a homogeneous design with 199 assemblies – 54 driver assemblies, 78 reflector assemblies, 48 shield assemblies, 10 control rod assemblies, and 9 test assemblies. Figure II.1-1 shows the reference core configuration. In order to increase the flexibility of core loading and the space for irradiation test, nine test assembly locations were allocated. The core barrel inner diameter is 2.27 m, and the equivalent core outer diameter is 1.31 m. Two independent safety-grade reactivity control systems are employed for reactivity control and reactor shutdown. The primary control system consists of one central assembly and six assemblies in the fifth row, and the secondary control system consists of three assemblies in the third row. Reactivity control for normal operation, load following and shutdown is accomplished by bank (uniform) movement of seven primary control rod assemblies in the fuel region of the core.

Enrichment zoning strategy was chosen to flatten the power distribution, and two enrichment zones were used to simplify the refueling operation. The 54 driver assemblies are divided into two enrichment zones: the inner and outer cores composed of 24 and 30 driver assemblies, respectively. The fuel enrichments (i.e., TRU fractions) of inner and outer cores are 16.5 and 20.7%, respectively. Among the total nine test assembly locations, three assemblies located in the fourth row were designated for material test assemblies. Since the compositions of these material test assemblies are not known at this point, reflector assemblies were used for the core performance calculations. Six fuel test assemblies are located in the third and fourth rows. The fuel test assemblies are assumed to be identical to the driver fuel assembly except that LWR-SF TRU is used instead of weapons grade plutonium. The fuel alloy is U-TRU-10%Zr, and the TRU compositions of WG-Pu and LWR-SF TRU are presented in Table II.1-1. The LWR-SF TRU composition was determined from 10-year cooled LWR spent fuel with 33 MWd/kg burnup.

The design of core assemblies maximizes the use of common structural components, with the exception of the assembly internals. All core assemblies use the same hexagonal duct and handling socket. Fuel, shield and control rod assemblies use sealed-type pins to contain the fuel and absorber materials and fission products. Reflector assemblies contain pin bundles of solid HT-9 rods. The bottom of the fuel pins similarly consists of solid HT-9 rods for lower axial shielding. Figure II.1-2 shows the assembly schematics and fuel pin design data. The key design parameters of the fuel, reflector, shield and control assemblies are presented in Table II.1-2.

The fuel assembly has an overall length of 328 cm and contains 217 fuel pins arranged in a triangular pitch array. Fuel pins are made of sealed cladding containing a metallic fuel column of 80 cm length. Sodium is filled as the initial thermal bond between the fuel column and the cladding. The fuel pin diameter and cladding thickness are 8.00 mm, and 0.52 mm, respectively. It is noted that this pin size is within the PRISM design range of 7.4-8.3 mm. The fuel smeared density is 75%. The fuel pin is helically wrapped

with wire to maintain the pin spacing so that the coolant can flow freely through the pin bundle. The wire-wrap helical pitch is 20.32 cm.

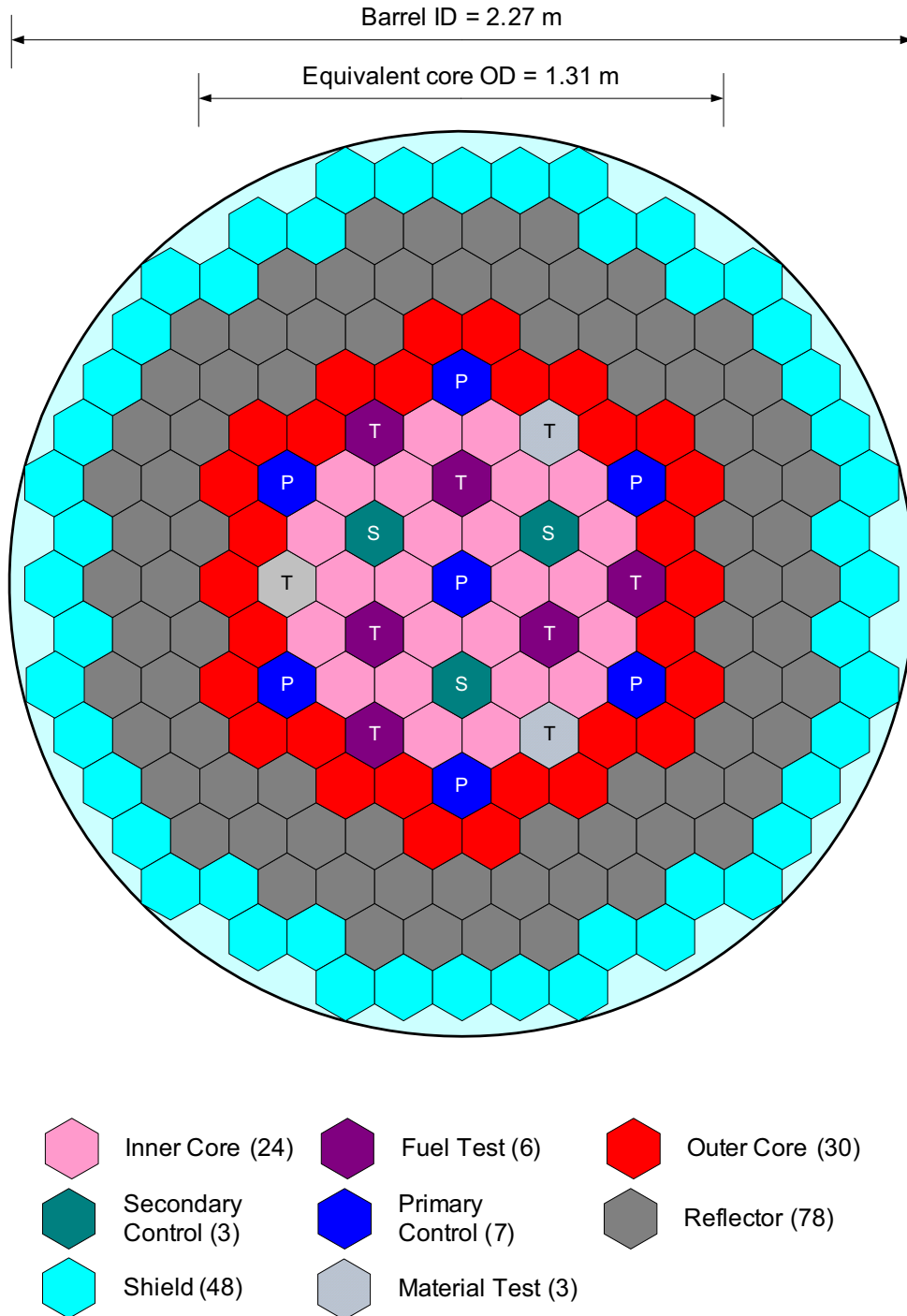


Figure II.1-1 Reference ABTR Core Configuration

Table II.1-1 TRU Isotopic Composition (%)

	WG-Pu	LWR-SF TRU
Np-237	0.00	4.60
Pu-238	0.01	1.35
Pu-239	93.81	51.77
Pu-240	5.81	23.67
Pu-241	0.35	7.80
Pu-242	0.02	4.67
Am-241	0.00	5.08
Am-242m	0.00	0.01
Am-243	0.00	0.88
Cm-243	0.00	0.00
Cm-244	0.00	0.17
Cm-245	0.00	0.01
Cm-246	0.00	0.00

A 120 cm long fission gas plenum is located above the fuel slug and sodium bond. The fuel assemblies are 14.198 cm across the outer hex flats and are positioned within the core at a 14.598 cm triangular pitch spacing with a 0.40 cm inter-assembly gap. The 80 cm high active core starts at 98 cm from the bottom of the assembly. Immediately below the core is a 60 cm shield region, with the shield being an integral part of the fuel pin in the form of an extended fuel-pin bottom end cap.

The reflector assembly contains 91 solid HT-9 pins arranged in a triangular pitch array. The HT-9 pin volume fraction is 76.5 % and the duct volume fraction is 7.8 %, yielding the total HT-9 volume fraction of 84.3 %. The shield assembly is mainly composed of HT-9 cladding and B₄C absorber. It consists of 19 thick HT-9 tubes containing boron carbide pellets. The natural boron is used with a smeared B₄C pellet density of 81%. The resulting B₄C and HT-9 volume fractions are 42.3 % and 30.4 %, respectively.

The control assemblies consist of an absorber bundle contained within a duct. The absorber bundle is a closely packed array of tubes containing compacted boron carbide pellets. The natural boron whose B-10 enrichment is 19.9 a/o is used. The pins are helically wrapped with wire and bundled into a triangular pitch, hexagonal pattern. The bundle of control rods is contained in an interior duct that channels flow through the bundle and protects the pins from damage as they slide within the outer fixed duct. The outer duct of the control rod assembly has the same external dimensions as the fuel assembly duct except for the nose-piece, which has unique discrimination features to preclude inadvertent installation into an unassigned core position. The duct directs coolant flow to the absorber bundle. The control system is designed to be operated with the absorber bundle partially inserted at all times.

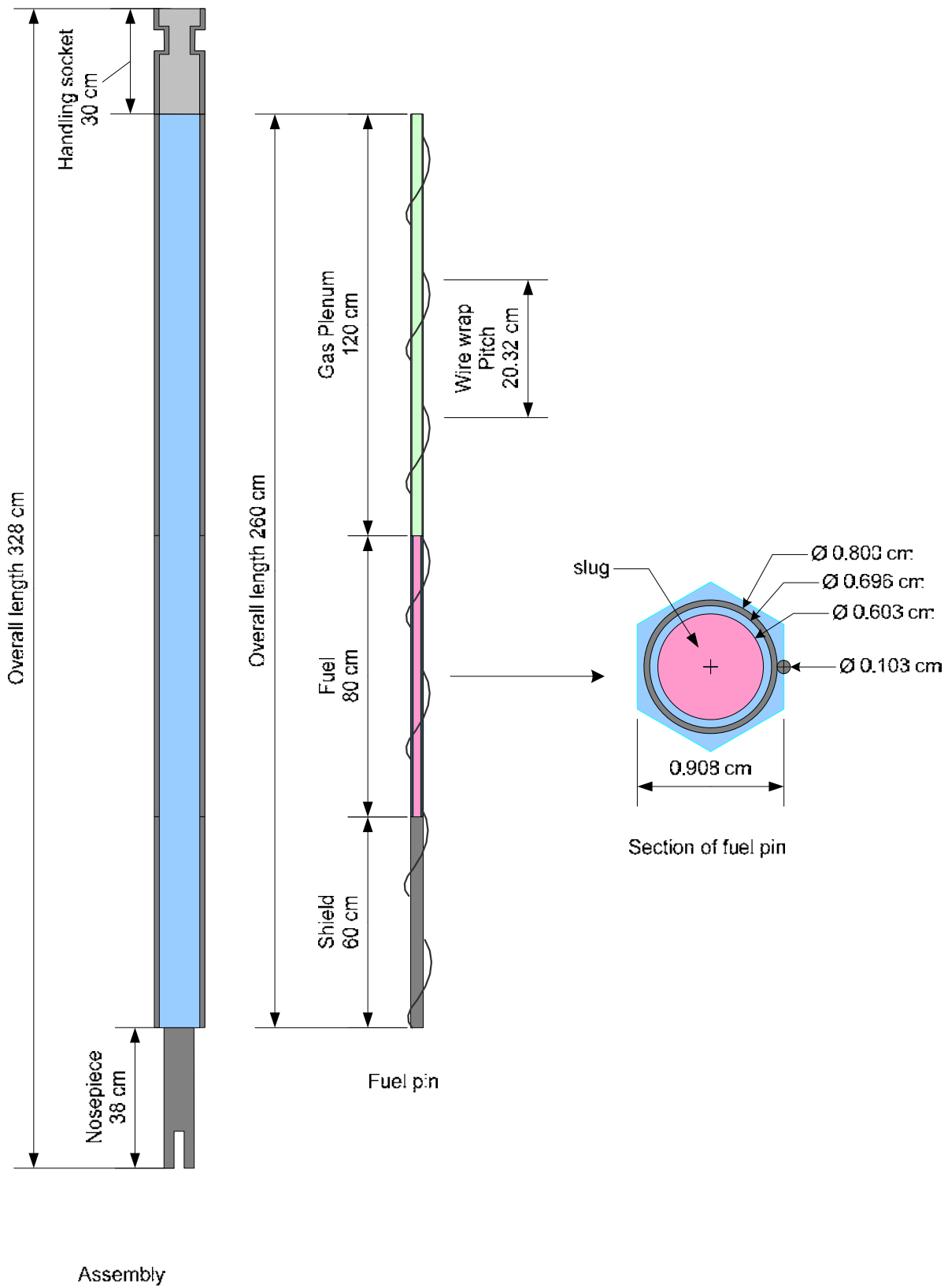


Figure II.1-2 Fuel Assembly Schematic and Fuel Pin Cross Section

Table II.1.1-2 Assembly Design Parameters

	Fuel	Reflector	Shield	Control
Assembly data – Number of pins – Assembly pitch, cm – Inter-assembly gap, cm – Duct outside flat-to flat distance, cm – Duct material – Duct thickness, cm – Gap between duct and interior duct, cm – Interior duct thickness, cm – Interior duct inside flat-to-flat distance, cm	217 14.598 0.400 14.198 HT9 0.300 - - -	91 14.598 0.400 14.198 HT9 0.300 - - -	19 14.598 0.400 14.198 HT9 0.300 - - -	91 14.598 0.400 14.198 HT9 0.300 0.400 0.300 12.198
Pin data – Pin material and type – Bond material – Overall pin length, cm – Pellet smeared density, % TD – Pellet diameter, cm – Cladding material – Clad outer diameter, cm – Pin pitch-to-diameter ratio – Cladding thickness, cm – Wire wrap diameter, cm	U-TRU-10Zr Na 260.0 75.0 0.603 HT9 0.800 1.130 0.052 0.103	HT9-solid pin - 260.0 - 1.405 - - 1.001 - (no wire-wrap)	B ₄ C (natural B) He 260.0 81.0 2.288 HT9 3.043 1.001 0.250 (no wire-wrap)	B ₄ C (natural B) He 260.0 85.0 0.895 HT9 1.110 1.124 0.070 0.133
Volume fraction, % – Fuel or Absorber – Bond – Structure – Coolant	33.6 11.2 23.1 32.1	- - 84.3 15.7	42.3 9.9 30.4 17.3	31.0 5.5 26.8 36.7

II.1.1.2 Fuel Cycle Performance Characteristics

Fuel cycle analyses were performed with the DIF3D/REBUS-3 code system [2,3]. The region-dependent 21-group cross section set generated with the ETOE-2/MC²-2/SDX code system [4-6] based on ENDF/B-V.2 was used. Using 3-dimensional hexagonal-z geometry models, equilibrium cycle analyses were performed with scattered loading. The material thermal expansion at operating condition was modeled by adjusting the hexagonal pitch, axial meshes, and the fuel and structure volume fractions appropriately. The irradiation-induced swelling of metal fuel was considered, and the bond sodium was displaced into the lower part of the fission gas plenum. Block nuclide depletion was performed by dividing each fuel assembly into five axial depletion zones. For flux calculations, the hexagonal-Z nodal diffusion theory option of DIF3D [7] was mainly employed. The required TRU enrichment (i.e., TRU fraction in heavy metal) was determined from the equilibrium cycle analysis such that the multiplication factor at the end of cycle (EOC) is 1.0. Enrichment zoning strategy was employed to flatten the power distribution, but no attempt was made yet to optimize the reactivity swing and discharge burnup. The fuel cycle length was estimated such that the burnup reactivity swing is within the reactivity control capability of the primary control system. The discharge burnup was determined by adjusting the fuel residence time such that the peak fast fluence is within the fast fluence limit of HT-9 cladding (4.0×10^{23} n/cm²).

Linear power limits were estimated by simple thermal-hydraulic calculations based on a single channel model. The coolant inlet and bulk outlet temperatures were 355 °C and 510 °C, respectively. The average flow rate was determined such that the coolant temperature rise across the core is 155 °C. A chopped cosine shape was assumed for the axial power distribution. Hot channel factors of 2.67, 1.10, and 1.24 were used for the film, cladding, and coolant regions, respectively. The fresh fuel thermal conductivity was determined as a function of U, Pu, and Zr weight fractions using the correlation for U-Pu-Zr fuel [8], and a porosity correction factor of 0.5 was applied to take into account the irradiation effects. It was noted that this metal fuel correlation significantly underestimates the thermal conductivity for high TRU fractions greater than 30%. The fuel solidus temperature was also estimated as a function of constituent mole fractions using the correlation for U-Pu-Zr fuel [9]. The fuel-cladding eutectic temperature was conservatively assumed to be 650 °C. The linear power limit was determined such that the peak fuel centerline temperature is lower than the fuel solidus temperature and the peak cladding inner-wall temperature is lower than the fuel-cladding eutectic temperature.

The start-up core performances characteristics of the reference cores are provided in Table II.1-3, which were obtained from REBUS-3 equilibrium cycle calculations without recycling the ABTR spent fuel. As mentioned in Section II.1.1.1, WG-Pu was used as TRU feed for driver assemblies, while the LWR-SF TRU was used for fuel test assemblies. The cycle length was selected as 4 months to limit the burnup reactivity swing within the reactivity control capability of the seven primary control assemblies. In order to achieve a reasonably high discharge burnup, a 60-month fuel residence time is

used for the outer core drivers. The fuel residence time of inner core drivers is set to 48 months to equalize the average discharge burnup of inner and outer core drivers approximately. A 15-batch fuel management scheme is used for outer core drivers, and a 12-batch scheme is used for inner core drivers. For the simplicity of REBUS-3 calculations, the fuel cycle management scheme for the inner core drivers was also used for test fuel assemblies. It is noted that the small number of drivers makes it difficult to achieve a reasonably high discharge burnup with a 1/6- or 1/3-core symmetry fuel management, thus a 1/2-core symmetry fuel management scheme was used.

Table II.1-3 Start-up Cycle Performance Characteristics

Cycle length, months	4
Number of batches (inner core/outer core/test assembly)	12 / 15 / 12
Fuel form	U-Pu-10Zr
TRU feed (fissile content, %)	WG-Pu (94.2)
TRU enrichment (inner core/outer core/test assembly), %	16.5 / 20.7 / 18.7
Conversion ratio, fissile/TRU	0.58 / 0.65
Initial core loading (heavy metal/TRU), MT	4.03 / 0.73
Specific power of active core, kW/kg	59.4
Power density of active core, kW/l	258.0
Discharge burnup (average/peak), MWd/kg	97.7 / 130.8
Peak fast fluence, 10^{23} n/cm ²	3.25
Burnup reactivity swing (% Δ k)	1.20
Power peaking factor, BOEC/EOEC	1.53 / 1.52
Peak linear power, kW/m	38.5
Linear power limit, kW/m	44.0
Core average flux, 10^{15} n/cm ² -sec	2.38
Test assembly flux, 10^{15} n/cm ² -sec	2.84
Fast flux fraction	0.70

The TRU enrichments are 16.5 and 20.7% for the inner and outer core zones, respectively. The resulting TRU conversion ratio is 0.65, and the burnup reactivity swing is 1.2 % Δ k over the 4-month cycle. The heavy metal and TRU loadings are 4.03 and 0.73 metric tons, respectively. The specific power density is 59.4 kW/kg, and the power density is 258.0 kW/l. The core average total flux is 2.38×10^{15} /cm²s, and the average flux of the fuel test assemblies is 2.84×10^{15} /cm²s. The average discharge burnup is about 98 MWd/kg, and the local peak discharge burnup is 131 MWd/kg. The peak fast fluence is 3.25×10^{23} n/cm², which is well within the HT-9 cladding limit of 4.0×10^{23} n/cm². The peak linear power is within the linear power limit with a 14% margin.

Table II.1-4 provides the heavy metal inventories and the mass flow rates of the start-up core. The annual consumption rates of TRU and total heavy metal are 25.9 and 84.6 kg, respectively. Two new outer core and two new inner core drivers are needed each

cycle. Since there are three cycles per year, the metal fuel production line would need to produce 12 new assemblies each year once the ABTR is up and running. The heavy metal mass per assembly is 70.1 kg, and the TRU mass per assembly is 11.6 kg for inner core drivers and 14.5 kg for outer core drivers. For the assumed fuel management scheme for fuel test assemblies, one and one-half assemblies are replaced per year on the average, and each test assembly contains 13.1 kg TRU.

Table II.1-4 Start-up Cycle Heavy Metal Inventories and Mass Flow Rates

Isotope	Inventory, kg		Mass flow, kg/year	
	BOEC	EOEC	charge	discharge
U-234	0.0	0.0	0.00	0.01
U-235	5.2	5.0	1.52	0.84
U-236	0.3	0.4	0.00	0.14
U-238	3289.6	3270.2	768.35	710.29
Np-237	3.6	3.6	0.89	0.88
Pu-236	0.0	0.0	0.00	0.00
Pu-238	1.6	1.7	0.28	0.56
Pu-239	628.6	617.0	156.83	121.80
Pu-240	80.2	83.1	13.74	22.29
Pu-241	8.9	9.0	2.09	2.26
Pu-242	4.0	4.0	0.96	1.03
Am-241	3.8	3.8	1.00	0.90
Am-242	0.1	0.1	0.00	0.05
Am-243	0.7	0.8	0.18	0.20
Cm-242	0.1	0.1	0.00	0.04
Cm-243	0.0	0.0	0.00	0.00
Cm-244	0.2	0.2	0.03	0.06
Cm-245	0.0	0.0	0.00	0.01
Cm-246	0.0	0.0	0.00	0.00
Total heavy metal	4027.2	3999.0	945.9	861.3
Total TRU	732.0	723.4	176.0	150.1

Figure II.1-3 shows the batch-average and fresh assembly power distributions determined by REBUS-3 equilibrium cycle calculations with scattered loading. The batch-average power estimates the average power of each assembly position by using a homogenized mix of all the burned stages of fuel. The real power of each assembly position varies over the fuel residence time depending on the burned stage of fuel. The fresh assembly power of Figure II.1-3 denotes the power of each assembly position when it is occupied by a fresh assembly. It is noted that the power distributions of Figure II.1-3 were obtained from the neutronics calculations only, in which the gamma energy is locally deposited at the position of its creation. (Coupled neutron and gamma heating calculations will be performed in the future along with detailed thermal-hydraulic analyses.) The results show that the fuel assembly power depends on the position more than the burned stage. The higher assembly powers are observed near the core center. It is

noted that the enrichment ratio of inner core to outer core was 1.25 and was not optimized in this study.

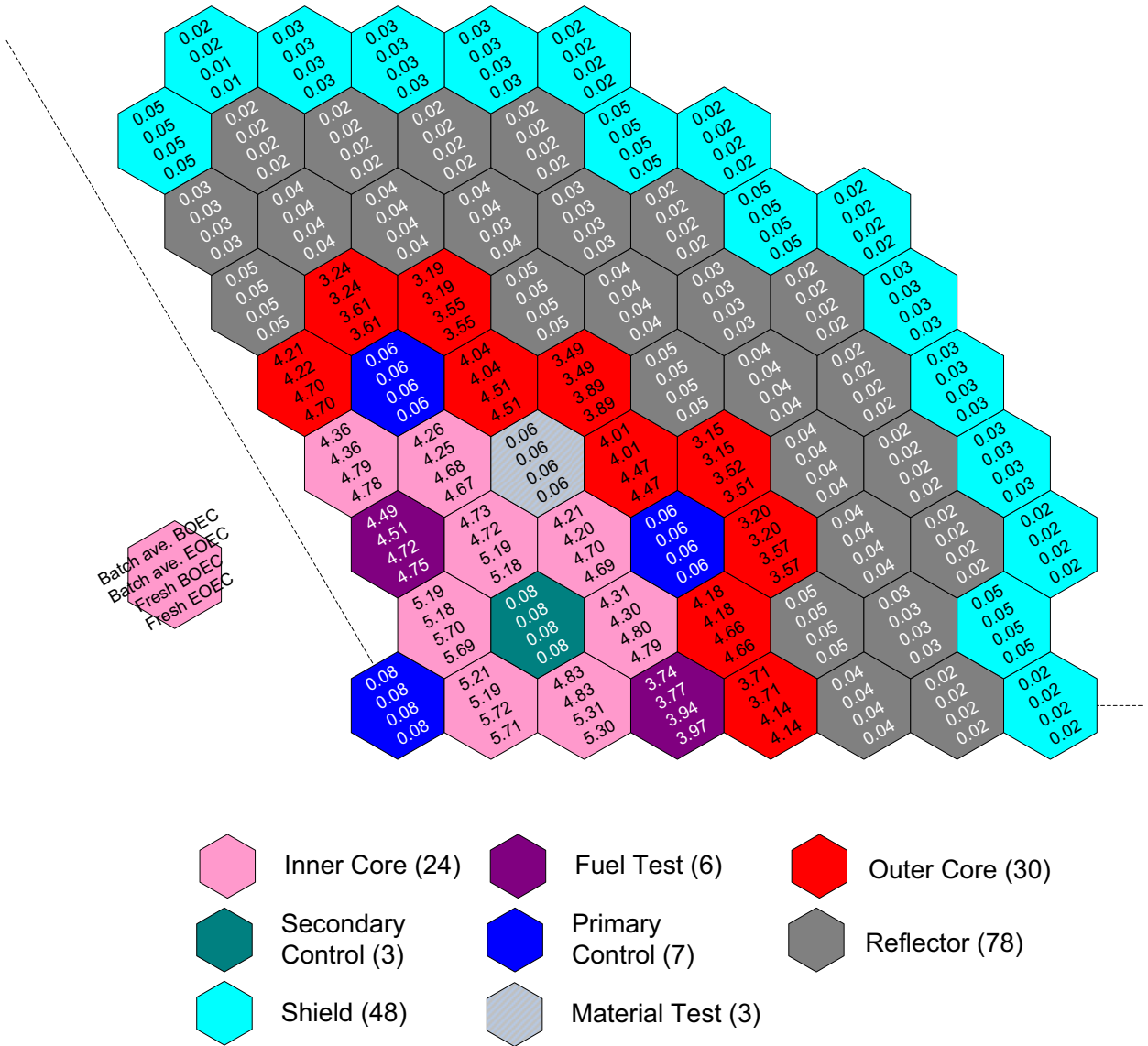


Figure II.1-3 Batch-Average and Fresh Assembly Power Distributions (MW)

II.1.1.3 Kinetics Parameters and Reactivity Coefficients

Kinetics parameters and reactivity coefficients of the reference core were calculated for the core configurations at the beginning of equilibrium cycle (BOEC) and the end of equilibrium cycle (EOEC). The coolant, fuel, and structure density coefficients and the coolant void coefficient were determined using the VARI3D perturbation code [10]; the linear perturbation theory option was used for density coefficients, while the exact perturbation theory option was employed for the coolant void coefficient. The effective delayed neutron fraction and prompt neutron lifetime were also calculated using the VARI3D code. The radial and axial expansion coefficients and the control rod worth were determined by direct eigenvalue differences of the base and perturbed conditions using the DIF3D code.

Table II.1-5 shows the kinetics parameters and reactivity coefficients estimated for the BOEC and EOEC configurations of the reference ABTR metal core. The effective delayed neutron fraction (β_{eff}) is 0.0033, and the prompt neutron lifetime is 0.33 μs . The radial expansion coefficient represents the reactivity effects of uniform, radial thermal expansion of the grid plate (SS-316) that is governed by the coolant inlet temperature. The axial expansion coefficient represents the reactivity effects of uniform, axial thermal expansion of fuel for the case that the fuel is bonded to the cladding. The radial and axial expansion coefficients are about -0.60 cents/ $^{\circ}\text{C}$ and -0.05 cents/ $^{\circ}\text{C}$, respectively

The sodium void worth and sodium density coefficient are positive because the positive spectral hardening effect over-weighs the negative leakage effect. However, the total sodium void worth is only $\sim 1.8\%$, when the flowing sodium inside the assembly duct of all the fuel assemblies is voided in the active core and above. The Doppler coefficient is about -0.10 cents/ $^{\circ}\text{C}$, and the voided Doppler coefficient is about -0.07 cents/ $^{\circ}\text{C}$. The voided Doppler coefficient is slightly less negative than the flooded Doppler coefficient due to hardened neutron spectra.

Table II.1-5 Kinetics Parameters and Reactivity Coefficients

	Unit	BOEC	EOEC
Effective delayed neutron fraction		0.0033	0.0033
Prompt neutron lifetime	μs	0.33	0.33
Radial expansion coefficient	cent/ $^{\circ}\text{C}$	-0.59	-0.60
Axial expansion coefficient	cent/ $^{\circ}\text{C}$	-0.06	-0.05
Fuel density coefficient	cent/ $^{\circ}\text{C}$	-0.75	-0.76
Structure density coefficient	cent/ $^{\circ}\text{C}$	0.03	0.03
Sodium void worth	$\%$	1.75	1.85
Sodium density coefficient	cent/ $^{\circ}\text{C}$	0.03	0.03
Doppler coefficient	cent/ $^{\circ}\text{C}$	-0.10	-0.10
Sodium voided Doppler coefficient	cent/ $^{\circ}\text{C}$	-0.07	-0.07

II.1.1.4 Spent Fuel Characteristics

To provide necessary data for designing the fuel-unloading machine and shielded fuel cask, spent fuel characteristics were estimated. Using the ORIGEN-2 code [11], the decay heat, photon and neutron sources were calculated for a time span from charge to 3 years after discharge. The one-group cross sections determined from REBUS-3 equilibrium cycle calculations were used for actinide isotopes, and the FFTF one-group cross section library of the ORIGEN-2 code package was used for other isotopes. It was confirmed that the use of the actinide cross sections derived from REBUS-3 calculations yields consistent depletion results between ORIGEN-2 and REBUS-3 calculations (the difference in the heavy metal masses at discharge burnup between ORIGEN-2 and REBUS-3 calculations was generally less than 1.0%).

It was observed that the decay heat depends more on the TRU feed than on the discharge burnup. Table II.1-6 presents the decay heat of ABTR metal fuel assemblies depleted up to the peak discharge burnup. To estimate a bounding case, LWR-SF TRU feed and low conversion ratio transmutation test fuels were also considered. (The design and performance parameters of these transmutation fuels are discussed in Sections III.4.4 and III.4.5.) The decay heat per assembly at discharge is about 0.23 MW, which is equivalent to about 5.5% of the average fission power; the LWR-SF TRU fuel yields a slightly higher decay heat relative to the WG-Pu fuel. Compared to the WG-Pu fuel, the LWR-SF TRU fuel shows a higher decay heat at charge and after a sufficient time elapse because of the higher content of the dominant long-lived decay heat sources (Pu-238, Am-241, and Cm-244). Figure II.1-4 shows the decay heat of ABTR discharged fuels as a function of post-irradiation decay time for the peak discharge burnup. The first two digits of each legend represent the TRU enrichment in percent, and the last three digits denote the discharge burnup in MWd/kg. The TRU enrichment denotes the round-off number of the values in Table II.1-6. The decay heat decreases rapidly with post-irradiation decay time, since short-lived fission products are dominant contributors to decay heat.

The spontaneous neutron and photon sources were evaluated for the spent metal fuel assembly of 24.8% LWR-SF TRU enrichment and 130.6 MWd/kg burnup, which has the largest decay heat. The spontaneous neutron source per assembly was about 1.32×10^9 /sec at the peak discharge burnup, and the dominant contributors were Cm-244 (55%) and Cm-242 (44%). The half-lives of Cm-244 and Cm-242 are 18.1 years and 162 days, respectively, and hence the spontaneous neutron source decreases in proportion to the Cm-242 decay during the time of interest for shielding design. Figure II.1-5 shows the energy-dependent photon sources per assembly. The photon source per assembly is about 1.15×10^{18} /sec at the peak discharge burnup, but it decreases to less than 2.0 % of this value after one year decay, because the short-lived fission products are dominant contributors to the photon source (~81% at discharge). The average photon energy at the peak discharge burnup is ~0.33 MeV, but it varies in the range of 0.25 to 0.40 MeV depending on the post-irradiation time.

Table II.1-6 Decay Heat of Spent Fuel Assembly with Peak Discharge Burnup

TRU feed		WG-Pu		LWR-SF TRU		
TRU Conversion ratio		Medium (~0.65)	Low (~0.31)	Medium (~0.57)	Low (~0.24)	
Charge TRU enrichment (%)		18.8	34.9	24.8	46.7	
Discharge burnup (MWd/kg)		130.8	130.8	130.6	130.5	
Initial HM/TRU mass per assembly (kg)		70.1/13.2	34.5/12.0	70.1/17.4	34.5/16.1	
Fuel residence time (EFPD)		2202	1086	2197	1087	
Decay heat fraction of rated power (%)		5.4	5.3	5.5	5.5	
Decay heat per assembly (kW)	Fresh fuel	0.03	0.03	0.37	0.34	
	Time after discharge	0 day	223.8	218.8	230.5	226.4
		1 day	11.0	20.2	25.8	25
		1 month	6.4	5.9	9.8	10.2
		2 month	4.7	4.2	7.8	8.1
		1 year	1.7	1.3	2.9	2.7
		2 year	0.9	0.7	1.6	1.4
		3 year	0.6	0.4	1.2	0.9

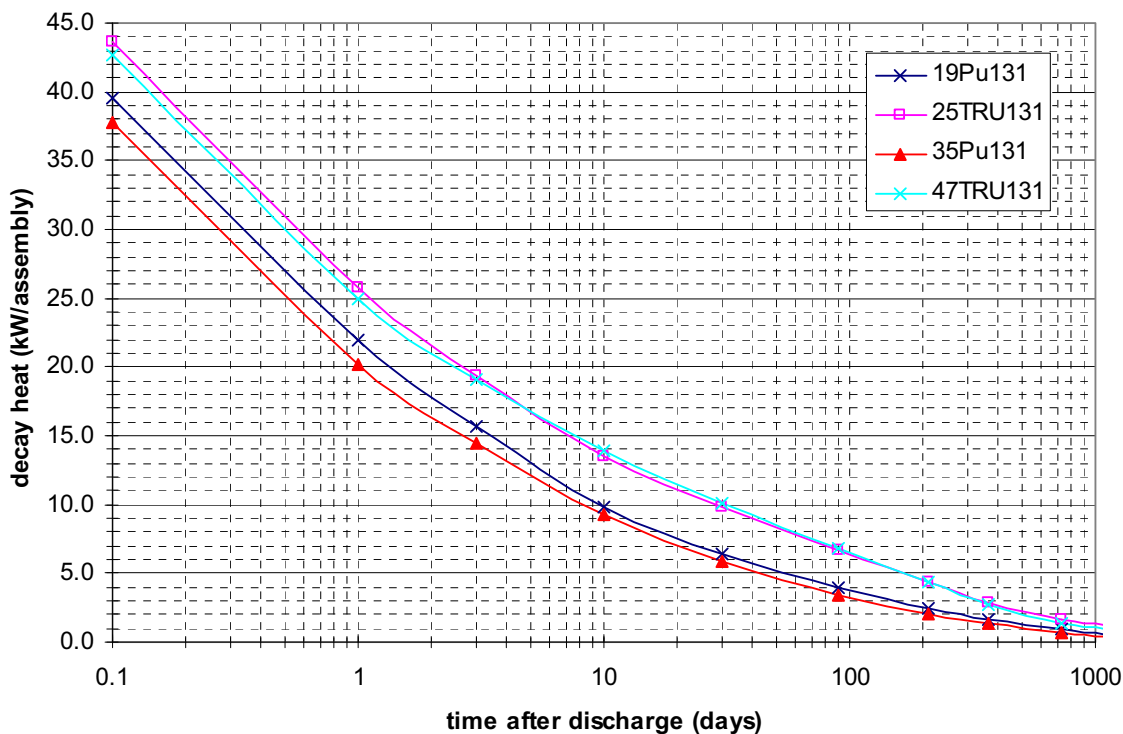
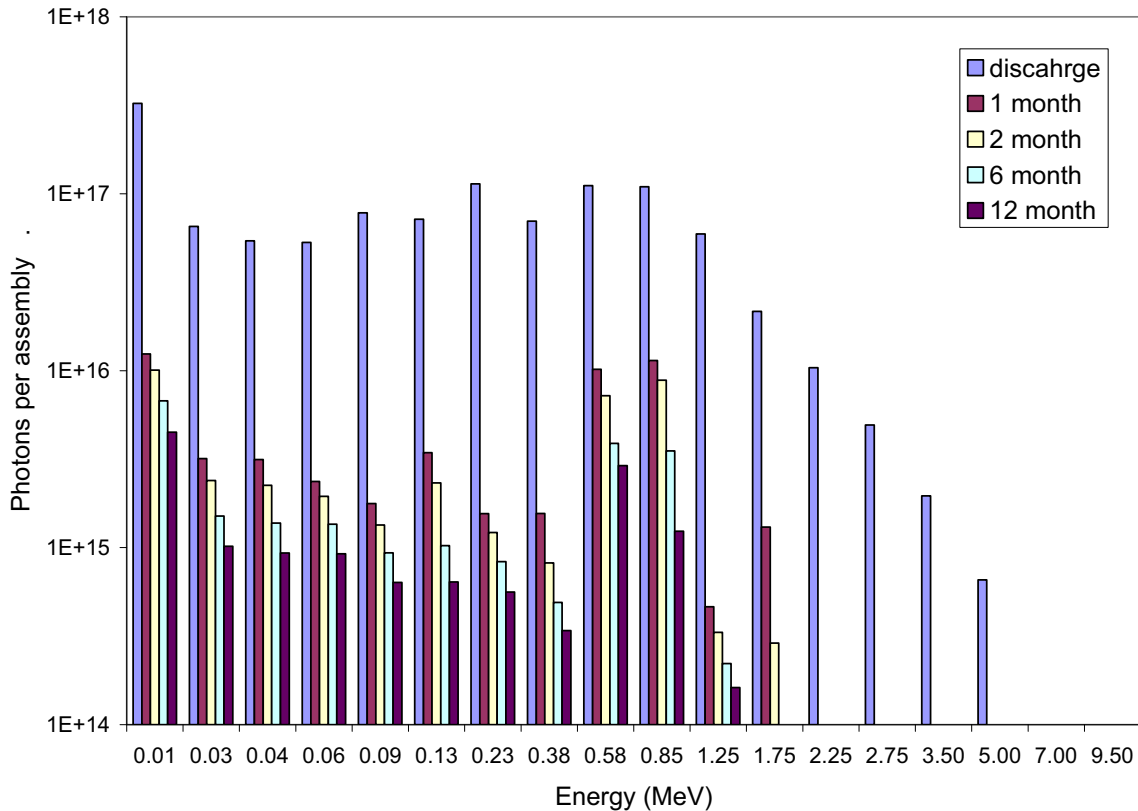


Figure II.1-4 Decay Heat of Spent Fuel



**Figure II.1-5 Photon Source Spectrum of Spent Fuel
(24.8% LWR-SF TRU Enrichment and 130.6 MWd/kg Burnup)**

II.1.2 Upper Internals Structure

The upper internals structure (UIS) is a package of hardware suspended from the rotatable plug to about 3 in. above the core assemblies. The functions of the UIS are to:

1. Support shroud tubes containing the primary and secondary control rod drivelines;
2. Preserve critical alignments between these drivelines and the core lattice, under normal and off-normal (including seismic) conditions;
3. Route and support thermocouples for temperature surveillance of core assemblies;
4. Route and support other instrumentation such as loose-parts monitors and delayed-neutron sampling stations;
5. Produce sufficient coolant mixing to mitigate thermal transients to downstream components;
6. Provide an opening for the In-Vessel Fuel Handling Machine to access inner core positions without interfering with the control rod drive lines and the upper core instrumentation package.

In the present design, outlet thermocouples cover most of the fuel assemblies, and some of the reflector assemblies, and no shield assemblies. Instrument posts of several different geometric configurations are needed when the requirement exists to monitor all heat generating core assemblies. When this requirement is relaxed, however, instrument posts can be dispensed with. In addition to the obvious cost reduction, this is an important design change because thermal striping studies on the CRBR UIS have shown the instrument posts to be the components most vulnerable to thermal fatigue under steady state operating conditions. Additional thermal striping tests are needed for confirmation, but at this time it is believed that the elimination of instrument posts could allow the entire UIS to be constructed of austenitic stainless steel.

Figure II.1-6 illustrates the present reference UIS design. The outer boundary is an 1.3 meter diameter shroud (essentially the outside diameter of the core assemblies) with large-hole penetrations over part of its length. The penetrations release the core effluent horizontally to the hot pool from which it travels upward and then to the inlets of the two IHXs. Within the shroud are ten 4 in. outer diameter control rod shroud tubes. Three inches is the nominal gap between the core assemblies and the bottom of the shroud tubes and UIS shroud. The shroud tubes are perforated for the release of coolant to the hot pool at an elevation close to the free surface. The radial position of the shroud tubes is fixed by at least three horizontal guide plates, welded to the UIS shroud. The lower guide plate is close to the core assemblies and is perforated to permit about 85% of the core effluent to reach the region between guide plates. The balance either goes up the shroud tubes or leaks through the 3 in. peripheral gap. In the region between guide plates are located five loose-parts monitors (high-temperature submersible microphones attached to the outside of selected shroud tubes) and delayed neutron sampling stations attached to all shroud tubes. The latter are part of the failed element detection and location (FEDAL) system. With minimal horizontal mixing of core effluent upstream of the sampling stations, it is expected that the location of a badly breached fuel element can be coarsely identified by the relative signal strengths from these sampling stations. Flow tests are necessary to better establish the expected performance of this part of the FEDAL system.

The upper guide plate is not perforated except for clearances at the 10 shroud penetrations to permit sliding due to differential thermal expansion. The upper guide plate is located high within the upper internal structure. Thus, almost all of the core effluent is forced to enter the hot pool at least 4 ft below the nominal hot pool operating level. This should meet the objective of maintaining a quiet entrainment-free surface. If future flow tests reveal an undesirable degree of surface agitation, the upper guide plate can be dished, concave downward, to further suppress any upward flow vectors of sodium leaving the UIS.

Core assembly outlet sodium temperature is monitored by chromel-alumel, stainless steel sheathed, ungrounded thermocouples. These thermocouples are replaceable and installed in helium-filled wells. The thermocouple wells are positioned 3 in. above the centerline of adjacent fuel assemblies. The outside surface of the control rod shroud tubes serves also to support the delayed neutron sampling lines and the leads and

oxygen vent lines for the loose parts-monitoring microphones. In the stagnant zone above the upper guide plate, all of these instrument lines are gathered into six instrument conduits which penetrate the rotatable plug.

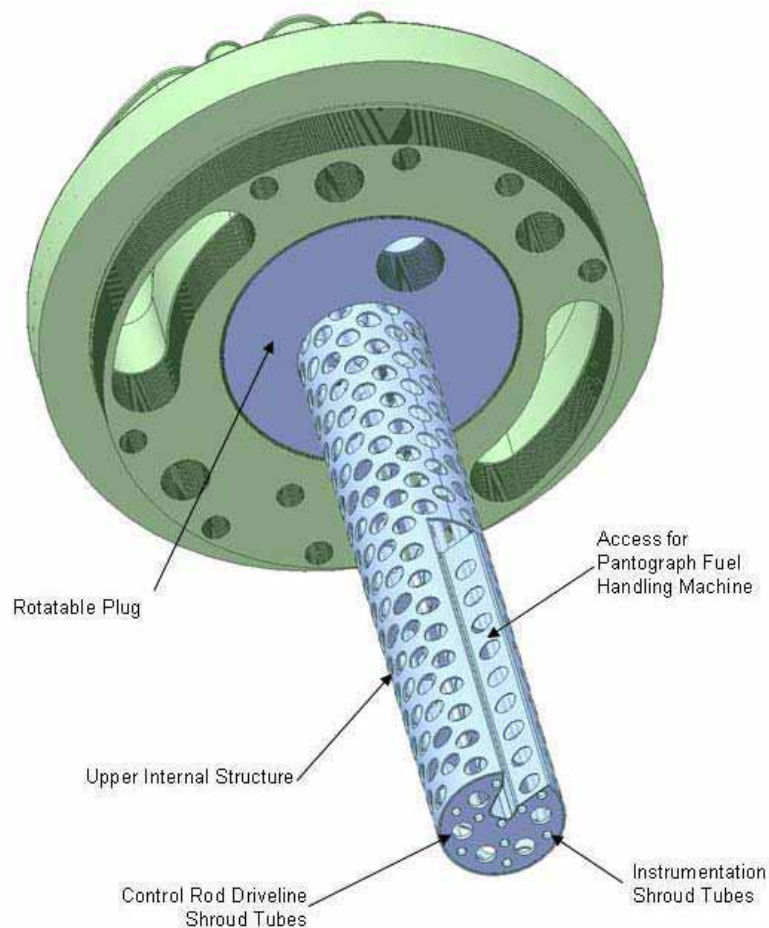


Figure II.1-6 Schematic of Upper Internal Structure

The UIS design provides backup mechanical hold-down protection, even though this is not considered a design requirement. In the event of a hydraulic liftoff of a fuel or internal blanket assembly, due to a non-mechanistic failure of the hydraulic hold-down system, the assembly would be stopped in 3 in. by the bottom of a shroud or dummy shroud tube if the assembly in question is one of the assemblies that are instrumented. Any of the others would be stopped by the middle guide plate. Radial reflectors and radial shield assemblies have a sufficiently low pressure drop that their liftoff is precluded by dead weight.

Aside from being a convenient shape to support surveillance thermocouples, the funnel-shaped lower ends of the control rod shroud tubes capture part of the coolant from the adjacent assemblies. The drivelines are exposed to this effluent for most of their

length, before the coolant is released to the hot pool through holes near the top of the shroud tubes. In a hypothetical unprotected loss-of-flow transient, it is expected that this hot effluent will cause some beneficial insertion of absorber material into the core by thermal expansion of the drivelines.

II.1.3 Lower Internals Structure

The lower internals structure consists of the core barrel, core grid, and the inlet plenum structure. The entire assembly is supported on the core support structure as shown in Figure II.1-7.

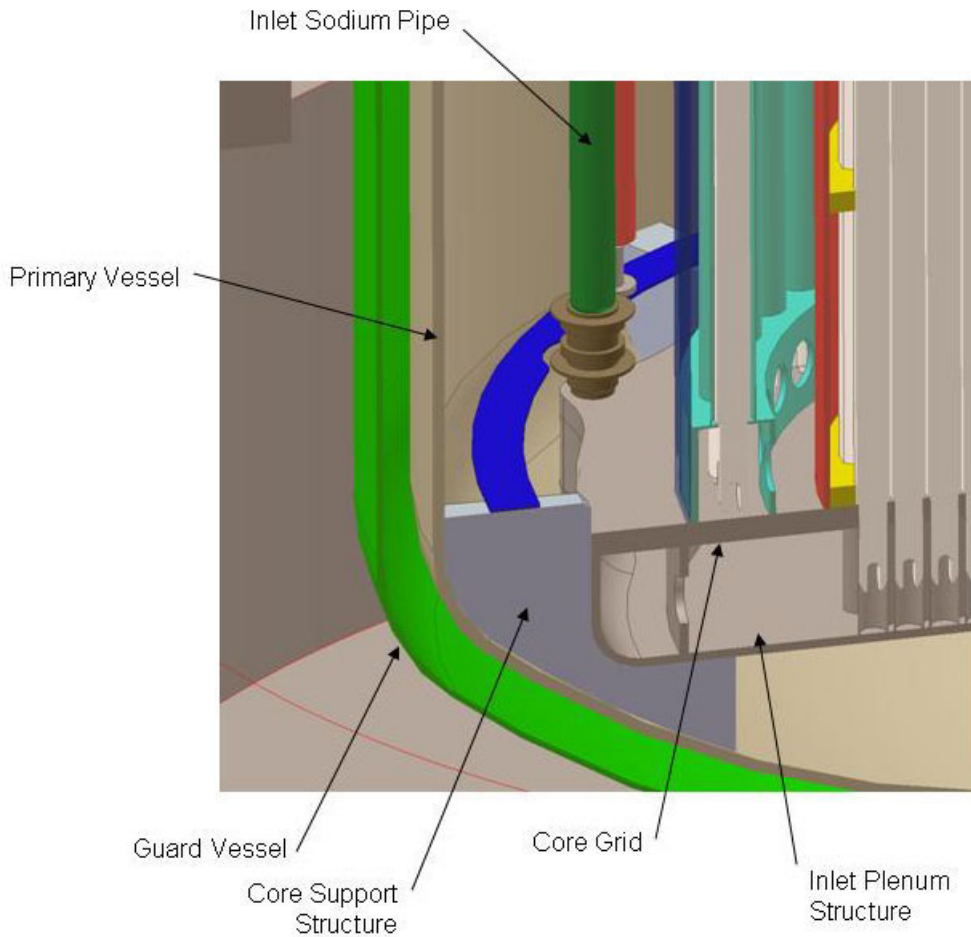


Figure II.1-7 Schematic of Lower Internal Structure

The lower internals structure supports the reactor inlet plenum, the core assemblies, the fixed radial shielding, the core barrel, the redan, and various shields, brackets and baffles. It is designed to withstand seismic events with acceptable stresses and deflections. The lower internals structure contains the inlet coolant flow distribution system that controls the rate of flow to the core assemblies. This distribution system consists of a doughnut-shaped manifold, or torus, and associated

ducts/piping, that encircles the inlet coolant plenum. For the baseline EM pump configuration, the pumps plug directly into the torus. For the mechanical pump configuration, the four pumps connect to pipes that are supported by the lower internals structure. A total of 12 short, smaller pipes distribute the coolant from the torus into the inlet plenum. This plenum or grid assembly currently contains a high pressure plenum only.

II.1.4 Core Restraint System

The core restraint system consists of distributed passive hardware features which, acting together, must meet the following functional requirements:

1. Establish the positions of the individual core assemblies in the horizontal plane;
2. Control horizontal movements of core assemblies arising from thermal expansion effects, irradiation-induced swelling, and irradiation-enhanced creep, in such a way that reactivity effects are acceptable and control rod driveline alignments are maintained within specified tolerances;
3. Accommodate horizontal seismic motions within alignment and stress specifications; and
4. Maintain sufficient clearances in the horizontal plane to allow for fuel handling within specified vertical withdrawal and insertion force limits.

The design choices representing the major decisions in the design of a passive core restraint system are:

1. Length and stiffness of the core assembly lower adapters;
2. Lower Internals Structure interface with the core assembly lower adapters -- clearances, seals, and number of support points (1 or 2);
3. Number, location, configuration and height of the core assembly load pads;
4. Rigidity of the peripheral boundary -- stiff radial shield assemblies or a rigid, shaped, core former ring attached to the core barrel;
5. Allowable vertical core assembly insertion and withdrawal loads.

The major challenge in core restraint design is to find the "design window" which contains sufficient clearance for fuel handling (even when core assemblies are bowed due to swelling and creep effects) and sufficient tightness or stiffness for adequate radial-position control. The thermal contraction produced by the cooldown to refueling conditions is very important in creating this window of design feasibility. The tool used in core restraint design is the NUBOW-3D computer code. It calculates the elastic and inelastic effects on the shape of individual core assemblies in a three-dimensional representation of the whole core or typical sector thereof, the reactivity effects associated with short-or long-term movements from one set of equilibrium positions to another, and the side loads at all contact points. Under refueling conditions, the sum of these side loads, times the coefficient of friction yields the required initial withdrawal force over and above the dead weight.

The two core restraint system design strategies are referred to as the "limited free bow" approach and the "free-flowering core." The first, used in FFTF and CRBR, employs a short lower adapter horizontally restrained in the lower internals structure (LIS) at one point (the lower end), and rigid core formers at the two elevations of core assembly load pads -- one near the top end and one about 4 in. above the fueled zone. The second, used in EBR-II, Phenix and SuperPhenix, employs a long lower adapter horizontally restrained in the LIS at two points, and the "fence" of stiff and essentially isothermal radial shield assemblies constitutes the peripheral restraint.

The ABTR design borrows features from both approaches. The relatively long lower adapter fits into a cylindrical perforated sleeve in the inlet plenum. A ball-and-cone seat at the transition from the cylindrical lower adapter to the hexagonal duct provides the coolant seal, load support, and a positive horizontal restraint point. Close clearance between the bottom of the lower adapter and the lower internal structure sleeve provides limited-movement horizontal restraint.

A rigid core former ring at the elevation of the top load pads provides positive peripheral restraint. The ring has enough clearance, relative to a tight array of assemblies, to permit removal and replacement of individual assemblies by the in-vessel transfer machine (IVTM), yet is tight enough so that the freedom of assemblies to move does not have adverse reactivity or alignment implications. The inner diameter of the ring is shaped so as to achieve flush contact with the outermost assemblies. The core former ring is welded to the inner diameter of the core barrel, to which the Upper Internals Structure is attached during operation with a system of retractable keys, thus assuring control and safety rod drive-train alignments. Each core assembly is equipped with a second load pad centered 4 in. above the fueled zone of the reactor, but no peripheral core former ring is present at this elevation. Normally the core assemblies contact one another only at the two load pads, which completely circumscribe the hexagonal ducts. The duct is 5.590 in. across flats and the lattice pitch (also the hot across-flat dimension of the load-pads) is 5.747 in. The 0.157 in. clearance between ducts is provided to prevent general contact at end of life due to swelling, creep (rounding of the flats), and differential bowing, but the adequacy of this clearance needs to be confirmed by analysis.

The IVTM, described elsewhere, has certain capabilities important to meeting the functional requirements of the core restraint system. The gripper assembly contains a "holddown and spreader" feature which facilitates fuel handling even when the core assemblies are distorted. The holddown provision prevents inadvertent lifting of any of the six assemblies surrounding the one being removed. The spreader feature, pioneered in EBR-II, has proven very useful in concentrating available clearances to the immediate vicinity of the core assembly being removed or the hexagonal hole into which a new assembly is being inserted. All components of the IVTM, and the core assemblies themselves, have ample margin beyond the planned administrative limit on insertion/withdrawal forces of greater than 1000 lb. excluding dead weight.

II.1.5 Reactivity Control and Shutdown System

As mentioned in Section II.1.1, two independent safety-grade reactivity control systems were employed: a primary and a secondary system. The primary system is required to have sufficient reactivity worth to bring the reactor from any operating condition to cold sub-critical at the refueling temperature with the most reactive control assembly stuck at the full power operating position. Any operating condition means an overpower condition together with a reactivity fault. The maximum worth of a control assembly is used as the base of this reactivity fault. The primary system also serves to compensate for the reactivity effects of the fuel burnup and axial growth of metal fuel. The reactivity associated with uncertainties in criticality and fissile loading is accommodated by the primary control system.

The secondary system is required to shut down the reactor from any operating condition to the hot standby condition, also with the most reactive assembly inoperative. It does not have to duplicate the primary system capability to hold down the excess reactivity for the fuel cycle since this excess reactivity is not additional reactivity to be overridden at an accident. Although the secondary system must shut down the reactor without insertion of the primary control assemblies, it is not necessary to assume that the primary assemblies are removed from the core during an accident situation. Since reactivity uncertainties are accommodated by the primary system, they are not a part of the secondary system requirements. However, the reactivity fault is included in the secondary system requirements since the secondary system should override the uncontrollable withdrawal of one primary control assembly that is being used for burnup control.

The reactivity control requirements include the axial expansion effect and temperature defect. The fuel axial growth is expansion with fuel burnup resulting from the accumulation of fission products. A 5% axial swelling was assumed for metal fuel. Temperature defect is the reactivity change from hot full power critical to zero-power refueling temperature. The calculated temperature and power defects are summarized in Table II.1-7. The refueling temperature was conservatively assumed 205 °C.

Table II.1-7 Temperature and Power Defects (\$)

Contribution	Hot full power to hot standby		Hot standby to cold shutdown	
	BOEC	EOEC	BOEC	EOEC
Doppler	0.18	0.18	0.14	0.15
Axial expansion	0.05	0.04	0.09	0.08
Radial expansion	0.46	0.47	0.89	0.90
Sodium density	-0.02	-0.02	-0.04	-0.04
Total	0.66	0.67	1.08	1.09

The reactivity worth was calculated for various combinations of control assemblies inserted, and one stuck-rod worth was estimated for each control assembly. The maximum single rod reactivity faults were also estimated from the reactivity worth curves of primary system control assemblies. To account for the interaction effects of control assemblies, the maximum worth of each control assembly was determined by withdrawing it from the configuration where all the primary or secondary control assemblies are inserted. Table II.1-8 presents the calculated control assembly worth for various combinations of control assemblies. Among the primary control assemblies, the central control assembly has the largest worth because of higher neutron flux in the core center. The estimated worth of the central assembly is ~8\$.

Table II.1-8 Control Rod Worth (\$)

	Number of inserted CRs	BOEC	EOEC
Primary System			
- Central rod	1	6.53	6.62
- All CR's in 5 th row	6	15.95	16.18
- Central and 5 CR's in 5 th row	6	20.32	20.61
- All primary rods	7	23.52	23.87
Secondary System			
- 2 CR's in 3rd row	2	10.53	10.68
- All secondary rods	3	16.38	16.61
One Stuck Rod Worth			
- Central rod		7.58	7.68
- One of 5th row		3.21	3.26
- One of 3rd row		5.84	5.93

Figures II.1-8 and II.1-9 show the primary system reactivity worth curves at BOEC and EOEC. The solid curve denotes the core reactivity as a function of control rod tip position from the bottom of the active core for the case where all the primary control assemblies are moving together. At the full power operating condition, only the fuel cycle excess reactivity is held down by the primary control system. As indicated by the dashed vertical line, the critical control rod position is 63.4 cm from the bottom of the active core. The dashed curve indicates the reactivity worth of the most reactive control assembly, which is the central assembly. The reactivity addition by the complete withdrawal of the central control assembly is 0.90\$. In order to limit the transient over-power initiator, it is necessary to reduce the central control rod worth or to introduce some means to limit the magnitude of rod withdrawal or the rod withdrawal speed. For example, the PRISM design introduced a rod stop system to limit the maximum withdrawal worth to 0.3\$, and the FFTF used a control circuit that limits the rod withdrawal speed to 9.8 inch/min.

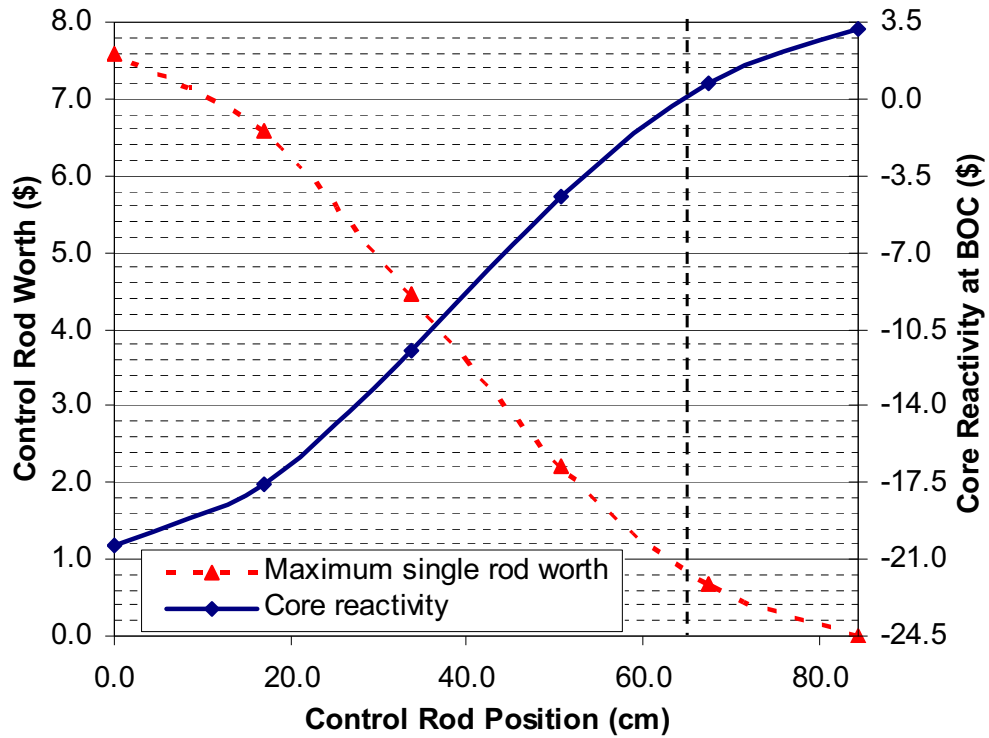


Figure II.1-8 Reactivity Worth of Primary Control System at BOC

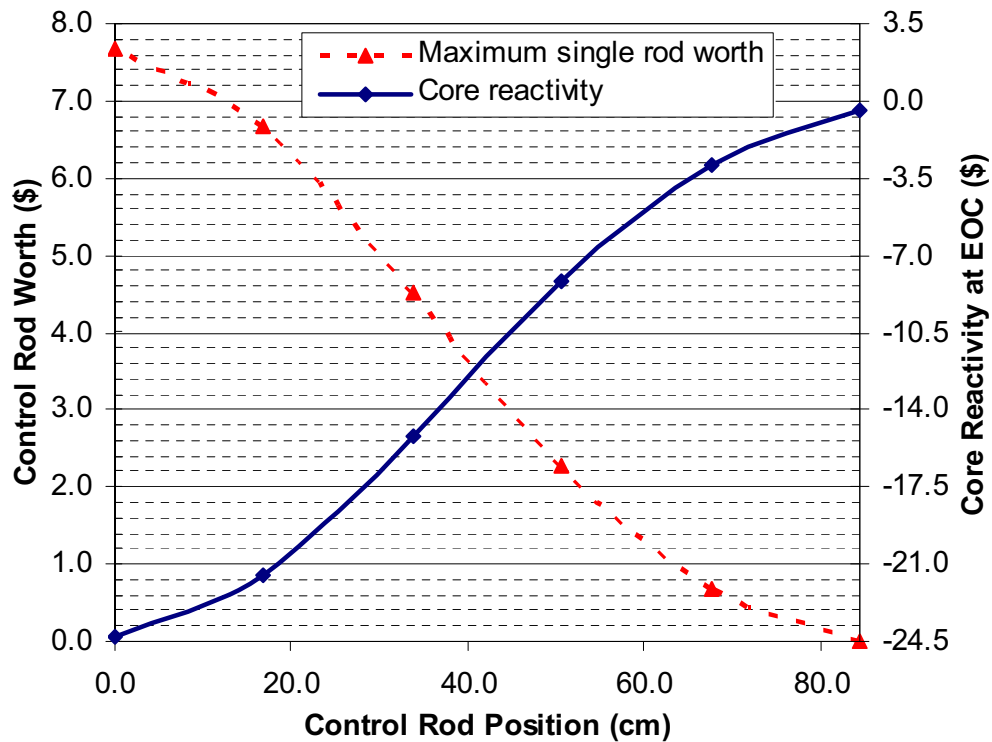


Figure II.1-9 Reactivity Worth of Primary Control System at EOEC

Table II.1-9 summarizes the reactivity worth requirements for both primary and secondary control systems. The estimated temperature and power defect from hot full power to cold shutdown at BOEC is 1.74\$. The overpower margin is allocated to permit the reactor to operate at 115% of the rated power, which is equivalent to 15% of the power defect. The fuel cycle excess reactivity is 3.77\$. Since the fuel cycle analysis was performed with expanded core geometry, the reactivity associated with the axial fuel growth is added at BOEC. The uncertainties consist of 20% of total temperature defect, 30% of total burnup reactivity, 20% of fuel axial growth, and an assumption of 1.00\$ each for criticality prediction and fissile loading (tolerance for manufacture uncertainty). The total uncertainty is obtained by statistically combining all the uncertainties.

Table II.1-9 Reactivity Control Requirements (\$)

	Primary system		Secondary system	
	BOEC	EOEC	BOEC	EOEC
Temperature defect	1.74	1.75	0.66	0.67
- Full power to hot standby	0.66	0.67	0.66	0.67
- Hot standby to refueling	1.08	1.09		
Overpower margin (15%)	0.10	0.10	0.10	0.10
Fuel cycle excess reactivity	3.77			
- Burnup reactivity	3.58			
- Fuel axial growth	0.19			
Uncertainties (RMS)	1.81	1.46		
- Temperature defect (20%)	0.35	0.35		
- Burnup reactivity (30%)	1.08	0.00		
- Fuel axial growth (20%)	0.04			
- Criticality prediction	1.00	1.00		
- Fissile loading	1.00	1.00		
Reactivity fault	0.90		0.90	
Total	8.32	3.31	1.66	0.77

In Table II.1-10, the reactivity control requirements are compared with the available reactivity worth of the control systems. The shutdown margins of the primary and secondary systems were determined with the assumption that the most reactive assembly is stuck. The shutdown margin of the primary system is 7.63\$ at BOEC and 12.88\$ at EOEC; the shutdown margins are more than adequate. These results suggest that the central assembly could be removed to reduce the transient over-power initiator. Simple estimation based on the values in Table II.1-8 showed that the shutdown margin of the primary system without the central assembly would be ~4.5\$ at BOEC and ~9.5\$ at EOEC.

The control-rod driveline expansion coefficients for reactivity feedback were estimated from Figures II.1-6 and II.1-7. Control rod expansion coefficients are governed principally by the total rod worth and the insertion depth of the rods. The calculated

control-rod expansion coefficients are 30.9 cents/cm at BOEC and 14.5 cents/cm at EOEC.

Table II.1-10 Reactivity Control Requirements and Available Reactivity Worth

	Primary system		Secondary system	
	BOC	EOC	BOC	EOC
Number of control assemblies	7	7	3	3
Reactivity worth of system (\$)	23.52	23.87	16.38	16.61
Worth of 1 stuck assembly (\$)	7.58	7.68	5.84	5.93
Reactivity worth available (\$)	15.95	16.18	10.53	10.68
Maximum requirement (\$)	8.32	3.31	1.66	0.77
Shutdown margin (\$)	7.63	12.88	8.87	9.92

References

1. T. K. Kim, W. S. Yang, E. A. Hoffman, R. N. Hill, "Core Design Studies for Advanced Burner Test Reactor," ANL-AFCI-169, Argonne National Laboratory, June 30, 2006.
2. K. L. Derstine, "DIF3D: A Code to Solve One-, Two-, and Three-Dimensional Finite Difference Diffusion Theory Problems," ANL-82-64, Argonne National Laboratory (1984).
3. B. J. Toppel, "A User's Guide to the REBUS-3 Fuel Cycle Analysis Capability," ANL-83-2, Argonne National Laboratory (1983).
4. "NSEC No. 350 ETOE-2 Documentation," National Energy Software Center Note 83-84, August 25, 1983.
5. H. Henryson II, B. J. Toppel, and C. G. Stenberg, "MC²-2: A Code to Calculate Fast Neutron Spectra and Multi-group Cross Sections," ANL-8144, Argonne National Laboratory (1976).
6. W. M. Stacey, Jr., et al, "A New Space-Dependent Fast Neutron Multigroup Cross Section Preparation Capability," *Trans. Am. Nucl. Soc.*, 15, 292 (1972).
7. R. D. Lawrence, "The DIF3D Nodal Neutronics Option for Two- and Three-Dimensional Diffusion Theory Calculations in Hexagonal Geometry," ANL-83-1, Argonne National Laboratory (1983).
8. G. Hofman, L. Leibowitz, J. M. Kramer, M.C. Billone, and J. F. Koenig, Private Communication, Argonne National Laboratory, November 1985.
9. A. D. Pelton and L. Leibowitz, Private Communication, Argonne National Laboratory, August 1988.
10. C. H. Adams, "Specifications for VARI3D – A Multidimensional Reactor Design Sensitivity Code," FRA-TM-74, Argonne National Laboratory (1975).
11. A. G. Croff, "ORIGEN-2 – A Revised and Updated Version of the Oak Ridge Isotope Generation and Depletion Code," ORNL-5621, Oak-Ridge National Laboratory (1980).

II.2 Reactor Enclosure System

II.2.1 Reactor Vessel

The reactor vessel contains essentially the entire inventory of the radioactive primary sodium coolant. It also provides support for the reactor core support structure, redan, thermal barriers, shielding and other internal structures. There are no penetrations in the reactor vessel; all equipment -- IHXs, pumps, piping, instrumentation, cold traps, fuel handling ports, and other components -- penetrate the primary coolant system enclosure through the top deck structure. The arrangement is shown in Figures II.2-1 and II.2-2.

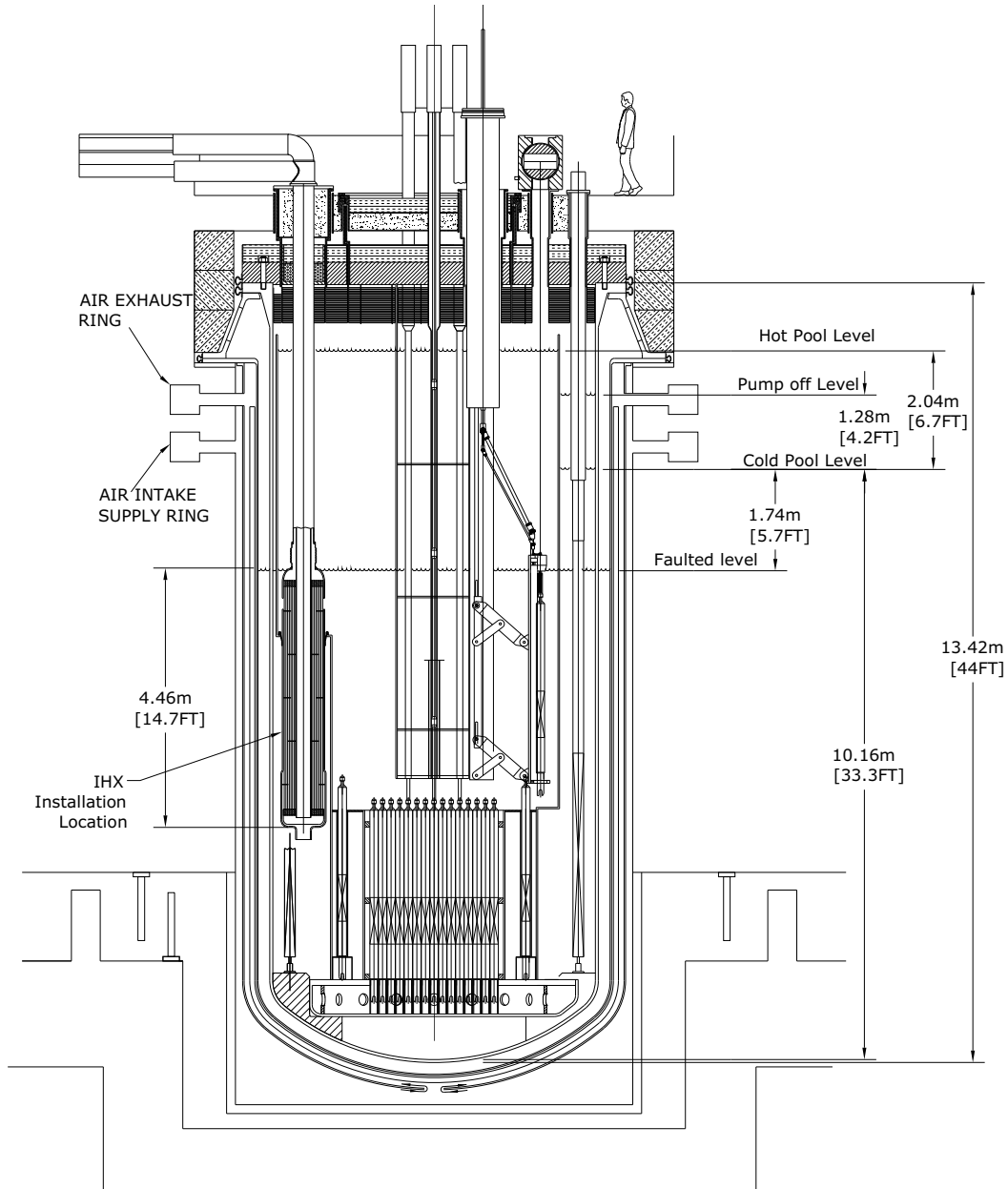


Figure II.2-1 Vertical View of Primary System

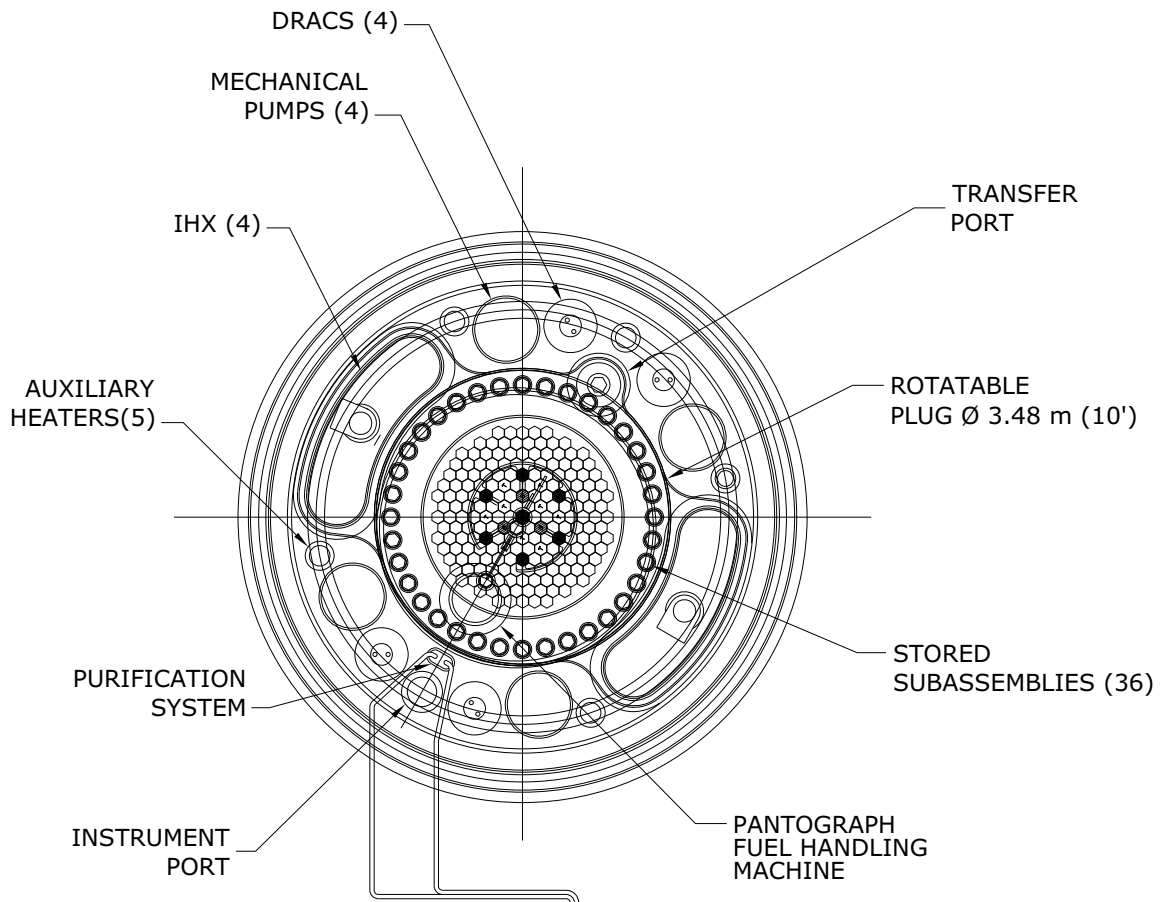


Figure II.2-2 Plan View of the Primary System

The reactor vessel is constructed of austenitic stainless steel. It has an inside diameter of 18.3 ft and wall thickness of approximately 2 inches. The overall height of the vessel is about 44 ft from its bottom to the top of the deck. The bottom head consists of a torospherical shell. The vessel is suspended at its top flange from the same conical support skirt which provides support for the deck. The skirt provides separation between the reactor vessel and the guard vessel and contains several access ports to permit periodic inspection of the area and to provide access to the annulus between the reactor vessel and the guard vessel. The reactor vessel is fastened to the support skirt. This detail is employed to avoid the structural bi-metallic weld which would otherwise be required between the reactor vessel and deck structure. Shear keys are provided at the support flange connection to resist seismic loadings.

A major design consideration with most pool reactor vessels results from the temperature distribution in the upper (support skirt) region of the vessel. This thermal condition arises because the upper part of the vessel is exposed either to the outlet sodium temperature (hot pool) or, at least, the cooler inlet sodium, while the top of the vessel (support flange) is much closer to room temperature. Many designs employ active

cooling of the vessel wall or thermal baffles, or a combination of these. The reference design in this study attempts to eliminate, or greatly reduce, this problem by minimizing the amount of vessel exposure to the hot, outlet sodium pool. This is done by minimizing the surface area of the hot sodium exposed to the reactor vessel and employing a thermal baffle. The special shape and configuration of the redan structure and reactor vessel baffles described in Sections II.2.5 and II.2.6, respectively, provide these features.

The height of the reactor vessel is established from the fuel assembly length, the intermediate heat exchanger length, and the need to keep the intermediate heat exchanger inlet covered by sodium during a leak of the reactor vessel where sodium would drain into the guard vessel. The “faulted” primary sodium level is indicated in Figure II.2-1. The diameter of the reactor vessel is established from the core diameter and IHX characteristics with respect to sodium hydraulic and heat transfer requirements and the requirement to be able to remove the primary components, such as the IHX, primary sodium pumps, and direct reactor auxiliary cooling system (DRACS) heat exchangers. The reactor vessel and its cover are designed to the requirements of the ASME B&PV Code, Section III, Division 1, Subsection NH for the combined loads of the entire volume of primary sodium, the primary system equipment, and the core support structure. In addition, the design will meet ASME B&PV Code requirements for normal and transient thermal loads as well as loads and displacement resulting from design basis earthquakes.

The reactor vessel assembly is designed to:

1. Accommodate high static loads at design temperatures.
2. Minimize the dead load deflections and thermal bowing of the reactor vessel and its cover to facilitate equipment alignment.
3. Provide a type of structure which can be erected on site to stringent tolerance requirements.
4. Ensure symmetrical radial thermal expansion of the primary tank about the vertical center of the entire primary tank assembly.

The reactor vessel contains the reactor core, entire primary coolant, intermediate heat exchangers, primary (electromagnetic or mechanical) pumps, DRACS heat exchangers, and internal structures. The diameter and overall height of the reactor vessel are 4.6m and 14.8m, respectively. The reactor vessel and guard vessel are made of austenitic stainless steel. The complete reactor vessel assembly is located below grade in a steel-lined concrete cavity of the reactor containment building. The reactor vessel and its cover constitute the primary structural boundary that envelopes and supports the reactor core, primary sodium coolant, reactor cover gas, auxiliary core components, primary sodium pumps, IHXs, and other associated reactor equipment. In addition to providing the primary structural boundary, support and containment, the reactor vessel and reactor vessel enclosure provide internal and interfacing equipment alignment features. All penetrations into the reactor vessel are through the top cover. There is an inert gas (argon) blanket between the reactor vessel cover and the bulk sodium free surface.

II.2.2 Reactor Vessel Enclosure

The reactor vessel enclosure forms the top closure for the reactor vessel. It supports the primary pumps, intermediate heat exchangers (IHXs), cold traps, rotatable plug, the direct reactor auxiliary system heat exchangers, and other equipment. The rotatable plug, in turn, supports the upper internal structure, in-vessel fuel handling equipment, and the control rod drivelines, as well as various instruments needed to monitor inside the reactor vessel.

The reactor vessel enclosure is constructed of austenitic stainless steel. The enclosure, along with the reactor vessel, is supported by the conical support skirt that transfers the entire weight of the enclosure and the reactor vessel to the concrete support structure, as illustrated in Figure II.2-3. The enclosure is bolted to the reactor vessel and there are seals welded around the interface between the enclosure and the reactor vessel to eliminate the release of cover gases through the reactor vessel/enclosure interface.

The reactor vessel enclosure is a solid piece of stainless steel about 10 inches in thickness. It is 21.7 feet in outer diameter. Openings are machined in the cover for those primary systems components that penetrate through to the primary vessel, such as the components mentioned above. Nozzles are welded to these openings that provide support for the primary system components and a location for sealing the components to the vessel enclosure. Reflective thermal insulation is attached to the bottom of the reactor vessel enclosure to reduce the amount of heat being conducted through the enclosure itself. Fiberglass insulation is added above the cover to reduce the amount of heat lost to the surrounding concrete.

The reactor vessel enclosure fulfills several important functions. These are:

1. The reactor vessel and some portion of the enclosure form the primary coolant boundary, and contain all of the radioactive materials produced by the reactor during operation. These materials include the sodium coolant and any gaseous or solid radioactive materials released from the fuel elements due to cladding failure.
2. Provides support for two IHXs, four primary pumps, four DRACS heat exchangers, two cold traps, the rotatable plug, and various other equipment and instrumentation. A gas tight seal is provided between the enclosure and all penetrations.
3. Provides sufficient stiffness to limit the vertical deformation during the safe shutdown earthquake (SSE) to a very small number (TBD).
4. Minimize heat loss to the inside of the reactor building.
5. Provide adequate rigidity to meet alignment needs for the primary sodium pumps, intermediate heat exchangers, rotatable plug, and the upper internal structure.

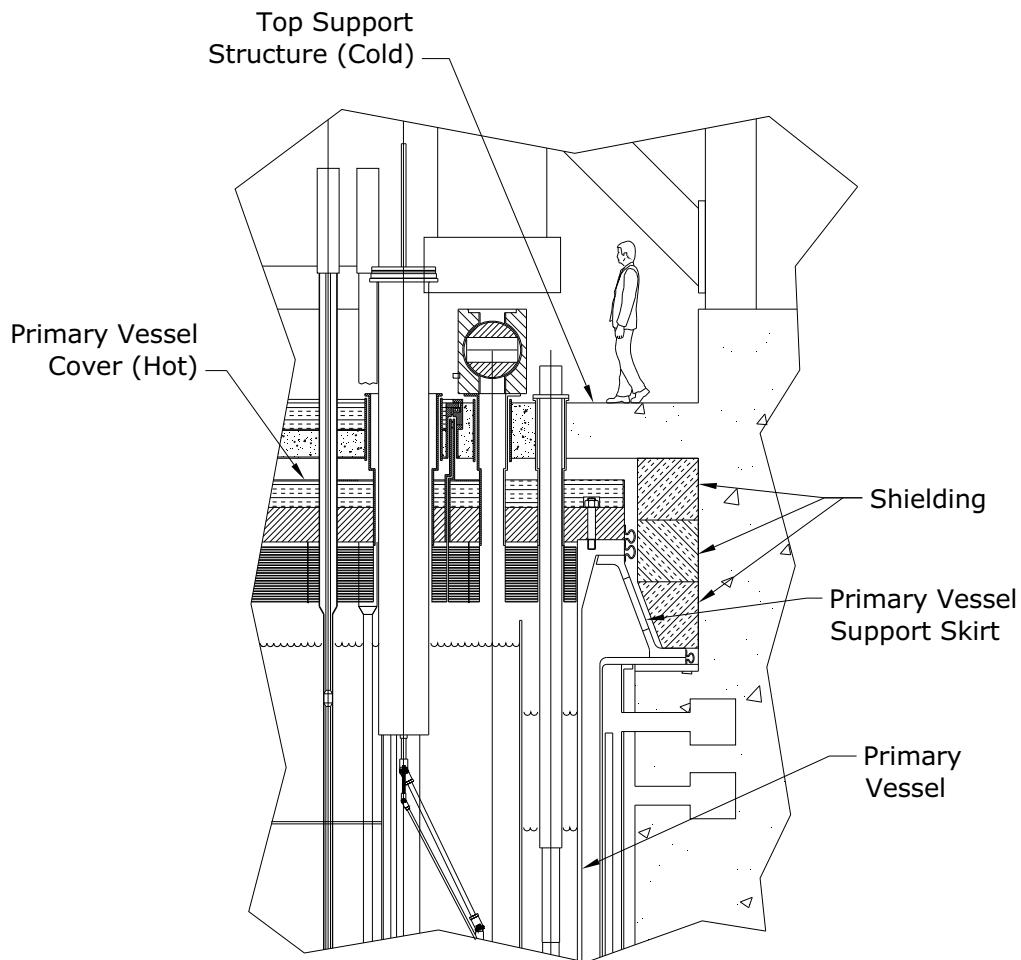


Figure II.2-3 Reactor vessel cover and reactor vessel support skirt

II.2.3 Rotatable Plug

The principal function of the rotatable plug is to serve as part of the fuel handling system. Their number and their size depend largely on the type of other components in the fuel handling chain. Specifically, the type of in-vessel transfer machine (IVTM) and the location of the fuel transfer point determine the distance of lateral movement that the rotatable plugs have to provide. After consideration of various options, the fuel handling system described in Section II.7 was chosen. This system uses a pantograph-style IVTM, and a transfer point to the vertical fuel unloading machine that is located on the reactor vessel enclosure just radially outside the rotatable plug. Thus the rotatable plug in concert with the pantograph in-vessel fuel handling machine has to provide a lateral movement that covers a circle of 8 ft diameter. Further requirements affecting the rotatable plug size are derived from the reactor control drive pattern and the upper internals structure

(UIS) design. In order to provide the most favorable control drive pattern, the option of having a "split" control area has been discarded. Similarly, the "splitting" of the UIS presents serious structural and seismic problems.

Design features regarding shielding arrangements and the interfaces among the rotatable plugs are essentially the same as described for the reactor vessel enclosure. The plug has a stressed-skin box-beam structure and contains 12 in. of magnetite concrete shielding. The underside of each plug has steel shielding and reflective sandwich insulation. Plug interfaces are provided with elastomer seals. The UIS is attached to the bottom of the rotatable plug.

The rotatable plug supports the vertical push-pull IVTM.

The rotatable plug incorporates devices for locking its positions during reactor operation, and devices against lift-off due to excessive reactor vessel pressures. Equipment associated with, or part of the rotatable plug requires a variety of services--connections for electricity, control, instrumentation, inert gas etc., that are provided via the festoon cable system.

II.2.4 Guard Vessel

The guard vessel provides the secondary containment for the primary sodium in the very unlikely event that the reactor vessel develops a leak. The guard vessel is sized such that the gap (8.5 inches) between it and the reactor vessel is:

1. Wide enough to accommodate in-service inspection devices
2. Narrow enough to prevent the primary sodium from dropping to an unacceptable level within the reactor vessel if the reactor vessel should develop a leak. The sodium level must remain high enough to keep the IHX inlet covered to provide a path for natural convection cooling of the core during a leak in the reactor vessel.

The guard vessel is constructed of austenitic stainless steel. If carbon steel were acceptable, it would facilitate the use of magnetically-operated remote devices needed to carry out the periodic in-service inspection (ISI) required for the reactor vessel and associated structures and components. With austenitic stainless steel, the equipment used for ISI would require use of friction or scissors-like devices to scan the entire outer surface of the reactor vessel.

Insulation is provided on the exterior of the guard vessel to reduce the heat lost to the guard vessel cooling system. A guard cooling shroud is provided on the outside of the insulation that forces air to flow around the supporting concrete structure and up over the guard vessel insulation to prevent overheating of the concrete support structure during normal and off-normal conditions.

II.2.5 Redan

The core barrel and redan assembly, illustrated in Figure II.2-4 is a single integrated unit that provides the internal structure for the reactor core assemblies and provides a barrier between the hot and cold sodium pools. The core barrel is a right circular cylinder fabricated from stainless steel. It is attached to the inlet plenum and lower support structure. It also provides support for the core restraint system.

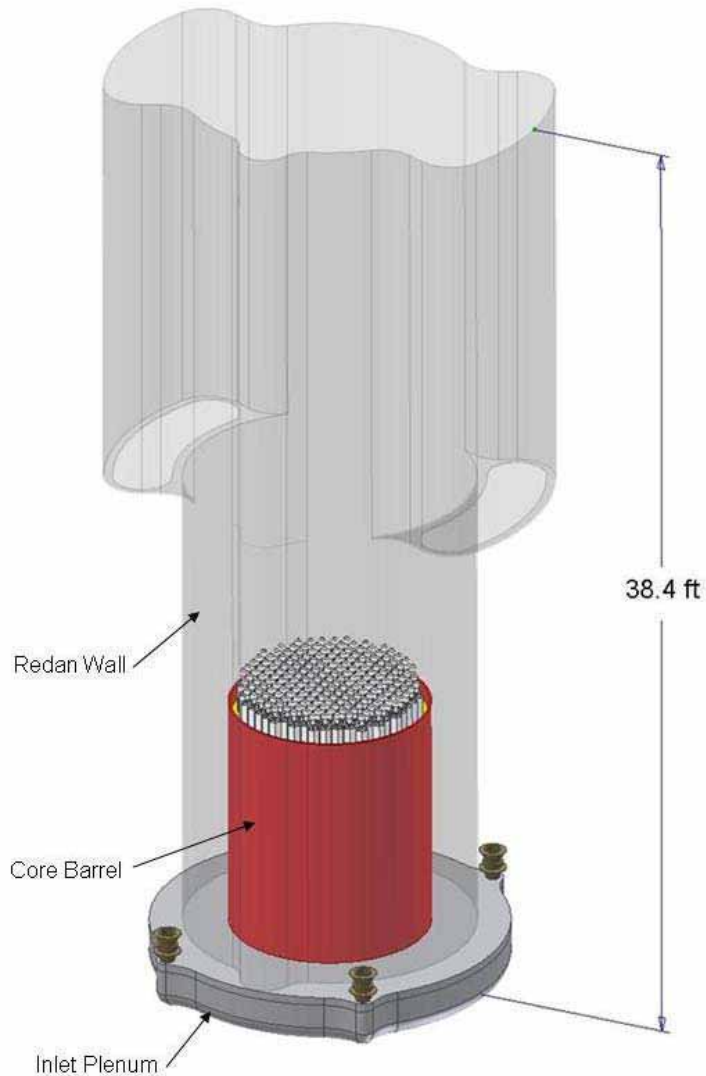


Figure II.2-4 Schematic of Redan Structure

The redan is a single integrated unit that separates the hot pool from the cold pool, and provides for communication of the hot sodium from the discharge of the reactor core to the inlet of the intermediate heat exchanger. It consists of multiple plates welded together that form a contoured shape around the intermediate heat exchangers and the upper internal structure.

The intermediate heat exchangers and upper internal structure are located within the redan. The primary pumps and DRACS heat exchangers are located outside the redan in the cold pool. The redan contains the hot sodium from the core outlet and helps to minimize leakage from the hot sodium to the cold sodium sides of the redan.

The redan is supported vertically by the lower internal structure and seal welded to the core barrel. The redan is one of the permanent structures within the primary reactor vessel. A mechanical labyrinth seal between the IHX and redan reduces the leakage of hot primary sodium from the hot pool into the cold pool.

II.2.6 Core Support Structure

The core support structure, shown in Figure II.2-5, provides support for the lower internals structure, the core assemblies, the core barrel assembly, the primary sodium inlet pipes, brackets, and baffles. It is designed to the requirements of the ASME B&PV Code, Section III, Division 1, Subsection NG, Core Support Structures. The core support structure consists of a steel web structure that is formed to the contours of the reactor vessel bottom head and becomes an integral part of the reactor vessel. All core support structure components are under compression, therefore there is no need for performing ISI on these components.

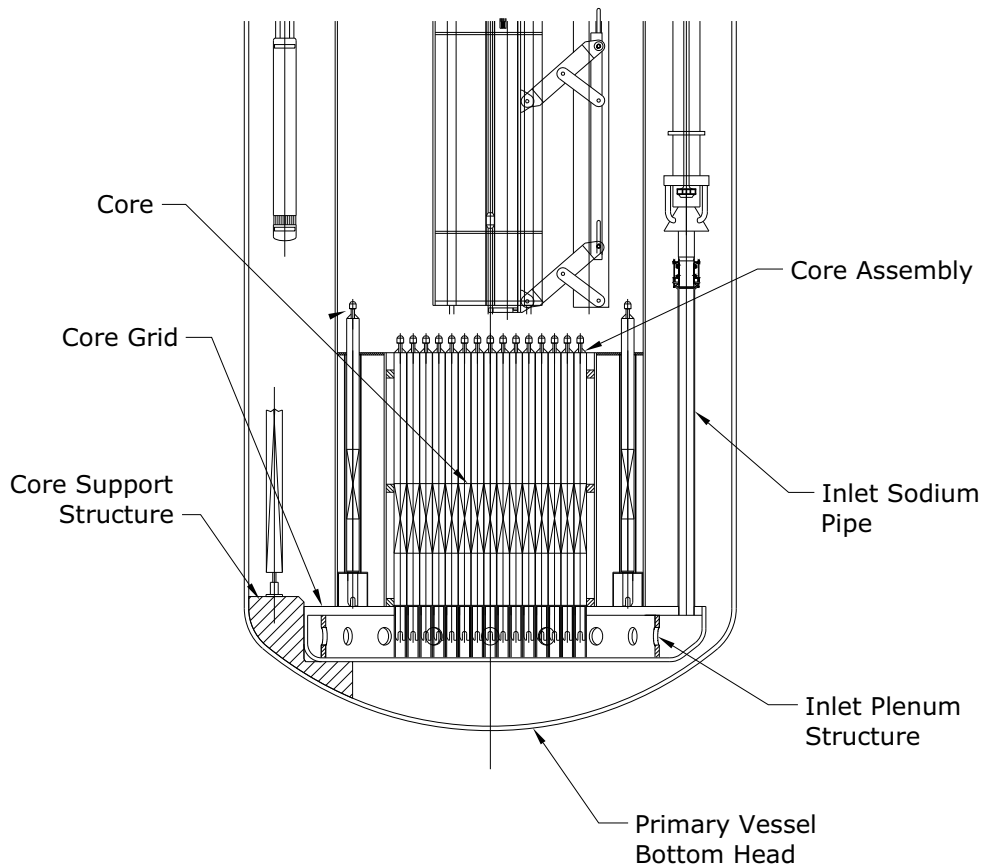


Figure II.2-5 Core Support Structure

II.2.7 Reactor Containment Boundary

The ABTR primary containment boundary is comprised of the reactor vessel, reactor vessel enclosure, the tubes in the intermediate heat exchanger and in the direct reactor auxiliary heat exchanger, and the sodium purification piping and components. These components maintain the containment for the primary radioactive sodium and form the first containment boundary. This initial boundary also includes the instrument thimbles and the cover gas piping system.

If this first boundary is breached, then the next secondary confinement is composed of the reactor guard vessel, the reactor containment, the intermediate sodium piping and sodium-to-CO₂ heat exchangers, the direct reactor auxiliary cooling system intermediate piping and systems, the stainless steel-lined compartments around the reactor vessel support, the purification system cell confinement, and the reactor building (which is maintained at a negative pressure with HEPA-filtered ventilation).

If there is a breach in a thimble or cover gas system, the gas operates at a slightly higher pressure than the sodium and therefore, there will be no release of sodium to the environment. The reactor building always operates at a negative pressure compared to the outside environment. All effluents are filtered via high-efficiency particulate air filters before they are released into the environment.

II.2.8 Integrity of Primary Coolant Boundary

It has been postulated that a structural failure or leak which would develop in the reactor vessel could prove to be a major economic setback. The purpose of this discussion is to show that current, proven technology can be applied to ensure a leak-tight primary coolant boundary over the plant lifetime, reducing the probability of such a leak occurring to a very low level.

In the pool-type design, the reactor and the entire radioactive primary coolant are contained in a single reactor vessel. This arrangement results in a direct and simple containment for the primary sodium, with no penetrations in the reactor vessel wall below the primary sodium surface. The ABTR design avoids, wherever possible, the use of dissimilar materials and the oftentimes difficult welding techniques associated with these dissimilar materials.

The surrounding environment of sodium is common to all of the primary system components, which mitigates pipe (duct) expansion stresses and minimizes effects of pipe leaks. A very high level of structural and leak-tight integrity of the reactor vessel and its surrounding guard vessel is achieved with the use of both proven design features and intrinsic characteristics of the sodium system. This basic foundation is supported by established fabrication, field construction, and quality control procedures, comprehensive testing plus inspections and finally, regular in-service monitoring and surveillance.

Inherent characteristics of the sodium system that mitigate potential challenges to the reactor vessel include non-corrosiveness of sodium to structural materials. The operating pressure of the bulk sodium is very low, generally limited to the hydrostatic head of sodium. This leads to low stresses in the reactor vessel structure and permits large design margins and the use of thin-walled plates for fabrication which, in turn, enhances the reliability of nondestructive examination methods which may be used for in-service inspection.

To ensure system safety, design features are included, such as the backup guard vessel, that give unimpaired capability for removal of reactor decay heat in the event of reactor vessel leakage.

Design features that promote the integrity of both the reactor vessel and the guard vessel are viable due to the following basic characteristics of the pool-type arrangement:

1. There are no attachments or penetrations in the shells and bottom head of either the reactor vessel or the guard vessel, except for the core support structure.
2. The vessels have simple geometries, e.g., right circular cylinders and smooth, curved bottom heads.
3. The core support structure is attached to the bottom head of the reactor vessel with a set of formed steel webs contoured to the shape of the reactor vessel bottom head. This eliminates welds at points of high stress.

In addition, the austenitic stainless steel material, used throughout the reactor vessel assembly (with the possible exception of the guard vessel), has several favorable characteristics:

1. Excellent compatibility with the sodium coolant.
2. Excellent ductility/toughness properties, even at total neutron fluences higher than expected at the reactor vessel boundaries.
3. No appreciable high temperature aging degradation with a primary sodium coolant temperature of about 510°C.
4. Excellent weldability.
5. High fracture toughness prevents rapid crack propagation and makes a leak-before-break strategy feasible.

Another unique feature is that the reactor vessel is interfaced with the cold pool, which results in a low and approximately constant temperature for the reactor vessel wall, and for the guard vessel as well. This approach has two very important benefits:

1. The reactor vessel temperature is almost always at the low sodium-inlet temperature (about 355 to 410°C) except for the upper sections of the reactor vessel which sees the increased temperature of the hot sodium pool.
2. Deleterious effects of large and frequent temperature transients are avoided by maintaining this temperature relatively constant.

With regard to radiation damage, adequate shielding in the core barrel as well as the distance to the reactor vessel wall results in total neutron fluences well below any level which would be of concern during the 60 year design life for the plant.

II.3 Primary Heat Transport System

II.3.1 System Requirements and Description

The basic function of the primary heat transport system (PHTS) is to transport heat from the reactor to the intermediate heat transport system (IHTS) under normal and off-normal operating conditions. The arrangement of the PHTS is shown in Figures II.2-1 and II.2-2.

The PHTS consists of four primary pumps, two intermediate heat exchangers (IHXs) and expansion joints between the pumps and the reactor inlet plenum. The four pumps and two IHXs are located symmetrically around the reactor. The four pumps are located in the cold pool between the redan and the reactor vessel. Each of the two IHXs is located within the redan and penetrates through the redan from the hot pool to the cold pool. Each of the IHX plena is open to the reactor vessel cover gas at the top and each is closed at the bottom by a seal. The sodium level in the plena around each IHX is essentially the same as in the main redan. Thus, the IHXs have no primary piping associated with them; the hot primary sodium enters the IHX inlet through openings in the IHX shell and is discharged to the cold region at the bottom of the IHX.

In this pool configuration the pumps as well as the IHXs are supported from the reactor vessel deck which is maintained near ambient temperature. The flexible seal between each IHX and the redan accommodates thermal and seismic motions. The flexible coupling between the discharge of each pump and the reactor inlet plenum which is fixed to the lower core support structure accommodates thermal and seismic motions. The flexible coupling is designed to accommodate the small amount of differential thermal expansion between the pump and the lower support structure, including the differential thermal expansion of these items from shutdown to full power conditions.

A total sodium flow of 10^7 lbs/hr removes the heat from the core and passes into the upper plenum at an average temperature of 510°C . The core effluent mixes with the hot sodium in the plenum and flows up into the redan to two IHXs. Approximately 125 MWt of heat is transferred from the primary to the secondary coolant in each IHX. The primary sodium leaves the IHX at 355°C and enters the cold pool region of the reactor vessel. Four pumps take the sodium from the cold pool and discharge it through inlet piping to the inlet plenum below the reactor core.

The PHTS must satisfy all normal and off-normal conditions specified in the duty cycle for the plant. In addition to full power 4-loop operation, the PHTS must provide heat removal for 50% power operation when only one IHTS loop is available or 75% when one primary pump is out-of-service. The system, along with the core and the IHX, is arranged to remove decay heat under natural circulation conditions. Maintainability and inspectability are important considerations in the design of the PHTS.

II.3.2 Primary Sodium Pump

Both mechanical and electromagnetic (EM) pumps can be adopted for the ABTR. In the ABTR design, the location of the suction of the primary pump is critical to ensure sodium circulation under a variety of operating conditions. In addition, the diameter of the pump is an important parameter, since it affects the diameter of the reactor vessel.

Although there are many different types of mechanical pumps, only centrifugal pumps have been used in the sodium cooled fast reactors and therefore are considered as the primary candidate. Similarly, annular linear induction pumps (ALIPs) are considered as the primary candidate for the EM pump option.

II.3.2.1 Mechanical pump

In general, mechanical pumps have a longer history than that of EM pumps. Development of mechanical pumps specifically for the sodium cooled reactor application started with EBR-I, in which a 500 gpm mechanical pump was used to pump NaK. Since then, essentially all sodium cooled fast reactors have utilized mechanical pumps for the primary system, although some EM pumps were used in the secondary systems.

Mechanical pumps have the following advantages over EM pumps:

1. Mature technology,
2. High efficiency (70-85 % for those used in nuclear reactors).

However, mechanical pumps have the following inherent disadvantages when compared to EM pumps:

1. Moving parts are involved,
2. Expected to be more prone to cavitation,
3. Need of bearings,
4. Need of seals for rotating shaft,
5. Need of penetration through the reactor vessel for rotating shaft,
6. The existence of a Na/cover gas interface somewhere along the length of the rotating shaft,
7. Only vertical installation is practical.

The operating experience indicates that hydrodynamic and hydrostatic bearings in liquid sodium have become less of a problem [1]. Operations of BOR-60, BN-350, and BN-600 showed that wear in the bearing was virtually absent and replacements were not needed within several tens of thousands of hours of operation. The single factor requiring periodic maintenance that necessitates removal of the pump internals is erosion of the impeller due to cavitation for BN-350 and BN-600 [2].

The EBR-II mechanical pumps experienced shaft binding after less than 200 hrs of operation. Rubbing had occurred between the shaft and lower labyrinth seal. Although the initial cause was not definitely established, possible causes include insufficient initial clearance and warping of the shaft prior to operation [3-4]. In FFTF, thermal shock deformed the sodium bearing housing, causing a rotation problem. Other rotation problems were caused by condensation of sodium between the shaft and the thermal shields and deformation of the shaft due to a non-uniform circumferential temperature distribution in the shaft.

In Rapsodie, reduction of the gaps in the sodium bearing due to thermal shock produced a rotation problem. In Phenix, two causes of rotation problems were a failed shaft sleeve due to thermal transients and a shifting of the bearing parts. In PFR, the separation of the surface of the sodium bearing caused a rotation problem.

In BN-350, condensation of sodium vapor in the narrow gaps hindered start-up of the primary pump after long downtime due to incorrect estimate of component temperatures. Also, cavitation damage of impellers was reported. At the end of the reactor lifetime, the pump repair interval was extended, due to maturity of sodium technology, to about 10 years. In BN-600, during the initial period of operation, several problems relating to failures of the primary and secondary pumps due to their increased vibration, shaft fissuring, coupler damage, and non-reliable drive performance were experienced. Although all problems were later successfully resolved, replacement of the pump shafts was required. In BOR-60, although one primary mechanical pump was replaced due to high vibration caused by inappropriate thermal treatment of the shaft components during fabrication, maximum operation time for primary and secondary mechanical pumps was impressive: 220,000 and 180,000 hrs, respectively [5].

The long history of the mechanical pumps in sodium cooled fast reactors indicates that although some minor maintenance would be required on a periodic basis, the overall reliability has been demonstrated and the mechanical pump would be a logical choice for the ABTR as well.

However, one potential issue unique for the ABTR is that the ABTR reactor vessel is much longer than vessels of other previously developed pool type reactors. This is schematically illustrated in Figure II.3-1, and the actual design data are summarized in Table II.3-1.

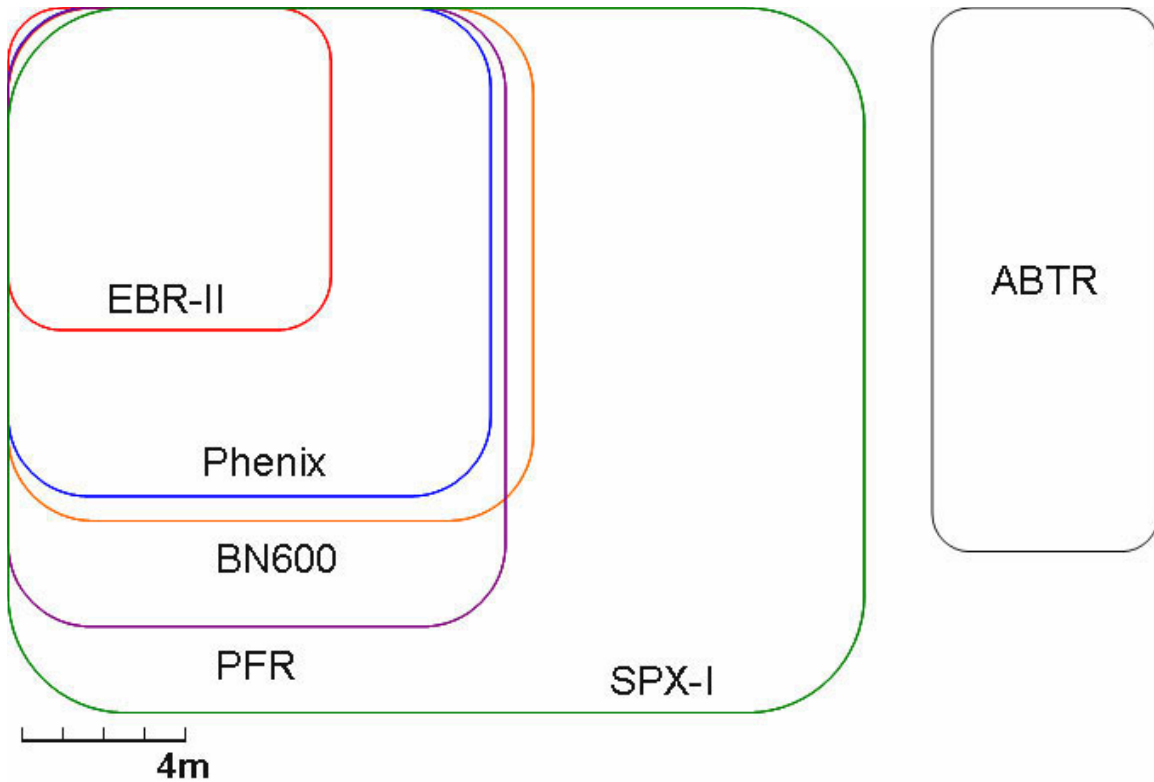


Figure II.3-1 Schematic comparison of pool type reactor vessels

Table II.3-1 Dimensions for various pool type reactor vessels

Reactor	Diameter, m	Height, m	H/D ratio
EBR-II	7.92	7.92	1.00
Phenix	11.82	12.00	1.02
SuperPhenix	21.00	17.30	0.82
PFR	12.20	15.20	1.25
BN-600	12.86	12.60	0.98
PRISM	9.07	19.35	2.13
ABTR	5.57	13.37	2.40

This fact drives the mechanical pumps for the ABTR to be longer than the other pumps. In fact, values for the ratio of the pump length to the pump diameter for several mechanical pumps used in the above pool type reactors are between approximately 5 and 6, however, the L/D ratio for the mechanical pump preliminarily designed for the ABTR is approximately 15, as compared in Table III.3-2, possibly making satisfactory performance of the pump much more difficult to achieve. The calculational procedure to obtain these pump dimensions for an ABTR pump is presented in Section III.1.1.

Table III.3-2 Dimensions of mechanical pump for various pool type reactors

Reactor	Flowrate, m ³ /min	Pump head, MPa	Pump diameter, m	Pump length, m	L/D ratio
EBR-II	19.0	0.54	1.28	6.88	5.4
PFR	70.7	0.73	1.91	10.80	5.7
Phenix	67.2	0.70	1.32	8.10	6.1
SuperPhenix	300.0	0.55	2.50	14.89	6.0
ABTR	22.1	0.76	0.53	7.85	14.8

As described in Section III.1.1, the mechanical pump was designed using a series of nomographs developed by Byron Jackson [6]. In the first nomograph, the specific speed and rotation speed are determined. In the second nomograph, the required power is determined. Then, in the third nomograph, the shaft diameter is determined. In the fourth nomograph, the pump case diameter, which is related to the impeller diameter, is determined. In the fifth nomograph the size of the pump outer barrel is determined, however, for the pool type configuration, the outer barrel is not used and the pump casing is suspended directly in the pool of Na. Finally in the sixth nomograph, the suction and discharge nozzle diameters are determined. This procedure estimates only the diameter of the pump. The length of the pump can be estimated from another consideration, namely the submergence depth to be greater than 0.9-1.2 m to prevent vortexing [7]. A summary of input data is presented in Figure II.3-2.

Gravity, g (m/s ²)	9.81	Flow rate (kg/s)	=	320	=	5849.40	GPM
μ ₀ : Magnetic Permeability (Wb/A-m)	1.26E-06	Pressure (Pa)	=	760000	=	293.13	feet
Gas Constant, R (J/mol-K)	8.3145	Temperature (K)	=	628	=	670.73	F
Reference							
	Na						
Molecular weight (g/mol)	22.98977						
MP (°C)	97.72						
MP (K)	370.87						
operating temperature, T (K)	628						
Density, ρ (kg/m ³)	867.1						
Dynamic Viscosity, η (Pa-s)	3.02E-04						
Surface Tension, σ _s (N/m)	0.174						
Thermal Conductivity, k (W/m-K)	73.87						
Specific Heat, C _p (J/K-kg)	1293.4						
Electrical Conductivity, σ _e (1/Ω-m)	5.05E+08						
Vapor Pressure, P (Pa)	12.61						
Vapor Pressure, P (Torr)	0.0959						
Est. Vapor Density, ρ _g (kg/m ³)	0						
Latent Heat of Evaporation (J/kg)							
Dynamic Viscosity, η _g (Pa-s)							

Figure II.3-2 Input data for mechanical pump design nomograph

The resulting design parameters are summarized in Table II.3-3, and the ABTR mechanical pump is schematically compared with that of EBR-II in Figure III.3-3.

Table III.3-3 Mechanical pump design parameters

Flow rate, m ³ /s	0.369
Pump head, psig	110
Power, kW	336
Efficiency, %	83.46
Pump length, m	6.45
Pump diameter, m	0.533
Suction nozzle diameter, m	0.406
Discharge nozzle diameter, m	0.305
Drive motor length, m	1.4
Drive motor diameter, m	0.75

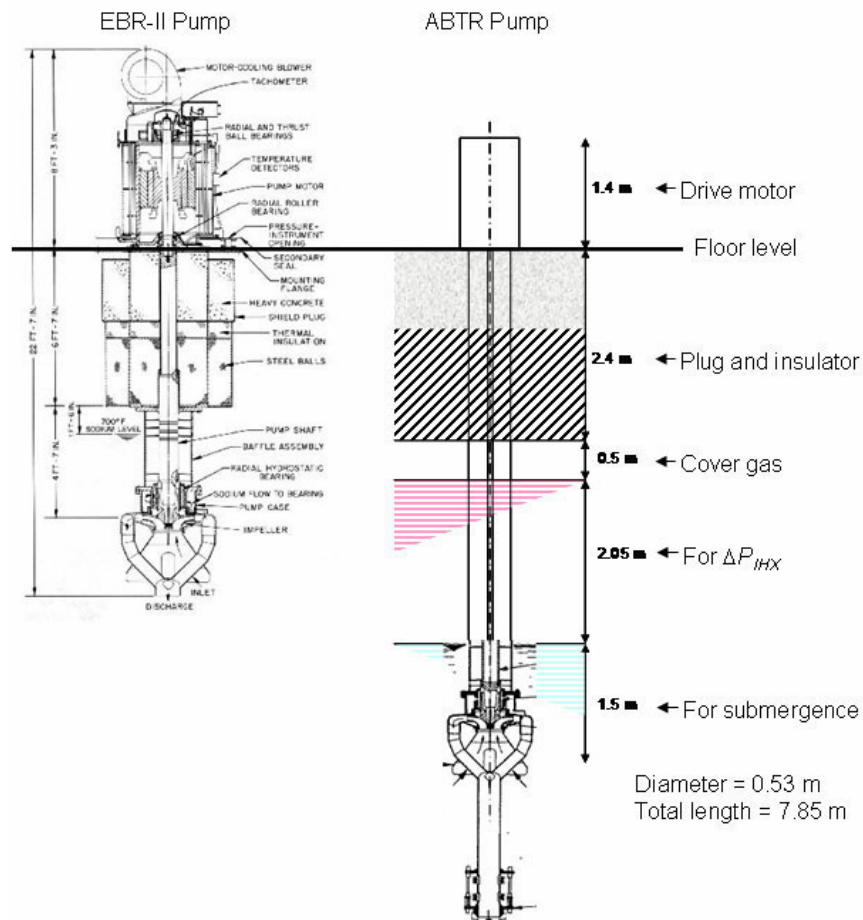


Figure II.3-3 Schematic comparison of ABTR and EBR-II pumps

II.3.2.2 Electromagnetic Pump

The first application of EM pump in sodium cooled fast reactor goes back to the nuclear powered submarine *Seawolf*, which used four flat linear induction pumps (FLIPs) rated at 3,300 gpm at 85 psi. These 4 units were operated at 43 % efficiency for 10,000 hours of maintenance free operation. The EBR-II used 5000 gpm and 6500 gpm FLIP units in the intermediate heat transport system. Although the operating history was satisfactory, the pump duct developed fatigue cracks after 1,385 hours of operation. They were caused by low inlet pressure and electrically induced pressure pulsation [3]. In DFR, 24 linear induction pumps were used as primary pumps. In BR-10, mechanical pumps were replaced with EM pumps, whose reported lifetime was 170,000 hours without any major repairs [7]. Among the many different types of EM pump designs, the EM pump type most favored for use in reactor systems is the annular linear induction pump (ALIP) type. Electromagnetic pump's advantages over mechanical pump are as follows:

1. Design using no penetration through the boundary between working fluid and ambient, thus a design without seals is possible,
2. No moving parts are involved,
3. Installation in any orientation is possible.

On the other hand, EM pumps have some disadvantages over mechanical pumps.

1. Lower pumping efficiency (~40 %),
2. Lesser reactor plant experience, especially for large EM pumps.

A known issue is that large scale EM pumps tend to cause flow instability. This topic is still being studied; however, the instability may be avoided by selecting the right operating parameters [8]. In addition, although no experience of using a large EM pump in the nuclear reactor exists, recently an EM pump with a capacity of 160 m³/min (42,267 gpm) at 280 kPa (40.6 psi) has tested for 2,550 hrs and confirmed applicability of the EM pump in the nuclear plants [9].

Traditionally, electrical insulators and magnetic materials in ALIPs limited the operating temperature of the pump. Until recently, ALIPs for liquid sodium service usually required external cooling to maintain acceptable temperatures in electrical insulators and magnetic materials; and removed thermal energy was wasted. However, recent development of high temperature insulators and magnetic materials that can operate at as high as 700°C allows operation of EM pumps using those components at temperatures as high as 350°C without any cooling [9-11]. This means the ALIPs immersed in a pool type reactor can utilize almost 100% of the input power provided to the pumps, making low pumping efficiency of the ALIPs less important. The impact on the overall plant efficiency due to the differences in pumping efficiency between mechanical and EM pumps is estimated to be only 0.4 % [12]. However, as shown by the history of EM pump development depicted in Figure II.3-4, the important developments occurred only recently and there exists no experience with ALIPs in sodium primary system.

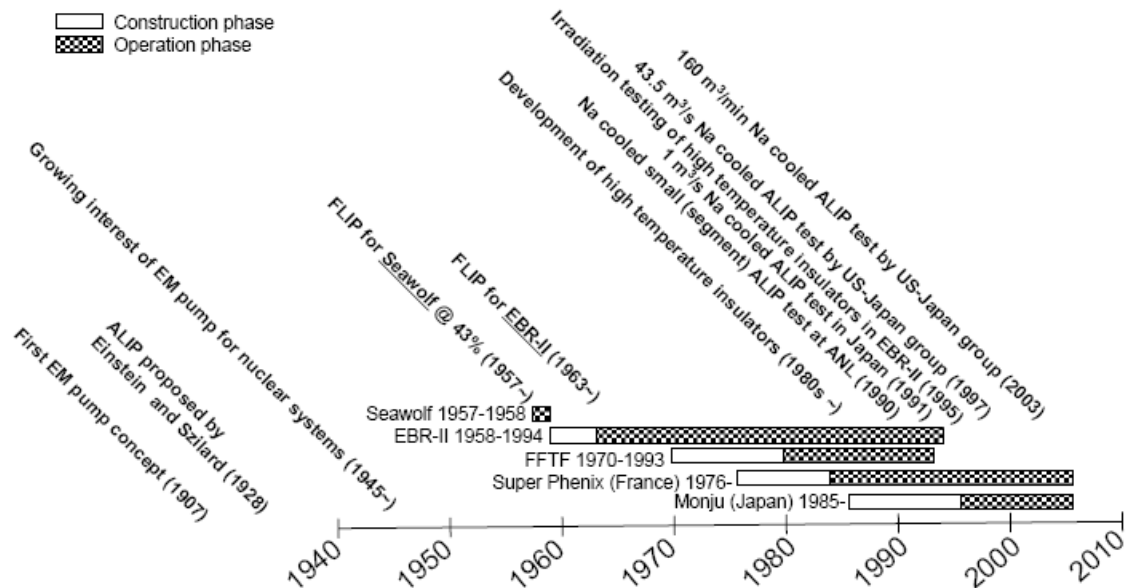


Figure II.3-4 History of EM pump development

The ALIP shown in Figure II.3-5 is a standard design obtained using a code developed at ANL. The code is based on the calculational scheme originally developed to estimate the performance of various ALIPs, for example, for the EBR-II and TREAT. An annular linear induction pump that can be calculated using the current code is a single stator design. A single stator ALIP comprises a core, coolant passage (or duct), coolant duct wall, stator core, and coils (see Figure II.3-5). For the ABTR, however, the pump of choice is a return type and includes the return duct that is placed outside of the stator. All magnetic core pieces are assumed to be made of a magnetic material with high saturation value, such as Permendur 2V or other cobalt alloy. Since the coolant bulk outlet temperature is 510°C, typical stainless steel can be used for the coolant ducts. The conductor part of the coil is made of copper. The electrical insulation around the conductor is made of mica tape backed with alumina cloth and inorganic silicone-base binder, the state of art electrical insulation for high temperature applications. Integrity of a similar coil was experimentally demonstrated at elevated temperatures up to 800°C. Similar coils were also used in a large sodium-immersed self-cooled ALIP [9].

In this design, the magnetic structures do not need to be thermally insulated from the coolant duct, due to the low coolant temperature that is well below the curie point of Permendur 2V (940°C) [11]. In fact, the coolant duct serves as the heat sink, since some of input energy is thermally dissipated as losses within the ALIP during operation and needs to be removed to avoid overheating of various components. Since this thermal energy is transferred to the coolant, these thermal losses in the ALIP are completely recovered in the system.

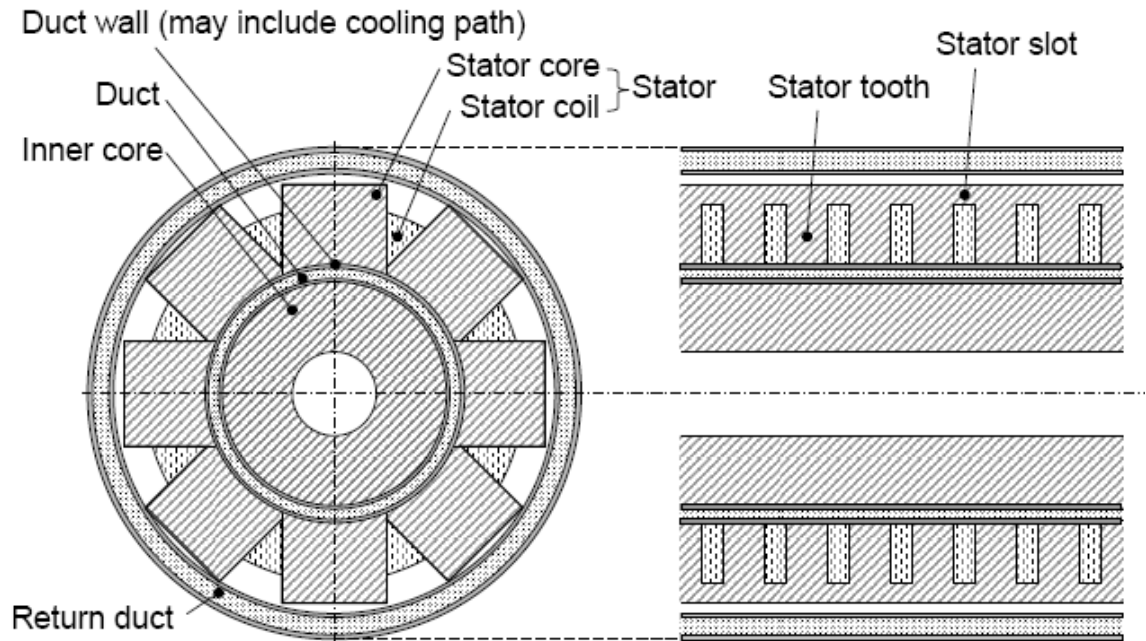


Figure II.3-5 Schematic of a single stator ALIP

The EM code described in Section III.1.2 does not include end effects, which degrade the efficiency of ALIPs [13]. However, for large ALIPs with a large number of poles, thus a large number of coils, sufficient tailoring of magnetic field at the ends of the pump can be easily achieved without altering the performance of a majority of the coils, yielding insignificant pump performance degradation [13]. In addition to the end effect, the skin effect will attenuate the electromagnetic field in the coolant, thus reducing the performance of the large scale ALIPs, unless a double stator design is employed [12], however, the current design code does not include the details of the skin effect. A schematic of a typical double stator ALIP is shown in Figure II.3-6.

Figure II.3-6 It should be noted that the combination of the attenuation of the electromagnetic field due to the skin effect and increase of the electromagnetic field due to the cylindrical configuration is somewhat balanced, which means that the net effect depends on the size of the pump and could be very small [14]. These effects will be investigated for more details in future work. Also noted is that since the ALIP for the ABTR must have both inlet and outlet at the bottom of the pump (return configuration), the internal hydrodynamic pressure drop of the pump is assumed twice that for a straight design ALIP in the code.

Important inputs for the code are the flow rate, pressure head, the length of the pump, various duct dimensions (wall thicknesses), and input voltage. For the flow rate and pressure head inputs, the nominal values for the ABTR design are used. Based on these inputs, the code calculates all other dimensions and parameters for the best efficiency. The calculated parameters include dimensions of the inner core, the duct gap size, and the stator assembly including number of coils and poles, mass of each

component, and performance parameters including input power, dissipated power in components, and efficiency. Also obtained is the optimum drive frequency.

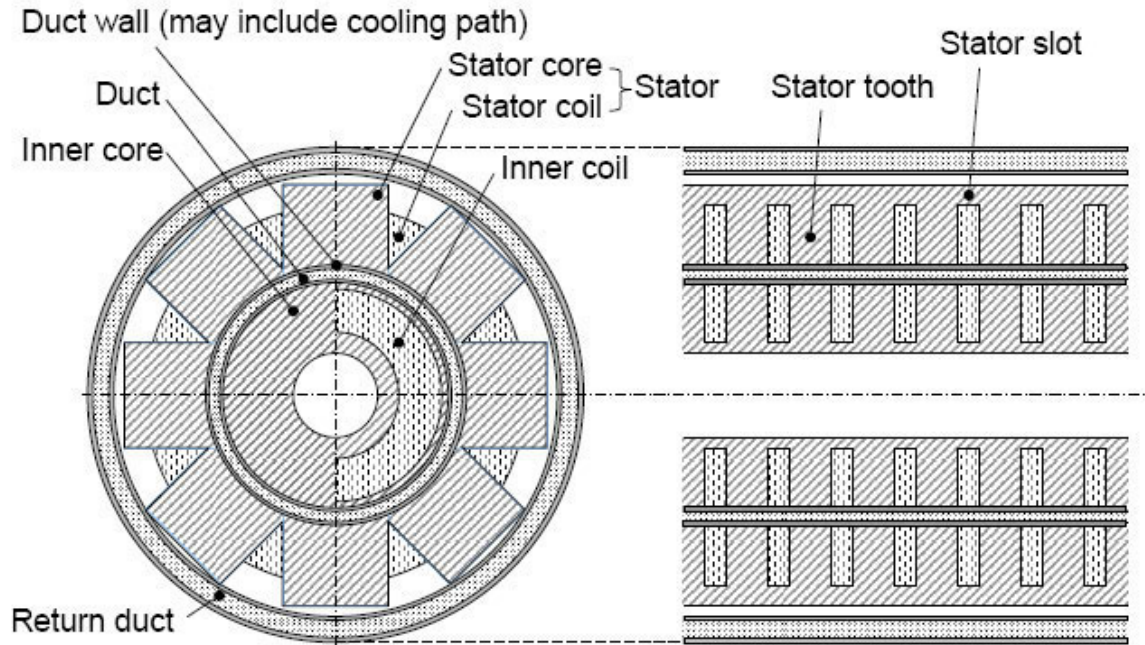


Figure II.3-6 Schematic of a double stator ALIP

Several calculations showed that most heat dissipation occurs in the coolant, duct wall, and coils. This fact allows us to construct a simple 1-D thermal model to conservatively estimate the critical temperatures, such as maximum wall and coil temperatures to ensure safe operation of the ALIP. This thermal model is integrated with the code for calculating the pump performance. The geometry for the thermal model is illustrated in Figure II.3-7.

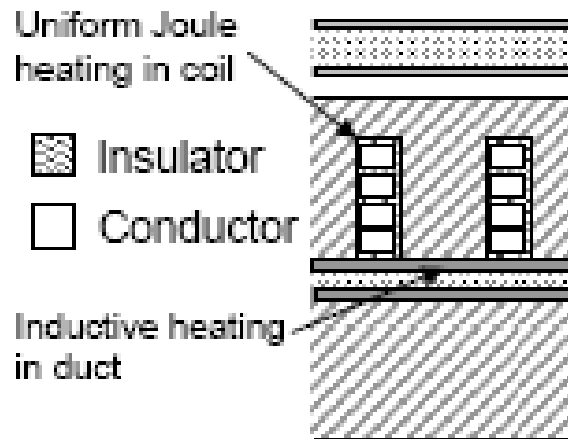


Figure II.3-7 Heat generations in the ALIP

In this thermal model, only radial heat flow is assumed and the outside surface of the ALIP is assumed to be thermally insulated for simplicity and assuring conservative estimation. Bulk thermal conductivity of the coil is estimated from the dimensions of the coil, thermal conductivity of the coil (copper), and that of insulator (mica).

For the ABTR, the diameter of the pump is limited to 0.6 m, so that the ALIP can be installed in the opening for the mechanical pump designed in the previous section. The key design parameters for the EM pump are summarized in Table II.3-4. (Additional detailed data are presented in Section III.1.2.

Table II.3-4 EM pump design parameters

Power, kW	609
Efficiency, %	46
Mass, kg	2271
Number of Poles	14
Number of Coils	42
Temperature, °C	355
Flow Rate, m ³ /s	0.369
Discharge Pressure, psig	110
Length, m	2.4
Pump Diameter, m	0.585

II.3.3 Intermediate Heat Exchanger

The intermediate heat exchangers (IHXs) transfer heat from the radioactive sodium coolant in the primary heat transport system to the nonradioactive sodium coolant in the intermediate heat transport system. Two sodium-to-sodium heat exchangers rated at 125 MWt each are used to transfer the 250 MWt core power at full-power conditions corresponding to core inlet and outlet temperatures of 355 and 510°C, respectively.

There are several factors that are important in the evaluation of the overall IHX design. These factors include material of construction, tube configuration (straight vs. bent), shell vs. tube-side primary flow, elevation of the IHX within the primary system, shape of the IHX (in plan view), primary flow-side pressure drop (i.e., low pressure loss is needed to ensure adequate natural convection primary sodium flow during loss-of-flow events), and the possible inclusion of a second internal coil near the upper region of the IHX to serve as a shutdown heat removal system. The various design choices that have been made, along with the underlying rationale for these choices, are described below.

The heat exchanger arrangement selected is a shell-and-tube counter-current flow arrangement with the primary flow on the shell-side, and secondary sodium flow on the

tube side. Major features of these heat exchangers are graphically depicted in Figure II.3-8, while key design information is provided in Table II.3-5. The tube-side secondary flow was selected to simplify cleaning of the heat exchanger tubes in the event of a leak in the CO₂ Brayton cycle system. Moreover, this configuration maximizes the ability of the IHX to accommodate any pressure transients that may arise if a secondary heat exchanger tube were to rupture, since for a given tube wall thickness the tubing is much stronger in tension (internal pressure source) versus compression (external pressure source).

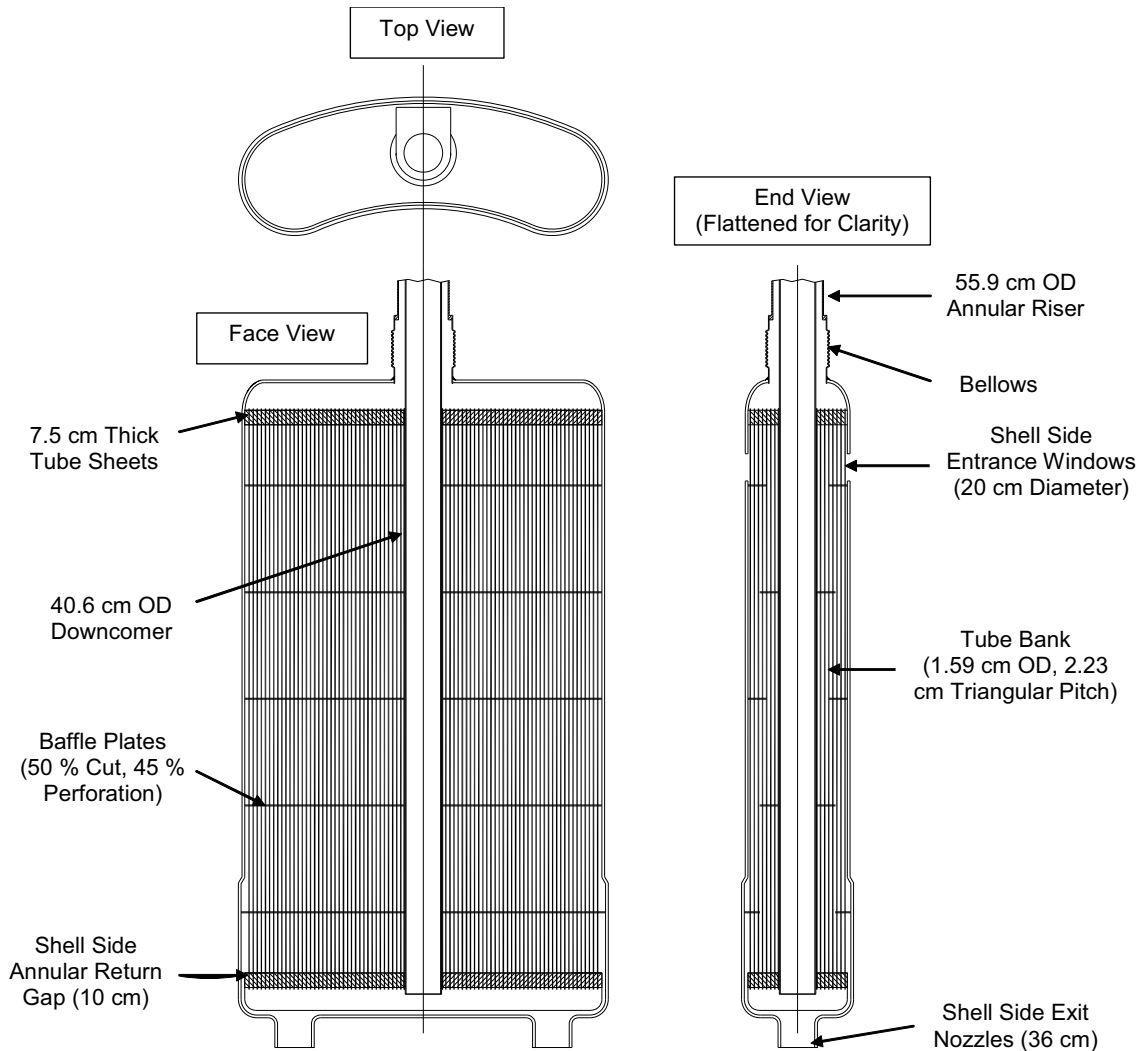


Figure II.3-8 Intermediate Heat Exchanger Design

The installation of the IHXs inside the reactor vessel is illustrated in Figure II.3-9. Each unit is vertically suspended from two rigid pipes that are welded to the IHX shroud. These pipes extend upward from the hot pool and are welded to the underside of a removable integral plug in the reactor vessel head. The IHXs pass through horizontal plate sections of the redan, which is contoured (in plan view) to accommodate the kidney-shaped IHX design that has been selected to minimize the reactor vessel diameter.

Table II.3.-5 Intermediate Heat Exchanger Design Parameters

Heat transfer capacity	125 MWt
Thermal design margin	+10%
Heat transfer area	634 m ²
Primary sodium temperature, inlet/outlet	510/355 °C
Primary sodium mass flowrate	628 kg/s
Secondary sodium temperature, inlet/outlet	333/488 °C
Secondary side sodium mass flowrate	628 kg/s
Tube outer diameter	1.59cm
Tube wall thickness	0.889 mm
Tube pitch	2.23 cm
Active Tube Length	3.85 m
Number of tubes	3300
Tube sheet – area	1.42 m ²
Tube sheet – thickness	75 mm
Downcomer piping – OD	40.6 cm
Downcomer piping – thickness	12.7 mm
Downcomer piping – length	10.8 m
Outlet piping – OD	55.9 cm
Outlet piping – thickness	12.7 mm
Outlet piping – length	6.6 m
Shell (primary) side pressure drop	12.6 kPa
Tube (secondary) side pressure drop	5.7 kPa
Shell height	4.84 m
Shell outside circumference	4.35 m
Shell thickness	19 mm
Cross-sectional area	1.5 m ²
Tube material	9Cr-1Mo

Primary sodium enters the shell side of each IHX through a series of 20 cm diameter circular openings in the shell approximately 30 cm below the upper tube sheet. These openings allow sodium from the hot plenum to enter the IHX with minimal head loss. Also, introduction of the sodium below the upper tube sheet minimizes the thermal shock to this relatively thick component during transients. The sodium then flows downward through the shell and vents through a 10 cm wide gap around the lower tube sheet that leads to the two parallel 36 cm diameter exit nozzles that discharge directly into the cold pool.

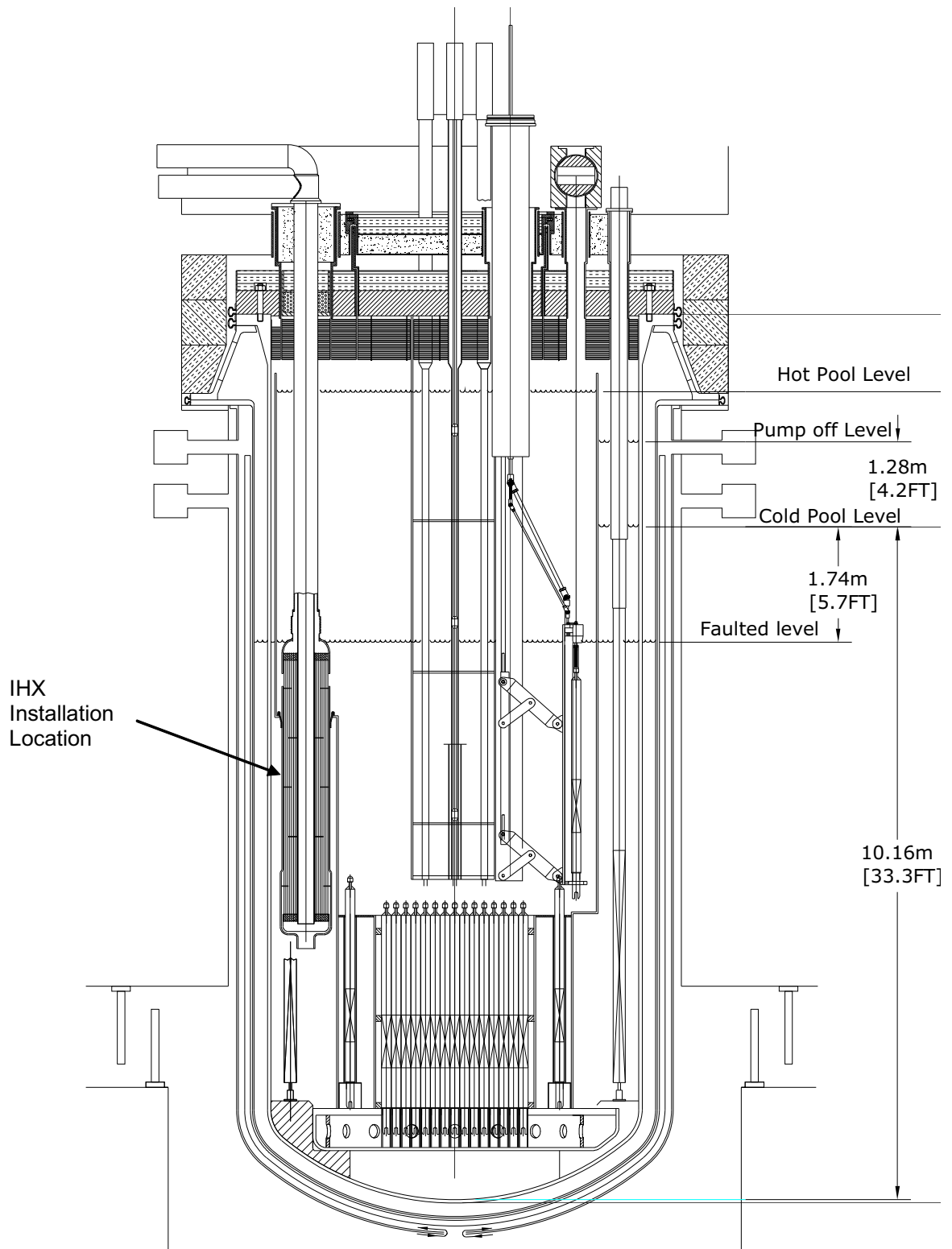


Figure II.3-9 Illustration of IHX Installation inside the Reactor Vessel

The IHX shell contains a seal where it seats on the horizontal deck of the redan to prevent sodium bypass from the hot to cold pools. Minor leakage of these seals is permissible. As shown in Figure II.3-8, the shell side includes a series of horizontally mounted, disk and donut-type baffle plates uniformly spaced at 64 cm intervals along the length of the tube bank. Aside from providing lateral support for the tubes, these plates promote cross-flow and mixing that enhances thermal performance on the shell (primary) side. The plates are made from 6.4 mm steel plate and occlude 50 % of the vertical flow path at each plate location. The plates are orificed (45 % equivalent porosity) to reduce flow pressure drop; a schematic showing the orifice design is provided in Figure II.3-10. This approach is similar to that used in the GE PRISM Mod B IHX design.

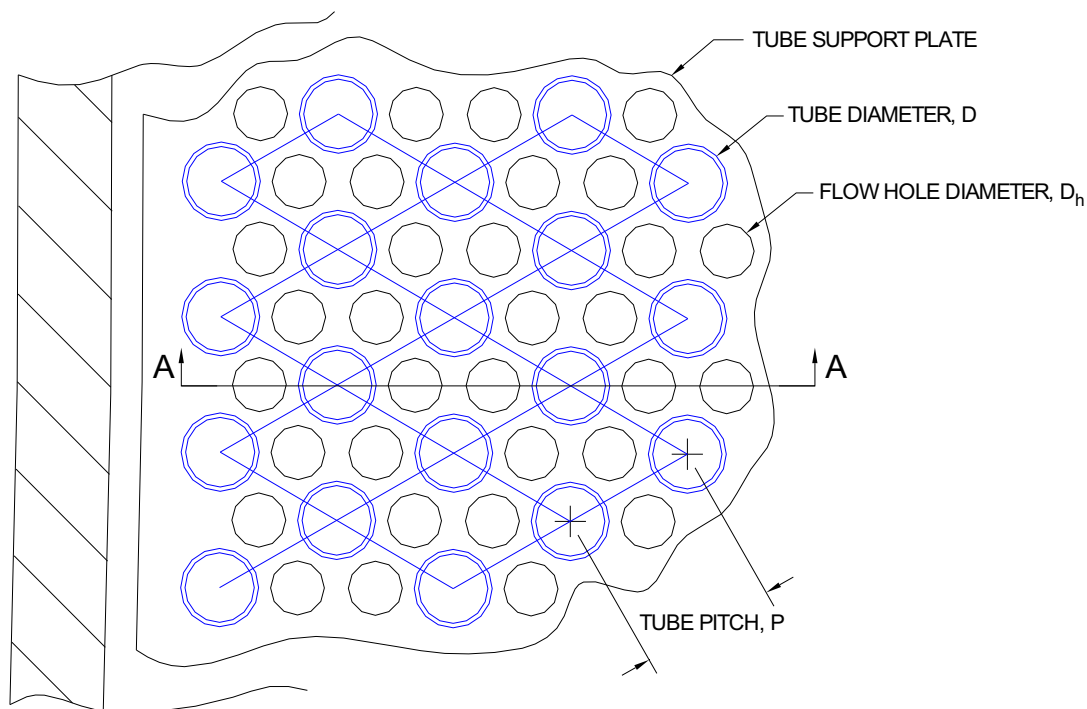


Figure II.3-10 Plan View of Orifice Baffle Plate Design

As shown in Figure II.3-8, cold intermediate sodium enters the IHX through a central 44.6 cm downcomer. The downcomer delivers the cold sodium through the lower tube sheet into a header manifold, where it then turns 180° and rises through the tube bank in counter current flow to the shell side primary sodium. The hot intermediate sodium exits the tubes into an upper header manifold, and then flows through an annular riser which is concentric to the downcomer. The downcomer is double walled with an annular gap for thermal insulation between the hot and cold streams. As shown in Figure II.3-8, both the downcomer and the 55.9 cm OD annular riser pipes are equipped with bellows just above the shroud to accommodate any differences in thermal expansion between the piping and the body of the IHX itself (each unit is rigidly attached to the removable plug in the reactor vessel head). The upper tube sheet is welded to the shroud, while the lower tube

sheet floats. Thus, the design accommodates differential thermal expansion within the tube bank also.

The inner wall of the shell operates near the bulk temperature of the sodium in the hot plenum. Since primary sodium flow is on the shell side of the IHX, there is no need for an insulating annulus to eliminate heat losses to the bulk sodium or to alleviate high thermal stresses in the shell.

Modified 9Cr-1Mo steel was chosen as the material of construction primarily because the thermal conductivity is higher than that of the austenitic steels such as Type 304 stainless steel. Since the heat transfer in sodium-to-sodium heat exchangers can be dominated by the tube wall thermal resistance, using modified 9Cr-1Mo steel results in considerable reduction in the required heat transfer area. The use of Type 304 stainless steel tubes would result in the need for as much as 20% more heat transfer area as compared to modified 9Cr-1Mo tubes with the same design characteristics. In addition, modified 9Cr-1Mo has a lower thermal expansion coefficient compared to Type 304 stainless steel. The higher thermal conductivity material results in lower temperature differences in component sections and, coupled with the reduced thermal expansion, results in lower thermal stresses in structural members. This is advantageous during thermal transients. Straight tubes are selected to simplify fabrication and reduce flow induced vibration problems.

The design of the IHX has been selected such that the primary flow of sodium on the shell side provides a low pressure drop. Low pressure drop on the primary side is important from two viewpoints: 1) minimizing the pressure-related structural requirements for the IHX shell, and 2) promoting the ability to establish natural circulation of the primary sodium in the case of a loss-of-flow event. Adequate natural convection flow for shutdown heat removal is essential. One key element of the DRACS shutdown heat removal system relies on natural circulation of the primary sodium through the core and IHX to the sodium pool surrounding the core barrel. Thus, the IHX has been sized and positioned to locate the primary sodium inlet below the faulted sodium level (primary sodium leak from the primary vessel to the annulus between it and the guard vessel).

Aside from the overall thermal-hydraulic design of the IHXs, additional analysis is needed to verify that the thermal stresses in various regions of these units will remain below acceptable levels to ensure that the plant design lifetime requirement can be met without undue risk of stress-related failure(s). Furthermore, shielding may need to be incorporated into the design if calculations indicate excessive activation of the secondary sodium by virtue of the close proximity of the IHXs to the core.

Note that as part of the design process, a set of parametric thermal-hydraulic calculations were performed that formed the technical basis for sizing of these units so that they would fit inside the available space between the redan and reactor vessel inner surface, while achieving the desired 125 MWt rating. In addition, a specialized model was developed in order to accurately evaluate flow pressure drop on the shell side of the

IHX, including the effect of the orificed baffle plates. These various design calculations are documented in Section III.8.

II.3.4 Internal Piping

There is very little primary piping within the reactor vessel assembly for either the mechanical or electromagnetic pump applications. If the electromagnetic pump is adopted as the primary pump, there is no internal piping within the reactor vessel. The discharge of the EM pump flows into an articulated coupling that connects the EM pump to the inlet plenum structure. If the mechanical pump option is adopted as the primary pump, it is expected that the coolant that flows through the pump will flow into a multi-pipe header that connects the articulated coupling to the inlet plenum structure. This primary piping would consist of a main header for each pump with multiple pipes leading from each pump header into the inlet plenum structure. The main header is connected to a flexible coupling. The other end of the internal piping is welded to the core inlet plenum.

Each primary piping assembly is supported to take the appropriate mechanical, thermal and hydraulic loads. The pump hangs from the reactor vessel enclosure and is connected to the inlet plenum or inlet pipe header (depending upon pump application) by a special, nonrigid, easily disconnected, low leakage articulated coupling. This articulated core inlet pipe coupling is shown in Figure II.3-11.

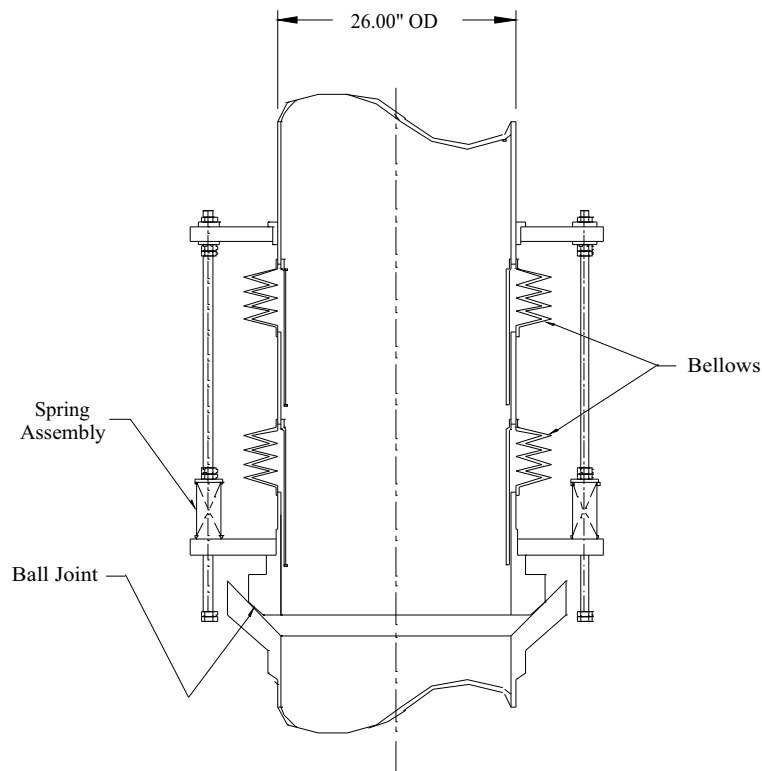


Figure II.3-11 Articulated Core Inlet Pipe Coupling

The flexible coupling allows lateral and vertical movement without losing metal-to-metal contact and accommodates relative displacements between the pump and the inlet plenum. The coupling has a slip joint to extend or retract the coupling length with a ball joint at the bottom end. The ball joint at the bottom end is unattached and connects with the mating seat on the reactor core vessel inlet plenum. During installation, the pump is lowered vertically into the reactor vessel. When the bottom ball joint contacts with the mating seat on the inlet plenum, the coupling is compressed, creating spring pressure in the coupling. The spring pressure maintains the coupling in position and seals the ball joint against the mating joint of the inlet plenum.

The coupling allows the pump to be removed or installed without cutting the inlet interface. The coupling can permit some leakage but must provide flexibility to accommodate thermal movements, be sufficiently stable to avoid flow induced vibrations, and accommodate seismic loads. No valves or movable flow control devices are part of the inlet piping or flexible coupling. Pipe insulation is not required.

References

1. R. W. Atz, and R. S. Baker, *Sodium-NaK Engineering Handbook*, Vol. IV, Sodium Pumps, Valves, Piping, and Auxiliary Equipment, Chap. 1, Gordon and Breach, Science Publishers, Inc., New York, NY, 1978.
2. *Status of Liquid Metal Cooled Fast Reactor Technology*, Chap. 8, IAEA, Vienna, Austria, 1999.
3. Davis, J. R., et al., Operating Experience with Sodium Pumps at EBR-II, ANL/EBR-027, 1970.
4. Monson, H. O., et al., "Components for sodium reactors," Proceedings of the Third International Conference on the Peaceful Uses of Atomic Energy, Geneva, v 8, pp588-599, 1964.
5. Korolkov, A. S., "Operating experience with BOR-60: basic results and prospects," TM-27172 and TM-26984, TWG-FR/123, Working Material, IAEA, pp218-225, 2005.
6. Charnock, H. O. and Holz, H. B., "Sodium Systems Components," Sodium Technology, Session IV, Atomic International, North American Rockwell, 1970.
7. Nikulin, M. P., et al., "Experience Gained during BR-10 Reactor Operation," TM-27172 and TM-26984, TWG-FR/123, Working Material, IAEA, pp211-217, 2005.

8. R. Stieglitz, "MHD-features of the Main Service and Bypass Pump in the MEGAPIE Design," ISSN 0947-8620, Forschungszentrum Karlsruhe GmbH, Karlsruhe, 2003.
9. H. Ota et al., "Development of 160 m³/min Large Capacity Sodium-Immersed Self-Cooled Electromagnetic Pump," J. of Nucl. Sci. and Tech. v41, No4, pp511-523, 2004.
10. M. Ishida, Y. Ikeda, and N. Naohara, "Development of Insulating System for FBR Electro-Magnetic Pump," Proc. of the 4th Int'l Conf. on Properties and Applications of Dielectric Materials, Brisbane Australia, pp471-474, July 3-8, 1994.
11. Abraham Weitzberg et al., Liquid Metal Cooled Reactor Concept for Nuclear Space Initiative Electric Propulsion Missions, Draft Input for DOE Report, October, 2002
12. *Electromagnetic Pumps for Large Pool-Concept LMFBR*, General Electric Company, NP-1265, Research Project 620-28, December 1979.
13. L. R. Blake, "Conduction and Induction Pumps for Liquid Metals," Proc. I.E.E., Paper No. 2111U, v104A, pp49-67, July 1956.
14. Kliman, G. B., "Large Electromagnetic Pumps," Electric Machines and Electromechanics: An International Quarterly, v.3 pp129-142, Hemisphere Publishing Corp., 1979.

II.4 Intermediate Heat Transport System

II.4.1 System Requirements and Description

The intermediate heat transport system (IHTS) circulates secondary sodium coolant, transporting heat from the radioactive sodium in the primary heat transport system (PHTS) to the power generation system. Currently, both supercritical CO₂ (S-CO₂) Brayton and Rankine steam cycle power generation systems are under consideration for the ABTR. Note that the IHTS description provided in this section is based on the reference S-CO₂ power conversion system. However, the piping layout would be similar for a steam system, with the exception that the printed circuit heat exchangers (PCHEs) for the Brayton cycle would be replaced with steam generators for the Rankine cycle.

The IHTS is composed of two completely independent loops, as shown in Figure II.4-1. This figure shows the plan view of the piping runs to the secondary PCHEs. The flowrate through both loops is controlled to maintain the primary sodium coolant temperature at design operation conditions. With the exception of the short pipe runs of the hot and cold sodium piping connected to the IHX and running from the IHX to the PCHEs, the entire IHTS is contained within the S-CO₂ generation facility that is part of the reactor building.

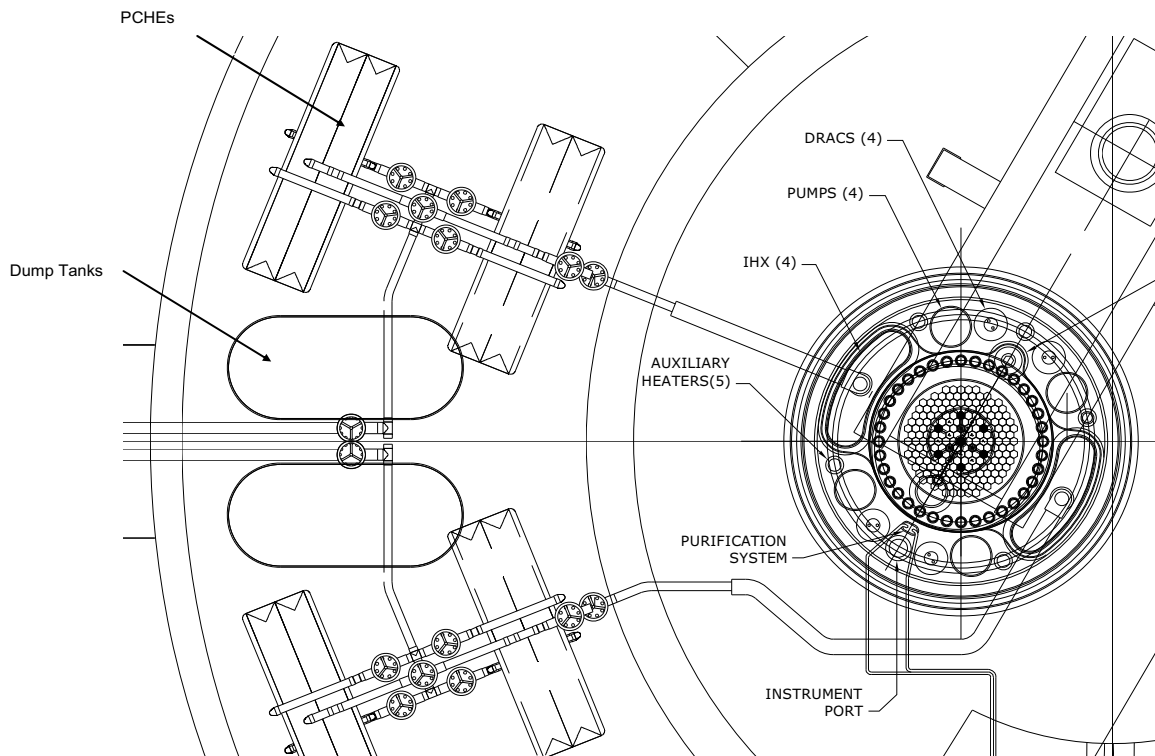


Figure II.4-1 Plan View of IHTS Layout

The secondary sodium exits the upper portion of the IHX after being heated to 488°C. The sodium then exits the reactor containment and traverses the short distance to the adjacent S-CO₂ production facility inside the reactor building. Here, the hot sodium enters the bottom of the PCHEs and transfers heat to the S-CO₂ before exiting at the top of these units. After exiting at the top of the heat exchangers, the secondary sodium circulates to the intermediate electromagnetic (EM) pump where it is pumped back to the reactor containment and cold side of the IHX. The tube walls of the IHX constitute the principal barrier for isolation of the activated primary sodium from the sodium in the secondary system. In the unlikely event of an IHX tube leak, sodium leakage will occur from the IHTS to the PHTS due to the fact that the secondary system is maintained at a pressure of at least 0.6 bar (8.5 psig) in excess of the primary system. The excess pressure is due to sodium hydrostatic head (~7.1 m) that is provided by the higher elevation of the secondary loop relative to the primary loop (see Figure II.4-2). Radiation detectors on the outlet (hot leg) piping from the IHX monitor for indications of contamination of the secondary loop sodium.

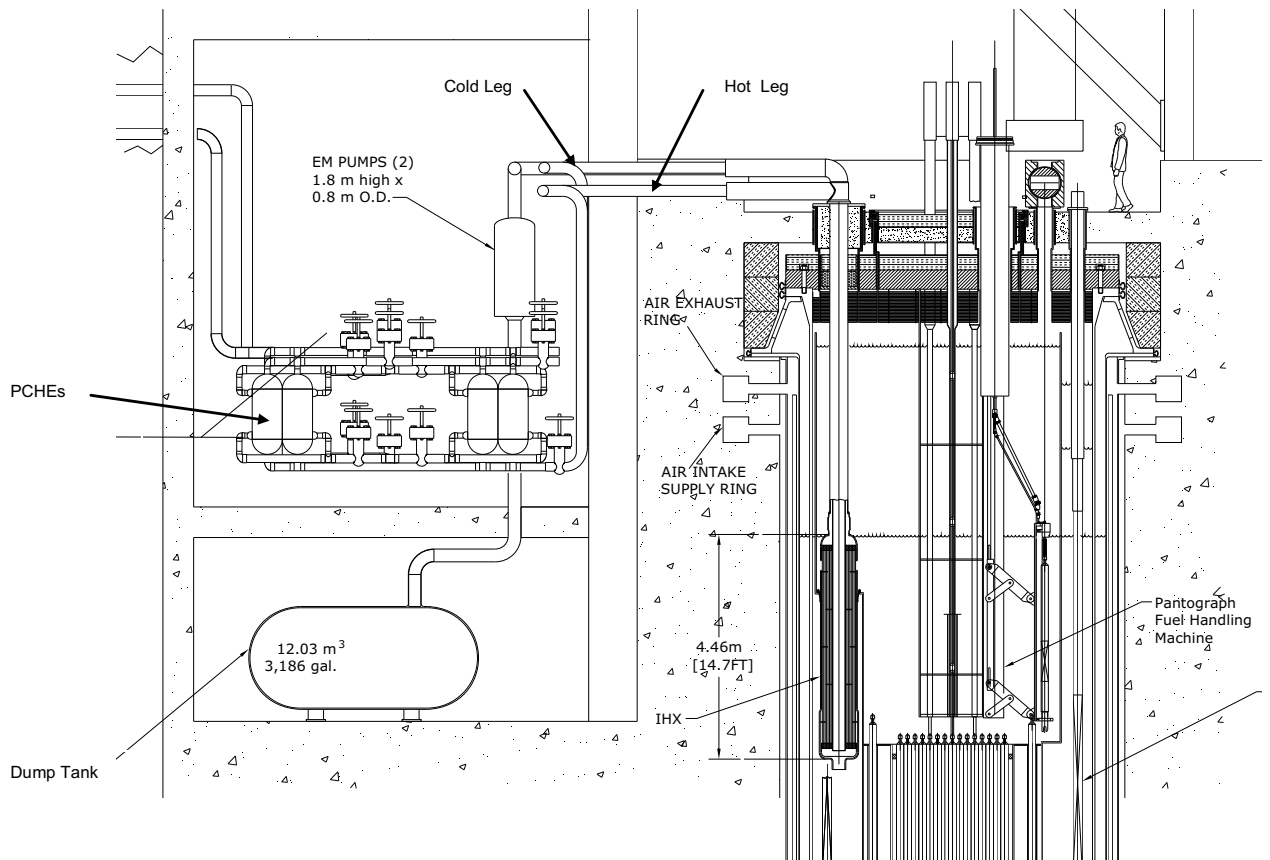


Figure II.4-2 Elevation View of IHTS Layout

Major components in each of the two loops include the EM pump, PCHE, sodium storage tank, and the piping connecting these components to each as well as the IHX and PCHE. Design details of the IHX and PCHE units are provided in Sections II.3.3 and II.5.1, respectively. Details regarding the balance of key system components are provided below.

Auxiliary systems that connect to the IHTS main loop that are necessary to achieve operational requirements include a circulating sodium purification system, trace heating, thermal insulation, and instrumentation that monitors key system parameters including flowrate (with permanently installed magnetic flowmeter in each cold leg), and temperature differential across the IHTS (with thermocouples installed at the PCHE inlet and outlet legs).

II.4.2 Intermediate Sodium Pump

One sodium pump is used in each IHTS loop. Each unit is a vertically mounted, double stator, EM pump design. The pump operates in the cold leg at nominally 326 °C.

The pump installation location is shown in the plant elevation view provided in Figure II.4-2, while design details are summarized in Table II.4-1. The pump design is very similar to the reference primary EM pump (see Section II.3.2), which minimizes the developmental requirements for ABTR. Flowrate through the pump is modulated by adjusting the drive voltage and frequency for continuous flow control over the design range.

As in previous designs, each pump is installed in a tank with the piping inlet and exits at the top and bottom of the tank, respectively. Both pumps are completely separate so that the two IHTS loops can be operated independently to produce the desired operational characteristics.

Each pump is self-cooled by transfer of waste heat from electrical heat losses in the stators directly to the IHTS sodium. Since all waste heat is transferred to the intermediate sodium, overall efficiency is increased. This increase is not factored into the calculated overall pump efficiency of nominally 40 % that is shown in Table II.4-1.

As noted earlier, the overall pump design is quite similar to the primary EM pump. However, motor-generator sets to provide flow coast down capability are not required for these units, as opposed to the primary system pumps.

II.4.3 IHTS Piping

The IHTS piping consists primarily of the main system hot and cold legs which make the necessary connections between the IHX and the PCHE. The hot leg piping connects to the secondary sodium outlet of the IHX directly to the PCHE sodium inlet. The IHTS

cold leg piping connects the sodium outlet from the PCHE to the EM pump tank inlet and then from the pump tank discharge to the secondary cold sodium inlet to the IHX.

Table II.4-1 Intermediate Sodium EM Pump Characteristics

Flow rate	0.738 m ³ /s
Pump head	0.21 MPa
Power	406 kW
Efficiency	37.58 %
Drive voltage	560 V
Drive current per phase	579 A
Drive frequency	17 Hz
Number of poles	6
Number of coils	18
Mass	2531 kg
Pump height (length)	1.8 m
Pump diameter	0.807 m
Inner core - inner diameter	0.140 m
Inner core - outer diameter	0.21 m
Duct - inner diameter	0.385 m
Duct - outer diameter	0.39 m
Material	304 SS

The IHTS piping is constructed from 40.6 cm OD, 1.27 cm thick-walled (16 inch Schedule 30) 304 stainless steel piping, primarily because of the lack of corrosion issues for sodium and the ease of fabrication with this material. The use of this piping diameter and schedule maintains the sodium flow velocity through the secondary piping system below ~ 7 m/sec (actual value is 6.5 m/sec at full power conditions), which is a rule-of-thumb design criterion for these types of systems. The use of 304 stainless steel requires dissimilar metal welds connecting the austenitic Type 304 stainless steel to the ferritic steels used in the IHX. The welding technology for joining these dissimilar metals is well established.

Inside the reactor building, the IHTS piping is enclosed in secondary piping so that in the unlikely event of failure of the main system piping, the sodium is contained which greatly reduces the possibility of a major sodium leak. In addition, the reactor building containing the IHTS is seismically isolated on the same platform as the reactor itself, which eliminates differential motions between these two structures during seismic events. This simplifies the design for piping hangers and supports that would otherwise need to be equipped with snubbers or other motion-dampening devices if the reactor building were not integral to the nuclear island.

II.4.4 IHTS Sodium Storage Tank, Expansion Tank, and Cleanup System

A small secondary loop is included in the IHTS to maintain sodium volume and to provide a purification pathway for the secondary sodium. The loop supplies sodium from a cold trap to the EM pump tank to maintain a constant level of sodium in the IHTS loop. The recirculation system uses a fill and overflow approach to maintain the sodium level constant. Spillover into the EM pump tank overflow line flows through the secondary piping to the storage tank. Sodium is then pumped from the storage tank by a small recirculation pump through interconnecting piping to the cold trap. After circulating through the trap, the sodium circulates back to the pump tank.

The circulating sodium to the storage tank keeps the tank at system temperature during normal operations. When flow is not available, trace heating is used to keep system components above the sodium freezing point.

Pressurized argon cover gas is maintained in the pump tank upper plenum. Subsystems must also be provided to control the argon cover gas pressure and supply.

II.5 Power Conversion System

II.5.1 Supercritical CO₂ Brayton Cycle

II.5.1.1 Supercritical CO₂ Brayton Cycle Arrangement

The reference power conversion system consists of a Brayton cycle utilizing supercritical carbon dioxide (S-CO₂) as the working fluid. The S-CO₂ Brayton cycle avoids the sodium-water reaction problem that the design and licensing safety evaluation must deal with for the conventional Rankine steam cycle. However, the technology for the S-CO₂ Brayton cycle is less well developed than that for the Rankine steam cycle.

The S-CO₂ Brayton cycle is an innovative power conversion technology for nuclear reactors having potential benefits above and beyond gas (e.g., helium) Brayton cycles or Rankine steam cycles operating at the same reactor core outlet temperature. The S-CO₂ Brayton cycle has been under development for several years in the U.S., Japan, Korea, and France because it offers significantly improved thermal efficiency as well as reduced turbomachinery costs. The current Generation IV Nuclear Energy Systems Initiative Energy Conversion Program plans to design, assemble, and operate a small-scale (e.g., ~ 1 MWt heat input) demonstration of the S-CO₂ Brayton cycle; two vendors are currently investigating approaches to a demonstration.

The benefits of the S-CO₂ Brayton cycle follow from the high supercritical carbon dioxide density and low work to compress S-CO₂ immediately above the critical point ($P_{\text{crit}} = 7.377 \text{ MPa}$, $T_{\text{crit}} = 30.98 \text{ }^\circ\text{C}$, $\rho_{\text{crit}} = 468 \text{ Kg/m}^3$). However, the rapid variation in thermophysical properties near the critical point impacts the cycle arrangement (i.e., the flow split between heat rejection and direct recompression) as well as compressor design, recuperator design, and cooler design.

The S-CO₂ Brayton cycle is selected as an alternative power converter for the ABTR for several reasons including the following:

- Elimination of the potential for energetic sodium-water interactions which result in the formation of combustible hydrogen gas;
- Potential for reduction in power conversion system costs. The S-CO₂ Brayton cycle incorporates a turbine and two compressors that are remarkably small compared with those of either a Rankine steam cycle or a gas Brayton cycle. The small turbine and compressor sizes are expected to significantly reduce the costs of the turbomachinery components. Also, the S-CO₂ Brayton cycle incorporates fewer components than the Rankine cycle – The condenser, feedwater heaters, and deaerator are eliminated;
- Higher thermal efficiency achievable with the S-CO₂ Brayton cycle including the potential to reach 45 % cycle efficiency with an increase in the ABR core outlet temperature to values of some sodium-cooled fast reactor concepts. A higher efficiency enhances the revenue from the sale of electricity.

Figure II.5-1 shows a comparison of cycle efficiency versus temperature for a S-CO₂ Brayton cycle and a helium ideal gas Brayton cycle. Over the temperature range of interest to the ABTR, the S-CO₂ cycle clearly provides a significantly greater efficiency.

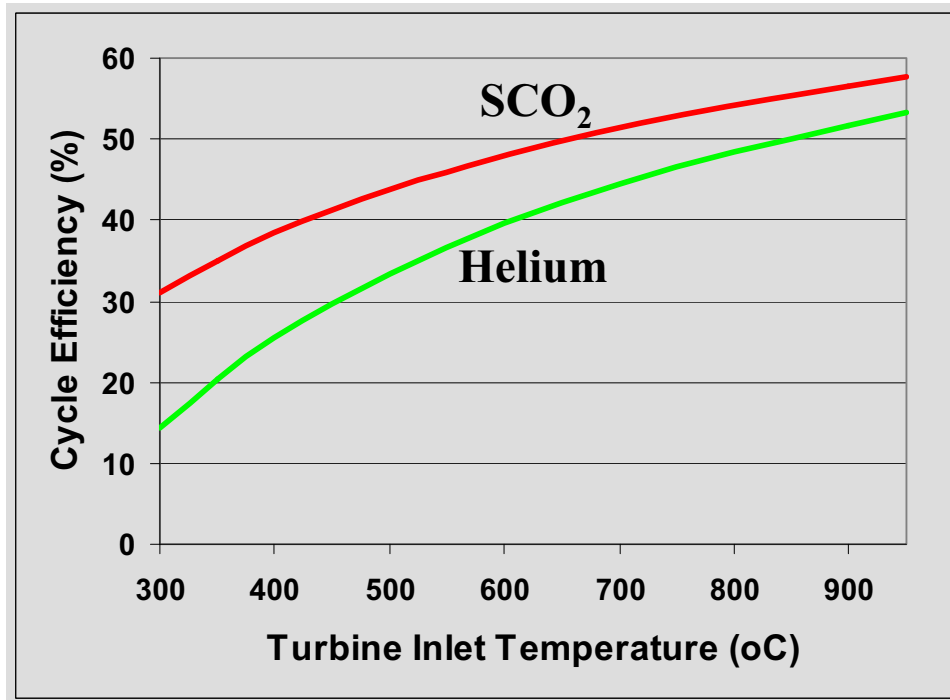


Figure II.5-1 Comparison of Efficiencies versus Temperature for S-CO₂ Brayton Cycle and Traditional Helium Ideal Gas Brayton Cycle

Figures II.5-2 and II.5-3 provide schematic illustrations of the S-CO₂ Brayton cycle coupled to the reactor through an intermediate sodium circuit. During normal operation, the supercritical CO₂ at about 20 MPa pressure is heated by the intermediate sodium loop in the sodium-to-CO₂ heat exchangers. It then expands to a lower pressure of about 7.7 MPa in the turbine where thermal energy is converted to mechanical rotational energy that drives the generator as well as the two main compressors that are all located on a common shaft (Figure II.5-2). The CO₂ then passes through two recuperators, designated the high temperature recuperator (HTR) and low temperature recuperator (LTR), where energy is transferred from the hot CO₂ to preheat CO₂ that has been compressed before it returns to the sodium-to-CO₂ heat exchangers. Preheating the CO₂ increases the cycle efficiency. A portion of the expanded low pressure CO₂ stream equal to 71 % of the total CO₂ flow passes through the cooler where heat is rejected from the cycle. Actual pressure, temperature, and flow rate conditions calculated for the cycle as well as the primary and intermediate sodium coolant systems are shown in Figure II.5-3. This figure also presents the energy exchange rates in the components. The largest heat exchange rates in the S-CO₂ Brayton cycle occur in the HTR and LTR. Hence, large heat transfer areas are required for these two specific components.

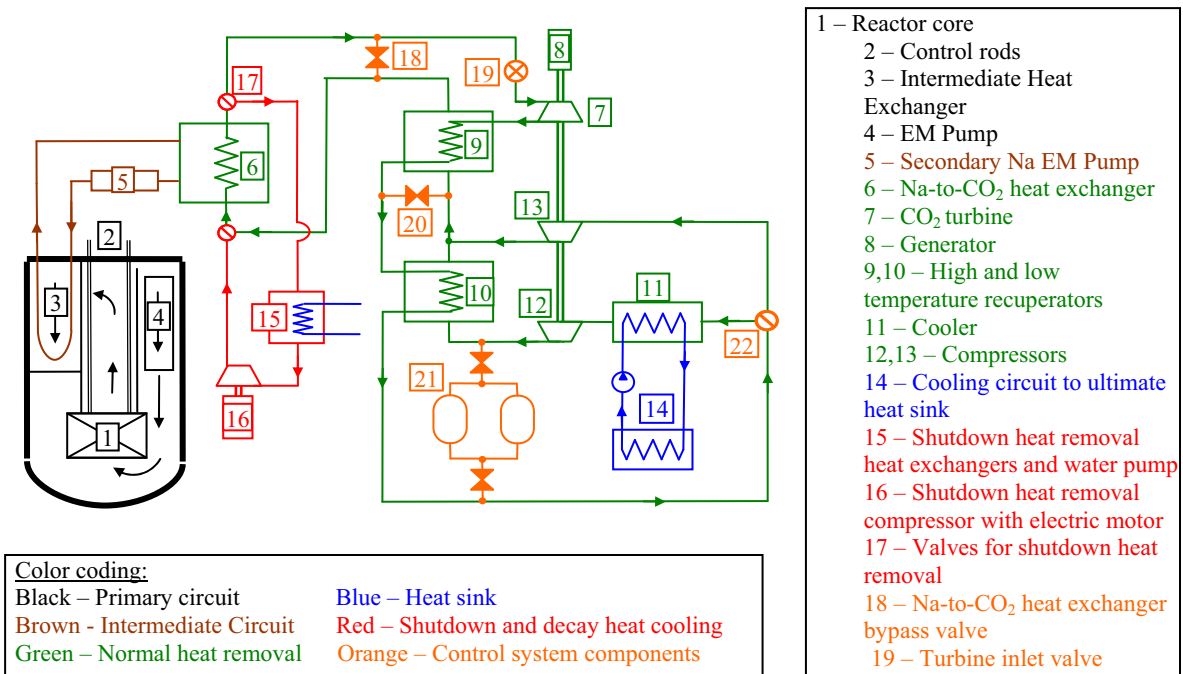


Figure II.5-2 Schematic Illustration of S-CO₂ Brayton Cycle Showing Heat Transfer Paths and Control Mechanisms

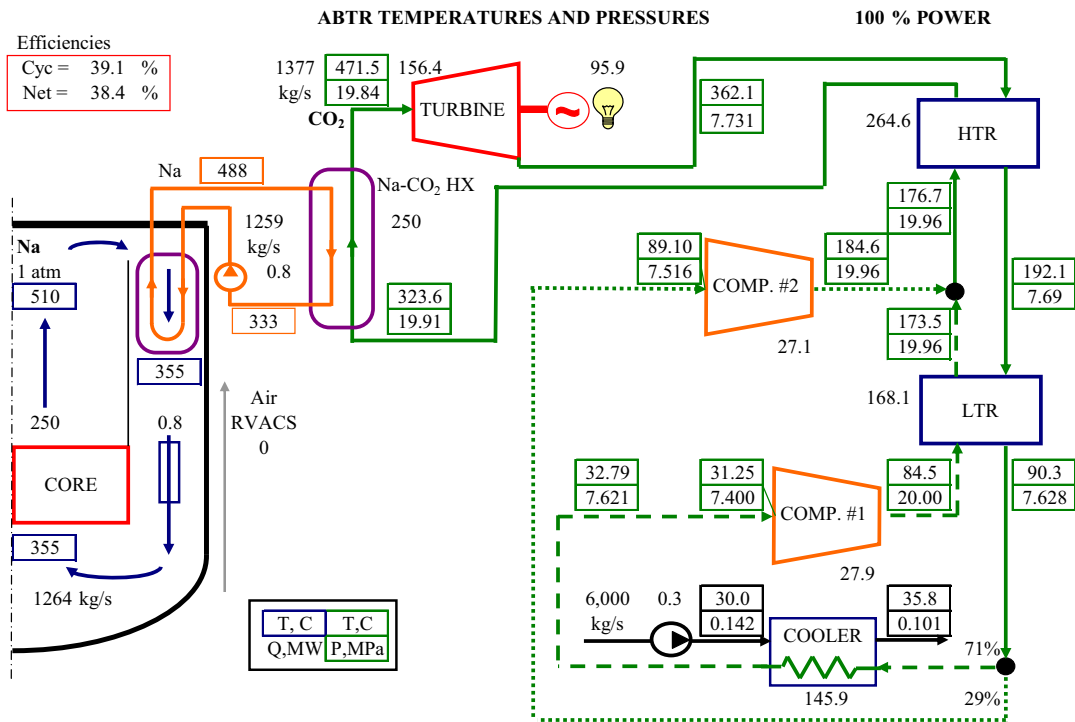


Figure II.5-3 S-CO₂ Brayton Cycle Temperatures, Pressures, Flow Rates, and Heat Exchange Rates

The CO₂ is expanded in the turbine such that the pressure at the compressor inlet is 7.4 MPa which is immediately above the critical pressure (7.377 MPa). This is done to take advantage of the low compressional work for CO₂ immediately above the critical point. The low work of compression is the salient feature of the cycle that contributes most to its improved efficiency over traditional gas Brayton cycles. In part, this is due to the high density of CO₂ immediately above the critical point (Table II.5-1) which is closer to that of an ordinary liquid than a gas in a traditional gas Brayton cycle. Thus, there is an incentive to cool the CO₂ to as near the critical temperature as feasible. The general dependency of cycle efficiency upon the temperature of CO₂ exiting the cooler as well as the required size of the cooler is illustrated in Figure II.5-4.

Table II.5-1 Comparison of Densities and Specific Heats

Fluid	Location	Pressure MPa	Temperature °C	Density kg/m ³	Specific Heat KJ/kg-K
S-CO ₂	Critical point	7.38	30.98	468	Infinite
	Compressor inlet	7.40	31.25	369	58.5
	Compressor outlet	20.00	84.5	566	2.58
	Turbine inlet	19.84	471.5	138	1.23
	Turbine outlet	7.73	362.1	65.0	1.15
Helium	Cooler outlet	2.6	27	4.17	5.19
	Compressor outlet	7.0	104	8.93	5.19
Water		0.1	20	998	4.18
Sodium		0.1	420	828	1.36

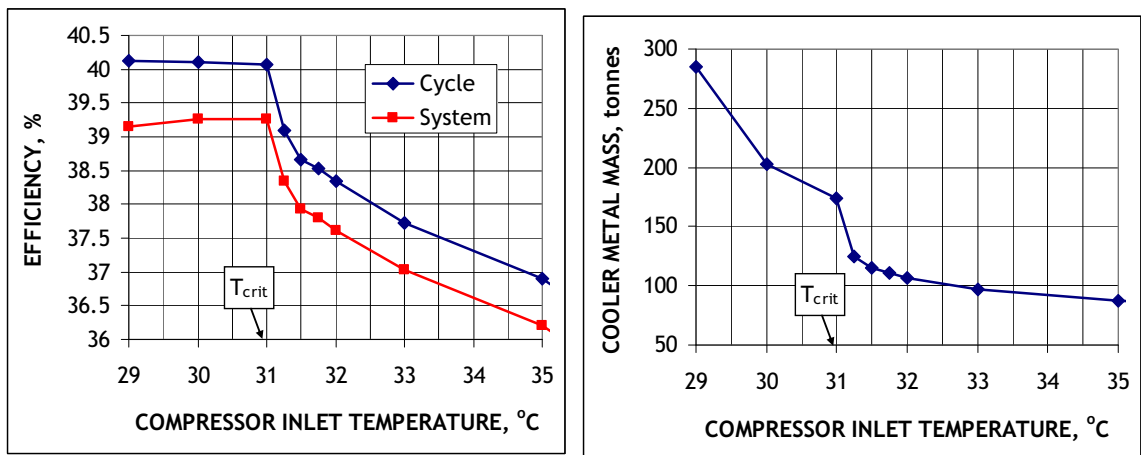


Figure II.5-4 Illustration of S-CO₂ Brayton Cycle Efficiency and Required Cooler Mass vs. Compressor Inlet Temperature

The cycle splits the CO₂ flow such that only a portion rejects heat in the cooler because of the dependency of the specific heat of CO₂ upon pressure immediately above the critical point. In particular, the specific heat of CO₂ immediately above the critical temperature and at 20 MPa is significantly greater than that at 7.6 MPa. The high

pressure CO₂ from Compressor No.1 entering the low temperature recuperator has a specific heat of 2.57 KJ/kg-K. The low pressure CO₂ exiting the low temperature recuperator has a specific heat of 1.37 KJ/kg-K. Splitting the flow reduces the flow rate through the low temperature recuperator of the cold stream from Compressor No. 1 resulting in a CO₂ cold stream temperature rise in the low temperature recuperator that more closely approaches the temperature drop of the hot stream. This enhances the S-CO₂ cycle efficiency. If the CO₂ flow were not split, then the CO₂ cold stream temperature rise would be significantly lower than the CO₂ hot stream temperature drop resulting in significantly reduced cycle efficiency. The flow split fraction, currently equal to 71 %, is chosen to optimize the cycle efficiency. Figure II.5-5 shows the effect of the flow split fraction upon the calculated S-CO₂ Brayton cycle and net plant efficiencies; the latter subtracts out the electrical power requirements for the primary and intermediate circuit sodium pumps as well as the circulating water pumps. The remaining 29 % of the CO₂ flow is directly recompressed in Compressor No. 2 and then merged with the remainder of the CO₂ flow before passing through the high temperature recuperator. The difference in specific heats between the cold and hot streams is not as pronounced over the temperature regime of the high temperature recuperator relative to the temperatures of the low temperature recuperator. A cycle efficiency of 39.1 % is calculated for the S-CO₂ Brayton cycle with the sodium core outlet temperature of 510°C. The plant efficiency is 38.4 %.

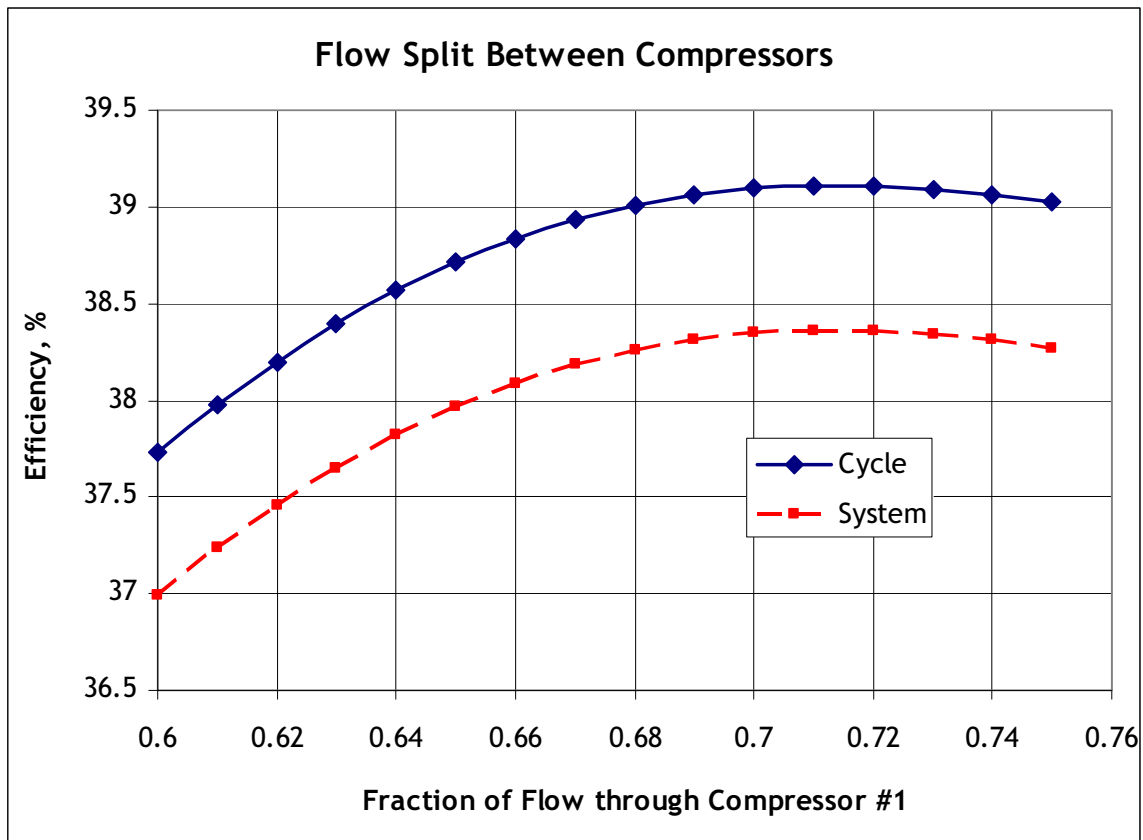


Figure II.5-5 Dependency of S-CO₂ Brayton Cycle and Plant Efficiencies upon Flow Split between Compressor No. 1 and Compressor No. 2

Figure II.5-6 shows a temperature-specific entropy diagram for the S-CO₂ Brayton cycle. Beginning at the turbine inlet, the CO₂ follows either of two paths through either Compressor No. 1 or Compressor No. 2 depending upon whether or not it rejects heat in the cooler. Pressures and temperatures of CO₂ at various locations in the S-CO₂ Brayton cycle are presented in Figure II.5-7.

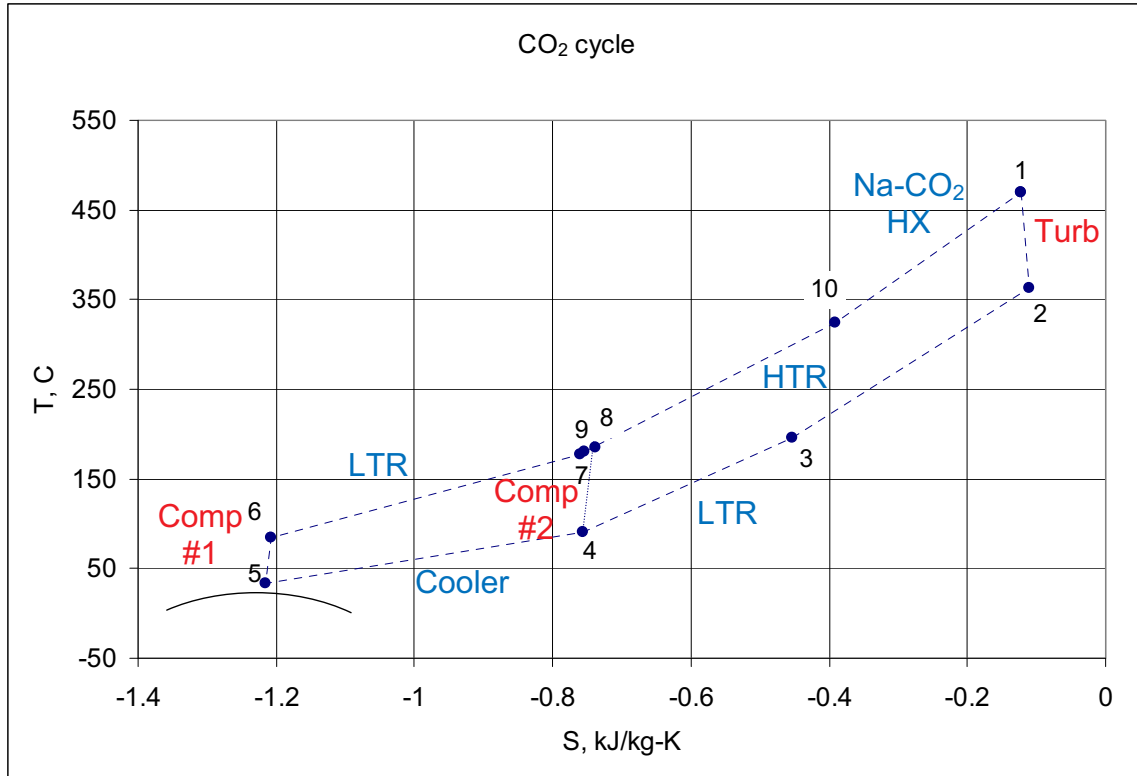


Figure II.5-6 Temperature-Specific Entropy Diagram for S-CO₂ Brayton Cycle

A more detailed drawing for the S-CO₂ Brayton cycle is shown in Figure II.5-8. This figure includes the shutdown heat removal path in which the S-CO₂ Brayton cycle components (i.e., turbine, recuperators, compressors, etc.) are isolated enabling the performance of maintenance or repair work on the components. Under nominal shutdown conditions, the CO₂ from the sodium-to-CO₂ heat exchangers passes through a special shutdown heat removal circuit incorporating a shutdown heat removal cooler where heat is rejected and is returned to the heat exchangers by a shutdown cooling circuit pump. The shutdown heat removal circuit is pressurized by means of a pressurizer. Figure II.5-8 also shows the CO₂ charging system. Liquid CO₂ is delivered to the site by truck and held in a storage tank. When charging or makeup of the S-CO₂ Brayton cycle is required, the liquid CO₂ is vaporized in an evaporator and delivered to the S-CO₂ Brayton cycle through operation of a charging compressor. Piping is manufactured from austenitic stainless steel which has excellent corrosion resistance to CO₂ at the normal operating temperatures. Figure II.5-8 also includes the locations of pressure, temperature, and flow sensing instrumentation.

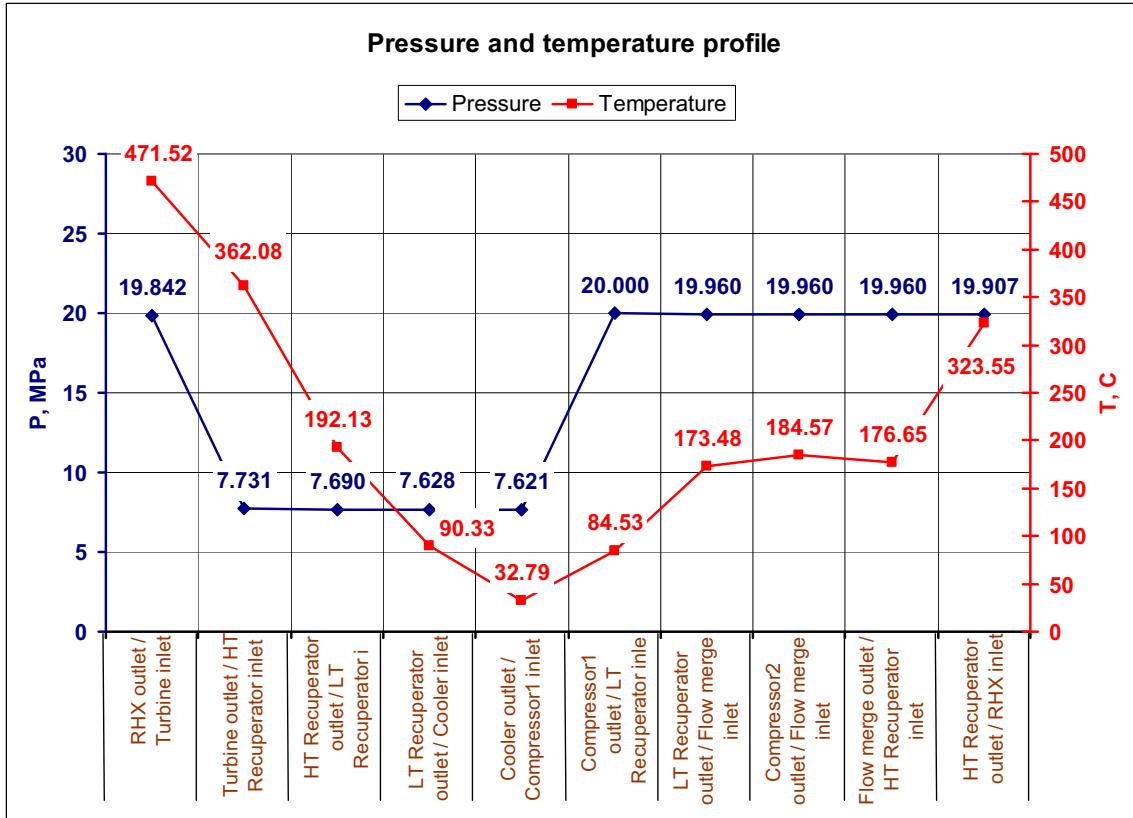
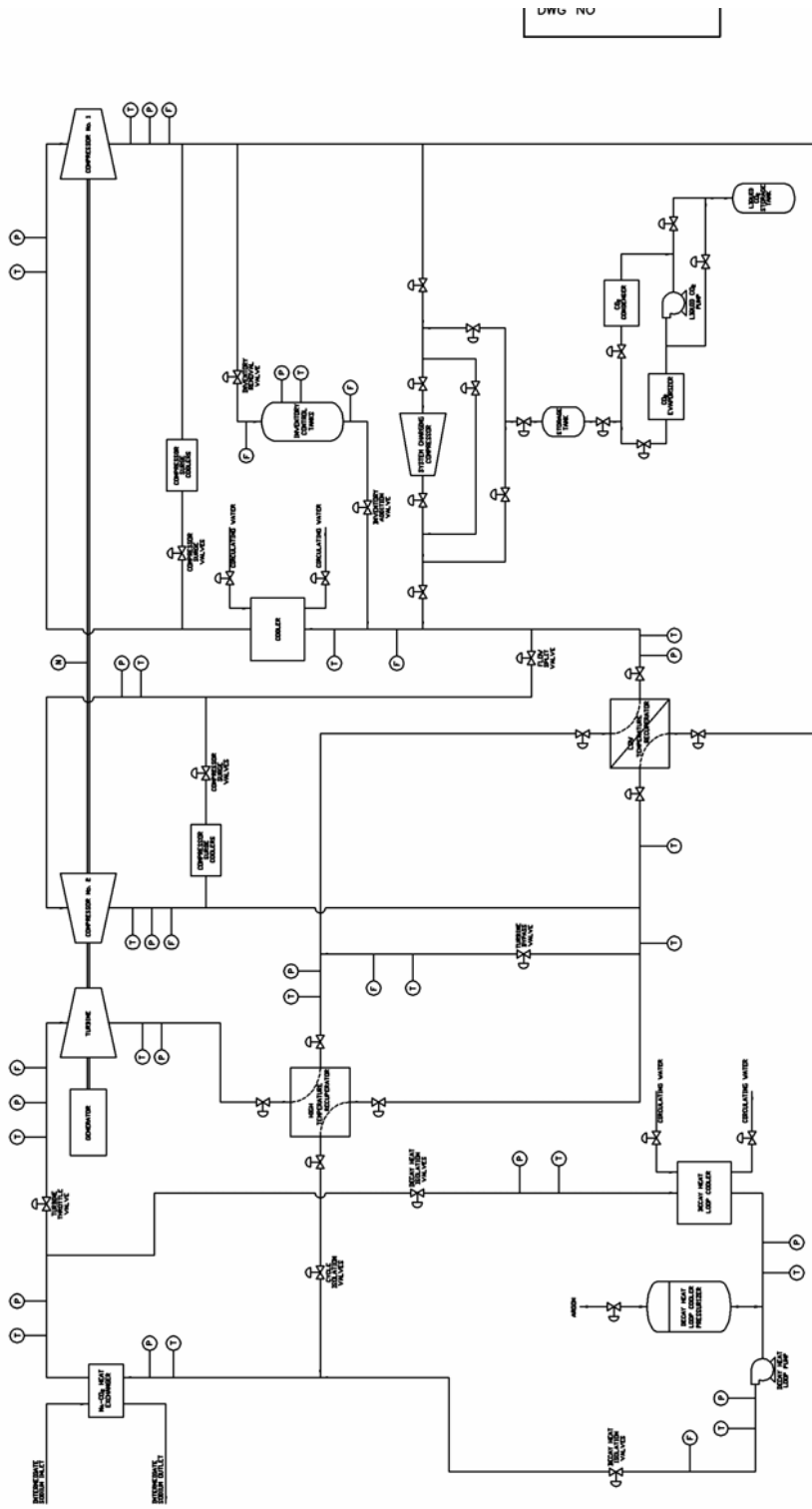


Figure II.5-7 Carbon Dioxide Pressures and Temperatures in S-CO₂ Brayton Cycle

Figure II.5-9 shows both the reactor building and the turbine generator building including the arrangement of S-CO₂ Brayton cycle components inside of the building. The turbine generator building has a main floor and a basement. The turbine, generator, compressors, recuperators, cooler, shutdown compressor, and shutdown heat removal components are located on the main floor. The inventory control tanks are located in the basement (Figure II.5-10). The small size of the power conversion unit, housing the turbine and two main compressors, is evident as well as the small size of the turbine generator building relative to the reactor building. The recuperators and coolers are distributed among transportable recuperator and cooler modules. The recuperator and cooler modules consist of a compact heat exchanger product known as a printed circuit heat exchanger (PCHETM, Heatric, a subsidiary of Meggit (UK), Ltd.). The turbine generator building incorporates a bridge crane for lifting and transporting of components and parts. Ventilation equipment is located adjacent to the building to deliver air for cooling of the generator. The liquid CO₂ storage tank and evaporator are also located adjacent to the turbine generator building. The main floor of the turbine generator building incorporates holes that enable dense CO₂ to sink into the lower level of the building, in the event of a CO₂ leak. The four sodium-to-CO₂ heat exchangers illustrated in Figure II.5.2-9 also consist of PCHETMs and are located inside the portion of the reactor building located between the reactor and the turbine generator building. The sodium-to-CO₂ heat exchangers are thus located in the seismically-isolated portion of the plant while the turbine generator building is not seismically isolated.



AS 584

ITEM NO.	NOT ASSIGNED	REV.	
THIS DRAWING IS THE PROPERTY OF ARGONNE NATIONAL LABORATORY		TITLE	
ABTR SUPERCRITICAL CO ₂ BRAYTON CYCLE		DATE	
RECORD NUMBER	DATE OF ISSUE	DATE OF LOAN	
ISSUED BY KRAJTL	CHECKED	PROJECT MGR	
RESPONSIBLE ENGINEER	APPROVED		
NATIONAL			
UNLESS OTHERWISE NOTED ALL DIMENSIONS ARE INCHES DECIMAL TOLERANCE ± .015 ± .010 ± .005 FRACTIONAL TOL. 1/16 FRACTIONAL TOL. 1/32 FRACTIONAL TOL. 1/64 FINISH ALL SURFACES AND SHARP EDGES UNLESS OTHERWISE SPECIFIED SEE NOTE 1 OF THIS DRAWING			
DRAWN BY: []			
CHECKED BY: []			
DATE: []			
SCALE: []			
SHEET [] OF []			

Figure II.5-8 Detailed Layout of S-CO₂ Brayton Cycle Including Instrumentation

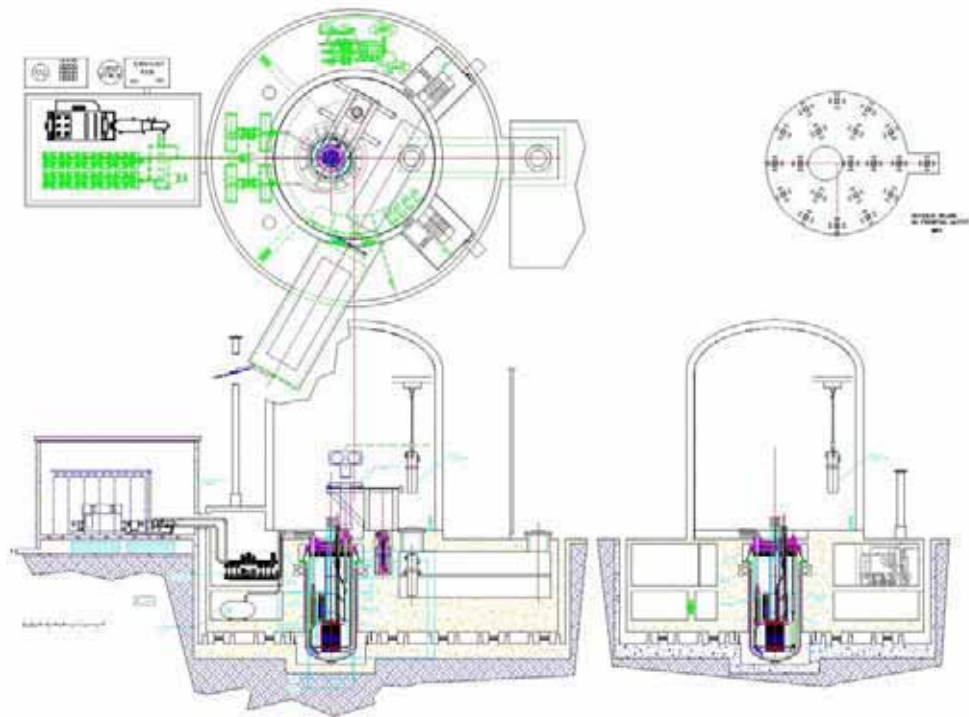


Figure II.5-9 Illustration of General Arrangement of Reactor Building with Containment and Turbine Generator Building Showing Layout of S-CO₂ Brayton Cycle Components

INVENTORY CONTROL TANKS

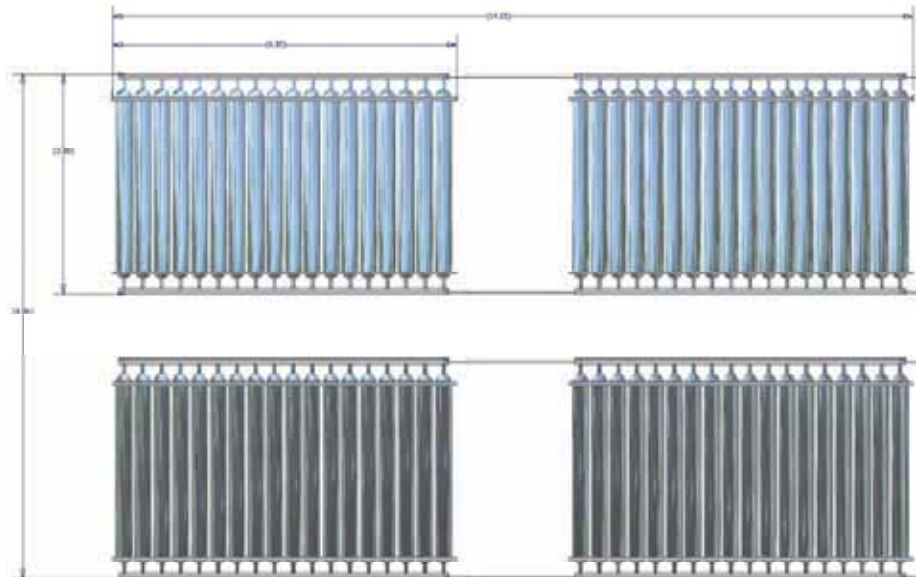


Figure II.5-10 Illustration of Arrangement of S-CO₂ Brayton Cycle Inventory Control Tanks in Basement/Subfloor of Turbine Generator Building

II.5.1.2 Turbine Generator

The turbine and compressors are located on a common shaft inside of a power conversion unit, inside of a common housing. The turbine is a six-stage axial flow turbine. It has a remarkably small size and weight relative to turbines belonging to gas (e.g., helium) Brayton cycles or steam turbines of similar power rating. The small turbine size is directly related to the high density of the CO₂ (Table II.5-1). In particular, the turbine power reflects the mass flow rate multiplied by the work performed per fluid mass. Because the S-CO₂ density is so high, the mass flow rate with S-CO₂ is much higher than that with an ideal gas such as helium in a gas Brayton cycle or steam in a Rankine steam cycle.

Hence, the size of the turbine required to accommodate the S-CO₂ mass flow rate is small compared with the turbine sizes required for a gas Brayton cycle or a Rankine steam cycle operating at the same reactor power level and core outlet temperature. Dimensions and conditions for the turbine are presented in Table II.5-2, which are based upon pre-conceptual turbine design and optimization analyses in which the number of stages is varied to determine an optimal number. The detailed design analyses are presented in Section III.3.

Table II.5-2 Turbine Design Parameters

Power	156.4	MW
Number of stages	6	
Rotational speed	60	rps
Length (stages)	1.02	m
Length (diffuser)	1.64	m
Length (total)	2.67	m
Max diameter	0.87	m
Hub radius, min/max	27.0/34.1	cm
Tip radius, min/max	41.4/43.5	cm
Blade height, min/max	7.3/16.5	cm
Blade chord, min/max	7.4/11.0	cm
Max Mach number	0.40	
CO ₂ temperature, inlet/outlet	471.5/362.1	°C
CO ₂ pressure, inlet/outlet	19.84/7.73	MPa
CO ₂ flow rate	1377	kg/s
Efficiency	93.4	%
CO ₂ mass	24.1	kg

The turbine is manufactured largely from Inconel-based alloys that are selected for their strength and low coefficients of thermal expansion as well as their resistance to oxidation by CO₂ over the normal operating temperature range. The turbine also incorporates a diffuser which increases the overall length beyond that of the rotor and stator stages.

The generator is a commercial “off-the-shelf” component. A generator marketed by Siemens was selected only as representative. The Siemens turbogenerator is a two-pole air-cooled unit designed to the International Standard, IEC 34, and in compliance with the harmonized standards according to European Commission machine guideline, 89/392/EEC.

The generator consists of a base frame, stator core, stator winding, cover, rotor shaft, rotor winding, rotor-retaining rings, bearings, and field connections. The rotor shaft consists of forged steel. It is supported on each end by bearings mounted to the base. The base frame and anchoring elements transmit the forces occurring in the machinery to the floor. Other functions of the base include damping of vibration and noise, support of the cooling system enclosure, and support of wiring and cabling.

An oil system for lubrication and an excitation system are also required for operation and are located inside of the turbine generator building. Heat losses arising in the generator interior are dissipated through air. The air cooling system is a self-contained ducted system. Air is drawn by axial-flow fans arranged on the rotor via lateral openings in the stator housing. The rotor is directly air cooled with heat losses transmitted directly from the winding copper to cooling air. The stator is indirectly air cooled.

II.5.1.3 Compressor

The S-CO₂ Brayton cycle requires two main compressors. The two main compressors operate at different conditions and therefore have different numbers of stages, dimensions, and efficiencies. In particular, Compressor No.1 receives CO₂ that has been expanded to a pressure immediately above the CO₂ critical pressure and a temperature immediately above the CO₂ critical temperature. The pre-conceptual evaluation of the S-CO₂ Brayton cycle has included investigation of both axial flow and centrifugal (i.e., radial flow) compressors. Axial flow compressors were initially considered based upon the experience with axial flow steam turbines. It was found that centrifugal compressors offer significant benefits relative to axial flow compressors including: 1) a wider stable operating range near the critical point; and 2) fewer stages in each compressor potentially further reducing costs. Figures II.5-11 and II.5-12 illustrate the configuration of single-stage and two-stage centrifugal compressors. In a multi-stage centrifugal compressor, the exhaust from one stage is ducted to the inlet of the next stage. The wider operating range for centrifugal compressor designs is demonstrated in Figures II.5-13 and II.5-14 which compare the pressure ratios and efficiencies versus the relative flowrate (i.e., the flowrate normalized by the nominal steady state value) calculated for optimized centrifugal and axial pre-conceptual designs. The operating range is limited by stall at low flowrates and choking at high flowrates.

The compressors are mainly fabricated from Inconel alloys and austenitic stainless steel for strength, low thermal expansion, and resistance to corrosion by CO₂. A charging compressor is also provided to add CO₂ to the supercritical CO₂ Brayton cycle from the liquid CO₂ storage tank and evaporator. Dimensions and conditions for the two main compressors are shown in Tables II.5-3 and II.5-4.

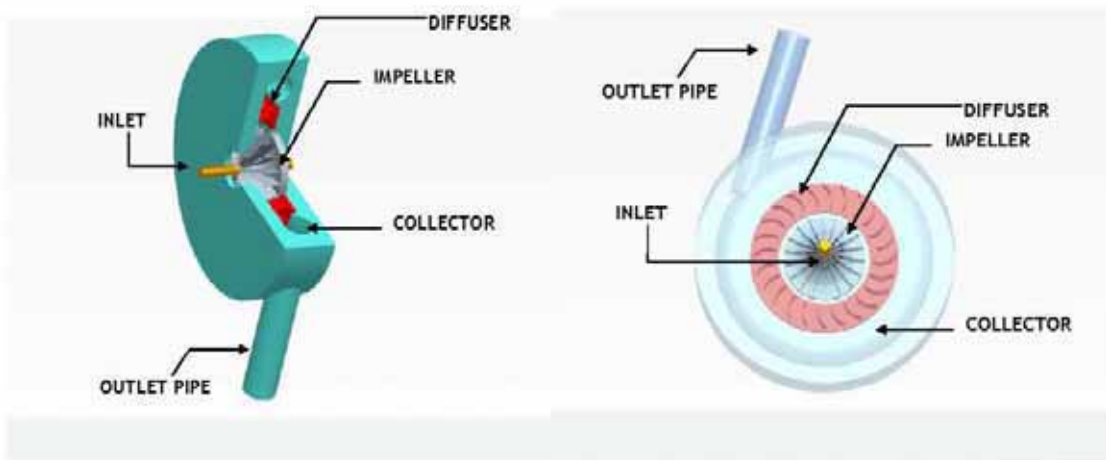


Figure II.5-11 Illustration of a Single-Stage Centrifugal Compressor

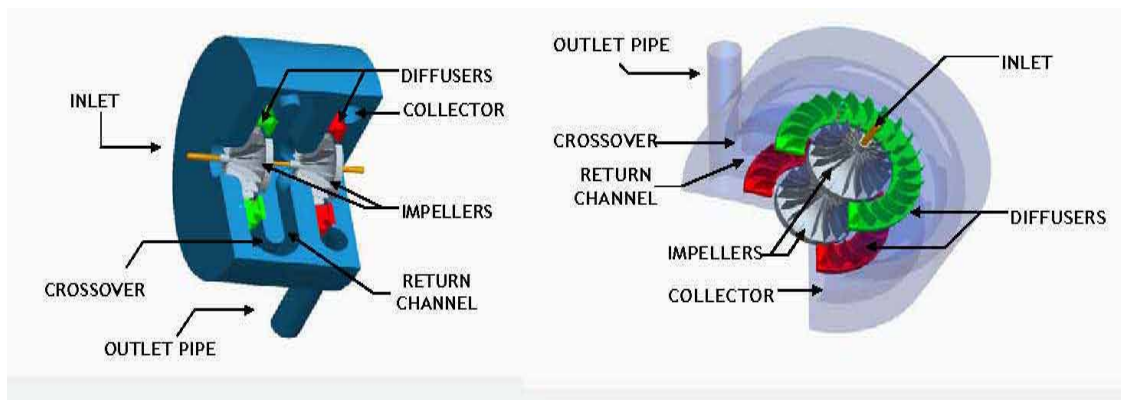


Figure II.5-12 Illustration of a Two-Stage Centrifugal Compressor

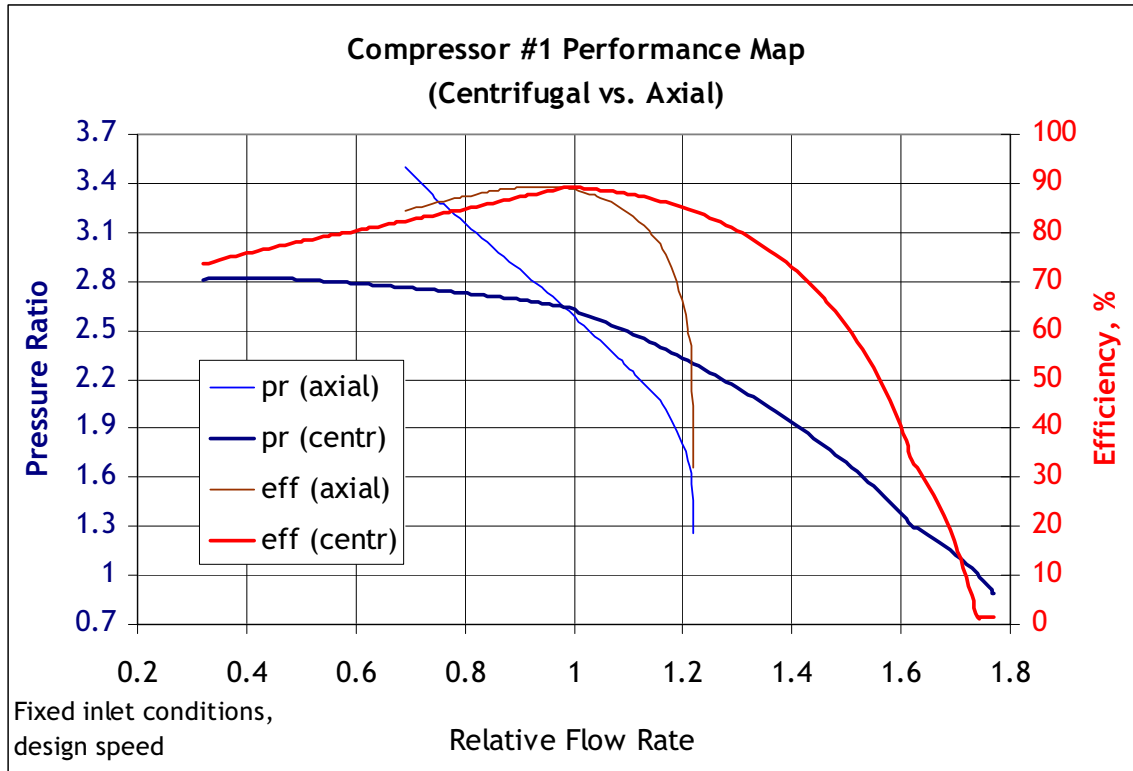


Figure II.5-13 Comparison of Performance of Centrifugal and Axial Flow Pre-Conceptual Designs for Compressor No. 1 Operating Near the Critical Point

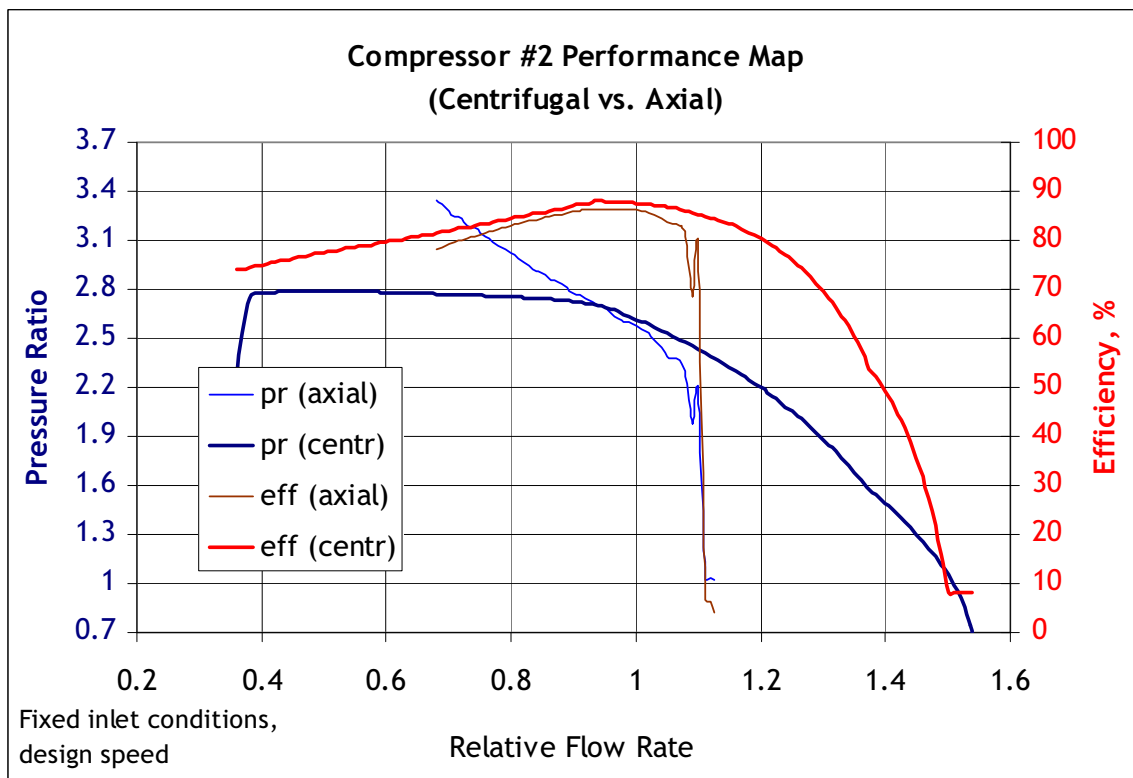


Figure II.5-14 Comparison of Performance of Centrifugal and Axial Flow Pre-Conceptual Designs for Compressor No. 2 Directly Recompressing CO₂ Away from the Critical Point

Table II.5-3 Compressor No. 1 Dimensions and Conditions

	27.89	MW
Number of stages	1	
Rotational speed	60	rps
Length	0.38	m
Max diameter	2.06	m
Hub radius min/max	9.8/9.8	cm
Impeller radius min/max	56.9/56.9	cm
Blade height min/max	1.4/9.0	cm
Blade length min/max	31.0/50.8	cm
Max Mach number	0.47	
CO ₂ temp inlet /outlet	32.79/84.5	°C
CO ₂ pressure inlet /outlet	7.62/20.0	MPa
CO ₂ flow rate	977.6	kg/s
Efficiency	89.1	%
CO ₂ mass	62.5	kg

Table II.5-4 Compressor No. 2 Dimensions and Conditions

Power	27.08	MW
Number of stages	2	
Rotational speed	60	rev/s
Length	0.55	m
Max diameter	2.19	m
Hub radius min/max	13.6/21.6	cm
Impeller radius min/max	59.1/64.8	cm
Blade height min/max	0.9/7.0	cm
Blade length min/max	31.5/49.1	cm
Max Mach number	0.51	
CO ₂ temperature inlet/outlet	90.33/184.6	°C
CO ₂ pressure inlet/outlet	7.63/19.96	MPa
CO ₂ flow rate	399.3	kg/s
Efficiency	87.5	%
CO ₂ mass	40.8	kg

II.5.1.4 Sodium-to-CO₂ Heat Exchanger

Each of the two loops of the intermediate sodium circuit incorporates a sodium-to-CO₂ heat exchanger, in which heat is transferred from the sodium in the intermediate circuit to the CO₂ in the S-CO₂ Brayton Cycle. The sodium-to-CO₂ heat exchangers incorporate compact heat exchanger products known as a printed circuit heat exchanger (PCHETM, Heatric a subsidiary of Meggit (UK), Ltd.). Printed circuit heat exchangers

have been selected for the sodium-to-CO₂ heat exchangers, recuperators, and cooler for the following reasons:

- Expected long life and low potential for failure (i.e., high reliability). Each PCHE is effectively a monolithic block of stainless steel, containing embedded flow channels. The concerns about tube failures typical of shell-and-tube heat exchangers are not present. This reduces the requirements for inspection through decrease of the potential for failure of the boundary between the sodium and CO₂ streams;
- Significantly smaller volume relative to shell-and-tube heat exchangers;
- The monolithic blocks resulting from diffusion bonding and the microchannel flow geometries are compatible with the S-CO₂ Brayton cycle high pressures, high pressure differences between hot and cold streams, temperature ranges, and flow requirements (i.e., low pressure drops through the PCHEs)
- Heatric claims only slow leakage failure involving the formation of small cracks in a PCHE fatigue test only after between 1000 and 2000 startup- and shutdown-type cycles with 25 °C per millimeter maximum temperature gradients in the metal and a high pressure difference between the streams. After 1000 cycles, they obtained interstream gas leaks identified by a very small leakage rate of 1×10^{-7} mbar liters per second. They continued to cycle a PCHE that was leaking and obtained more cracks but no unzipping failure. No solid material was found entering the system. The cracks were too small to be seen with the naked eye and had to be observed under a microscope.
- Any failures should be small cracks giving rise to small intermixing of hot and cold streams in a recuperator slightly decreasing the preheating effect and cycle efficiency, slow loss of CO₂ inventory into water in a cooler, or slow interaction of CO₂ with sodium and slow loss of CO₂ inventory into sodium in a sodium-to-CO₂ heat exchanger.

Each PCHE is manufactured by diffusion bonding of plates of austenitic stainless steel into which semicircular channels have been chemically etched. Type 316 austenitic stainless steel is selected for its resistance to corrosion by both CO₂ and sodium. The individual etched plates are assumed to be diffusion bonded together by heating to a sufficiently high temperature maintained for a suitable time in the presence of a sufficiently high force applied to a stack of plates. The plate stacking arrangement for a general PCHE is illustrated in Figure II.5-15, developed by the PCHE manufacturer, Heatric, a subsidiary of Meggitt (UK), Ltd. The sodium and CO₂ streams are assumed to flow through alternating rows of semicircular channels as shown in Figure II.5-16, also from Heatric. The sodium and CO₂ flow through the alternating rows of channels in opposite directions providing for countercurrent heat exchange. A largely countercurrent flow configuration is provided by the Heatric platelet PCHE configuration with zigzag semi-circular flow channels illustrated in Figure II.5-17. Carbon dioxide flows through zigzag channels while straight channels are provided for sodium flow. The zigzag channel configuration enhances the heat transfer from the CO₂.

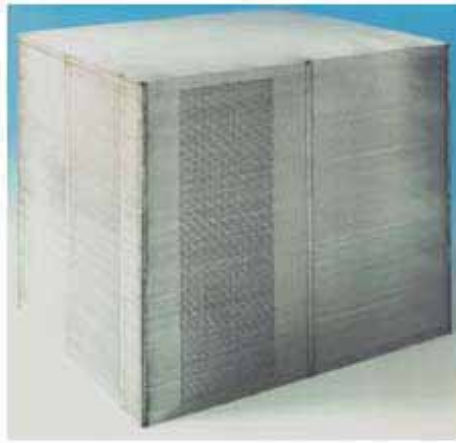
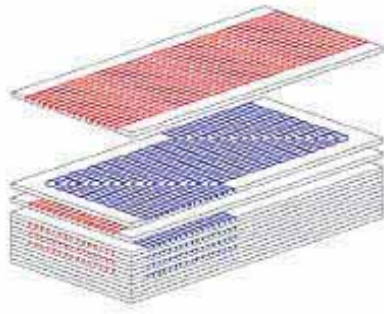


Figure II.5-15 Illustration of Stacking of Chemically Etched Plates to Form Core of PCHE™ by Diffusion Bonding (Heatric, a subsidiary of Meggitt (UK), Ltd.)

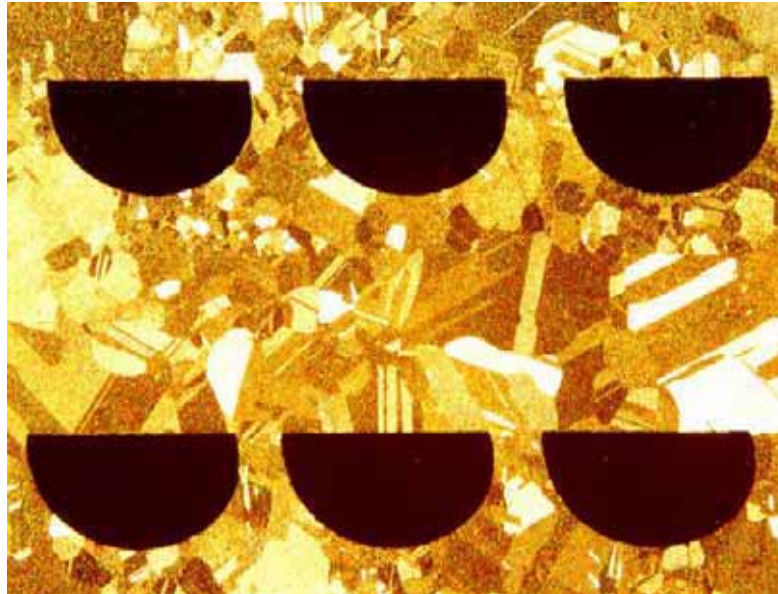


Figure II.5-16 Micrograph of Diffusion-Bonded PCHE™ Core with Semi-Circular Channels (Heatric, a subsidiary of Meggitt (UK), Ltd.)

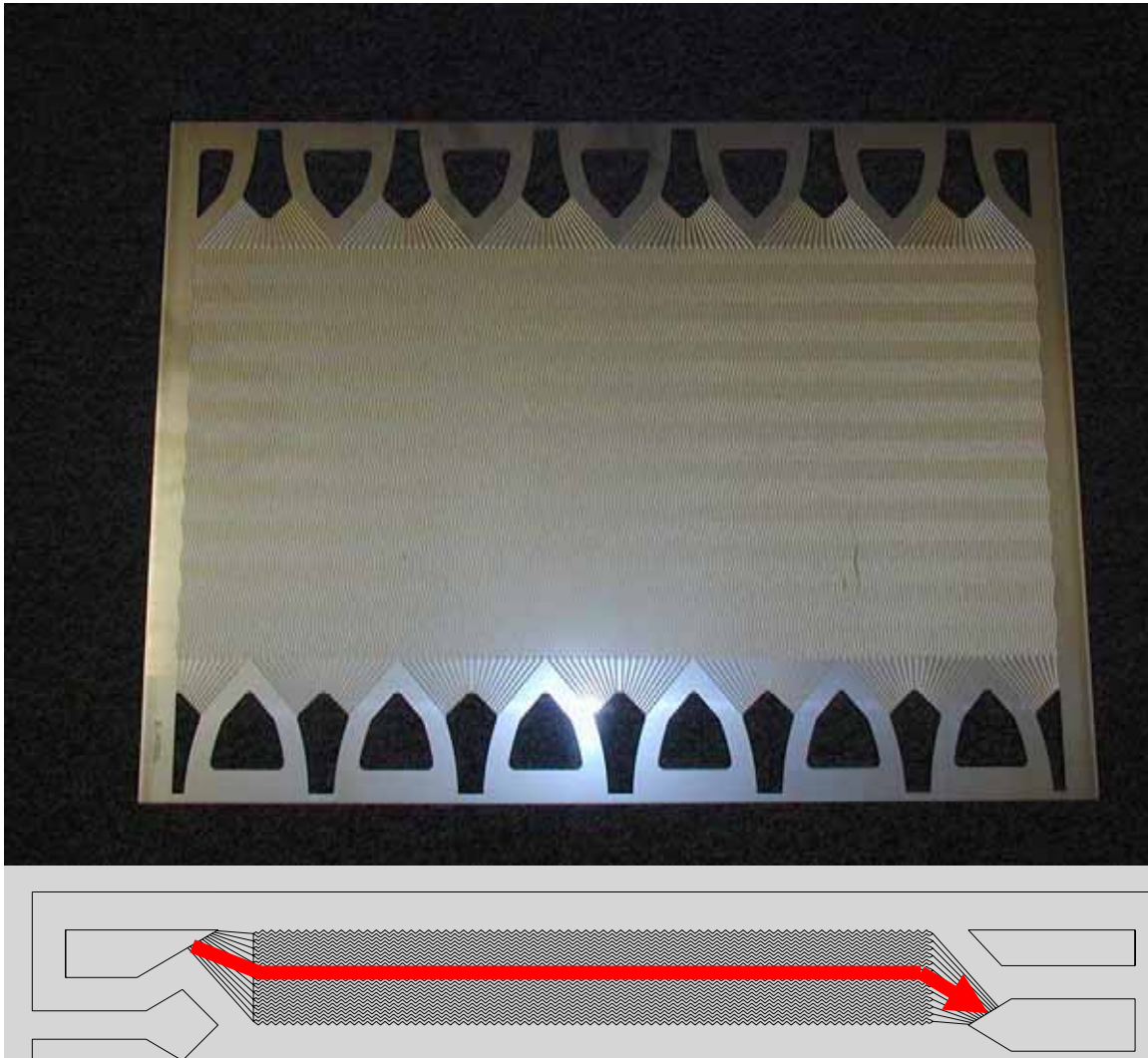


Figure II.5-17 PCHETM Platelet Configuration with Zigzag Semi-Circular Flow Channels (Heatric, a subsidiary of Meggitt (UK), Ltd.)

The current PCHE manufacturing process limits the width and length of each plate or platelet incorporated into a PCHE to 0.6 m by 1.5 m. Individual PCHE cores can be welded together side-by-side to provide a block having more channels; however, cores cannot be welded together end-to-end to increase the channel length. Headers are welded onto the completed core.

A deterministic computer code model has been developed at Argonne National Laboratory to perform PHCE pre-conceptual design analyses and to calculate PCHE heat exchange and pressure drop performance. An example of four sodium-to-CO₂ heat exchanger modules consisting of a number of PCHEs is illustrated in Figure II.5-18.

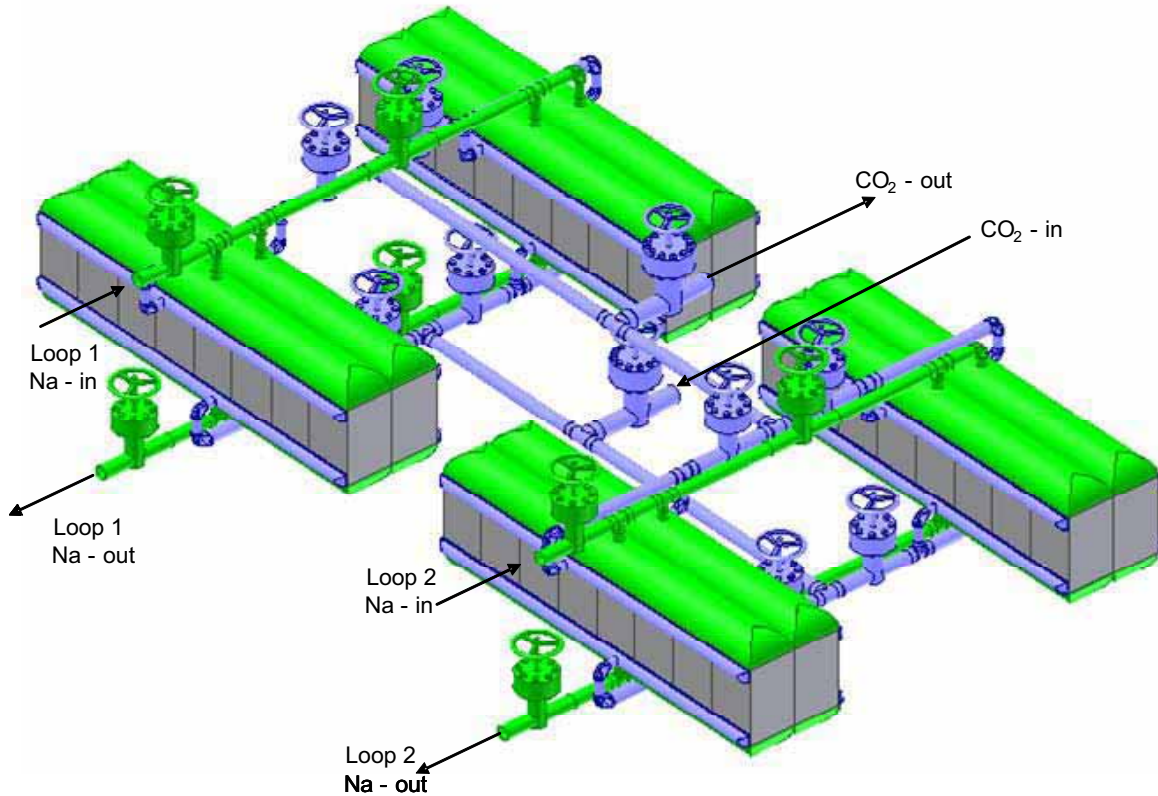


Figure II.5-18 Illustration of Four Sodium-to-CO₂ Heat Exchangers Consisting of PCHEs

For the sodium-to-CO₂ heat exchangers, each semicircular channel is selected to have a diameter of 2.0 mm, a lateral pitch of 2.4 mm, and a plate thickness of 2.0 mm. A semicircular channel diameter of 2.0 mm is determined on the basis that for this minimal size, the effects of oxide layer growth upon austenitic stainless steel due to oxidation by CO₂ will not significantly degrade either the heat transfer performance or the strength of the stainless steel ligaments between the sodium and CO₂. The length of each individual PCHE unit is held fixed while the number of PCHE units comprising the four sodium-to-CO₂ heat exchangers is varied to determine how the cycle efficiency depends upon the total PCHE mass in the four sodium-to-CO₂ heat exchangers for different fixed unit lengths. The heat exchanger cost is approximately proportional to mass to lowest order.

Table II.5-5 shows the detailed parameters of the sodium-to-CO₂ heat exchangers, which are comprised of a total of 64 PCHE units.

II.5.1.5 Recuperator

The low temperature recuperator (LTR) and high temperature recuperator (HTR) are regenerative heat exchangers that provide for preheating of the compressed CO₂ before it is delivered to the sodium-to-CO₂ heat exchangers using part of the thermal energy of the hotter CO₂ expanded from the turbine. Preheating significantly enhances the efficiency of the cycle. The largest heat exchange rates in the S-CO₂ Brayton cycle occur in the LTR and HTR. Therefore, large heat transfer areas must be provided for each of the LTR

and HTR. Each recuperator is fabricated by Type 316 stainless steel and consists of a set of PCHEs which are selected for use with the S-CO₂ Brayton cycle for the same reasons as stated for the sodium-to-CO₂ heat exchangers. Each zigzag semicircular channel of the HTR is selected to have a diameter of 1.5 mm, a lateral pitch of 2.3 mm, and a plate thickness of 2.0 mm. Dimensions and conditions for the HTR are provided in Table II.5-6. The HTR is comprised of 64 PCHE units.

Table II.5-5 Sodium-to-CO₂ Heat Exchanger Design Parameters per PCHE Unit

Heat transfer capacity	3.91	MWt
Unit width	0.60	m
Unit height	0.60	m
Unit length	1.00	m
Heat transfer area	133.5	m ²
Material	SS316	
Semi-cir. channel diameter	2.0	mm
Semi-cir. channel pitch	2.4	mm
Plate thickness	2.0	mm
Number of sodium channels	236	
Number of CO ₂ channels	204	
Void fraction for channels	0.309	
Sodium temperature, inlet/outlet	488/333	°C
Sodium flow rate	21.5	kg/s
CO ₂ temperature, inlet/outlet	323.6/471.5	°C
CO ₂ pressure, inlet/outlet	19.91/19.84	MPa
CO ₂ flow rate	21.5	kg/s
Effectiveness	94.3	%
Metal mass	1.728	tonnes
CO ₂ mass	6.5	kg

The LTR semicircular channels are also selected to have a diameter of 1.5 mm, a lateral pitch of 2.3 mm, and a plate thickness of 2.0 mm. Figures II.5-33, II.5-34, and II.5-35 show the results of pre-conceptual optimization analyses for the LTR from which it is determined that a LTR PCHE unit length of 0.8 m optimizes the S-CO₂ Brayton Cycle efficiency while maintaining a reasonable recuperator effectiveness and CO₂ turbine inlet temperature. The tradeoff between LTR cost and S-CO₂ Brayton Cycle efficiency is illustrated in Figure II.5-36. For the selected point, the LTR consists of 128 PCHE units. Dimensions and conditions for the LTR are provided in Table II.5-7. The LTR is comprised of 64 PCHE units.

Table II.5-6 High Temperature Recuperator Design Parameters per PCHE Unit

Heat transfer capacity	4.13	MWt
Unit width	1.50	m
Unit height	0.60	m
Unit length	0.60	m
Heat transfer area	134.6	m ²
Semi-cir. channel diameter	1.5	mm
Semi-cir. channel pitch	2.3	mm
Plate thickness	2.0	mm
Hot side number of channels	564	
Cold side number of channels	461	
Void fraction for channels	0.192	
Hot side temperature, inlet/outlet	362.1	°C
Hot side pressure, inlet/outlet	7.73/7.69	MPa
Hot side flow rate	21.5	kg/s
Cold side temperature, inlet/outlet	176.7/323.6	°C
Cold side pressure, inlet/outlet	19.96/19.91	MPa
Cold side flow rate	21.5	kg/s
Effectiveness	91.7	%
Metal mass	3.109	tonnes
CO ₂ mass	9.6	kg

Table II.5-7 Low Temperature Recuperator Design Parameters per PCHE Unit

Heat transfer capacity	1.31	MWt
Unit width	0.60	m
Unit height	0.60	m
Unit length	0.80	m
Heat transfer area	79.4	m ²
Semi-cir. channel diameter	1.5	mm
Semi-cir. channel pitch	2.3	mm
Plate thickness	2.0	mm
Hot side number of channels	218	
Cold side number of channels	178	
Void fraction for channels	0.185	
Hot side temperature, inlet/outlet	192.1/90.3	°C
Hot side pressure, inlet/outlet	7.69/7.63	MPa
Hot side flow rate	10.8	kg/s
Cold side temperature, inlet/outlet	84.5/173.5	°C
Cold side pressure, inlet/outlet	20.00/19.96	MPa
Cold side flow rate	7.6	kg/s
Effectiveness	94.6	%
Metal mass	1.767	tonnes
CO ₂ mass	10.0	kg

II.5.1.6 Control System

The S-CO₂ Brayton cycle is controlled by means of a combination of control mechanisms illustrated in Figure II.5-19. At power levels near 100 % nominal and for sufficiently slow load changes, inventory control is used to control the S-CO₂ Brayton cycle such that the heat removed from the reactor matches the load demand from the electric grid. For more rapid transients, turbine bypass control is employed. Inventory control involves the removal or addition of CO₂ from the cycle. The purpose is to decrease or increase the CO₂ flow rate in the circuit without significantly altering the cycle efficiency. By changing the flow rate, the amount of heat transported by the cycle is changed without significantly changing the temperatures. Maintaining the same approximate temperatures maintains the same approximate cycle efficiency.

The inventory control system consists of inventory control tanks and valves that remove CO₂ from the high pressure part of the cycle between Compressor No. 1 and the low temperature recuperator into the inventory control tanks, or that admit CO₂ from the inventory control tanks to the low pressure part of the cycle between the cooler flow split valve and the cooler.

The inventory control tanks are illustrated in Figure II.5-19. The tanks consist of a large number of cylindrical tanks fabricated from piping segments onto which are welded hemispherical heads containing nozzles. In particular, each pipe is a 12-inch Schedule 80 (0.69 inch wall thickness) austenitic stainless steel pipe 3.0 m long and internally polished. Austenitic stainless steel is selected for its resistance to corrosion by CO₂. Manifolds connect the pipes together to achieve a single distributed volume. This approach minimizes the cost of the inventory control system volume compared to fabrication of a single tank providing the total volume.

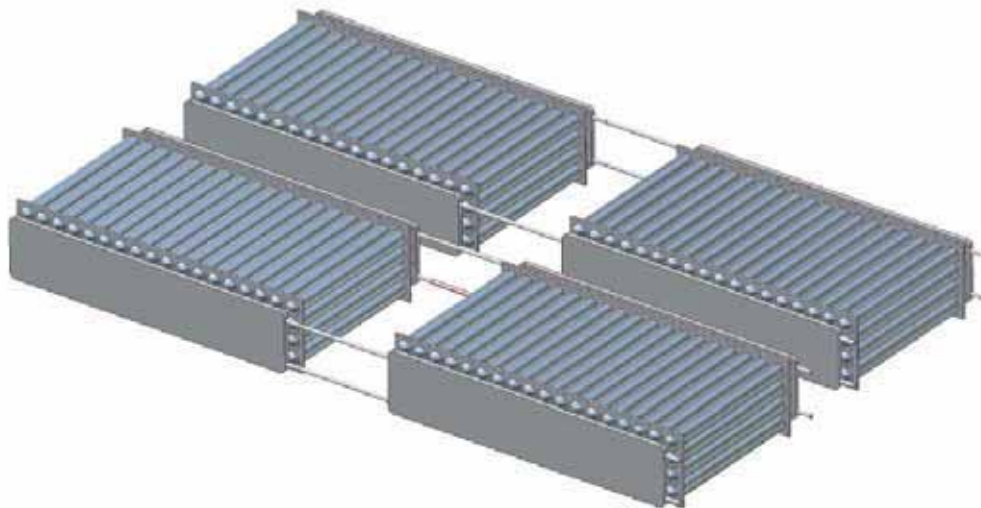


Figure II.5-19 Illustration of Inventory Control Tanks

For fast control action, such as turbomachinery shaft speed control, turbine bypass control is utilized. This control mechanism allows a portion of the flow to bypass the turbine, if necessary, in order to reduce the flow rate through the turbine thereby reducing the turbine output power. Turbine bypass control is also used when inventory control reaches the limiting condition at which the inventory tanks are full.

At all power levels, the flow split of CO₂ to the cooler may be varied from the nominal value of 71 % as a means of maintaining high cycle efficiency.

II.5.1.7 Cooler and Heat Rejection System

The S-CO₂ Brayton cycle heat rejection system consists of a cooler where heat is rejected from CO₂ to water, a water circulating system involving pumps, and cooling towers where heat is rejected from the water to the atmosphere.

A CO₂ temperature and pressure at the inlet to Compressor No.1 of approximately 31.25°C and 7.4 MPa are selected. This temperature enhances the cycle efficiency while limiting the cooler mass/volume to a reasonable value as shown in Figure II.5-4. The CO₂ accelerates in the inlet nozzle of the compressor. As a result, the temperature and pressure of the CO₂ decrease while passing through the nozzle. Thus, the CO₂ temperature and pressure at the cooler outlet is selected to provide the desired conditions at the compressor inlet. A cooler outlet temperature of 32.79°C and pressure of 7.62 MPa provide the desired compressor inlet temperature and pressure of 31.25°C and 7.4MPa, respectively. Immediately above the critical pressure and temperature, the supercritical CO₂ specific heat exhibits a spike as shown in Figure II.5-20.

Within the spike, removal of a given amount of enthalpy results in a relatively smaller reduction in temperature. As the CO₂ is cooled within the spike, the behavior is similar to that of a phase transition in that energy is removed at an approximately unvarying temperature. This behavior is utilized to achieve the CO₂ temperature at the compressor inlet of 31.25°C that is very close to but still above the critical temperature (30.98°C) without concern of overcooling the CO₂ to below the critical temperature. Cooling CO₂ below 31.25 °C would require a significantly larger cooler mass as shown in Figure II.5.-4. Overcooling the CO₂ to below the critical temperature would require heating the CO₂ from subcritical to supercritical conditions as is done in a Rankine cycle. The S-CO₂ cycle normally operates at temperatures above the critical temperature to avoid the need for the “feedwater heaters” that are part of the Rankine cycle.

The cooler consists of a number of PCHE units. Each PCHE is selected to incorporate 2.0 mm diameter zigzag semicircular channels for countercurrent CO₂ and water flow. The channel lateral pitch is selected to equal 2.4 mm and the plate thickness 1.66 mm. The CO₂ inlet temperature to the cooler is equal to the temperature of CO₂ exiting the low temperature recuperator. The CO₂ cooler outlet temperature is selected to equal 32.79°C. Dimensions and conditions for the cooler are provided in Table II.5-8. The cooler is fabricated by Type 316 stainless steel and comprised of 48 PCHE units.

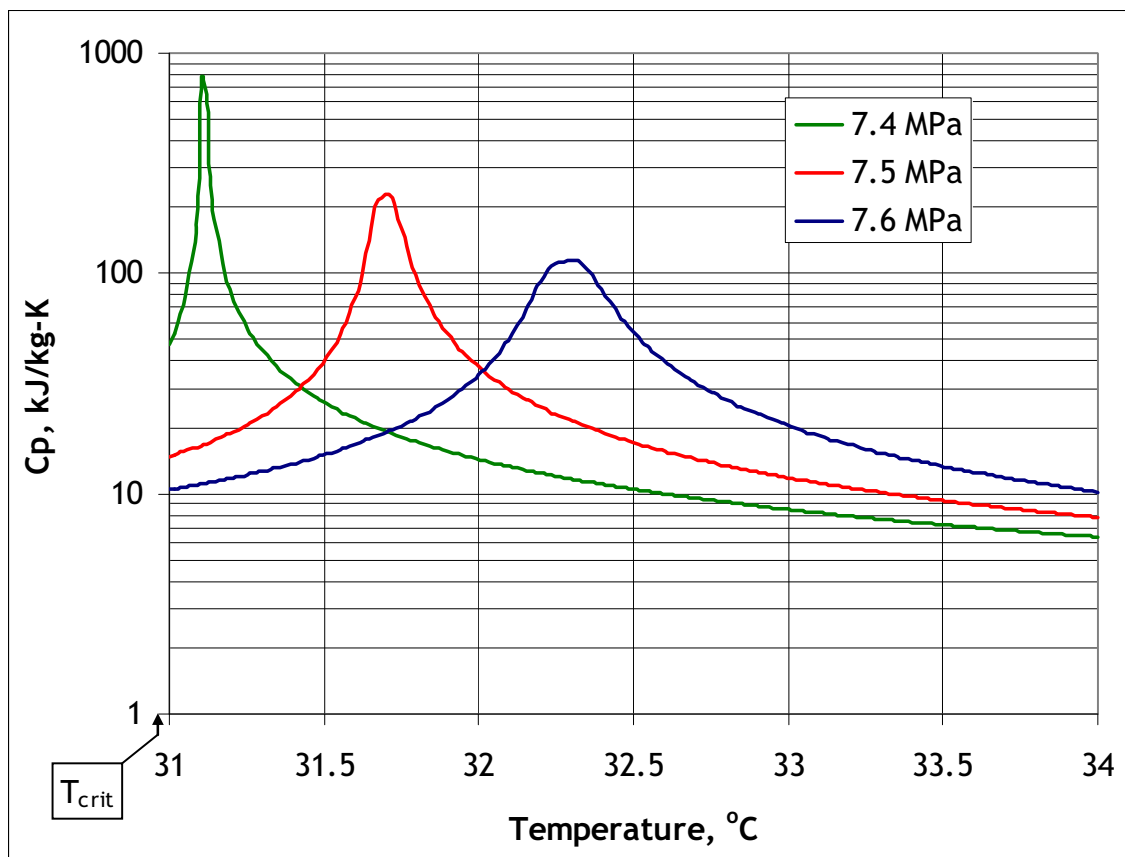


Figure II.5-20 Behavior of CO₂ Specific Heat Immediately Above the Critical Point

The heat rejection system rejects heat to the atmosphere with four commercially-available, open- evaporative, forced-air counter flow cooling towers. Internally, each cooling tower uses nozzles to evenly distribute water downward over a packing fill. A drift eliminator ensures that the water drops do not leave the cooling tower. The cooling tower uses induced draft, axial fans that have a low air inlet speed which creates a highly efficient distribution of air. The location of the fan on the outlet also causes the hot air to flow far away, which reduces any recirculation. Besides the fans, the cooling towers are also highly efficient due to the use of film fills, which maximize the contact surface between the water and air. The type of packing can be altered depending on the characteristics needed in accordance with the process and surrounding conditions.

The cooling towers have a high efficiency (less than 1 KW electric per 100 KW cooling) due to evaporation. Each unit has a maximum capacity to cool 6300 m³/h of water to remove 37.1 MW of thermal energy. Power for the units is supplied from the generator and thus factors into the overall plant efficiency. Typically, a unit this size is 14.8 square meters in footprint and 10 meters tall.

Table II.5-8 Cooler Design Parameters per PCHE Unit

Heat transfer capacity	3.04	MWt
Unit width	1.50	m
Unit height	0.60	m
Unit length	0.574	m
Heat transfer area	188.9	m ²
Semi-cir. channel diameter	2.0	mm
Semi-cir. channel pitch	2.4	mm
Plate thickness	1.66	mm
CO ₂ side number of channels	432	
Water number of channels	529	
Void fraction for channels	0.350	
CO ₂ side temperature, inlet/outlet	90.3/32.8	°C
CO ₂ side pressure, inlet/outlet	7.628/7.621	MPa
CO ₂ side flow rate	20.4	kg/s
Water side temperature, inlet/outlet	30.0/35.8	°C
Water side pressure, inlet/outlet	0.142/0.101	MPa
Water side flow rate	125	kg/s
Water pumping power	0.272	MW
Effectiveness	95.4	%
Metal mass	2.608	tonnes
CO ₂ mass	15.4	kg

In order to reduce corrosion in the cooling towers, the manufacturer will use materials such as stainless steel, polyester, and synthetics for all components that are in contact with water. Because of this, a long life-span is expected that does not depend on water treatment or water cleanings.

The cooling towers each employ modular construction and can be transported to the site. Rail or truck (i.e., by common carrier) are typical transportation modes for the commercial product. Once on site, the towers can be quickly assembled and installed on an existing concrete foundation. Should a replacement cooling tower be required, another tower could be assembled next to the existing unit and lifted in place fully-assembled, minimizing the shutdown time for replacement of the cooling tower.

The S-CO₂ Brayton cycle heat rejection system also incorporates a special shutdown cooler in which heat is rejected from the CO₂ to the circulating water during normal shutdown of the reactor.

II.5.1.8 Carbon Dioxide Release Mitigation System

Carbon dioxide is a toxic substance for humans at concentrations in air above 1.0 volume % and causes death in humans within one minute for exposure to concentrations of 17 to 30 volume %. In particular, the OSHA time weighted average permissible exposure limit is 1.0 volume % concentration in air. The time weighted average temporary exposure limit, usually for exposures of 15 minutes duration, is 3 volume %. Exposures of humans at 3 % concentration for an hour will cause mild headache, sweating, and dyspnea (i.e., shortness of breath or labored respiration) at rest. Concentrations of 4 to 5 % cause headache, dizziness, increased blood pressure, and uncomfortable dyspnea within a few minutes. Exposure at 6 % concentration also causes hearing and visual disturbances within one to two minutes. Unconsciousness or near-unconsciousness will result from exposure to concentrations of 7 to 10 % for a few minutes. At concentrations between 10 and 15 %, exposures of one to several minutes results in dizziness, drowsiness, severe muscle twitching, and unconsciousness. A concentration of 17 to 30 % produces loss of controlled and purposeful activity, unconsciousness, convulsions, and death within one minute.

Carbon dioxide has a higher density than air at the same temperature. Thus, CO₂ is a heavy gas that will collect in basements and other low areas and spread upon floors or the ground. It is necessary to protect personnel from the effects of accidental CO₂ releases.

The Brayton cycle building incorporates a CO₂ release mitigation system for small CO₂ leak rates. In particular, the turbine generator building has a low pressure capability and blowers are provided to remove the gaseous mixture from the building. The CO₂ and air removed from the turbine generator building is mixed with outside air to a concentration below 1 volume % and is released to the atmosphere through a stack.

II.5.2 Steam Rankine Cycle

As an alternative to the supercritical CO₂ Brayton cycle, a Rankine steam cycle power conversion system is also under consideration for ABTR. This system utilizes heat from the intermediate heat transport system (IHTS) to produce steam. The steam is delivered to the turbine, which drives the electrical generator. This is the reference power conversion technology for traditional sodium-cooled fast reactors. The technology is well developed and, with the exception of the steam generators, the system components are largely off-the-shelf items available from commercial vendors. However, the possibility of sodium/water reactions remains a safety concern with the traditional steam cycle. Sodium and water react exothermically and produce hydrogen, which may ignite in the presence of oxygen. Thus, the steam generator design needs to incorporate a sodium water reaction pressure relief system (SWRPRS) to provide for the possibility of steam generator tube rupture(s) that would lead to this type of interaction. At this point in the preconceptual design process, attention has been focused on the power production side of the system. The system design will be upgraded to include a SWRPRS in future work if the decision is made to carry the steam cycle power conversion system along as an alternative to the CO₂ Brayton cycle.

Steam generator concepts that have been developed over the years include the double-walled straight tube design that operated successfully for over 30 years for EBR-II, the hockey-stick design that was developed by Rockwell for the SAFR concept, and the helical coil steam generator (HCSG) that was developed by GE for the PRISM Mod-B Concept. For the purposes of this pre-conceptual design, a modified version of the HCSG design is adopted, as it is readily scaled to different reactor power levels.

The main components of the steam generation system include two sodium heated steam generators, one for each IHTS loop, a feedwater system, and a steam distribution system. The sodium side of each steam generator is connected to the hot and cold legs of the main sodium piping on the secondary (tube) side of each IHTS loop.

The steam cycle selected for application to the ABTR is a superheated cycle with dual reheat. Five feedwater heaters are used to increase cycle efficiency. The steam generator is a once-through design with feedwater entering the bottom of the steam generator at a temperature of 216°C, and superheated steam exiting from the top at a temperature of 454 °C. The high pressure turbine receives steam at 2250 psia, and the low pressure turbine exhausts to a condenser at a pressure of 2 inches of mercury. The power conversion system produces approximately 95 MW of electric power. The steam cycle system design parameters are summarized in Table II.5-9.

II.5.2.1 Steam Generator

As noted earlier, a steam generator design similar to that utilized in the GE PRISM Mod B plant concept is proposed for the ABTR if a steam cycle is adopted. The steam generator is a helical coil, vertically oriented, sodium-to-water, countercurrent flow, shell-and-tube type unit featuring once-through operation. Two 125 MWt steam generators are utilized for ABTR; one for each IHTS loop.

The steam generator design utilizes the identical tube diameter, thickness, and pitch-to-diameter ratio as for the PRISM Mod B helical-coil design. Moreover, the tube length and helical pitch are the same. Thus, if the water and sodium mass flowrates per tube are conserved, then 92 tubes per unit are selected to achieve the required 125 MWt heat exchange rate based on a linear scaling of the PRISM design (viz., 630 tubes for 845 MWt rating). A diagram that illustrates key elements of the scaled steam generator design is provided in Figure II.5-21, while key design data are summarized in Table II.5-10. Aside from the thermal power rating, the thickness of structural elements (i.e., upper and lower tube sheets, as well as shell and elliptical head thicknesses) have been scaled to approximately preserve peak mechanical stresses for a given pressure loading. Moreover, the diameters of inlet and exit piping on both the sodium and steam sides of the HCSG have been scaled to approximately preserve flow velocities, which then approximately preserves pressure drops at the various points within the steam generator.

Table II.5-9 Steam Cycle System Design Parameters (PRISM Mod-B Basis)

IHTS Loop Operational Data	
Number of Intermediate Loops	2
Secondary Loop Heat Capacity	125 MWt
Loop Hot Leg Temperature	477 °C
Loop Cold Leg Temperature	326 °C
Loop Temperature Drop	151 °C
Loop Sodium Mass Flowrate	645 kg/sec
Helical Coil Steam Generator (HCSG) Operational Data	
SG Inlet Pressure	167 bar
SG Feedwater Inlet Temperature	216 °C
SG Feedwater Mass Flowrate	55.9 kg/sec
Steam Exit Temperature	454 °C
Steam Exit Pressure	155 Bar
Saturation Temperature at Exit Pressure	345 °C
Steam Exit Superheat	109 °C

During full power operation, feedwater flow to the steam generator is regulated by a 15 cm (6 inch) main control valve. The main feedwater line breaks into four 10 cm (4 inch) feedwater nozzles located on the bottom head of the unit. These nozzles supply water to the inlet of the steam generator at 216 °C temperature and 167 bar pressure. The GE design incorporates flow restrictors with a pressure drop of 6.5 bar at the tube inlets to increase static and dynamic flow stability over a wide load range.

After entering the steam generator, the water flows up through the tube side of the 3.18 cm OD, 98.5 m long tube bank while absorbing energy from the sodium on the shell side of the unit in a counter-current flow configuration. The water then exits the steam generator as superheated steam at a temperature of 454 °C and pressure of 155 bar through four 15 cm diameter (6 inch) steam nozzles located in the top head of the unit. These four nozzles are then headered into the 20 cm diameter (8 inch) main steam line leading to the turbine generator building. To aid in plant control and monitoring, flowrate and temperature measurements are made both at the feedwater inlet and steam exits to the steam generator.

On the shell side of the unit, sodium is headered from the 40.6 cm diameter (16 inch) IHTS hot leg supply line from the IHX into four 20.3 cm diameter (8 inch) nozzles that provide the pathway for the sodium to enter through the upper elliptical head of the unit. The sodium then flows in a counter-current flow configuration on the shell side of the heat exchanger while delivering heat to the steam/water mixture on the interior of the tubes. The sodium then exits the steam generator through a single 40.6 cm diameter (16 inch) pipe that constitutes the cold leg of the IHTS.

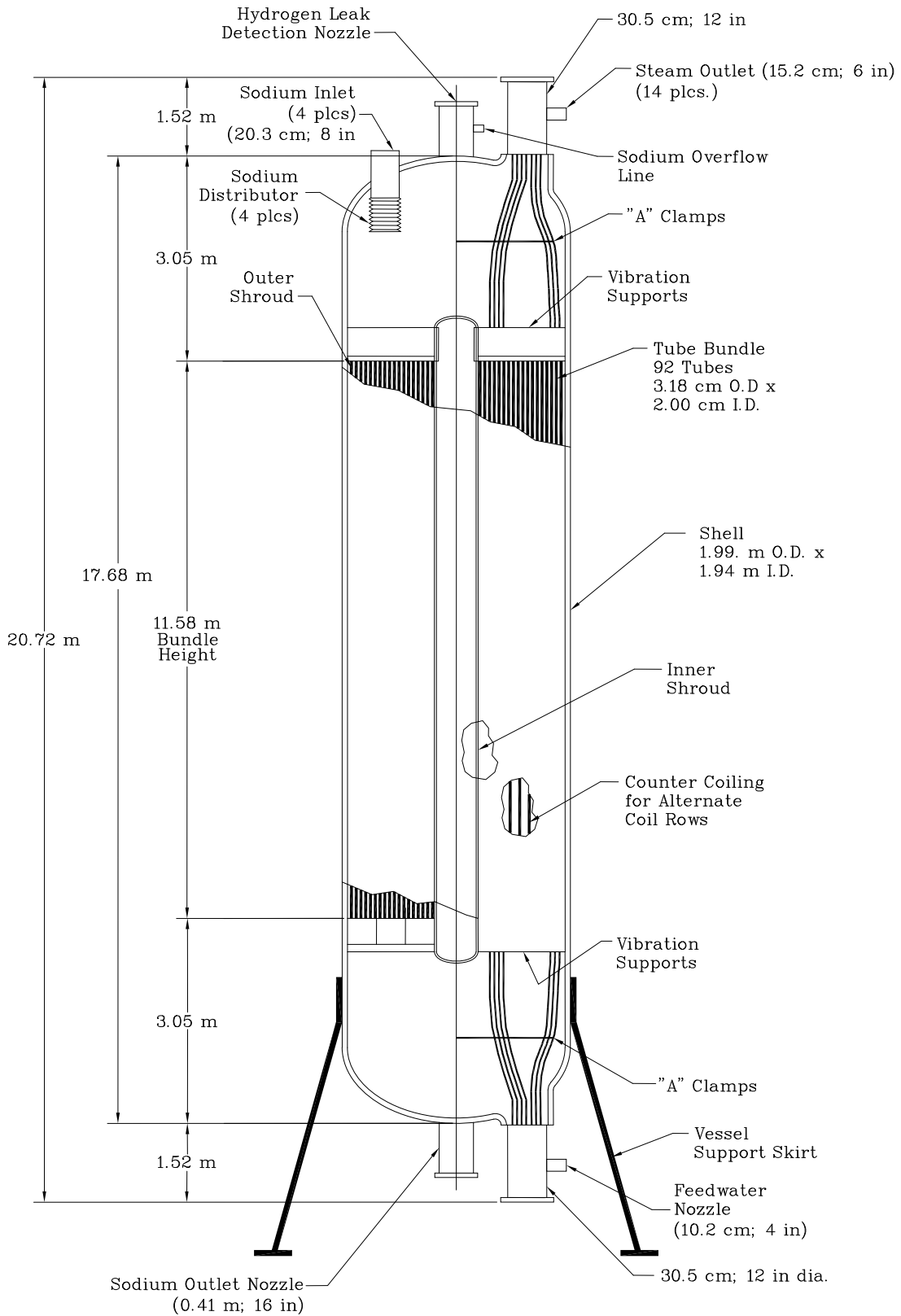


Figure II.5-21 HCSG Design Characteristics (GE PRISM Mod B basis)

Table II.5-10 Scaled Once-Through HCSG Design Data (PRISM Mod-B Basis)

Operational Mode	Single Pass
Configuration	Cross-Flow; Shell and Helical Coil; Tube Side Water/Steam Flow
Number of Tubes	92
Tube OD	3.18 cm
Tube ID	2.00 cm
Overall Tube Length	98.5 m
Tube Material of Construction	2-1/4 Cr-1 Mo
Overall Tube Heat Transfer Surface Area	903 m ²
Heat Transfer Surface Area Margin	20%
Tube Bundle Transverse Pitch	5.72 cm
Tube Bundle Longitudinal Pitch	4.76 cm
Tube Pitch Angle	7.55°
Number of Tube Coil Rows	4
Helical Coil Bundle Height	11.6 m
Vessel Outside Diameter	199 cm
Inner Shroud Outside Diameter	97.2 cm
Steam Generator Height	20.72 m
Water Side Tube Pressure Drop	11.72 bar
Inlet Restrictor Pressure Drop	6.55 bar
Sodium Side Pressure Drop	0.19 bar
Shell Thickness	3.81 cm
Elliptical Head Thickness	4.45 cm
Tube Sheet Thickness	8.89 cm

II.5.2.2 Steam Cycle

A Rankine superheated steam cycle power conversion system concept has been developed for the ABTR. Layouts of key system components, piping, and instrumentation have been roughed out for the purposes of the ABTR pre-conceptual design phase. The overall system layout is shown in Figure II.5-22, while system piping and instrumentation are shown in Figure II.5-23. The power conversion system, which is based on standard technology currently employed in fossil-fueled power plants, includes both high pressure, intermediate pressure, and low pressure turbines. Other key system components include a moisture separator and two steam reheaters, as well as three low-pressure and two high-pressure feedwater heaters. The pre-conceptual design and analysis activities have included a calculation of the overall system electrical production cycle efficiency using the plant performance software GateCycle (GE Energy). For a given system configuration, this tool calculates design and off-design performance of power plants incorporating Rankine or gas turbine cycles. Based on the system design requirements provided in Table II.5-9, the calculated overall cycle efficiency for the

system shown in Figure II.5-22 is 37.8 %. The system heat balance is shown in Figure II.5-24.

The main steam system transports superheated steam from the two steam generators through a common steam header pipe to the high-pressure turbine inlet valves. Steam is extracted from the high- and intermediate- pressure turbines and is piped to the steam reheaters which condition the steam transported from the intermediate-pressure turbine exhaust to the low pressure turbine inlet. The main steam system includes a turbine bypass to the condenser to prevent a reactor trip in the event of a turbine trip.

II.5.2.3 Auxiliary Systems

Main auxiliary system components include the feedwater and condensate systems, and the circulating water system. The water quality and chemistry of the plant must be carefully controlled. High purity feedwater is required to prevent deposition of impurities on heat transfer surfaces and to preclude intergranular stress-corrosion cracking of the heat transfer surfaces. This requires careful attention to the design and material selection for each component of the system, i.e., on-line water monitoring, full-flow filters, full-flow demineralizers, and pH control.

The main function of the condensate system is to condense and collect turbine exhaust steam and water, to reject excess heat, to transport the condensate collected at the condenser hotwells to the deaerator, and to provide the initial condensate/feedwater heating. The main function of the feedwater system is to transport the feedwater collected at the deaerator storage tank to the steam generators at the required flow rate, temperature, and pressure for all operating conditions. This system not only includes the feedwater and condensate systems, but also the condensate demineralizer system. The function of the demineralizer system is to improve the chemistry of the condensate stream in order to make it acceptable for a once-through steam generation system. The feedwater and condensate systems are shown in Figure II.5-25. This design is based on standard components commonly used in the power generation industry. The design and maintainability of the feedwater system is as important as the design of the steam generator system.

A makeup water system is also provided. This system supplies makeup water that meets the feedwater chemistry requirements. The makeup water system utilizes standard components commonly used in power plants.

The circulating water system rejects waste heat from the main condenser shells to the atmosphere through a cooling tower. This system is shown in Figure II.5-26.

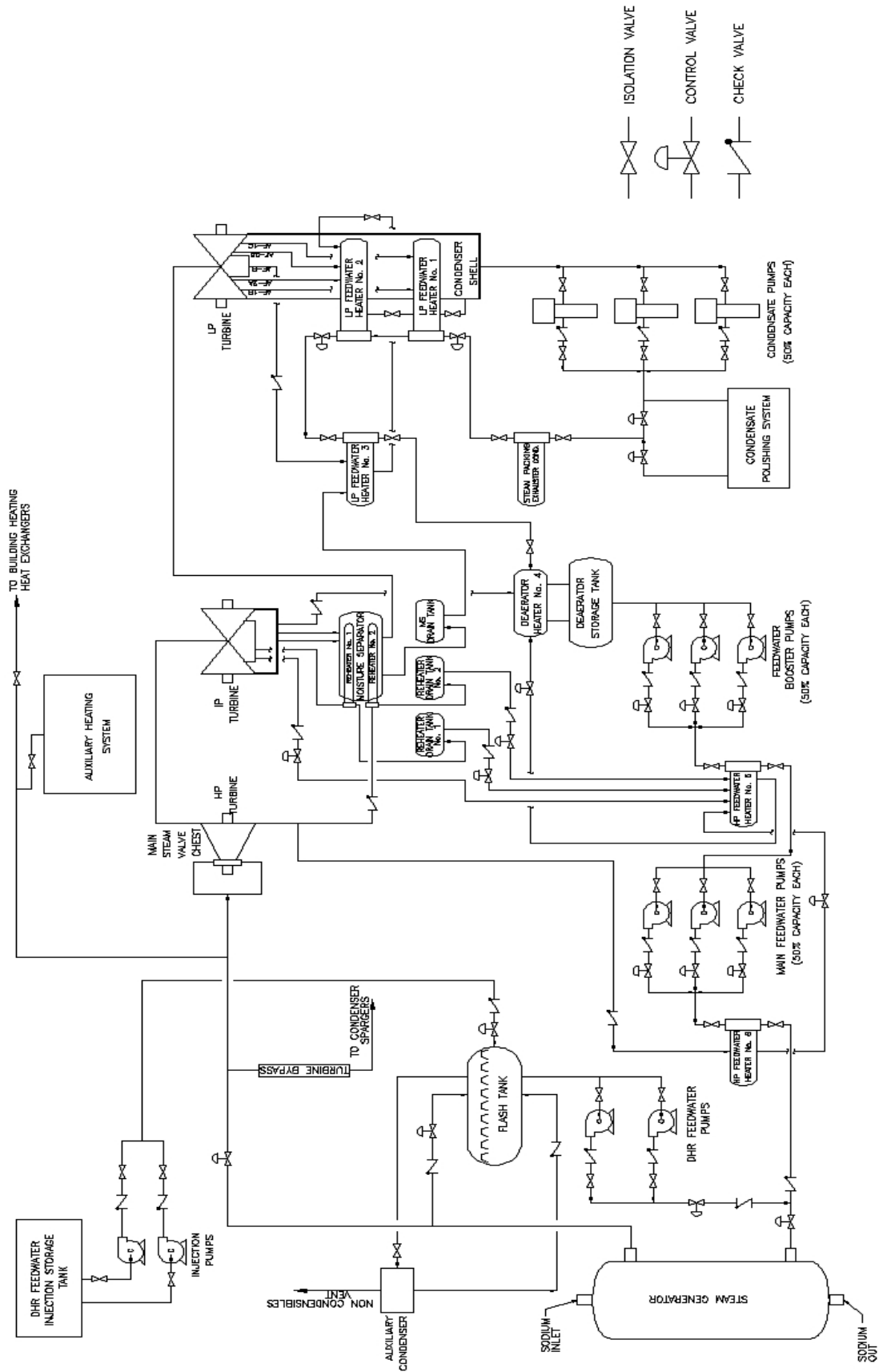


Figure II.5-22 ABTR Steam Cycle Power Conversion System

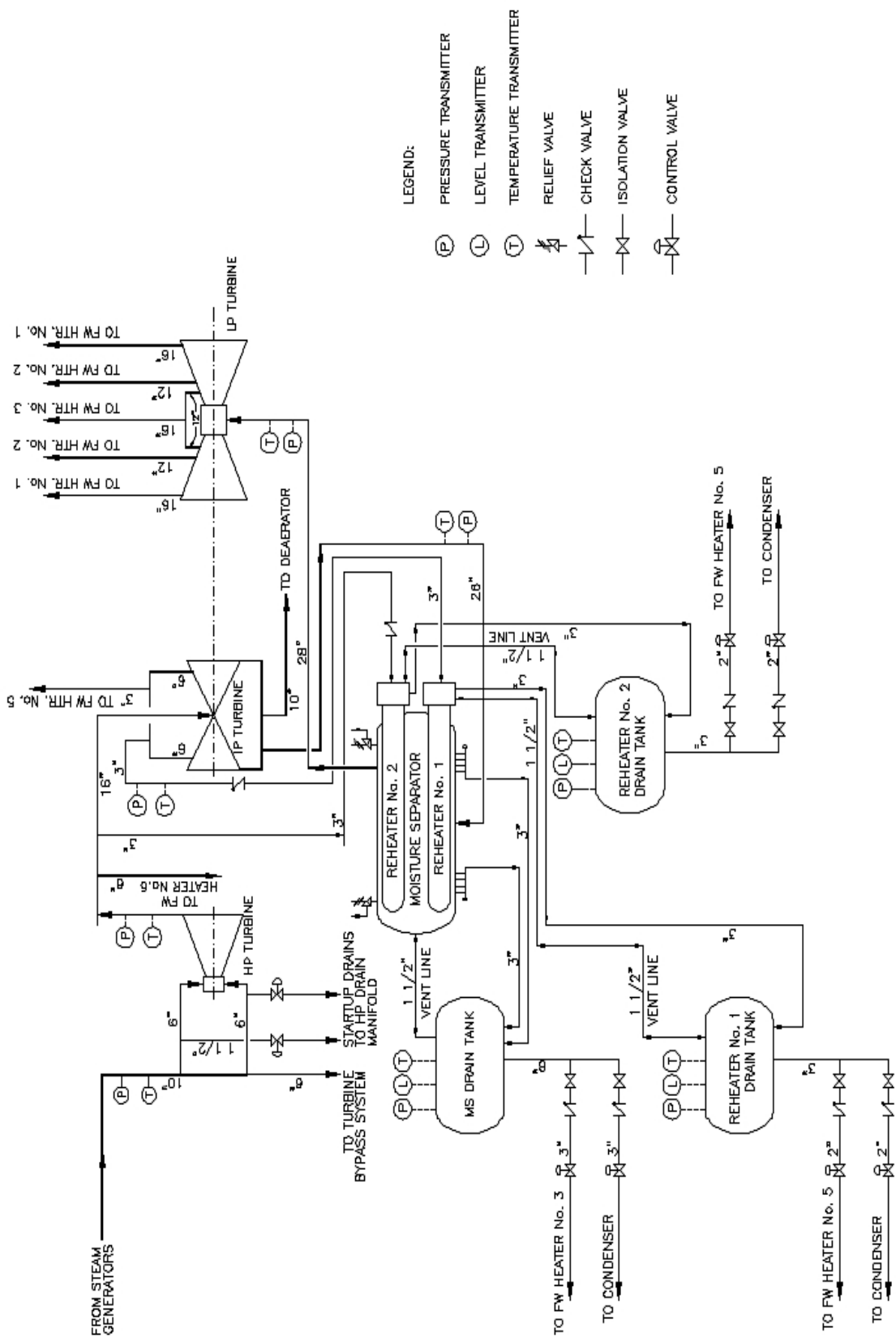


Figure II.5-23 Steam Cycle Piping and Instrumentation Drawing

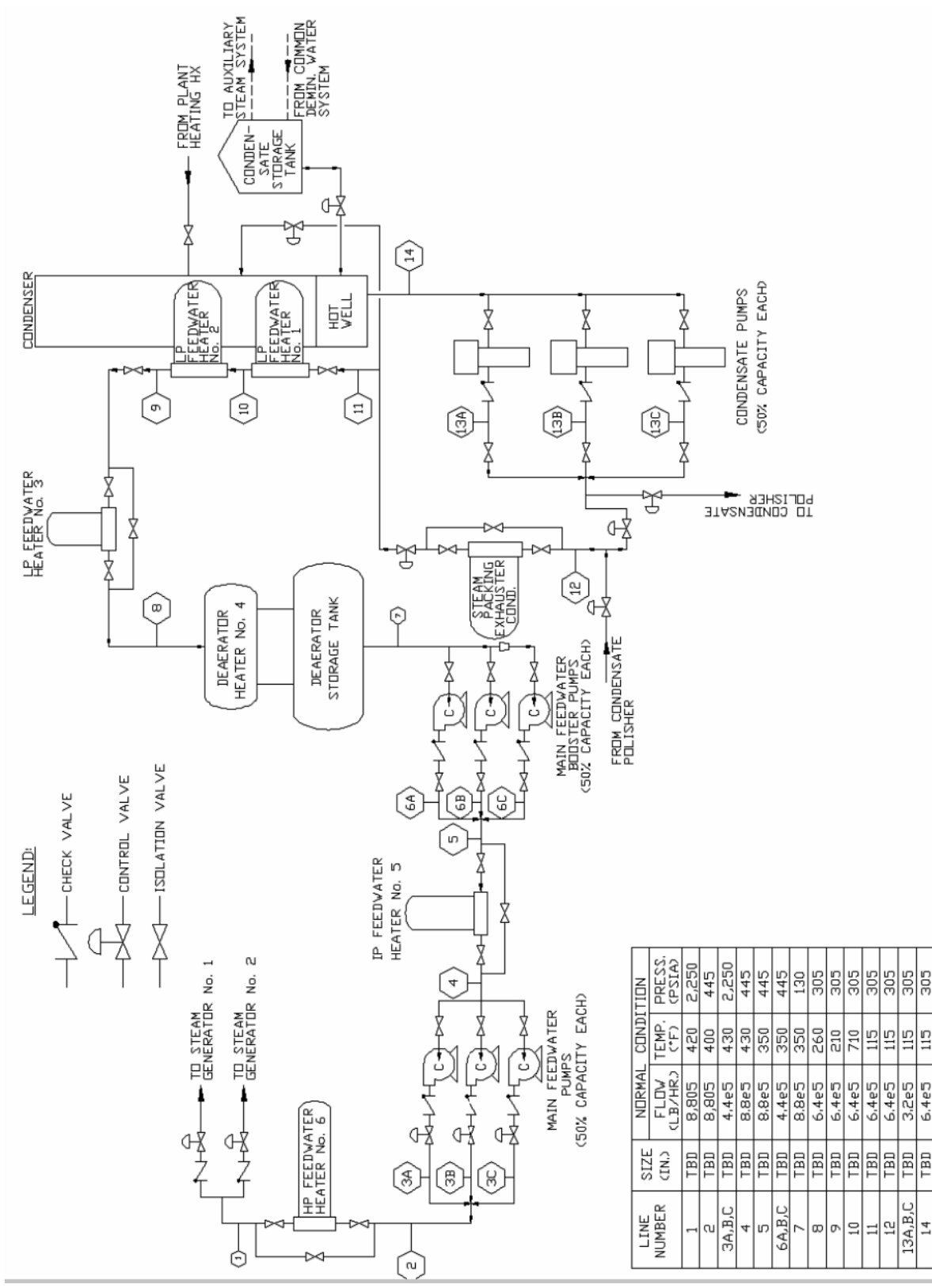
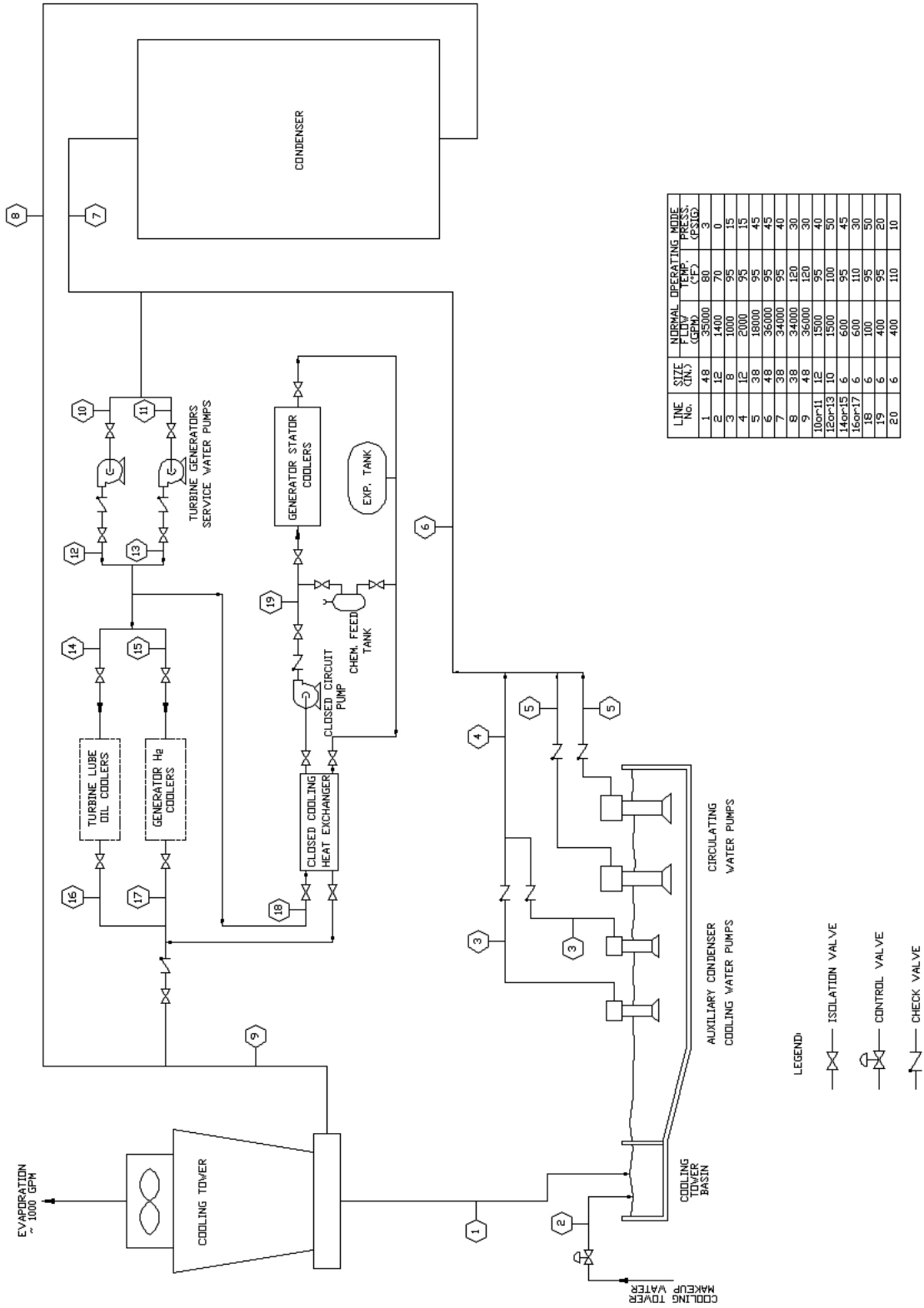


Figure II.5-25 Flow Diagram for the Condensate and Feedwater Systems



LINE No.	SIZE (IN.)	NORMAL FLOW (GPM)	OPERATING TEMP. (°F)	MODE PRESS. (PSIG)
1	4.8	35000	50	0
2	12	1400	70	0
3	8	1000	95	15
4	12	2000	95	15
5	3.8	18000	95	45
6	4.8	36000	95	45
7	3.8	34000	95	40
8	3.8	34000	120	30
9	4.8	36000	120	30
10or-11	12	1500	95	40
12or-13	10	1500	100	50
14or-15	6	600	95	45
16or-17	6	100	95	50
18	6	400	95	20
19	6	400	110	10
20	6	400	110	10

LEGEND:

- |—|— ISOLATION VALVE
- |—|— CONTROL VALVE
- |—|— CHECK VALVE

Figure II.5-26 Flow Diagram for the Circulating Water Systems

II.6 Shutdown Heat Removal System

The shutdown heat removal system is completely independent from the normal decay heat removal through the intermediate heat transport system, and is activated only when the normal heat removal system is disabled. The system consists of three independent, redundant, and diverse heat removal loops, with a fourth provided as a spare. Each loop consists of a small in-vessel direct reactor auxiliary cooling system (DRACS), a secondary natural draft heat exchanger (NDHX), an expansion tank, and an exterior stack that forms the natural draft pathway for dissipating the decay heat to the atmosphere. A schematic diagram showing key elements of the system is shown in Figure II.6-1.

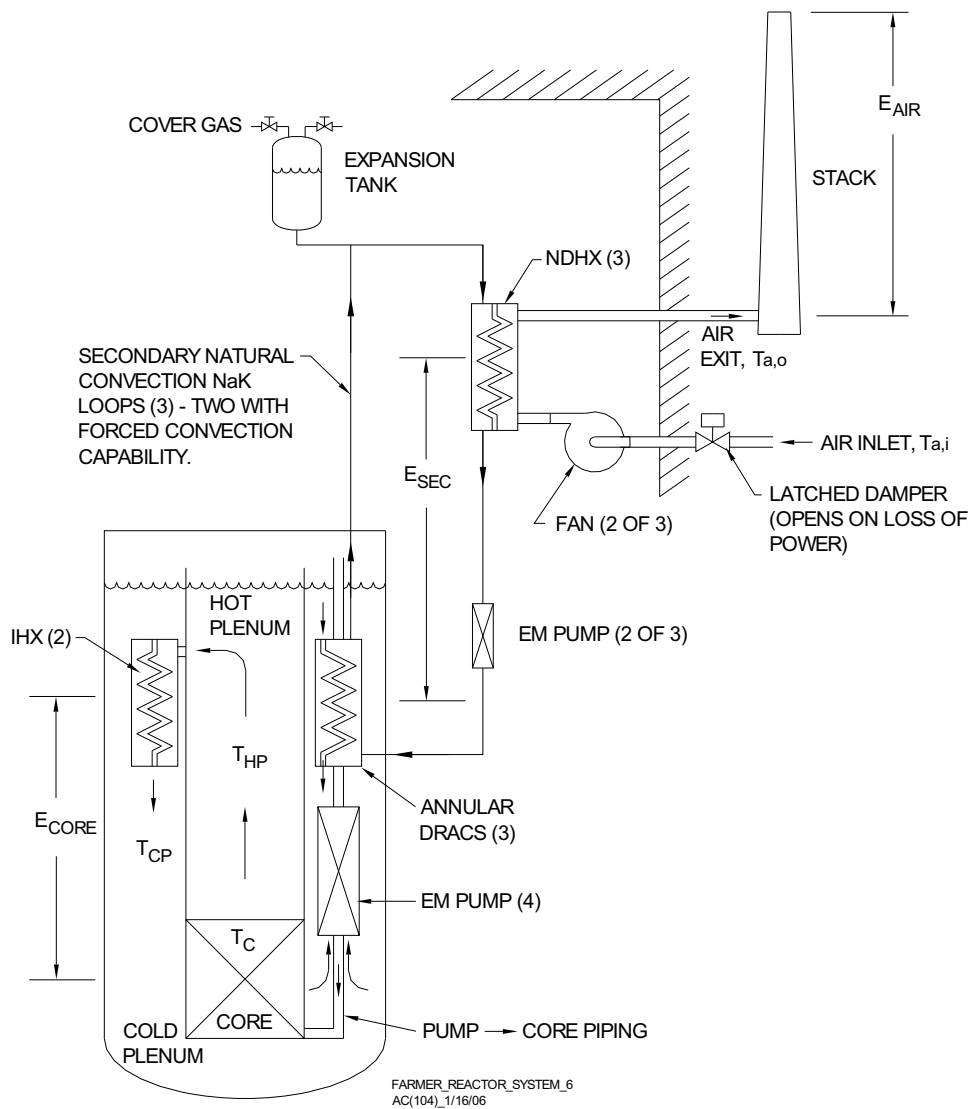


Figure II.6-1 Schematic Diagram of Shutdown Heat Removal System

The DRACS heat exchangers are positioned directly in the sodium cold pool. Moreover, there are no valves or other mechanical devices that isolate the primary sodium from the DRACS. Thus, during full power operation, primary cold pool sodium circulates at a modest flow rate through the shell side of the DRACS. However, when activated, buoyancy-driven natural convection flow of the primary sodium through the DRACS is initiated.

The core decay heat is transferred by natural convection flow of primary sodium from the reactor hot pool through the IHX flow path to the cold pool. Heat from the primary sodium cold pool is then transferred through the DRACS to the secondary sodium-potassium (NaK) eutectic passing through the heat exchanger tubes. All three loops are capable of operating in a natural convection mode, in which buoyancy driven convection causes the secondary NaK to circulate through the natural draft heat exchangers where the airflow transfers the heat from the NaK to the atmosphere. The secondary NaK flow circuits (one for each of the three independent systems) are completely passive without any valves or constrictions to limit the flow during normal operation or shutdown conditions.

On the tertiary (air) side of the systems, the natural convection circuits are passive except for magnetically latched dampers that prevent air flow on the air inlet side of the three NDHXs. Upon loss of electrical power to the electro-magnetic latch, the dampers fail by gravity in the open position. The DRACS are brought into full operation by opening of these dampers. The dampers are designed to provide an air leak rate that corresponds to nominally 1 % of the full design flow rate in the closed position, which results in a parasitic heat loss of ~ 18 kW during full power operation. This minor heat loss is included in the design to maintain the correct natural convection flow patterns in the primary, secondary, and tertiary sides of the system so that proper natural convection flow patterns are established immediately upon system activation. Moreover, continuous heat addition to the system is desirable in regions where the ambient temperature can fall below the NaK freezing temperature of nominally -13 °C.

Alternatively, two of the three DRACS loops are capable of operating in a forced convection mode to control (i.e., limit) the heat removal rate from the reactor vessel during planned shutdowns (e.g., fuel shuffling operations). As shown in Figure II.6-1, the secondary NaK sides of these two loops are equipped with EM pumps, so that the loop flowrates can be modulated by adjusting the applied voltage to the pumps. The tertiary air loops on these two units are also equipped with fans so that the heat removal rate through the NDHXs can be adjusted as needed. The EM pumps and fans are selected since these devices have large open flow areas that do not significantly impede natural convection when the loops are operated in that manner.

The three DRACS are designed to remove 625 kW each at normal operating conditions. The thermal rating for each DRACS thus corresponds to 0.25 % of the core full power rating of 250 MWt. The three DRACS are thus capable of removing 1.88 MW of decay heat at design conditions. Since the DRACS are located inside the reactor vessel, any leakage from the DRACS or ancillary piping will not lead to coolant drain

down. The DRACS are annular in shape, and are concentrically mounted around the vertical piping that supports the three main (EM) reactor coolant pumps. This approach is adopted to minimize the number of penetrations through the reactor vessel head.

Key design parameters for the DRACS are summarized in Table II.6-1, while a drawing that illustrates key features is provided in Figure II.6-2. The DRACS is a shell-and-tube, counter-current flow-type heat exchanger with primary flow on the shell-side, and NaK flow on the tube side. Primary sodium from the cold pool enters the shell side of the DRACS through an annular ring opening in the shroud located just below the upper tube sheet. The sodium flows by natural convection down through the tube bundle while dissipating heat. The sodium then returns to the cold pool through a second annular ring opening located just above the lower tube sheet. Cold secondary NaK enters the DRACS through a 5.1 cm diameter downcomer. The downcomer delivers the cold NaK through the lower tube sheet into a header manifold, where it then turns 180° and rises through the tube bank in counter current flow to the shell side primary sodium. The hot secondary NaK exits the tubes into an upper header manifold, and then flows through an annular riser which is concentric to the downcomer. The downcomer is double walled with an annular gap for thermal insulation between the hot and cold streams.

Table II.6-1 DRACS Design Parameters

Heat transfer capacity	625 kWt
Heat transfer area	4.32 m ²
Primary sodium temperature inlet	510 °C
Primary sodium temperature outlet	355 °C
Primary sodium mass flowrate	3.14 kg/s
Secondary NaK temperature outlet	484 °C
Secondary NaK temperature inlet	328 °C
Secondary NaK mass flowrate	4.38 kg/s
Tube outer diameter	2.22 cm
Tube wall thickness	0.9 mm
Tube Pitch	3.79 cm
Active Tube length	2.50 m
Number of tubes	25
Upper Tube Sheet - Area	0.032 m ²
Upper Tube Sheet - Thickness	25 mm
Lower Tube Sheet - Area	0.032 m ²
Lower Tube Sheet - Thickness	25 mm
Outlet piping – OD	5.1 cm
Shell OD	30.0 cm
Shell thickness	6.4 mm
Material	9Cr-1Mo

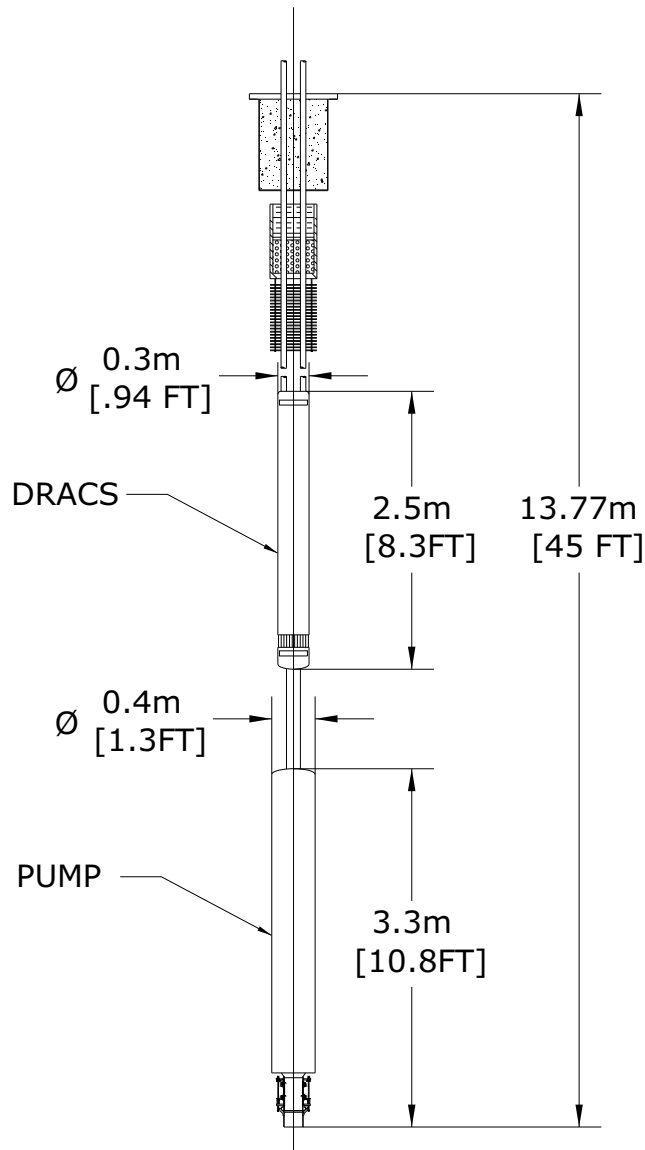


Figure II.6-2 Details of DRACS Design

Both the downcomer and the annular riser pipes are equipped with bellows just above the shroud to accommodate any differences in thermal expansion between the piping and the body of the DRACS itself (which is rigidly attached to the vertical piping that supports the EM pumps). The upper tube sheet is welded to the shroud, while the lower tube sheet floats. Thus, the design accommodates differential thermal expansion within the tube bank also.

Consistent with the thermal rating of the DRACS, each NaK-to-air NDHX is designed to remove 625 kW decay heat. The unit is a horizontal tube, cross-flow design. Key design parameters are summarized in Table II.6-2. The unit is equipped with fire suppression plate and catch basin to mitigate the effects of a NaK tube bundle leak. The

damper to the unit is magnetically latched to fail open under gravity upon loss of electric power. The unit will also have a manual hand-wheel operation capability.

Table II.6-2 NDHX Design Parameters

Heat transfer capacity	625 kW
Tube length	2.83 m
HX tube OD	4.22 cm
Tube wall thickness	3.55 mm
Fin height	3.2 mm
Tube horizontal center-to-center spacing	7.62 cm
Tube vertical center-to-center spacing	10.2 cm
Stack riser cross-sectional area	8.25 m ²
Stack height	5.0 m

Air flow through each NDHX is induced through a dedicated exhaust stack, one for each unit. Each stack is 5 m high and 8.75 m² in cross section. The stacks are of lightweight steel construction and are insulated. Each secondary NaK loop contains an expansion tank to accommodate changes in system volume due to variations in temperature. The tank has one NaK nozzle on the bottom and one gas nozzle on the top, which supplies argon cover gas to the tank and permits pressure control. The tank is located at the high point in the loop. The resultant NaK static head is sufficient to operate the loop with expansion tank cover gas pressures at, or slightly below, atmospheric pressure. In the event of a leak in the DRACS, loss of radioactive primary sodium into the secondary NaK loop will not occur. In the event of a leak in the NDHX, the resultant spill is minimized because of the low expansion tank operating pressure.

Design calculations for sizing of the DRACS heat exchangers, as well as scoping analyses of system response under a postulated loss of flow/loss of heat sink event, are provided in Section III.2.

II.7 Fuel Handling System

The fuel handling system (Figures II.7-1 and II.7-2) includes several pieces of machinery and mechanisms required to move core assemblies into and out of the primary tank and provide an effective means to transfer those assemblies to an external fuel cycle facility.

The primary function is to receive, prepare, and load fuel assemblies into the reactor core. Subsequently, the system enables the removal of the core assemblies at the end of their life, transfer them out of the reactor, and reload the core with fresh assemblies. Other functions include rearranging core assemblies, minor loading adjustments, refinements, and moving fuel assemblies from the storage rack positions to an unloading position.

The fuel handling system includes several major components including the rotatable plug, pantograph fuel handling machine (PFHM), storage rack, fuel unloading machine (FUM), intra-building casks and intra-building transfer tunnel.

II.7.1 Rotatable Plug Assembly

Located on the reactor cover is the rotatable plug (Figure II.7-3). It is 3.05 m (10 ft) in diameter and located 14.7 cm (5.8") eccentric of the reactor cover. The primary function is to provide the necessary support for the control rod drives and provide the PFHM access to all core sub-assembly positions.

It consists of a 38.1 cm (15") thick solid austenitic stainless steel cover. Above that is 30.8 cm (12") of insulating material. Then as part of the deck, is 12" of heavy concrete topped off with 30.8 cm (12") of insulation covered with a stainless steel plate. Below the cover are the heat shields. These consist of 56.5 cm (22 1/4") thick, austenitic stainless steel plates with a 2.22 cm (7/8") gap between the plates.

Also supported from the cover plate are the upper internal structure (UIS) (Figure II.7-4) and the PFHM. The UIS gives the control rod guide tubes the necessary support. This consists of a 1.32 m (52") diameter, heavy wall perforated tube with baffle plates. The control rod guide tubes penetrate these baffles and extend to just above the reactor core. The UIS is slotted to give the PFHM access to all core positions.

The Rotatable Plug is mounted on a motor driven bearing and employs an elastomer seal around its perimeter to provide a gas tight seal with the cover.

This seal maintains the integrity of the primary vessel atmosphere while the reactor is operating. The rotatable plug is only rotated during fuel handling operations (reactor shutdown). Once the reactor is safely shutdown, the control rod drive lines are disconnected from the control rods and raised slightly into their respective guide tubes in the UIS. Only then can the plug be rotated and the PFHM operated.

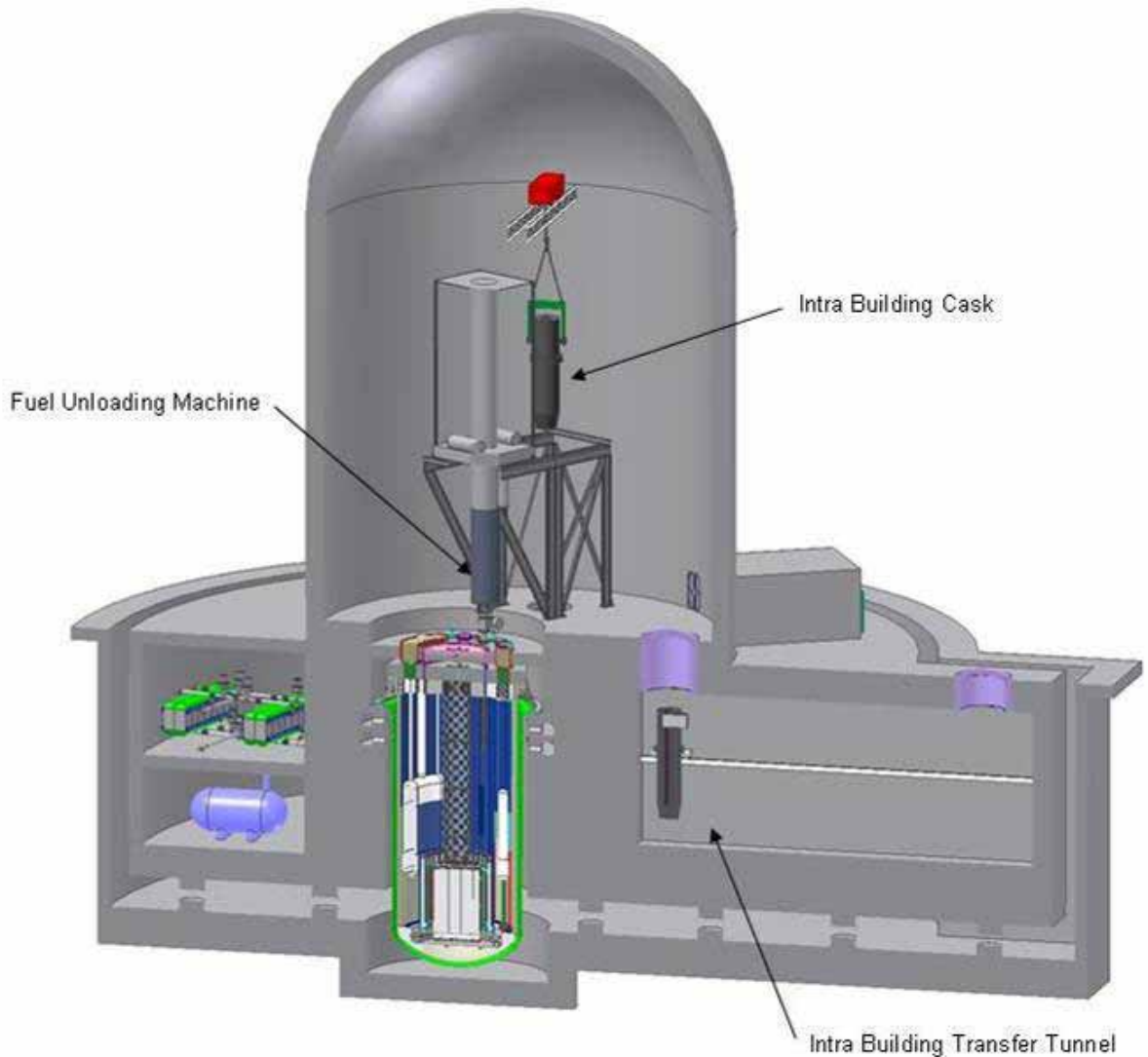


Figure II.7-1 Schematic of Fuel Handling System

Although a dual rotatable plug design with straight pull fuel handling was considered (Figure II.7-5), the single plug design with a PFHM, described above, was chosen as the reference design for several reasons. First and predominantly is cost. The complexity of a dual plug design and the added number of components dictate approximately twice the amount of hardware to operate and maintain over the single plug design. Second is reliability. Minimizing the number of components on the reactor cover will result in the simplicity of operation. The single plug design achieves this better than a dual plug. Third is space. A dual plug system has been found to increase the diameter of the reactor vessel by approximately one meter over a single plug system. This translates to added cost also. Although a dual rotatable plug design can use a “straight pull” fuel handling machine, the benefits of the single rotatable design outweigh any slight disadvantage of a PFHM. The dual plug system will be maintained as alternate concept in case the PFHM proves unfeasible.

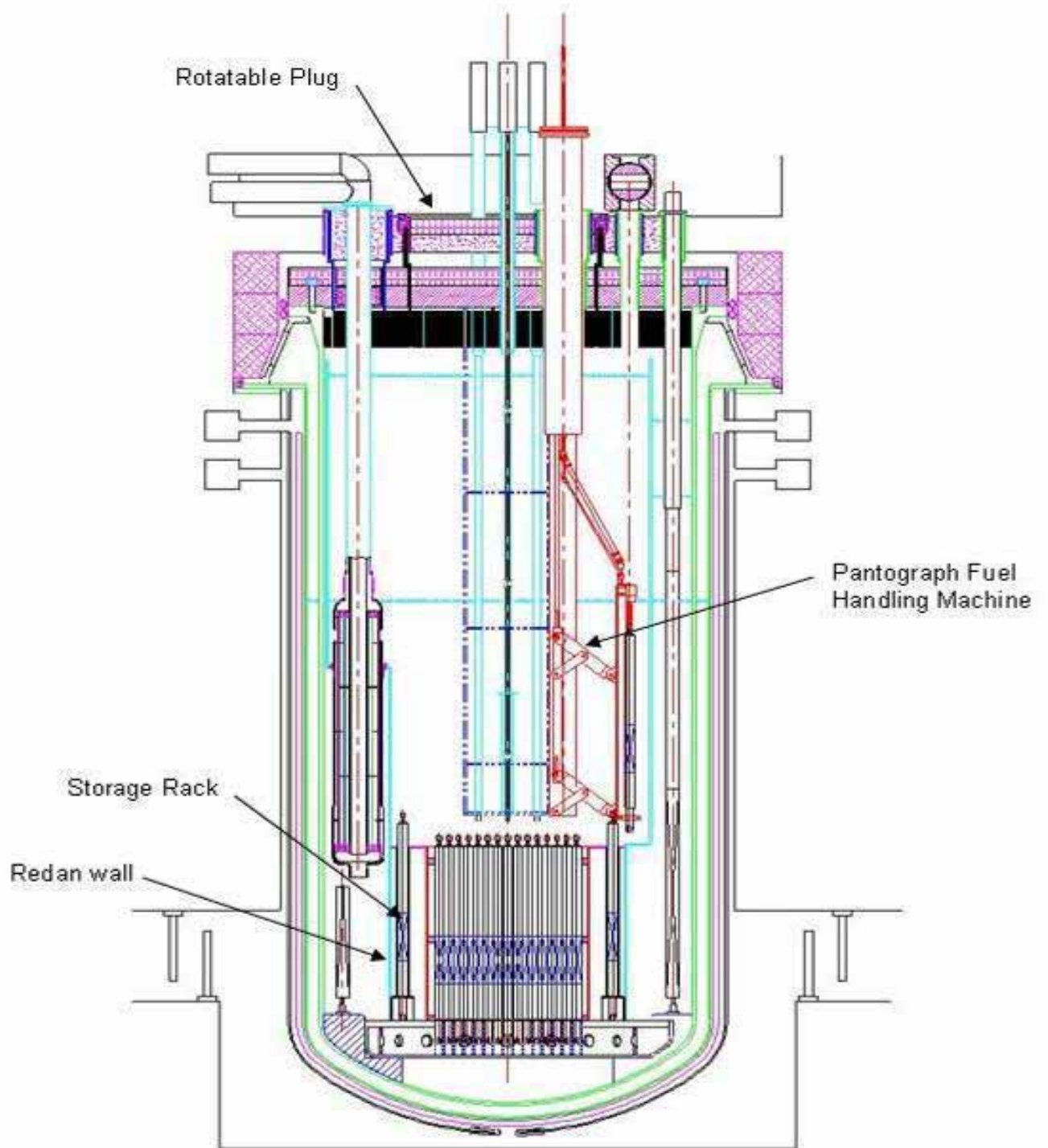


Figure II.7-2 Fuel Handling System

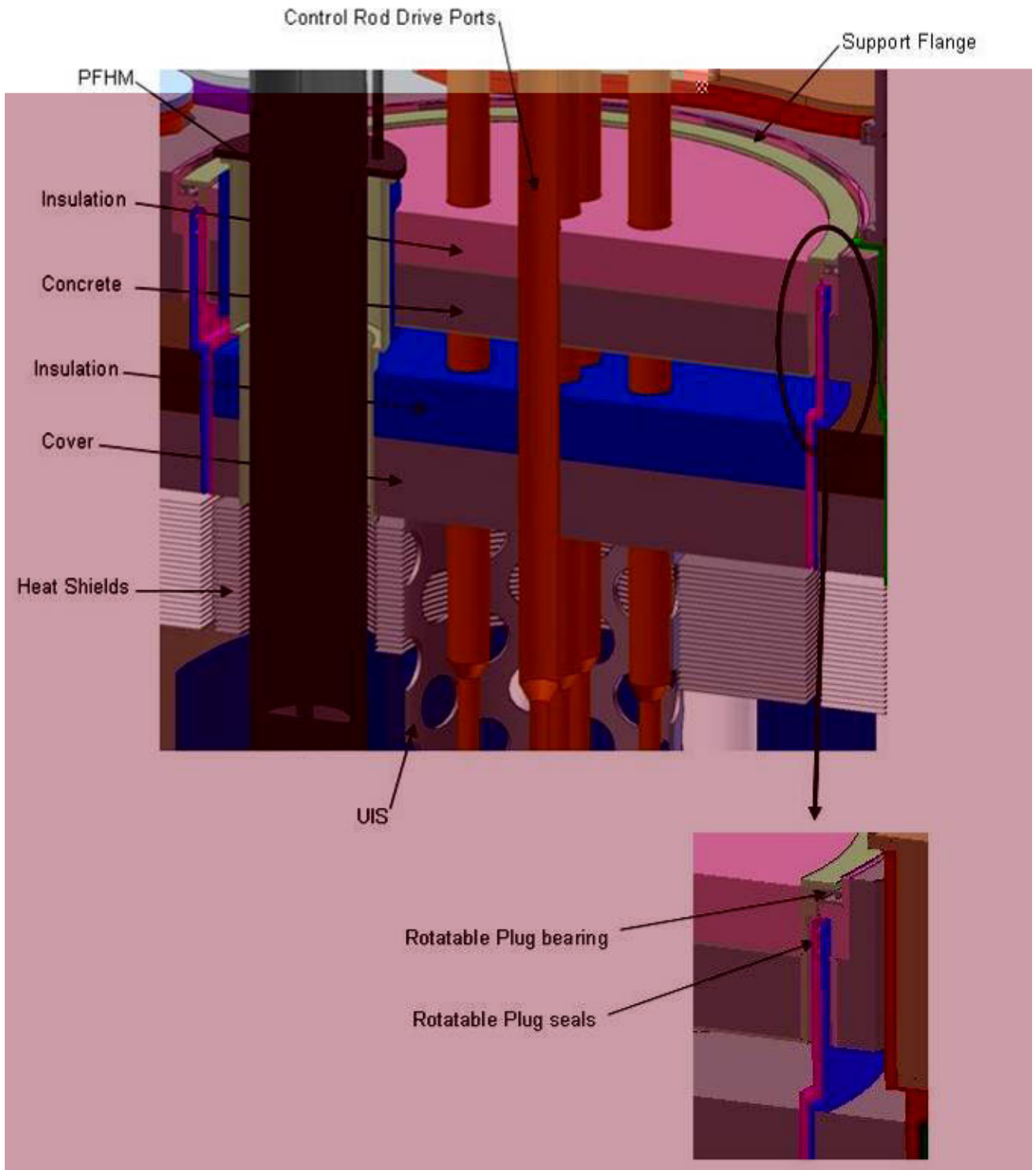


Figure II.7-3 Rotatable Plug

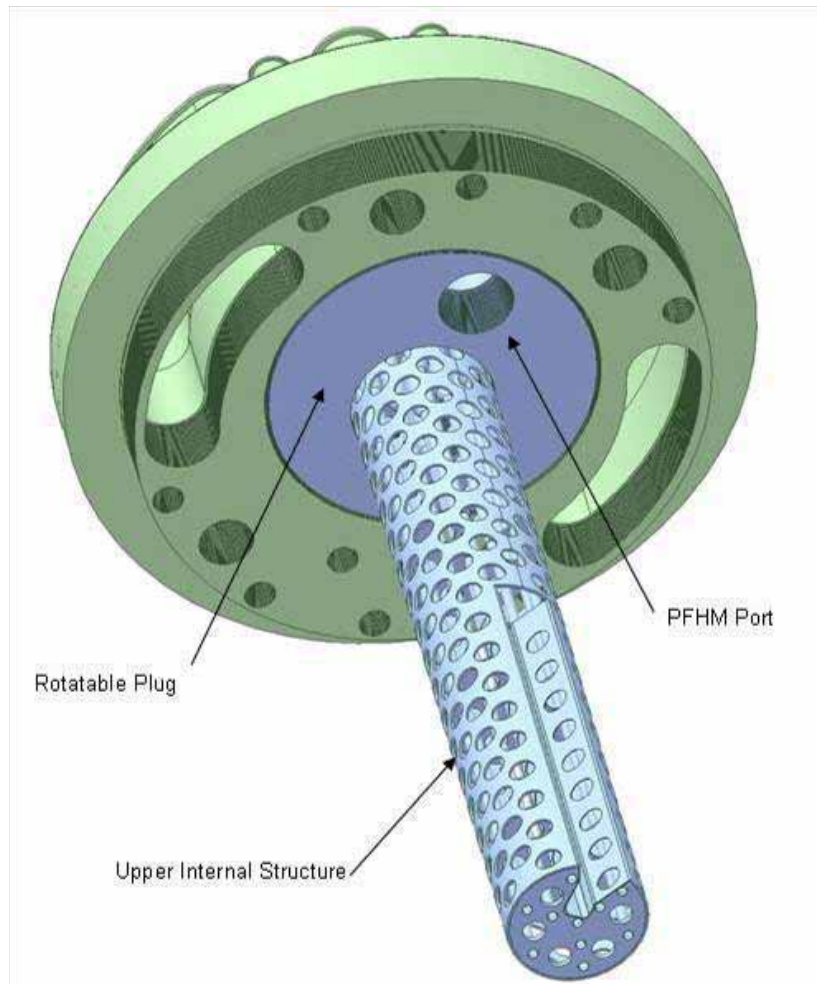


Figure II.7-4 Rotatable Plug Structures

II.7.2 Pantograph Fuel Handling Machine

The primary function of the pantograph fuel handling machine (PFHM) is to transfer fresh assemblies (fuel, shield, and reflector) into the core, and to remove spent core assemblies from the core barrel. It is also used to place them into a storage rack and place or retrieve core assemblies from the transfer position inside the redan (Figure II.7-2).

The PFHM has six motions: rotation, pantograph travel, gripper travel, gripper rotation, gripper locking, and hold down travel (Figure II.7-6). It can be positioned over any core assembly in the core by a combination of rotating the PFHM, extending or retracting the pantograph arm, or rotating the rotatable plug. When extended, the PFHM arm extends through a slot in the UIS to reach the core sub-assemblies (Figure II.7-7).

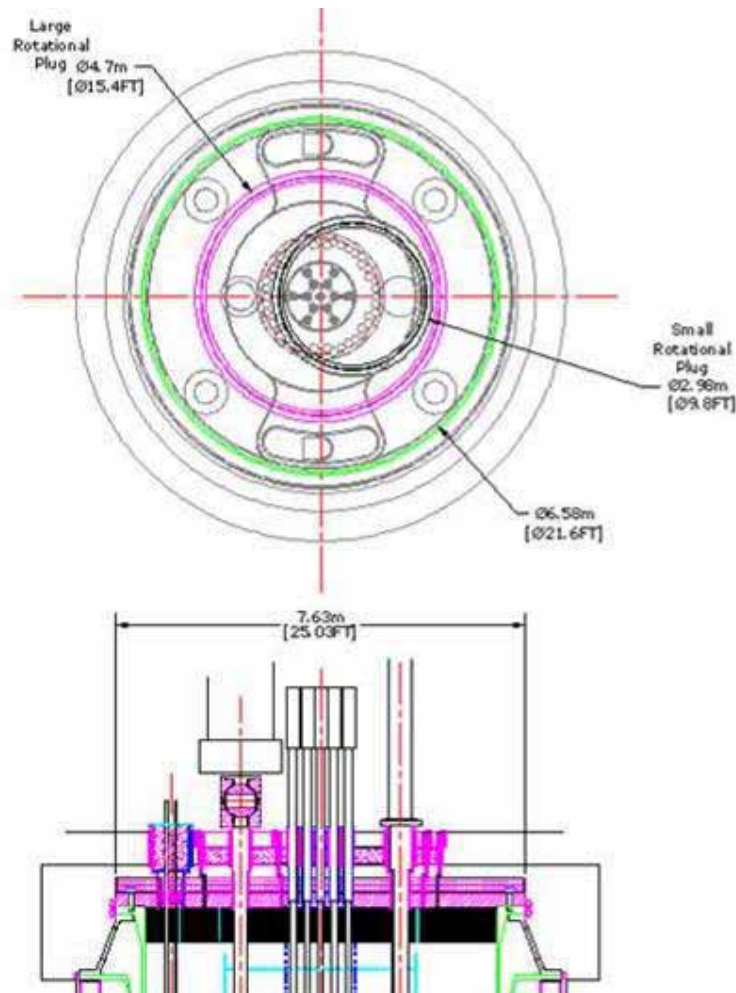


Figure II.7-5 Dual Rotatable Plug Concept

The PFHM is located and supported on the rotatable plug. It is secured to the plug with a bolted flange to resist any loads associated with the fuel handling operation. Using the pantograph arm, the PFHM is capable of reaching up to 1.14 m (45") from the center of rotation. At that distance it is designed to exert up to 28.8 kN (6000 lbs) of force to remove or insert a sub-assembly in the core barrel. The PFHM operates using three major components: the upper section, support tube, and the pantograph arm that includes the gripper.

The upper section is 91.4 cm (36") diameter and located above the reactor cover inside a cylindrical cover. It contains all the necessary drives and controls to operate the machine. This is the only area expected to require routine maintenance. The controls used are commercially available motion controllers. These include servo motors and resolvers for position feedback, linked to computer software with graphical depiction of position and administrative controls for every operation. Load sensing and object interference detection are accomplished through a system of voltage monitors on the drives. Each drive has manual override capability.

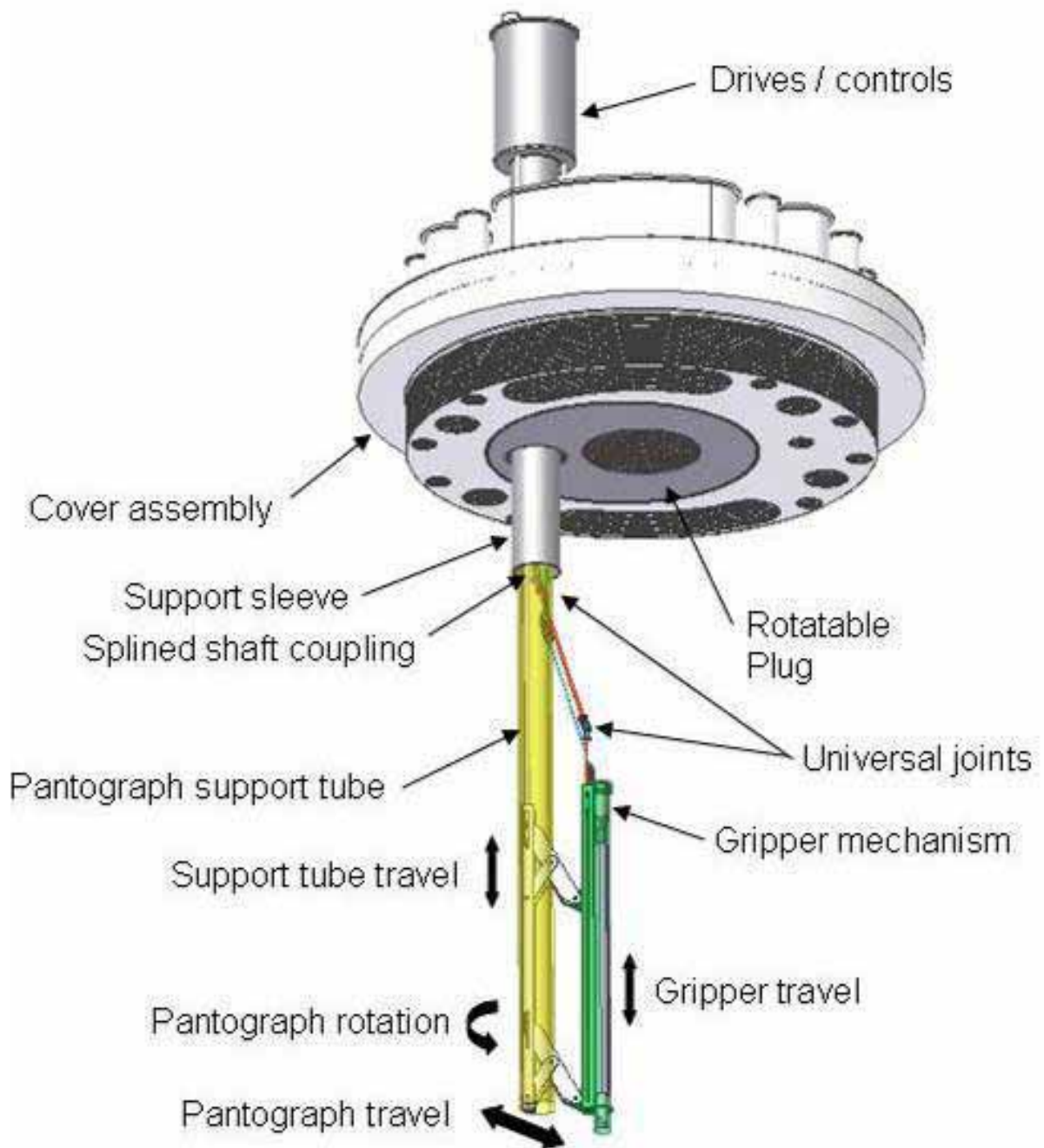


Figure II.7-6 Pantograph Fuel Handling Machine

The support tube section provides the physical support for the pantograph. It also houses the linkages required to move the pantograph arm and gripper mechanism. It consists of a 45.7 cm (18”) diameter, heavy wall tube with a vertical slot to allow the

pantograph arm to retract fully. The support tube section is mounted on a bearing to allow full rotation of the pantograph.

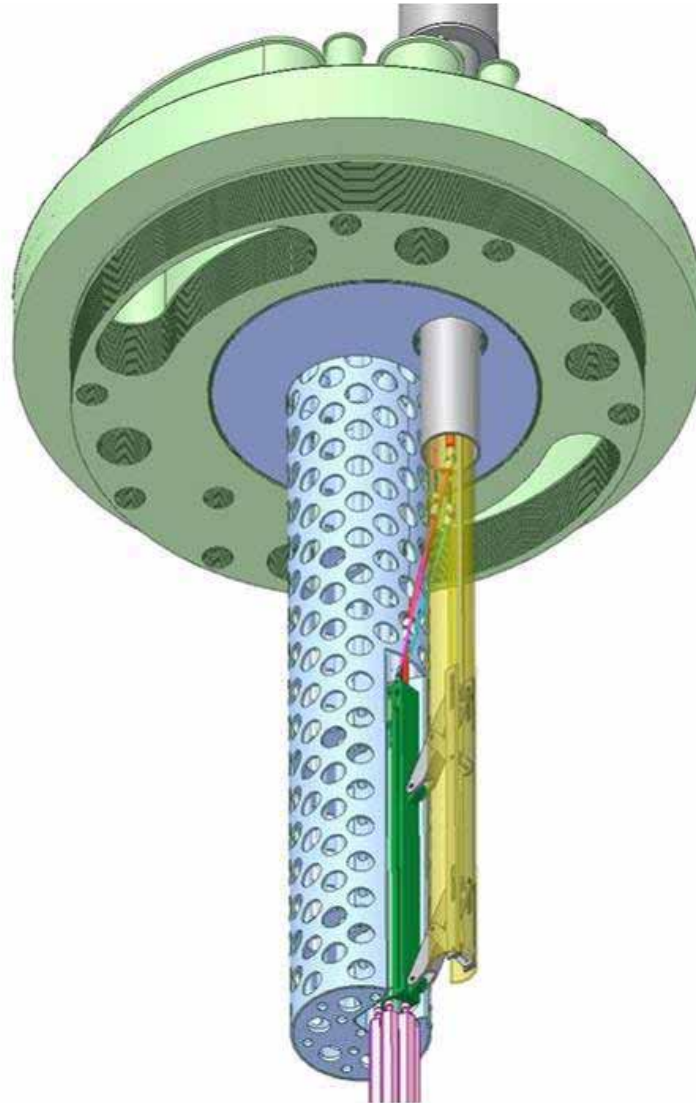


Figure II.7-7 Pantograph fuel handling machine and upper internal structure

The gripper mechanism, located on the pantograph arm, is driven by a 5.1 cm (2") diameter screw drive and travels vertically 3.48 m (137") inside 20.3 (8") diameter guide tube. This guide tube, which is fixed to the arm, is used to hold down adjacent fuel assemblies (Figures II.7-8 and II.7-9) and spread them slightly allowing the fuel assembly to be easily accessed without disturbing adjacent assemblies. This is accomplished by lowering the entire PFHM. The gripper mechanism is then lowered to the core assembly with its jaws open. On contact with the end of the assembly, a 2.54 cm (1") diameter spline shaft is rotated which operates gears to raise the cam spindle and close the jaws around the end (Figure II.7-10). The gripper is then raised, with the core assembly safely inside the guide tube. The gripper can then be rotated to re-orient the assembly for reinsertion, or removed and replaced. The PFHM is then raised to disengage the guide

tube from the top of the core assembly and can then move on to perform the next operation.

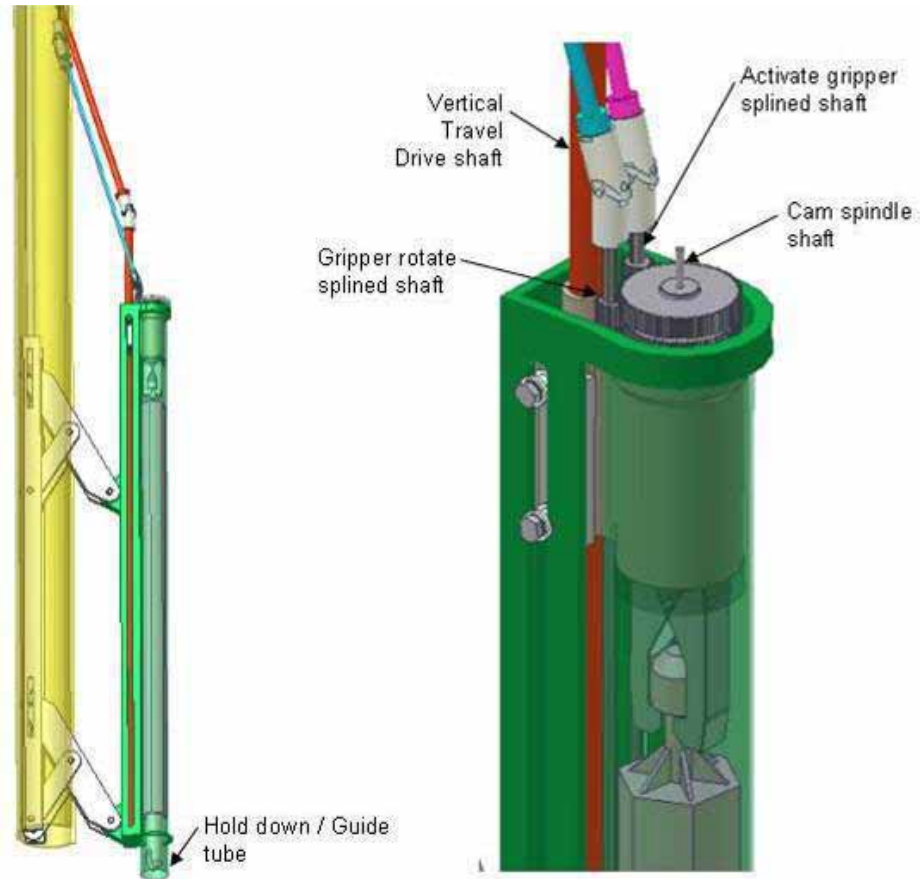


Figure II.7-8 Pantograph fuel handling machine guide tube

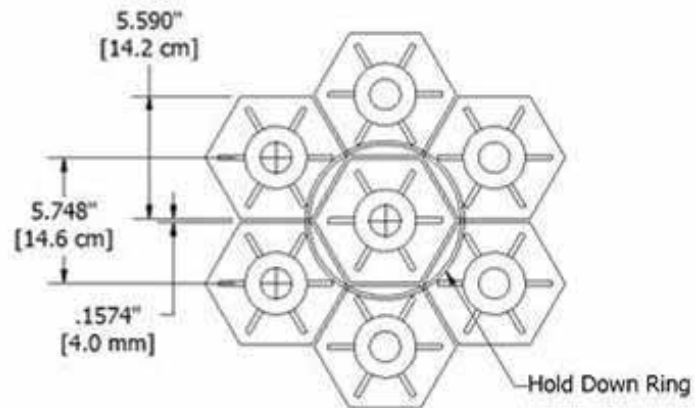


Figure II.7-9 PFHM Guide Tube Hold Down

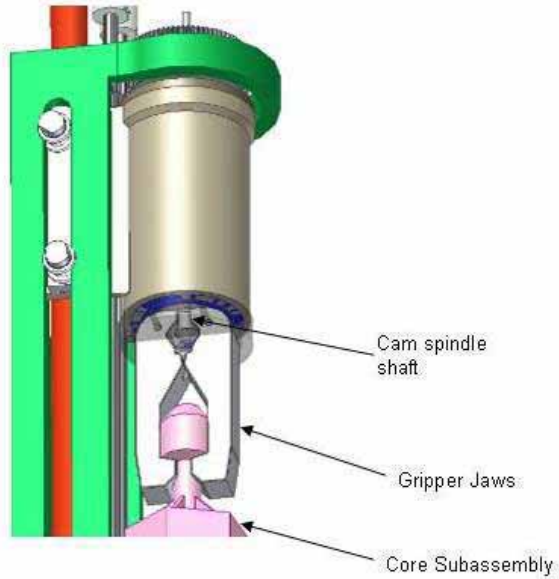


Figure II.7-10 PFHM Gripper Jaws

Several existing gripper designs were researched and evaluated for potential application to ABTR. They were; EBR-II, GE PRISM, ANL PRISM, UKAEA Prototype Fast Reactor, AFR-300 concept, MONJU, as well as various modifications to these designs (Figure II.7-11). At this time the ABTR reference design is a multi jaw gripper as described above. However, an alternate gripper design, similar to the gripper design used at MONJU (Figure II.7-12), may also have merit and should be evaluated further for adaptability to the PFHM.

It should also be noted that the PFHM is not normally removed from the reactor. Although the penetration in the rotatable plug is large enough to facilitate removal of the PFHM, only under off normal or maintenance conditions is this expected.

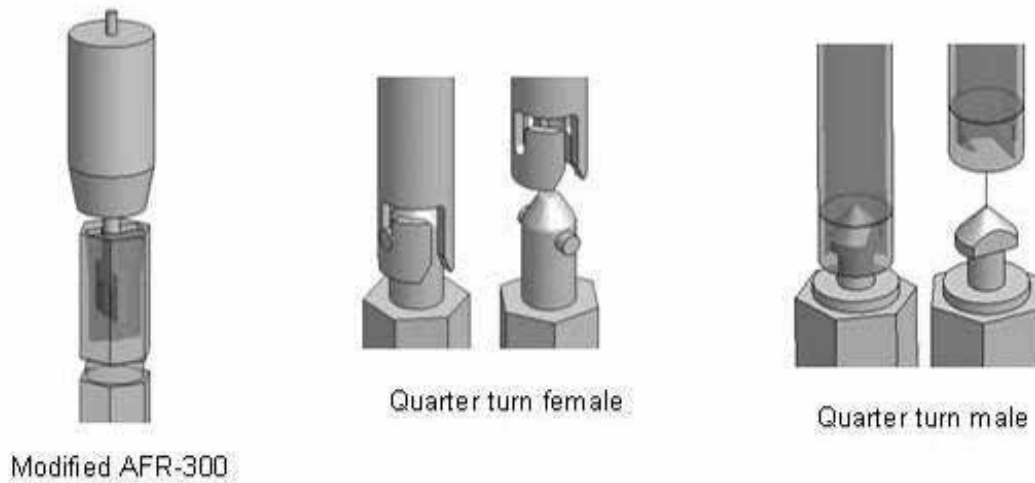


Figure II.7-11 PFHM Gripper Concepts

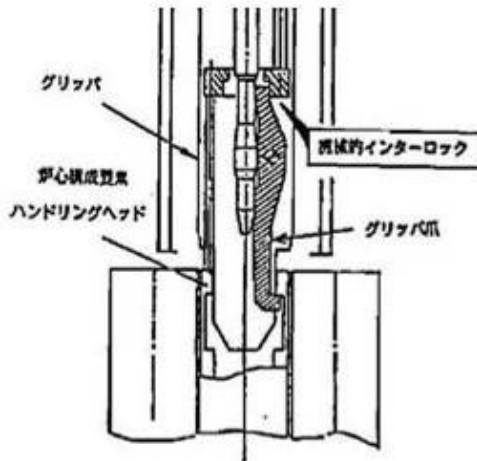


Figure II.7-12 MONJU Gripper Design

II.7.3 Fuel Storage Rack

The purpose of the rack is to provide a location for fresh fuel assemblies to be preloaded into the reactor vessel, and to store spent core assemblies removed from the core and allowed to decay in storage before removal from the reactor. Currently, the storage rack is located between the outside of the core barrel and the inside wall of the redan (Figure II.7-13). The open construction of the rack and its proximity to the redan and cold sodium pool induce natural convection of sodium to facilitate adequate cooling of spent fuel assemblies. There are a total of 36 positions in the rack. One position is located directly below the fuel unloading machine (FUM) that is located on the cover of the reactor. This position is used to cue core assemblies that are ready for removal from the reactor by the FUM.

II.7.4 Fuel Unloading Machine and Transfer Port

The fuel unloading machine (FUM) uses a shielded cask mounted on a self-propelled frame (Figure II.7-14). The frame traverses on rails between the transfer port and the inter-building cask (IBC) pit area. The FUM is equipped with a gripper for inserting and retrieving core assemblies from the cue position of the storage rack. The bottom of the machine has a movable seal to engage with the transfer port or an IBC. Also located in this area is a shielded door to maintain an inert atmosphere inside the FUM and protect or shield the surrounding area from the radiation from the core assemblies during transport. The FUM also provides for proper heating, cooling and an inert gas atmosphere for transferring fuel assemblies between the core and an IBC. The heated inert gas is also used to blow off residual sodium during spent fuel assembly removal operations and return it to the primary vessel.

The transfer port is located on the reactor enclosure. It provides an interface between the FUM and the primary vessel. The Transfer Port provides the needed radiation

shielding and inert atmosphere seal to prevent oxidation of residual sodium during transfer. This seal also assists in maintaining a pure argon atmosphere inside the reactor vessel.

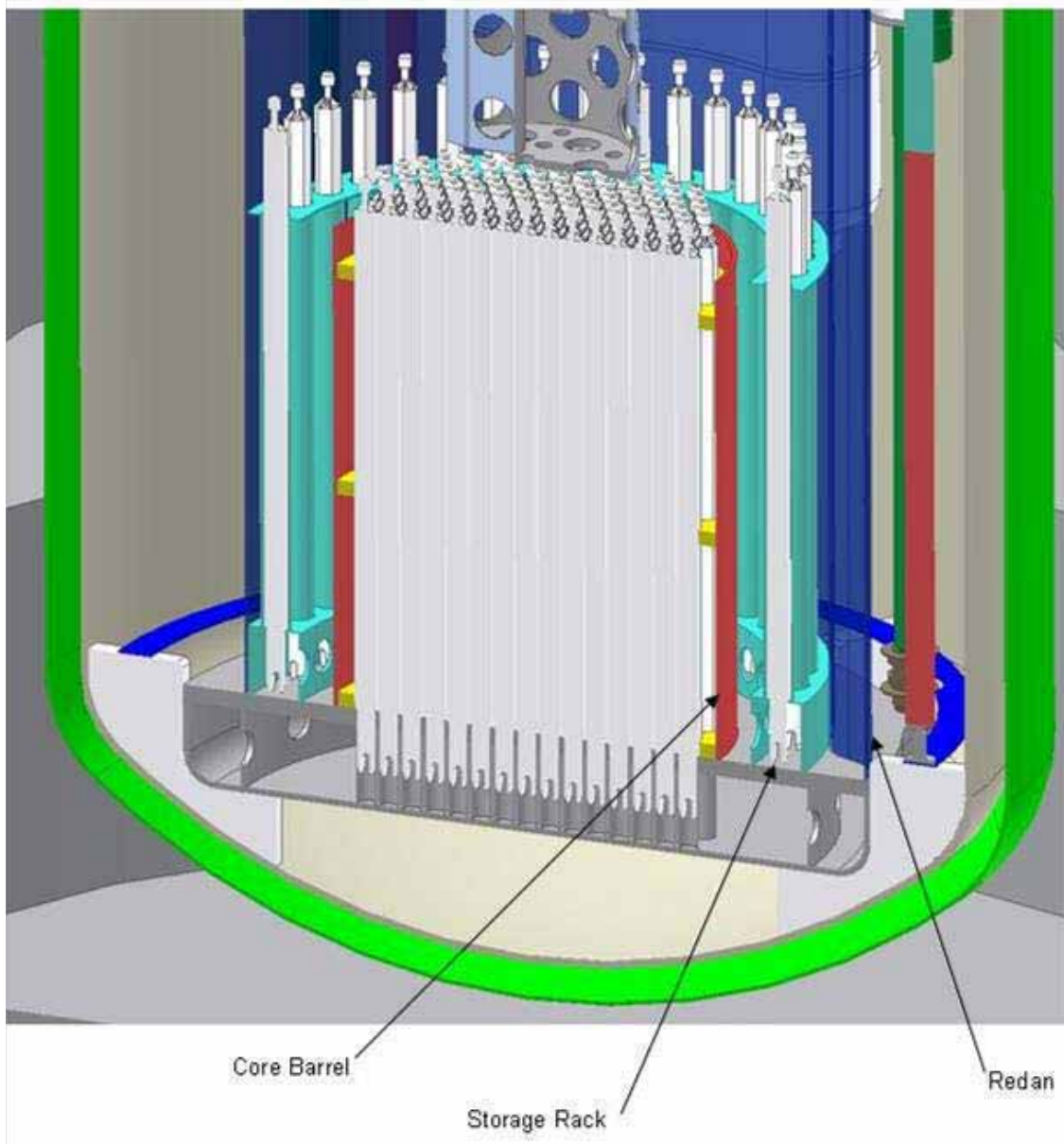


Figure II.7-13 Storage Rack

An alternate design to the FUM and the storage rack is a concept similar to Phenix (Figure II.7-15). In this arrangement, a rotating arm removes a sub-assembly from the core barrel and places it in an “internal storage area”. The sub-assembly is allowed to decay in this area for a predetermined amount of time. The sub-assembly is then removed from the reactor using an immersed handling bucket. This sodium filled bucket holds a

type of IBC has the necessary shielding and inert gas atmosphere but without any active cooling for the subassembly. Another type has all the same features but with active cooling to maintain the core assemblies below a temperature where there would be fuel cladding interaction. The IBC is illustrated in Figure II.7-16.

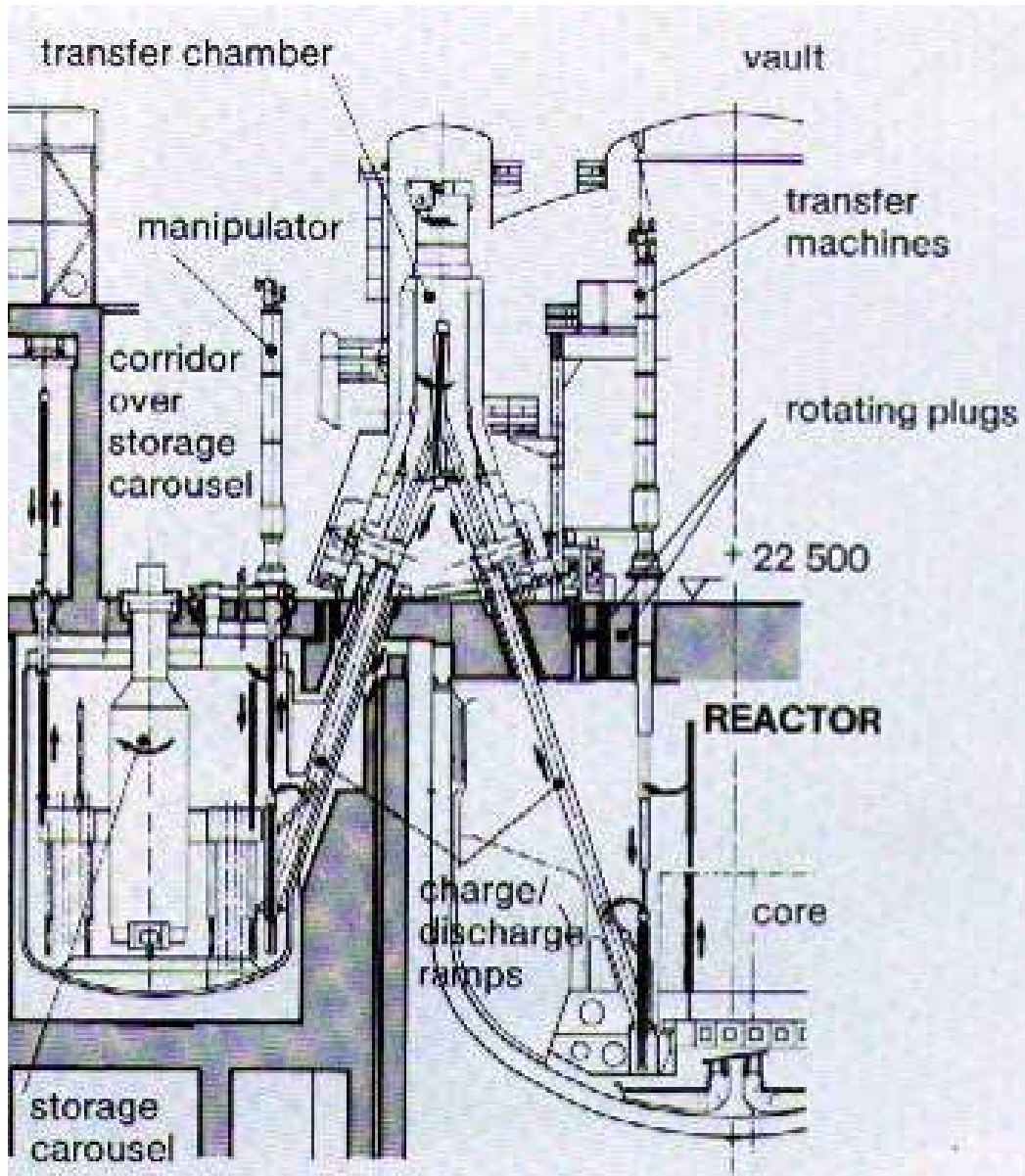


Figure II.7-15 Phenix A-frame transfer concept

An empty IBC is located in the IBC pit area under the travel of the FUM (Figure II.7-12). The core sub-assemblies that have been irradiated in the reactor are transferred by the FUM to the IBC located in the pit. Once filled, the IBC can then be moved by the reactor building overhead crane to the intra-building transfer tunnel (IBTT) where it is transported from the reactor building.

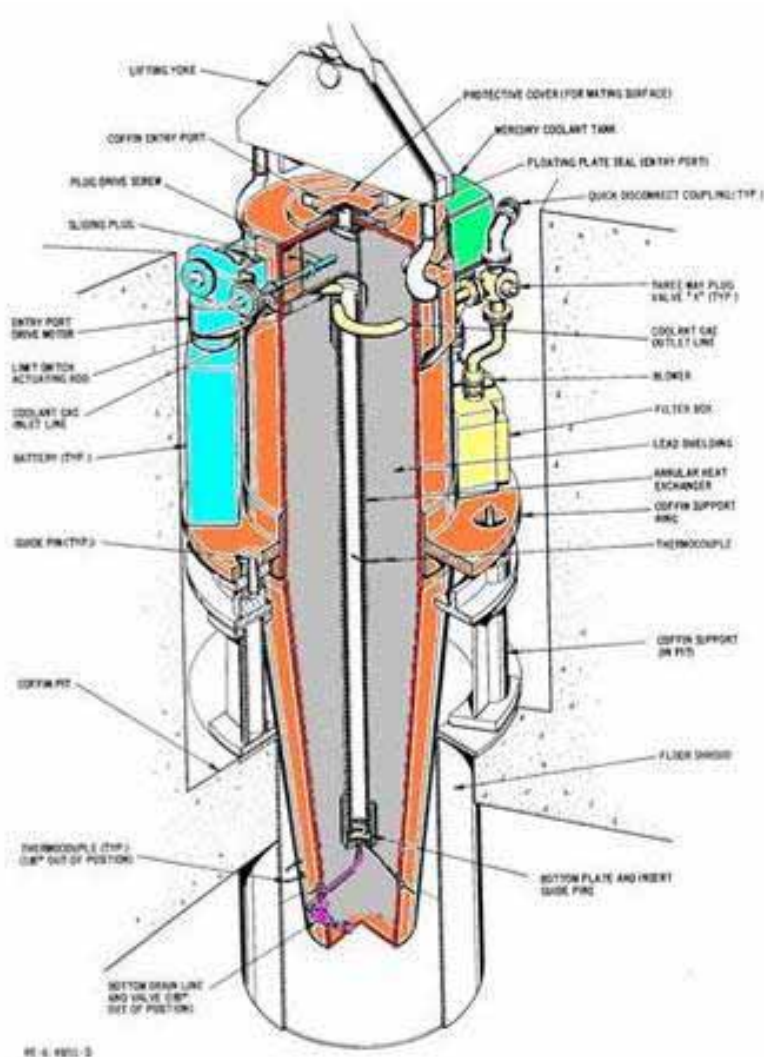


Figure II.7-16 Intra Building Cask

II.7.6 Intra-Building Transfer Tunnel

The intra-building transfer tunnel is a sealed transfer tunnel used to maintain containment of the reactor facility while transporting IBC's to the fuel cycle facility (Figure II.7-1). The tunnel atmospheric pressure is kept slightly below the reactor building. Each end of the tunnel is hermetically sealed and has interlocked doors to maintain containment. The tunnel door in the reactor facility is opened and an IBC is brought from the IBC pit area and placed on the tunnel carriage system. The tunnel door is then closed and sealed. This carriage includes a conveyance system to move the IBC between facilities. Once the carriage reaches the other end, the door is opened and the IBC is removed. At this time another empty IBC can be transferred back to the reactor for reloading, or the door can simply be closed and sealed while the empty carriage returns.

The intra-building transfer tunnel is located on the nuclear island and therefore utilizes the base isolation system.

II.7.7 Fuel Handling Operation

Prior to reactor startup, fuel assemblies will be preloaded in the core barrel and in the storage rack. At the time of core assembly replacement, the reactor is shutdown and the control rod drives are disconnected and retracted. The rotatable plug is then unlocked and rotated so that the PFHM can access a core position. The arm of the PFHM is extended and centered over the assembly. The entire PFHM is then lowered approximately 38.1 cm (15") to engage the hold down tube with the adjacent assemblies. The gripper mechanism is then lowered to engage the head of the assembly. The gripper cam spindle is actuated and the gripper jaws are locked around the head. The gripper mechanism is then raised and the assembly withdrawn from the core into the guide tube. The assembly can then be rotated and reinserted, or the machine is ready for the next operation. If the assembly is to be placed in the Storage Rack, the PFHM is raised to its original position, and by rotating the rotatable plug and movement of the PFHM, the spent core assembly is positioned over the rack. The PFHM arm is extended over a storage rack position, and the assembly is lowered into place. Once safely in the rack, the gripper jaws are released using the cam spindle, and the PFHM is free to perform the next operation.

Once the decay heat in an assembly has fallen to a sufficiently low level and is ready for removal from the reactors, the assembly is moved from the storage position to the transfer position. The PFHM is used to remove the assembly from the rack. It is then rotated into position for placement in the transfer position under the FUM. The PFHM can be operated within 350 degrees of the Rotatable Plug movement while the reactor is shutdown and other fuel handling operations outside the reactor are taking place.

As the next step in the assembly removal procedure the FUM is positioned over the transfer port on the cover. The lower section of the FUM is lowered to engage and seal on the transfer port. Once the gap between the doors has been purged with inert gas, the shielding doors on both the port and the FUM are opened. The FUM gripper mechanism is lowered into the reactor above the transfer position of the storage rack. The gripper is then secured onto the assembly and withdrawn into the FUM. As it enters the FUM hot inert gas is used to blow off residual sodium and back into the reactor vessel. The shielding doors on both the port and the FUM are then closed and purged with gas. Next the FUM seal is raised free of the transfer port. While inside the FUM, the assembly is kept cool and inerted during transfer. The FUM is then moved off the reactor cover and positioned over an empty IBC in the pit area. In the same manner as the transfer port, the FUM engages the IBC. Using the gripper inside the FUM, the assembly is placed into the IBC. The gripper retracts back into the FUM and all doors are sealed and purged. The FUM is now ready for the next transfer operation.

The sealed IBC is then moved by the reactor building overhead crane to the intra-building transfer tunnel. The tunnel door is opened and the overhead crane places the IBC on the tunnel carriage. The interlock door is closed and the carriage carries the IBC to the

end of the tunnel and toward the fuel handling facility. The interlocked door at the end is opened and the IBC is removed and placed in the assembly washing station where the residual sodium is removed. Once the residual sodium is removed, the IBC containing the washed core assembly is moved to the air cell where the assembly is removed and placed into storage racks awaiting disposition. The IBC can then be returned to the reactor building for subsequent fuel handling transfers.

II.7.8 Refueling Time

In EBR-II, the spent and new fuels were transported between the core and the in-vessel basket during the normal refueling operation with reactor shutdown (unrestricted fuel handling). The spent assemblies were then unloaded from the reactor vessel to the fuel examination facility by the inter-building coffin (IBC) while the reactor was operating (restricted fuel handling). The durations of unrestricted and restricted fuel handling procedure in EBR-II are shown in Tables II.7-1 and Table II.7-2, respectively [1]. The unrestricted and restricted fuel handling operations took approximately one hour and ten hours per subassembly, respectively.

Table II.7-1 Restricted fuel handling in EBR-II

Item		Time(min)
Preparing		150
Spent Fuel handling	Core to FHM gripper	13
	FHM gripper to TA	6
	TA to basket	11
New Fuel Handling	Basket to TA	10
	TA to FHM gripper	6
	FHM gripper to core	17
Concluding		85
Total		298

ABTR stores the new and spent fuels at the positions around the core barrel to reduce the diameter of the reactor vessel since the basket storage method used in EBR-II requires a large space in the reactor vessel. Thus ABTR must rotate the plug to load and unload fuels to and from the positions around the core barrel with reactor shutdown. Therefore ABTR refueling may take as long as the restricted fuel handling of ten hours per subassembly.

The number of refueling items depends on the number of core components and their number of batches. ABTR has 24 inner and 30 outer core assemblies with the batch numbers of 12 and 15 respectively. Thus ABTR changes two inner and two outer core subassemblies during every refueling. Including other items such as test fuel assemblies and control rods, following items are expected to be exchanged:

- Inner core subassembly: 2
- Outer core subassembly: 2
- Test Fuel subassembly: 0 or 1
- Test Material subassembly: 0 or 1
- Control Rods: 0 or 1
- Total: 7 (maximum).

Table II.7-2 Unrestricted fuel handling in EBR-II

Item		Time(min)
New Fuel Handling	Load new assembly in temporary coffin	30
	Transport FUM to temporary coffin	5
	Load new assembly in FUM and	
	Transport FUM to fuel transfer port	130
	Prepare assembly insertion	3
	Assembly insertion	33
	FUM gripper to transfer arm	7
	Transfer arm to basket	12
Spent Fuel Handling	Basket to Transfer arm	10
	Transfer arm to FUM	35
	Conclude unloading	5
	Transport FUM to coffin pit	10
	FUM to IBC	15
IBC Handling	Transport IBC to FEF	165
	Return IBC to coffin pit	135
Total		595

The maximum refueling time is estimated to be 70 hours. The refueling time can be reduced by installing extra IBC's, or additional new fuel handling facilities. An extra IBC can reduce the refueling time dramatically since it allows that a parallel operations of IBC transportation and fuel transportation between the reactor vessel and IBC. The critical path with two IBC's is the IBC transportation time of 300 minutes, while the spent fuel transportation time from the FUM to IBC is 15 minutes. Therefore, the refueling time per subassembly is estimated to be 315 minutes (5 hours 15minutes).

Three or more IBC's can only reduce the refueling time from 315 minutes to 295 minutes, since the critical path with three IBC's becomes the fuel transportation time between the reactor vessel and the IBC, as shown in Table II.7-3. Further reduction of refueling time with three IBC's can be achieved by adding a fuel preheating step before the temporary coffin (TC) operation. In the EBR-II refueling scheme, the new fuel was preheated at the FUM, and it took 90 minutes. Thus, preheating an IBC can shorten the refueling time by 90 minutes. In this case, the refueling time per assembly is estimated to be 205 minutes, as shown in Table II.7-4. Instead of three IBC's, a combination of two IBC's and a new fuel buffer zone in the reactor building yields the shortest refueling time of 205 minutes. The new fuel buffer zone can be used to store fresh fuel for one refueling operation, and the fuel preheating operation can be carried out in this facility. For example, Fast Flux Test Facility (FFTF) was equipped with a core component conditioning station (CCCS). In FFTF, new fuels were transported from shipping casks to the CCCS and preheated in the CCCS prior to entry into the sodium system [2].

II.7.9 Spent Fuel Cooling During Transfer Operations

In ABTR, spent fuel is transported from the reactor vessel to the fuel cycle facility with an IBC with gas cooling. The current ABTR design has thirty six (36) in-vessel storage (IVS) positions for spent fuel. The cooling time in the reactor vessel depends on the number of refueling items and IVS positions. In every refueling, four driver assemblies and one test fuel assembly are unloaded from the core. Therefore the cooling time in the reactor vessel becomes 7 reactor cycles (28 months). In this case, the maximum decay heat of the spent fuel is estimated to be 1.5 kW per subassembly, as shown in Figure II.7-17.

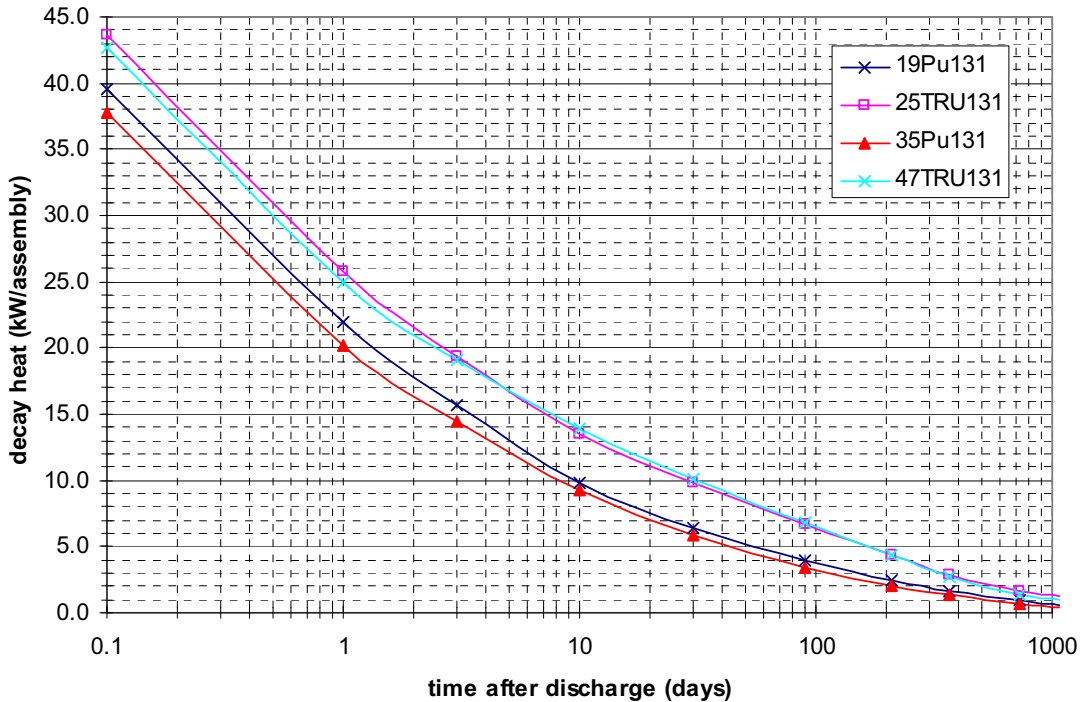


Figure II.7-16 Decay Heat of Spent Fuel

Table II.7-3 Refueling Chart with two IBCs

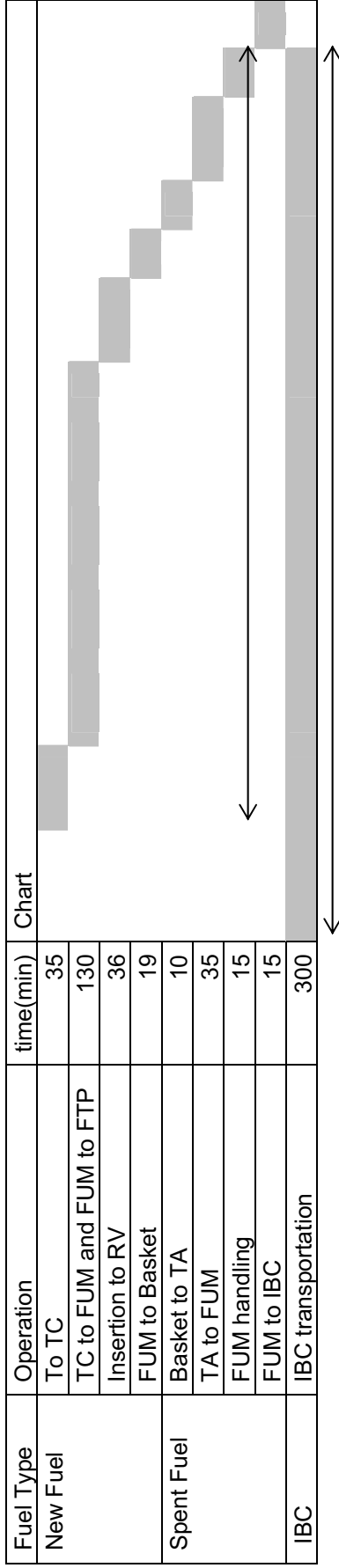
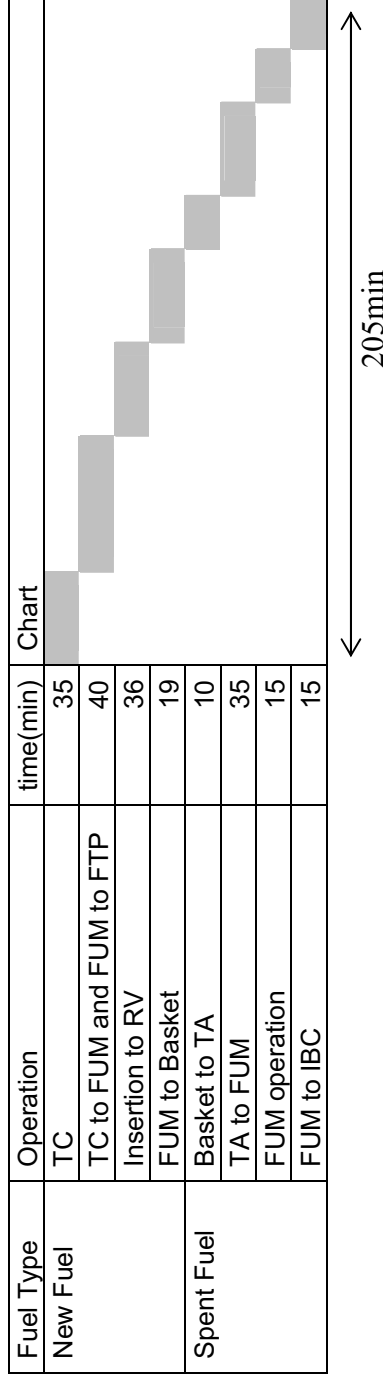


Table II.7-4 Refueling Chart with three IBCs and new fuel preheating before TC



TC: Temporary Coffin
 FHM: Fuel handling Machine
 TA: Transfer Arm
 FTP: Fuel Transfer Port
 IBC: Inter Building Coffin

An analysis has been performed to determine at what assembly decay heat level the assemblies can be moved with the IBCs while relying on passive natural convection cooling and radiation alone. This analysis provided in Section III.9 shows that the maximum assembly power level which the cladding can be maintained below 600°C by combined natural convection and radiation heat transfer mechanisms is ~0.6kW. Thus, active cooling of spent fuel during transfer operations will be required.

II.7.10 New Fuel Cooling During Transfer Operations

ABTR will use pure Plutonium fuel for the initial core loading and gradually install TRU fuel with minor actinide content as operations progress. It means that a new fuel has possibility to give high decay heat. Table II.7-5 shows decay heat levels of various ABTR fuel types. Though the decay heat of the Plutonium fuel is in the range of 0.03 kW per subassembly, the maximum decay heat of the TRU fuels reaches 0.37 kW per subassembly. Although, this value is much smaller than that of spent fuels, the temperature limit of new fuel cladding must be much lower than that of the spent fuel, since no damage to the cladding can be tolerated before core loading. In reference [3], the temperature of new fuel cladding is limited to 375°C to maintain the cladding temperature below the creep temperature of high Chromium steel. The same criteria can be applied to ABTR since high Chromium steel (HT-9) is also proposed as the cladding material. The analysis provided in Section III.9 shows that the maximum assembly power level which the cladding can be maintained below 375 °C by combined natural convection and radiation heat transfer mechanisms is ~0.2kW. Thus, active cooling of TRU fuel during transfer operations will be required.

Table II.7-5 Decay Heat of New Fuel

Case	19Pu131	35Pu131	25TRU131	47TRU131
TRU enrichment, %	18.81	34.86	24.83	46.70
Peak discharge burnup (MWd/kg)	130.84	130.83	130.55	130.45
Specific power density (kW/kg)	59.42	120.51	59.42	120.06
Resident time (EFPD)	2202	1086	2197	1087
Total HM mass in core (MT)	4.03	1.98	4.03	1.98
Total driver fuel (including test)	63	63	63	63
HM mass per assembly (kg)	70.06	34.54	70.06	35.54
Decay heat (W/kg)	0.4	0.8	5.3	9.9
Decay heat (kW/assembly)	0.03	0.03	0.37	0.34

Reference

1. EBR-II design descriptions, Volume II, Chapter 5 (1971)
2. D.M. Romrell, D.M. Art, R.D. Redekopp and J.B. Waldo, "FFTF Fuel Handling Experience (1979-1986)", Proc of Fast Breeder Systems, Richland, Washington, Sept. (1987)

II.8 Instrumentation and Control Systems

II.8.1 Flux Monitoring System

The neutron flux monitoring system has several functions: 1) to provide measurements that aid in reactor startup and enable efficient plant control, 2), to monitor reactivity changes during core loading or servicing and 3) to detect abnormal conditions that could threaten the integrity of the fuel. As part of a test reactor, this system also provides neutron flux measurements to characterize irradiation conditions for the test fuel. Thus, the flux monitoring system provides control signals for normal plant operation, signals to the plant protection system, and measurements for the fuel testing program. The system is capable of measuring the neutron flux level at all times and power levels while the core is loaded with fuel.

The main monitoring system functions over a reactor power range of ~1W to over 300 MWt and it consists of three subsystems, each having three redundant neutron detectors designed to measure flux over a specific range. The source range subsystem employs detectors with the lowest flux range and is used when the core power is less than a few kilowatts. The detectors are high sensitivity, BF₃-filled counters that generate a signal proportional to the thermal flux level. The source range subsystem is used during low flux operations such as initial core loading, startup, shutdown, and refueling. The system issues a warning if there is an unplanned approach to criticality such as might occur with a refueling error.

The power range subsystem is active when the reactor is near its nominal full power rating. The detectors are fission chambers optimized for high flux levels and a reactor power in the range of ~100 kW to 300 MW. An intermediate range subsystem with the same type of detectors bridges the other two and is used at power levels between about ~100 W and 1 MW. The range overlap between subsystems allows the operator to verify detector function before switching to a new subsystem.

The detectors of the main monitoring system are located below the reactor vessel at the end of guide tubes that enhance neutron flow to the sensors. (See Figure II.8-1) Lead shielding is used to block gamma rays from ²⁴Na and a layer of borated graphite shields the detectors from (γ,n) reactions. The precise size and orientation of the guide tubes will be selected to optimize the sensor signal/noise ratio. Previous experience with Superphénix has shown that such an ex-vessel detector configuration can be designed to have very little sensitivity to coolant temperature.

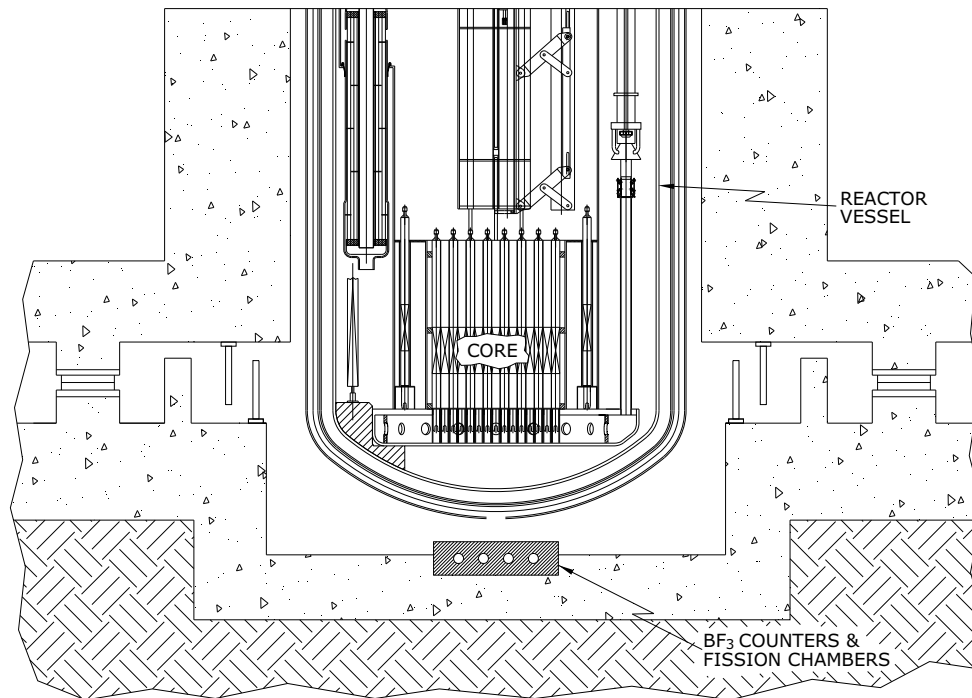


Figure II.8-1 Ex-vessel flux monitoring system layout

A system of in-vessel flux monitors supplements the main system. These detectors are held within steel thimbles mounted on the rotating plug. The system includes BF_3 detectors for low flux levels to be used during the initial fueling and startup when the reactor shutdown power, along with the neutron flux to the ex-vessel detectors, is at a minimum. These sensors may be retracted from the thimbles for high power operation to prevent a loss of sensitivity due to activation. Additional thimbles can be reserved to test detector designs or record flux levels at a particular location as an element of a fuels test.

II.8.2 Heat Transport Instrumentation System

The instrumentation system provides information on the state of the heat transport system so that the operator can control the reactor in a safe, economic, and efficient manner. A subset of the instruments is dedicated to the plant protection system so that the reactor can be shut down automatically following excursions beyond accepted operating set points.

Temperature

The majority of the sodium coolant temperature measurements are made with chromel-alumel, insulated junction type thermocouples. The sensors are mounted within stainless steel thermowells for protection and to provide a robust boundary for the sodium. Both the thermocouples and thermowells are swaged at the tip to create the

desired time response for each measuring station. In addition, the sensors are spring loaded against the bottom of the thermowell to improve time response.

Individual thermocouples will be used to measure the outlet temperature of each core subassembly. A total of 66 chromel-alumel type thermocouples are used for the 60 fuel and 6 test subassemblies. These sensors provide protection against local cooling deficiencies caused by flow blockages or equipment malfunctions. Abnormal conditions within a subchannel can be indicated by either excessively high temperatures or the presence of increased signal noise caused by subchannel boiling. In addition to the safety function, the thermocouples on each assembly permit determination of the core power distribution through the use of an energy balance.

Certain system calibration operations benefit from higher sensor accuracy than that obtainable with thermocouples. These include in-situ flow meter calibration and measurements to establish an accurate relationship between neutron flux readings and core power output. Higher accuracy is obtained by using resistance temperature detectors (RTDs). Like the thermocouples, the RTDs are mounted within stainless steel thermowells for protection against the sodium.

Level

Level is measured in the hot and cold pools, the intermediate loop expansion tanks, and the two main system dump tanks. A subset of the pool sensors is made up of short range units to measure level under normal operating conditions when the reactor vessel sodium inventory is at its nominal level. Some of these sensors are reserved for the plant protection system to measure hot-to-cold pool level difference. This is one of the methods used to confirm proper operation of the primary pumps. Other sensors are long range, extending down near the bottom of the reactor vessel, and are used for filling and draining operations. Level meters are also used in the intermediate loop to monitor sodium inventory and provide an early alert to large-scale leaks. Each level meter uses an inductive sensor mounted within a steel well for protection.

Flow rate

At this conceptual design stage, both mechanical and electromagnetic (EM) type pumps are being considered for the main coolant pumps. If mechanical pumps are chosen, the flow rate will be inferred from measurements of motor speed and the pump performance curve. For EM pumps, the flow rate is a function of the supplied current, which can be accurately measured with electrical equipment outside the vessel. Level meters in the hot and cold pools are used as backup flow indicators. For full flow operating conditions, the level difference between the hot and cold pools is about 2 m.

Flow rates through the intermediate heat transport loops are measured with permanent magnet flow meters located on the cold legs. A U-shaped magnet assembly provides the magnetic field and electrodes attached directly to the pipe wall carry the flow rate signal.

The electrodes are made of the same material as the pipe to avoid thermally-induced potentials.

Core thermal power

Thermal power of the entire core is found using flow rate and the average temperature rise of the coolant:

$$P_{core} = \dot{m} c_p \Delta T_{avg}$$

where \dot{m} is the core mass flow rate and c_p is the specific heat of the sodium. The power outputs of individual subassemblies can be calculated using coolant temperature measurements at the subassembly outlets:

$$P_i = \alpha_i \dot{m} c_p \Delta T_i$$

where ΔT_i is the difference between the measured outlet temperature for the i^{th} subassembly and the average inlet temperature. The parameter α_i accounts for the flow distribution through the various subassemblies and it is determined by a core design code.

Pressure

The intermediate loop will be operated at a pressure slightly higher than that of the primary system so that tube leaks in the IHX will not result in a transfer of radioactive sodium from the primary to secondary side. The operating pressure of the intermediate loop will be measured with pressure transducers connected to the main piping via NaK-filled capillaries. The pressure of the cover gas within the reactor vessel is measured with conventional pressure transmitters.

II.8.3 Radiation Monitoring System

The radiation monitoring system measures and records radiation levels in the plant and surroundings to ensure the safety of plant personnel and the general public during normal operating conditions and in the event of a plant malfunction. The system detects and measures the concentrations of airborne radioactivity and monitors activity levels in liquid and gaseous effluents. The system also provides alarms when radiation levels exceed acceptable limits.

A portion of the radiation monitoring system serves the plant safety system by providing sensor signals that can be used as trips in the event of accidental radiation release. Radiation monitors trigger containment isolation in the event of a sizable radiation release within the containment. The radiation monitoring system is also used to survey the reactor cover gas to check for elevated fission gas levels that could indicate fuel failures, and to detect fuel handling and criticality accidents.

II.8.4 Impurity Monitoring and Analysis System

The overall performance and reliability of the plant can be affected by the level of impurities within the sodium coolant. This occurs through its influence on the properties of structural materials and cladding, component performance, the malfunction of mechanisms, and other factors. The role of the impurity monitoring system is to continuously measure the sodium impurity level within the pool and intermediate heat transport loop. The impurity monitoring system is able to enhance plant availability and economic performance by predicting or preventing problems associated with chemical impurities.

The principal measurement system for impurity monitoring is the well-known plugging meter. With this system, a small amount of sodium is shunted to a bypass loop where it passes through a temperature-regulated section containing an orifice. Under a constant driving pressure supplied by an electromagnetic pump, the flow rate through the bypass loop is determined by the size of the orifice. Cooling the sodium within the temperature-regulated section causes impurities to precipitate and collect within the orifice, which reduces the flow rate. The saturation temperature of the impurities is close to the temperature at which the initial decline in flow rate is observed and this temperature is an indication of the sodium impurity level. Once the flow decline is detected, the cooling system is deactivated to allow an increase in sodium temperature, dissolution of the impurities, and reestablishment of the nominal flow rate in preparation of another measurement. The system automatically cycles between flow rate set points and can repeat the measurements indefinitely. The plugging meter can also be run in a continuous, rather than cyclic mode in which the temperature is regulated to maintain partial plugging.

Figure II.8-2 shows the basic layout of the impurity monitoring and analysis system. Plugging temperature indicators are used for both the pool and intermediate loop. To monitor sodium from the pool, fluid is pumped continuously from the reactor vessel cold pool. A fraction of the flow is shunted to the plugging temperature indicators and returned to the sampling line. A similar system is operated on the intermediate heat transport loop cold leg. Plugging temperature indicators are placed both before and after the cold trap to measure the general level of system impurities and to monitor cold trap performance.

The plugging temperature indicators can generally provide only the saturation temperature of the precipitating impurities, but not their chemical composition. For a more detailed analysis of the coolant, a sodium sampling system is used. The system diverts a portion of the sample stream to a system of valves that permit the collection of the sample in a receptacle that is then taken to a laboratory for detailed laboratory analysis. The analysis provides the concentrations of tritium, corrosion products, particulates, and fission products. Because the primary sodium is radioactive, the corresponding sodium sampling system must be operated remotely and shielded sample

receptacles must be used to protect personnel. A cell is included in the Reactor Building for the impurity monitoring and analysis equipment.

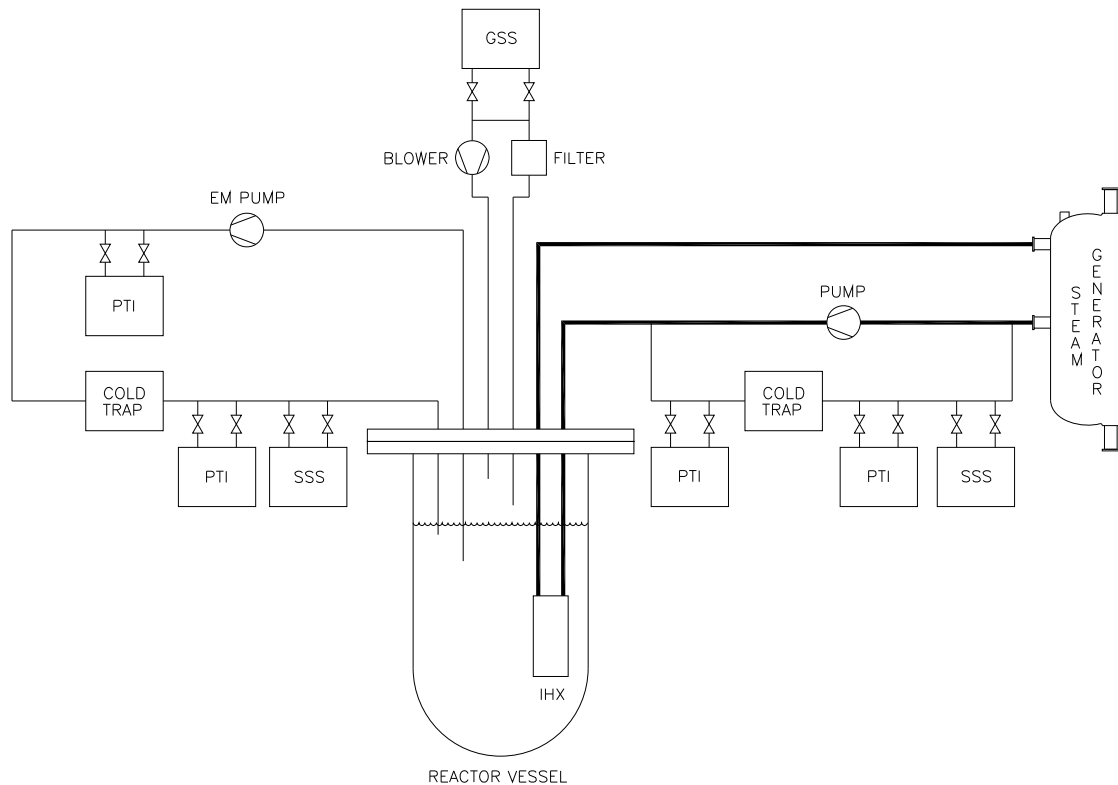


Figure II.8-2 Schematic of impurity monitoring system.

Figure II.8-2 also shows a cover gas sampling system that is used to monitor the impurity level in the argon cover gas within the reactor vessel. Cover gas is pumped continuously in a circuit with a filtering stage to eliminate sodium vapor and aerosols. A portion of the clean gas is shunted to the CSS where sensors such as oxygen and humidity sensors measure the air and water content of the gas. These sensors are able to provide a prompt indication of air leakage into the vessel. The system is also equipped to extract samples for laboratory analysis by filling evacuated bottles. The bottles are shielded to protect personnel since fission gases may be present in the cover gas.

II.8.5 Leak Detection System

The leak detection system is required to assure safe reactor operation, protect equipment, and enhance plant availability through early fault detection. This system is not required to shutdown the plant, remove decay heat, or prevent off site radiation exposure and so it is not classified as a safety system. The leak detection system is required to detect small leaks (10-100 g/hr) within a time frame of tens of hours, and large leaks (> 1 kg/min) within minutes. The system is also designed to provide the

general location of the leak. A wide assortment of sensors is necessary to monitor the diverse elements of the plant and to provide prompt detection.

Leakage faults can be divided into three general categories, each requiring a particular set of instruments for fault detection:

- Loss of sodium from the primary system or intermediate heat transport loop into the guard vessel or reactor vessel, respectively, depending upon the fault location
- Water leakage from the tube side of the steam generator into sodium
- Sodium leakage between the intermediate heat transport loop and the reactor pool.

The first class of faults is dealt with using a combination of level sensors, cable detectors, and an assortment of atmospheric monitors distributed throughout the reactor enclosure. Level sensors in the pool and intermediate loops register large-scale losses of sodium. Cable detectors, which are placed in the guard vessel and below tanks and intermediate loop piping, can discern more moderate leaks. These detectors are stainless steel sheathed cables with a central conductor and mineral oxide insulator. Holes in the sheath allow leaked sodium to come in contact with the conductor, causing an electrical short between the electrode and sheath which alters the signal from the no fault condition. Aerosol detectors are used to identify both small leaks and moderate-sized ones that are missed by cable detectors. Two types of aerosol detectors are employed. One is a sodium ionization detector that uses a hot filament to ionize liquid metal aerosols and vapor. An increase in aerosol concentration produces a corresponding rise in ion current, indicating the presence of a leak. The second type of detector operates as an aerosol collection system in which sample gas is passed through a membrane filter at a constant flow rate. Any aerosols present in the sample gas are filtered, which raises the pressure drop across the filter and provides an indication of a leak.

Water leakage from the high pressure secondary side into the sodium of the intermediate heat transport loop is detected by measuring the level of hydrogen within the sodium. Hydrogen detection is based upon the diffusion of hydrogen through a thin-walled nickel membrane. A carrier gas flows by the membrane at a low rate so that an equilibrium hydrogen concentration is established within the gas. The carrier then flows to a hydrogen measurement system. Hydrogen concentration within the sodium is proportional to the square root of the measured hydrogen pressure. The system measures hydrogen concentrations in the range of ~0.1-10 ppm. Oxygen is measured with ceramic electrolytes that act as electrochemical cells to provide a low level voltage signal that can be related to oxygen concentration. These sensors operate on the same principle as conventional electrochemical oxygen sensors with one electrode immersed in the sodium and the other a reference gas (or oxide).

Leakage between the intermediate heat transport loop and the reactor pool can, in principle, occur in either direction through a breach in the IHX. However, the operating pressure of the intermediate loop is, under normal conditions, higher than the pool

pressure to prevent leakage of radioactive sodium into the intermediate loop. Though such leakage is unlikely, radiation monitors on the cold legs between the steam generator and IHXs are able to detect this type of leak. A significant increase in measured activity would provide an indication of probable leaks in the IHX. For the more likely case of leakage from the intermediate loop into the pool, level meters are relied upon to show the accompanying changes in coolant inventory.

II.8.6 Data Handling and Signal Transmission System

The data handling and transmission system is a distributed computing system linking the plant control system with all remaining aspects of plant monitoring, trending, and data analysis. It also provides remote access to plant data and operational status.

Figure II.8-3 shows the basic architecture of the data handling and signal transmission system. The system uses an Ethernet-based network to link PCs to plant databases containing both current and historical plant data. The databases are updated continually by the plant control system (PCS) and are for the use of supervisors, maintenance personnel, regulatory agencies, etc. Though the PCS computers have access to the databases via the Ethernet, other computers will not, in general, be able to access the PCS via the network. In general, access to plant data by anyone other than the operators within the control room is obtained through the data bases on the LAN and not directly through the main control room computers. Remote access privileges to the PCS computers are available to a very limited number of authorized personnel. In all cases, the type of plant data available for access depends upon user privileges.

II.8.7 Plant Control System

The purpose of the PCS is to maintain the neutron flux, coolant flow rates, and other plant processes at levels that meet requirements imposed to ensure safety, efficiency, and protection of plant equipment. The PCS is responsible for plant control during start-up, power generation, shutdown, and standby. It monitors and regulates the neutron flux and compensates reactivity changes resulting from fuel burnup, temperature effects, and other factors. The PCS is responsible for coordinating the operation of nuclear island systems with those of the power conversion system and the auxiliary systems.

A simplified block diagram showing the PCS architecture is included in Fig. II.8.3. The lowest level of the PCS hierarchy is made up of sensors, actuators, and programmable logic controllers (PLCs) linked through a high-speed data bus. Low level control of the actuators is handled by the PLCs while programming of the PLCs and higher level computing functions are managed by computers within the main control room. A main console within the control room provides operator access to the PCS. Redundant systems are used to ensure that operators are able to monitor and direct the PCS under both normal operating and accident conditions.

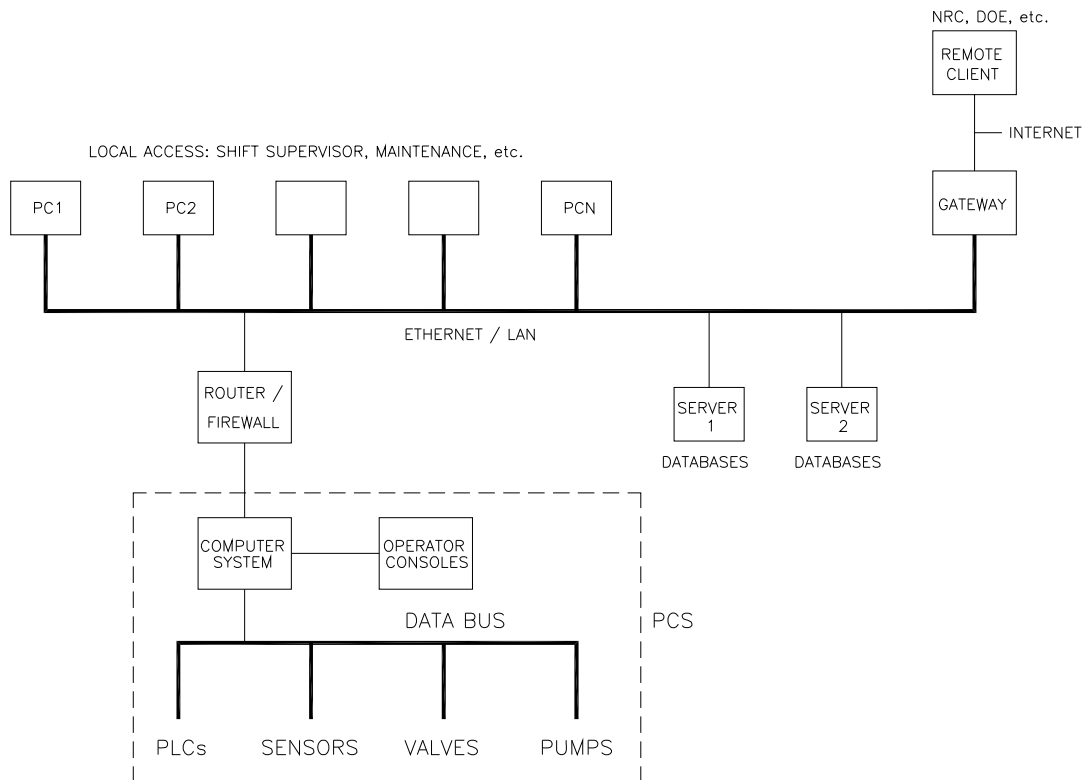


Figure II.8-3 Schematic of data handling and signal transmission system

II.8.8 Plant Protection System

The plant protection system is designed to shut down the reactor when one or more process variables move beyond predetermined thresholds. The system, therefore, limits damage to the reactor, including the fuel, and prevents the release of radioactive materials to the environment by retaining them within either the reactor vessel or primary containment. The plant protection system operates independently of the plant control system.

The sensors used for the plant protection system are separate from those used for plant control. The following parameters are monitored by the plant protection system and used to trip the reactor when an abnormal condition is detected:

- Neutron flux and coolant temperature at core outlet: Protect against overpower transients and prevent high fuel temperatures.
- Sodium level: Scram the reactor upon low pool level indicating coolant leakage from reactor vessel into guard vessel. Scram the reactor on low level in the intermediate heat transport loop expansion tank indicating loss of coolant from the loop.

- Pump status and rate of change of flow rate: Protect against loss of flow and uncontrolled flow changes.
- Intermediate loop pressure and S/G hydrogen levels: Loss of S/G integrity would be indicated by an abnormal pressure increase on the shell side of the S/G and/or detection of hydrogen produced by sodium/water reactions.
- Delayed neutron emission levels in the primary coolant and fission gas concentration in the cover gas: These parameters are indicators of fuel integrity.
- Acoustic signals: Ultrasonic sensors detect the presence of subcooled boiling, which can indicate flow blockages within subassemblies.

The plant protection system also allows the reactor to be scrammed manually. Switches in the control room can be used by the operator to shutdown the reactor at any time.

II.8.9 Communications System

A diverse set of equipment will be available for communication among plant personnel and between the plant and outside agencies. Diversification ensures the ability to communicate during both normal plant operations and in the event of severe plant disruption. The communications system consists of:

- Public address system for intra-plant communications. The system delivers site-wide or localized messages along with alarms such as fire, high radiation, and evacuation alarms.
- Microwave communications system to provide a wireless link between the plant and neighboring DOE facilities.
- Portable radio systems for two-way communications at any plant location. These systems are used for maintenance operations, traffic control, and fire protection. A separate system is used by plant security personnel.
- Security intercom system for closed communications between security personnel at the main security station and remote security stations.
- Offsite law enforcement radio system for communication with outside law enforcement agencies.
- Conventional telephone network for routine intra-plant and inter-office communications.

II.8.10 Industrial Security and Safeguards System

The industrial security and safeguards system is designed to protect plant equipment and personnel, and to prevent the theft of special nuclear materials. The system is designed to defend against the design basis threats specified in regulations. The key requirements for the security and safeguards systems are:

- Allow plant access only to authorized personnel and material
- Prevent the theft of special nuclear materials
- Prevent the sabotage of critical plant equipment
- Deter, detect, and delay unauthorized activities and assaults on the plant

II.8.11 Auxiliary Sodium Systems

In order to ensure long term, safe operations of the sodium systems, the chemistry of the system must be controlled and monitored by a set of auxiliary systems that are common to all liquid metal reactors. Although the chemistry does not affect the nuclear operation directly, it is important for the hydrodynamics of the system as well as for the corrosion and contamination control. One goal is to ensure stable hydrodynamics on the long term to promote an efficient and constant heat transfer, which can be affected by oxide formation or mass transfer within the non-isothermal circuit. Another goal is to ensure the maintenance and component handling easiness by reducing the activated corrosion products.

The following auxiliary sodium systems are included:

- Sodium purification system for purification and monitoring of sodium circuits, such as crystallization and plugging indicators
- Cover gas purification system for purification and monitoring of the argon cover gas
- Sodium sampling and analysis system for contamination monitoring
- Primary and secondary sodium storage system
- Sodium reaction system for component handling, cleaning, and decontamination (located in the Maintenance Building)

The sodium purification deals not only with the hydrogen and oxygen impurities introduced during the initial startup or maintenance operations, but also with other potential source of impurities such as the sodium/CO₂ interaction products.

To minimize the required size of the security force, the plant is divided into nuclear and non nuclear areas, each operated with appropriate levels of security. All safety grade components and systems are located within the nuclear island to minimize the area requiring the highest level of protection.

II.9 Buildings and Structures

Figures II.9-1 shows the overall site plan for the ABTR. Table II.9-1 lists all the site buildings and provides their dimensions and footprint. This site plan is independent of the ultimate ABTR site and does not take into account any existing facilities at a particular DOE site.

Table II.9-1 Site Buildings with Dimensions

Building Name	Footprint (ft ²)	Length (ft)	Width (ft)	Height (ft)
Security Gate House	900	30	30	16
Control/Personnel Building	6,319	89	71	30
Reactor Building	7,832	89	89	-
Brayton Cycle Building	3,336	72	46	49
Emergency Generator Building	375	25	15	12
Balance of Plant Service Building	2,250	50	45	20
Cooling Towers (each)	2,352	48	48	33
Radwaste/ Maintenance Facility	6,000	100	60	40/80
Lift Station	1,200	40	30	16
Wastewater Treatment Plant	1,200	40	30	16
Interior Security Perimeter Fence	105,896	435	244	-
Exterior Security Perimeter Fence	242,704	616	394	-

II.9.1 Reactor Building

The reactor building, as schematically indicated in Figure II.9-2, encloses the entire primary reactor system and is constructed on a seismically-isolated basemat structure. The building is a reinforced-concrete containment structure that contains an inner reactor containment dome, and is designed for a maximum leak rate of 0.1 %/day at an internal pressure of 10 psig. The reactor building is a conventional reactor containment structure with the reactor vessel assembly located below grade. All of the primary radioactive systems are located below grade within the reactor building.

The major functions of the reactor building are as follows:

- Contain radioactive material following the unlikely event of an accidental radioactivity release from the primary reactor system.
- House and structurally support the reactor vessel, guard vessel, the shield/air baffle cooling system, support structure of the primary system and temporary fuel handling equipment, biological shielding, and associated equipment and structures.
- Provide adequate space for the operation, maintenance, and removal of equipment housed within the containment structure during periodic maintenance.

- Facilitate sodium and non-sodium fire protection for all safety equipment; this includes separation of redundant systems required for safe shutdown and for maintaining the reactor in safe shutdown condition.
- Provide protection for all safety equipment from the environment and natural phenomena such as floods, winds, tornadoes, and earthquakes.
- Maintain pressure within the containment boundary at less than 0.5 psig negative with respect to the exterior, except during pressurization accidents.
- Limit leakage from the containment boundary to no more than 0.1% of its contained volume per day at an internal pressure of 10 psig.
- Maintain the integrity of the containment boundary during all design loadings, including a maximum long term containment atmosphere temperature of 50°C under normal operating and design basis accident containment atmosphere conditions.

Containment Design Requirements

The reactor building will be designed to the rules of the current ASME Boiler and Pressure Vessel Code, Section III, Division 2, “Code for Concrete Reactor Vessels and Containments,” Subsection CC for concrete containment. These rules provide for: material, design, fabrication, construction, examination, testing, marking, stamping, and preparation of reports for prestressed and reinforced concrete containment. The containment components covered by the ASME B&PV Code include: (1) structural concrete pressure resisting shells and shell components; (2) shell metallic liners; (3) and penetration liners extending the containment liner through the surrounding shell concrete.

Additionally, the reactor building must be designed for natural hazards, such as an earthquake, wind and flood. The design must also conform to the NRC regulatory guides (Federal Regulations 10 CFR 50 and 10 CFR 100) for seismic and other natural hazards.

Penetrations and Transfer Openings

A large number of penetrations through the reactor building shell are required for access of personnel, equipment, freight, electrical conductors, and service fluids. These penetrations are grouped into three broad classifications: large mechanical penetrations, small mechanical penetrations, and electrical penetrations. These penetrations use pressure-tight seals consisting of appropriate materials. These seals are protected from the building atmosphere since this atmosphere could become hot enough to destroy the seals should a major sodium/air reaction occur. All seals are designed to withstand the same maximum pressure of 10 psig for the building. To provide adequate assurance that the total leak rate of the reactor containment boundary remains less than the design value of 0.1% of the free volume per day, selected penetrations are leak tested annually.

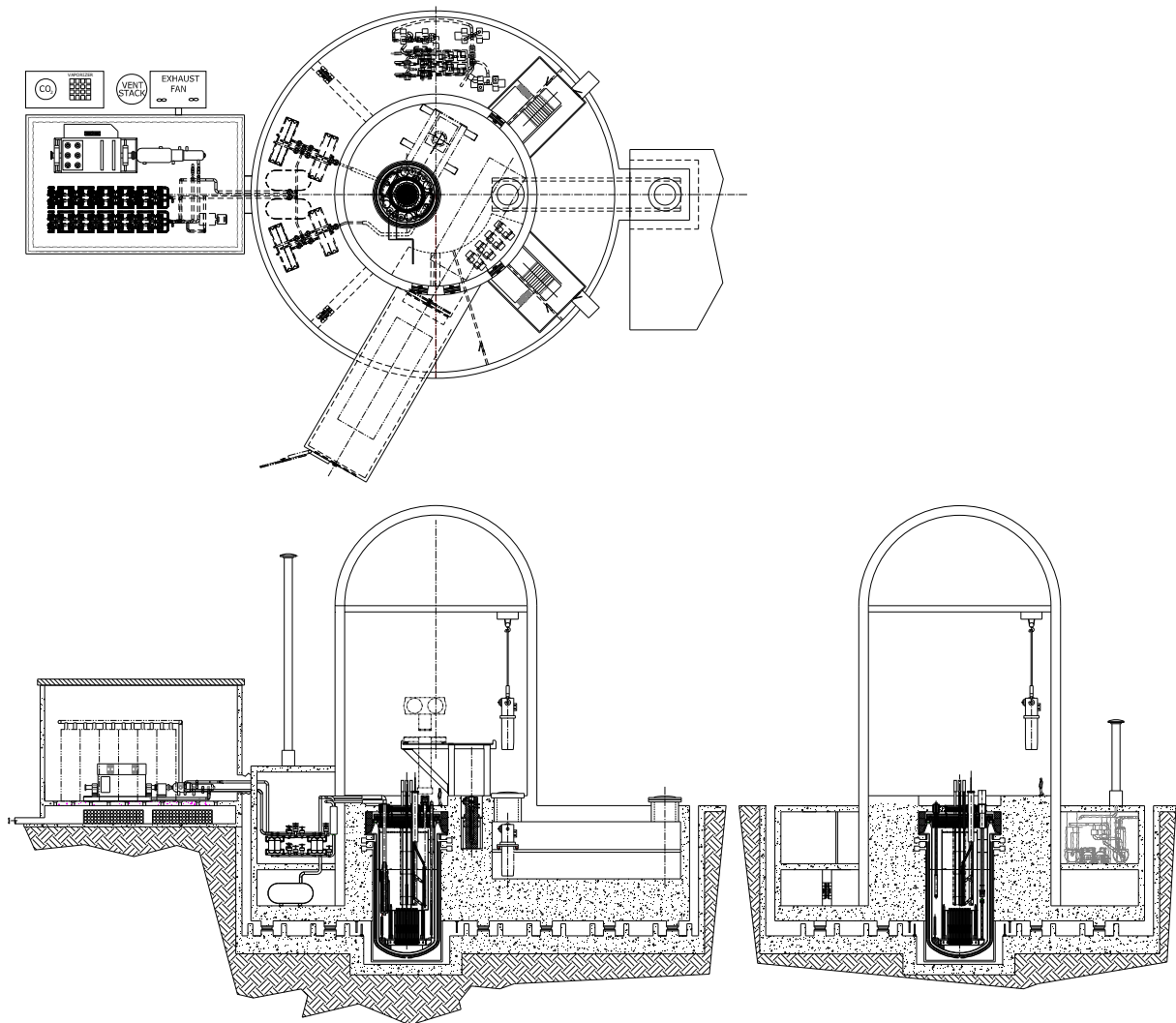


Figure II.9-2 Plan view and vertical views of the reactor building

The large penetrations are comprised of three airlocks (personnel, emergency personnel, and equipment airlocks). The airlocks allow equipment and personnel access to the reactor plant while maintaining building containment integrity at all times. All airlocks are cylindrical steel-welded shells that have a sealed door at each end. The doors are electrically or mechanically interlocked to allow only one door at a time to be opened. The equipment airlock is the largest of the three; it connects the reactor building to an equipment transfer location outside the facility. The personnel airlock is smaller than the equipment airlock; it connects the operating floor area of the reactor plant to the control/personnel service building and serves as the normal personnel entrance and exit. The emergency airlock is the smallest of the three. It provides an emergency exit from the reactor building should the personnel airlock become blocked. All airlock doors are periodically pressure tested.

Cooling Requirements

The shutdown heat removal system transfers the decay heat from the bulk sodium in the reactor vessel directly to the atmosphere through heat exchangers located on the outside of the reactor building. Therefore, there are no unusual cooling requirements for the reactor building internal atmosphere. A standard heating, ventilation and air conditioning (HVAC) system maintains the internal atmosphere around 22°C at all times.

II.9.2 Balance of Plant Building System

The balance of plant building is approximately 13m x 22m x 15m high and consists of an upper and lower level. The upper level is fabricated on a slab or grate with sheet metal over frame construction and no windows. The building's heating and air conditioning system maintains an ambient temperature for the enclosed equipment and maintains a slightly negative atmosphere pressure relative to outside. This negative pressure ensures that minor CO₂ leaks in the Brayton cycle system (if a Brayton cycle system is adopted) will be contained within the structure. The building also includes an overhead bridge crane with a capacity sufficient to provide maintenance or removal of equipment.

All ventilation equipment is located adjacent to the building to deliver air for cooling of the generator and ambient temperature control for the building.

The lower level is located below grade. It is sized to contain 2 m³ of CO₂. There are holes in the upper floor which open to this area. In the event of a leak, this enables dense CO₂ to sink and collect in the lower level. Sensors on the lower level detect the gas and turn on exhaust fans to evacuate the CO₂ through a stack for dispersal. Another option may be ducts to carry the gas away from the site or to a scrubber device. The lower level also contains the inventory control tanks and the letdown tanks which are part of the Brayton cycle system on the upper level. Access to this lower level will be for inspection of the tanks or maintenance purposes only.

II.9.3 Control Room and Personnel Building

The reactor control building is a multi-story building adjoining the reactor building. This concrete and steel tornado-hardened, Seismic Category 1 structure, houses the control room, technical support center, and the central computer for the overall plant. It also includes space for switchgears, cable routing rooms, motor-generator sets, heating, ventilating and air conditioning equipment, compressed air and other auxiliary systems. Fire protection/suppression systems are also provided.

II.9.4 Radwaste/Maintenance Building

The radwaste/maintenance building is a slab-on-grade sheet metal high bay structure that provides two areas, a waste management area and a maintenance area. The waste

management area is sized and designed to handle the collection, treatment, staging and shipment for disposal of all regulated wastes generated at the site. Waste will be generated from on-going and periodic maintenance work during the life of the plant. Equipment will exist in this building to condition the waste streams that are expected to be generated from the plant.

The maintenance side of the building provides space and equipment for the routine and planned maintenance of the facility and equipment. The maintenance building also has a location in the structure where large components will be assembled prior to installation in the reactor building. A rail spur provides easy access and delivery of components such as the reactor vessel module, primary pumps, intermediate heat exchangers, and Balance of Plant system equipment to the maintenance area during installation and checkout of the primary and secondary systems. After the facility has been constructed, the maintenance building will then have space and equipment for performing routine and non-routine maintenance of the reactor primary and secondary systems.

II.9.5 Security Building

The security building is a single-story reinforced concrete non-seismic category structure located outside of the administration and service building with a reinforced concrete slab located at grade. The windows are made from bullet-proof glass.

The security building provides a controlled means of access to the plant site to prevent inadvertent access, industrial sabotage or the theft of nuclear materials. All personnel must pass through this building and be checked by the associated security systems for ingress and egress to sensitive plant structures/areas, or areas where radioactive materials are stored. The plant security system is monitored and operated from this building. A truck trap is located adjacent to this building that allows for security force control and containment of trucks requiring access to the site for deliveries or pickups.

II.9.6. Emergency Generator Building

A gas or diesel generator building is located adjacent to the reactor control building. It houses a two modular 1 MWe generator that provides emergency power to the primary and secondary systems upon demand. The emergency generator buildings are shipped as single integrated units that can be quickly installed at that site and made operable to support the construction activities during the facility construction, emergency power during reactor operations, and as an alternative source of power during reactor decommissioning.

II.9.7 Balance of Plant Services Building System

The balance of plant service building provides space for equipment that supports the Brayton cycle building, cooling towers, and other services. This includes recirculation

pumps, water conditioning equipment, air compressors, electrical switchgears, motor control centers, plant heating systems, and other support equipment.

II.9.8 Lift Station and Waste Treatment Plant Building

The lift station building provides pumps and filtration system to pump water from the river (or other suitable cooling water source) to the plant for use in cooling and domestic water services. All wastewaters go through the wastewater treatment plant where the water is conditioned prior to being discharged into the river.

II.9.9 Seismic Isolation System

When an earthquake occurs, the seismic waves travel through the ground where the reactor is supported causing the reactor structures to shake back and forth with the ground. For this reason, reactor structures must be designed to sustain the inertia force generated by the vibration. The earthquake motion obviously depends on the characteristics of the site where the reactor is located. This makes the seismic design of the reactor site-dependent. However, it is desirable to standardize the reactor structure design regardless of seismic conditions. To make this standardization feasible, the site specific seismic design has to be decoupled from the structural design. This can be achieved by incorporating a base isolation system into the reactor structure. These base isolators can be tuned (adjusting its period of vibration) so that the reactor structure will experience about the same magnitude of the seismic loading irrespective of the site.

The fundamental principle of base isolation is to provide a layer with low horizontal stiffness between the structure and the foundation so that the structure is decoupled from the horizontal components of the earthquake motion. This layer gives the reactor structure a fundamental frequency that is much lower than that of the same reactor structure without this soft layer. Also, this fundamental frequency is much lower than the predominate frequencies of the ground motion. As a result, the ground motion transmitted into the structure is modified (the isolator functions as a low pass filter). The high frequency contents in the ground motion will be filtered out along with the high energy associated with these frequencies. Since the base isolator has low horizontal stiffness, a large horizontal displacement will take place during the earthquake. This large displacement needs to be accounted for in the structural design; therefore, in ABTR a trench with a seismic gap of 90 cm is built around the reactor structure to accommodate this horizontal displacement.

There are three technical challenges for designing a base isolation system for ABTR. These challenges are listed below.

1. The footprint of the ABTR reactor structure is small. Therefore, the number of base isolators that need to be installed as well as the size of the base isolator are limited. As a result, the load carried by each base isolator is high. The preliminary design of ABTR indicates that this load is about 600 metric tons. If a

safety factor of 1.5 is considered, 900 metric tons would be the design load for each isolator.

2. The ABTR site will be used in a remote rural area where the weather temperature may be below freezing during winter. The mechanical properties of the isolator must be stable during the temperature change.
3. The weight of the ABTR reactor structure is not a constant during the entire life of the ABTR. The fundamental natural frequency of the base isolator system must be insensitive to this weight change.

Seismic isolators are classified as either elastomeric or sliding. Elastomeric isolators include high-damping rubber bearings (HDR), low-damping rubber bearings (RB) or low-damping rubber bearings with a lead core (LRB). Sliding isolators include flat assemblies, the friction-pendulum system (FPS) or the multiple friction-pendulum system (MFPS). The difference between the FPS and MFPS is that the FPS has a single concave surface whereas the MFPS consists of two facing concave surfaces. As a result, the MFPS can accommodate a larger relative displacement at the isolator level.

In ABTR the sliding isolators are chosen in favor of the elastomeric isolators for the following reasons.

1. With a design load of 900 metric tons, the size of the elastomeric isolator would be about two meters in diameter. This may cause difficulties for the manufacturer of the rubber bearing because the damping of the rubber bearing comes from a chemical compound added into the natural rubber. The bigger the rubber bearing, the longer the curing time. This makes quality control of the bearing difficult.
2. The mechanical properties of the rubber bearing will be degraded in a cold temperature environment. This is based on the actual performance of rubber bearings in real earthquakes. During the 1995 Kobe earthquake in Japan, the rubber bearings installed in the Matsumura Gumi Laboratory building did not attenuate the ground motion because the ambient temperature was 0°C, and the isolator area was not heated [1].
3. The fundamental natural frequency of the elastomeric isolator is a function of the weight of the structure. As a result, the performance of the base isolator system depends on the weight of the structure.

Among the sliding isolators, the MFPS is chosen to be used in the ABTR. The MFPS consists of doubled concave sliding surfaces and an articulated slider with a hinge mechanism. The hinge mechanism is to guarantee that the super structure always remains vertical during an earthquake. The system mimics the kinematics of a pendulum, forcing the structure to rise slightly as it moves horizontally. This movement generates a restoring force to return the super structure back to its original position. The energy is dissipated by friction. The isolator is made of stainless steel and is capable of carrying a large load. The fundamental frequency of the isolator is independent of the weight of the structure (it depends on the radius of curvature of the concave surface), and the operating temperature of the isolator is from -125 °C to 250 °C. Therefore, the MFPS meets all the three challenges mentioned above. In addition, since the movement of the structure

always starts from the mass center of the structure, the torsional response is minimized [2]. Note that the MFPS possesses characteristics of both elastomeric and sliding type base isolators in reducing the seismic response. The advantages of MFPS over HDRB are summarized below.

1. Period is independent of the structural weight
2. Design is simpler
3. Torsional effect is minimum
4. No buckling concerns
5. Durable (made of stainless steel)
6. Wider working temperature range
7. Quality control is easier

The reactor design can be standardized by incorporating the MFPS in the reactor structure. The period of the MFPS may be adjusted for the same reactor design to be used at a different site.

Note that the MFPS is a 2D isolator. It means that it provides reduction for the horizontal seismic loading only. It does not reduce the vertical seismic loading. A three-dimensional seismic isolation is not proposed herein for the following two reasons.

1. The reason for inserting the steel shim plates into the laminated rubber bearing is to increase the vertical stiffness of the isolator. However, isolation in the vertical direction is achieved by reducing the vertical stiffness. These two ideas contradict each other.
2. The vertical isolators will introduce additional rocking vibration to the structure. In 1969, the Swiss Full Base Isolation-3D system was installed for an elementary school in Skopje, Yugoslavia. The building bounced and rocked backwards and forwards during an earthquake [3]. Therefore, the vertical isolator is not recommended in any building codes.

However, several 3D isolators were developed in Japan recently [4]. These 3D isolators are currently under review. The 3D isolators may be proposed in the future if they are proved to be effective in reducing the seismic loadings with no adverse side effects.

The seismic isolator used in the ABTR is the multiple friction pendulum system (MFPS) shown in Figure II.9-3. It consists of a lower and an upper sliding surface shown in Figure II.9-4, and two sliders (shown in Figure II.9-5) in between the two sliding surfaces. Every component is made of stainless steel. The isolator is designed for a vertical load of 900 metric tons. With a safety factor of 1.5, the allowable vertical load for each isolator is 600 metric tons. The seismic response spectrum used in the design is the site-independent response spectrum given in ASCE 4-98 [5] for horizontal motion. The response spectrum is scaled to 0.3g Peak Ground Acceleration (PGA) with 5% damping. The size of the isolator is 100 cm in width by 100 cm in length (square shape) with a height of 35 cm. The radius of curvature for the lower and upper sliding surfaces

of the isolator is designed such that the period of the isolator is 3 seconds, and the maximum allowable seismic displacement is 30 cm. A moat (silo) with a seismic gap of 90 cm is built around the reactor structure to accommodate this displacement with substantial margin. Each seismic isolator is inserted at the mid-height of a 120 cm by 120 cm reinforced concrete column that transfers the weight of the super-structure through the isolator to the foundation. These columns provide a 152 cm high space for inspection and maintenance. Each isolator unit is surrounded by four 50 cm by 50 cm concrete pedestals (fail-safe system). The clearance from the isolator to the pedestal is 85 cm. These pedestals function as a physical barrier, in case of a higher than expected maximum earthquake. This is to avoid collision between the reactor structure and the moat wall. These pedestals also serve as temporary supports for the reactor structure when an isolator unit needs to be replaced. In addition, rubber pads will be installed on the moat wall in the radial direction to serve as bumpers in case the concrete pedestals cannot stop the reactor structure from colliding with the moat wall.

The weight of the ABTR reactor structure is estimated to be 11000 metric tons. Each isolator carries 600 metric tons; therefore, a total of twenty (20) isolators are used to support the reactor structure. These isolators are housed in between the basement concrete slab and the foundation concrete slab shown in Figure II.9-6. The arrangement of these isolators is shown in Figure II.9-7.

References

1. Trevor E Kelly, "Base Isolation Structures – Design Guidelines", Holmes Consulting Group Ltd., July 2001.
2. C. S. Tsai, T. C. Chiang and B. J. Chen, "Seismic Behavior of MFPS Isolated Structure under Near-Fault Sources and Strong Ground Motions with Long Predominant Periods", Seismic Engineering-2003, PVP Vol. 466, ASME, Cleveland, Ohio, 2003.
3. Naeim, F. and Kelly, J. M., Design of Seismic Isolated Structures, John Wiley, New York, 1999.
4. Takahashi, Kenji, et, al, "A Development of 3D Seismic Isolation for Advanced Reactor System in Japan – Part 2", SMiRT 18-K10-2, Beijing, China, 2005
5. ASCE4-98, Seismic Analysis of Safety-Related Nuclear Structures and Commentary, ASCE Standard.

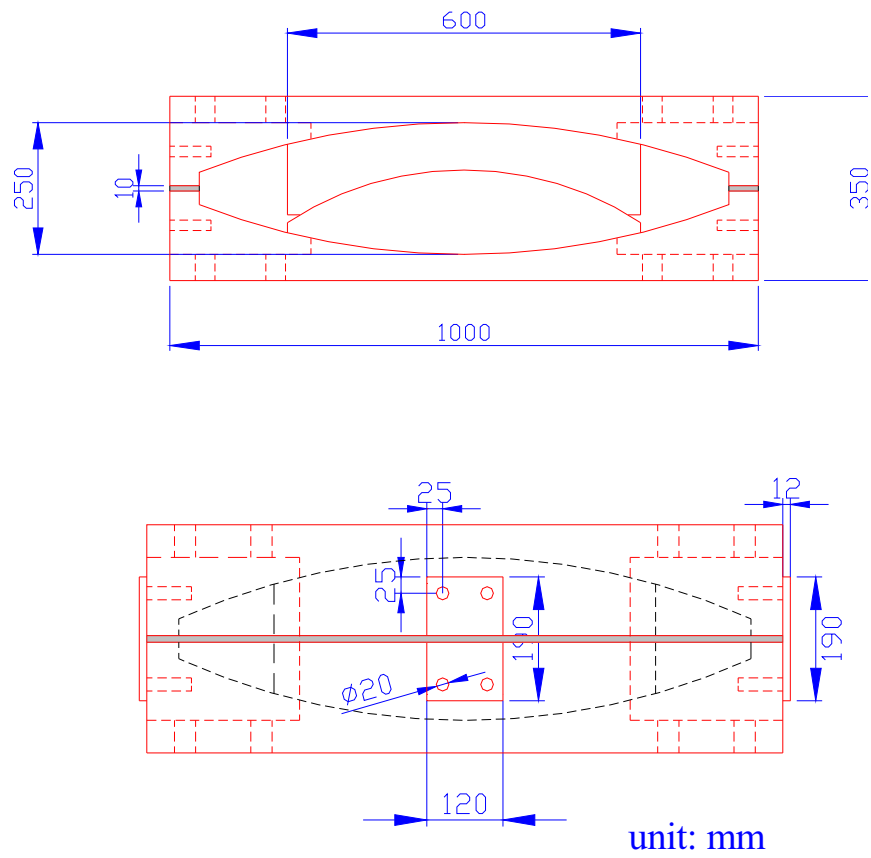


Figure II.9-3 Multiple Friction Pendulum System

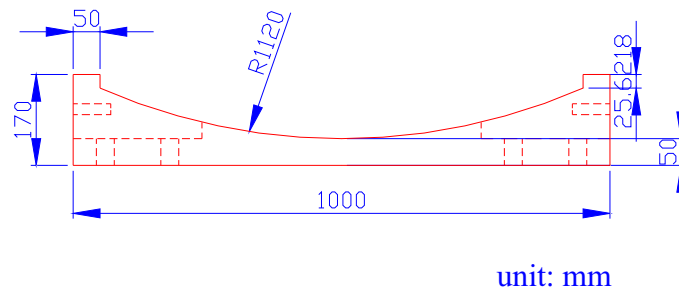
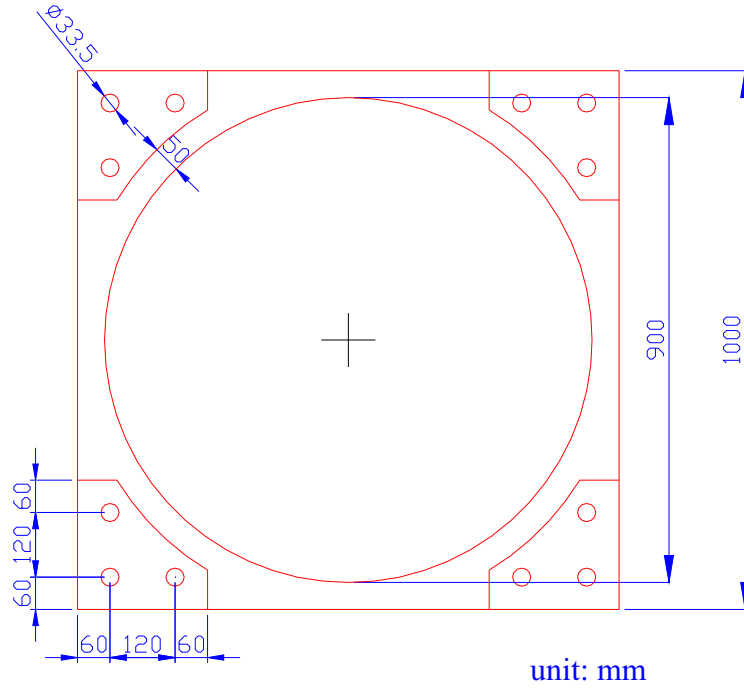


Figure II.9-4 Lower and Upper Concave Sliding Surface

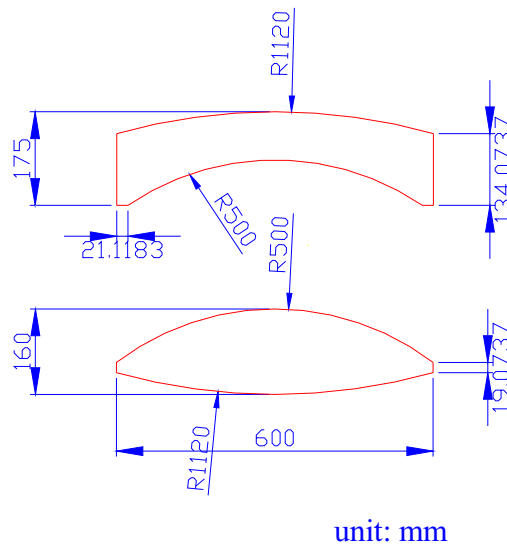


Figure II.9-5 Sliders

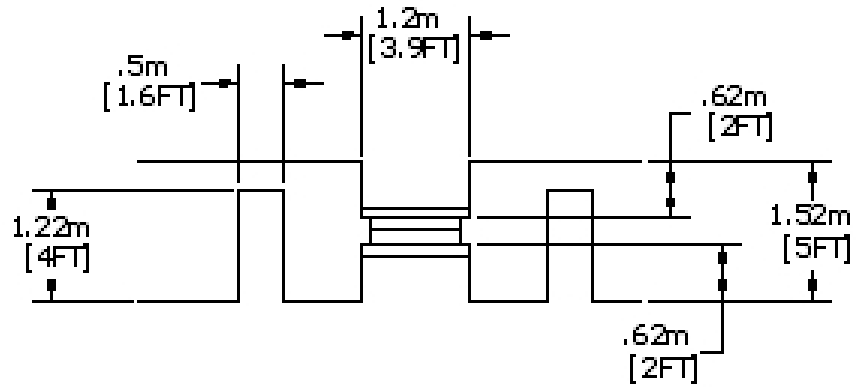


Figure II.9-6 A Typical MFPS Installation: One MFPS isolator with Four Concrete Pedestal Stoppers (Fail-Safe System)

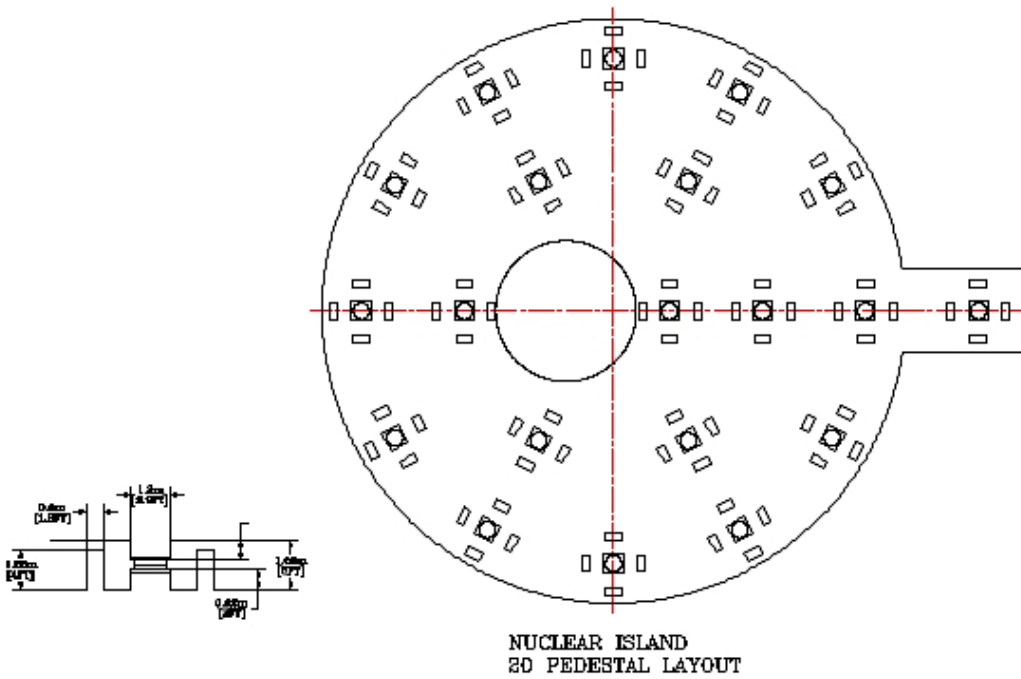


Figure II.9-7 Seismic Isolator Layout

II.10 Balance of Plant Systems

II.10.1 Compressed Gas System

The compressed gas system distributes compressed gases throughout the reactor plant from the point of storage or compression to the point of use. Five subsystems are:

- Service Air System
- Instrument Air System
- Hydrogen System
- Carbon Dioxide System
- Argon Cover Gas System

The service air system provides compressed air for use by various plant systems such as the fuel handling system, maintenance systems, unloading devices, tools, miscellaneous cleaning, and inspection services. The system also delivers breathable air to required stations. The service air system receives compressed air from the instrument air system. The service air system is a distribution system of piping and valves that takes compressed air from the instrument air header and distributes it to the users. The service air system operates at all times providing compressed air during normal plant operation or when the plant is shut down. The service air system is not safety related.

The instrument air system provides clean, oil-free dry air for operation of instruments and controls, pneumatic piston and diaphragm valve operators and air locks in all areas of the plant. The instrument air system operates at all times to provide compressed air during normal plant operation or when the plant is shutdown, since compressed air is required during plant shutdown as well as during normal plant operation. The instrument air system also supplies the service air system. The instrument air system is not safety related. Safety-related items requiring instrument air are supplied from local safety-class accumulators.

The hydrogen system stores and supplies hydrogen gas to the main generator for cooling the generator stator core and rotating field during operation (if needed). The hydrogen system is not safety related.

The carbon dioxide system stores carbon dioxide in liquid form, processes the carbon dioxide liquid to carbon dioxide gas, and supplies the gas to the main generator for purging. The carbon dioxide system is not safety related.

The argon cover gas system stores argon in liquid form, processes the argon liquid to argon gas, and supplies the gas to the reactor building and fuel handling facility for inert gas operations, such as reactor vessel cover gas, cell inerting, IBC inert gas, and fuel unloading machine inert gas, among others.

II.10.2 Chilled Water System

The chilled water system provides chilled water during normal plant operation for air conditioning and removal of heat from the following areas or systems:

1. Nuclear island (NI) HVAC and balance of plant (BOP) HVAC system.
2. Process cooling in the NI maintenance building.
3. Recirculating gas system.

The system includes chillers, pumps, expansion tanks, piping, valves, and related components. A refrigerant pumpout and storage system is also provided for maintenance. The system does not include air cooling coils in air conditioning units nor heat transfer equipment in process cooling systems. Cooling water for the chiller condensers is provided by the plant service water system.

The chilled water system is not safety grade and is only needed for routine plant operation. The total loads have not been evaluated in detail, but based on previous ALMR designs it is estimated that the total cooling load will be 1000 tons of refrigeration. The system will consist of three 500 ton cross-connected chiller systems. Two of the systems will normally be in operation with one system on standby.

The chilled water system consists of a single large central system to serve buildings with both constant and seasonal cooling loads. The system has three centrifugal chillers each of approximately 50 percent total system capacity and connected in parallel so that one chiller is available as a standby. Each chiller has a circulating pump, piping, valves and controls. The normal chilled water system has a single loop with branches to several buildings. The chillers and their accessory equipment are located in the Balance of Plant Services Building. The piping supply loop runs from the Balance of Plant Services Building through the control building around the reactor containment building with branches to the buildings served by the system. Branch piping within the buildings is direct return except where long runs would make balancing difficult.

The type of system selected is consistent with large industrial type systems that are commercially available today. The chilled water system described above is sized for a pool plant and is therefore smaller than a similar loop-sized plant. The reduced system size results from elimination of the primary heat transport system cell cooling load.

II.10.3 Essential Chilled Water System

The essential chilled water system provides chilled water for removal of heat during plant normal and off-normal operation from the following systems:

1. Portions of the nuclear island (NI) HVAC system.
2. Portions of the control and personnel services building heat removal system.

The essential chilled water system shall be designed as two independent closed chilled water loops each with a 100 percent capacity water chiller, heat exchangers, recirculating pump, expansion tank, piping, valves, instrumentation, and controls. The components of one loop shall be separated from the components of the other loop, in accordance with single failure criteria. The essential chilled water chillers shall be designed with a minimum of 25 percent refrigeration margin. The essential chilled water system shall be available during or following all normal, upset, emergency, and faulted events of plant operation.

The essential chilled water system supplies and distributes chilled water (42°F) to the various components that are required for maintenance of the safe shutdown condition. This system operates during normal and emergency plant operation. The essential chilled water system has two 100 percent capacity redundant closed loops, each with one mechanical refrigeration centrifugal water chiller, one circulating pump, one expansion tank, and one air separator, complete with interconnecting piping, valves, instrumentation, and controls. Chillers and pumps are located in the Control and Personnel Services Building (east and west). Piping loops with separation as required are run with branches to the various buildings served. All returns are direct. Temperature control valves are located near each piece of equipment served.

The essential chilled water system described above is smaller compared with loop plants. The system size has, however, been reduced by 40% because of the elimination of the primary heat transport system cells.

II.10.4 Radioactive Waste System

The radioactive waste system provides the equipment and facilities for collecting, processing, monitoring, storing, and disposing of liquid and solid radioactive wastes. The radioactive waste system consists of liquid radioactive waste subsystem and solid radioactive waste subsystem. The radioactive waste system is located in the radwaste/maintenance building. Equipment within the building will be located and arranged in a manner which isolates the operating and maintenance galleries from the equipment to achieve as low a level of personnel radiation exposure as is reasonably achievable.

The liquid radioactive waste subsystem collects radioactive liquid waste for processing, recycle or disposal; provides sample points and equipment to monitor the chemical and radioactive content of liquid wastes; processes and concentrates radioactive liquid waste; stores processed or reclaimed liquid for reuse or disposal; and controls discharges to assure compliance with applicable regulatory standards.

The solid radioactive waste subsystem receives and measures the radiation levels of small low activity level components from other systems and determines temporary storage, processing or disposal requirements; compacts, packages, and prepares compactible radioactive solid wastes for disposal; establishes the necessary interfaces with other systems for packaging and disposal of large noncompactible radioactive

solids; and develops an inventory control system that provides for accountability of radioactive materials.

The following general design requirements shall apply:

1. The general system design shall provide as-low-as-reasonably achievable (ALARA) radiation protection for maintenance and plant operating personnel
2. The system shall have the capability to monitor and record discharges to the environment.
3. The equipment and its associated supports are to be classified as nonseismic.
4. The quality of the discharged water shall comply with the governing water quality standards.
5. Prior to discharge to the environment, a laboratory analysis of all liquids to be discharged to the environs shall be performed to assure that the activity requirements for such discharges are met.
6. An acid and caustic solution supply, neutralization and pH control system shall be provided, with the capability to adjust the pH of all liquid wastes which are collected, prior to further processing.
7. Receive radioactive sodium generated by the fuel handling and fuel receiving, storage and shipping systems.
8. Provide control functions for the LRWS and SRWS to maintain the design, operating and performance parameters during all operating modes.

II.10.5 Nuclear Island Heating, Ventilating, and Air Conditioning System

The nuclear island (NI) heating, ventilating, and air conditioning (HVAC) system maintains environmental conditions within design limits throughout the noninert areas of the nuclear island buildings, and in conjunction with the radiation monitoring system (RMS) and plant protection system (PPS) limits the release of radioactive materials from the nuclear island buildings.

The NI HVAC system maintains the temperature, humidity, pressure, and cleanliness of the air atmospheres in the various building spaces during normal plant operation; maintains, as necessary, the temperature, humidity, pressure, and cleanliness of the air atmospheres in the areas containing safety-related equipment during normal plant operation and during off-normal conditions; in conjunction with the RMS and PPS, maintains the release of airborne radioactive materials to the outside environment below acceptable limits during normal operation and off-normal conditions; and limits the intake of hazardous airborne materials into certain safety-related and occupied areas, such as the control room.

All safety-related ventilation trains shall consist of two redundant 100% capacity equipment trains that are designed to Seismic Category I requirements. No single failure

of any active component of the safety-related subsystems will result in loss of that subsystem's safety-related functions.

II.10.6 Balance of Plant Heating, Ventilating, and Air Conditioning System

The balance of plant (BOP) HVAC system provides heat, ventilation, cooling, humidity control, pressure, and control of airborne contamination or any combination of these functions to the BOP buildings or portions of buildings as required for proper operation of equipment and for personnel comfort.

The BOP HVAC system consists of several subsystems serving various areas of the BOP buildings, each performing specialized functions as required for the area served. Each subsystem consists of combinations of various basic components as required to satisfy the performance requirements for that sub-system. These basic components include air handling units, fans or blowers, cooling and heating coils, filters of various efficiencies, duct work, dampers, isolation valves, carbon absorbers, instrumentation and controls, and other accessories as required.

Facilities served by the BOP HVAC system include:

1. Balance of plant building
2. Fuel handling facility
3. Nuclear island cooling tower pump house
4. Fire protection pump house
5. Switchyard relay house
6. Circulating water pump house
7. Balance of plant services building
8. Radwaste/maintenance building
9. Gate house
10. Emergency generator buildings
11. Water treatment plant
12. Sewage treatment plant
13. Well water pump house

II.10.7 Fire Protection System

The fire protection system provides the means to prevent, control, and mitigate the consequences of plant fires through the following general functions - detect fires, or incipient fires, activate alarms, suppress fires, extinguish fires, isolate and confine fires, protect personnel from smoke and heat and protect safety-related systems and components to assure continued readiness and operation.

The fire protection system is comprised of two subsystems: the sodium fire protection system, which addresses sodium or sodium-potassium fires; and the non-sodium fire protection system, which addresses fires of non-alkali metal origin or involvement.

The sodium fire protection system provides the means for detecting, locating, confining, suppressing, and extinguishing sodium and NaK fires. Special requirements imposed by the presence of sodium and NaK in the plant result in employing special fire protection methods. These methods include passive catch pans and fire-suppression decks, and manually operated portable fire extinguishers.

Fire detectors and associated instrumentation are used to inform the plant operator of the existence and location of a fire. The effectiveness of these fire protection methods for limiting fire losses and the spread of airborne contaminants is augmented by fire barriers, fire doors, fire dampers, low-leakage penetrations, and similar isolation devices provided by the building design, and by the heating and ventilation system.

The fire protection water supply system provides water at the design pressure and quantity to the sprinkler, deluge, and water spray systems, and the yard hydrants. The water storage tanks, fire pumps, and hydrants are all nonseismic Category I components. One seismically qualified (Seismic Category I) pump, taking its suction from two seismically qualified (Seismic Category I) storage tanks, provides water at the design pressure and quantity to special service wet standpipes located in buildings and areas of the plant containing systems, equipment and components essential for reactor safe shutdown.

II.10.8 Recirculating Gas Cooling System

The recirculating gas cooling system (RGCS) provides gas cooling capability to the inerted fuel handling machine - fuel transfer tubes system in the reactor building and to the fuel handling cell in the fuel handling facility. The RGCS provides heat removal from cell and equipment by forced circulation in closed loops.

The RGCS provides heat removal from the inert gas atmospheres of the fuel handling and storage cells in the fuel handling facility and the fuel handling machine in the reactor building and intra-building cask system.

Each RGCS subsystem acts as an extension of the cell pressure and leakage boundary and thereby limits potential release of radioactive materials to the environment. Connections are provided to the inerted gas system for pressure control and gas sampling and to the nuclear island heating, ventilating and air conditioning system for deinerting air supply and exhaust. The RGCS is capable of recirculating and cooling cell atmosphere air during periods when the cells are deinerted and occupied.

The fuel handling and storage cells subsystem operates to maintain temperatures within the cell. Heat loads include decay heat from fuel assemblies and lighting loads. Cell temperatures are also maintained within design limits in the event of a design basis fuel handling accident. This subsystem together with the cell liner and penetrations seals, maintains a very low leakage barrier to contain the products of a design basis accidental release of radioactive materials.

The safety-related cooling circuits consist of two-100 percent capacity equipment trains that are redundant, separated from each other, and are designed to Seismic Category I requirements. No single failure of any active component of a safety-related cooling circuit results in loss of the cooling.

II.10.9 Fuel Receiving, Storage, and Shipping System

The fuel receiving, storage, and shipping system located in the fuel handling facility receives, inspects, stores, and prepares new core assemblies, including fuel, reflector, control, and radial shield assemblies, for insertion into the reactor; makes selected measurements on irradiated core assemblies and prepares irradiated core assemblies for shipment to an off-site location; provides inventory control for all core assemblies at all times within the plant; and is capable of cooling fuel assemblies for an indefinite period during transfer operations.

Also provided is the instrumentation and control system that is used to operate the FRSSS and the fuel handling system. This system interfaces closely with the fuel handling system, the reactor service building, and the liquid metal auxiliary system.

New core assemblies enter the fuel handling facility are unloaded from their shipping containers and inspected, and are temporarily stored in the air cell. From the air cell, they are transferred to the reactor building for staging prior to core loading. After reactor shutdown for refueling, the fresh core assemblies are loading into the reactor vessel and stored outside the core barrel in the spent fuel storage positions.

II.10.10 Feedwater and Condensate System

This system is applicable only for the steam Rankine cycle. The feedwater and condensate system collects water from the main turbine and auxiliaries, where its available thermal energy has been extracted, conditions it, and returns it to the steam generator at design temperature and pressure. The feedwater and condensate system is not safety grade.

The feedwater and condensate system provides high purity feedwater to the steam generators. Condensate from the hotwell is delivered via the condensate pumps to the deaerating heater after being processed by the condensate polishing subsystem and the low-pressure heaters. The deaerating heater storage tanks provide the source of feedwater for the main feedwater pumps. The main feed pumps take the fluid, increase the pressure, pump it through the high-pressure heater shells to increase the temperature to the specified level, and deliver it to the steam generator system where it is converted to superheated steam. Some steam is returned to the feedwater heaters via the extraction steam subsystem, for heating condensate and feedwater, and to the main feedwater pump turbine drives. The exhaust from these turbines, along with the cascaded drains from the feedwater low- and high-pressure heaters, is returned to the main condenser. All heater

drains are cascaded to the condenser to ensure that feedwater chemistry specifications are met.

The steam generators are not required for shutdown heat removal. Thus, emergency feedwater pumps, protected condensate storage, and attendant safety-grade components, structures, and buildings are not required.

II.10.11 Main and Auxiliary Steam System

The main and auxiliary steam system transports the steam produced by the steam generators to its point of use and extracts its available thermal energy, primarily in the main turbine, but also in auxiliary equipment. Included within this system are those systems that are needed to support the operation of the main turbine generator.

The main steam system takes superheated steam from the steam generator system and transports it to the high pressure turbine of the turbine generator. The system includes provisions for steam dump to the condenser following a turbine generator load rejection or turbine trip to prevent a reactor trip. The steam dump also provides a flow path for main steam during plant startup until the steam reaches conditions or quality required for other uses.

The steam dump portion of this system takes steam from the manifold, bypasses the turbine, and dumps the steam into the condenser. The steam dump arrangement is a part of the turbine bypass system. The steam dump system includes desuperheaters and steam dump control valves to desuperheat the steam and control the flow of steam into the condenser in accordance with the control of the reactor.

The extraction steam system conducts steam from the high pressure, the intermediate pressure, and the low pressure turbines to the reheat tube bundles in the moisture separator/reheaters and the feedwater heaters. The extraction steam system also supplies steam to the auxiliary steam system. The extraction steam is required for feedwater heating to increase cycle efficiency. The system also removes moisture from the turbine to provide water erosion protection for the low pressure turbine blades. The turbine-generator converts the thermal energy generated in the reactor to electrical energy. The turbine is provided with two moisture separator/reheaters with two stages of reheat in each moisture separator/reheater unit.

The generator is a liquid-cooled stator type with a capability of 100 MWe gross at rated turbine conditions of inlet steam at 2,200 psig and 850°F exhausting at 1.6 in. of mercury absolute mean effective exhaust pressure with zero makeup and five stages of extraction.

The turbine generator auxiliary systems provide supportive services to the turbine-generator to provide needed cooling, sealing, lubricating, and control functions to sustain the operation and assure the maximum efficiency of the turbine generator.

The auxiliary steam system provides steam for various process uses and heating throughout the plant during plant startup, normal plant operation, and plant shutdown. The auxiliary steam system receives its steam from one of three sources. During normal operation, the steam is supplied from the extraction steam system through a pressure reducing valve. When the extraction steam pressure is too low, auxiliary steam is supplied from the main steam system through a pressure reducing valve. If neither extraction steam nor main steam is available, auxiliary steam is supplied by the auxiliary boiler.

II.10.12 Circulating Water System

The circulating water system provides cooling water flow to the main condenser and the turbine plant component cooling water heat exchangers to remove waste heat rejected by the turbine-generator cycle. The circulating water rejects this waste heat to the atmosphere by means of mechanical draft cooling towers.

The circulating water system is capable of removing the design heat load placed on the turbine condenser or Brayton Cycle heat exchanger. The system also removes the heat load rejected through the turbine plant component cooling water heat exchangers. The circulating water system is capable of removing the heat load from a 50 percent steam dump occurring at summer design condition. The safety classification of the circulating water system piping, equipment, and components is non-safety grade. Provisions are made to isolate portions of the system for major maintenance without removing the generating unit from operation.

The circulating water system provides cooling water for the main condenser and the turbine plant component cooling water heat exchangers. Circulating water pumps in separate bays in a pumphouse take suction from a flume connecting the cold water basins of the mechanical draft cooling towers. Cooled water is pumped through a pipeline to the main condenser and back to the cooling towers. Turbine plant component cooling water pumps, in a separate bay, pump water through a pipeline to the turbine plant heat exchangers and discharge into the circulating water pipe downstream of the main condenser.

II.10.13 Service Water System

The service water system consists of three subsystems, namely: the turbine plant water, the nuclear island service water, and the turbine plant component cooling water. All three of these subsystems are closed loop cooling systems and in total their function is to provide cooling for all plant systems and components except the main turbine condenser. With the exception of the nuclear island service water subsystem, the heat load is rejected to the recirculating water system. The nuclear island service water subsystem rejects heat to two separate cooling towers.

The turbine plant water and turbine plant component cooling water subsystems are non-safety grade. The nuclear island service water subsystem is safety grade. It is possible to isolate portions of the system for major maintenance without removing the generating unit from operation.

The nuclear island service water subsystem shall be designed to meet the single failure criteria.

II.10.14 Treated Water System

The treated water system receives raw water from the well water system and supplies various levels of treated water for the entire plant needs. The principle plant water needs are: makeup water for the main cooling towers, demineralized water, and potable water.

This system consists of piping, tanks, valves, instrumentation, and controls necessary to supply the quantity and quality of water to operate, maintain, and protect the plant.

II.10.15 Industrial Waste Water Treatment System

The waste water treatment system collects, treats, and disposes of all nonradioactive liquid plant wastes originating from the plant floor drain system, lube oil storage area drains, auxiliary boiler, chemical storage area drains, the makeup water treatment system, the condensate polishing system, and sanitary waste system.

The system is comprised of pumps, tanks, valves, instrumentation, and controls necessary to treat the waste water coming from the above nonradioactive liquid plant wastewaters.

II.10.16 Liquid Metal Auxiliaries System

The liquid metal auxiliaries system receives, melts, and transfers to storage all sodium delivered to the site; receives, stores, purifies, and distributes all NaK; provides the pumps and piping to transfer sodium and NaK; and provides the pumps and piping to fill and drain all sodium and NaK systems.

Separate, independent, purification capability is provided, as necessary, for the primary sodium, and for the sodium in each of the two intermediate heat transport system loops. There is no permanent connection between primary sodium components and intermediate sodium components.

The sodium and NaK receiving system receives all sodium and NaK needed by the plant. The sodium receiving system provides the capability to melt the contents of a sodium tank car, or sodium drum, and transfer it to the system to be filled. The capability to transfer NaK from drums to storage vessels and to circulate and purify NaK during system loading and cleanup is also provided by the system.

The primary auxiliary liquid metal system provides purification (cold trapping) for sodium used in the reactor vessel and the primary sodium plugging temperature indicator system and primary sodium sampling system.

Two NaK-cooled, primary sodium cold traps are supported by shield plugs in nozzles in the reactor vessel and immersed in the primary bulk sodium. An EM pump is located between the shield plug and the cold trap in each unit. During normal plant operation, one trap is in use and the second is on standby.

The intermediate auxiliary liquid metal system provides purification of the sodium in each of the two IHTS loops. The system also provides the piping to accomplish the filling and draining of each intermediate sodium loop.

II.10.17 Inert Gas Receiving and Processing System

The inert gas receiving and processing system provides inert gases and vacuum, as required by other systems of the ABTR, including: (1) cover gas, (2) cell-inerting atmospheres, (3) valve actuation gas in inerted cells, (4) cooling gas, (5) gas for certain seals, for component cleaning, and other services, and (6) vacuum for liquid metal transfer and gas analysis purposes.

The argon gas distribution subsystem is composed of liquid argon storage tanks, pressure control valves, stop valves, piping, vapor traps, filters, and relief systems. Argon is distributed to the reactor building, balance of plant building for use as a cover gas in the intermediate heat transport system (IHTS), IHTS cold traps, and SWRPRS rupture disc areas (for steam plant applications). Argon is distributed to the auxiliary buildings for use as the cover gas for DRACS NaK expansion and drain vessels. All the cover gas cell and equipment spaces that require argon use recycled argon to minimize consumption. The level of radioactivity in the recycled argon gas is reduced by the radioactive argon processing system to a level such that it will not cause a radiation hazard.

The nitrogen gas distribution subsystem is composed of liquid nitrogen storage tanks, vaporizers, pressure control valves, stop valves, piping, filters, and relief systems. Nitrogen gas is used for inerting the annulus between the reactor vessel and the guard vessel. It is also used for steam generator water-side purging.

The radioactive argon processing subsystem is composed of a vacuum vessel, vacuum compressors, a surge vessel, charcoal absorber vessels, piping, pressure control valves, stop valves and particulate filters. It is located in shielded cells in the lower level of the reactor building. The radioactive argon processing subsystem cleans up the argon gas that is normally vented from the reactor cover gas space, and the FUM and IBC such that the gas can be safely recycled with an acceptable radiation hazard to personnel external to the recycled helium piping.

II.10.18 Other Auxiliary Systems

II.10.18.1 Reactor Vessel Heating System

Four electrical reactor vessel immersion heaters provide supplementary heating of the bulk primary sodium to maintain a minimum sodium temperature of 120°C whenever the reactor is not operating at sufficient power to make up for the total heat losses from the primary system. Heaters are also required during the initial sodium fill and startup.

Each heater is installed through a heater nozzle in the reactor vessel cover. Power to the heaters is supplied from 480V 3-phase AC power or, if necessary, by an emergency diesel generator.

II.10.18.2 Shield and Thimble Cooling System

Normally, the heat induced in the biological shield, air baffle tank, and primary support structure, by losses from the reactor vessel bulk sodium, is dissipated by the shield cooling system. The shield cooling system consists of two basic systems operating in parallel: an air recirculating and cooling system and an exhaust air system. Power is normally supplied by the 480V distribution system. If this were to fail, power to the exhaust air system would be supplied by an emergency generator, and to the air recirculating and cooling system by another diesel generator. This shield cooling system also has alternate blowers and air conditioning equipment which is automatically switched on if a failure of the primary units were to occur.

A total heat load generated for the most part by heat losses from the reactor vessel sodium to the surrounding biological shields, is dissipated by the forced circulation of cooling air provided by the shield cooling system. The reactor vessel top support structure, the insulated top surface of the reactor vessel cover, and component nozzles are cooled primarily by the reactor building air which is drawn into the system and flows through ducts to cool these areas.

Recirculated air is made available from the cooling coils and blower and provides cooling for the radial and lower biological shields and the reactor vessel. Since the shield cooling system operates at a slightly lower pressure than the building atmosphere, a certain amount of air in-leakage occurs which simplifies the cooling of certain areas which cannot be connected to a closed system.

A thimble cooling system is provided to maintain the neutron detection instruments, which are positioned in thimbles (not currently shown) next to the core barrel, at a temperature of less than 65°C. Backup cooling includes a standby turbo compressor. If this also fails, thimble cooling can be manually transferred to the shield cooling exhaust system. Operating power for the thimble cooling system is normally supplied from the 480V power distribution system. The thimble cooling loads are automatically transferred to the emergency diesel generator during a loss of electrical power. If neutron detection

instruments can be found that withstand ambient core conditions, then the thimble cooling system can be eliminated.

II.10.18.3 Emergency and Backup Systems

There are emergency and backup systems required to ensure that plant monitoring capability is available and for personnel safety under a loss of electrical power situations. Backup power is also provided for investment protection in certain parts of the plant to reduce the possibility of damage due to high temperatures resulting from off-normal conditions.

The emergency and backup systems are integrated with the subsystems that they service, and are usually peculiar to that system. The majority of emergency backup systems are electrical. These include standby gas or diesel generators, battery backup banks, and standby operating components such as pumps, fans, and blowers. The subsystems that incorporate these emergency and backup components include: primary sodium circulation, shutdown cooling, thimble cooling, and shield cooling.

Flywheels are incorporated into the motor generator sets that provide electrical power to the primary EM pumps. The flywheels provide for an appropriate and specific primary flow coast down that matches the reduction in power during plant shutdown following a scram and assists in the transition from forced flow to convection flow through the reactor.

With failure of the main pumps (loss of flow), the reactor will scram, the motor generator set flywheel will ensure an appropriate pump coastdown to remove the fission product decay heat produced in the reactor. Transition to natural convection will still occur assisted by the motor generator set flywheels. The motor generator set flywheels are located on the pump motor generators sets to maintain power to the pumps during loss of normal and backup power.

The emergency power is supplied by the standby generator. If this power source also fails, a storage battery which is connected in parallel with the rectifier output will operate the pump effectively for approximately 30 minutes. As the batteries discharge, the resulting gradual flow reduction will provide a transition from forced flow to natural convection cooling.

II.11 Electrical Power Systems

II.11.1 Power Transmission System

The power transmission system provides the electrical subsystems for the control and distribution of power between the off-site power system and the station service AC power systems. The generating station can receive AC power from the main generator; from off-site backfeed through the main generator step-up transformers; or from off-site ties through reserve station service transformers.

The power transmission system provides the means for the control and transmission of generator output power to the utility grid through the main generating step-up transformers and the station switchyards.

The system shall be designed so that power can be supplied from the generator output during normal operation, or from the off-site power sources during startup and shutdown, or during maintenance or repair of parts of the normal system. An automatic bus transfer scheme shall be used to transfer from the unit station service transformer to the off-site source for certain loss of power events. The preferred transfer will be to the off-site supply feed through the generator step-up transformers. If this latter supply is lost or unavailable, station service system will automatically transfer to the reserve power supply. The generator load break switch shall be capable of full load current circuit interruption and fault current circuit interruption.

The power transmission system is a nonsafety-grade system and is classified as Quality Assurance Group D in accordance with Regulatory Guide 1.26.

The power transmission system supplies three alternate power connections for the plant station service load. A reserve supply is provided from the off-site system, via two three-winding reserve station service transformers, each 161 kV to 13.8 kV-4.16 kV. The two reserve sources are developed in a 161 kV switchyard. Each reserve source connection from the switchyard is installed in a duct bank or in a concrete lined trench, set in a sand filled earthen furrow, and bridged with precast concrete covers designed with drainage provisions, and protected along roadways, access ways, and removed from major building foundations. Either of these installation methods offers accessibility and protection and is able to accommodate future circuits. Separation of duct banks (or trenches) is required for each reserve source connection (i.e., each has a dedicated installation). Within a duct bank (or trench), control circuits are specified as separate from power circuits. The electrical power interface of the Class IE AC power systems and the power transmission system is located at the Class IE 4 kV switchgear breaker terminals.

II.11.2 Station Power System

The station power system receives power from the power transmission system, provides standby AC and DC power supplies, and distributes power to all building and

equipment loads of the power station. It also provides the plant grounding grids for safety grounding of electrical circuits and building structures. The electrical load of this system is commonly called "the hotel load."

The station power system shall receive power from the power transmission system and provide the transformers and associated switching and control equipment necessary to supply the maximum design station electrical power load.

The station power system shall provide standby AC and DC electrical power capacity sufficient to supply essential loads upon complete loss of power at the interfaces between the power transmission system and the station power system.

Those portions of the Station Power System that provide power to Class IE power systems as defined in IEEE Standard 308 shall meet the requirements of this Standard.

The interfaces between the Station Power System and the systems that receive power from the Station Power System shall be established by interface agreements between the responsible design organizations. These agreements shall be prepared with due consideration for minimizing fragmentation of design and construction responsibility. Similar interface agreements shall be prepared for connection of structures and equipment to the plant grounding grids.

The station power system provides electrical power to all station loads, grounding for electrically energized equipment and plant structures, and lightning protection for the plant. This system consists of standard industrial power plant type equipment necessary to distribute power to the loads. This equipment includes medium voltage and low voltage switchgear buses, medium voltage to low voltage step-down unit substations, distribution transformers and panels, station batteries, and standby turbine-generator units.

The station power system is designed to supply the plant loads at the appropriate utilization voltages. The nominal bus voltages selected are:

1. 13.8 kVAC, nominal, 3-phase, 3-wire, 60 Hz - Power supply for very large motor-driven equipment rated 13.2 kVAC, resistive loads, and unit substation transformers with transformer primary rated 13.8 kVAC nominal.
2. 4.16 kVAC, nominal, 3-phase, 3-wire, 60 Hz - power supply for large motor-driven equipment rated 4.0 kVAC and unit substation transformers with transformer primary rated 4.16 kVAC nominal.
3. 480 VAC/277 VAC, nominal, 3-phase, 4-wire, 60 Hz - power supply for heat tracing control panels and plant lighting.
4. 480 VAC, nominal, 3-phase, 3-wire, 60 Hz - power supply for small motor-driven equipment, lighting, heating loads, and welders.
5. 120/208 VAC, nominal, 3-phase, 4-wire, 60 Hz - power supply for control systems, instrumentation, lighting, communications, and small (generally fractional horsepower) motor-driven equipment.

6. 250 VDC, nominal 2-wire - power supply for DC motor-driven equipment.
7. 125 VDC, nominal 2-wire - power supply for control systems, instrumentation and annunciation.
8. 120/208 VAC nominal 3-phase, 4-wire, 60 Hz, uninterruptible power supply for control and instrumentation which must be continuously energized under all plant operating modes.

The station power system is radial in configuration, that is, there are no bus ties, double-ended substations, or primary selector switches.

Each medium voltage bus (13.8 kV and 4.16 kV nominal) has at least two transferable incoming supplies. One supply is from one of the two Unit station service transformers; the second supply is from one of the two Reserve Transformers. Power can be supplied to the 13.8 kV and 4.16 kV buses via the Unit station service transformers from the main turbine-generator (Plant Power Supply) with the generator circuit breaker closed, or from an off-site power source via the generating switchyard and main transformer with the generator circuit breaker open or from the reserve transformer. The off-site power via the generating switchyard is considered the preferred power supply, because it serves as the first access to the utility power transmission grid upon plant trip and is consistent with utility terminology.

The station power system delivers the maximum total continuous plant power requirements from the plant, preferred or reserve power supplies. All 480 VAC nominal unit substations are fed from medium voltage buses through unit substation transformers; and 480 VAC nominal motor control centers are fed from 480 VAC unit substations. Voltage at unit substations and motor control center buses is adjusted by no-load tap changers at the USS transformers to ensure acceptable voltage regulation.

The 120/208 VAC and 277/480 VAC nominal power and lighting panels are fed from the 480 VAC nominal motor control centers through dry type distribution transformers. Voltage at the power and lighting panels is adjusted by no-load tap changers at the distribution transformers to ensure acceptable voltage regulation.

The standby AC power system is divided into two load groups known as Division 1 and 2 that are powered from two gas turbine-generator units. One generator unit feeds Division 1 and one generator unit feeds Division 2. Division 1 and 2 are physically and electrically independent power systems. The gas turbine-generator units are housed in separate buildings as shown on Fig. II.9-1, and the buildings and equipment are Seismic Category I and Safety Grade. Standard LWR practice is to use diesel-generator units for on-site standby power. Gas turbine-driven generators are an acceptable alternative for a pool-type sodium-cooled fast reactor because the large thermal capacity in the sodium pool eliminates the fast starting requirements of the LWR plants. Tests conducted on sodium-cooled fast-reactor plants in the United States and in Europe have demonstrated that properly designed systems can safely withstand loss of normal power without operation of standby generators for extended periods of time. One standby generator has

the capacity to supply the Class IE and other essential loads if one generator is inoperative during the loss of off-site power.

A detailed system load analysis of the hotel power requirements has not yet been made, however, it is currently estimated that 6MWe is reserved for hotel loads. For purposes of comparison, Phenix a 254 MWe plant has a hotel load of 16 MWe.

II.11.3 Sodium Piping and Equipment Heating and Insulation System

The sodium piping and equipment heating and insulation system provides the piping and equipment insulation and insulation hardware, electrical heaters, the heater mounting devices, the electrical power controllers and the temperature sensors, required to insulate and heat the sodium or the NaK containing components of the following process systems:

1. Reactor vessel assembly system
2. Fuel receiving, storage, and shipping system
3. Intermediate heat transport system
4. Direct reactor auxiliary cooling systems
5. Steam generator system
6. Liquid metals auxiliaries system
7. Inert gas system
8. Impurity monitoring and analysis system

This system also provides a heating system for preheating the reactor vessel prior to sodium loading.

The sodium piping and equipment heating and insulation system provides the following heating and insulation functions for those process systems that contain sodium or NaK:

1. Preheat the sodium process systems solid metal parts, before the systems are filled with liquid metal sodium, from ambient conditions up to 232°C (450°F).
2. Heat the sodium process systems from plant extended shutdown conditions to reactor startup conditions, with the process systems filled with sodium.
3. The piping and equipment electrical heating system shall provide controlled heat to melt sequentially the frozen sodium.
4. Insulate to limit piping and equipment heat losses to the building and maintain insulation surface temperatures at or below 140°F.
5. The sodium piping and equipment heating and insulation system is nonsafety grade.

Electrical power is used for the piping and equipment heaters. The heating cable is either wrapped around the component or piping or placed in zig-zag pattern on the surface of the component. The heat rate required by different components is controlled by thermocouples which monitor piping and component temperatures and adjust the power supplied to the heaters.

The insulation system consists of an inner jacket of stainless steel, insulation layer of either mineral or reflective insulation depending on the operating temperature, and an outer protective jacket of stainless steel.

For smaller piping or components, the heaters are wrapped around the component. For tanks and large components, the heaters are arranged in banks.

II.12 In-Service Inspection

In-service inspection (ISI) is the examination required during the plant operation life to early detect potential failures. Its objectives are to 1) confirm integrity of function of parts necessary to safety, and 2) satisfy the needs to protect plant investment and high plant availability. In this regard, the in-service inspection approach for ABTR is established in such a way that inspectability of all components of the reactor system is ensured.

II.12.1 In-Service Inspection Requirements

The in-service inspection approach is based on the rules and requirements delineated in Division 3, Section XI of the ASME boiler and pressure vessel code, “Rules for inspection and testing of components of liquid-Metal cooled plants”. The code sections specify identification and classification of components subject to inspection, provisions for accessibility, examination methods and procedures, inspection plans and schedules, and repair requirements.

II.12.1.1 Components Subject to Inspection

The code specifies inspection requirements for nuclear safety grade components containing liquid-metal and cover-gas in liquid-metal cooled nuclear plants. The rules are established based upon anticipated characteristics of the systems which contain sodium coolant and protections against failure of the liquid-metal coolant boundaries. For example, it is anticipated that, due to the low vapor pressure of sodium and the inherent ductility and toughness of the coolant boundary material, reactor internal structures will not fail with sudden release of energy. Also, double walled pipes and vessels are used for protection against loss of core cooling, and inert gas is introduced within all the plant components containing free liquid metal surfaces.

Safety grade components of liquid-metal reactor containing other fluids may be provided by references to articles in Division 1.

II.12.1.2 Accessibility

Providing adequate access for inspection and maintenance is an important factor in the reactor design. Article IMA-1500 of the code specifies that accessibility provisions shall be made with the following considerations:

1. Access for the inspector, examination personnel, and equipment necessary to conduct the examination,
2. Capability for removal and storage of structural members, shielding components, insulating materials, and other equipment and components required to perform the visual observations, examinations, and tests,

3. Installation and support of handling machinery (e.g. hoists or other handling equipment) where required to facilitate removal, disassembly, and storage of equipment, components, and other examinations,
4. Performance of alternative or additional examinations to those specified herein in the event structural defects or indications are revealed that may require such alternative examinations,
5. Performance of necessary operations associated with repair or replacements of system components in the event structural defects or indications are that may require such repair or replacements.

II.12.1.3 Examination Methods

The code specifies four types of examination methods used during in-service inspection, namely visual, surface, continuous monitoring, and volumetric examinations.

Visual Examination is the primary method of inspecting for liquid metal retaining components. The code defines the following categories of visual examination:

1. VTM1: close range examination to detect discontinuities and imperfections on the surface of components, including such conditions as cracks, wear, corrosion, or erosion.
2. VTM2: examination of exterior surfaces in such a way that accumulation of liquids, liquid drops and smoke are discernable. The removal of external covering, such as insulation, is not required for VTM-2 visual examination.
3. VTM3: examination to determine the general mechanical and structural conditions of components and their supports by verifying parameters such as clearance, settings, and physical displacements; and to detect discontinuities and imperfections, such as loss of integrity as bolted or welded connections, loose or missing parts, debris, corrosion, wear, or erosion.

Continuous monitoring (CM) of the region outside the liquid-metal and cover-gas containment boundary can provide detection of leakage. Other operation parameters, such as pressure, coolant flow, temperature, flux, vibration can be monitored to supplement other examination methods.

Surface examination is used to detect the presence of surface or near-surface cracks. It may be conducted by either a magnetic particle or a liquid penetrant method.

Volumetric examination is used to detect cracks and discontinuities throughout the volume of the material. The recognized techniques are radiographic examination, ultrasonic examination, and eddy-current examination.

These examination methods may be substituted by alternative examination methods, a combination of methods, or newly developed techniques, if they are demonstrated to be equivalent or superior, and accepted by the inspector.

II.12.1.4 Inspection Plans and Schedules

The code requires that inspection plans shall be developed, which delineate the following:

1. Classification of the components and the boundaries of the system classifications,
2. Identification of components subject to examination and testing;
3. The code requirements by category, item number for each component and the examination or test to be performed,
4. The code cases proposed for use and the extent of their application,
5. Schedule for performance of examination and tests.

It is also required that all the liquid metal retaining components shall be continuously monitored for leakage. These requirements are delineated in this section for reactor internals and vessel, and summarized in Table II.12-1.

Reactor internals are required to be inspected via VTM-3 visual examination methods. VTM-3 inspection may be conducted via direct or remote visual examination, dimensional gauging, and ultrasonic scanning. The key guidelines principles for the inspection requirements are summarized as following.

1. For integrally welded components, observe dimensional or positional relationships that ensure a coolable and controllable core geometry and adequate coolant circulation.
2. Observe the location of each removable or non-welded component and verify the as-installed location of visible fasteners.
3. Components for which the applicable requirement above cannot be met shall be examined by some other methods capable of determining the general condition and functionality of the component.

Reactor vessel is required to be continuously monitored for liquid-metal leakage and periodically inspected via VTM-2 visual inspection as. The visual inspection is required for the following weld joints: longitudinal and circumferential shell welds, meridional and circumferential head welds, shell-to-flange welds, shell-to-head welds.

The code specifies inspection time intervals during which the inspection should be performed. Accordingly, the inspection schedules for ASME class 1 liquid metal or cover gas retaining components may follow the programs given in Table II.12-2 or II.12-3. The in-service inspection of the subject components shall be completed during each of the inspection intervals for the service lifetime of the plant. Each inspection interval may be decreased or extended by as much as 1 year. Deferral of inspections to the end of the interval is permitted. During each interval, 100% of the reactor internal structures must be examined. For the reactor vessel, 33% of the vessel welds must be examined, so that essentially 100% if the vessel welds are inspected by the end of the third interval.

Table II.12-1 In-Service Inspection Plan Requirements for Liquid-metal Cooled Reactor Components

Code Item	Components Examined	ISI Method	Schedule & Extent	
			1 st inspection interval	Successive Intervals
B1.10	Reactor Vessel (RV)	VTM-2	33%	33%
B5.10	Reactor Vessel: Circumferential shell welds joining dissimilar metals	Cont. monitoring	100%	100%
	Guard Vessel	* Volumetric	100%	100%
F1.10	Reactor Support - bolts & welds	VTM-3	100%	100%
B12.20	In-vessel components above sodium level	Cont. monitoring	100%	100%
B12.10	Integrally welded Reactor Internals: Core support / Retainer/ Inlet manifold and plenum / Thermal barriers	VTM-3	100%	100%
B12.20	Removable reactor internal components	Cont. monitoring	100%	100%
B3.10	EM Pumps, IHX	VTM-3	100%	100%
B3.20	Reactor Cover (rotating plugs and deck)	Cont. monitoring	External or adjacent to surface monitored	External or adjacent to surface monitored
B3.30	Control rod drive and other above cover mechanisms containing cover gas			
B3.40	Primary cover gas systems - vessel welds, piping welds, valves and stem seals, other gas tight components)			
B6.10	Reactor Closure Bolting	Cont. monitoring	External or adjacent to surface monitored	External or adjacent to surface monitored
B8.10	Liquid metal retaining heat transport loop piping protected by guard pipe	VTM-2	33% (100% for **)	33% (100% for **)
B8.14	- circumferential / longitudinal welds			
B9.10	- branch pipe connection welds**	Cont. monitoring	100%	100%
C2.30	- piping boundary			
	Guard pipes on intermediate liquid metal boundary - all guard pipe welds	VTM-3	100%	100%

Table II.12-2 Inspection Program A (Table IMB-2411-1)

Inspection Interval	Inspection Period, Calendar Years of Plant Service	Minimum Examinations Completed, %	Maximum Examinations Credited, %
1 st	3	100	100
	7	33	67
2 nd	10	100	100
	13	16	34
3 rd	17	40	50
	20	66	75
	23	100	100
4 th	27	8	16
	30	25	34
	33	50	67
	37	75	100
	40	100	...

Table II.12-3 Inspection Program B (Table IMB-2411-1)

Inspection Interval	Inspection Period, Calendar Years of Plant Service	Minimum Examinations Completed, %	Maximum Examinations Credited, %
1 st	3	16	34
	7	50	67
	10	100	100
2 nd	13	16	34
	17	50	67
	20	100	100
3 rd	23	16	34
	27	50	67
	30	100	100
4 th	33	16	34
	37	50	100
	40	100	...

II.12.2 Examination Techniques

II.12.2.1 Description of Examination Techniques

The following examination techniques are adopted for the conduct of in-service inspection of ABTR.

Continuous Monitoring: The in-service inspection approach heavily utilizes continuous monitoring of various operating conditions. Sodium vapor sensors can monitor the presence of sodium vapor in the atmosphere. Sodium liquid detectors can monitor the presence of liquid sodium in bottom of a vessel. Gas pressure gauge is used for leakage test of a vessel by directly pressurizing. Radiation sensors monitor an area for cover-gas leaks. In addition, various sensors are available for monitoring the conditions of reactor internals – flow, pressure, vibration, temperature, coolant level, and pump power. These technologies are readily available.

Remote Operated Robotic Vehicle (ROV) can be equipped with cameras and light sources to inspect parts of the components inaccessible by human, such as reactor/guard vessel surfaces and reactor support skirt. This robotic device should be able to navigate in small areas of vertical vessel walls, to precisely position the camera, and to endure high temperature and radiation. Currently, this technology is not available on commercial basis.

Electromagnetic Acoustic Transducer (EMAT) can be used for volumetric inspection of structural elements, such as reactor vessel. Compared to ultrasonic transducers, this device is particularly suitable for remote inspection because it does not require corpuent fluid and is adequate for high temperature use.

Eddy Current Examination can be used for detection of structural failures in pipes and tubes of NSSS systems.

Periscope/Camera: Periscope or camera systems, inserted through the access port in the reactor head closure, can be used to visually observe the cover gas area within containment boundary. Special provision is needed to keep the camera lens clear from sodium vapor build-up.

Dimensional Gauging Probe: In areas where dimensional gauging is not possible with direct visual observation, positioning mechanisms can be used to indirectly verify structural integrity of structural components. In-vessel fuel handling machine or an equivalent indexing mechanism can be used for this purpose.

Under-Sodium Viewer (USV): Due to the opacity of sodium, the reactor internals below sodium level cannot be observed with optical means. To this end, conceptually, under-sodium viewing devices may be effectively utilized to carry out visual inspection of the components submerged under sodium. Typically, these are ultrasonic metrology devices that emit high frequency sound waves and receive the reflecting waves to perceive environmental objects. Special design provisions are made to match the acoustic impedance with sodium, and to withstand high temperature use. This device can be used for mapping the core, horizontal baffle and vessel liner during and following fuel handling, and also be used as a core sweep at the start of refueling. Currently, the

benefits of using this device are uncertain because of the immature state-of-the art of the technology.

II.12.2.2 Evaluation of Examination Techniques

To ensure inspectability of the reactor system, it is important to adopt proven and readily available inspection techniques. While most of the above techniques mature, the some techniques are based on immature technology basis, and require improvement. In particular, the following techniques need particular attention.

Under-sodium Viewing

Due to the opacity of the sodium coolant, the under-sodium viewing technique is important for ensuring full inspectability of reactor internals and internal components. Visual inspection is needed not only for the normal VTM-3 inspection, but also for supplemental close-up viewing. With available USV technology, many difficult inspection processes will be made possible or simplified. Otherwise, inspections may require complex design provisions and procedures, which may involve draining of sodium to expose the parts. In spite of the apparent benefits, however, the current state-of-the-art of the technology exhibits some significant limitations against its deployment.

The first limitation attributes from unavailability of high temperature ultrasonic transducer. The typical transducer materials have relatively low Curie temperature, and thus they will lose the piezoelectric characteristics in the high temperature environment inside the reactor. Some piezoelectric material, such as LiNbO_3 (Lithium Niobate), can withstand high temperature, but their sensitivity is known to be impractically low. In addition, the bonding between the piezoelectric element and the face plate tends to fail easily at high temperature.

Another limitation attributes from the inaccuracy of measurement. To make accurate ultrasonic measurement, the object's surface has to be flat and in the transducer should be faced normal to the object surface. It is difficult to measure the pose of the parts with curved or oblique surface, especially when it is specular. Since most parts are of such nature, it is not possible to use current ultrasonic techniques for general imaging. To circumvent such technical difficulty, flat plates may be provided at predefined locations in order to facilitate accurate positional measurement at these locations. However, such design provisions require substantial installations and may be impractical for general purpose inspection. Due to such difficulties, the current ultrasonic viewing techniques have limited success only in ranging mode operation, which intends to identify the presence of an object, such as for path clearance during fuel handling.

To this end, technology development is needed to develop sensor configuration for high temperature use, and to improve measurement accuracy. Such improvements may be leveraged and improved upon recent advances in sensor and signal processing technologies.

Remote Operated Robotic Vehicle for Reactor Vessel Inspection

The ASME code requires visual inspection of the reactor vessel (RV) welds. An annular gap is provided between the reactor vessel and the guard vessel (GV), in order to allow access for the remote operated robotic vehicle to perform remote visual inspection. Since this ISI gap contains sodium in case the reactor vessel leaks, it determines the faulted sodium level in the reactor. Therefore, minimizing the ISI gap will bring about significant benefit of reducing the sodium level variations in faulted conditions. This is a significant benefit in terms of reactor design, because it allows for reducing the height of the reactor, more compact reactor, and alleviating design requirements for many reactor internal components. In this regard, introducing small size robotic vehicle is a significant benefit.

Since no commercially available robotic system can meet the unique requirements of reactor vessel inspection, such as having small size, and being tolerant to high temperature and radiation. Recently, reactor vessel inspection robots have been developed for a few sodium cooled reactors, such as Monju in Japan and Super Phoenix in France, but the developed systems are much larger in size. Therefore, development of a new robotic system is necessary, with emphasis on size-reduction, adaptation to high temperature use, and design of the locomotion mechanism and the camera system. Recent advances in robotics and inspection technologies may be leveraged for the needed development.

II.12.3 In-service Inspection Approach for ABTR

In-service inspection approaches for ABTR are established based on the following general guidelines, which is consistent with the ASME code section XI:

- In-service inspection will be conducted during refueling or service outage,
- Available examination technologies are adopted,
- Access provisions are provided for all components of the reactor system,
- Design provisions are made to reduce possible areas and modes of failures,
- All liquid metal and cover gas containment boundaries will be continuously monitored for leakage,
- Continuous monitoring of reactor operating variables will be utilized to supplement or replace other inspection methods, whenever possible,
- Problem areas observed in the normal in-service inspection will be further investigated.

The in-service inspection approaches cover for both normal and supplemental inspections. The supplemental inspections may be follow-up examinations in the event the normal inspections indicate deviations from normal operating or structural conditions.

II.12.3.1 Approaches for Accessibility

The ABTR design has incorporated access provisions for in-service inspection according to the code requirements. These design provisions include:

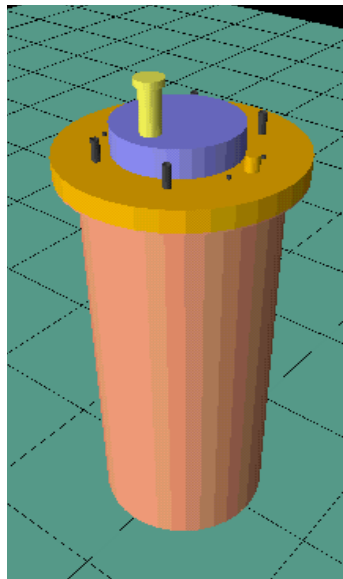
1. Annular space (ISI gap) between reactor vessel and guard vessel for inspection,
2. Entry ports in the reactor support skirt for access to the ISI gap,
3. Access provisions to allow inspection of reactor deck structure,
4. Space for installing work platforms and lighting and shielding and insulation during inspection and maintenance,
5. Verification that welds requiring inspection are not in inaccessible locations,
6. Access provisions for inspection within the reactor vessel. These provisions include access ports in the reactor deck and the rotating plug, passage holes in the horizontal baffle plates, and passage to the bottom of the core support structure.

In addition to accessibility, design focus was directed to reducing the possible areas and modes of failure. By reducing the possible failure modes, it is possible to reduce inspection requirements. For example, the core support load path is arranged in such a way that critical in-vessel structures are normally in compression, while the principal tensile load path is only in the reactor vessel wall, which will be continuously monitored for leaks that would indicate crack propagation.

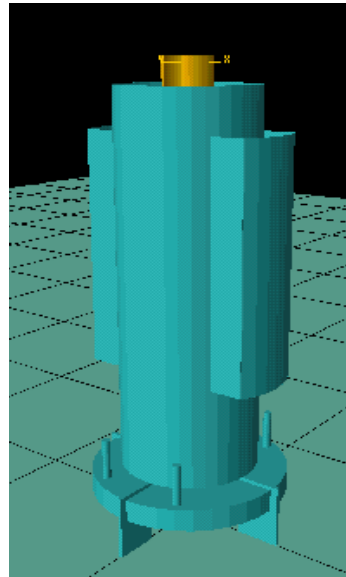
II.12.3.2 Proposed Inspection Methods and Procedures

This section specifies the in-service inspection approaches for the reactor system components, with emphasis given to nuclear safety grade components of the reactor internals, the reactor vessel and the reactor closure, which are shown in Figure II.12-1. The inspection of the non-nuclear safety grade components of the remaining nuclear steam generation system, such as intermediate heat transport system and steam generation system, is considered far less difficult, and not detailed in this report.

The inspection methods and procedures are established in accordance with possible failure modes of associated components. While the ASME code provides general guidelines, each individual examination that makes up the inspection has to be established in consideration of its own unique limitations on access and geometry. Even a single component can fail in various ways, and each case may require different inspection techniques. These aspects cannot be generalized, and inspection methods must be considered individually associated with possible failure modes. Therefore, the failure modes of the reactor components are first postulated, and subsequently the inspection techniques are established that are capable of detecting the onset of these failures. Table II.12-4 presents a list of failure modes and the suggested in-service inspection approaches for ABTR. Both normal examination methods and follow-up examination methods are presented for each failure modes.



(a) Reactor vessel and closure



(b) Reactor internal structure

Figure II.12-1 Areas Subject to Inspection

Inspection of Reactor Internals

Normal in-service inspection of reactor internals and internal components require VTM-3 visual inspection. The sodium surface and the in-reactor vessel components above the sodium level will be examined using periscope or camera, inserted through the multiple access ports in the closure head deck.

For components below the sodium level, normal in-service inspection approach is based on continuous monitoring, dimensional gauging and under-sodium viewing. Continuous monitoring of sodium levels, outlet temperature of a limited number of core assemblies, vibration and the pressure in the pump discharge manifold will provide indication of the integrity of the pressurized components (core barrel, inlet plenum, and primary piping discharge manifolds) in hard-to-access areas of the reactor pool as will statistical analysis of primary pump power.

The structural components of the core support and restraints will be inspected with dimensional gauging. Dimensional gauging will be performed by indexing with the fuel handling machine or other dedicated indexing mechanism on several specified locations on several specified locations on the top of the former ring and other structural components in the hot pool. This technique can determine possible shifts in elevation of components. The verification of the proper location of a component, such as the top of core barrel, can also imply a proper location for the core support structure. Figure II.12-2

illustrates the concept of dimensional gauging with such indexing mechanisms. Under-sodium viewer can also be used to map the core top, and used to investigate the condition of many difficult to reach areas. The under-sodium viewer is inserted through ports in the rotating plug, and additional access to vessel internals components are provided through ports in the outer radius in the fixed part of the closure head deck. For accurate measurement, gauge blocks and gauge marks are set at key locations to serve as reference marks for under-sodium viewer. The rotating plug can move the fuel-handling machine and the under-sodium viewer to various locations inside the reactor vessel.

Large cracks or separation of the reactor vessel liner will be detected by continuous monitoring of vessel temperatures and pump well level. The inspection will be supplemented with visual inspections, for which camera/periscope will be used for above sodium-level portion, and under-sodium viewer will be used for below sodium-level portion.

Failures in redan, such as at various connections to storage basket, intermediate heat exchanger, and pump wells, are checked by dimensional gauging. This can be performed with fuel handling machine or under-sodium viewer, and indexing various wells and penetrations.

Upper internals structure (USS) is associated with various failure modes as delineated in Table II.12-4. Its structural integrity is checked primarily via continuous monitoring with acoustic sensors, and use of an under-sodium viewer.

Anomalies in the control rod drives can be tested through periodic test operations and by monitoring the drive motor current.

The integrity of the instrument drywells will be verified by continuous monitoring for leakage with reactor cover radiation monitors, and visually inspecting for distortion using periscope/camera.

Continuous monitoring will be the primary source of information on the operation of the primary pumps and intermediate heat exchanger. For this purpose, cover gas leak will be monitored with radiation monitor, and pump oil leakage will be monitored.

DRACS may fail by sodium leakage, sodium blockage, and air-side blockage. Currently, the requirements for its inspection are not explicitly specified in the ASME code. To ensure safe and reliable operation, continuous monitoring of the relevant operation parameters is recommended. The detailed scope and procedures shall be developed.

Problems observed in the normal in-service inspection will be further investigated by follow-up examinations. These follow-up examinations may include close-up viewing with optical instruments and under-sodium viewing of difficult-to-access areas. Such procedures require more extensive access and may involve removal of components and lowering sodium level, as delineated in Table II.12-4, supplemental inspection column.

Such extensive ordeals may be alleviated if accurate under-sodium imaging technology is available. However, the current state-of-the-art of the technology does not meet such expectations. The results of the follow-up examination will be used to verify structural failure and plan detailed maintenance procedures. Maintenance approaches are identified for most of the components in the reactor vessel. Some major structures do not have outlined maintenance plan because it is considered improbable that a relevant structural failure can be repaired.

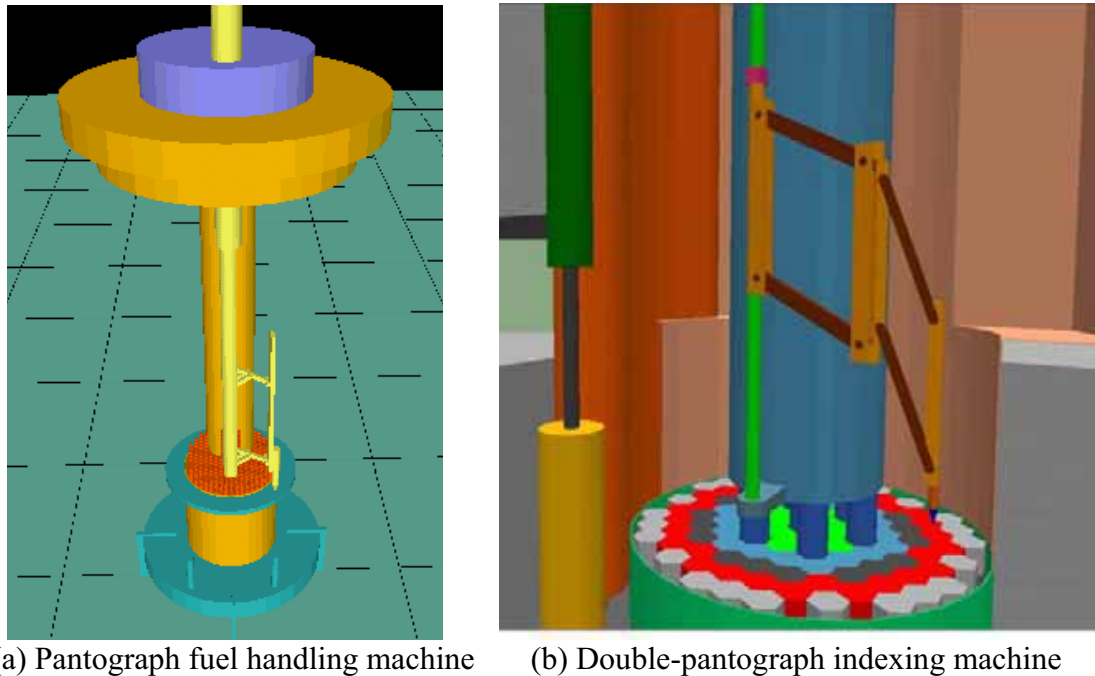


Figure II.12-2 Dimensional Gauging with Indexing Mechanisms

Inspection of Reactor Vessels and Closures

Inspection of the reactor vessel will be conducted via visual examination (VTM-2) of all welds and continuous monitoring. The reactor vessel will be continuously monitored for sodium and gas leakage. Sensors and measurement techniques are readily available for this purpose. The visual inspection is performed using a camera system mounted on a remotely operated robotic vehicle. This robotic device will be installed in the annulus between the reactor vessel and the guard vessel, as shown in Figure II.12-3. Currently, there is no commercially available system for this purpose.

VTM-3 visual inspection is required for the guard vessel. This is conducted using a TV camera mounted on the remote operated robotic vehicle. Continuous monitoring of pressure in the reactor vessel/guard vessel annulus will provide initial detection of leak. Follow-up examinations will consist of close-up visual examination of the annulus, and analyzing a gas sample from the annulus.

Sodium vapor sensors are adopted to monitor the annulus region between the reactor vessel and the guard vessel for sodium vapor. Sodium liquid detectors monitor the presence of liquid sodium in the reactor vessel/guard vessel annulus bottom. Gas pressure gauge is used for leakage test, in which reactor vessel/guard vessel annulus is pressurized. Radiation sensors monitor the reactor closure for cover-gas leaks. In addition, various sensors are utilized to monitor the conditions of reactor internals – flow, pressure, vibration, temperature, coolant level, and pump power.

VTM-3 visual inspection is required for normal inspection of the reactor support in the head access area. For this purpose, the reactor support skirt welds and bolts will be inspected with remote visual examination using a camera on the remote operated robotic vehicle.

The reactor closure, including the deck and rotatable plug, will be continuously monitored for leaks, using radiation detectors in the head access area. Analysis of reactor cover gas and the primary sodium purity will provide follow-up indications.

Further inspection will be performed if abnormal conditions are detected during normal inspection. Such supplemental inspection will involve broader TV viewing to pinpoint the problem area, and subsequent close-up visual inspection (VTM-1) and volumetric inspection with electromagnetic acoustic transducer to characterize the condition of the defects.

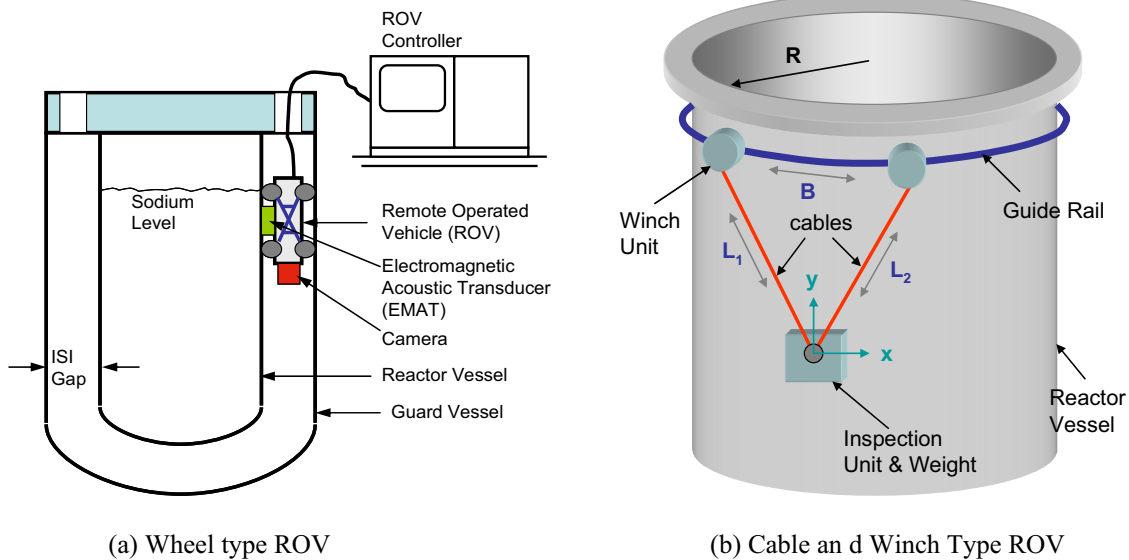


Figure II.12-3 Reactor Vessel Inspection with ROV

Table II.12-4 Postulated Failure Modes and In-Service Inspection Considerations (1/6)

Component / System	Postulated Failure	Normal Inspection (NI) Method, to detect problem	Code Requirements (Div.3, Section XI, ASME B&PV)	Supplemental Inspection (SI), if a problem is indicated
1. Reactor Vessel	Weld crack (below Na level) Weld crack (cover-gas region) Exterior surface deterioration	1.1 CM: Sodium leak, Radiation, RV/GV annulus pressure 1.2 Periodic visual inspection with ROV and camera	VTM-2 inspection on all welds plus Continuous monitoring	1.1 Broader TV viewing to pinpoint the area 1.2 VTM-1 inspection with zoom lens or fibroscope 1.3 Localized inspection w/ ultrasonic transducer
2. Guard Vessel	Weld crack Interior surface deterioration	2.1 CM: Cover gas leak, Radiation, Pressure 2.2 same as 1.2 3.1 Visual inspection with ROV and camera	VTM-3 inspection for low-alloy steel	2.1 Same as 1.1-1.3. 2.2 additional inspection from the outside
3. RV/GV Support	Crack or distortion		Visual VTM-3	3.1 Surface inspections, Volumetric inspections, and VTM-1 exam.
4.Reactor Internals - Core support	Massive weld failure Support to reactor vessel weld failure	4.1 Check height of core barrel with IVHM or USV 4.2 Measure loads to remove fuel assy. 4.3 Test operation of control rods 4.4 same as 1.2 4.5 same as 4.1 thru 4.3	VTM-3 inspection	4.1 Access to the bottom of the reactor vessel, and use USV in the core support region if there has been structural movement. 4.2 Same as 4.1

Table II.12-4 Postulated Failure Modes and In-Service Inspection Considerations (2/6)

Component / System	Postulated Failure	Normal Inspection (NI) Method, to detect problem	Code Requirements (Div.3, Section XI, ASME B&PV)	Supplemental Inspection (SI), if a problem is indicated
- Shield barrel and inlet plenum	Massive or barrel-to-plenum weld failure Massive plenum top and bottom plate failure	4.6 same as 4.1 thru 4.3 4.7 same as 4.1 thru 4.3 4.8 CM with overcore thermocouple	VTM-3 inspection	4.3 Same as 4.1 4.4 Same as 4.1 4.5 Examine plate surface with USV. 4.6 Drain Na and examine with remote optical instruments.
	Module sleeve weld failure	4.9 Vibration/Acoustic Sensors for loose part 4.10 Core outlet temp. for flow distribution		4.7 Same as 4.1 4.8 same as 4.6
	Separation of shield barrel with weld crack	4.11 Indexing on shield barrel with IVHM and USV		4.9 Examine shield barrier below redan using USV
- Core restraints	Broken retaining pins	4.12 Index reference points on the core restraints with IVIM 4.13 Loose parts monitor 4.14 USV core sweep		4.10 Imaging with USV. Further examination will require core removal and partial drain.
	Formal ring breakup	4.15 same as 4.12 – 4.14		4.11 Same as 4.10

Table II.12-4 Postulated Failure Modes and In-Service Inspection Considerations (3/6)

Component / System	Postulated Failure	Normal Inspection (NI) Method, to detect problem	Code Requirements (Div.3, Section XI, ASME B&PV)	Supplemental Inspection (SI), if a problem is indicated
- Pump well	Well weld failure	4.16 Examine well position with Periscope /camera above the Na level. Use USV to check position below Na level.	VTM-3 inspection	4.12 Remove pump, examine interior of well with camera/periscope above Na level, and USV below Na surface
- Pump discharge pipes	Large Na leak (weld fail at pump or plenum)	4.17 Monitor pump well level, pump speed, pump discharge flow, core outlet temperature		4.13 Remove pump, examine pipes from within using USV. 4.14 If needed, remove fuel, drain Na, and examine pipe optically
- Vessel thermal liner	Large liner crack Separation of liner from vessel	4.18 Monitor pump well level and vessel temp. 4.19 Examine above Na level region with camera /periscope 4.20 same as 4.18 4.21 USV of selected points on the liner and on top of horizontal baffle assembly		4.15 Remove core, drain Na, and examine areas with periscope 4.16 Same as 4.15

Table II.12-4 Postulated Failure Modes and In-Service Inspection Considerations (4/6)

Component / System	Postulated Failure	Normal Inspection (NI) Method, to detect problem	Code Requirements (Div.3, Section XI, ASME B&PV)	Supplemental Inspection (SI), if a problem is indicated
- Redan	Fail at redan connections to fuel storage basket, IHX, and pump well	4.21 Dimension gauging with IVHM and USV on the redan and various wells and penetrations 4.22 Monitor level in pump well	VTM-3 inspection	4.17 Remove high burnup assemblies, drain Na to partially expose the redan, and examine with optical devices
- Instrument drywells	Lower baffle support skirt structural failure Drywell leakage	4.23 same as 4.21 4.24 CM with reactor cover radiation monitors		4.18 Same as 4.17 4.19 Pressurize drywell and check for pressure decay 4.20 Remove probe and examine for Na leakage
- Inlet modules	Drywell distortion Module weld failure Binding on fuel assay	4.25 Camera/periscope, USV 4.26 same as 4.1-4.3 4.27 CM of core outlet temperature 4.28 same as 4.2		-- 4.21 Remove any hot or binding fuel assay, and inspect with USV 4.22 Same as 4.21

Table II.12-4 Postulated Failure Modes and In-Service Inspection Considerations (5/6)

Component / System	Postulated Failure	Normal Inspection (NI) Method, to detect problem	Code Requirements (Div.3, Section XI, ASME B&PV)	Supplemental Inspection (SI), if a problem is indicated
<p>- Upper Internals Structure (UIS)</p>	<p>UIS support cylinder weld fail or distortion</p>	<p>4.29 Examine exposed surface above Na level with camera/periscope. Check location and general shape with USV below Na level</p>		<p>4.23 Remove core, lower Na level, and inspect cylinder with remote optics and periscope.</p>
	<p>Distorted control rod drive (CRD), shroud tubes, weld & bearing failures</p>	<p>4.30 Periodic testing of CRDs 4.31 Monitor drive motor current 4.32 Loose part monitor 4.33 USV core sweep</p>		<p>4.24 Remove driveline and insert fiber-optic device in opening to examine shroud tubes.</p>
	<p>Failure of spokes or connection to drywells at support plates</p>	<p>4.34 same as 4.30-4.33</p>		
	<p>Erosion of UIS surface</p>	<p>4.35 Loose parts monitor 4.36 analyze particulate from Na purification sys. for metal particle</p>		
	<p>Failure of connection pins, loose sleeves on instrument hold-down, loose shock liner plates</p>	<p>4.37 Loose part monitor 4.38 USV core sweep</p>		<p>4.25 Scan top of core for loose parts with USV. 4.26 Lower Na level, and examine underside of redan with optics</p>

Table II.12-4 Postulated Failure Modes and In-Service Inspection Considerations (6/6)

Component / System	Postulated Failure	Normal Inspection (NI) Method, to detect problem	Code Requirements (Div.3, Section XI, ASME B&PV)	Supplemental Inspection (SI), if a problem is indicated
5. Reactor Cover (deck and rotatable plug)	Cover gas seal leakage Dip seal loss Inflatable seal failure	4.39 Reactor cover radiation monitor	Continuous monitoring	4.27 Liquid penetrant examination of seal and support flange. 4.28 Periodically examine and clean seal
6. Primary Pump	Deck seal leak Pump shaft seal leak Support flange failure	4.40 Reactor cover radiation monitor 4.41 Pump oil leakage monitor	Continuous monitoring	4.29 Liquid penetrant examination of seal and support flange
7. IHX	Deck seal leak IHX inlet/outlet leak IHX to primary Na leak	4.42 Reactor cover radiation monitor	Continuous monitoring	4.30 Same as 4.28
8. Primary cover gas	Cover gas leak Gas valve failure	4.43 Reactor cover radiation monitor	Continuous monitoring	4.31 Pressure test and visual examination of piping and seals
9. DRACS	Na Leakage Sodium blockage Air-side blockage	4.44 CM (details to be developed)	None (NI exceeds Code requirements)	

PART III

DETAILED DESIGN ANALYSES AND TRADE-OFF STUDIES

III.1 Primary Pump Design Analyses

III.1.1 Mechanical Pump Design

A schematic of a mechanical pump, indicating major essential components is shown in Figure III.1-1. Since the design called “Fermi” type was considered superior to that called “Hallam” (see Figure III.1-2), a Fermi type design was used in this study. The mechanical pump shown in Figure III.1-1 is a Fermi type. To estimate the size of this type of mechanical pumps, Byron Jackson has developed a series of nomographs [1]. A size estimation of a mechanical pump for ABTR was done using the nomographs shown in Figure III.1-4 Figure III.1-9 Mechanical. In these nomographs, sodium flow rate, head pressure, and operating temperature are needed as inputs (see Figure III.1-3).

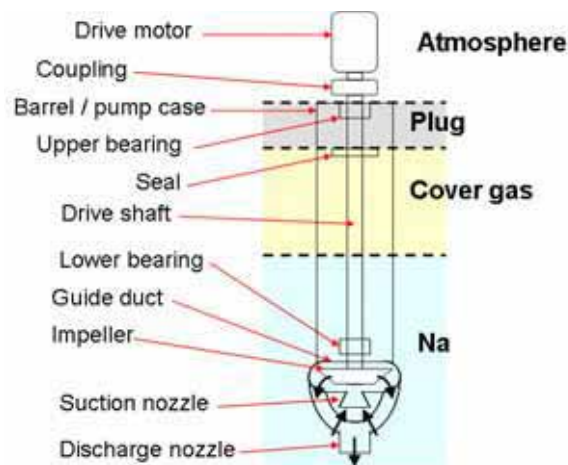


Figure III.1-1 Schematic of mechanical pump

In the first nomograph, the specific speed and rotation speed are determined. In the second nomograph, the required power is determined. Then, in the third nomograph, the shaft diameter is determined. In the fourth nomograph, the pump case diameter, which is related to the impeller diameter, is determined. In the fifth nomograph the size of the pump outer barrel is determined, however, for the pool type configuration, the outer barrel is not used and the pump casing is suspended directly in the pool of Na. Finally in the sixth nomograph, the suction and discharge nozzle diameters are determined. A summary of those parameters obtained as well as input values are presented in Figure III.1-10. This procedure estimates only the diameter of the pump. The length of the pump can be estimated from another consideration, which is that the submergence depth needs to be greater than 0.9-1.2 m to prevent vortexing [2].

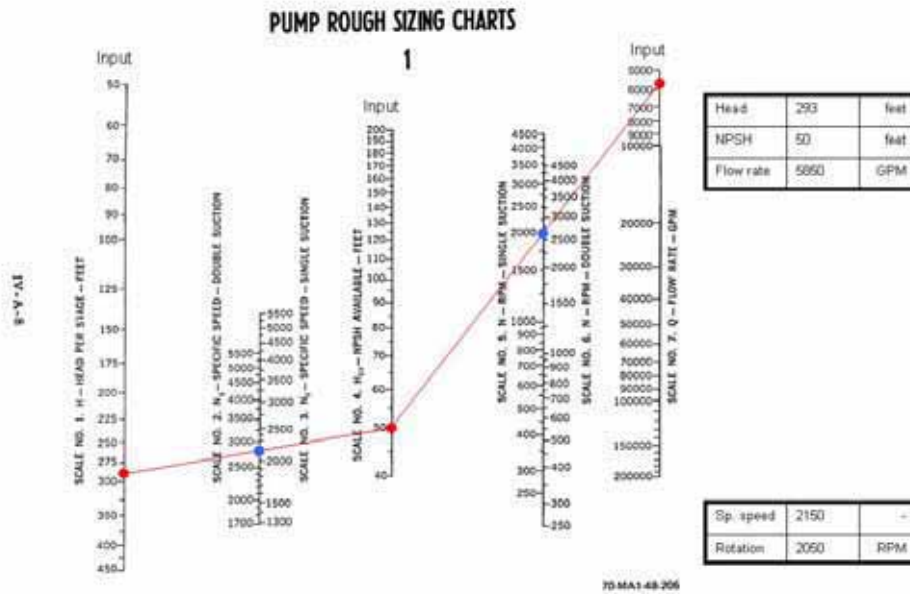


Figure III.1-4 Mechanical pump design nomograph-1

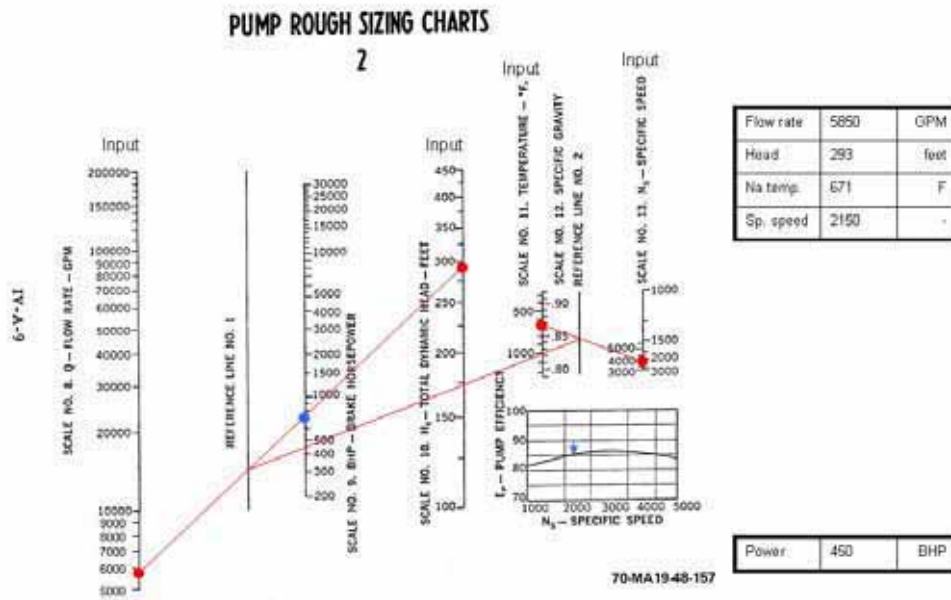


Figure III.1-5 Mechanical pump design nomograph-2

PUMP ROUGH SIZING CHARTS

3

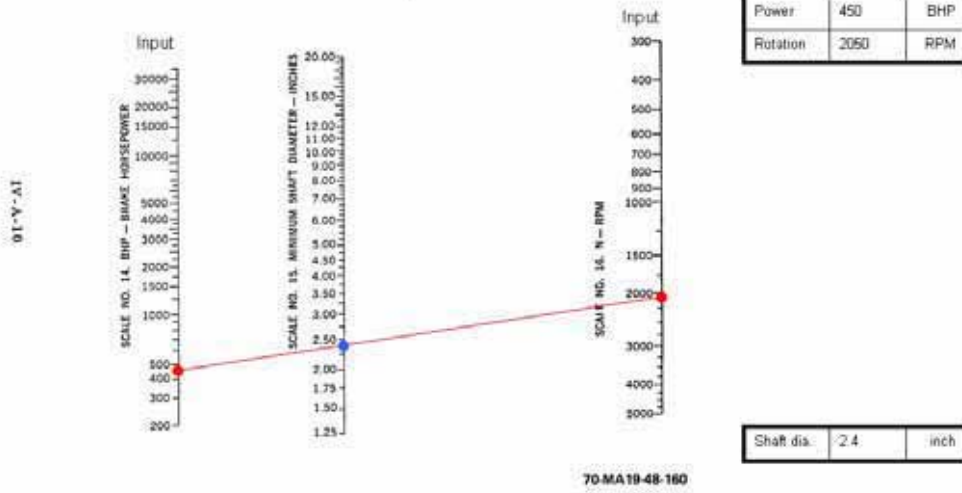


Figure III.1-6 Mechanical pump design nomograph-3

PUMP ROUGH SIZING CHARTS

4

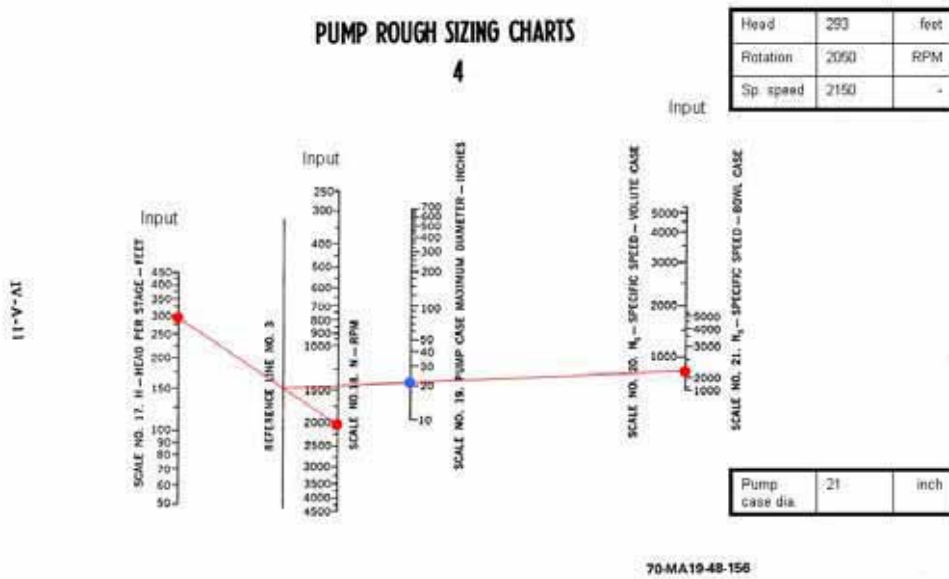


Figure III.1-7 Mechanical pump design nomograph-4

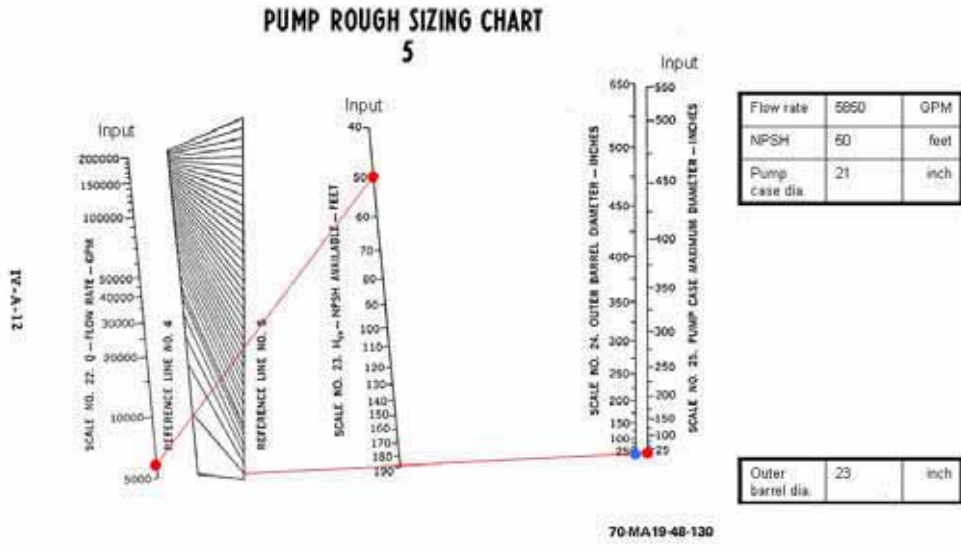


Figure III.1-8 Mechanical pump design nomograph-5

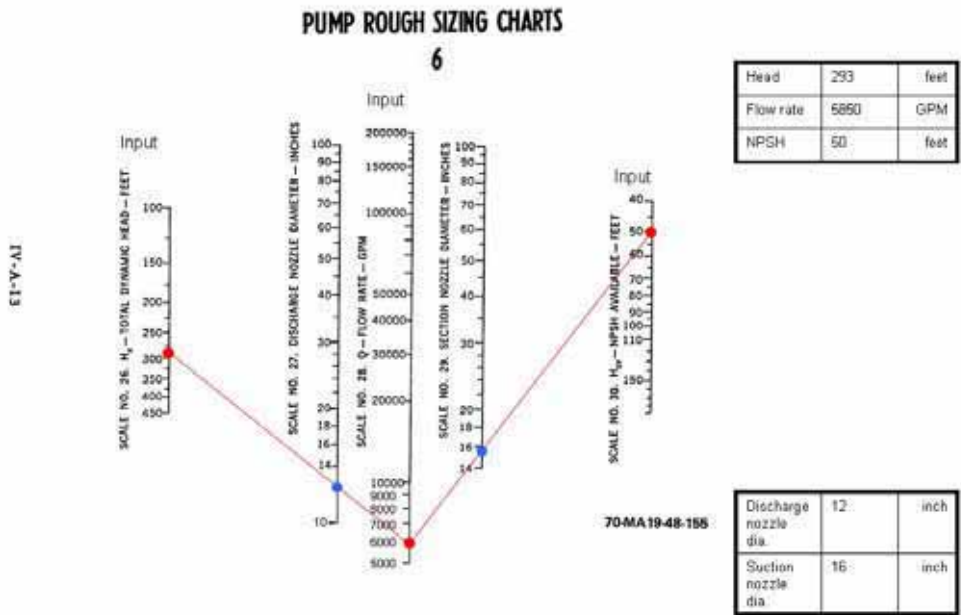


Figure III.1-9 Mechanical pump design nomograph-6

Input			Estimated Parameters		
Head	293 ft	(= 760 kPa, or 110 psi)	Specific speed	2150	
NPSH*	50 ft	(= 15 m)	Rotation	2050 rpm	
Flow rate	5850 GPM	(= 320 kg/s or 0.369 m ³ /s)	Power	450 BHP	(= 336 kW)
Na temp.	671 F	(= 628 K)	Shaft dia.	2.4 in	(= 6.1 cm)
*Of which 41 ft (or 12 m) corresponds to atmospheric pressure of 101325 Pa.			Pump case dia.	21 in	(= 53.3 cm)
			Outer barrel dia.	23 in	(= 58.4 cm)
			Discharge nozzle dia.	12 in	(= 30.5 cm)
			Suction nozzle dia.	16 in	(=40.6 cm)

Figure III.1-10 Estimated design parameters for an mechanical pump

III.1.2 Electromagnetic Pump

The EM pump design optimization studies were carried out using an ANL developed code based on the calculational model developed to estimate the performance of various ALIPs. At the design operating condition (nominal operating condition for the ABTR design) and a given pump length, the code estimates the diameter of the pump without return duct, mass, and efficiency of the ALIP. To optimize some parameters for the pump, the code repeatedly calculates the performance of the pump at a fixed operating condition and pump length while varying the following parameters:

1. Diameter of the pump duct,
2. Number of coils,
3. Number of coils per pole per phase,
4. Drive frequency.

In this analysis, the diameter of the pump is limited to within 0.6 m, such that the ALIP can be installed in the opening for the mechanical pump design presented in Section II.3.2.1. An example design for a primary pump is shown in Table III.1-1. Performance curves are shown in Figure III.1-11 and III.1-12.

Table III.1-1 EM Pump design parameters

	Items	Spec. (SI)	Unit	Spec. (Eng units)		Remarks
Primary sodium pump	Type	ALIP				return, single stator
	Quantity	4		4		
	Mass flow rate	320	kg/s	-	-	
	Volumetric Flow rate	0.369	m ³ /s	5849	gpm	
	Pump head (psig)	0.76	MPa	110	psig	It is currently estimated that the core pressure drop is ~60 psig and the IHX primary side pressure drop is 5-10 psig, so the EM pump specified here may be oversized.
	Temperature	355	C	671	F	cold pool temperature
	Power	609	kW			
	Efficiency	46.05	%	46	%	Neglecting skin effect, actual value should be lower
	Drive voltage	560	V	560	V	
	Drive current	1052	A	1052	A	
	Drive frequency	45	Hz	45	Hz	
	Pole count	14		14		
	Coil count	42		42		
	Net positive suction head available		m of sodium	0	feet of sodium	Roughly, the expected cover gas pressure will be ~1 atm which is equivalent to ~40 feet of sodium head plus 4-5 feet of sodium to the inlet of the sodium pump - see drawing
	Mass	2271	kg	4996	lbm	
	Pump height (length)	2.4	m	7.9	ft	
	Pump diameter	0.58498	m	1.9	ft	
	Inner core - inner diameter	0.094	m	0.3	ft	
	Inner core - outer diameter	0.142	m	0.5	ft	
	Inner core - containment thickness	0.5	mm	0.0	inches	
	Duct - inner diameter	0.23542	m	0.8	ft	
	Duct - outer diameter	0.24	m	0.8	ft	
	Duct - wall thickness	2.29	mm	0.1	inches	
	Pump housing - inner diameter	0.4774	m	1.6	ft	
	Pump housing - outer diameter	0.4874	m	1.6	ft	
	Pump housing - wall thickness	5	mm	0.2	inches	
	Return path - thickness	0.0465	m	0.2	ft	
	Casing - inner diameter	0.5804	m	1.9	ft	
	Casing - outer diameter	0.58498	m	1.9	ft	
	Casing - wall thickness	2.29	mm	0.1	inches	

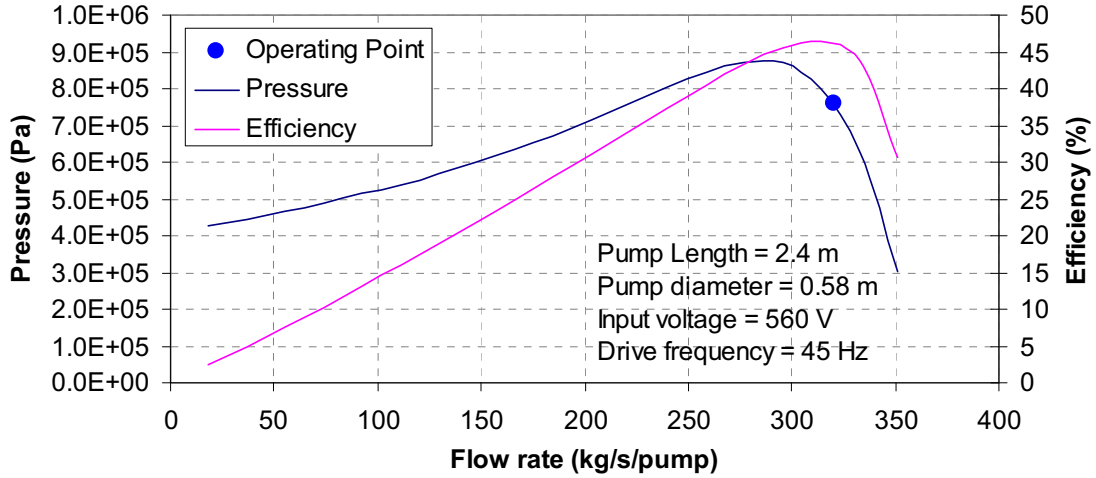


Figure III.1-11 Performance Curve of 2.4 m ALIP

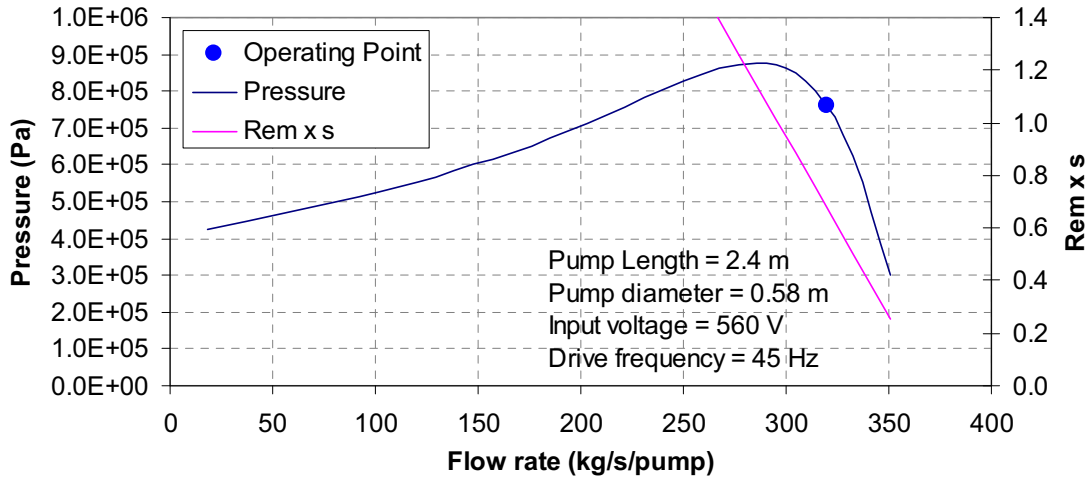


Figure III.1-12 Stable Range of Operation for 2.4 m ALIP

The operating point (primary coolant flow rate of 320 kg/s and pressure head of 760 kPa) is shown as a blue dot in these figures. It must be noted that stable operation of the pump requires that $Rem \times s < \sim 1.5$ where Rem is the magnetic Reynolds number and s is the slip defined below [3-4]:

$$Rem = 2\pi f \frac{\mu}{\rho} \left(\frac{L_p}{\pi} \right)^2 \left(\frac{\tau}{\tau_a} \right), \text{ and } s = \frac{v_s - v_f}{v_s},$$

where f is the drive frequency, μ is the magnetic permeability and $\mu \cong \mu_0$ that is the magnetic permeability of vacuum, ρ is the resistivity of the working fluid, L_p is the pole pitch, τ is the flow channel height, τ_a is the total non-magnetic gap height, v_s is the synchronous velocity defined as $v_s = 2L_p f$, and v_f is the fluid velocity.

Once all dimensions and design parameters are calculated, performance curves of the pump as a function of the drive voltage and frequency are generated and compared with the system curve (flow rate vs pressure drop curve) for the ABTR design to check the stability of the pump at various off-normal conditions. However, the system curve for the ABTR has not yet been developed. Similar stability analyses were conducted for Small Modular Fast Reactor (SMFR) [5], which has somewhat similar hydraulic design parameters as those for ABTR, except pressure drop. In the following, results for the SMFR were used to explain the method of stability analysis and significance of it.

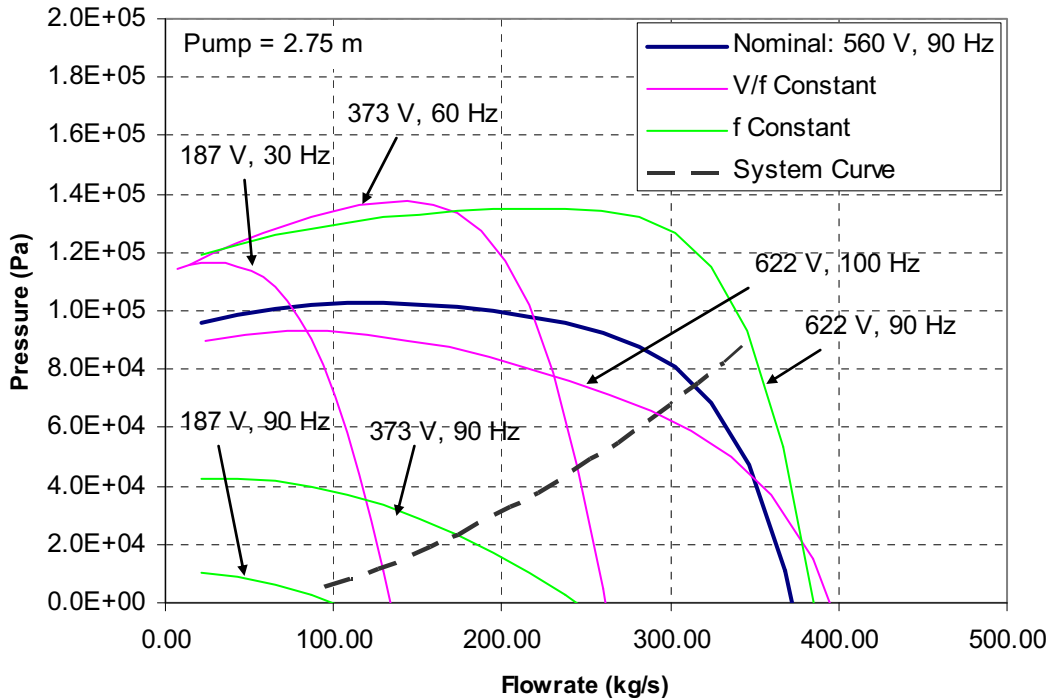


Figure III.1-13 Comparison of Different Control Methods.

One typical method to control an induction motor is constant V/f control. In this method, the ratio of the drive voltage, V to drive frequency, f is kept constant while the drive voltage is reduced from the rated value. This method is used to provide maximum torque at reduced motor speed for an induction motor. Another method is constant frequency control in which the drive frequency is kept constant while changing drive voltage. For hydrodynamic pump applications, since pressure head required at reduced flow rate is generally smaller than that at nominal operating conditions, large pressure head is not required while the pump operates at the reduced flow rates and thus constant frequency method may be suitable. An example comparison of V/f constant control and f constant control is shown in Figure III.1-13. This figure shows that when a flow rate greater than the nominal value is required, the V/f constant control cannot meet the required pumping characteristics. For example, the ALIP performance line for the 622 V and 100 Hz operation crosses the system curve at a flow rate smaller than that at the

nominal condition. On the other hand, the f constant control provides adequate pumping characteristics at a flow rate greater than the nominal value (see the ALIP performance line for the 622 V and 90 Hz operation). However, it is shown that both methods can provide satisfactory pumping characteristics at reduced flow rates. It is also confirmed that the coil temperatures are well below the maximum demonstrated temperature of 1023 K at any operating conditions. The highest coil temperature occurs when the pump is driven at increased drive voltage using the f constant control method ($< \sim 900$ K at 622 V and 90 Hz operation and $< \sim 940$ K at 650 V and 90 Hz operation).

The next figures show the region in which the ALIP operation is stable ($Rem \times s < \sim 1.5$) for V/f constant control (Figure III.1-14) and f constant control (Figure III.1-15). Figure III.1-14 shows that when a flow rate greater than the nominal value is required, an ALIP controlled using the V/f constant control method becomes unstable. On the other hand, an ALIP controlled using the f constant control method becomes unstable, when a flow rate smaller than the nominal value is required, as shown in Figure III.1-15. Table III.1-2 summarizes the applicability of different control methods.

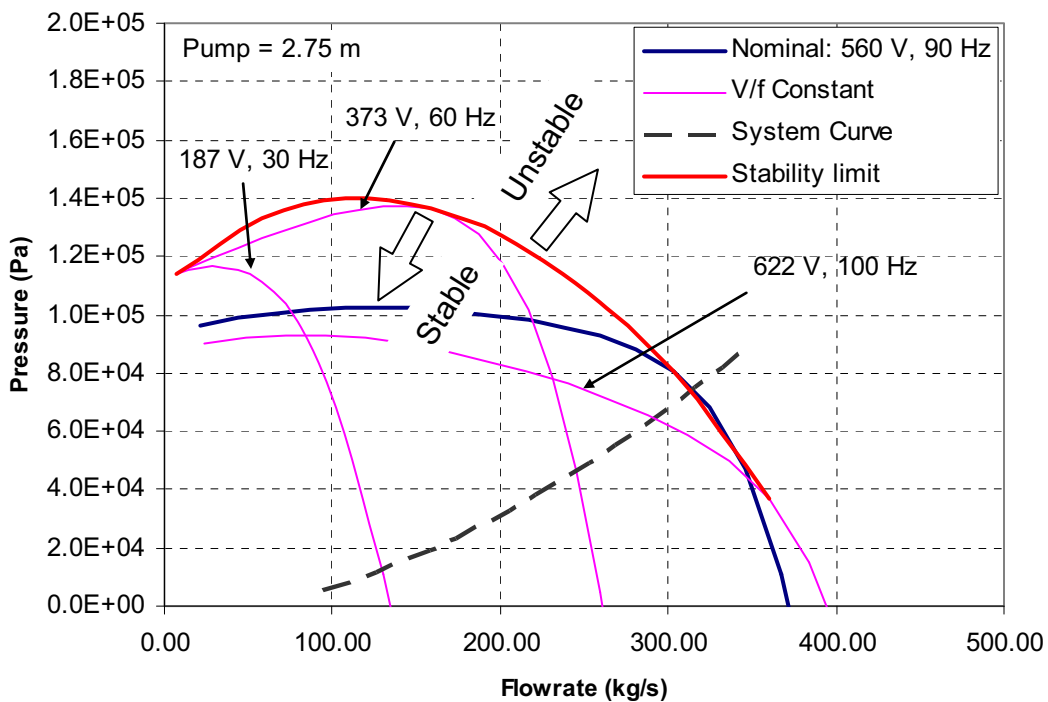


Figure III.1-14 Stability Diagram for V/f Constant Control

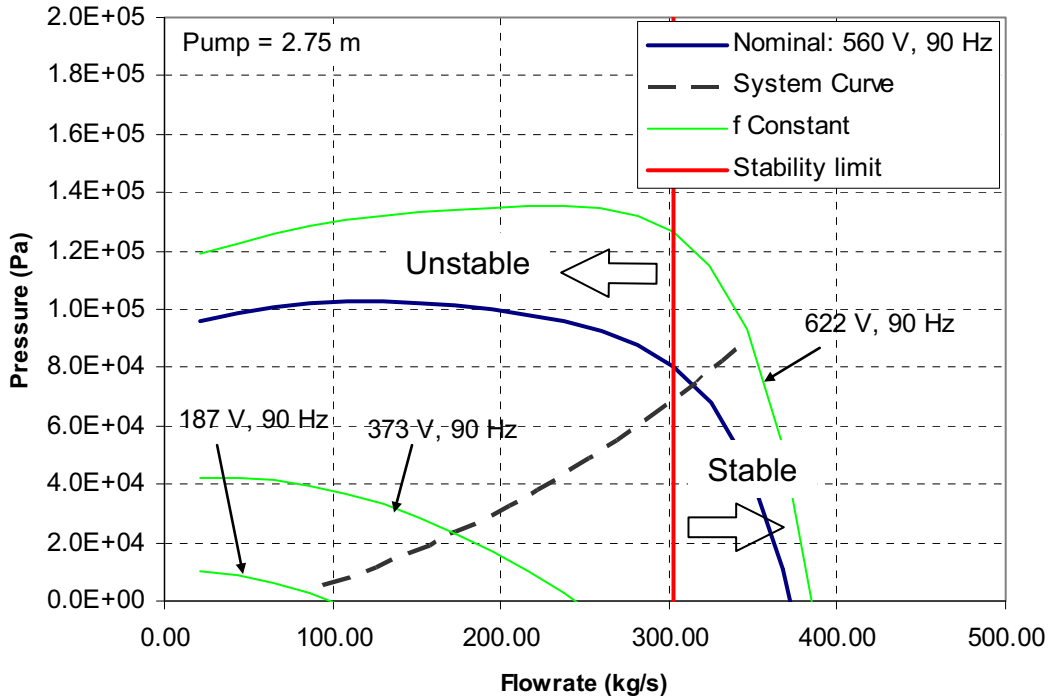


Figure III.1-15 Stability Diagram for f Constant Control

Table III.1-2 Applicability of Different Control Methods

	Reduced Flow Rate		Increased Flow Rate	
	Pumping	Stability	Pumping	Stability
V/f Constant	Good	Good	No Good	No Good
f Constant	Good	No Good	Good	Good

These results indicate that the V/f constant control method is appropriate for ALIP operation at reduced flow rates below the nominal operating condition and the f constant control method is suitable for ALIP operating at increased flow rates above the nominal operating condition (see Figure III.1-16). Detailed pump operation curves for a 2.75 m ALIP using this mixed control method are shown in Figure III.1-17. It has shown that all discussions above are also applicable to other pumps with similar size and performances as well.

These results show that using the V/f constant control at reduced flow rates below the nominal operating condition and the f constant control at increased flow rates above the nominal operating condition, the designed ALIPs for various pump lengths are all capable of meeting the flow rate-pressure requirements for the SMFR design. To employ this mixed control method, the power supply for the ALIP must be able to vary both voltage and frequency simultaneously. It must be noted that the ALIP may be designed

such that the nominal operating condition of the pump is set at 110 % flow rate point and the ALIP is controlled using only the V/f constant control in the entire operating range to simplify the control scheme. Once the system curve for the ABTR is developed, a similar analysis needs to be performed to confirm that the pump designed for the ABTR can be stably operated at all conditions; however, since the size and performance of the ABTR pumps are very similar to the SMFR pumps, the analysis is expected to show that the ABTR pumps can be stably operated using similar control methods described here.

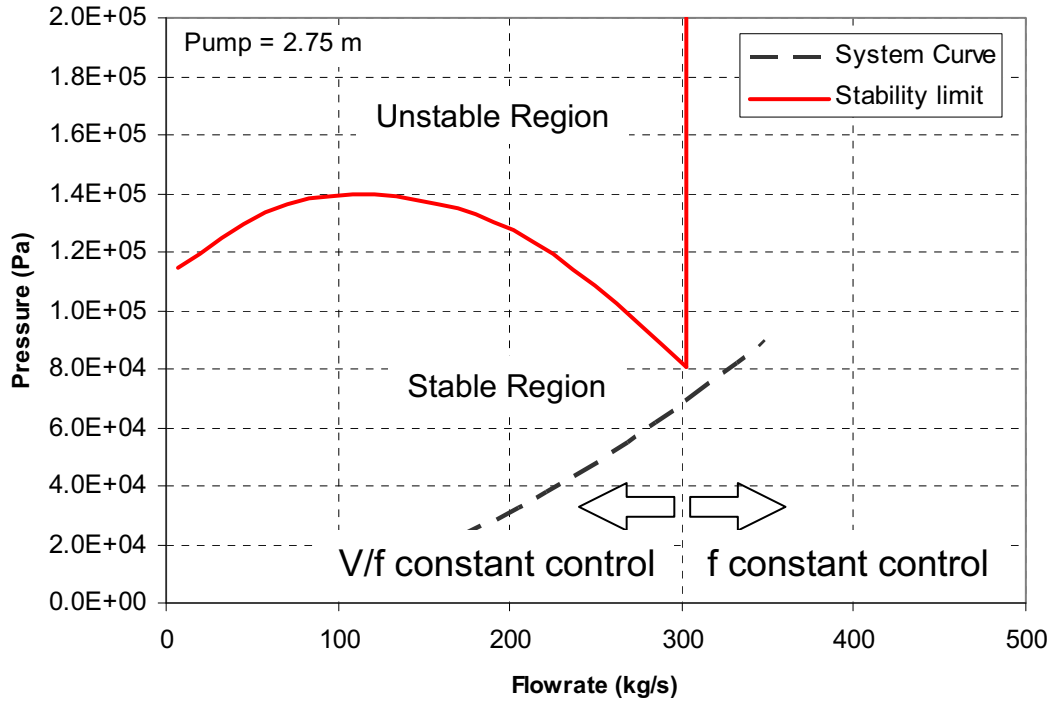


Figure III.1-16 Overall Stability Diagram

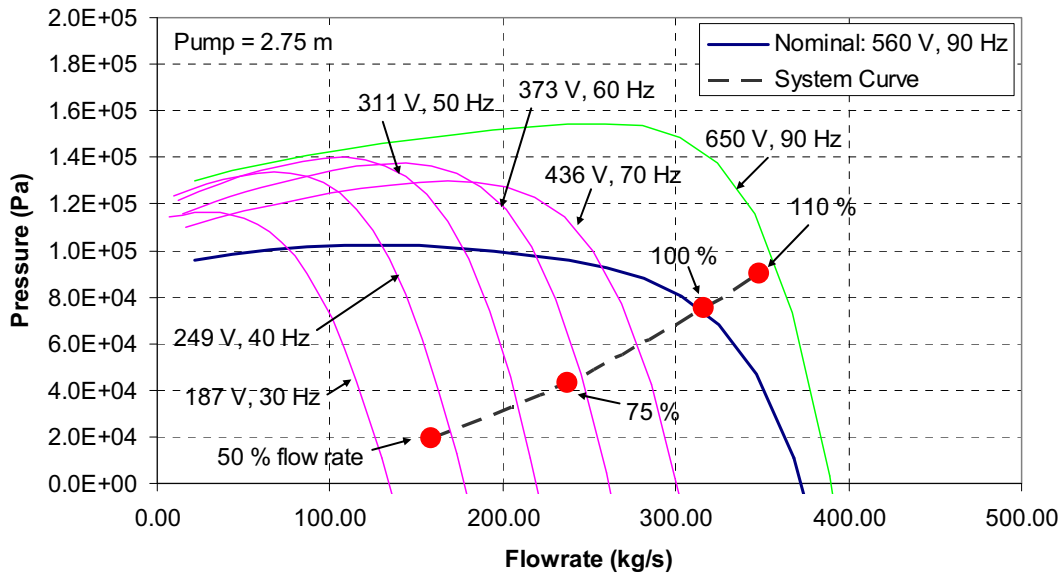


Figure III.1-17 Pump Operation Curves and System Curve for 2.75 m ALIP

References

1. Charnock, H. O. and Holz, H. B., "Sodium Systems Components," Sodium Technology, Session IV, Atomic International, North American Rockwell, 1970.
2. Babcock, W., "State of Technology Study – Pumps Experience with High Temperature Sodium Pumps in Nuclear Reactor Service and Their Application to FFTF," BNWL-1049 UC-80, Reactor Technology, Battelle Memorial Institute Pacific Northwest Laboratories, Richland, Washington, 1969.
3. H. Ota et al., "Development of 160 m³/min Large Capacity Sodium-Immersed Self-Cooled Electromagnetic Pump," J. of Nucl. Sci. and Tech. v41, No4, pp511-523, 2004.
4. R. Stieglitz, "MHD-features of the Main Service and Bypass Pump in the MEGAPIE Design," ISSN 0947-8620, Forschungszentrum Karlsruhe GmbH, Karlsruhe, 2003.
5. ANL-SMFR-1, Small Modular Fast Reactor Design Description, 2005.

III.2 IHX and DRACS Sizing Calculations

As noted in Sections II.3.3 and II.6, thermal hydraulic analyses were performed in order to form the technical basis for the sizing of both the IHX and DRACS in-vessel heat exchangers and the results are summarized here.

In terms of the thermodynamic analysis required to estimate the overall unit size needed to achieve the specified thermal rating, the forced convection heat transfer coefficients on the shell and tube sides are calculated using the well-known Lockhart-Martinelli correlation which was developed on the basis of forced convection heat transfer from liquid metals:

$$Nu = \frac{hD_e}{k} = 5.0 + 0.025(Re \cdot Pr)^{0.8}$$

where

Nu	=	Nusselt number,
h	=	forced convection heat transfer coefficient,
Pr	=	Prandlt number = $\mu c/k$,
k	=	sodium thermal conductivity ~ 69 W/m-K,
c	=	specific heat ~ 1283 J/kg-K,
Re	=	Reynolds number = $\rho Du / \mu$
D	=	equivalent diameter of flow channel = tube ID for tube-side flow,
	=	(4·channel flow area)/wetted perimeter for shell side.

For pitch-to-diameter (P/D) ratios of > 1.1, the above correlation results in errors of no more than 10 % on the shell side of the IHX.

Aside from the thermodynamic calculations, the pressure drop on the tube side of the heat exchangers is calculated to facilitate pump selection and design considerations. In particular, the pressure drop is calculated using the standard Bernoulli equation modification to account for frictional drag as well as tube bank entrance and exit form losses; i.e.,

$$\Delta P_t = (K_{entr} + K_{exit} + fL / D_i) \frac{1}{2} \rho u^2$$

where

u	=	flow velocity,
K_{entr}	=	tube entrance loss coefficient (typically taken as ~0.5),
K_{exit}	=	tube exit loss coefficient (typically taken as ~1.0),
f	=	friction factor evaluated from Blasius correlation = $0.3164/Re^{1/4}$,
Re	=	Reynolds number = $\rho D_i u / \mu$
D_i	=	tube inner diameter,
L	=	tube bundle length,
μ	=	sodium viscosity ~ $2.76 \cdot 10^{-4}$ kg/m-sec, and
ρ	=	sodium density ~ 850 kg/m ³ .

The pressure drop analysis on the shell side is complicated by the fact that an orificed baffle plate design has been adopted in order to minimize pressure drop. Although well-established correlations have been developed for evaluating pressure drop for the case of impervious plates [1], suitable correlations for the case of orificed plates could not be identified in the literature. On this basis, a correlation was developed and validated against other IHX designs that feature orificed baffle plates. The specific correlation is presented below; complete modeling details can be found in reference [2].

For the case of orificed baffle plates, the flow pressure drop is evaluated through the following correlation:

$$\Delta P_s = \frac{C}{2\rho} (N_b + 1) \left(\frac{\mu N_T}{D_o} \right)^{0.135} (FG_c)^{1.73}$$

where

$$\begin{aligned} D_o &= \text{tube outside diameter,} \\ G_c &= \text{mass flux through bundle in cross flow} = \frac{\dot{m}}{B(P - D_o)N_T}, \\ N_t &= \text{number of tubes in cross-flow, perpendicular to flow direction,} \\ N_b &= \text{number of baffle plates,} \\ P &= \text{tube pitch,} \\ B &= \text{baffle plate pitch (i.e., distance between plates),} \\ \dot{m} &= \text{shell-side mass flowrate,} \\ C &= \begin{cases} 3.59 + 8.34(1.44 - P/D_o), & P/D_o < 1.44, \\ 3.59, & P/D_o \geq 1.44 \end{cases} \end{aligned}$$

and F is the fraction of the total shell side mass flowrate that remains in a cross-flow configuration during flow past an individual baffle plate. This fraction is evaluated through the following transcendental equation:

$$1 - F = \omega F^{0.865}$$

where

$$\omega = \frac{\pi}{2} N_x^{1.5} \left(\frac{C}{K_h} \right)^{0.5} \frac{D_h^2}{[(P - D_o)B]^{0.865}} \left(\frac{\mu N_T}{D_o \dot{m}} \right)^{0.135}$$

and

$$\begin{aligned} D_h &= \text{orifice hole diameter,} \\ K_h &= \text{orifice hole form loss coefficient} \sim 1.5, \text{ and} \\ N_x &= \text{number of tube rows in cross flow, parallel with flow direction.} \end{aligned}$$

In terms of the approach for carrying out the parametric calculations, the number of heat exchanger tubes is treated as the independent variable. The required tube length is then calculated as the key model output, and the minimum heat exchanger cross-sectional area is given by tube unit cell cross-sectional area multiplied by the total number of tubes.

This approach provides the overall heat exchanger size to be selected on the basis of the available cross sectional area, or the available elevation space, whichever is desired.

In terms of the design calculations for the IHX, tube diameter was selected to be identical to the PRISM IHX. For completeness, the calculations were carried for a variety of P/D ratios with the temperature differentials on the primary and secondary sides fixed at the design levels shown in Table II.3-5. The thermal conductivity of the 9Cr-1Mo tubes was taken as 28 W/m-°C.

The results of the calculations for the IHX are shown in Figures III.2-1 through III.2-4, which provide the tube sheet planar area, tube length, and pressure drop across the shell and tube sides vs. number of heat exchanger tubes for a range of P/D ratios from 1.2 to 1.8. To compromise between the planar area of the reactor vessel occupied by the IHXs and the primary side pressure drop, an intermediate value of the P/D ratio of 1.4 was selected for the current design. Given the equipment distribution within the reactor vessel, ~1.6 m² of cross sectional area is available to accommodate each IHX. Factoring in the shell thickness of 1.9 cm, as well as the downcomer pipe planar area, then the available area for the tube sheet is reduced to ~1.5 m². Thus, from Figure III.2-1, an IHX with a total of ~ 3300 tubes is selected to fit into the available space. From Figure III.2-2, for the case of P/D=1.4, the active tube length must be at least 3.5 m to achieve the target thermal rating of 125 MW per IHX. For these purposes, the IHX tube length is increased to 3.85 m (see Table II.3-5) to provide a 10% design margin in the heat exchanger thermal capacity. With the tube length specified, the minimum required elevation space to accommodate the IHXs in the vessel plan view is determined. From Figures III.2-3 and III.2-4, the pressure drop across the primary and secondary sides of the tube bank are found to be 12.6 and 5.7 kPa, respectively, for the case of P/D = 1.4. The primary side pressure drop thus sets the pressure head required to drive the 628 kg/sec sodium flowrate through the IHX at ~ 1.5 m at full power conditions.

Figures III.2-5 through III.2-7 provide the analogous plots of planar area, tube length, and pressure drop across shell and tube sides vs. number of heat exchanger tubes for the 625 kW DRACS heat exchangers that are incorporated as part of the shutdown heat removal system described in Section II.6. Key design parameters for these units are summarized in table II.6-1.

References

1. D. Q. Kern, process heat transfer, McGraw-Hill Book Co., New York, NY, 1950.
2. M. T. Farmer, Intra-Laboratory Memo to C. Grandy, ANL, May 18, 2006.

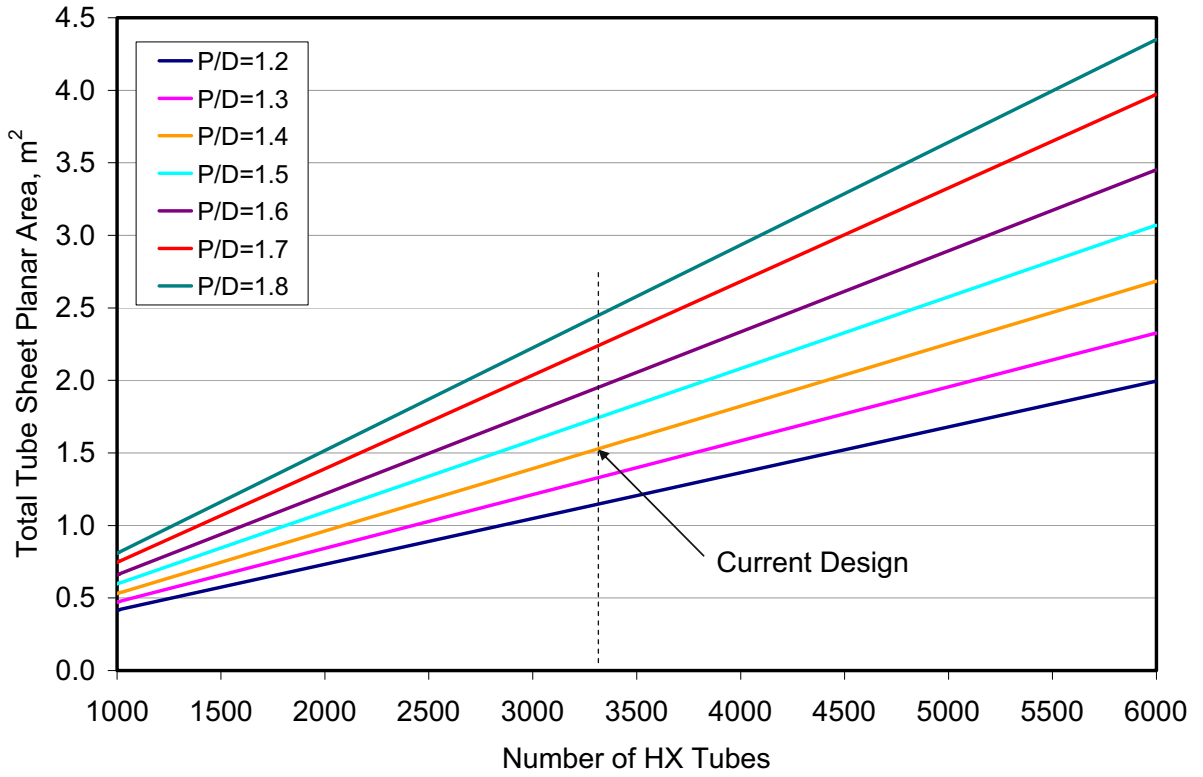


Figure III.2-1 IHX tube sheet planar area vs. no. of tubes for various p/d ratios

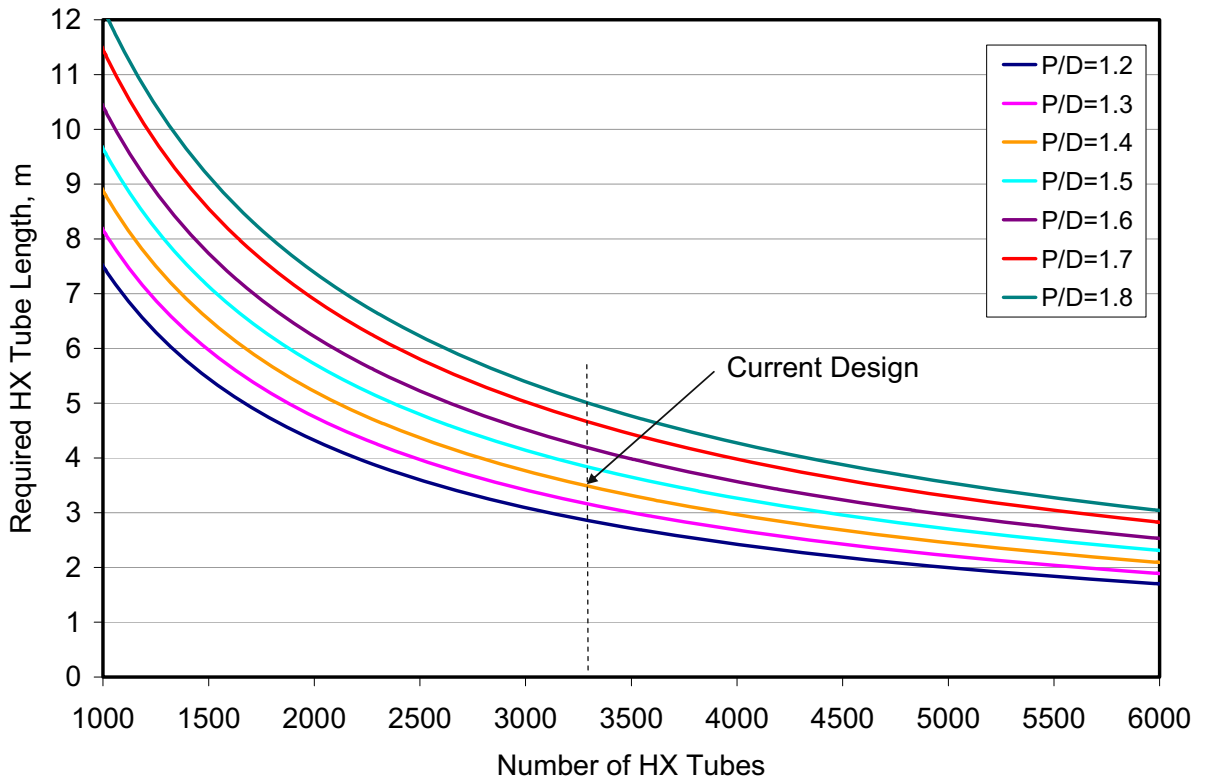


Figure III.2-2 IHX tube length vs. no. of tubes for various p/d ratios

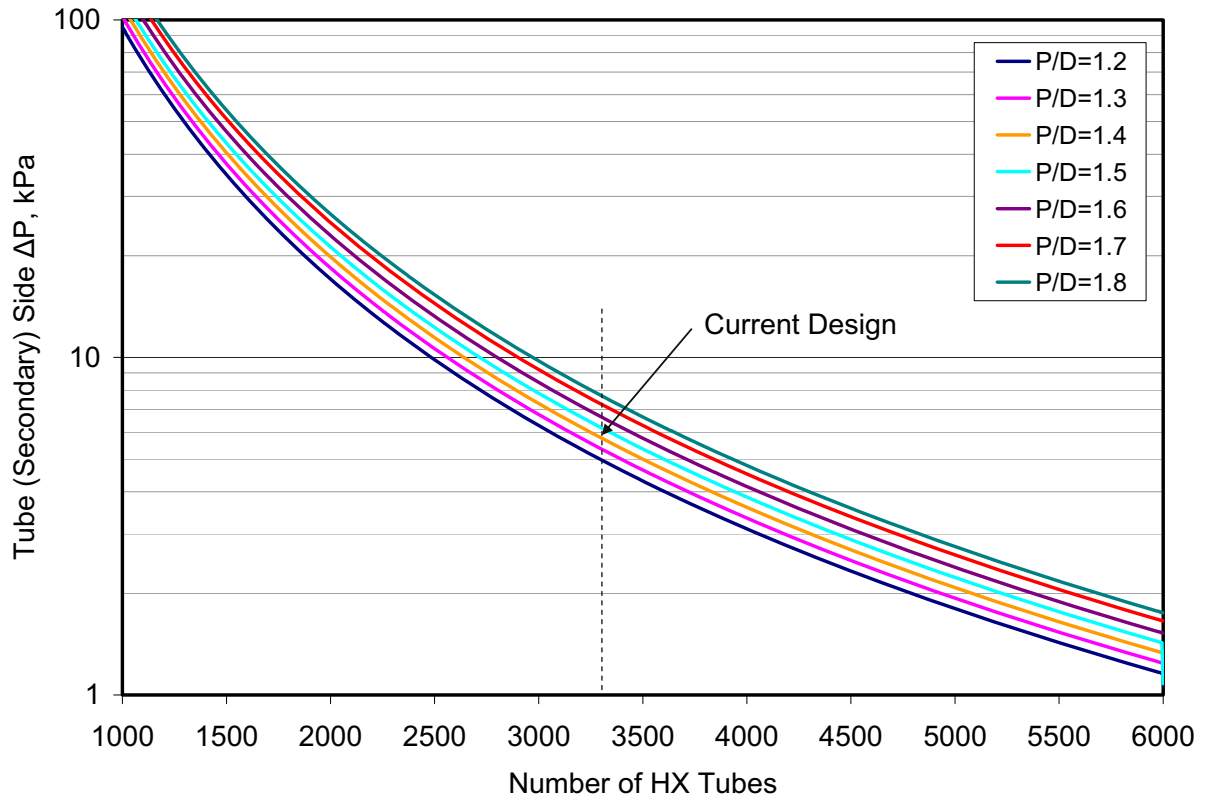


Figure III.2-3 IHX secondary (tube) side Δp vs. no. of tubes for various p/d ratios

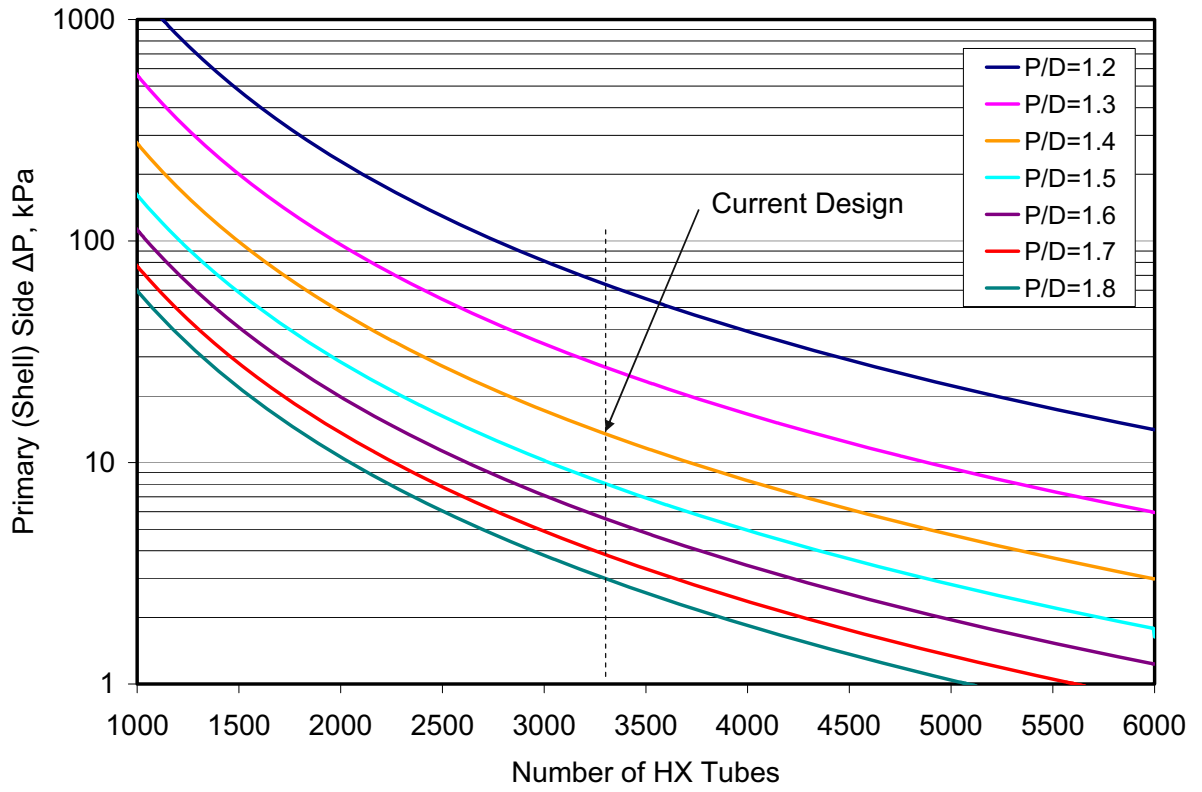


Figure III.2-4 IHX primary (shell) side Δp vs. no. of tubes for various p/d ratios

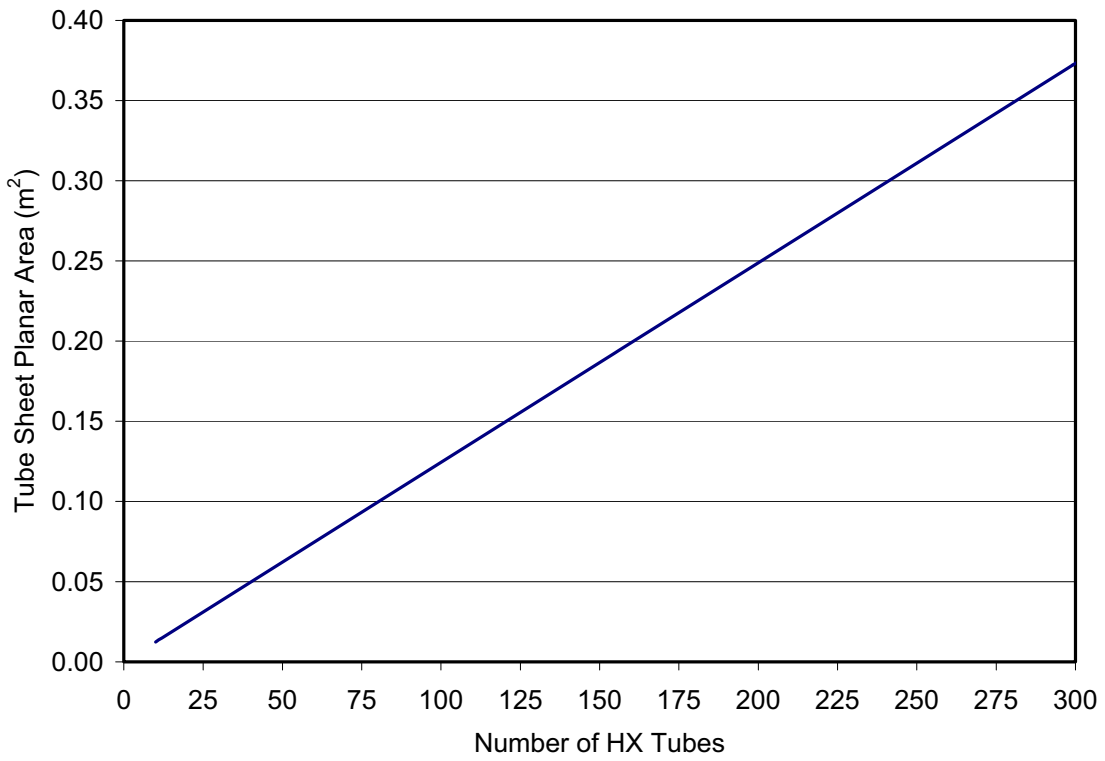


Figure III.2-5 DRACS HX tube sheet planar area vs. number of tubes

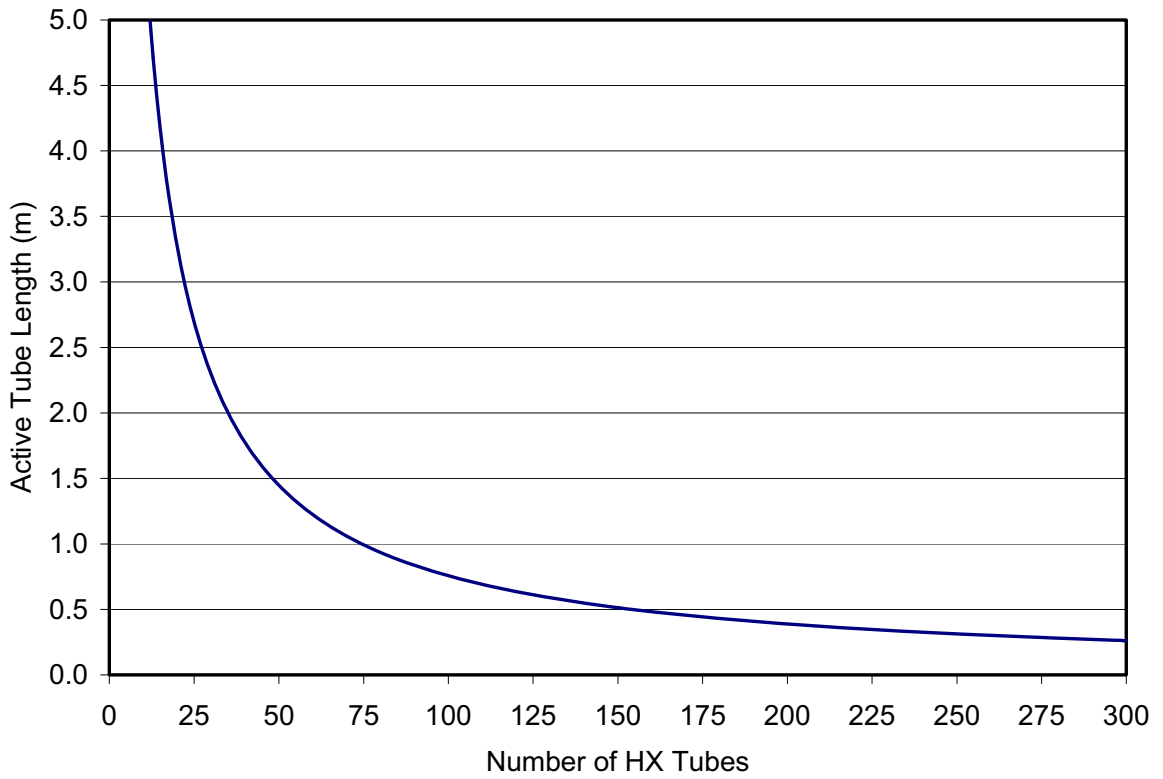


Figure III.2-6 DRACS HX tube length vs. number of tubes

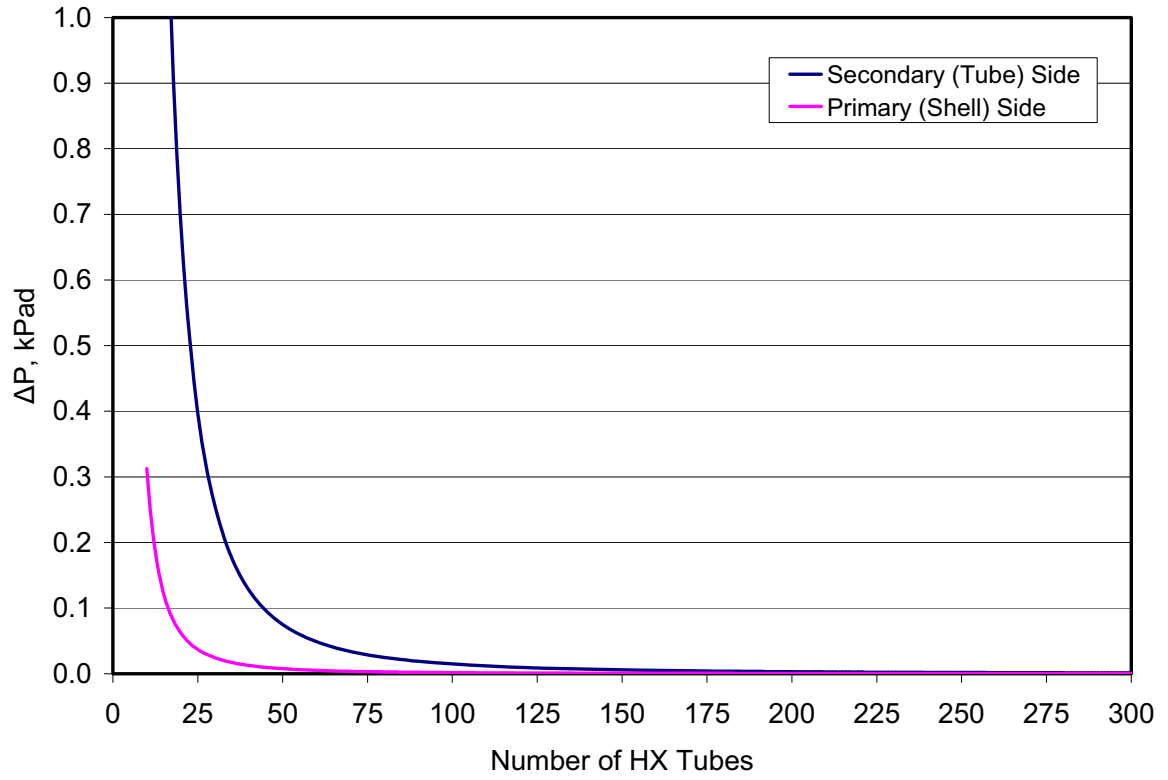


Figure III.2-7 DRACS HX primary (shell) and secondary (tube) side Δp vs. no. of tubes

III.3 Supercritical CO₂ Brayton Cycle

III.3.1 Turbine Generator

The turbine design and optimization analyses are presented in this section. As shown in Figure III.3-1, six stages is selected as the optimal number. The turbine is manufactured largely from Inconel-based alloys that are selected for their strength and low coefficients of thermal expansion as well as their resistance to oxidation by CO₂ over the normal operating temperature range. The turbine also incorporates a diffuser which increases the overall length beyond that of the rotor and stator stages.

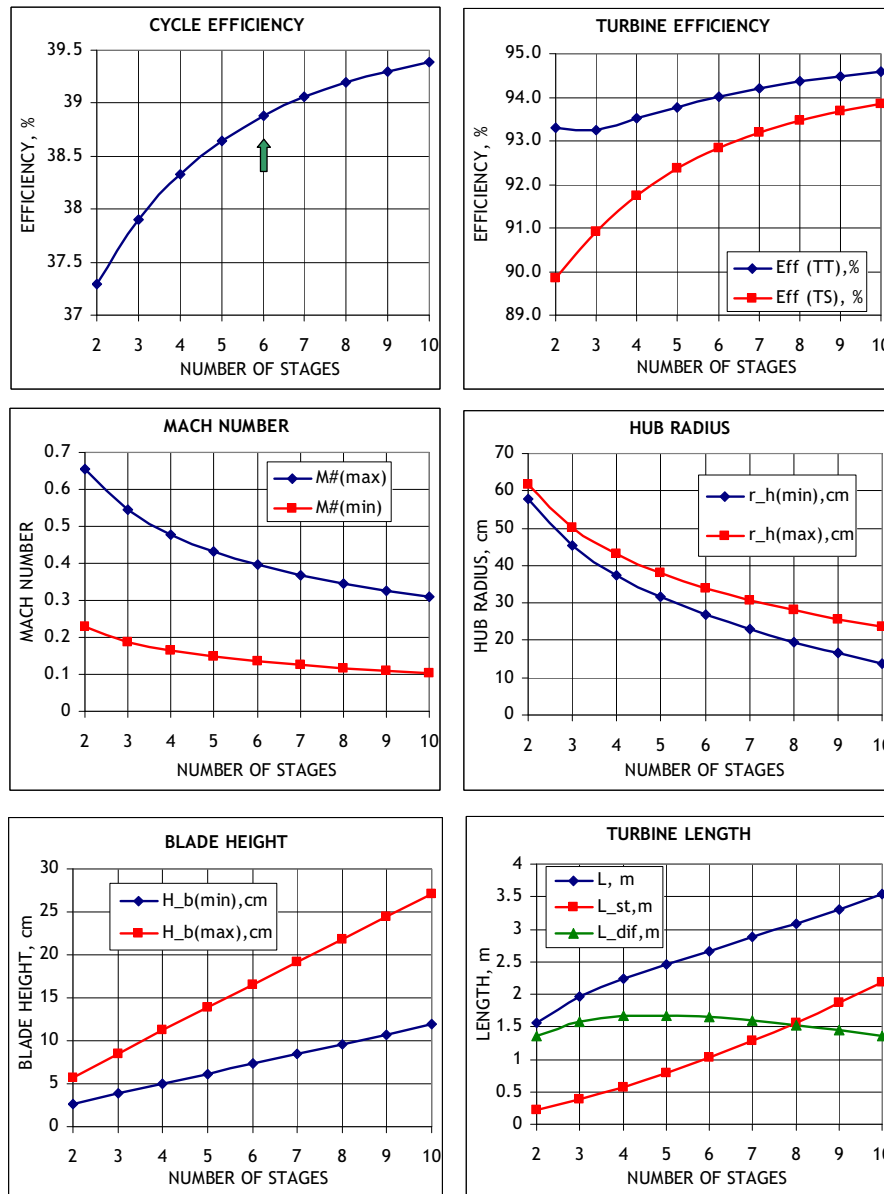


Figure III.3-1 Results of Turbine Pre-Conceptual Design and Optimization Analyses

III.3.2 Compressor

The results of pre-conceptual design and optimization analyses for the compressor are presented in Figures III.3-2 and III.3-3. Pre-conceptual designs having only one and two stages have been selected for Compressors No. 1 and 2, respectively. A comparison of performance for single-stage and two-stage pre-conceptual designs for Compressor No.1 is provided in Figure III.3-4. It is observed that nearly the same efficiency is attained with a single stage as with two stages while the operating range is wider with a single stage. In addition, the amount of alloy materials is reduced decreasing the compressor cost. Similar to the turbine, the compressors possess remarkably small dimensions due to the high density of supercritical CO₂ and the small number of stages. The compressors are mainly fabricated from Inconel alloys and austenitic stainless steel for strength, low thermal expansion, and resistance to corrosion by CO₂. Figures III.3-5 and III.3-6 provide examples of the optimization of compressor pre-conceptual design as well as sensitivity of compressor and cycle efficiencies to the diffuser incidence angle and return channel loss coefficient, respectively.

III.3.3 Sodium-to-CO₂ Heat Exchanger

It is observed from Figures III.3-7 through III.3-9 that a PCHE unit length of 1.0 m optimizes the S-CO₂ Brayton cycle efficiency while maintaining a low pressure drop on the sodium flow side and a reasonably high turbine inlet temperature on the CO₂ side; this value is therefore selected for the unit length. For a fixed PCHE unit length, increasing the number of PCHE units increases the cycle efficiency. However, it also increases the total cost of the sodium-to-CO₂ heat exchangers. Thus, there is a tradeoff between cycle efficiency and cost. Figure III.3-10 shows the relationship between the total cost of the sodium-to-CO₂ heat exchangers and the S-CO₂ Brayton cycle efficiency. A cost of \$ 60 per Kilogram of PCHE metal alloy mass is assumed. This number should be taken as only illustrative to demonstrate the tradeoff involved. For the selected point, 64 PCHE units are incorporated into the sodium-to-CO₂ heat exchangers.

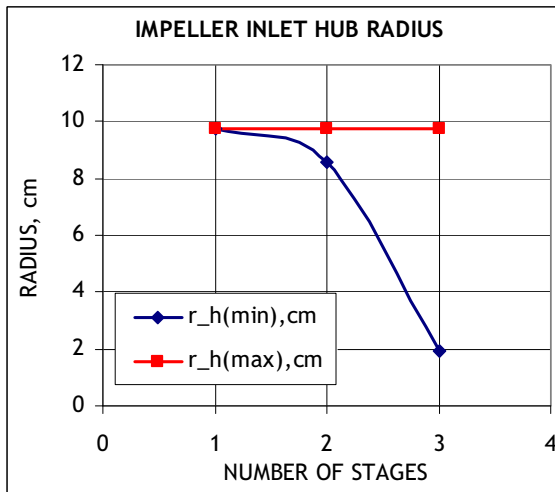
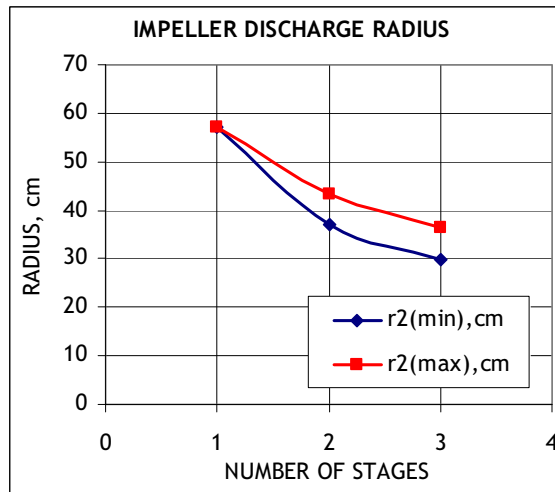
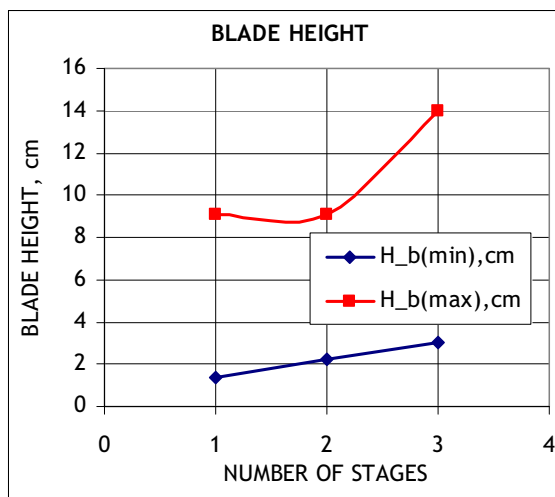
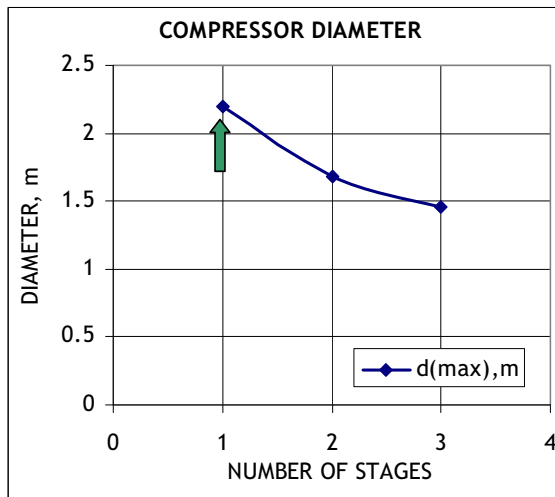
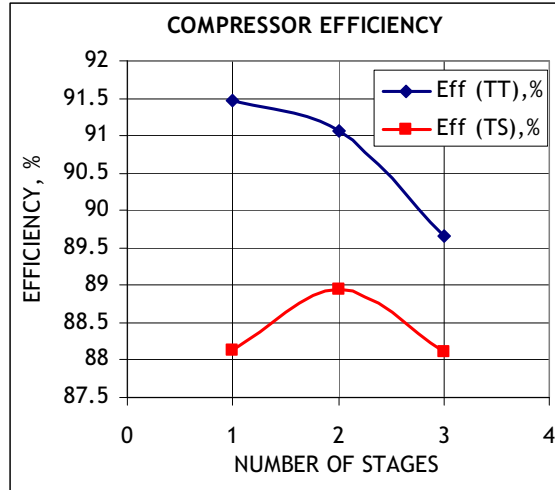
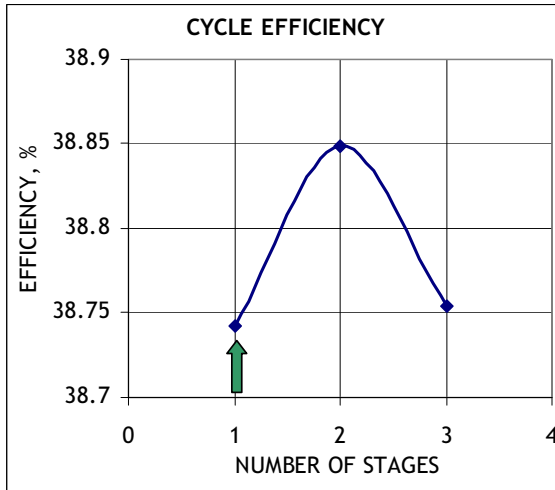


Figure III.3-2 Results of Compressor No. 1 Pre-Conceptual Design and Optimization Analyses

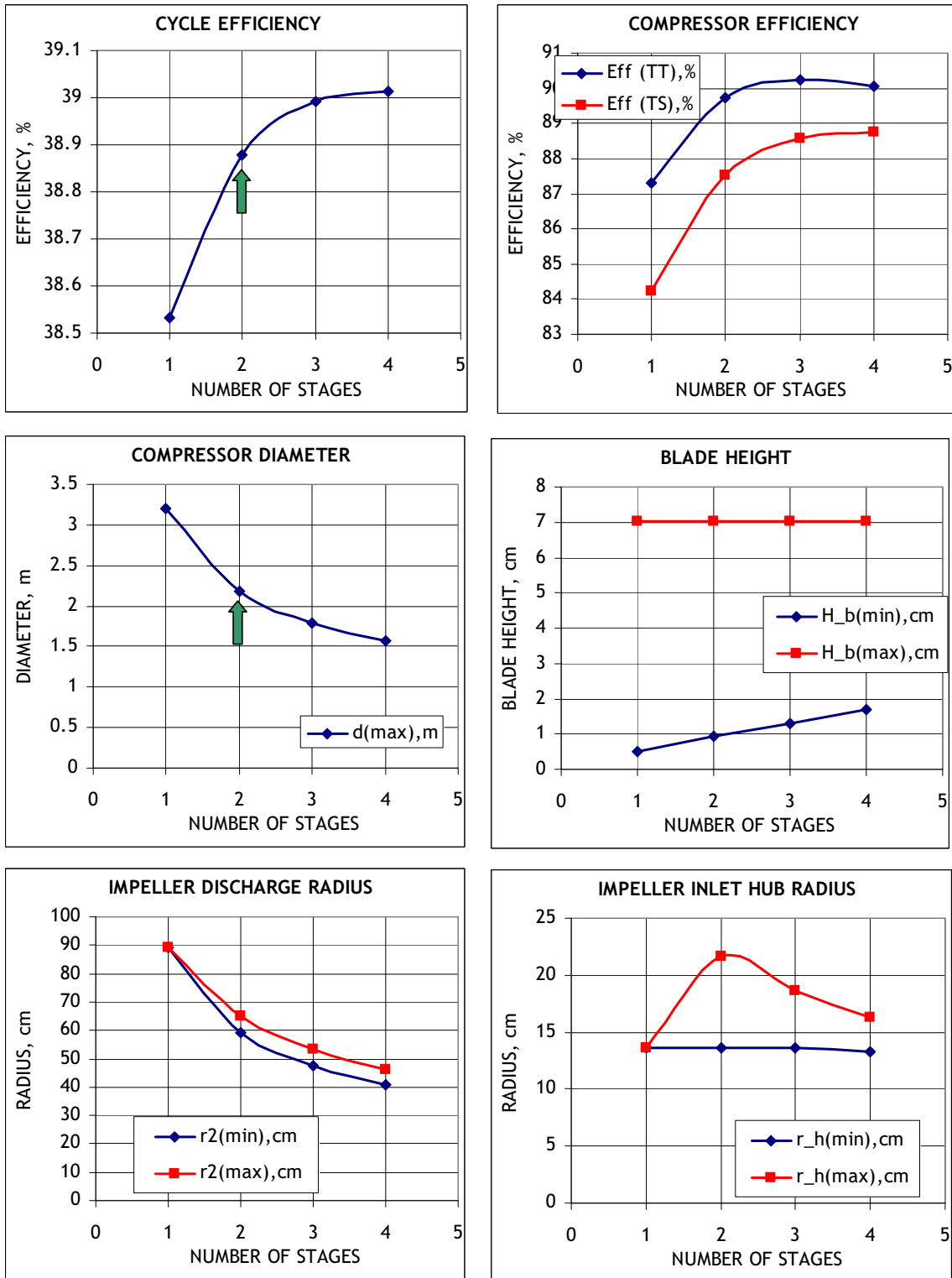
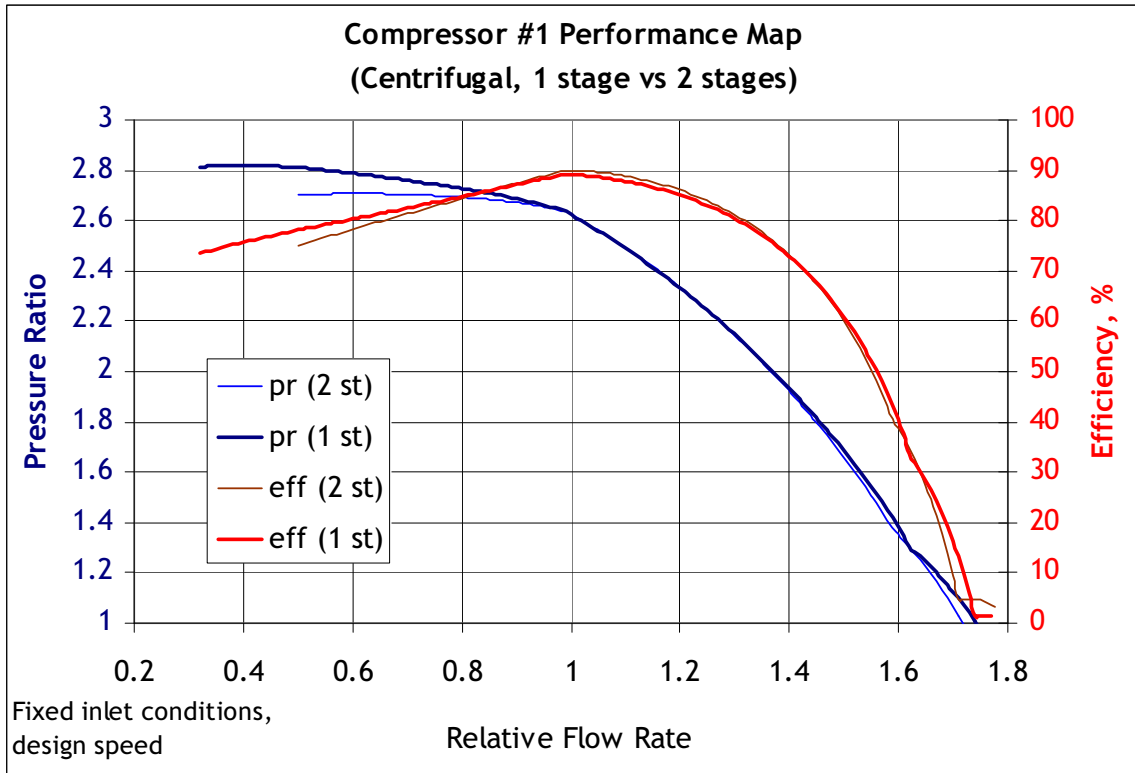


Figure III.3-3 Results of Compressor No. 2 Pre-Conceptual Design and Optimization Analyses



**Figure III.3-4 Comparison of Performance Maps for Compressor No. 1
Single-Stage and Two-Stage Pre-Conceptual Designs**

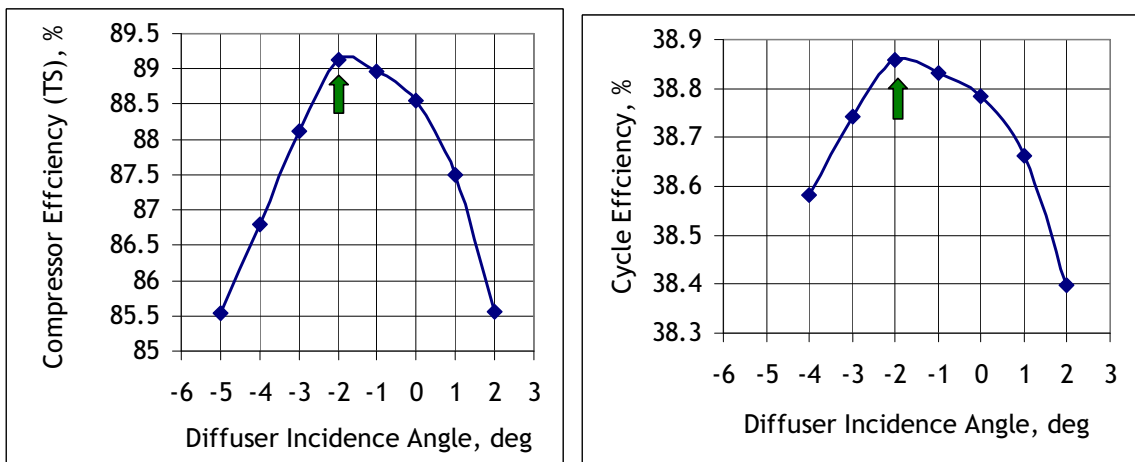


Figure III.3-5 Optimization of Diffuser Incidence Angle for Compressor No. 1 Pre-Conceptual Design

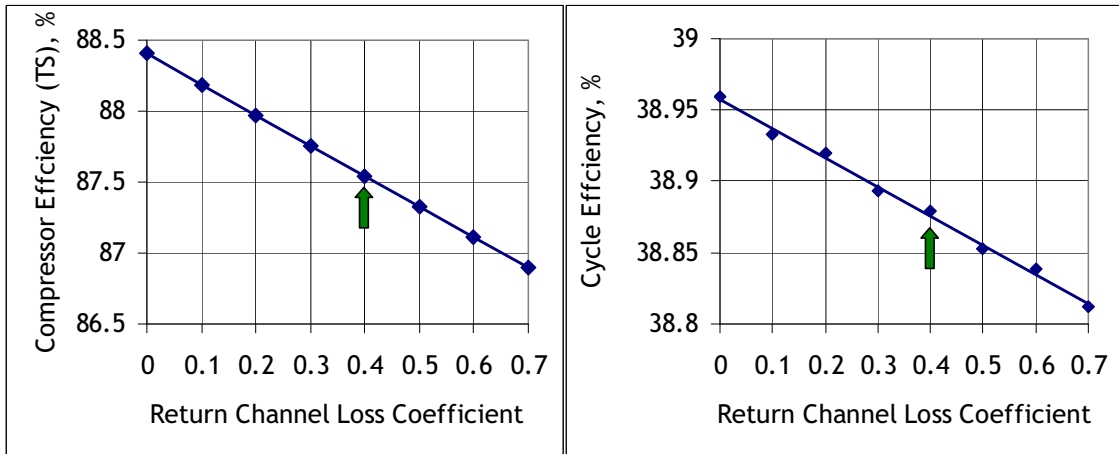


Figure III.3-6 Dependency of Compressor and Cycle Efficiencies upon Return Channel Loss Coefficient for Compressor No. 2

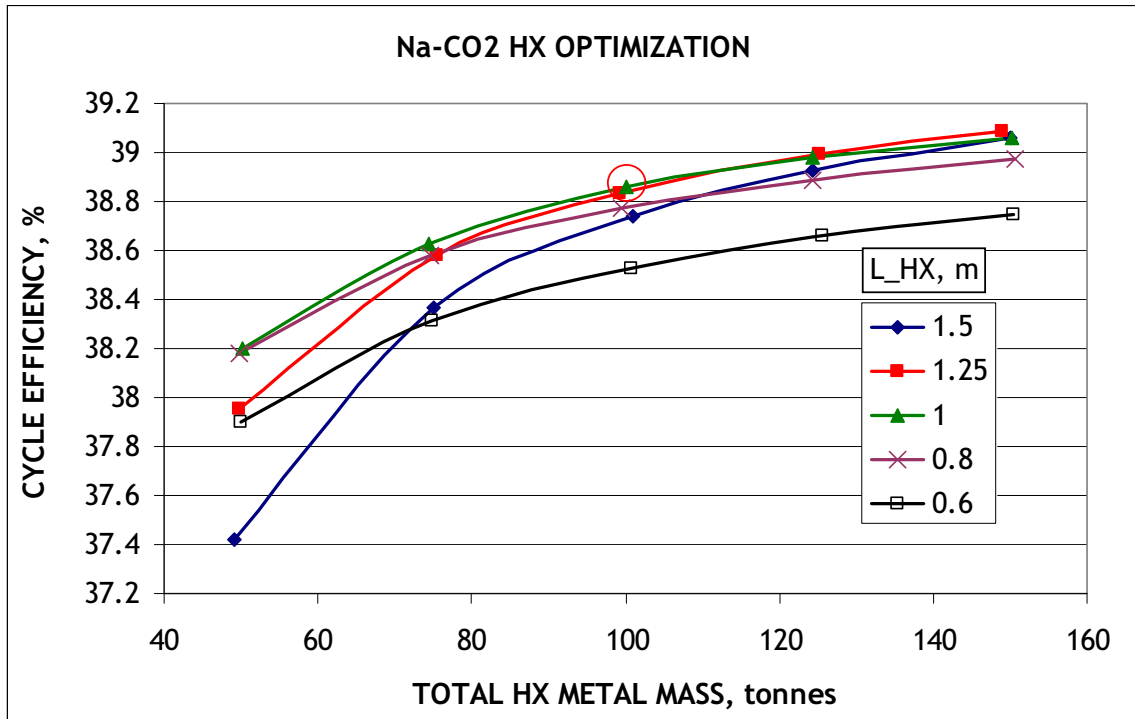


Figure III.3-7 Dependency of S-CO₂ Brayton Cycle Efficiency upon Total Sodium-to-CO₂ Heat Exchanger Metal Alloy Mass for Fixed PCHE Unit Length

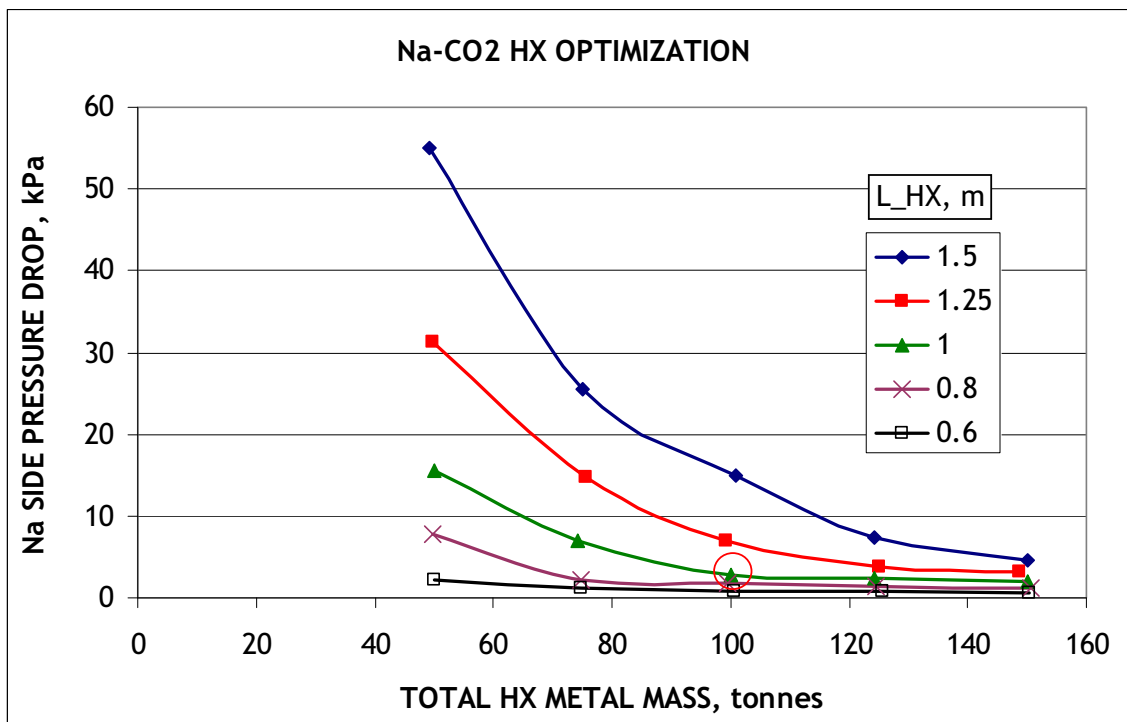


Figure III.3-8 Dependency of Sodium Side Pressure Drop upon Total Sodium-to-CO₂ Heat Exchanger Metal Alloy Mass for Fixed PCHE Unit Length

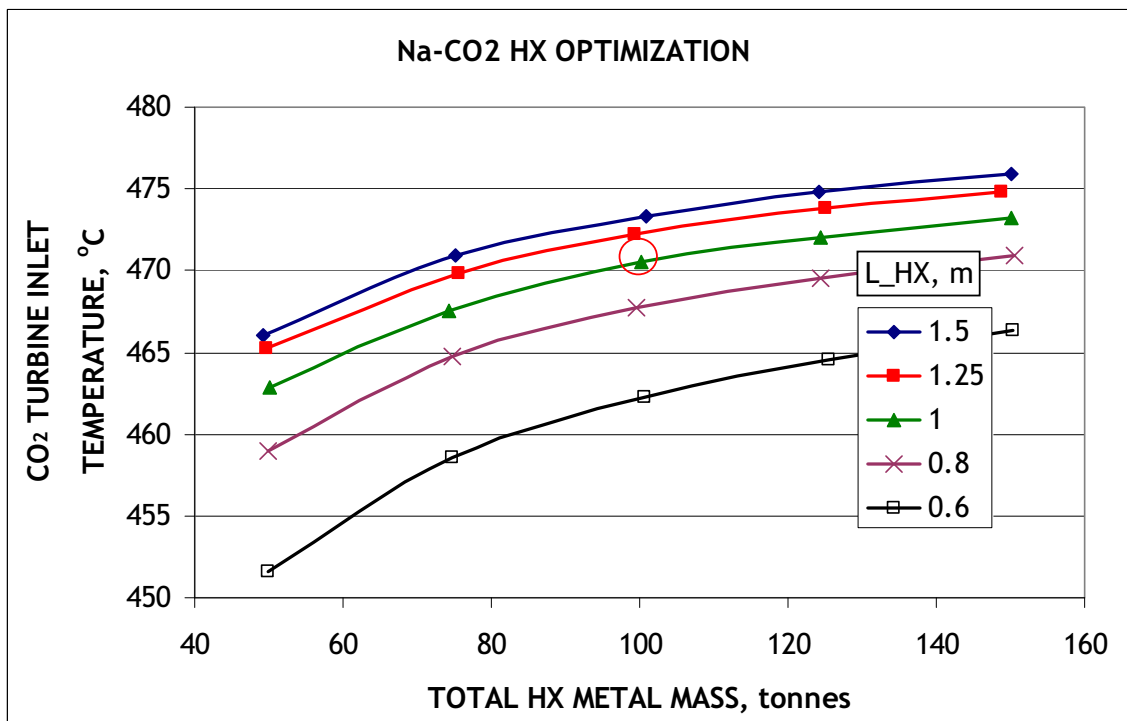


Figure III.3-9 Dependency of CO₂ Turbine Inlet Temperature upon Total Sodium-to-CO₂ Heat Exchanger Metal Alloy Mass for Fixed PCHE Unit Length

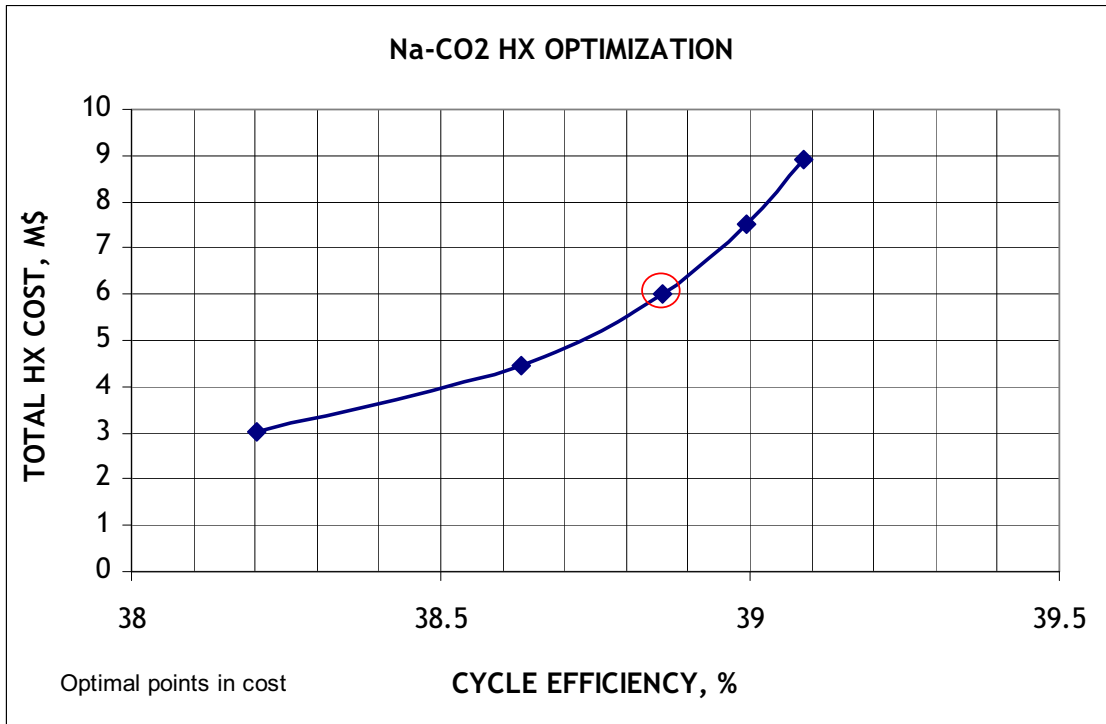


Figure III.3-10 Tradeoff Between Total Sodium-to-CO₂ Heat Exchanger Cost and S-CO₂ Brayton Cycle Efficiency (Assuming Illustrative Cost of \$ 60/Kg of PCHE Metal Alloy Mass)

III.3.4 Recuperator

Each zigzag semicircular channel of the high temperature recuperator (HTR) is selected to have a diameter of 1.5 mm, a lateral pitch of 2.3 mm, and a plate thickness of 2.0 mm. Figures III.3-11, III.3-12, and III.3-13 show the results of pre-conceptual design and optimization analyses for the HTR from which it is determined that a HTR PCHE unit length of 0.6 m optimizes the S-CO₂ Brayton cycle efficiency while maintaining a reasonable recuperator effectiveness and CO₂ turbine inlet temperature. The tradeoff between HTR cost and S-CO₂ Brayton cycle efficiency is illustrated in Figure III.3-14. For the selected point, the HTR consists of 64 PCHE units.

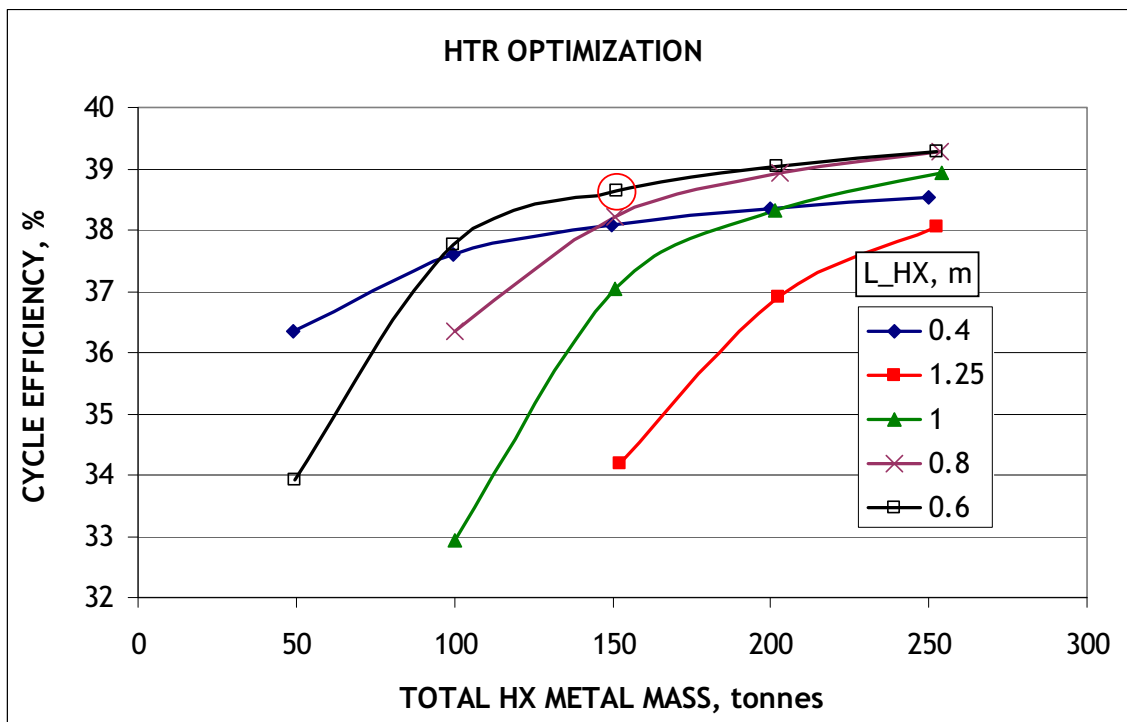


Figure III.3-11 Dependency of S-CO₂ Brayton Cycle Efficiency upon Total High Temperature Recuperator Metal Alloy Mass for Fixed PCHE Unit Length

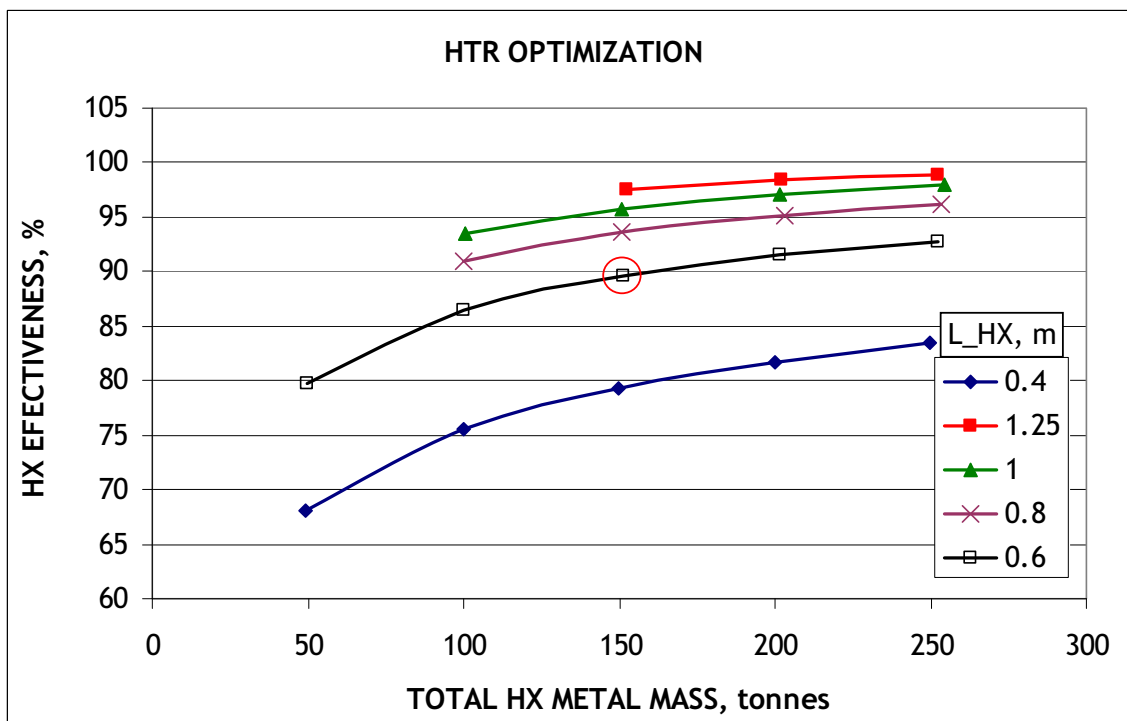


Figure III.3-12 Dependency of High Temperature Recuperator Effectiveness upon Total High Temperature Recuperator Metal Alloy Mass for Fixed PCHE Unit Length

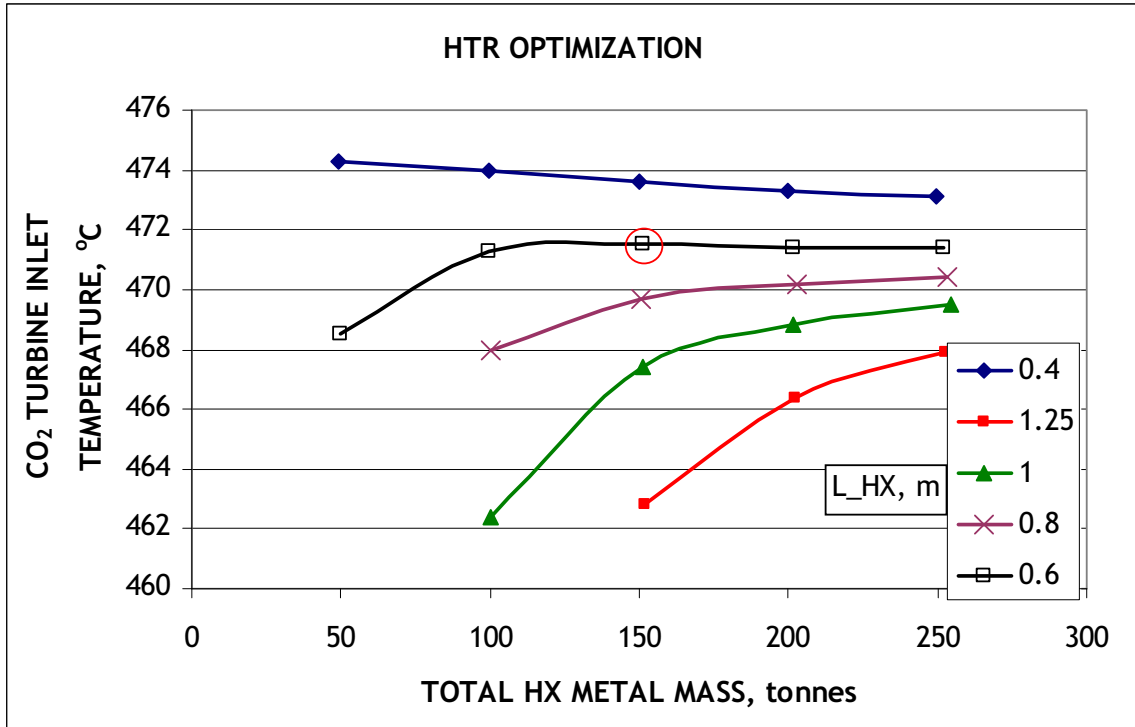


Figure III.3-13 Dependency of Turbine Inlet Temperature upon Total High Temperature Recuperator Metal Alloy Mass for Fixed PCHE Unit Length

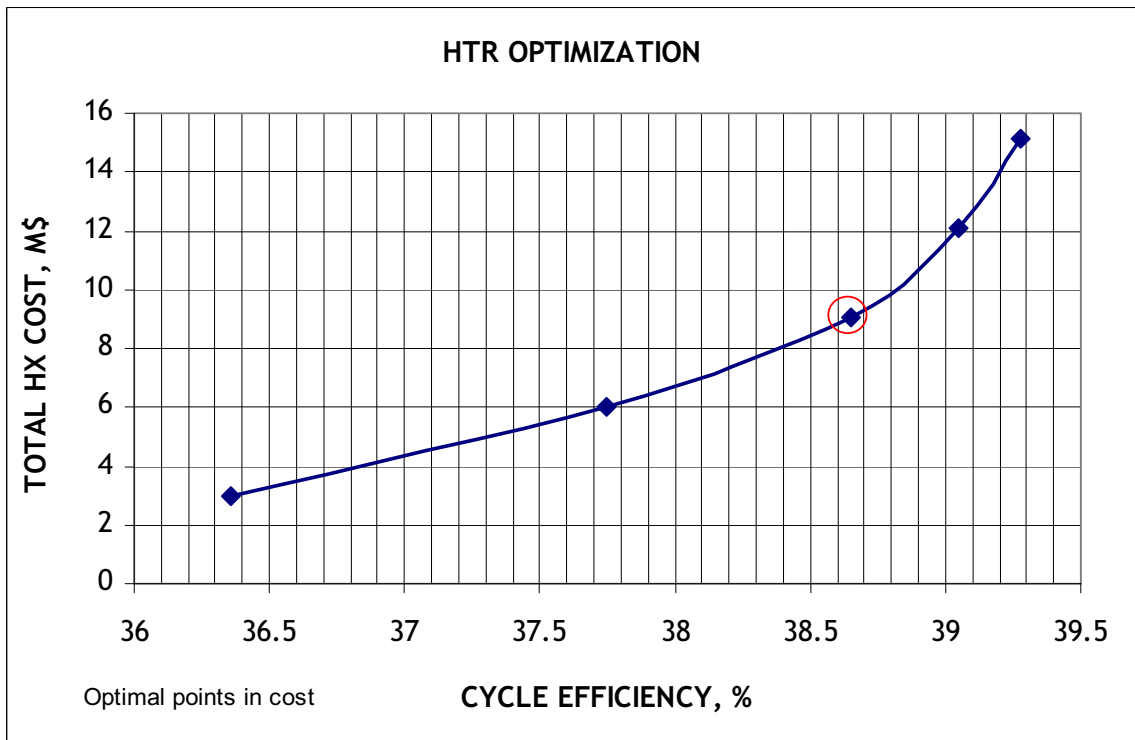


Figure III.3-14 Tradeoff Between Total High Temperature Recuperator Cost and S-CO₂ Brayton Cycle Efficiency (Assuming Illustrative Cost of \$ 60/Kg of PCHE Metal Alloy Mass)

The low temperature recuperator (LTR) semicircular channels are also selected to have a diameter of 1.5 mm, a lateral pitch of 2.3 mm, and a plate thickness of 2.0 mm. Figures III.3-15, III.3-16, and III.3-17 show the results of pre-conceptual optimization analyses for the LTR from which it is determined that a LTR PCHE unit length of 0.8 m optimizes the S-CO₂ Brayton cycle efficiency while maintaining a reasonable recuperator effectiveness and CO₂ turbine inlet temperature. The tradeoff between LTR cost and S-CO₂ Brayton cycle efficiency is illustrated in Figure III.3-18. For the selected point, the LTR consists of 128 PCHE units.

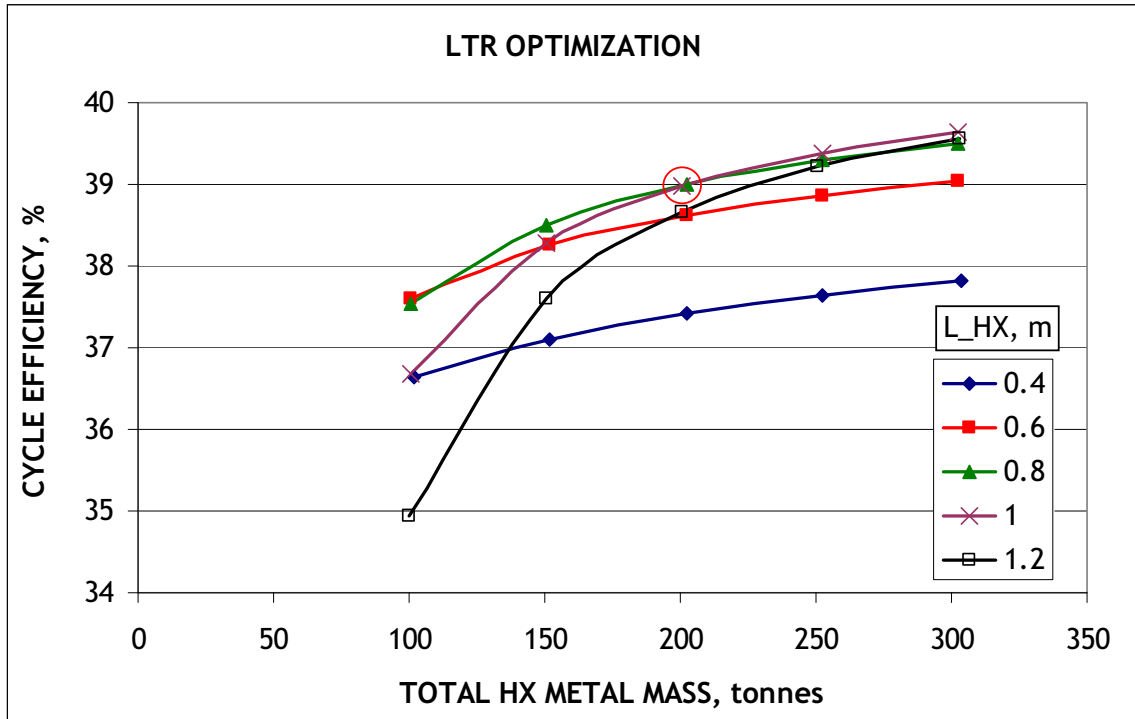


Figure III.3-15 Dependency of S-CO₂ Brayton Cycle Efficiency upon Total Low Temperature Recuperator Metal Alloy Mass for Fixed PCHE Unit Length

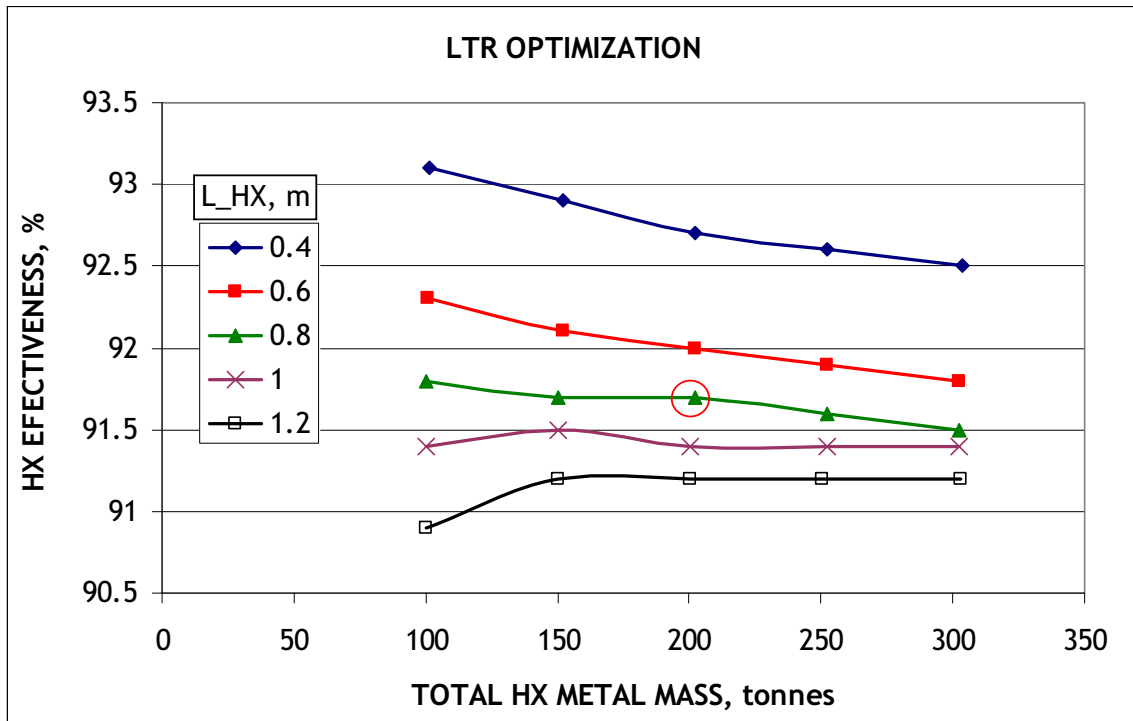


Figure III.3-16 Dependency of Low Temperature Recuperator Effectiveness upon Total High Temperature Recuperator Metal Alloy Mass for Fixed PCHE Unit Length

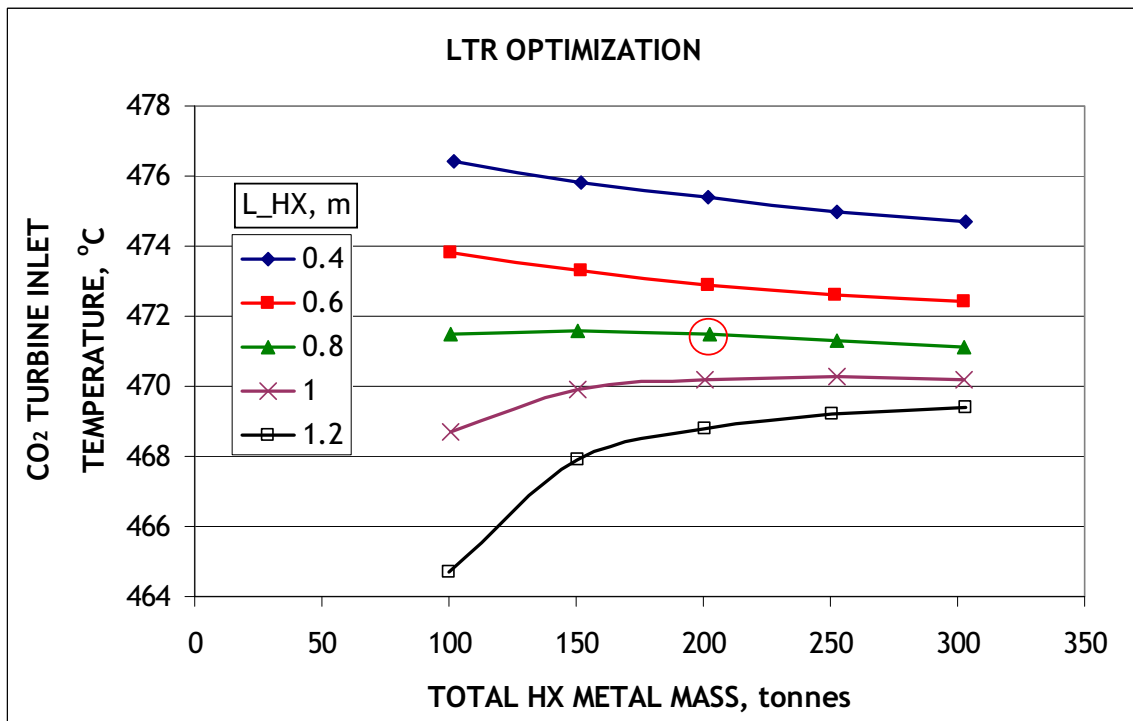


Figure III.3-17 Dependency of Turbine Inlet Temperature upon Total Low Temperature Recuperator Metal Alloy Mass for Fixed PCHE Unit Length

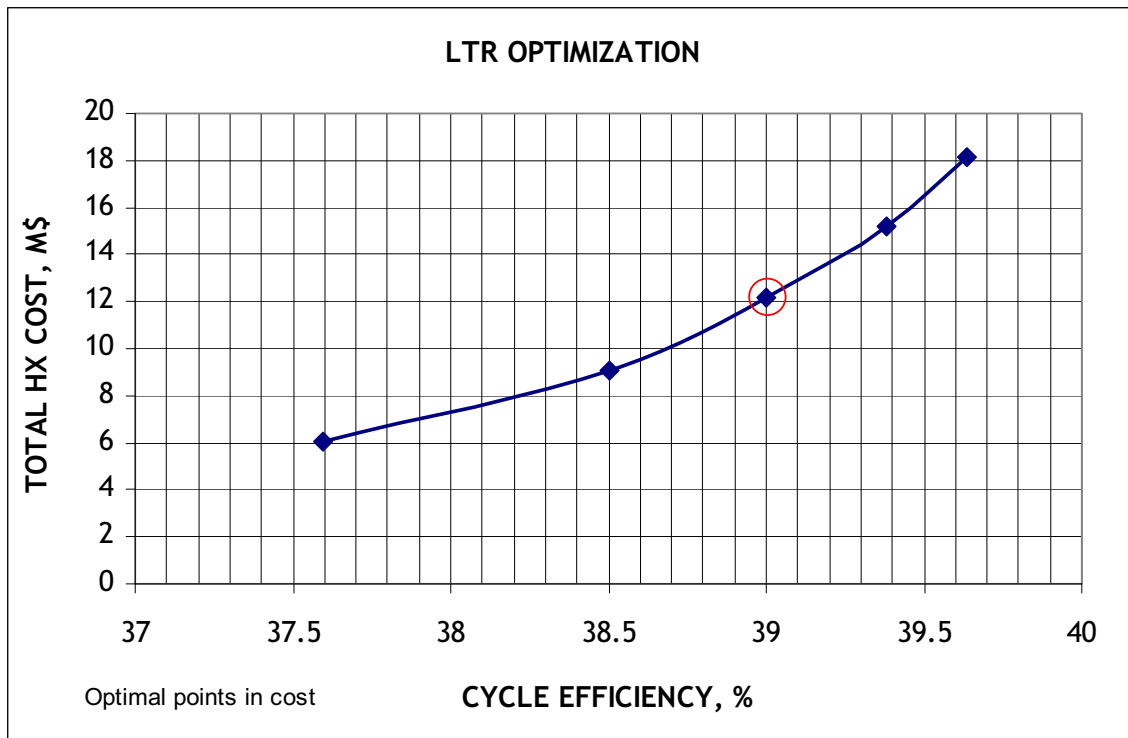


Figure III.3-18 Tradeoff Between Total Low Temperature Recuperator Cost and S-CO₂ Brayton Cycle Efficiency (Assuming Illustrative Cost of \$ 60/Kg of PCHE Metal Alloy Mass)

III.3.5 Cooler

For a specified cooling water inlet temperature, cooling water flowrate, and CO₂ flowrate, there is a unique PCHE unit length that provides the desired CO₂ outlet temperature. Thus, the cooler pre-conceptual design, optimization, and tradeoff analyses have been performed to determine an optimal water flowrate and number of PCHE units. A water cooler inlet temperature of 30 °C is selected. Figure III.3-19 shows the required PCHE unit length versus the total cooler metal alloy mass as the number of PCHE units is varied for different values of the water flowrate. Figures III.3-20 through III.3-23 present the dependencies of the S-CO₂ Brayton cycle efficiency, plant efficiency, water side pressure drop, and water side pumping power upon the total metal alloy mass. Similarly, Figures III.3-24 and III.3-25 provide the tradeoffs between S-CO₂ Brayton cycle efficiency and plant efficiency versus total cooler metal alloy mass. The selected point with a water flowrate of 6000 Kg/s corresponds to 48 PCHE units having a length of 0.57 m which is just less than 0.6 m which is one of the PCHE plate side manufacturing limitations. The resulting water side pressure drop and pumping power requirements are low. Most significantly, the point lies at the location on the plant efficiency versus cooler cost curve beyond which further increasing the number of PCHE units and cooler cost would only slightly improve the plant efficiency.

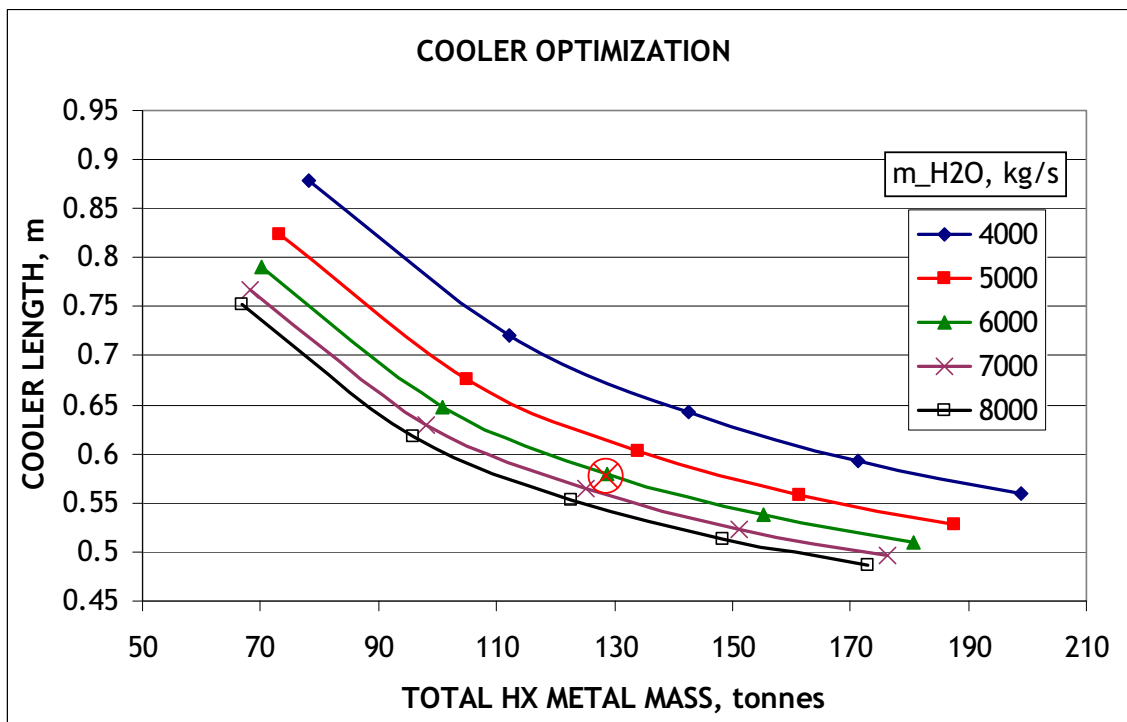


Figure III.3-19 Cooler PCHE Unit Length versus Total Cooler Metal Alloy Mass for Various Values of the Cooling Water Flowrate

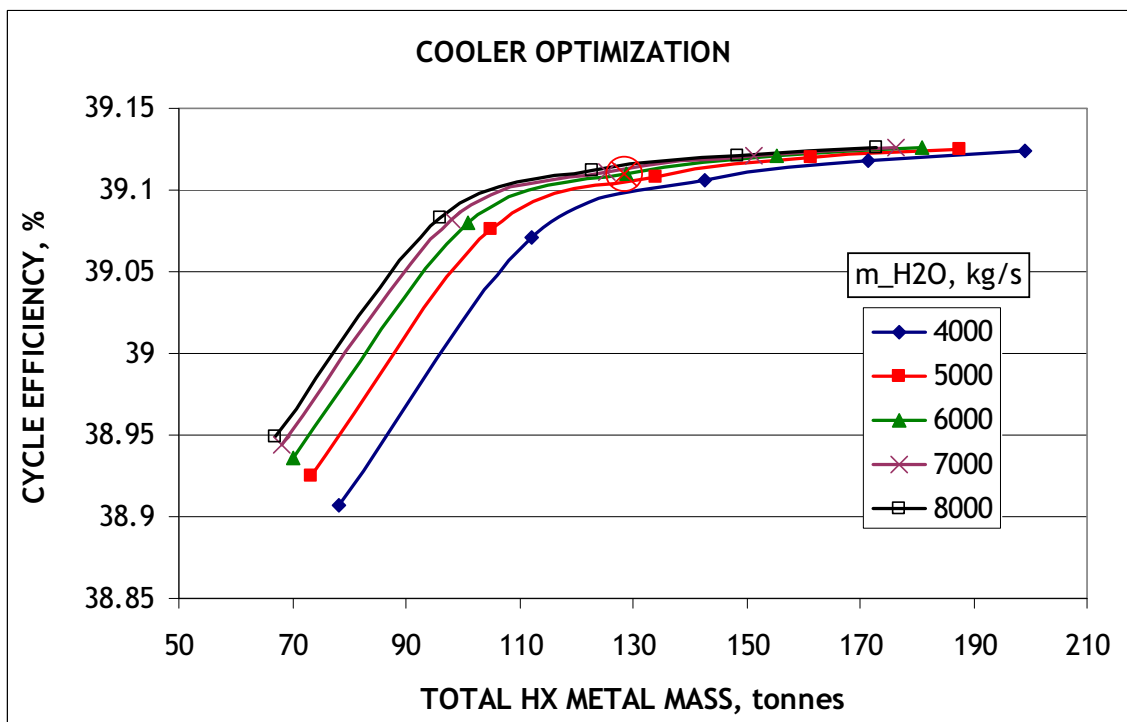


Figure III.3-20 S-CO₂ Brayton Cycle Efficiency versus Total Cooler Metal Alloy Mass for Various Values of the Cooling Water Flowrate

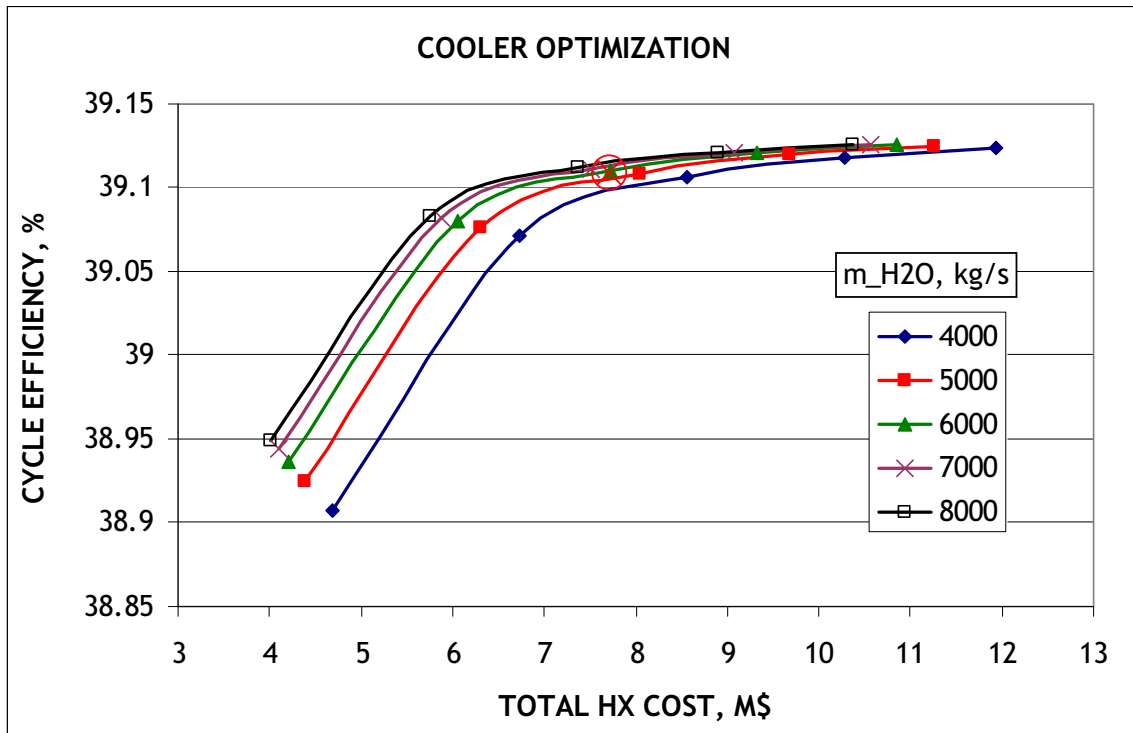


Figure III.3-21 Plant Efficiency versus Total Cooler Metal Alloy Mass for Various Values of the Cooling Water Flowrate

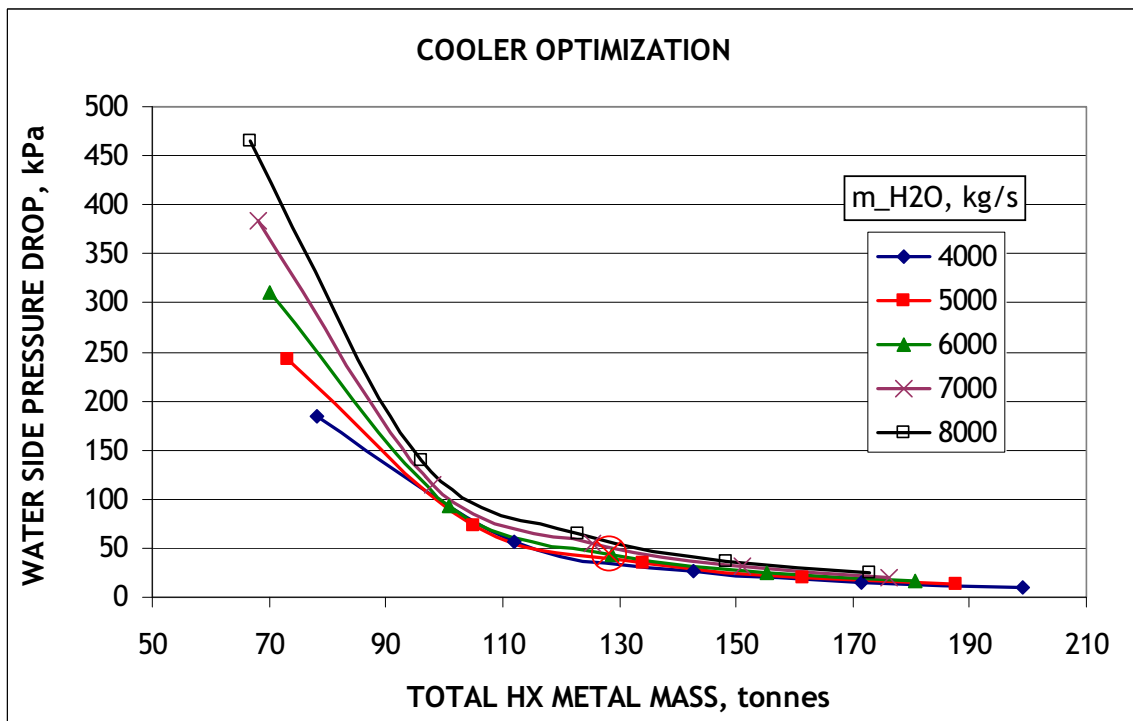


Figure III.3-22 Water Side Pressure Drop versus Total Cooler Metal Alloy Mass for Various Values of the Cooling Water Flowrate

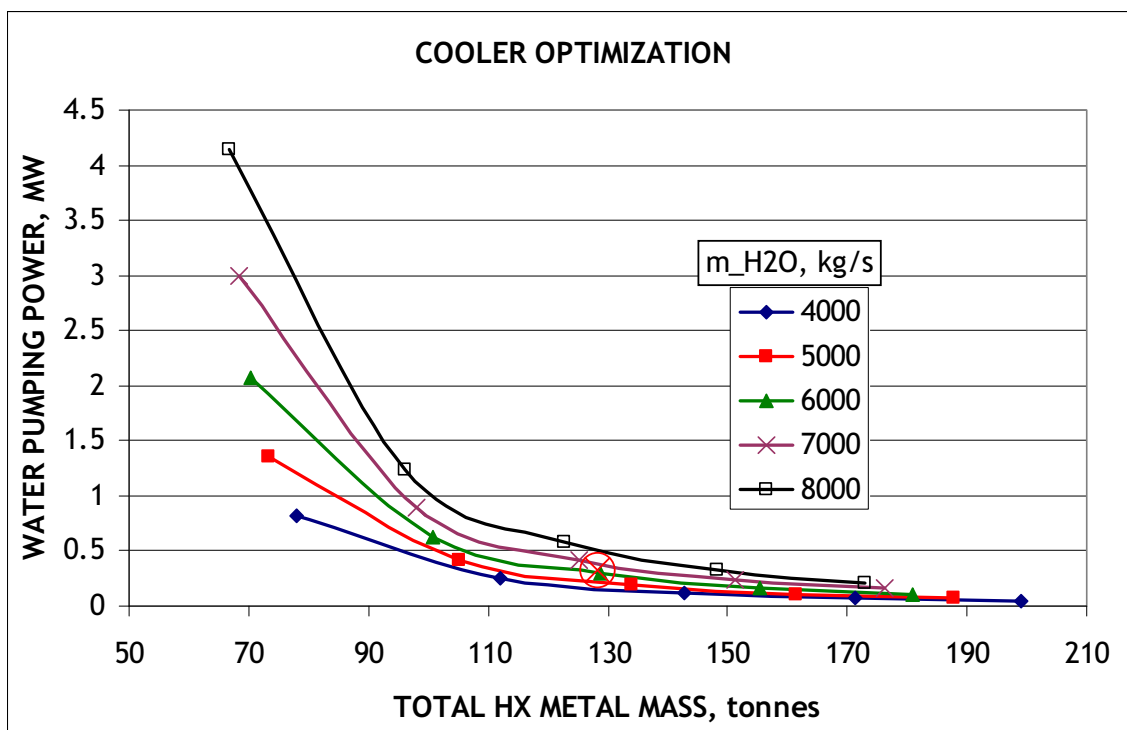


Figure III.3-23 Water Side Pumping Power versus Total Cooler Metal Alloy Mass for Various Values of the Cooling Water Flowrate

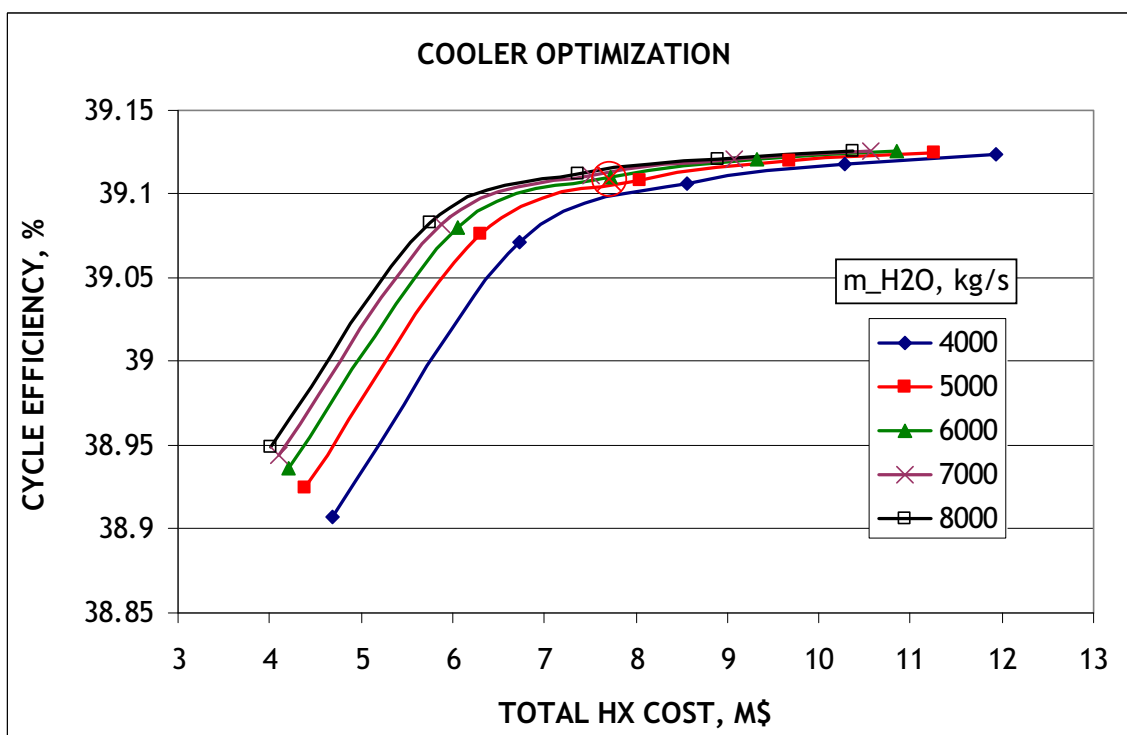
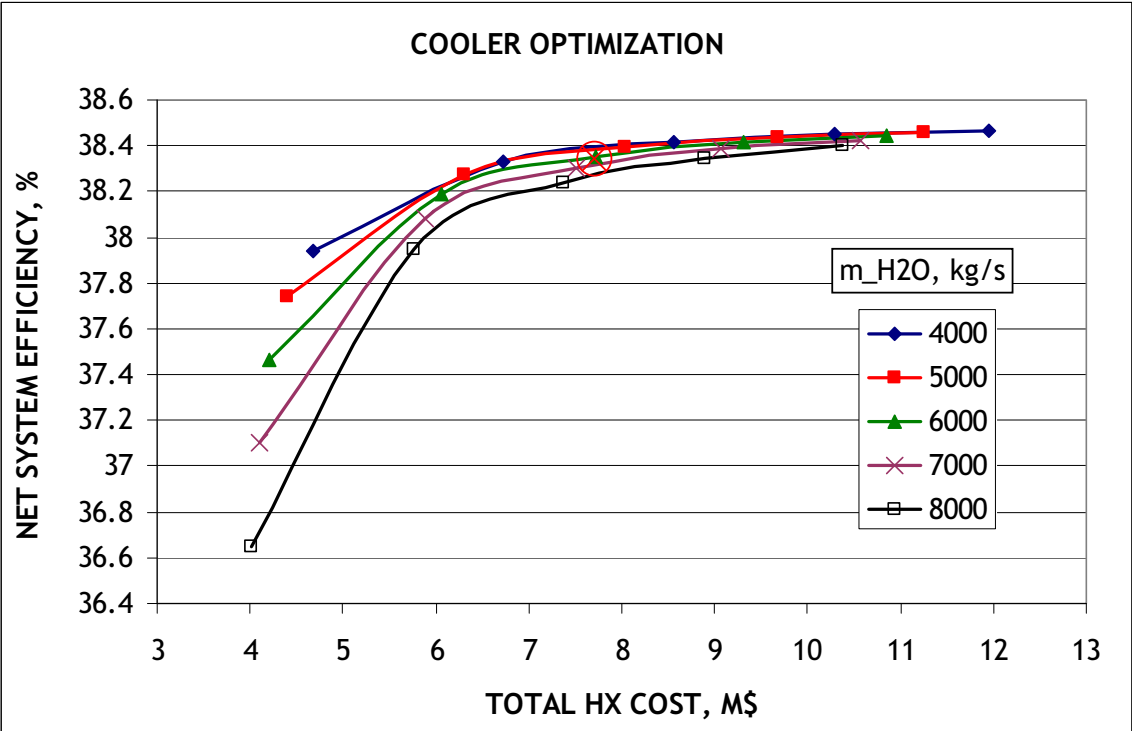


Figure III.3-24 Dependency of S-CO₂ Brayton Cycle Efficiency upon Cooler Cost (Assuming Illustrative Cost of \$ 60/Kg of PCHE Metal Alloy Mass)



**Figure III.3-25 Dependency of Plant Efficiency upon Cooler Cost
(Assuming Illustrative Cost of \$ 60/Kg of PCHE Metal Alloy Mass)**

III.4 Core Design Trade-off Studies

The design descriptions and performance characteristics of the reference metal core design were discussed in Section II.1.1. As mentioned there, various option and trade-off studies were performed to determine the appropriate power level and conversion ratio of the reference design. Based on the results of these trade-off studies, the reference core design was developed for ternary metal alloy, U-TRU-Zr fuel with WG-Pu feed. An alternative design was also developed for mixed oxide, UO_2 -TRUO₂ fuel. The performance characteristics of the metal and oxide core designs loaded with LWR-SF TRU drivers were evaluated. Additional design studies were performed to develop fuel assembly designs that yield a low TRU conversion ratio when employed in the reference core configuration.

The results of these trade-off and design studies are presented in this Section. The trade-off studies to determine the power level and conversion ratio are discussed in Sections III.4.1 and III.4.2, respectively. The alternative oxide core design is discussed in Section III.4.3. The performances of the LWR-SF TRU fuel and the low CR assembly designs are provided in Sections III.4.4 and III.4.5, respectively.

III.4.1 Trade-off Study for ABTR Power Level Determination

The ABTR reactor size should be large enough to provide a prototypic irradiation environment similar to commercial scale Advanced Burner Reactors (ABR's). On the other hand, a smaller reactor size would result in a lower project cost and a shorter project schedule. Hence, the reactor size should be selected balancing these considerations. Trade-off studies were performed in order to determine an appropriate power level. Using a ternary metal fuel (U-TRU-10Zr), fuel cycle analyses were performed for 4 different power levels of 125, 250, 400, and 840 MWt. TRU isotopic composition of a 10-year cooled LWR spent fuel (LWR-SF) with 33 MWd/kg burnup was used in this study. Various assembly designs were examined, including the FFTF, PRISM Mod-B/92 and PRISM Mod-B/93 Burner designs. The fuel pin diameter was varied in a wide range from 5.8 mm to 10.5 mm. Various core performance parameters were examined, including the required TRU enrichment, heavy metal and TRU loadings, core volume, conversion ratio, core average and test assembly flux levels, fast fluence to burnup ratio, burnup reactivity swing, and specific power.

Core configurations were developed for 4 different power ratings of 125, 250, 440, and 840 MWt, based on the SMFR [1], SMFR-2 [2], FFTF [3], and PRISM Mod-B [4] designs, respectively. The planar core layouts are shown in Figure III.4-1. For consistent comparison, the active core height was fixed to 80 cm, and the number of assemblies were adjusted to attain a similar linear power around 26 kW/m except for the 125 MWt core, for which a symmetric core configuration with a linear power of ~26 kW/m could not be made because of limited assembly locations and thus the resulting linear power was somewhat lower (~22 kW/m).

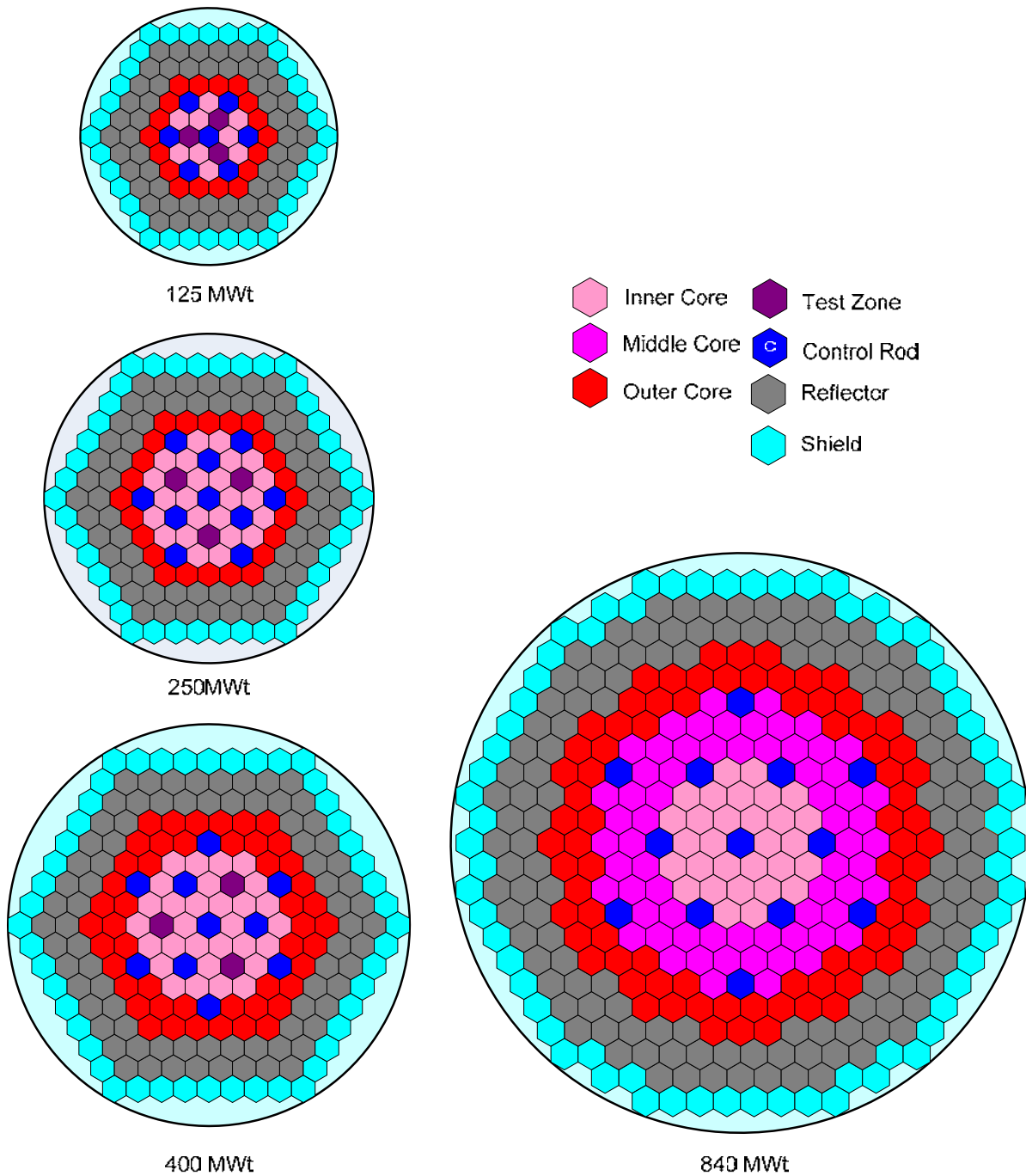


Figure III.4-1 Core Configurations for Power Level Trade-off Study (in scale)

Five different assembly designs were developed for the parametric study as provided in Table III.4-1. The first three assembly designs were adopted from the FFTF, PRISM Mod-B/92 and PRISM Mod-B/93 Burner designs. The fuel pin diameter was varied in a wide range from 5.8 mm to 10.5 mm, but the number of fuel pins per assembly was fixed

to 217. A similar wire-wrap diameter was used, and thus the pin pitch-to-diameter ratio decreases with increasing fuel pin diameter while the assembly size increases with increasing pin diameter. The fabricated fuel volume fraction varies from 25.5 to 32.4 %. The core average power densities and pin bundle pressure drops of the four cores loaded with these assembly designs are shown in Table III.4-2. Except for the 125 MWt core that has a lower linear power, the average power densities are similar for the same pin diameter and decreases as the pin diameter increases. The pin bundle pressure drop increases with decreasing pin diameter.

Table III.4-1 Fuel Assembly Design Parameters

Assembly Design	D5.8 ^{a)}	D7.4	D8.3	D9.5	D10.5
Assembly pitch, cm	12.225	14.735	16.142	17.930	19.416
Pin diameter, mm	5.842	7.442	8.306	9.5	10.5
Duct thickness, mm	3.01	4.45	3.94	3.94	3.94
No. of fuel pins	217	217	217	217	217
Pitch-to-diameter ratio	1.268	1.199	1.196	1.172	1.155
Wire wrap diameter, mm	1.42	1.33	1.57	1.57	1.57
Volume Fraction, %					
- Fuel	25.5	27.2	29.3	31.6	32.4
- Bond	8.5	9.1	9.8	10.5	10.8
- Structure	23.0	26.9	24.2	23.0	23.4
- Coolant	43.0	36.8	36.7	34.8	33.4
Remarks	FFTF	PRISM Mod-B/92	PRISM Mod-B/93		

a) Read as pin diameter is about 5.8 mm

Fuel cycle performance parameters were determined from REBUS-3 calculations. Equilibrium cycle analyses with scattered loading were performed using 3-dimensional hexagonal-z geometry models. A 3-batch fuel management scheme and a 12-month cycle length with 90% capacity factor were used. The characteristics of the equilibrium fuel cycle performance are summarized in Table III.4-3 and Figures III.4-2 to III.4-5.

For fixed core size and enrichment, the effective multiplication factor increases with increasing fuel volume fraction because of increased infinite multiplication factor and reduced leakage. For a given core composition, the effective multiplication factor increases with increasing core size due to reduced leakage. As can be seen in Figure III.4-2, therefore, the TRU enrichment required to achieve the targeted cycle length decreases with increasing pin diameter (i.e., fuel volume fraction) and power rating (i.e., core size). For a fixed core size, the TRU enrichment required to achieve the core criticality decreases with increasing fuel volume fraction, but the product of TRU enrichment and fuel volume fraction increases as the fuel volume fraction increases. Similarly, the TRU enrichment required to achieve the core criticality decreases with increasing core size, but the product of TRU enrichment and core volume increases as the core size increases. As a result, the total TRU loading increases with increasing power rating and fuel pin

diameter, as shown in Figure III.4-2. The total heavy metal (HM) loading is proportional to the fuel volume fraction and the core size. As discussed above, the core configurations except for the 125 MWt core were developed to yield the similar power density for the same fuel pin size. Thus, for the same fuel pin diameter, the 250 MWt, 400 MWt and 840 MWt cores produces similar specific powers (see Table III.4-3), and the 125 MWt core yields a somewhat lower value. For the same power rating, the specific power density decreases as the pin diameter increases.

Table III.4-2 Power Density and Pin Bundle Pressure Drop

Core power rating		125 MWt	250 MWt	400 MWt	840 MWt
Ave. linear power density, kW/m		22.2	26.2	26.4	25.8
Average power density (kW/l)	D5.8	368.4	433.7	437.4	427.8
	D7.4	252.9	298.0	300.7	294.3
	D8.3	210.6	248.2	250.5	245.3
	D9.5	170.7	201.2		
	D10.5	145.5	171.6		
Pin bundle pressure drop (psi)	D5.8	37.9	53.3	53.3	49.9
	D7.4	25.9	26.8	36.7	37.9
	D8.3	16.9	24.3	24.1	21.8
	D9.5	12.5	18.0		
	D10.5	9.8	14.3		

The TRU conversion ratio is proportional to the uranium to TRU atomic ratio, thus it increases with increasing power rating and fuel pin size (see Figure III.4-3) because the TRU fraction decreases with increasing power rating. The ratio of average discharge burnup to peak fast fluence decreases with increasing power rating and fuel pin size since it is proportional to the TRU enrichment (see Figure III.4-4). For a fixed cycle length, the average discharge burnup is proportional to the specific power density, and hence it shows the same trend as the specific power density. The burnup reactivity swing decreases as the conversion ratio increases, thus it decreases as the power rating and the fuel pin size increase. Under the assumption that the maximum reactivity hold-down of each primary control rod is \$0.8, the cycle length was estimated by limiting the burnup reactivity swing within the reactivity control capability of the primary control system. As shown in Figure III.4-5, the estimated cycle length increases with increasing power rating and fuel pin size.

Table III.4-3 Summary of Fuel Cycle Performance Characteristics

Assembly	D5.8				D7.4				D8.3				D9.5		D10.5		
	125	250	400	840	125	250	400	840	125	250	400	840	125	250	125	250	
Thermal power (MW)	125	250	400	840	125	250	400	840	125	250	400	840	125	250	125	250	
Active core diameter (m)	0.78	1.00	1.22	1.76	0.94	1.21	1.48	2.12	1.03	1.33	1.62	2.32	1.14	1.47	1.24	1.59	
Assembly lattice pitch (cm)	12.22				14.73				16.14				17.93		19.42		
Pin diameter (mm)	5.84				7.44				8.31				9.50		10.50		
Pin pitch-to-diameter ratio	1.27				1.20				1.20				1.17		1.16		
Cladding thickness (mm)	0.38				0.56				0.56				0.60		0.70		
Average power density (kW/liter)	368.4	433.7	437.4	427.8	252.9	298.0	300.7	294.3	210.6	248.2	250.5	245.3	170.6	201.2	145.5	171.6	
Charge enrichment (%)	low enrichment				42.1	37.0	30.3	23.8	32.2	28.4	23.6	19.0	27.5	24.4	20.3	16.6	23.4
	medium enrichment				47.6	41.8	34.3	26.8	36.4	32.1	26.7	21.5	31.1	27.5	23.0	18.8	26.5
	high enrichment				52.6	46.2	37.9	29.7	40.2	35.6	29.5	23.8	34.4	30.4	25.4	20.8	29.3
Fuel loading (MT)	1.08	1.81	2.88	6.20	1.69	2.86	4.55	9.78	2.20	3.73	5.92	12.73	2.95	5.00	3.55	6.03	
Specific power (kW/kg)	111.5	131.2	132.2	129.2	72.0	84.7	85.3	83.4	55.7	65.53	66.0	64.5	42.4	50.0	25.2	41.5	
Average discharge burnup (MWd/kg)	107.9	126.7	127.4	123.9	69.1	81.2	81.7	79.6	53.4	62.7	63.1	61.5	40.0	47.0	33.2	39.0	
Peak fast fluence (10^{23} n/cm ²)	2.41	3.45	4.02	4.68	1.90	2.67	3.04	3.39	1.66	2.31	2.61	2.84	1.42	1.96	1.25	1.72	
TRU conversion ratio	0.18	0.27	0.37	0.53	0.30	0.41	0.52	0.69	0.38	0.50	0.62	0.79	0.48	0.60	0.54	0.66	
Burnup reactivity swing (Δk)	0.061	0.077	0.078	0.069	0.043	0.049	0.045	0.034	0.033	0.036	0.031	0.019	0.024	0.024	0.020	0.019	
Estimated max. cycle length (month)	2.2	3.1	3.0	4.8	3.2	4.8	5.2	9.7	4.0	6.5	7.7	17.3	5.5	5.5	6.9	7.2	
BOEC power peaking factors	1.45	1.50	1.49	1.46	1.50	1.56	1.54	1.48	1.52	1.59	1.56	1.49	1.54	1.62	1.56	1.64	
Average linear power (kW/m)	22.2	26.2	26.4	25.8	22.2	26.1	26.4	25.8	22.2	26.1	26.4	25.8	22.2	26.1	22.1	26.1	
Peak linear power (kW/m)	36.1	45.5	45.7	42.3	36.1	45.0	44.5	40.8	35.8	44.7	43.8	39.9	35.8	44.6	35.8	44.6	
Linear power limit (kW/m)	20.9	29.7	40.0	46.7	35.8	43.3	49.7	47.7	42.7	50.2	51.0	48.6	43.8	52.8	44.2	53.3	

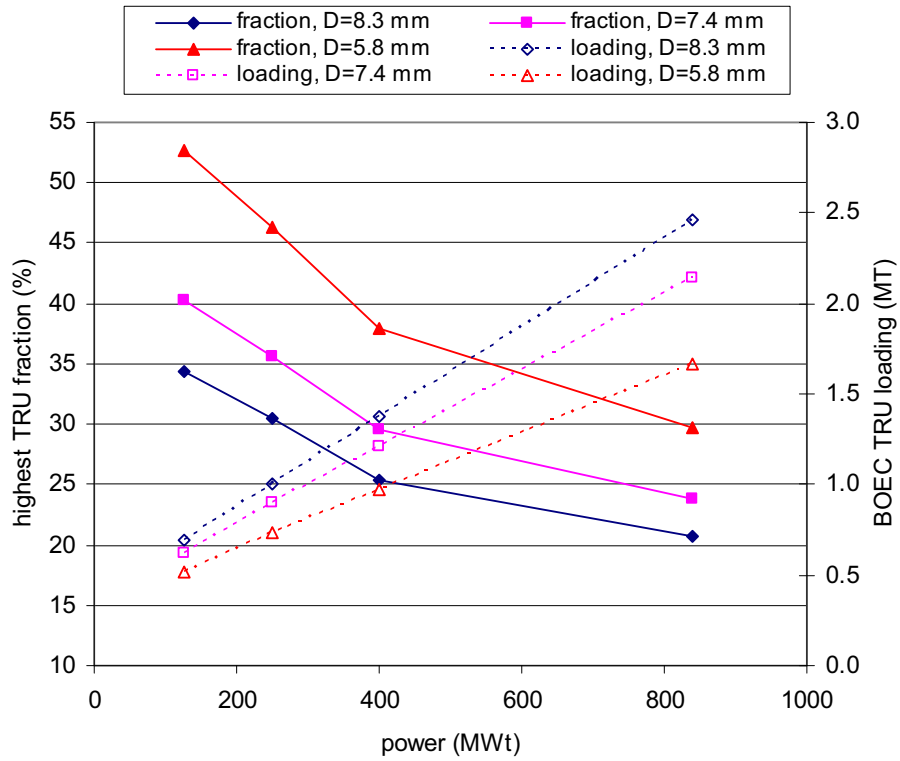


Figure III.4-2 TRU Enrichment and Loading vs. Power Level

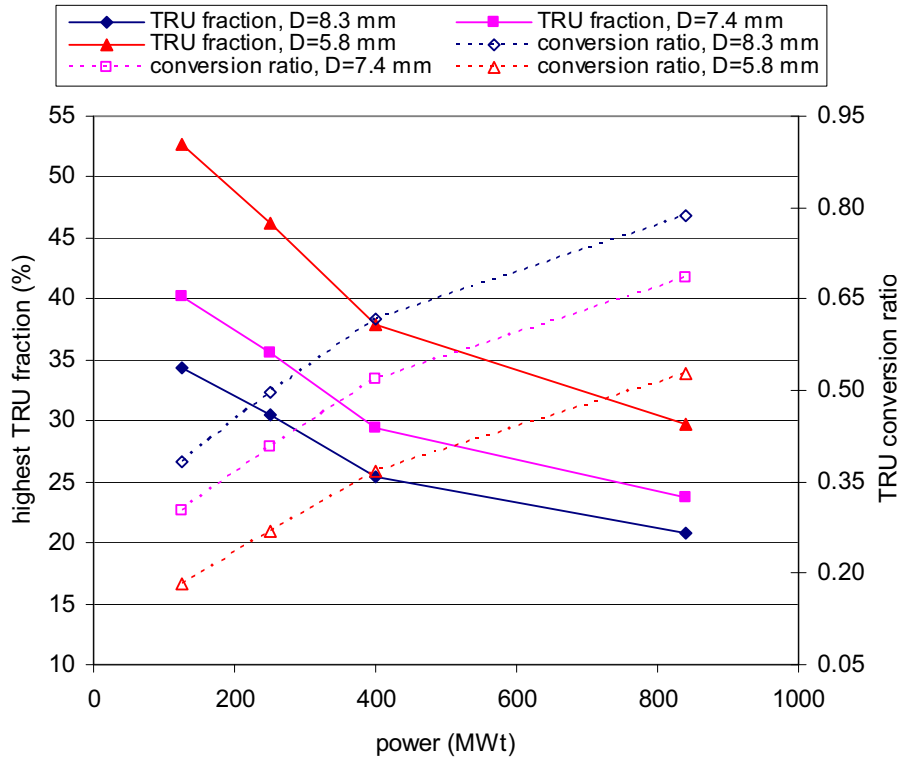


Figure III.4-3 TRU Enrichment and Conversion Ratio vs. Power Level

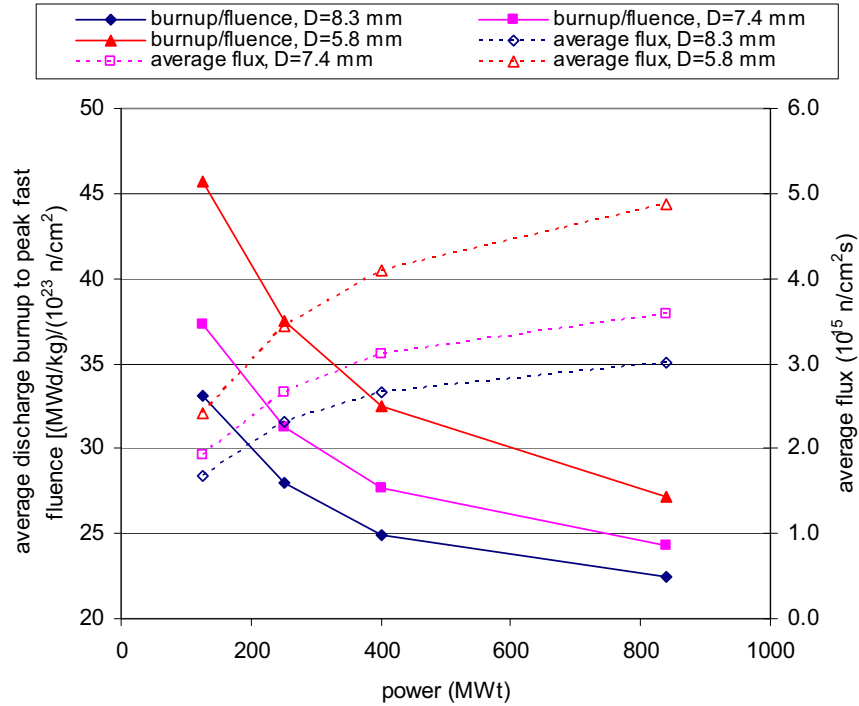


Figure III.4-4 Discharge Burnup to Peak Fast Fluence and Average Flux vs. Power Level

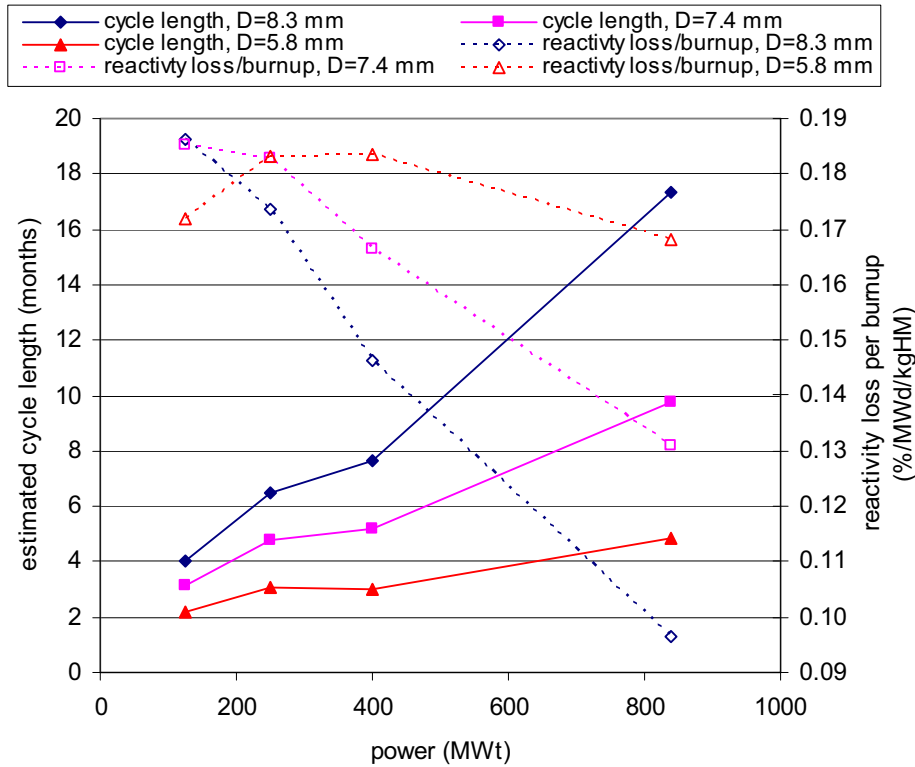


Figure III.4-5 Estimated Cycle Length and Reactivity Loss vs. Power Level

The core average flux level is proportional to the power density and inversely proportional to the TRU loading. Thus, the average flux increases as the linear power increases and as the TRU enrichment and the fuel pin size decreases. As a result, the average flux level increases with increasing power rating and decreasing fuel pin size (see Figure III.4-4). For a fixed linear power, the ratio of average flux to TRU conversion ratio is inversely proportional to the square of fuel pin radius and $1 - e_{TRU}$, where e_{TRU} is the TRU enrichment, thus it increases as the fuel pin size and power rating decreases.

In summary, all the performance parameters are monotonically improved with increasing power level. However, the TRU conversion ratio, TRU loading, and core size also increase with power level; and this is not desirable for the ABTR low cost burner mission. Of particular interest for fuels testing duration, the average flux level decreases significantly as the power level decreases. It is also noted that the TRU enrichment for the cases of small power rating and fuel pin size is higher than 30%, which is beyond the current irradiation experience. In addition, since the fuel solidus temperature decreases as the TRU fraction increases, the peak linear power limit is violated for some of these cases. The maximum average flux level achievable within the linear power limit appears to be $\sim 1.9 \times 10^{15}$ and $\sim 2.5 \times 10^{15}$ n/cm²s for the 125 and 250 MWt cores, respectively. The corresponding conversion ratios of the 125 and 250 MWt cores are 0.30 and 0.41, respectively. These results suggest that ~ 250 MWt is a reasonable compromise to allow a low project cost, at the same time providing a reasonable test bed for demonstrating the ABR design features.

A higher power level would result in a higher average flux level, which would reduce the irradiation time of ABR test fuel assemblies, but the construction cost would also increase. For example, compared to the proposed power level of 250 MWt, the 400 MWt power level of FFTF would increase the flux level by only $\sim 16\%$, but the construction cost and schedule would be increased substantially. The heavy metal mass flow would also increase by $\sim 60\%$ and hence resulting in additional burden on the startup core fabrication capability. Therefore, a reactor size of 250 MWt was selected for the ABTR as a good compromise between the construction cost/schedule and the required performance characteristics to meet the ABTR mission goals.

III.4.2 Design Studies of Range of Conversion Ratios

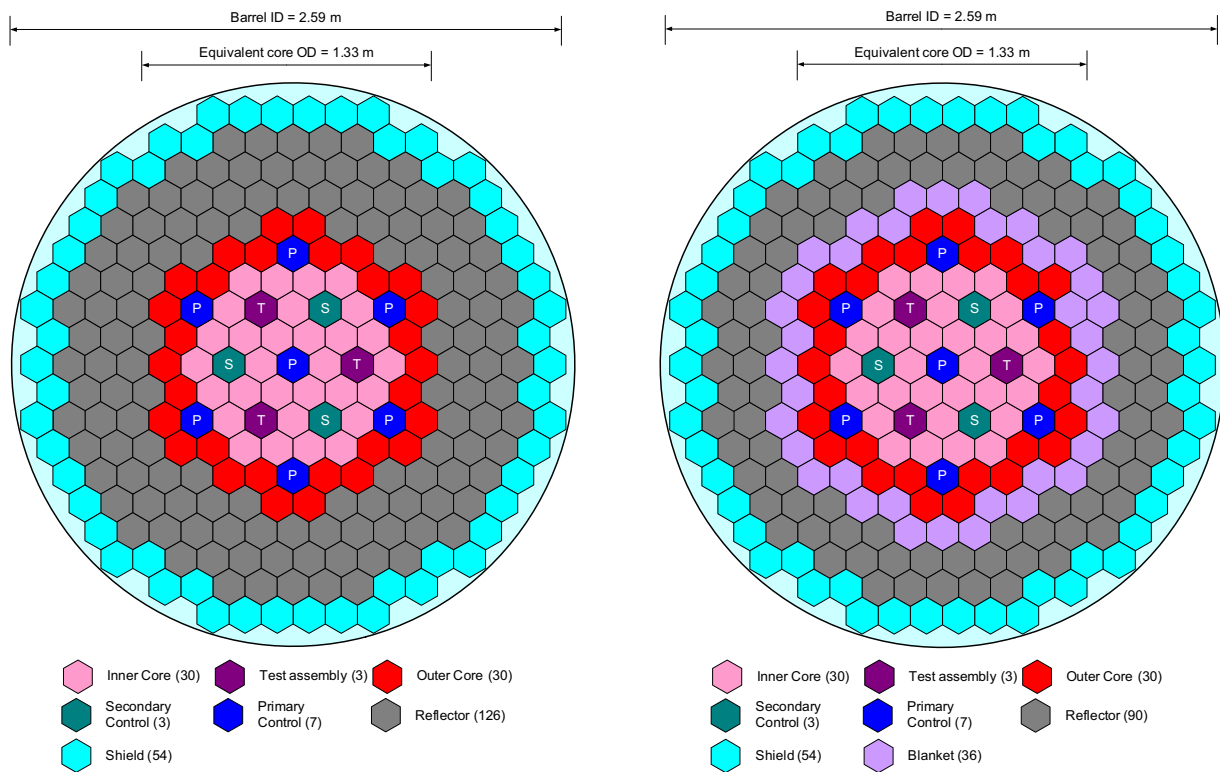
The role of the advanced burner reactor is to transmute the recycled TRU elements which are the dominant contributors to spent fuel radio-toxicity, long-term heat and dose. In order to demonstrate a high TRU consumption rate, it is desirable to have a low conversion ratio (CR). However, a low conversion ratio requires a high TRU enrichment, which is beyond the current irradiation experience with plutonium-based fast reactor fuels [5-7]. Using U-TRU-Zr ternary metal fuel, initial design studies have been performed to evaluate the feasibility of the ABTR design to accommodate a wide range of conversion ratios by changing the assembly design only for fixed core configuration and assembly pitch.

The major design variables to be used in changing the conversion ratio of a given core design are the fuel pin size and the number of fuel pins per assembly. The TRU conversion ratio is proportional to the uranium to TRU atomic ratio, and hence it decreases with increasing TRU enrichment. For a fixed core size, the required TRU enrichment to achieve the core criticality and a desired cycle length increases with decreasing fuel volume fraction. As the TRU enrichment increases, the linear powers limit decreases because of the decreased solidus temperature and reduced thermal conductivity of ternary metal fuel. Thus, to achieve a low conversion ratio, a larger number of smaller fuel pins needs to be used to reduce the fuel volume fraction while maintaining the peak linear power within the appropriate limit. On the other hand, to achieve a high conversion ratio, a smaller number of larger fuel pins needs to be used to increase the fuel volume fraction.

Using the 250 MWt core design described in Section III.4.1 as a reference design, parametric studies were performed to develop the core configuration and assembly designs that achieve the conversion ratios of ~0.25, ~0.7, and ~1.05. Various design constraints were imposed, including those on the peak linear power, peak fast fluence, peak discharge burnup, and burnup reactivity swing. In order to employ wire-wrap spacers, the fuel pin pitch-to-diameter ratio was limited to be less than 1.3. To satisfy the peak linear power limit for the low conversion ratio core (CR=0.25), the number of fuel assemblies was increased to 63 (including 3 test fuel assemblies) from 51 of the reference core. In addition, when the TRU enrichment is higher than 30%, the Zr fraction was increased to 20 wt. % from a nominal value of 10 wt. % in order to increase the solidus temperature. An additional row of reflectors was also introduced to reserve space for the blanket assemblies of the high conversion ratio core (CR>1.0). Table III.4-4 provides the assembly design data for three conversion ratios, and Figure III.4-6 shows the resulting core configurations.

Table III.4-4 Assembly Design Parameters for Different Conversion Ratios

Target conversion ratio	Low (~0.25)	Medium (~0.7)	High (> 1.0)
Height (core/plenum) , cm	80 / 120	80 / 120	80 / 120
Pin outer diameter, mm	6.25	9.41	11.0
Number of fuel pins per assembly	271	169	127
Assembly lattice pitch, cm	14.834	14.834	14.834
Inter-assembly gap, mm	4.45	4.0	4.0
Duct thickness, mm	4.45	3.0	3.0
Pin pitch-to-diameter ratio	1.29	1.11	1.10
Cladding thickness, mm	0.75	0.41	0.41
Average linear power, kW/m	16.8	27.1	34.0
Pin bundle pressure drop, psi	11.5	50.2	51.6
Volume fraction (driver/blanket), %			
- Fuel	18.9	38.5	40.7 / 46.1
- Bond	6.3	12.8	13.6 / 8.1
- Structure	33.1	18.7	17.3 / 17.3
- Coolant	41.7	29.9	28.4 / 28.4



Burner Core **Breeder Core**
Figure III.4-6 Core Configurations for Range of Conversion Ratios

The core is composed of 60 driver assemblies, 3 test fuel assemblies, and 10 control assemblies. The 60 driver assemblies were divided into two enrichment zones (inner and outer cores) to flatten the power distribution while simplifying the refueling operation. Each of inner and outer cores has 30 driver assemblies. Three test assemblies were loaded with the ternary fuel used in the driver assemblies with different enrichment. The active core is 80 cm high and the gas plenum is 120 cm high. The equivalent active core diameter is 1.33 m and the inner diameter of core barrel is 2.59 m. The core is surrounded successively by 126 radial reflectors and 54 shield assemblies. For the high conversion ratio core ($CR > 1.0$), the innermost row of reflectors (36 assemblies) were replaced with radial blankets. Internal blankets were not used to ease the orifice design for appropriate flow allocation for different core configurations. A binary metal fuel (U-10Zr) with depleted uranium was used for blankets. The fuel smeared density was 85% for blankets and 75% for driver assemblies. Fuel pin diameters for the low, medium, and high conversion ratios are 6.25, 9.41, and 11.0 mm, respectively. The corresponding numbers of fuel pins per assembly are 217, 169, and 127, respectively. For the low conversion ratio core, slightly thicker duct and cladding were used to reduce the fuel volume fraction further.

Table III.4-5 presents the startup core performance characteristics for the three conversion ratio designs, obtained from REBUS-3 equilibrium cycle calculations. In these calculations, the LWR-SF was used as TRU feed, without recycling the ABTR

spent fuel. The cycle length was adjusted to limit the burnup reactivity swing within the reactivity control capability of the seven primary control rods. The number of batches (i.e., fuel residence time) was adjusted to maximize the discharge burnup within the fast fluence limit of HT-9 cladding ($4.0 \times 10^{23}/\text{cm}^2$) and the discharge burnup limit (150 MWd/kg). The cycle lengths of low, medium, and high conversion ratio designs are 3, 6, and 12 months, respectively. A 10-batch fuel management scheme was used for the low and medium conversion ratio designs. For the high conversion ratio design, 5- and 10-batch schemes were used for drivers and blankets, respectively. The calculated TRU conversion ratios are 0.25, 0.72, and 1.03 for the low, medium, and high conversion ratio designs, respectively.

Table III.4-5 Start-up Core Performance Characteristics of Various Conversion Ratios

Target conversion ratio	Low (~0.25)	Medium (~0.7)	High (>1.0)
Cycle length, months	3	6	12
Number of batches (driver/blanket)	10	10	5 / 10
TRU enrichment (IC/test/OC), %	40.6/45.9/50.8	17.8/20.1/22.2	16.5/18.7/20.4
Conversion ratio, fissile/TRU	0.33 / 0.25	0.77 / 0.72	1.05 / 1.03
HM loading (driver/blanket), Mt	2.08	5.05	5.37 / 3.80
TRU loading, Mt	0.93	1.00	1.08
Specific power of active core, kW/kg	114.8	47.7	41.3
Power density of active core, kW/l	236.1	237.7	219.1
Discharge burnup (ave./peak), MWd/kg	94.3 / 138.8	78.4 / 122.4	67.9 / 108.0
Peak fast fluence(driver/blanket), $10^{23}/\text{cm}^2$	2.08	3.82	3.51 / 3.81
Burnup reactivity swing (% Δk)	1.65	0.89	1.03
Power peaking factor, BOEC/EOEC	1.53 / 1.51	1.62 / 1.60	1.66 / 1.62
Stage factor, BOEC/EOEC	1.15 / 1.15	1.10 / 1.10	1.07 / 1.06
Peak linear power, kW/m	29.6	48.1	58.8
Linear power limit, kW/m	31.1	57.0	70.2
Core average flux, $10^{15}/\text{cm}^2\text{-sec}$	2.61	2.18	2.00
Test assembly flux, $10^{15}/\text{cm}^2\text{-sec}$	3.32	2.81	2.57

Table III.4-6 presents the recycled core performance characteristics for the three conversion ratio designs, obtained from REBUS-3 equilibrium cycle calculations. In these calculations, the recycled TRU from the ABTR spent fuel was used as the primary TRU feed, and the TRU recovered from 10-year cooled LWR spent fuel with 33 MWd/kg burnup was used as the makeup feed. For the reprocessing of ABTR spent fuel, one-year cooling time and half-year reprocessing time were assumed. The same cycle lengths and number of batches as the start-up cores were used. The fissile fractions of the charged TRU for the low, medium, and high conversion designs were 37.7, 55.3, and 72.4%, respectively, while that of the LWR spent fuel was 59.5%. The difference in the fissile fraction of charged TRU increases the TRU enrichment of the low conversion ratio core by ~29% relative to the start-up core and decreases it by ~13% for the high

conversion ratio design. The TRU enrichment of the medium conversion ratio core increased only slightly. The changes of the TRU enrichment and the fissile fraction in charged TRU alter the conversion ratios of the recycled cores relative to the start-up cores. For the low conversion ratio core, the TRU conversion ratio decreases to 0.18 from 0.25 because of the increased TRU enrichment, but the fissile conversion ratio increases to 0.44 from 0.33 because of the reduced fissile fraction in charged TRU. By the same reasons, the fissile conversion ratio increases from 0.77 to 0.83 for the medium conversion ratio core, and the TRU conversion ratio decreases to 0.81 from 1.03 for the high conversion ratio core. The TRU conversion ratio of the medium conversion ratio core is not changed noticeably because of similar TRU enrichments, and the fissile conversion ratio of the high conversion ratio core is reduced slightly because of similar fissile loadings.

Table III.4-6 Recycled Core Performance Characteristics of Various Conversion Ratios

Target conversion ratio	Low (~0.25)	Medium (~0.7)	High (>1.0)
Cycle length, months	3	6	12
Number of batches (driver/blanket)	10	10	5 / 10
Fissile fraction of charged TRU, %	37.7	55.3	72.4
TRU enrichment (IC/test/OC), %	52.4/59.2/65.5	18.2/20.6/22.8	14.3/16.2/17.9
Fissile/TRU conversion ratio	0.44 / 0.18	0.83 / 0.72	1.04 / 0.81
HM loading (driver/blanket), Mt	2.08	5.05	5.37 / 3.80
TRU loading, Mt	1.21	1.03	0.96
Specific power of active core, kW/kg	114.8	47.7	41.2
Power density of active core, kW/l	236.2	237.6	217
Discharge burnup (ave./peak), MWd/kg	94.3 / 139.8	78.4 / 123.0	67.7 / 107.2
Peak fast fluence(driver/blanket), $10^{23}/\text{cm}^2$	2.03	3.84	3.53 / 3.85
Burnup reactivity swing (% Δk)	1.29	0.78	1.1
Power peaking factor, BOEC/EOEC	1.55 / 1.53	1.62 / 1.61	1.65 / 1.61
Stage factor, BOEC/EOEC	1.12 / 1.12	1.09 / 1.09	1.07 / 1.07
Peak linear power, kW/m	29.2	47.8	58.4
Linear power limit, kW/m	29.3	57.2	69.6
Core average flux, $10^{15}/\text{cm}^2\text{-sec}$	2.58	2.2	2.03
Test assembly flux, $10^{15}/\text{cm}^2\text{-sec}$	3.24	2.83	2.61

Tables III.4-7, III.4-8, and III.4-9 summarize the heavy metal inventories and mass flow rates of the low, medium and high conversion ratio cores, respectively. For the start-up core that uses the external feed only without recycling the ABTR spent fuel, the required TRU mass per year is 398.1 kg, 209.4 kg, and 205.4 kg for the low, medium, and high conversion ratio cores, respectively. The TRU consumption rate is 60.0 kg/year for the low conversion ratio core and 20.4 kg/year for the medium conversion ratio core. For the recycled core, the required external TRU mass per year is reduced to 66.4 kg, 20.1 kg, and 0.0 kg for the low, medium and high conversion ratio cores, respectively.

In summary, the results indicate that it is feasible to design the ABTR to accommodate a wide range of conversion ratios by employing different assembly designs. A low conversion ratio increases the TRU consumption rate from ~20 kg/year (CR=0.72) to ~60 kg/year (CR=0.25) at 250 MWt power level. Because of much faster burnup reactivity loss, however, appropriate means for reactivity compensation must be employed (e.g., shorter cycles with more frequent refueling or increased number of control assemblies). More importantly, a TRU enrichment of ~50% is required, which is beyond the current irradiation experience. It is also noted that the TRU inventory requirement plays an important role in the dynamics of removing TRU from the current interim storage and the repository waste; the inventory is larger than the annual TRU burning rate and dominates the TRU feed requirement.

The TRU enrichments of the medium conversion ratio core are within the plutonium enrichments of the U-Pu-10Zr ternary fuel used in the EBR-II and FFTF metal-fuel irradiation test programs. Thus, the ABTR core will be based on conventional enrichment plutonium-based fuel for the initial core, gradually transitioning to full core loading of transmutation fuel after its qualification phase (resulting in ~0.6 CR). The low CR transmutation fuel tests can be accommodated in the designated test assemblies, and if fully developed, core conversion to low CR fuel can be envisioned. If necessary, this low conversion ratio core can be converted into a breeder in the future by employing driver assemblies with high fuel volume fraction and by replacing the innermost row of reflector with blanket assemblies.

Table III.4-7 Heavy Metal Inventories and Mass Flow Rates of Low Conversion Ratio Core

Isotope	Start-up Core						Recycled Core					
	Inventory, kg		Mass flow, kg/year				Inventory		Mass flow, kg/year			
	BOEC	EOEC	Charge	Discharge	External	BOEC	EOEC	Charge	Discharge	External		
U-234	0.1	0.2	0.0	0.1	0.0	0.4	0.5	0.0	0.4	0.0		
U-235	2.0	1.9	0.9	0.6	0.9	1.5	1.5	0.7	0.5	0.7		
U-236	0.1	0.1	0.0	0.1	0.0	0.1	0.1	0.0	0.1	0.0		
U-238	1152.6	1146.6	471.5	447.6	471.5	872.3	867.9	356.8	338.8	356.8		
Np237	39.7	38.6	18.1	13.4	18.1	27.8	27.0	12.6	9.5	3.0		
Pu-236	0.0	0.0	0.0	0.0	0.0	0.0	0.0	0.0	0.0	0.0		
Pu-238	17.5	18.4	5.3	9.0	5.3	56.1	55.7	23.4	21.7	0.9		
Pu-239	456.9	445.0	205.6	157.8	205.6	355.3	346.7	158.4	124.1	34.3		
Pu-240	234.0	233.4	94.4	92.0	94.4	426.2	422.1	177.6	161.4	15.7		
Pu-241	68.0	66.0	31.2	23.1	31.2	72.5	71.7	30.6	27.2	5.2		
Pu-242	47.4	47.4	18.8	19.0	18.8	124.6	123.9	51.2	48.1	3.1		
Am-241	47.1	46.2	20.3	17.0	20.3	64.7	63.4	28.3	23.1	3.4		
Am-242	1.0	1.2	0.0	0.7	0.0	4.8	4.8	1.9	1.9	0.0		
Am-243	9.3	9.4	3.6	3.9	3.6	40.8	40.7	16.6	16.0	0.6		
Cm-242	1.6	1.8	0.0	0.9	0.0	2.2	2.5	0.1	1.1	0.0		
Cm-243	0.0	0.1	0.0	0.0	0.0	0.2	0.2	0.1	0.1	0.0		
Cm-244	2.2	2.3	0.7	1.1	0.7	22.6	22.7	8.8	9.2	0.1		
Cm-245	0.2	0.2	0.0	0.1	0.0	5.8	5.8	2.3	2.3	0.0		
Cm-246	0.0	0.0	0.0	0.0	0.0	3.0	3.0	1.2	1.2	0.0		
Total HM	2079.9	2058.9	870.5	786.5	870.5	2081.0	2060.1	870.5	786.8	423.8		
TRU	925.0	910.0	398.1	338.1	398.1	1206.7	1190.1	513.1	447.0	66.4		

Table III.4-8 Heavy Metal Inventories and Mass Flow Rates of Medium Conversion Ratio Core

Isotope	Start-up Core						Recycled Core					
	Inventory, kg		Mass flow, kg/year				Inventory		Mass flow, kg/year			
	BOEC	EOEC	Charge	Discharge	External	BOEC	EOEC	Charge	Discharge	External		
U-234	0.3	0.3	0.0	0.1	0.0	0.4	0.5	0.0	0.2	0.0		
U-235	6.4	6.1	1.7	0.9	1.7	6.4	6.0	1.6	0.9	1.6		
U-236	0.4	0.5	0.0	0.2	0.0	0.4	0.5	0.0	0.2	0.0		
U-238	4040.2	4008.5	836.3	772.9	836.3	4013.5	3981.6	831.1	767.3	831.1		
Np237	40.2	38.7	9.5	6.5	9.5	16.2	15.7	3.7	2.8	0.9		
Pu-236	0.0	0.0	0.0	0.0	0.0	0.0	0.0	0.0	0.0	0.0		
Pu-238	20.1	21.4	2.8	5.3	2.8	27.2	27.0	5.7	5.2	0.3		
Pu-239	517.8	512.8	108.1	98.1	108.1	521.0	515.8	108.9	98.5	10.4		
Pu-240	243.0	241.8	49.6	47.2	49.6	299.4	296.9	62.0	57.2	4.8		
Pu-241	65.1	61.8	16.4	9.9	16.4	41.4	40.8	8.8	7.7	1.6		
Pu-242	49.5	49.4	9.9	9.8	9.9	55.6	55.1	11.5	10.6	1.0		
Am-241	48.9	47.9	10.7	8.6	10.7	33.5	32.8	7.4	5.9	1.0		
Am-242	1.3	1.5	0.0	0.5	0.0	2.4	2.4	0.5	0.5	0.0		
Am-243	9.9	10.0	1.9	2.1	1.9	17.5	17.4	3.6	3.4	0.2		
Cm-242	1.4	1.6	0.0	0.3	0.0	1.0	1.1	0.0	0.2	0.0		
Cm-243	0.0	0.1	0.0	0.0	0.0	0.1	0.1	0.0	0.0	0.0		
Cm-244	2.5	2.6	0.4	0.6	0.4	8.8	8.8	1.7	1.8	0.0		
Cm-245	0.2	0.2	0.0	0.1	0.0	2.1	2.1	0.4	0.4	0.0		
Cm-246	0.0	0.0	0.0	0.0	0.0	1.0	1.0	0.2	0.2	0.0		
Total HM	5047.4	5005.2	1047.3	963.1	1047.3	5047.9	5005.7	1047.3	963.0	852.9		
TRU	1000.0	989.8	209.4	189.0	209.4	1027.2	1017.1	214.5	194.4	20.1		

Table III.4-9 Heavy Metal Inventories and Mass Flow Rates of High Conversion Ratio Core

Isotope	Start-up Core						Recycled Core					
	Inventory, kg		Mass flow, kg/year				Inventory		Mass flow, kg/year			
	BOEC	EOEC	Charge	Discharge	External	BOEC	EOEC	Charge	Discharge	External		
U-234	0.2	0.4	0.0	0.1	0.0	0.1	0.2	0.0	0.1	0.0		
U-235	13.2	12.2	2.5	1.5	2.5	13.4	12.3	2.6	1.5	2.6		
U-236	0.7	0.9	0.0	0.2	0.0	0.7	0.9	0.0	0.2	0.0		
U-238	8082.0	7996.2	1280.6	1194.9	1280.6	8208.9	8119.6	1307.7	1218.4	1307.7		
Np237	41.5	39.0	9.3	6.8	9.3	7.1	7.1	1.3	1.4	0.0		
Pu-236	0.0	0.0	0.0	0.0	0.0	0.0	0.0	0.0	0.0	0.0		
Pu-238	18.5	20.6	2.7	4.9	2.7	8.9	8.9	1.8	1.8	0.0		
Pu-239	602.9	613.6	106.1	116.7	106.1	683.6	687.7	124.9	129.0	0.0		
Pu-240	241.7	240.3	48.7	47.3	48.7	206.5	207.8	40.5	41.8	0.0		
Pu-241	66.1	59.9	16.1	9.9	16.1	20.2	20.7	3.9	4.3	0.0		
Pu-242	48.5	48.4	9.7	9.6	9.7	11.7	11.7	2.3	2.4	0.0		
Am-241	49.6	48.0	10.5	8.9	10.5	12.2	12.0	2.5	2.3	0.0		
Am-242	1.1	1.5	0.0	0.4	0.0	0.9	0.9	0.2	0.2	0.0		
Am-243	9.5	9.7	1.8	2.0	1.8	2.8	2.8	0.6	0.6	0.0		
Cm-242	1.1	1.4	0.0	0.3	0.0	0.3	0.4	0.0	0.1	0.0		
Cm-243	0.0	0.0	0.0	0.0	0.0	0.0	0.0	0.0	0.0	0.0		
Cm-244	2.2	2.5	0.3	0.6	0.3	1.2	1.2	0.2	0.3	0.0		
Cm-245	0.2	0.2	0.0	0.1	0.0	0.3	0.3	0.1	0.1	0.0		
Cm-246	0.0	0.0	0.0	0.0	0.0	0.1	0.1	0.0	0.0	0.0		
Total HM	9179.2	9094.8	1488.5	1404.2	1488.5	9178.9	9094.5	1488.5	1404.2	1310.2		
TRU	1083.0	1085.2	205.4	207.5	205.4	955.8	961.5	178.3	184.0	0.0		

III.4.3 Alternative Core Design for Oxide Fuel

III.4.3.1 Oxide Fuel Assembly Design

The reference ABTR core design presented in Section II.1.1 was developed using a ternary metal fuel. An alternative ABTR design was developed for mixed oxide, UO₂-TRUO₂ fuel based on the same core configuration as the reference metal core design. The key design parameters of the oxide fuel assembly are compared with those of the metal fuel assembly in Table III.4-10.

Compared to the metal fuel, the active core height of the oxide fuel was increased to 90 cm from 80 cm to reduce the peak linear power density within the linear power limit. The gas plenum of the oxide fuel was proportionally increased to 135 cm from 120 cm. The fuel volume fraction of the oxide fuel is about 23.8% higher than that of the metal fuel because of the higher fuel smeared density. The smeared density of the mixed oxide fuel is 88.4% TD (theoretical density), while that of the metal fuel is 75%. The density of oxide fuel pellet was assumed 95% TD, and the gap between fuel pellet and cladding was assumed 0.12 mm.

Table III.4-10 Comparison of Key Design Parameters of Metal and Oxide Fuel Assemblies

	Metal fuel	Oxide fuel
Assembly data		
- Number of fuel pins	217	217
- Assembly pitch, cm	14.598	14.598
Pin data		
- Fuel form	U-TRU-10Zr	(U,TRU)O ₂
- Bond material	Na	He
- Height (core/plenum), cm	80 / 120	90 / 135
- Overall pin length, cm	260.0	285.0
- Fuel smeared density, % TD	75.0	88.4
- Pin diameter, cm	0.800	0.800
- Pin pitch-to-diameter ratio	1.13	1.13
- Cladding thickness, cm	0.052	0.052
Volume fraction, %		
- Fuel	33.6	41.6
- Bond	11.2	3.1
- Structure	23.1	23.1
- Coolant	32.1	32.1

III.4.3.2 Fuel Cycle Performance Characteristics

The start-up core performances characteristics of the oxide fuel core are compared with the metal fuel core in Table III.4-11. The WG-Pu was used as TRU feed for driver assemblies, while the LWR-SF TRU was used for fuel test assemblies. The axial irradiation swelling of oxide fuel was neglected, while 5% axial swelling was assumed for metal fuel. For the estimation of the linear power limit of oxide fuel, the thermal conductivity and melting temperature correlations of Reference 8 were used, and the porosity correction factor of 0.86 was applied for thermal conductivity.

Table III.4-11 Comparison of Start-up Cycle Performance Characteristics between Metal and Oxide Cores

	Metal core	Oxide core
Cycle length, months	4	4
No. of batches (IC/OC/test)	12 / 15 / 12	12 / 15 / 12
Equivalent core diameter /barrel ID, m	1.31 / 2.27	1.31 / 2.27
Fuel form	U-Pu-10Zr	UO ₂ -PuO ₂
TRU feed (fissile content, %)	WG-Pu (94.2)	WG-Pu (94.2)
TRU enrichment (IC/test/OC), %	16.5/18.7/20.7	19.2/21.7/24.0
Fissile/TRU conversion ratio	0.58 / 0.65	0.56 / 0.64
HM/TRU loading, Mt	4.03 / 0.73	3.67 / 0.78
Specific power of active core, kW/kg	59.4	64.9
Power density of active core, kW/l	258.0	241.3
Discharge burnup (average/peak), MWd/kg	97.7 / 130.8	106.7 / 146.6
Peak fast fluence, 10 ²³ n/cm ²	3.25	2.67
Burnup reactivity swing (%Δk)	1.20	1.35
Power peaking factor, BOEC/EOEC	1.53 / 1.52	1.61 / 1.60
Stage factor, BOEC/EOEC	1.13 / 1.13	1.15 / 1.15
Peak linear power, kW/m	38.5	38.4
Linear power limit, kW/m	44.0	42.0
Core average flux, 10 ¹⁵ n/m ² -sec	2.38	2.21
Test assembly flux, 10 ¹⁵ n/cm ² -sec	2.84	2.67
Fast flux fraction	0.70	0.60

Compared to the metal fuel core, the lower heavy metal density of oxide fuel decreases the heavy metal loading by ~9% despite a 23.8% larger fuel volume fraction. The lower heavy metal inventory increases the specific power from 59.4 kW/kg to 64.9 kW/kg. The increased active core height reduces the average power density from 258 W/cm³ to 241 W/cm³. The higher specific power density increases the average discharge burnup from 98 MWd/kg to 107 MWd/kg, but the lower power density reduces the core average flux level by ~8%. The neutron spectrum of the oxide fuel core is significantly

softer than that of metal fuel core, and thus the fast flux fraction is reduced to 0.60 from the value 0.70 of the metal fuel core. Combined with the lower flux level, the softer spectrum reduces the peak fast fluence from 3.25×10^{23} n/cm² to 2.67×10^{23} n/cm². The lower density oxide fuel core increases the average TRU enrichment from 18.8% to 21.8%, which results in slightly higher TRU (780 kg as compared to 730 kg in the metal core) despite a ~9% smaller heavy metal inventory. The combined effects of the increased TRU enrichment and the softer spectrum result in similar fissile and TRU conversion ratios. The burnup reactivity swing of the oxide core is ~10% larger than that of the metal fuel core. The peak linear power of the oxide core is similar to that of the metal fuel core, but the linear power limit is slightly lower for the oxide fuel because of the low thermal conductivity of the oxide fuel and the helium bonding.

Table III.4-12 provides the comparison of the heavy metal inventories and the mass flow rates between the metal and oxide fuel cores. Compared to the metal fuel core, the oxide fuel core increases the TRU consumption rate from 25.9 kg/year to 26.8 kg/year. The heavy metal mass per assembly is reduced to 64.2 kg from 70.1 kg. The TRU mass per assembly is increased to 12.3 kg from 11.6 kg for inner core drivers and to 15.4 kg from 14.5 kg for outer core drivers. For the assumed fuel management scheme for fuel test assemblies, each test assembly contains 13.9 kg TRU.

III.4.3.3 Kinetics Parameters and Reactivity Coefficients

Table III.4-13 compares the kinetics parameters and reactivity coefficients estimated for the BOEC and EOEC configurations of the reference ABTR metal and oxide cores. The softer spectrum of the oxide fuel yields a slightly smaller β_{eff} (0.0032 as compared to 0.0033 of the metal core), since the neutron importance increases with increasing energy. The prompt neutron lifetime is 0.42 μs for the oxide fuel core and 0.33 μs for the metal fuel core. Since the prompt neutron lifetime is proportional to the bi-linearly weighted average of the inverse of neutron velocity, the softer neutron spectrum of the oxide fuel yields a significantly longer prompt neutron lifetime.

The radial expansion coefficient represents the reactivity effects of uniform, radial thermal expansion of the grid plate that is governed by the coolant inlet temperature. It is about -0.60 cents/°C for the metal fuel core and about -0.55 cents/°C for the oxide fuel core. The radial expansion coefficient is more negative for the metal fuel core, since the axial leakage increase resulting from the radial core expansion is larger because of a shorter core height. The axial expansion coefficient represents the reactivity effects of uniform, axial thermal expansion of fuel for the case that the fuel is bonded to the cladding. It is slightly more negative for the oxide fuel core, since the radial leakage increase resulting from the axial core expansion is slightly larger because of slightly smaller fuel atom densities.

Table III.4-12 Comparison of Start-up Cycle Heavy Metal Inventories and Mass Flow between Metal and Oxide Cores

Isotope	Metal fuel core				Oxide fuel core			
	Inventory, kg		Mass flow, kg/year		Inventory, kg		Mass flow, kg/year	
	BOEC	EOEC	charge	discharge	BOEC	EOEC	charge	discharge
U-234	0.0	0.0	0.00	0.01	0.0	0.0	0.0	0.0
U-235	5.2	5.0	1.52	0.84	4.5	4.3	1.3	0.7
U-236	0.3	0.4	0.00	0.14	0.3	0.4	0.0	0.1
U-238	3289.6	3270.2	768.35	710.29	2889.2	2870.2	678.0	620.9
NP237	3.6	3.6	0.89	0.88	3.6	3.5	0.9	0.8
Pu-236	0.0	0.0	0.00	0.00	0.0	0.0	0.0	0.0
Pu-238	1.6	1.7	0.28	0.56	1.9	2.0	0.3	0.7
Pu-239	628.6	617.0	156.83	121.80	660.3	646.8	166.7	126.1
Pu-240	80.2	83.1	13.74	22.29	93.3	97.5	14.6	27.2
Pu-241	8.9	9.0	2.09	2.26	10.4	10.6	2.2	2.9
Pu-242	4.0	4.0	0.96	1.03	4.4	4.4	1.0	1.2
Am-241	3.8	3.8	1.00	0.90	4.0	4.0	1.1	0.9
Am-242	0.1	0.1	0.00	0.05	0.1	0.1	0.0	0.1
Am-243	0.7	0.8	0.18	0.20	0.8	0.8	0.2	0.2
Cm-242	0.1	0.1	0.00	0.04	0.2	0.2	0.0	0.1
Cm-243	0.0	0.0	0.00	0.00	0.0	0.0	0.0	0.0
Cm-244	0.2	0.2	0.03	0.06	0.2	0.2	0.0	0.1
Cm-245	0.0	0.0	0.00	0.01	0.0	0.0	0.0	0.0
Cm-246	0.0	0.0	0.00	0.00	0.0	0.0	0.0	0.0
Total HM	4027.2	3999.0	945.9	861.3	3673.3	3645.1	866.3	781.9
TRU	732.0	723.4	176.0	150.1	779.2	770.3	187.0	160.2

The sodium void worth and sodium density coefficient are positive because the positive spectral hardening effect over-weighs the negative leakage effect. However, the total sodium void worth is only ~1.4\$ for the oxide fuel core and ~1.8\$ for the metal fuel core, when the flowing sodium inside the assembly duct of all the fuel assemblies is voided in the active core and above. The oxide fuel core shows ~30% less positive sodium void worth and density coefficient, since the positive spectral hardening effect is reduced due to the moderation provided by oxygen. The Doppler coefficient is about -0.10 cents/°C for the metal fuel core and -0.20 cents/°C for the oxide fuel core. The voided Doppler coefficients become slightly less negative due to hardened neutron spectra. The oxide core shows significantly more negative Doppler coefficients than the metal fuel core because of significantly softer spectrum as shown in Figure III.4-7.

Table III.4-13 Comparison of Kinetics Parameters and Reactivity Coefficients between Metal and Oxide Cores

	Unit	Metal fuel core		Oxide fuel core	
		BOEC	EOEC	BOEC	EOEC
Effective delayed neutron fraction		0.0033	0.0033	0.0032	0.0032
Prompt neutron lifetime	μs	0.33	0.33	0.42	0.42
Radial expansion coefficient	cent/ $^{\circ}\text{C}$	-0.59	-0.60	-0.55	-0.56
Axial expansion coefficient	cent/ $^{\circ}\text{C}$	-0.06	-0.05	-0.06	-0.06
Fuel density coefficient	cent/ $^{\circ}\text{C}$	-0.75	-0.76	-0.51	-0.58
Structure density coefficient	cent/ $^{\circ}\text{C}$	0.03	0.03	0.03	0.04
Sodium void worth	$\$$	1.75	1.85	1.32	1.40
Sodium density coefficient	cent/ $^{\circ}\text{C}$	0.03	0.03	0.01	0.01
Doppler coefficient	cent/ $^{\circ}\text{C}$	-0.10	-0.10	-0.20	-0.20
Sodium voided Doppler coefficient	cent/ $^{\circ}\text{C}$	-0.07	-0.07	-0.16	-0.16

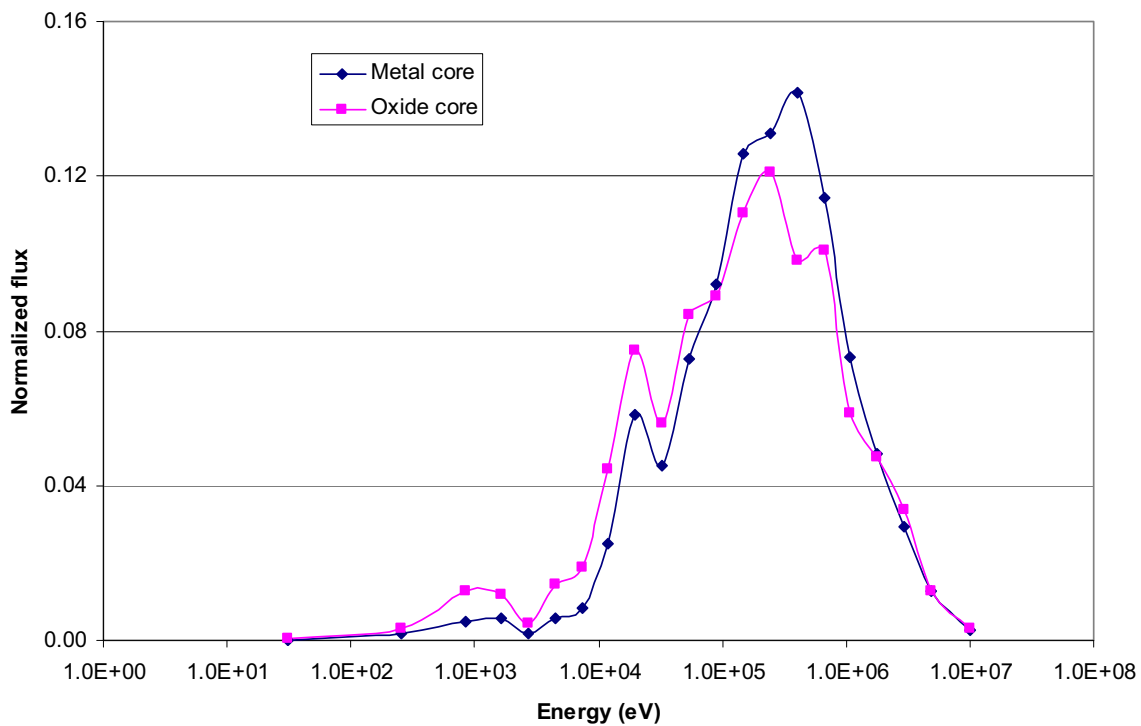


Figure III.4-7 Neutron Spectra of Metal and Oxide Fuel Cores

III.4.3.4 Reactivity Control Requirements and Shutdown Margins

The calculated temperature and power defects of metal and oxide fuels are compared in Table III.4-14. It is noted that the Doppler effect is noticeably larger for the oxide fuel core because of the significantly larger Doppler coefficient and the much higher fuel temperature. As a result, the total temperature defect of the oxide fuel is significantly higher than that of the metal fuel. Table III.4-15 presents the calculated control assembly worth for various combinations of control assemblies. As can be seen, the control assembly worth is larger in the oxide core because of a significantly softer spectrum. Among the primary control assemblies, the central control assembly has the largest worth because of higher neutron flux in the core center. The estimated worth of the central assembly is ~9.5\$ for the oxide fuel core and ~8\$ for the metal fuel core.

Figures III.4-8 and III.4-9 show the primary system reactivity worth curves of the oxide fuel core at BOEC and EOEC. As indicated by the dashed vertical lines in Figures II.1-8 and III.4-8, the critical control rod position is 63.4 cm for the metal fuel core and 67.8 cm for the oxide fuel core. The dashed curve indicates the reactivity worth of the most reactive control assembly, which is the central assembly. The reactivity addition by the complete withdrawal of the central control assembly is increased to 1.03\$ for the oxide fuel core from 0.90\$ for the metal fuel core. In order to limit the transient over-power initiator, it is necessary to reduce the central control rod worth or to introduce some means to limit the magnitude of rod withdrawal or the rod withdrawal speed.

Table III.4-16 summarizes the reactivity worth requirements for both primary and secondary control systems. The estimated temperature and power defects from hot full power to cold shutdown at BOEC are 1.74\$ and 2.71\$ for the metal and oxide fuel cores, respectively. The overpower margin is allocated to permit the reactor to operate at 115% of the rated power, which is equivalent to 15% of the power defect. The fuel cycle excess reactivity is 3.77\$ for the metal fuel core and 4.21\$ for the oxide fuel core. Since the fuel cycle analysis was performed with expanded core geometry, the reactivity associated with the axial fuel growth is added at BOEC. The uncertainties consist of 20% of total temperature defect, 30% of total burnup reactivity, 20% of fuel axial growth, and an assumption of 1.00\$ each for criticality prediction and fissile loading (tolerance for manufacture uncertainty). The total uncertainty is obtained by statistically combining all the uncertainties.

In Table III.4-17, the reactivity control requirements are compared with the available reactivity worth of the control systems. The oxide fuel core has slightly larger shutdown margins compared with the metal fuel core. The shutdown margin of the primary system is 8.15\$ at BOEC and 14.12\$ at EOEC. The shutdown margin of the secondary system is 9.36\$ at BOEC and 10.54\$ at EOEC. For both the metal and oxide fuel cores, shutdown margins are more than adequate. These results suggest that the central assembly could be removed to reduce the transient over-power initiator. Simple estimation based on the values in Table III.4-15 showed that the shutdown margin of the primary system without the central assembly would be ~4.5\$ at BOEC and ~9.5\$ at EOEC for both the metal and oxide fuel cores.

The control-rod driveline expansion coefficients for reactivity feedback were estimated from Figures III.4-8 and III.4-9. Control rod expansion coefficients are governed principally by the total rod worth and the insertion depth of the rods. The calculated control-rod expansion coefficients of the oxide fuel core are 32.9 cents/cm and 13.7 cents/cm at BOEC and EOEC, respectively.

Table III.4-14 Comparison of Temperature and Power Defects between Metal and Oxide Fuel Cores

Contribution	Metal fuel core				Oxide fuel core			
	Hot full power to hot standby		Hot standby to cold shutdown		Hot full power to hot standby		Hot standby to cold shutdown	
	BOEC	EOEC	BOEC	EOEC	BOEC	EOEC	BOEC	EOEC
Doppler (\$)	0.18	0.18	0.14	0.15	1.05	1.05	0.30	0.30
Axial expansion (\$)	0.05	0.04	0.09	0.08	0.05	0.05	0.09	0.09
Radial expansion (\$)	0.46	0.47	0.89	0.90	0.43	0.43	0.82	0.84
Sodium density (\$)	-0.02	-0.02	-0.04	-0.04	-0.01	-0.01	-0.02	-0.02
Total (\$)	0.66	0.67	1.08	1.09	1.51	1.52	1.20	1.21

Table III.4-15 Comparison of Control Rod Worth (\$) between Metal and Oxide Fuel Cores

	Number of inserted CRs	Metal fuel core		Oxide fuel core	
		BOEC	EOEC	BOEC	EOEC
		Primary System			
• Central rod	1	6.53	6.62	7.56	7.66
• All CR's in 5 th row	6	15.95	16.18	18.29	18.59
• Central and 5 CR's in 5 th row	6	20.32	20.61	23.66	24.02
• All primary rods	7	23.52	23.87	27.63	28.06
Secondary System					
• 2 CR's in 3rd row	2	10.53	10.68	12.13	12.29
• All secondary rods	3	16.38	16.61	19.15	19.41
One Stuck Rod Worth					
• Central rod		7.58	7.68	9.33	9.46
• One of 5th row		3.21	3.26	3.97	4.04
• One of 3rd row		5.84	5.93	7.03	7.12

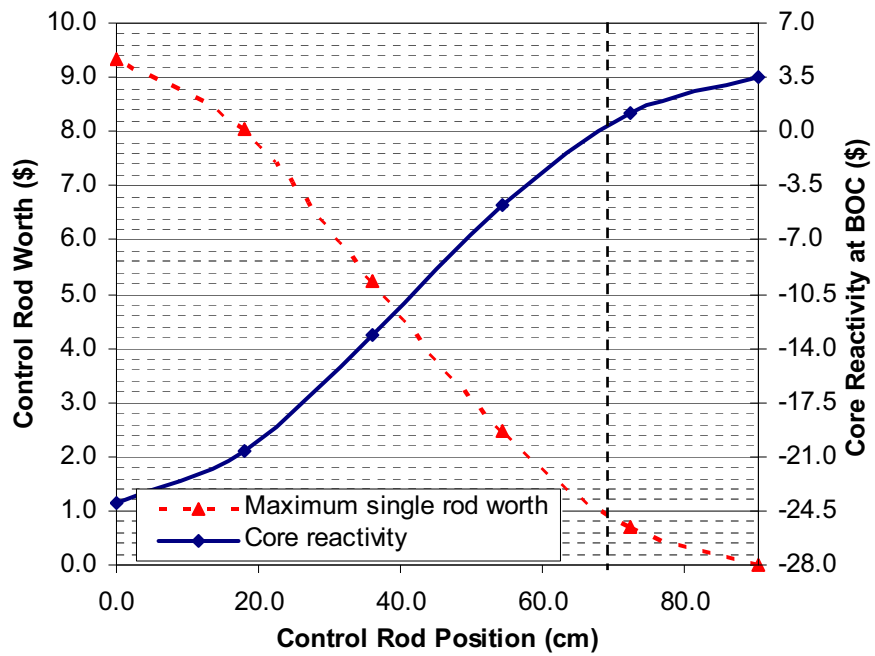


Figure III.4-8 Reactivity Worth of Primary Control System of Oxide Core at BOC

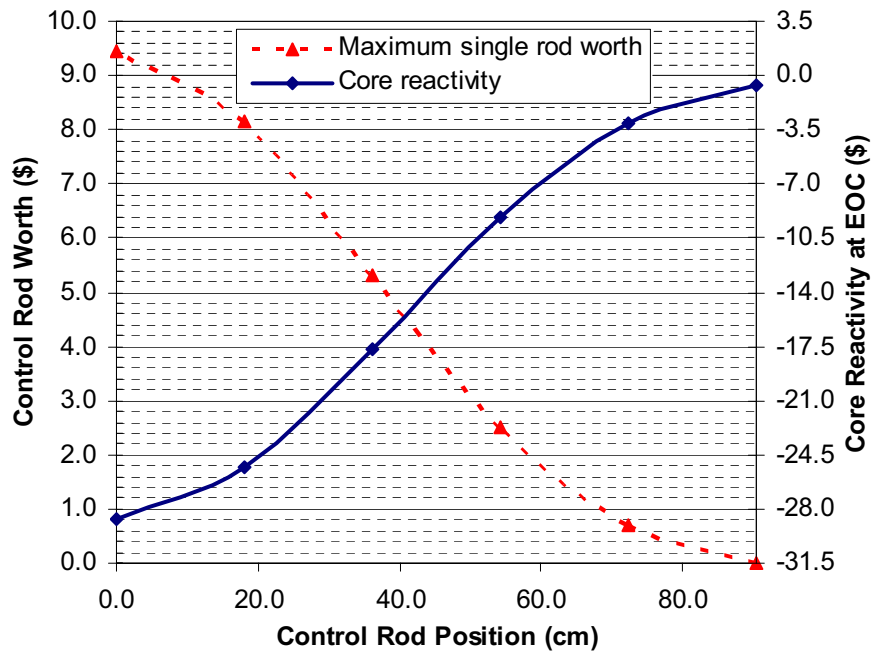


Figure III.4-9 Reactivity Worth of Primary Control System of Oxide Core at EOC

Table III.4-16 Comparison of Reactivity Control Requirements (\$) between Metal and Oxide Fuel Cores

	Metal fuel core				Oxide fuel core			
	Primary system		Secondary system		Primary system		Secondary system	
	BOEC	EOEC	BOEC	EOEC	BOEC	EOEC	BOEC	EOEC
Temperature defect	1.74	1.75	0.66	0.67	2.71	2.73	1.51	1.52
- Full power to hot standby	0.66	0.67	0.66	0.67	1.51	1.52	1.51	1.52
- Hot standby to refueling	1.08	1.09			1.20	1.21		
Overpower margin (15%)	0.10	0.10	0.10	0.10	0.23	0.23	0.23	0.23
Fuel cycle excess reactivity	3.77				4.21			
- Burnup reactivity	3.58				4.21			
- Fuel axial growth	0.19				0.00			
Uncertainties (RMS)	1.81	1.46			1.97	1.52		
- Temperature defect (20%)	0.35	0.35			0.54	0.55		
- Burnup reactivity (30%)	1.08	0.00			1.26	0.00		
- Fuel axial growth (20%)	0.04				0.00			
- Criticality prediction	1.00	1.00			1.00	1.00		
- Fissile loading	1.00	1.00			1.00	1.00		
Reactivity fault	0.90		0.90		1.03		1.03	
Total	8.32	3.31	1.66	0.77	10.15	4.47	2.76	1.75

Table III.4-17 Comparison of Reactivity Control Requirements and Available Reactivity Worth

	Metal fuel core				Oxide fuel core			
	Primary system		Secondary system		Primary system		Secondary system	
	BOC	EOC	BOC	EOC	BOC	EOC	BOC	EOC
Number of control assemblies	7	7	3	3	7	7	3	3
Reactivity worth of system (\$)	23.52	23.87	16.38	16.61	27.63	28.06	19.15	19.41
Worth of 1 stuck assembly (\$)	7.58	7.68	5.84	5.93	9.33	9.46	7.03	7.12
Reactivity worth available (\$)	15.95	16.18	10.53	10.68	18.29	18.59	12.13	12.29
Maximum requirement (\$)	8.32	3.31	1.66	0.77	10.14	4.47	2.76	1.75
Shutdown margin (\$)	7.63	12.88	8.87	9.92	8.15	14.12	9.36	10.54

III.4.4 Performances with LWR Spent Fuel TRU

The reference metal core design discussed in Section II.1.1 and the alternative oxide core design discussed in Section III.4.3 were developed using weapons-grade plutonium feed, since it is unlikely to recover enough TRU for the ABTR start-up core loading from the LWR spent fuel under the current time schedule. It is expected that the ABTR core will be converted gradually into LWR-SF TRU drivers, thus the performance characteristics of the ABTR reference and alternative core designs loaded with LWR-SF TRU drivers were evaluated. The assembly designs and core configurations described in Sections II.1.1 and III.4.3 were used, but the required TRU enrichments to achieve the same cycle length were re-calculated.

The heavy metal inventories and TRU consumption rates of the reference ABTR designs for two different TRU feed streams (i.e., WG-Pu and LWR-SF) are compared in Table III.4-18. The start-up cycle performance characteristics of the metal and oxide fuel cores are summarized in Tables III.4-19 and III.4-20, respectively. As discussed in Section III.4.3, the heavy metal inventory of the oxide fuel core is smaller than that of the metal fuel core for both TRU feeds, because of the lower heavy metal density. For each fuel form, the WG-Pu and LWR-SF TRU cores have similar performance characteristics (e.g., discharge burnup, flux level, peak fast fluence, specific power density, etc.) because of the same heavy metal loading. However, the low fissile content of the LWR-SF TRU fuel increases the required TRU enrichment by 32 to 33% to maintain the same cycle length; the average TRU enrichment increases from 18.8 to 24.8% for the metal core and from 21.8 to 29.1% for the oxide core. The increased TRU enrichment decreases the TRU conversion ratio from 0.65 to 0.57 for the metal core and from 0.64 to 0.55 for the oxide core, but the reduced fissile content increases the fissile conversion ratio by ~10 %. The decreased TRU conversion ratio increases the TRU consumption rate from 26 to 32 kg/year for the metal core and from 27 to 34 kg/year for the oxide core, and the increased fissile conversion ratio decreases the burnup reactivity swing by ~0.2 %Δk.

Table III.4-18 Heavy Metal Inventories and TRU Consumption Rates of Metal and Oxide Fuel ABTR Cores for WG-Pu and LWR-SF TRU Drivers

		Metal fuel core		Oxide fuel core	
		WG-Pu	LWR SF	WG-Pu	LWR SF
External TRU source		WG-Pu	LWR SF	WG-Pu	LWR SF
HM inventory (BOEC/EOEC), kg		4027/3999	4029/4001	3673/3645	3675/3647
TRU inventory (BOEC/EOEC), kg		732/723	975/964	779/770	1046/1035
TRU consumption rate (kg/yr)		25.9	32	26.8	34.3
HM mass per assembly, kg		70.1	70.1	64.2	64.2
TRU mass per assembly, kg	Inner core	11.6	15.3	12.3	16.4
	Outer core	14.5	19.1	15.4	20.5
	Fuel test	13.1	17.3	13.9	18.6

**Table III.4-19 Start-up Cycle Performance Characteristics of Metal Fuel Core
for WG-Pu and LWR-SF TRU Drivers**

External TRU source	WG-Pu	LWR-SF TRU
Fuel form	U-Pu-10Zr	U-TRU-10Zr
TRU feed (fissile content, %)	WG-Pu (94.2)	LWR-SF (59.6)
TRU enrichment (IC/test/OC), %	16.5/18.7/20.7	21.8/24.7/27.3
Fissile/TRU conversion ratio	0.58 / 0.65	0.64 / 0.57
HM/TRU loading, Mt	4.03 / 0.73	4.03 / 0.97
Specific power of active core, kW/kg	59.4	59.4
Power density of active core, kW/l	258.0	258.2
Discharge burnup (ave./peak), MWd/kg	97.7 / 130.8	97.7 / 130.6
Peak fast fluence, $10^{23}/\text{cm}^2$	3.25	3.28
Burnup reactivity swing ($\% \Delta k$)	1.20	1.02
Power peaking factor, BOEC/EOEC	1.53 / 1.52	1.64 / 1.63
Stage factor, BOEC/EOEC	1.13 / 1.13	1.12 / 1.11
Peak linear power density, kW/m	38.5	40.8
Linear power limit, kW/m	44.0	47.0
Core average flux, $10^{15}/\text{cm}^2\text{-sec}$	2.38	2.34
Test assembly flux, $10^{15}/\text{cm}^2\text{-sec}$	2.84	2.84
Fast flux fraction	0.70	0.70

**Table III.4-20 Start-up Cycle Performance Characteristics of Oxide Fuel Core
for WG-Pu and LWR-SF TRU Drivers**

External TRU source	WG-Pu	LWR-SF TRU
Fuel form	UO ₂ -PuO ₂	UO ₂ -TRUO ₂
TRU feed (fissile content, %)	WG-Pu (94.2)	LWR-SF (59.6)
TRU enrichment (IC/test/OC), %	19.2 / 21.7 / 24.0	25.6 / 28.9 / 32.0
Fissile/TRU conversion ratio	0.56 / 0.64	0.61 / 0.55
HM/TRU loading, Mt	3.67 / 0.78	3.68 / 1.05
Specific power of active core, kW/kg	64.9	64.9
Power density of active core, kW/l	241.3	241.5
Discharge burnup (ave./peak), MWd/kg	106.7 / 146.6	106.7 / 146.4
Peak fast fluence, $10^{23}/\text{cm}^2$	2.67	2.73
Burnup reactivity swing ($\% \Delta k$)	1.35	1.13
Power peaking factor, BOEC/EOEC	1.61 / 1.60	1.73 / 1.71
Stage factor, BOEC/EOEC	1.15 / 1.15	1.13 / 1.12
Peak linear power density, kW/m	38.4	40.5
Linear power limit, kW/m	42.0	41.5
Core average flux, $10^{15}/\text{cm}^2\text{-sec}$	2.21	2.16
Test assembly flux, $10^{15}/\text{cm}^2\text{-sec}$	2.67	2.67
Fast flux fraction	0.60	0.61

III.4.5 Low Conversion Ratio Core Designs

The reference metal and oxide fuel core designs were based on conventional enrichment plutonium-based fuel for the initial core, foreseeing gradual transition to full core loading of transmutation fuel after its qualification phase (resulting in ~ 0.6 CR). The low CR transmutation fuel tests can be accommodated in the designated test assemblies, and if fully developed, core conversion to low CR fuel can be envisioned. Thus, additional design studies were performed to develop fuel assembly designs that yield a low TRU conversion ratio when employed in the reference core configuration. To achieve the targeted low conversion ratio of ~ 0.25 , the TRU enrichment should be increased significantly. In order to increase the TRU enrichment in such a way that the initial excess reactivity is within the reactivity control capability of the primary control system, the fuel volume fraction and the cycle length were reduced. For the metal fuel, the Zr mass fraction was increased from 10% to 20% to compensate the decreasing melting temperature of metal fuel with increasing TRU fraction.

Table III.4-21 presents the assembly design parameters of the low conversion ratio assemblies. The fuel pin diameter was reduced from 8.00 mm to 6.25 mm, and the fuel pin pitch-to-diameter ratio was increased from 1.13 to 1.28. The cladding thickness was increased from 0.52 mm to 0.75 mm, and the wire-wrap diameter was increased from 1.03 mm to 1.73 mm. This wire-wrap is thicker than conventional wire-wrap designs, and the assembly design change from wire-wrap to grid spacer may need to be considered. The resulting fuel volume fraction was decreased from 33.6% to 19.5% for the metal fuel and from 41.6% to 24.2% for the oxide fuel. The structure volume fraction was increased from 23.1% to 31.6%, and the coolant volume fraction was increased from 32.1% to 42.4%. In order to limit the burnup reactivity swing within the reactivity control capability of the primary control system, the cycle length was reduced to 2 months from 4 months.

Table III.4-22 compares the heavy metal inventories and TRU consumption rates of the low CR core designs for two different TRU feed streams. Table III.4-23 summarizes the start-up core performances characteristics, which were obtained from REBUS-3 equilibrium cycle calculations without recycling the ABTR spent fuel. The performance characteristics of WG-Pu and LWR-SF TRU feeds are compared. As can be seen, the low conversion ratio assembly designs with the LWR-SF TRU feed yield a TRU conversion ratio of 0.24 for the metal fuel core and 0.28 for the oxide fuel core. The conversion ratios obtained with WG-Pu fuel are somewhat higher; 0.31 for the metal fuel core and 0.36 for the oxide fuel core. It is noted that the oxide fuel core has a larger heavy metal loading than the metal fuel core because of the increased Zr fraction in the metal fuel assembly. Compared to the reference medium CR core designs, the heavy metal loading is reduced from 4.03 to 1.98 MT for the metal fuel core and from 3.67 to 2.15 MT for the oxide fuel core, because of the reduced fuel volume fractions. As a result, the specific power density is increased about two times. The increased specific power combined with the reduced cycle length from 4 months to 2 months yields a similar discharge burnup. The low conversion ratio roughly doubles the LWR-SF TRU enrichment from 25% to 47% for the metal fuel core, but only from 29% to 45% for the oxide fuel. Thus the

LWR-SF TRU loading is reduced from 0.98 to 0.90 MT for the metal core and from 1.05 to 0.95 MT for the oxide core. The combined effects of the decreased conversion ratio and reduced cycle length increases the burnup reactivity swing by $\sim 0.1\% \Delta k$ for the metal fuel core but decreases that by $\sim 0.1\% \Delta k$ for the oxide fuel core. The decreased conversion ratios roughly double the TRU consumption rate for both the metal and oxide fuel cores.

Table III.4-21 Fuel Assembly Design Parameters of Low Conversion Ratio Cores

	Metal fuel core	Oxide fuel core
Fuel Form	U-TRU-20Zr	UO ₂ -TRUO ₂
Height (core/plenum), cm	80 / 120	90 / 135
Fuel smeared density, % TD	75	88.4
Pin diameter, mm	6.25	6.25
Number of fuel pins	271	271
Assembly lattice pitch, cm	14.598	14.598
Pin pitch-to-diameter ratio	1.28	1.28
Average linear power, kW/m	17.7	16.6
Pin bundle pressure drop, psi	20.5	21.2
Volume fraction, %		
- Fuel	19.5	24.2
- Bond	6.5	6.5
- Structure	31.6	31.6
- Coolant	42.4	42.4

Table III.4-22 Heavy Metal Inventories and TRU Consumption Rates of Low CR Cores

	Metal fuel core		Oxide fuel core	
	WG-Pu	LWR SF	WG-Pu	LWR SF
External TRU source	WG-Pu	LWR SF	WG-Pu	LWR SF
HM inventory (BOEC/EOEC), kg	1984/1970	1985/1971	2151/2137	2152/2138
TRU inventory (BOEC/EOEC), kg	663/654	903/893	691/683	948/938
TRU consumption rate (kg/yr)	55.0	61.4	50.4	57.8
HM mass per assembly, kg	34.5	34.5	37.3	37.3
TRU mass per assembly, kg	Inner core	10.6	14.2	10.9
	Outer core	13.2	17.7	13.7
	Fuel test	11.9	16.0	12.3

Table III.4-23 Fuel Cycle Performances Characteristics of Low Conversion Ratio Cores

	Metal Core		Oxide Core	
	U-Pu-20Zr	U-TRU-20Zr	UO ₂ -PuO ₂	UO ₂ -TRUO ₂
Fuel form	U-Pu-20Zr	U-TRU-20Zr	UO ₂ -PuO ₂	UO ₂ -TRUO ₂
TRU feed	WG-Pu	LWR-SF	WG-Pu	LWR-SF
Cycle length, months	2	2	2	2
No. of batches (IC/OC/etc)	12/15/12	12/15/12	12/15/12	12/15/12
TRU enrichment (IC/test/OC), %	30.6 / 34.6 / 38.3	41.1 / 46.4 / 51.3	29.3 / 33.1 / 36.6	39.6 / 44.7 / 49.5
Fissile/TRU conversion ratio	0.28 / 0.31	0.32 / 0.24	0.32 / 0.36	0.36 / 0.28
Zr mass fraction, %	20.0	20.0	-	-
HM/TRU loading in core, MT	1.98 / 0.66	1.98 / 0.90	2.15 / 0.69	2.15 / 0.95
HM/TRU mass per assembly, kg	34.5 / 11.9	34.5 / 16.0	37.3 / 12.3	37.3 / 16.6
Core specific power, kW/kg	120.5	120.0	111.5	111.5
Core power density, kW/l	256.8	257.1	240.2	240.4
Burnup (average/peak), MWd/kg	99.1 / 130.8	99.1 / 130.5	91.7 / 123.8	91.7 / 123.3
Specific power density, MW/t	120.5	120.1	111.5	111.5
Peak fast fluence, 10 ²³ /cm ²	1.75	1.76	1.50	1.52
Burnup reactivity swing, %Δk	1.31	1.14	1.24	1.06
Power peaking factor, BOEC/EOEC	1.48 / 1.46	1.59 / 1.58	1.54 / 1.53	1.65 / 1.64
Stage factor, BOEC/EOEC	1.13 / 1.13	1.12 / 1.12	1.13 / 1.13	1.11 / 1.11
Peak linear power density, kW/m	29.5	31.6	28.8	30.5
Linear power limit, kW/m	32.3	31.9	39.6	38.9
Core average flux, 10 ¹⁵ /cm ² sec	2.75	2.67	2.54	2.47
Test assembly flux, 10 ¹⁵ /cm ² sec	3.23	3.21	3.02	3.00
Fast flux fraction	0.68	0.67	0.61	0.62
Decay heat fraction of rated power, %	5.3	5.5	-	-
Decay heat at discharge, kW/assembly	219	226	-	-

References

1. Y. I. Chang, M. Konomura, and P. Lo Pinto, "A Case for Small Modular Fast Reactor," Proc. of GLOBAL 2005: Nuclear Energy Systems for Future Generation and Global Sustainability, Tsukuba, Japan, October 9-13, 2005.
2. W. S. Yang, Private Communication, Argonne National Laboratory, January 2006.
3. C. P. Cabell, "A Summary Description of Fast Flux Test Facility," HEDL-400, Hanford Engineering Development Laboratory, December 1980.
4. R. N. Hill, Private Communication, Argonne National Laboratory, June 1993.
5. E. C. E. Lahm, J. F. Koenig, R. G. Pahl, D. L. Porter, and D. C. Crawford, "Experience with Advanced Driver Fuels in EBR-II," *Journal of Nuclear Materials*, 204, 119 (1993).
6. R. B. Baker, F. E. Bard, R. D. Leggett, and A. L. Pinter, "Status of Fuel, Blanket, and Absorber Testing in the Fast Flux Test Facility," *Journal of Nuclear Materials*, 204, 109 (1993).
7. A. L. Pinter and R. B. Baker, "Metal Fuel Test Program in the FFTF," *Journal of Nuclear Materials*, 204, 124 (1993).
8. J. J. Carbajo, G. L. Yoder, S. G. Popov, and V. K. Ivanov, "A Review of the Thermo-physical Properties of MOX," *Journal of Nuclear Materials*, 299, 181 (2001).

III.5 In-Vessel Shielding Analysis

Preliminary in-vessel shielding analyses were performed to estimate 1) the fission power of spent ABTR fuels located in the in-vessel storage, 2) the neutron irradiation damage of the in-vessel structures, and 3) the secondary sodium activation in the intermediate heat exchangers. Using the TWODANT transport code [1], the neutron flux distributions were calculated for the BOEC and EOEC configurations. R-Z geometry models and S_{16} angular discretization were used. For neutron damage calculation, 28-group dpa (displacement per atom) cross sections were generated using the NJOY code [2] based on the ENDF/B-VI data. The time integrations were evaluated using the average values of BOEC and EOEC fluxes.

Figure III.5-1 shows the RZ geometry model used in the TWODANT calculations. In this preliminary analysis, the inside of the core barrel assembly was modeled in detail, but only major components were modeled outside the core barrel assembly. The core barrel is made of SS-316, and its radius and thickness are 120 cm and 2.54 cm, respectively. The in-vessel spent fuel storage is located outside the core barrel; there are 36 positions for the fresh or spent fuel assemblies, including the fuel unloading machine retrieval position. The distance from the outside of the core barrel to the center of the spent fuel storage positions is about 36.5 cm and the distance between the centers of the spent fuel storage positions is 27.4 cm. It was assumed that all the storage positions are occupied by spent fuel assemblies. The spent fuels were represented by a homogenized region, and the unloading machinery was ignored.

Four primary pumps and eight auxiliary heaters were homogenized together and located at 223.0 cm from the reactor center. Two intermediate heat exchangers (IHX) are homogenized and located at 239.0 cm from the core center and elevated to 340.0 cm from the bottom of reactor. Four direct reactor auxiliary cooling system (DRACS) and other internal structures were not modeled. The modeled components were assumed a homogeneous mixture of SS-316 and sodium. The volume fractions of the structural material and sodium were determined to conserve the total mass of the structural materials. The calculated volume fractions of the structural material of the pump (including auxiliary heaters) and IHX are 37.2% and 10.7%, respectively. The reactor vessel is made of SS-316, and its radius and thickness are 278.5 cm and 5.08 cm, respectively. The radius and thickness of the guard vessel are 330.0 cm and 2.54 cm, respectively, and it is made of SS-304.

Table III.5-1 provides the regionwise power distribution determined from the neutronics calculations only, in which the gamma energy is locally deposited at the position of its creation. Most of the power is generated inside the core, but non-negligible amount of power is generated outside the core. The spent fuel assemblies located in the in-vessel storage generates ~0.5% of the rated power. The fission power generated by each spent fuel assembly is ~33 kW, which is ~0.8% of the average assembly power in the core. As discussed in Section II.1.1, the decay heat of a spent fuel decreases below ~15 kW in a few days after discharge. Thus the fission power is the dominant contributor

to the power generated in spent fuels. This result suggests that appropriate coolant flow needs to be directed to the spent fuels stored in the in-vessel spent fuel storage.

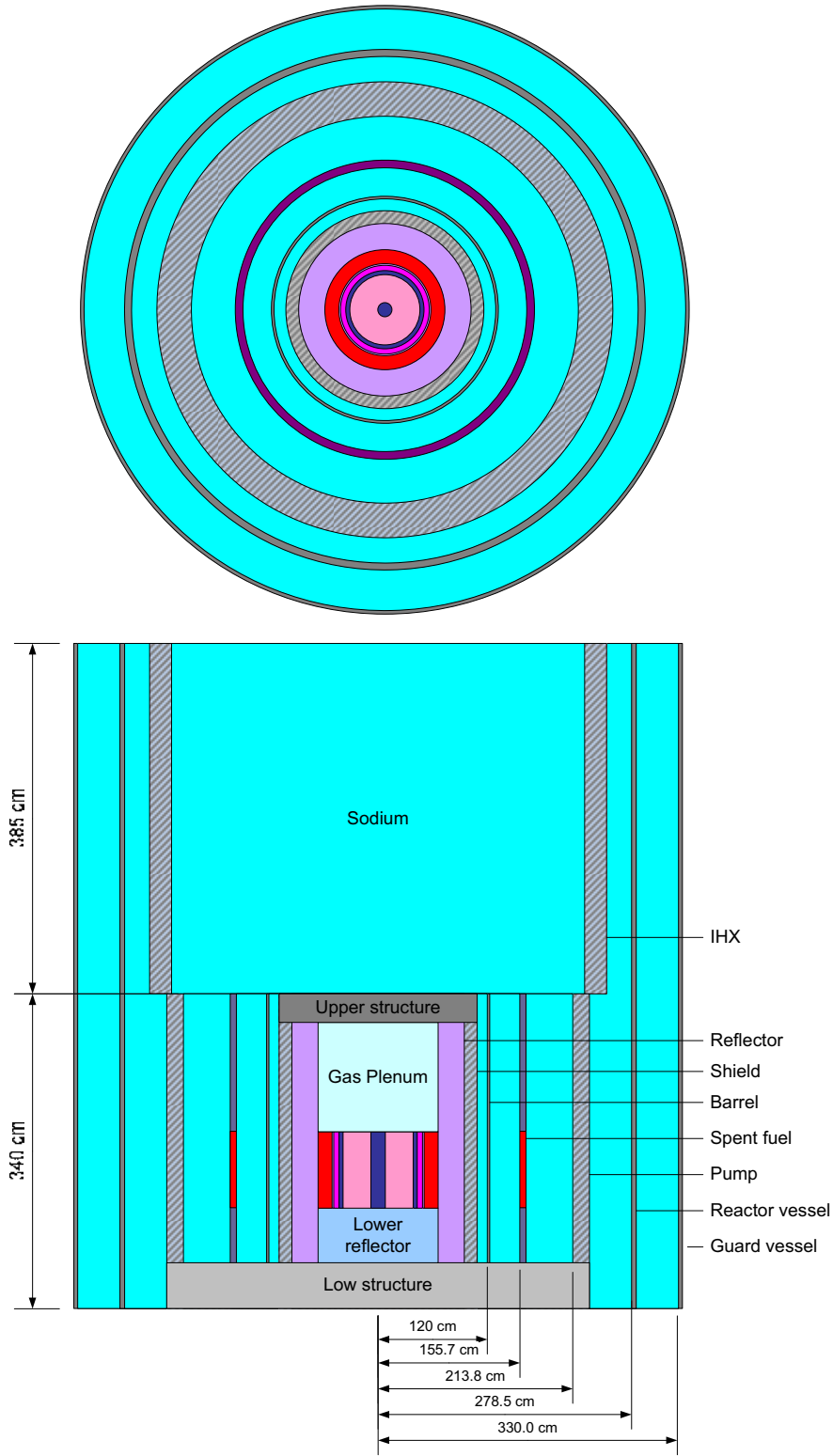


Figure III.5-1. RZ Model for In-Vessel Shielding Analysis

Table III.5-1 Regionwise Power Distribution of Reference ABTR Design

		Inner core	Outer core	Test fuel	Spent fuel	Other
Power (MW)	BOEC	118	104	21.2	1.16	4.77
	EOEC	117	105	21.4	1.18	4.73
Power fraction (%)	BOEC	47.4	41.8	8.5	0.47	1.91
	EOEC	46.9	42.2	8.6	0.47	1.89
Assembly power (MW)	BOEC	4.93	3.48	3.53	0.032	-
	EOEC	4.88	3.51	3.57	0.033	-
Peak power density (W/cm ³)	BOEC	428.5	311.3	286.2	2.75	-
	EOEC	411.8	303.6	279.7	2.78	-

The neutron irradiation damage of the in-vessel structures is the loss of ductility and fracture resistance due to the atom displacement within the material. The dpa is used to measure the neutron irradiation damage instead of the traditional fluence calculations, since it provides a simpler correlation with ductility that is generally only material dependent. It is recommended to ensure that the neutron fluence on the reactor vessel and core support structure during its service life does not reduce the residual total elongation of the material below 10%. For SS-316, based on the presently available data, this condition corresponds to ~5 dpa.

The neutron irradiation damages of the in-vessel structures are summarized in Table III.5-2, which were calculated for an assumed life time of 30 years with 90% capacity factor. As can be seen, the grid plate experiences the highest peak dpa. This peak value occurs at the center of the top surface of grid plate and is 4.4 dpa. In the inside of the grid plate, it is reduced to ~3 dpa. The peak fast fluence of the grid plate (1.1×10^{22} n/cm²) is only ~20% of the fast fluence inside the grid plate of the 4S design ($\sim 6 \times 10^{22}$ n/cm²). These results suggest that the in-vessel structure damages are well within the limits. It is noted that the fast fluence per dpa is consistent with the experimental value of $\sim 2 \times 10^{21}$ n/cm² obtained in EBR-II [3].

Table III.5-2 In-Vessel Structure Irradiation Damage

		Grid plate	Core barrel	Reactor vessel	Guard vessel
Fast fluence (n/cm ²)	Average	1.2E+21	2.1E+21	6.8E+18	5.2E+17
	Peak	1.1E+22	2.3E+21	1.5E+19	1.1E+18
Dpa	Average	0.49	0.82	3.0E-3	2.5E-4
	Peak	4.40	0.88	6.4E-3	5.2E-4
Fast fluence per dpa	Average	2.4E+21	2.6E+21	2.3E+21	2.1E+21
	Peak	2.5E+21	2.6E+21	2.3E+21	2.1E+21

The secondary sodium activation in the intermediate heat exchangers was estimated. Sodium in nature is composed entirely of Na-23. A (n,γ) reaction in sodium produces radioactive Na-24 that has a 14.95-hour half life and emits both 1.4 and 2.8-MeV gamma rays. A $(n,2n)$ threshold reaction produces Na-22 that has a 2.604-year half life and emits a 1.3 MeV gamma. The activation products are produced in the reactor and decay out outside the reactor. Thus, the activity of an activation product in the secondary sodium leaving the reactor can be determined as

$$\alpha = R(1 - e^{-\lambda t_1}) / (1 - e^{-\lambda t_2})$$

where

R = average production rate per cm^3

λ = decay constant

t_1 = transit time in IHX

t_2 = transit time over intermediate heat transfer (IHT) loop.

Using the characteristics of the secondary sodium loop shown in Table III.5-3, the sodium activation in the IHX was estimated. No IHX shielding was considered, and 21-group fluxes and Na-23 cross sections were used. Table III.5-4 shows the estimated activations of the secondary sodium. As can be seen, Na-24 is the dominant activation product, and its specific activity is ~ 0.3 Ci/kg. Considering that the secondary sodium activation was to be held below $0.07 \mu\text{Ci/kg}$ in CRBRP [3], the IHX must be shielded from neutrons in order to reduce the secondary sodium activity.

Table III.5-3 Secondary Sodium Loop Characteristics

	IHX	Secondary loop
Mass flow rate (kg/s)	629.3	
Volumetric flow rate (m^3/s)	0.74	
Volume (m^3)	4.27	9.70
Transit time (s)	5.8	13.1

Table III.5-4 Secondary Sodium Activation in IHX

	Na-24		Na-22	
	BOEC	EOEC	BOEC	EOEC
Volumetric activity, mCi/cm^3	0.26	0.27	4.82E-10	4.96E-10
Specific activity, Ci/kg	0.30	0.31	5.67E-10	5.83E-10
Total activity, Ci	2.49E+06	2.57E+06	4.68E-03	4.81E-03

References

1. R. E. Alcouffe, F. W. Brinkley, D. R. Marr, R. D. O'Dell, "User's Guide for TWODANT: A Code Package for Two-Dimensional, Diffusion-Accelerated, Neutral-Particle Transport," LA-10049-M, Los Alamos National Laboratory (1990).
2. R.E. MacFarlane, "NJOY 99/2001: New Capabilities in Data Processing," Presentation at the Workshop on Reactor Physics and Analysis Capabilities for Generation IV Nuclear Energy Systems, Argonne National Laboratory, Argonne, February 18-19, 2003.
3. A. E. Walter and A. B. Reynolds, *Fast Breeder Reactors*, Pergamon Press, New York, NY, 1981.

III.6 Thermal-Hydraulic Analysis

A computational fluid dynamics (CFD) analysis was performed to assess at steady-state flow patterns in the primary reactor system, sodium pool temperature distributions, and temperature distributions in the reactor vessel and the reactor vessel closure structures. For these analyses the CFD code STAR-CD was used.

The CFD model has about 2,330,000 computational cells, and includes the reactor pumps, the reactor plenum, the reactor core, lower reflector, upper shield, radial reflector, and radial shielding, the core barrel, the redan, the intermediate heat exchangers (IHXs), the reactor vessel, the guard vessel, the DRACS heat exchangers inside the sodium pool, the structures that form the closure of the reactor vessel, and the Argon gas space between the reactor and guard vessel and between the reactor vessel closure and the concrete support structures. To preserve the magnitude of the coolant velocities in the core, the core region was modeled as a cylindrical ring of fluid having the same flow area as the actual core. A more realistic representation would be to model the core as a porous region with volume porosity. At this time STAR-CD does not have this capability. The reactor pumps were modeled as momentum sources. The heat generation in the core was modeled as a volumetric heat source, and the IHXs and the DRACS were modeled as volumetric heat sinks. The redan was modeled as a solid of zero thickness that allows heat transfer by conduction between the hot and cold sodium pool, and heat transfer by radiation to the reactor vessel and the structures above the sodium pool through the Argon cover gas. Because at this time the STAR-CD code does not allow radiation from a liquid surface, a solid of zero thickness and zero thermal resistance was placed on the top of the sodium pool (separating the sodium from the Argon cover gas). The emissivity of this solid was set equal to that of the sodium pool surface [1].

Because the auxiliary cooling systems have not been sized yet, an adiabatic boundary condition was used on the outside surface of the guard vessel, and a temperature of 90°C was used on the concrete surfaces that form the model boundaries.

Figure III.6-1 shows the flow in the lower plenum (top view). Sodium from the outlet of the pump-pipes flows towards the center of the plenum, and from there it flows upwards into the core. Figure III.6-2 shows the sodium flow in the hot pool. The main flow pattern is a strong upward flow towards the inlet of the IHXs. The small flow reversal at the inlet of the hot pool is an artifact due to the simulation of the core coolant as a cylindrical ring. This artifact can be removed by simulating the core region as a porous medium with volume porosity, but at this time STAR-CD does not have this capability. The lower velocity profiles are oscillating and are not symmetric. The small flow reversal at the inlet of the hot pool may contribute to these patterns. A porous medium model with volume porosity would provide more realistic flow patterns at the level of the small velocities. Figure III.6-3 shows the coolant velocities in the hot pool on a vertical plane perpendicular to the axis passing through the centers of the IHXs. The flow is asymmetric and oscillating at low velocities as it is in Figure III.6-2.

Figures III.6-4 and III.6-5 show the temperature distribution in the hot pool. There is a central hot plume where the temperature is close to that of the core outlet, with a loss of about 2°C from the core outlet (510°C) to the top of the pool (Figure III.6-6). The small asymmetries in the temperature distribution are the result of the oscillating asymmetries in the flow distribution.

There is a heat transfer through the thin redan structure from the hot pool to the cold pool, which reduces the sodium temperature at the inlet of the IHX by about 2°C below the core outlet temperature (Figure III.6-7). Figure III.6-8 shows the temperature distribution in the reactor vessel. There is a significant azimuthal temperature variation in the section of the reactor vessel between the free surface of the cold and that of the hot pool, which reaches a peak temperature of 485°C in the neighborhood of the IHXs. There are also significant temperature variations in the redan, which may need to be considered in assessing its structural behavior.

Figure III.6-9 shows the temperature distribution in the reactor cover. There is a significant variation from the center to the periphery of the cover.

Reference

1. A. Yamaguchi and Y. Tajima, "Numerical Investigation of Mass and Heat Transfer in Sodium Pool Combustion," Numerical Heat Transfer, Part A, 41:697-709, 2002

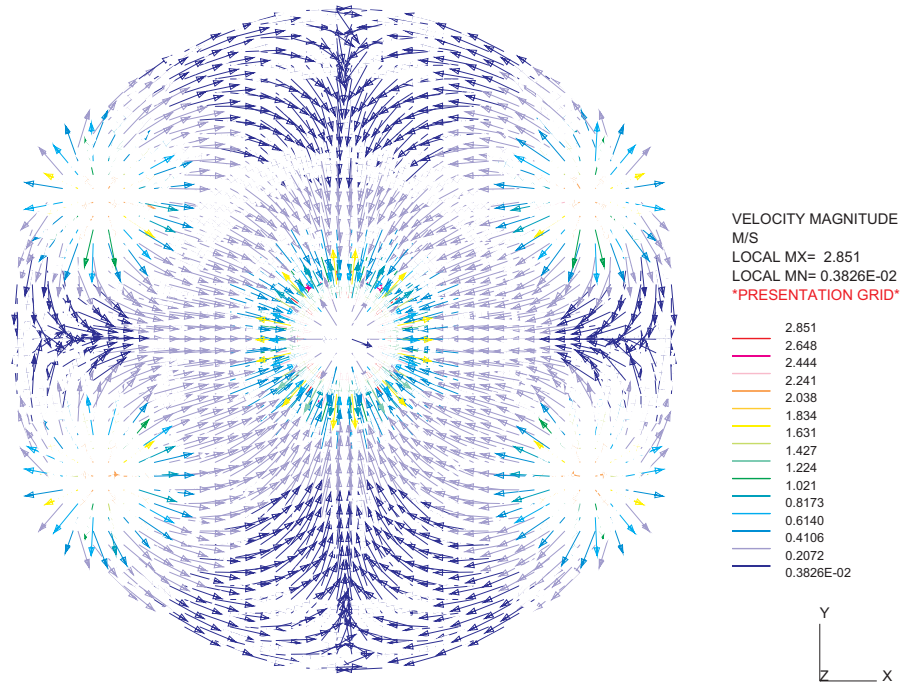


Figure III.6-1 Velocity distribution in the lower plenum

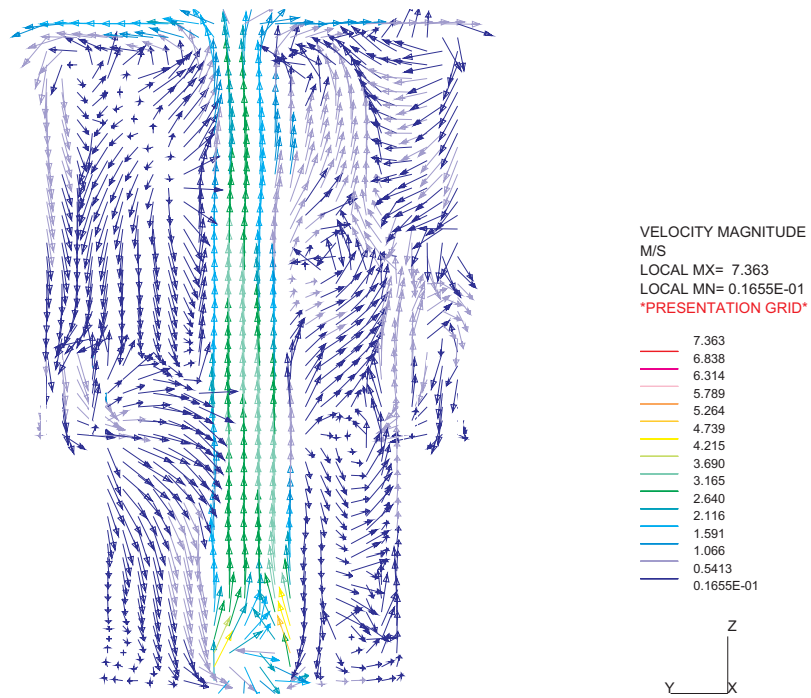
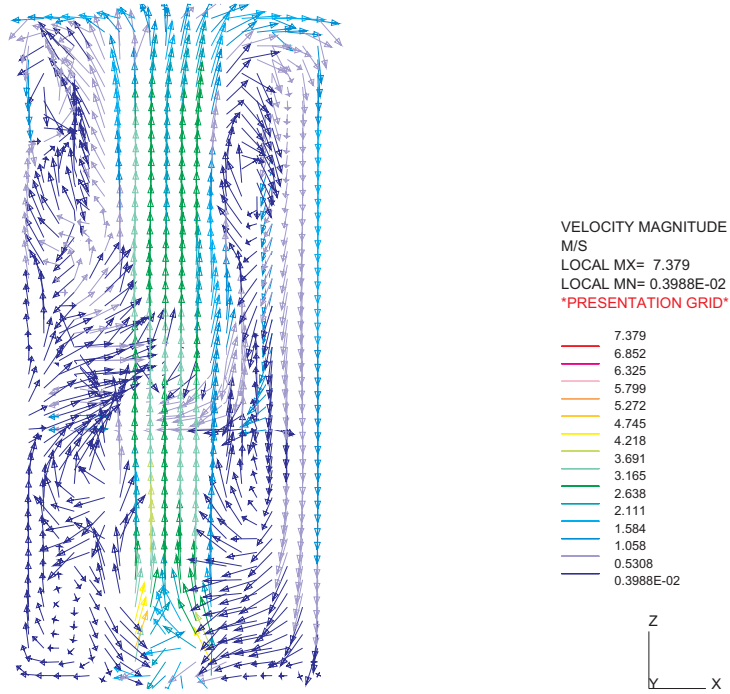
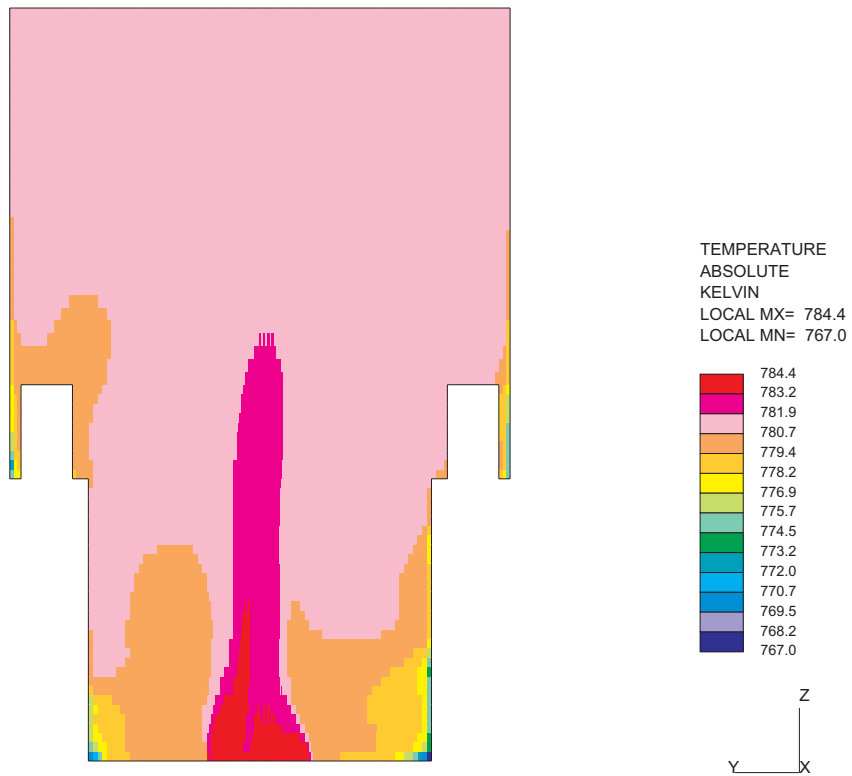


Figure III.6-2 Sodium velocity in the hot pool (plane passing through the IHX centers)



**Figure III.6-3 Sodium velocity in the hot pool
(plane perpendicular to the axis passing through the IHX centers)**



**Figure III.6-4 Temperature distribution in the hot pool
(plane passing through the IHX centers)**

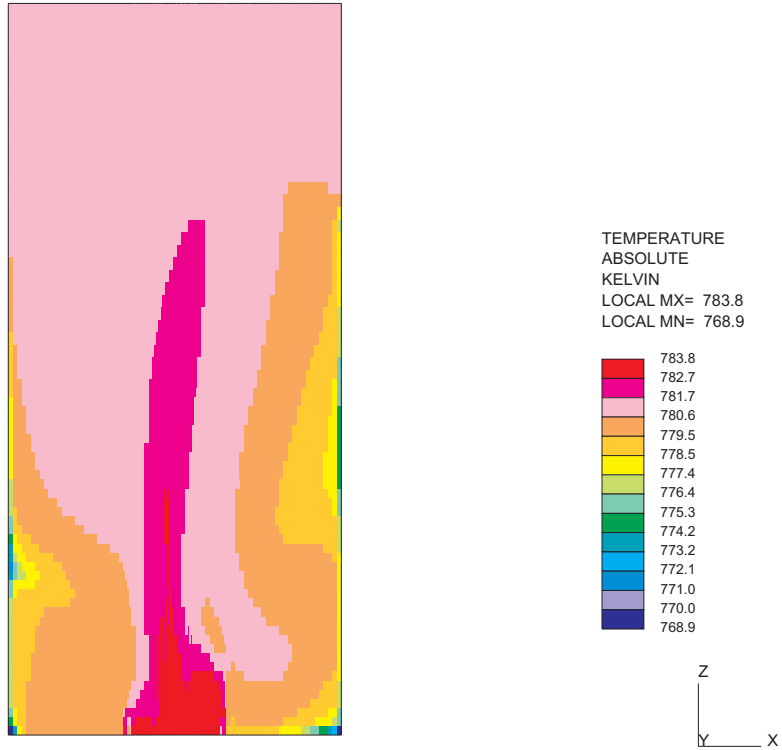


**Figure III.6-5 Temperature distribution in the hot pool
(plane perpendicular to the axis passing through the IHX centers)**

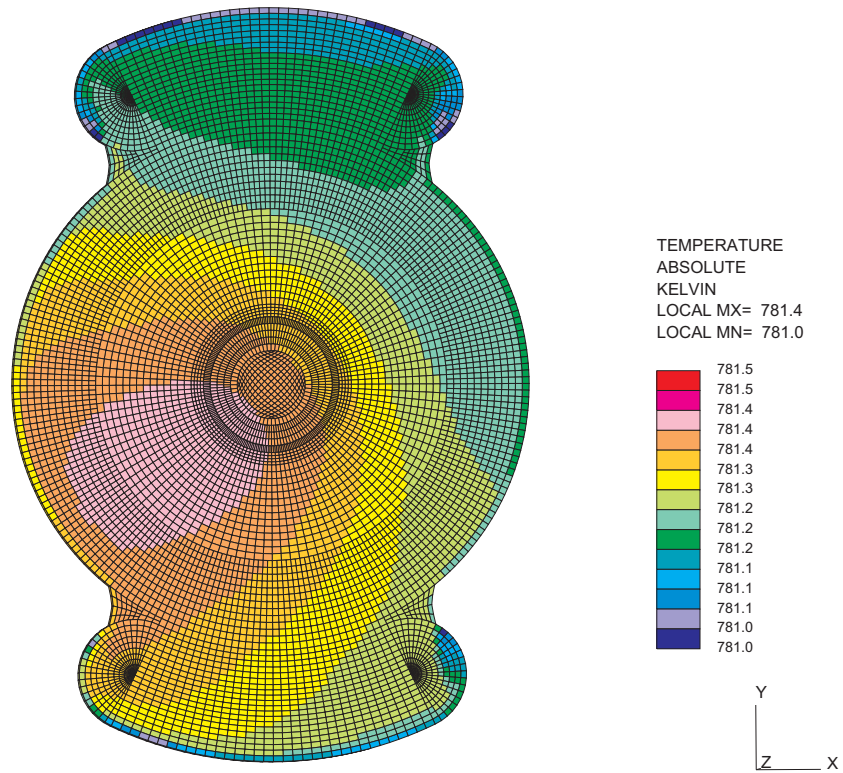


Figure III.6-6 Temperature distribution at the top of the hot pool

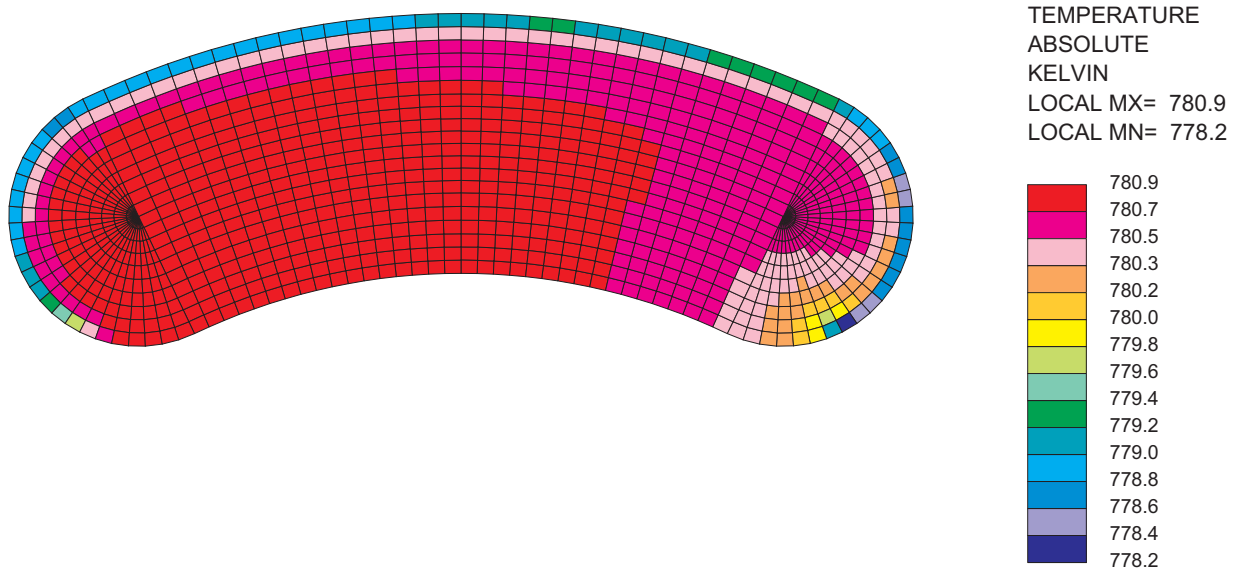


Figure III.6-7 Temperature distribution at the IHX inlet

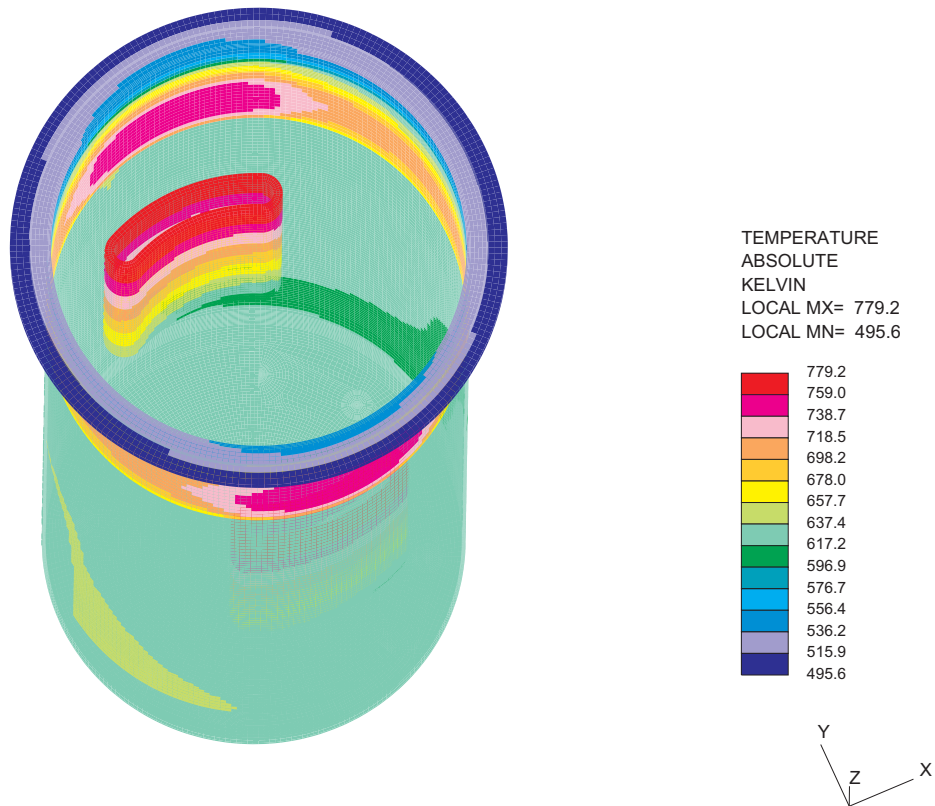


Figure III.6-8 Temperature distribution in the reactor vessel

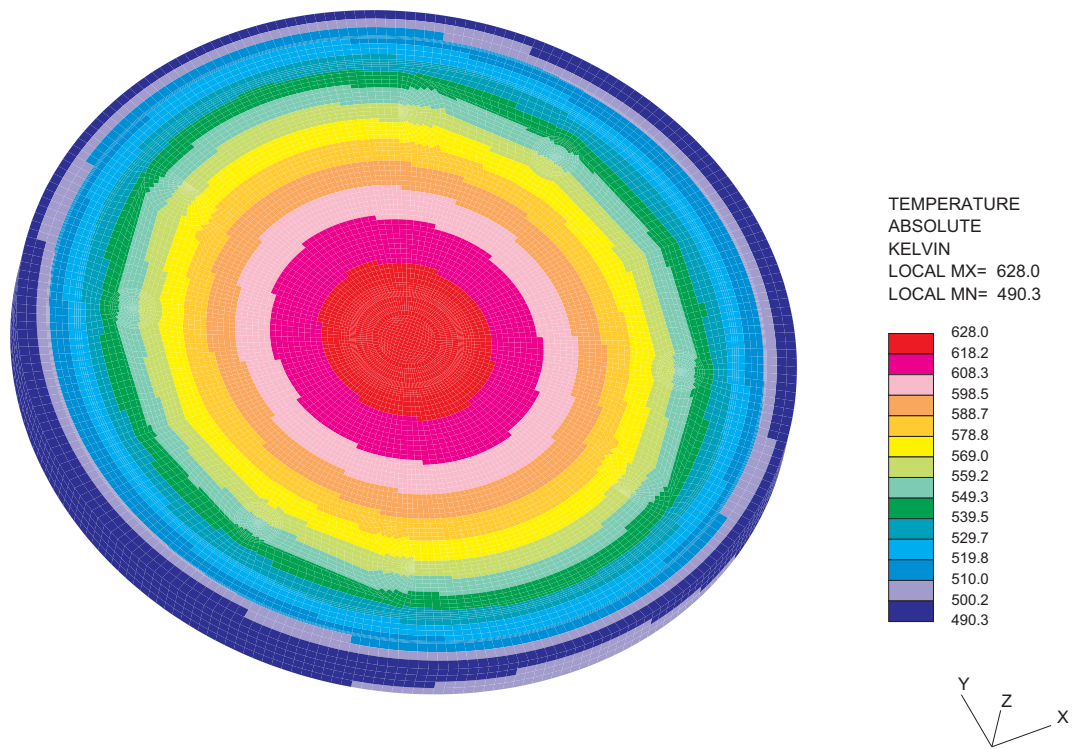


Figure III.6-9 Temperature distribution in the reactor cover

III.7 Safety Analysis

Preliminary analyses have been completed to assess the potential safety performance characteristics of the Advanced Burner Test Reactor (ABTR) design. The scope of the analyses presented here focuses on the ability of ABTR to provide inherent protection against damaging consequences in low probability accident sequences involving multiple equipment failures.

III.7.1 Introduction and Summary

Analysis Background

One of the primary goals in the ABTR design is to provide not only the customary safety margins in design basis events, but also to deliver superior safety performance in beyond design basis events involving multiple equipment failures or unplanned operator actions. Consequently, the preliminary analyses presented here examine the behavior of ABTR in response to an accident initiator that is normally considered to have a low occurrence frequency, but potentially severe consequences, especially when engineered safety systems are assumed to fail.

The accident initiator examined here is the total loss of normal power to the reactor cooling system while the plant is operating at full rated power. Within the plant, the effect of this initiator is the loss of normal operation of all reactor coolant pumps. According to design, the plant responds with a reactor scram, with activation of emergency power supplies (diesel generators and batteries), and with activation of the normal shutdown heat removal mode. The normal shutdown heat removal path is through the reactor coolant system and the power cycle (sodium-CO₂) heat exchanger, with auxiliary power supplied by the emergency power supplies. As a backup, a low-capacity emergency heat removal system is provided to remove heat directly from the reactor without the need for emergency power.

In the accident sequence analyzed here, the loss of power is accompanied by a complete failure of the emergency power supply system, resulting in a total loss of power to the reactor and intermediate coolant pumps. It is also assumed that the power generation plant immediately ceases operation, and provides no heat rejection capacity. The sole heat removal path following the loss of forced coolant flow is through the emergency heat removal system by natural circulation. This sequence was analyzed for the case with an immediate reactor scram, and for the case without reactor scram. These cases are identified as the protected loss-of-flow (PLOF) and the unprotected loss-of-flow (ULOF) cases respectively. The PLOF and ULOF accident sequences both assume multiple equipment failures, failures of safety grade protection and cooling systems, and no operator actions. These sequences are an extreme test of the ABTR to provide inherent self-protection against the consequences of the most severe accident initiators.

Results Summary

The detailed analysis results for the PLOF and ULOF accident sequences are presented in Section III.7.4, below. Although both sequences simulate accidents that for some reactor designs may cause damage to the fuel and possibly progress into severe accident conditions, in the ABTR these events cause no damage. For both accident sequences, reactor fuel, cladding, and coolant temperatures remain below safety limits.

In the PLOF sequence, the loss of forced coolant flow and normal heat removal is accompanied immediately by a reactor scram, which quickly brings the reactor power to decay heat levels. Early in the sequence, the emergency decay heat removal system does not have sufficient capacity to remove all the heat being produced, so system temperatures rise. However, due to the large heat capacity of the sodium-cooled pool-type concept, the ABTR is able to absorb a significant amount of energy with only a slight temperature increase, and the natural circulation capability of the ABTR promotes heat removal through the available emergency heat sink. After about 5 hours, the reactor decay heat falls to the capacity of the emergency heat removal system, and system temperatures begin to decrease. The analysis predicts that short coolant and cladding temperature spikes occur during the transition to natural circulation, but no fuel damage or cladding failures would occur.

In the ULOF accident, the reactor safety system fails to scram the reactor upon loss of forced coolant flow and normal heat removal, so the reactor remains at full power initially. Within the first minute, reactor temperatures increase as the coolant flow rate decreases, and inherent reactivity feedbacks reduce the reactor power. During this time, peak cladding temperatures rise to approximately 600°C. As coolant flow continues to decline, a second temperature peak occurs, and peak fuel and cladding temperatures reach approximately 660°C. This increase in temperature provides the necessary driving force to establish natural circulation flow. The development of natural circulation reduces the peak fuel and cladding temperatures back to around 600°C, after which temperatures remain stable.

The primary significance of the analysis results for the PLOF and ULOF accident sequences is that no fuel damage or cladding failures would occur, even when multiple safety systems are assumed to malfunction. The neutronic, thermal, and hydraulic performance characteristics of the ABTR design provide a defensive barrier to reactor damage for accident initiators that otherwise progress into severe accident conditions. Such superior safety characteristics are inherent to a metallic-fueled, sodium-cooled, pool-type reactor concept.

III.7.2 Analysis Scope

The analysis results reported here were selected on the basis that they show the safety margins and the inherent ability of a metallic-fueled, sodium-cooled, pool-type reactor system to provide protection against severe, damaging consequences. The accident sequences analyzed here are near the end of the spectrum of the most pessimistic, challenging, and potentially damaging events. The analysis results demonstrate the passive safety performance advantages of ABTR. This performance is possible because of the favorable heat transfer and reactivity feedback characteristics of metallic fuel, and the natural circulation shutdown heat removal capability that is possible with low pressure sodium coolant in a pool configuration.

Accident Sequences

The basic accident sequence analyzed here is the loss of normal power to the reactor and intermediate coolant pumps, with failure of the emergency power supplies. The result is an immediate loss of forced flow in the primary and intermediate coolant circuits. The equipment that provides a programmed flow coast down of the electromagnetic coolant pumps is assumed to operate. In addition, it is assumed that heat removal at the sodium-CO₂ heat exchanger ceases, so that the only heat removal path is through the emergency direct reactor auxiliary cooling system (DRACS).

The natural circulation DRACS consists of heat exchangers located in the cold pool region within the reactor vessel, air dump heat exchangers located outside containment, and the connecting piping. The working fluid in the DRACS is NaK, and fluid flow is by natural circulation. Multiple independent DRACS units are provided for defense in depth. The DRACS is designed to remove 0.5% of full power (1250 kW) at normal operating temperatures assuming failure of one DRACS unit. The DRACS system operates continuously, with heat losses limited in normal operation by dampers on the NaK-to-air heat exchangers. In all the accident sequences analyzed here, one DRACS unit is assumed to fail, leaving a system heat rejection capacity of 1250 kW.

The initial condition for the accident sequence is normal operation at full power and flow. With the loss of pumping power, flow in the primary circuit coasts down according to the programmed pump head decay. The energy for this flow coast down is provided by a safety grade energy storage device. Following flow coast down, natural circulation flow is established.

With the loss of power, forced flow in the intermediate coolant system is also lost. Further, it is assumed that heat rejection through the sodium-CO₂ heat exchanger ceases. The intermediate heat transport system (IHTS) is alternately a heat sink or source in the accident sequence, depending on its temperature and the primary system temperature at

the intermediate heat exchanger (IHX). During the transient, natural circulation flow in the IHX may reverse, depending on transient temperature conditions.

Two variations of the loss-of-flow accident sequence have been analyzed. In the first, it is assumed that the reactor safety system acts as designed to insert control rods and reduce reactor power immediately to decay heat. This sequence is called the protected loss-of-flow (PLOF) accident. In the second analysis, it is assumed that the reactor safety system fails to insert the scram control rods, and the loss of forced flow proceeds at full power. This sequence is called the unprotected loss-of-flow (ULOF).

In the PLOF sequence, the absence of normal shutdown heat removal through the reactor coolant system causes a slow system temperature rise following the reactor scram. This temperature increase occurs because the DRACS has insufficient heat removal capacity to overcome both the early decay heat production rate and the stored heat in the primary and intermediate systems. Eventually, the decay heat falls below the DRACS capacity, and the system temperature declines.

In the ULOF sequence, the system temperature rises significantly with the flow coast down, but the core temperature rise introduces negative reactivity that acts to reduce the reactor fission power. The reactor, with its negative feedback characteristic, seeks equilibrium with the available heat sink by reducing power. This has the effect of reducing the reactor temperature and establishing a quasi-equilibrium condition. However, until the decay heat falls below the available heat rejection capacity, the reactor system will continue to heat slowly, with the long term temperature rise buffered by the thermal heat inertia of the system. When decay heat production falls below the DRACS capacity, the system temperature declines.

Reactor State

Safety analyses were performed for the beginning-of-equilibrium-cycle (BOEC) reactor conditions described in Section II.1. Only the BOEC results are reported here because the EOEC results are similar, even though the reactor radial power distribution changes with irradiation.

For the BOEC safety analysis, it was assumed that sufficient irradiation had taken place to swell the fuel radially into contact with the cladding. Examination of EBR-II irradiated fuel has indicated that fuel-cladding contact will occur early in fuel life, depending on the initial geometry and local specific power. Fuel-cladding contact has the impact of lowering thermal resistance by eliminating the sodium-filled fuel-cladding gap.

For the PLOF analysis, the decay heat curve was taken as 100% of the ANSI 5.1 standard for Pu-239 [1]. For the ULOF analysis, the decay heat curve was combined with the computed fission power calculated using the reactivity feedback parameters determined by the reactor physics analysis of Section II.1 for the BOEC core.

III.7.3 Analysis Methods and Input Data

The analytical methods used to evaluate the ABTR performance are incorporated into the SAS4A/SASSYS-1 computer code [2] which was used to produce all the results presented here. In the following sections, the reactor and coolant system thermal-hydraulic models are described along with key input data relevant to the determination of ABTR safety performance.

Reactor Thermal Hydraulics

The thermal-hydraulic performance of the reactor core is analyzed with a geometric model consisting of a number of single-pin channels. In a multiple-channel, whole-core model, each channel represents a single fuel pin and its associated coolant and structure. The single pin is assumed to characterize the average pin in a fuel subassembly, and subassemblies with similar reactor physics and thermal-hydraulics characteristics are grouped, so a number of channels are selected to represent all the pins in the reactor core.

The geometry assumed in the channel thermal-hydraulic model is shown in Figure III.7-1. Heat generated in the fuel is assumed to travel through the cylindrically-symmetric pin to the upward-flowing coolant. The structure field is used to represent part of the hexagonal duct and the wire wrap. One-dimensional, radial heat transfer calculations are performed at many axial locations to model heat transfer from the fuel through the cladding to the coolant, and from the coolant to the structure, the gas plenum, and the reflectors. One-dimensional (axial) coolant mass flow is modeled with a momentum equation solution for the axial pressure profile, and convective heat transfer conditions are assumed at the interfaces between the coolant and the cladding, the reflectors, and the structure. Temperatures are calculated at multiple radial nodes in the fuel, the cladding, the reflectors, and the structure. A single bulk temperature is calculated at each axial location. Axial heat conduction is neglected.

Thermal, transport, and physical properties data for the coolant were taken as the temperature-dependent liquid sodium properties available in SAS4A/SASSYS-1. Cladding properties were taken as the HT9 data presented in Reference 3. Fuel properties were taken from the SSCOMP correlations in SAS4A/SASSYS-1 Version 3.0; these correlations are based on data generated in the Integral Fast Reactor (IFR) Program.

On the basis of the reactor physics calculations reported in Section II.1, the multiple-channel model depicted in Figure III.7-2 was selected for safety analysis calculations. This model approximates the full heterogeneity of the reactor physics model by assigning channels to represent each fuel enrichment zone. Channels 1 and 3 represent the average subassemblies in the inner and outer enrichment zones respectively, while channel 2 represents the average of the mid-core fuel test assemblies. A fourth channel represents all of the non-fuel subassemblies, including the mid-core materials test assemblies. A fifth channel is used to represent the peak-power inner-core subassembly with fresh fuel.

Table III.7-1 presents geometric input data employed in the multiple-channel whole-core model. In this data, it has been assumed that the irradiated fuel has swollen into contact with the cladding.

Figure III.7-3 shows the initial subassembly powers for the beginning of equilibrium cycle (BOEC) condition as described in Section II.1. The subassembly power for the peak assembly assumes fresh fuel in the peak power location. All other subassembly powers represent channel averages from BOEC fuel compositions at various stages of depletion. The initial subassembly flow rates shown in Figure III.7-4 were determined such that the mixed-mean coolant outlet temperature was 510°C for each region (inner core, outer core, fuel test, and reflectors). Flow for the peak subassembly was set so that the outlet temperature would be 510°C midway through depletion, with the remaining flow for the inner core allocated to channel 1. With fresh fuel in the peak subassembly location, the outlet temperature for the peak subassembly is higher than nominal. Initial coolant outlet temperatures at BOEC are shown in Figure III.7-5.

Based on the above input conditions, SAS4A/SASSYS-1 calculates the initial, steady-state thermal-hydraulic conditions in the reactor core prior to the onset of a transient. Peak coolant outlet, peak cladding, and peak fuel temperatures are shown in Figure III.7-5, III.7-6, and III.7-7, respectively. Coolant, cladding, and fuel temperatures that arise during a transient are discussed in the relevant sections below.

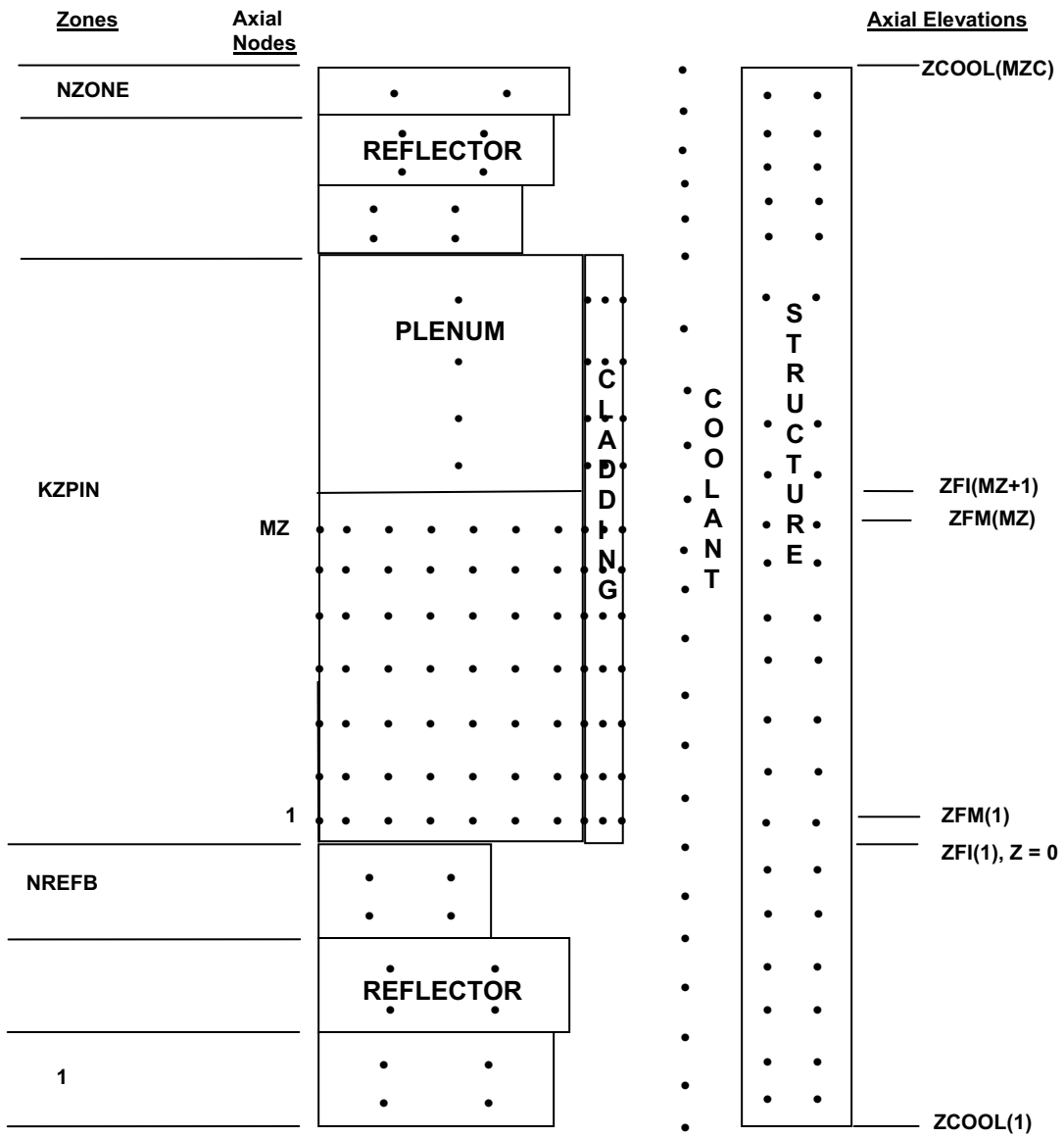


Figure III.7-1 Single-Pin Channel Model

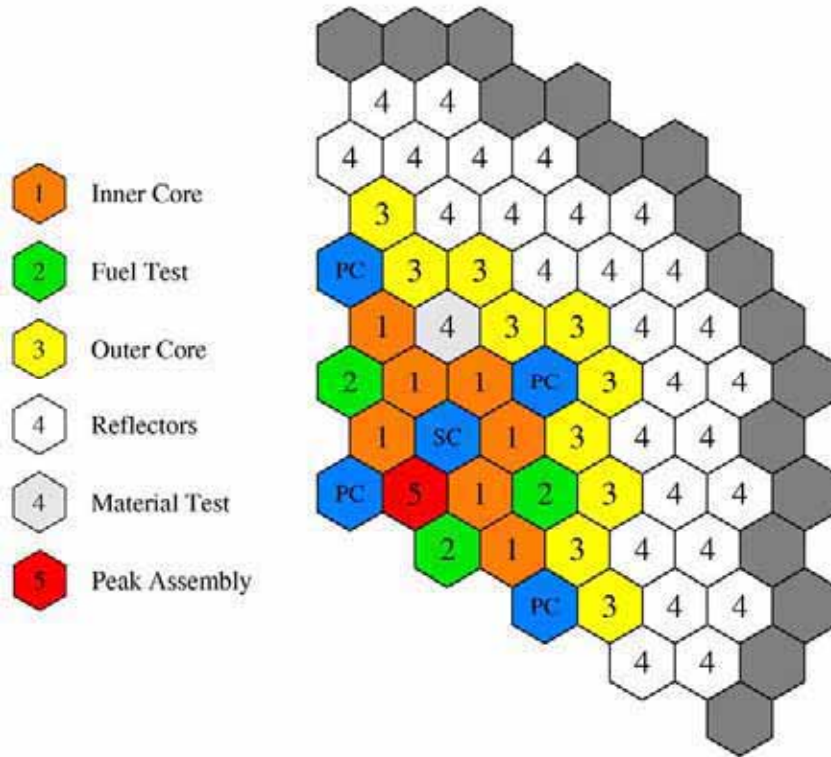


Figure III.7-2 Channel Assignment for Reactor Core Thermal-Hydraulic Model

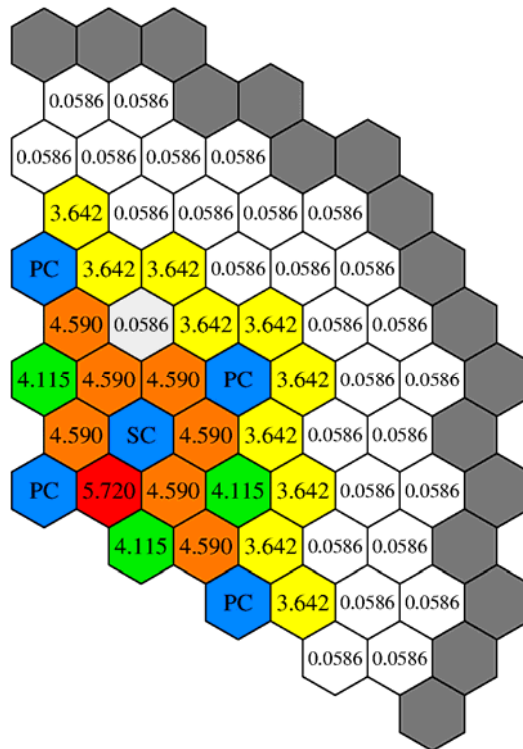


Figure III.7-3 BOEC Initial Subassembly Power (MW)

Table III.7-1 Fuel Assembly, Pin, and Coolant Channel Model Data

Pins per Assembly	217
Number of Fuel Assemblies	60
Channel 1 (Inner Core)	23
Channel 2 (Fuel Test)	6
Channel 3 (Outer Core)	30
Channel 5 (Peak Inner Core)	1
Fuel Height (mm)	800
Gas Plenum Height (mm)	1200
Upper Reflector Height (mm)	300
Lower Reflector Height (mm)	600
Axial Node Height (mm)	
Core	40
Gas Plenum	200
Upper Reflector	60
Lower Reflector	120
Hydraulic Diameter (mm)	2.972
Coolant Flow Area per Pin (mm ²)	22.69
Outer Fuel Radius (mm)	3.48
Inner Cladding Radius (mm)	3.48
Outer Cladding Radius (mm)	4.00
Structure Thickness ^a (mm)	3.45
Structure Perimeter ^b (mm)	2.46
Reflector Thickness (mm)	2.00
Reflector Perimeter (mm)	25.1

a. Structure thickness includes weighted contribution from the inter-assembly gap.

b. Structure perimeter includes contribution from wire wrap spacers.

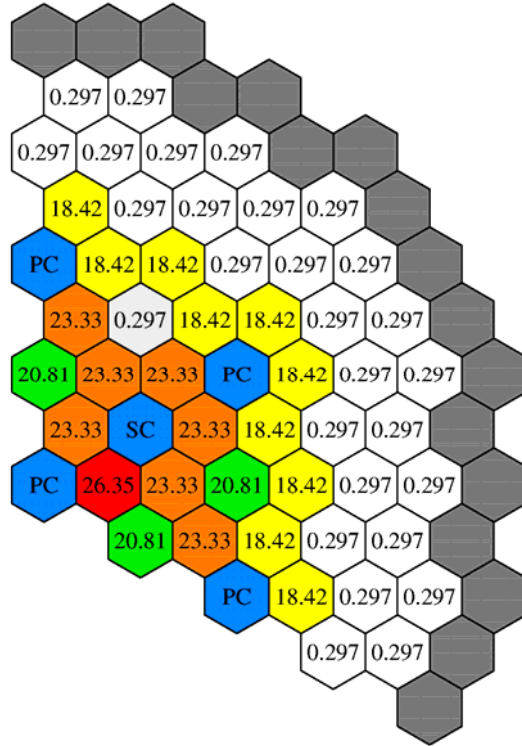


Figure III.7-4 Initial Subassembly Coolant Flow (kg/s)

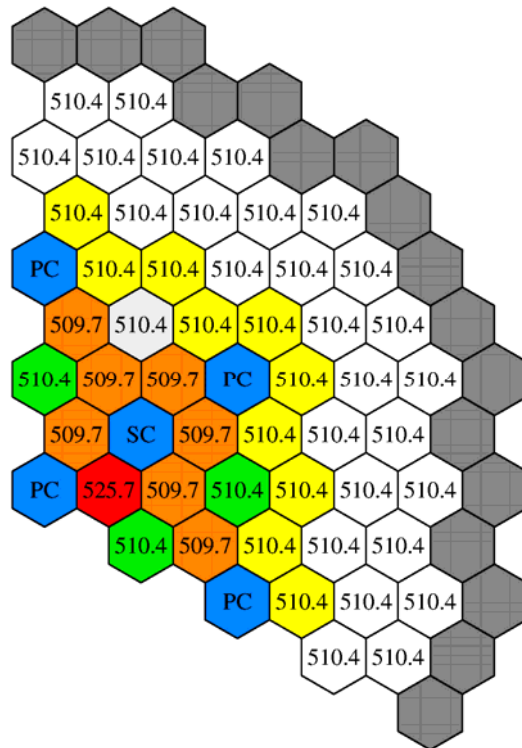


Figure III.7-5 BOEC Initial Coolant Outlet Temperature (°C)

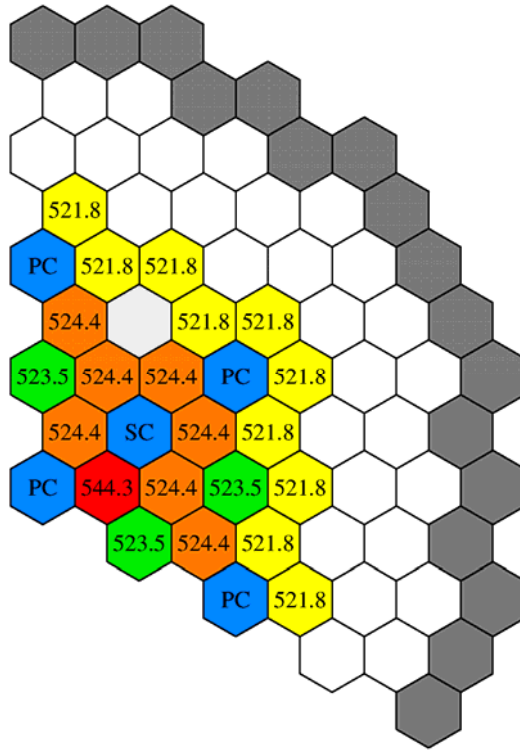


Figure III.7-6 BOEC Initial Peak Cladding Temperature (°C)

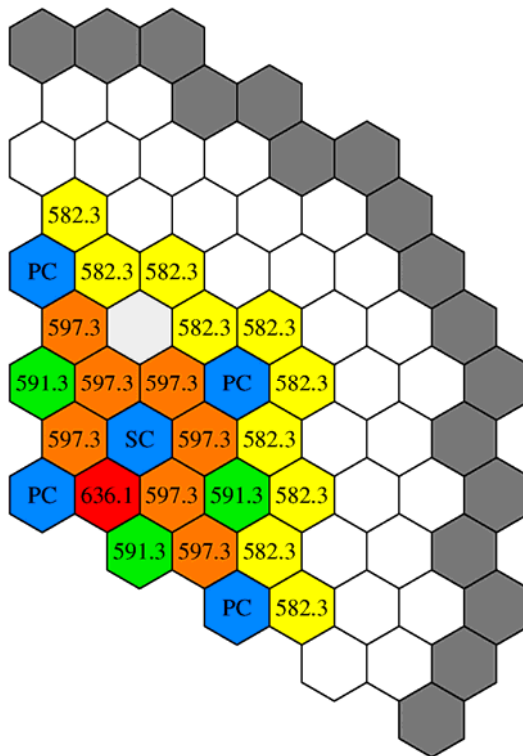


Figure III.7-7 BOL Initial Peak Fuel Temperature (°C)

Coolant Systems Thermal Hydraulics

The coolant systems thermal hydraulics model represents coolant flow and heat transfer in the primary and intermediate sodium systems, and in the emergency decay heat removal system, with a network of volumes and components connected by flow paths. The coolant systems model is shown in Figure III.7-8. From the inlet plenum, cold coolant flows through the core and is heated, then exits to the outlet plenum and travels to the shell side of the intermediate heat exchangers (IHXs), where it gives up its heat. Cold primary coolant exits the IHXs and flows to the cold pool. The primary coolant pumps take suction from the cold pool and deliver the coolant back to the inlet plenum. Emergency decay heat removal is provided by the direct reactor auxiliary cooling system (DRACS), a natural circulation system that removes heat by means of a heat exchanger in the upper region of the primary circuit cold leg and rejects heat through an air dump heat exchanger outside the containment. The working fluid in the DRACS system is NaK.

In the primary coolant circuit, volumes 1 and 2 represent the inlet and outlet plenums, and volumes 3 and 4 stand for regions of the primary circuit cold leg; the coolant in volume 4 is essentially stagnant. Volumes 5 and 6 simulate the gas expansion volumes in the intermediate loop and decay heat removal system, respectively. Design parameters assumed for the volumes in the model are shown in Table III.7-2. All of the volumes in the model are perfectly mixed (i.e. characterized by a single temperature) except for the upper region of the cold pool, which is treated by a stratification model for low flow conditions.

Volumes in the model are connected by one-dimensional flow segments, which are further subdivided into temperature elements for heat transfer calculations. Table III.7-3 shows the parameters assumed for the liquid segments. Flow segment 1 stands for the core channels, and flow segment 2 represents the shell side of the IHX. The ABTR has two IHXs, but only a single IHX is modeled, and it is assumed in this work that both primary circuits behave identically. Segment 4 represents the four primary coolant pumps and the discharge pipes connected to the inlet plenum. Segment 5 represents the primary coolant flow path through the decay heat removal heat exchanger, and segment 6 connects the upper region of the cold pool with the near stagnant lower region. Segment 7 represents the intermediate heat transfer loop, and includes the loop piping, the intermediate heat exchanger, and the intermediate coolant pump. Segment 8 represents natural circulation flow in the DRACS loop. In normal operation, heat addition takes place in segment 1, and heat is rejected in segments 3 and 5. Segment 2 is thermally connected through the IHX to the intermediate loop, and segment 5 is thermally connected to the DRACS loop through the DRACS heat exchanger.

In the model, liquid flow segments are divided into a number of elements for the purpose of heat transfer and pressure drop calculations. The liquid elements in the coolant systems model are described in Table III.7-4.

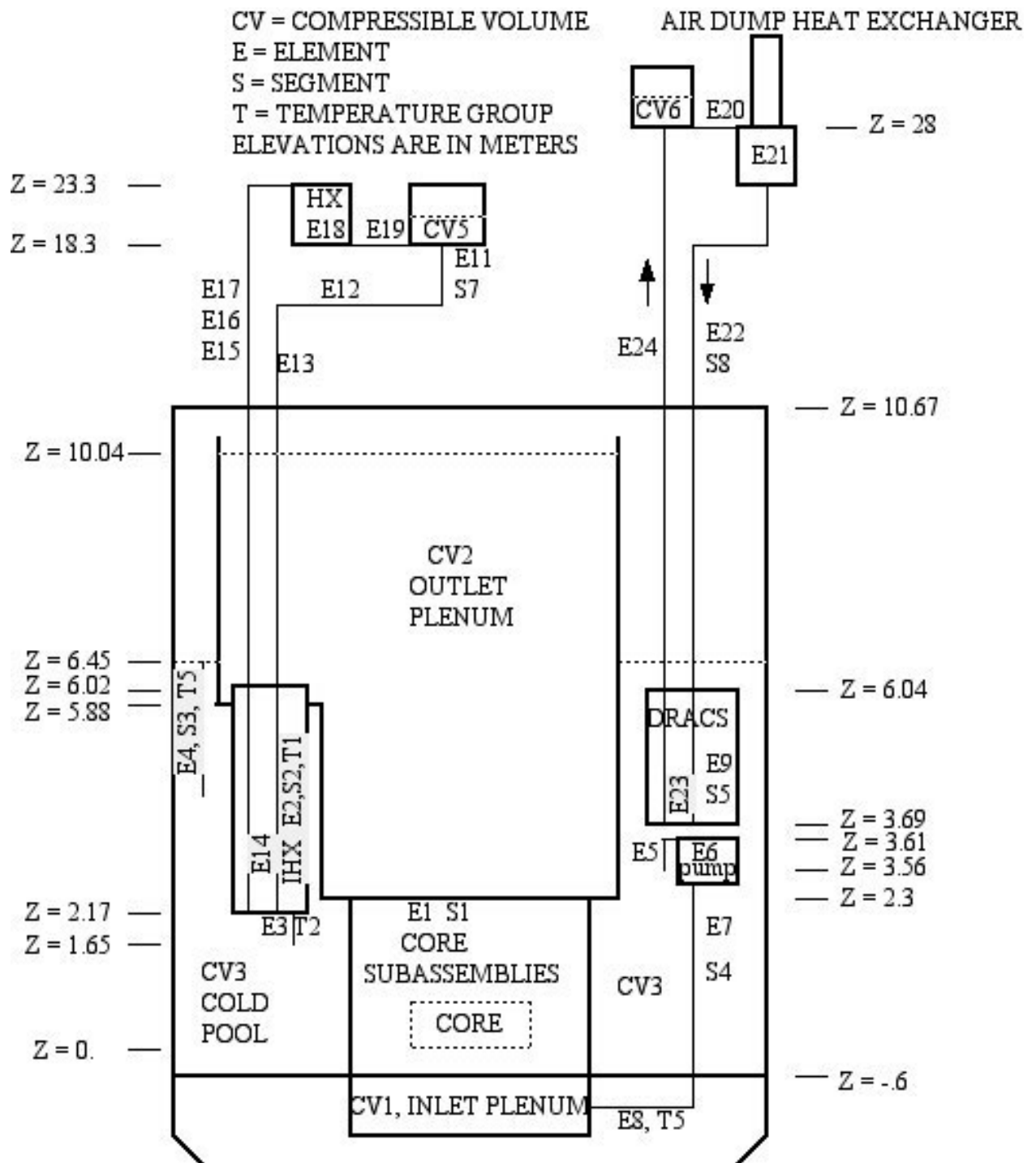


Figure III.7-8 Coolant Systems Thermal Hydraulics Model

Table III.7-2 Compressible Volumes Input Data

Volume Number	1	2	3	4	5	6
Volume Description	Inlet Plenum	Outlet Plenum	Upper Cold Pool Region	Lower Cold Pool Region	Intermed. Loop Junction	DRACS Loop Junction
Total Volume (m ³)	3.06	92.51	152.97	28.14	6.0	4.0
Initial Gas Volume (m ³)	-	6.17	60.6	-	1.0	0.6
Ref. Liquid Elevation (m)	-0.75	3.0	7.0	0.0	18.3	27.0
Liq/Gas Interface Area (m ²)	-	11.16	12.8	-	1.0	0.8
Wall Surface Area (m ²)	10.5	16.5	80.0	44.0	13.0	10.0
Wall Heat Capacity (MJ/K)	63.5	0.66	26.87	14.14	1.075	0.707

Table III.7-3 Liquid Segments Input Data

Segment Number	Description	Compressible Volume In/Out	Inlet Elevation (m)	Liquid Element In/Out	Initial Flow (kg/s)
1	Reactor Sub-Assemblies	1/2	-0.60	1/1	1264.4
2	IHX Shell Side	2/3	6.02	2/3	632.2
3	Intra-Volume Heat Transfer	3/3	4.0	4/4	0.0
4	Primary Pump	3/1	3.56	5/8	316.1
5	DHRX to Cold Pool	3/3	6.035	9/9	0.0
6	Cold Pool Transition	3/4	-0.85	10/10	0.0
7	Intermediate Loop	5/5	18.2	11/19	634.0
8	DRACS Loop	6/6	28.0	20/24	0.0

Table III.7-4 Liquid Elements Input Data

Element Number	Description	Outlet Elevation (m)	Length (m)	Flow Area (m ²)	Hydraulic Diameter (m)
1	Reactor	*	*	*	*
2	IHX Shell	2.17	3.85	0.766	0.0186
3	IHX Outlet	1.65	0.42	0.3	0.34
4	Cold Pool HT	6.4	2.4	0.44	0.16
5	Pump Inlet	3.61	0.05	0.13	0.41
6	Primary Pump	3.61	0.05	0.055	0.113
7	Pump Outlet	-0.77	4.38	0.132	0.34
8	Pump Discharge	-0.77	1.26	5.36	1.0
9	DRACS HX	3.69	2.35	0.024	0.037
10	CP Transition	-.87	0.02	0.092	0.34
11	IHTS Pipe	13.0	6.4	0.092	0.34
12	IHTS Pipe	13.0	4.3	0.092	0.34
13	IHTS Pipe	2.17	10.8	0.092	0.34
14	IHX Tube	6.02	3.85	0.517	0.014
15	IHTS Pipe	12.4	6.36	0.092	0.34
16	IHTS Pipe	12.4	5.2	0.092	0.34
17	IHTS Pipe	23.3	6.0	0.092	0.34
18	Na/CO ₂ HX	18.3	4.0	3.6	0.0075
19	IHTS Pump	18.3	1.0	0.092	0.34
20	DRACS Pipe	28.0	1.0	0.016	0.14
21	Air Dump HX	27.0	5.7	0.17	0.05
22	DRACS Pipe	3.7	23.3	0.016	0.14
23	Na/NaK HX	6.04	2.35	0.010	0.037
24	DRACS Pipe	26.9	20.9	0.016	0.14

* See core channel model in Table III.7-1.

Flows in the primary and intermediate circuits are driven by both forced circulation at the pumps and by buoyancy due to heat exchange, so transient natural circulation flows adjust to changing heat generation and transfer conditions. The natural circulation flow in the DRACS loop can change due to temperature changes in the DRACS heat exchanger and the air dump heat exchanger, and heat transfer at the air dump heat exchanger can be enhanced by opening air flow dampers (normally closed).

Reactor Kinetics and Reactivity Feedback

A point kinetics model is employed to calculate the response of reactor fission power to transient reactivity feedback in unscrammed sequences. At any time, the net reactivity

is the sum of a number of individual reactivity feedbacks that are determined by the transient thermal, hydraulic, mechanical, and neutronic state of the reactor. The feedback reactivities considered are fuel Doppler, coolant density, fuel and cladding axial expansion, radial core expansion, and control rod driveline thermal expansion. In addition to tracking fission power, a decay heat model is integrated with the point kinetics model to track shutdown events in sub-critical conditions.

Fuel Doppler feedback is calculated from the spatially-dependent fuel temperature distribution and the input spatial distribution of the fuel Doppler reactivity coefficient. In each single-pin channel, the axial distribution of the radial pin-average fuel temperature is used to calculate the reactivity feedback.

Coolant density reactivity feedback is calculated from the spatially dependent coolant density distribution and the input distribution of the coolant density reactivity coefficient calculated from perturbation theory. The reactivity feedback data is entered as a coolant void worth (the negative of the coolant mass worth).

Transient fuel and cladding temperatures are used to predict fuel and cladding axial dimension changes, and in each single-pin channel the reactivity feedbacks associated with fuel and cladding axial expansion are computed from first order perturbation theory.

A simple radial core expansion model accounts for core dilation due to thermal expansion of the hexcan load pads and thermal expansion of the core support grid plate. Reactivity feedback is then calculated from the computed core dimension change and an input linear reactivity coefficient based on stand-alone neutronics eigenvalue calculations.

For the control-rod driveline feedback model, it is assumed that the control rod drivelines are washed by the outlet coolant from the core. Thermal expansion of the drives due to a rise in core outlet temperature will cause the control rods to be inserted further into the core, providing a negative reactivity component. On the other hand, if the control rod drives are supported on the vessel head, and if the core is supported by the vessel walls, then heating the vessel walls will lower the core, leading to a positive reactivity component. In the present model, both control-rod driveline expansion and vessel wall expansion are treated.

III.7.4 Analysis Results

Analyses of the protected loss-of-flow (PLOF) and unprotected loss-of-flow (ULOF) accident sequences were performed with coupled heat transfer, thermal-hydraulics, and reactor kinetics models available in the SAS4A/SASSYS-1 code. These models have

been validated through many applications to EBR-II and FFTF transient tests. Additionally, temperature criteria for assessments of cladding damage thresholds have been established by results from testing of metallic fuel in EBR-II and TREAT. Consequently, there is high confidence that the detailed results from the PLOF and ULOF accident analyses presented here give a true characterization of the physical performance that could be obtained in the ABTR design.

Protected Loss-of-Flow (PLOF) Accident Sequence

Results from analysis of the PLOF accident sequence are shown in Figure III.7-9, -10, -11 and -12. Figure III.7-9 and -10 show the history of the reactor power, the decay heat power, the DRACS heat removal rate and the coolant flows through the highest temperature subassembly (Channel 5) and an average temperature subassembly (Channel 3). Recall that this transient is initiated by a complete loss of forced coolant flow in the primary and intermediate loops, save the pump coast-downs. Both the primary pumps and the intermediate pumps have enough inertia to give initial flow halving times of 7 seconds. The primary pump rotors completely stop turning at about 450 seconds after the start of the transient, leading to a transition to natural circulation. The transition to natural circulation goes more smoothly in the hotter Channel 5 than in the cooler Channel 3. Almost immediately at initiation, the reactor control system scrams the reactor, beginning the power reduction to decay heat shown in Figure III.7-9, and the dampers on the DRACS air dump heat exchangers open, permitting the DRACS to operate at its full capacity of 0.5%. As the cold pool temperature rises, DRACS heat removal capacity increases, eventually reaching the equivalent of 0.7% of normal reactor power. Not indicated in this figure is the loss of heat removal to the balance-of-plant, which is assumed to occur after the first 10 seconds. Figure III.7-9 shows that the reactor decay heat power equals the DRACS heat removal capacity at about 5 hours into the transient.

Figure III.7-11 shows the early reactor temperature histories during the coolant flow coast down and transition to natural circulation. During this and the following time, the only heat removal is through the DRACS. The rapid reactor power decrease due to the scram initially lowers the coolant and cladding temperatures in the core. Then the drop in core flow as the pumps coast down leads to a rise in core coolant and cladding temperatures. As mentioned above the transition to natural circulation is smoother in Channel 5 than in Channel 3. In channel 3 as the primary pumps stop turning the coolant flow rate temporarily drops to very low values, leading to higher peak coolant and cladding temperatures. This short-term cladding temperature rise may result in some fuel-cladding chemical interaction, but no cladding failure would occur.

Note that the “Cold Pool” temperature shown in Figure III.7-10 and -11 is the average temperature of the axial distribution computed with the volume stratification model. The pump inlet is in the lower part of the cold pool, and at this location the coolant temperature is lower than the average for the cold pool.

As the system temperature rises, as shown in Figure III.7-11 and -12, the DRACS heat removal capability increases due to an increase in NaK flow and heat rejection at the air dump heat exchangers. The decay heat production declines throughout the transient, until it becomes equal to the DRACS heat removal at 5 hours. The hot pool and cold pool temperatures reach long-term peak values at about this time, and then uniformly decrease as the whole system cools.

The significance of the PLOF analysis results is emphasized in Figure III.7-11 which shows the initial peak cladding temperature (522°C) in channel 3, compared to the short-term transient peak cladding temperature of 750°C and the long-term peak cladding temperature just above 500°C at around 4 hours. In the PLOF transient, no cladding failures would occur, and the long-term peak temperatures in the accident are lower than the normal operating temperatures. Stated in another way, the long-term temperature safety margins in the accident are greater than the margins at the normal operating conditions. This very significant result is obtained as a result of the natural circulation capabilities of the reactor coolant system and the DRACS.

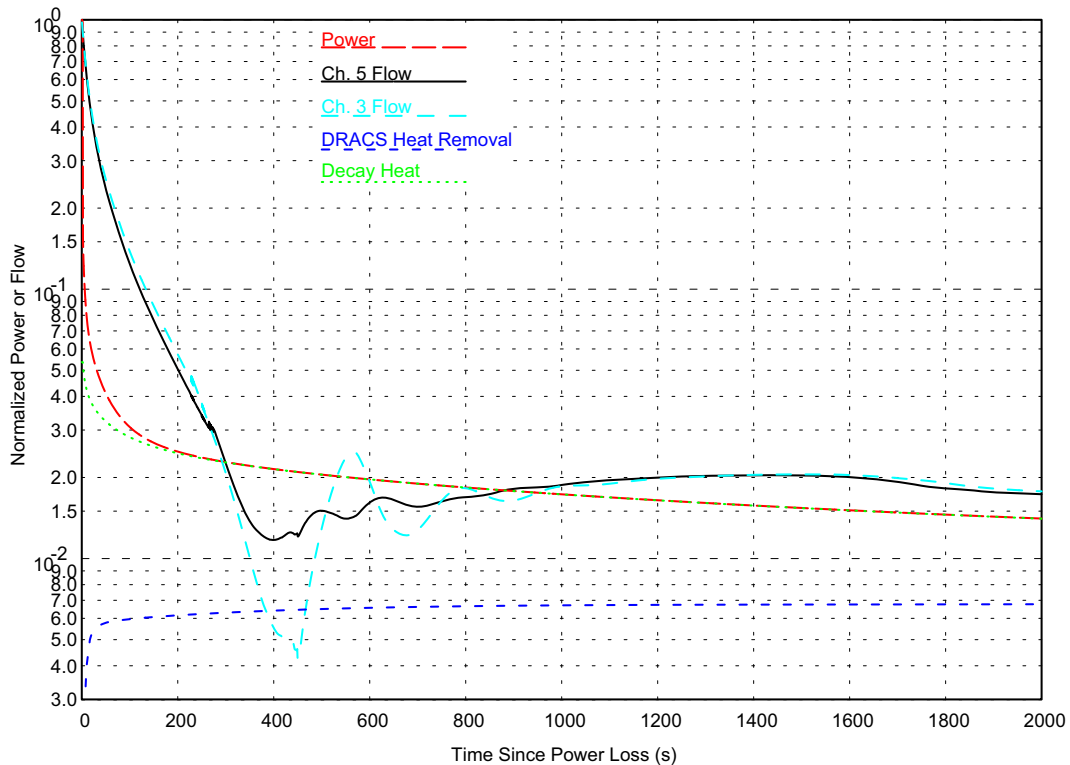


Figure III.7-9 PLOF Power and Flow History, Early Times

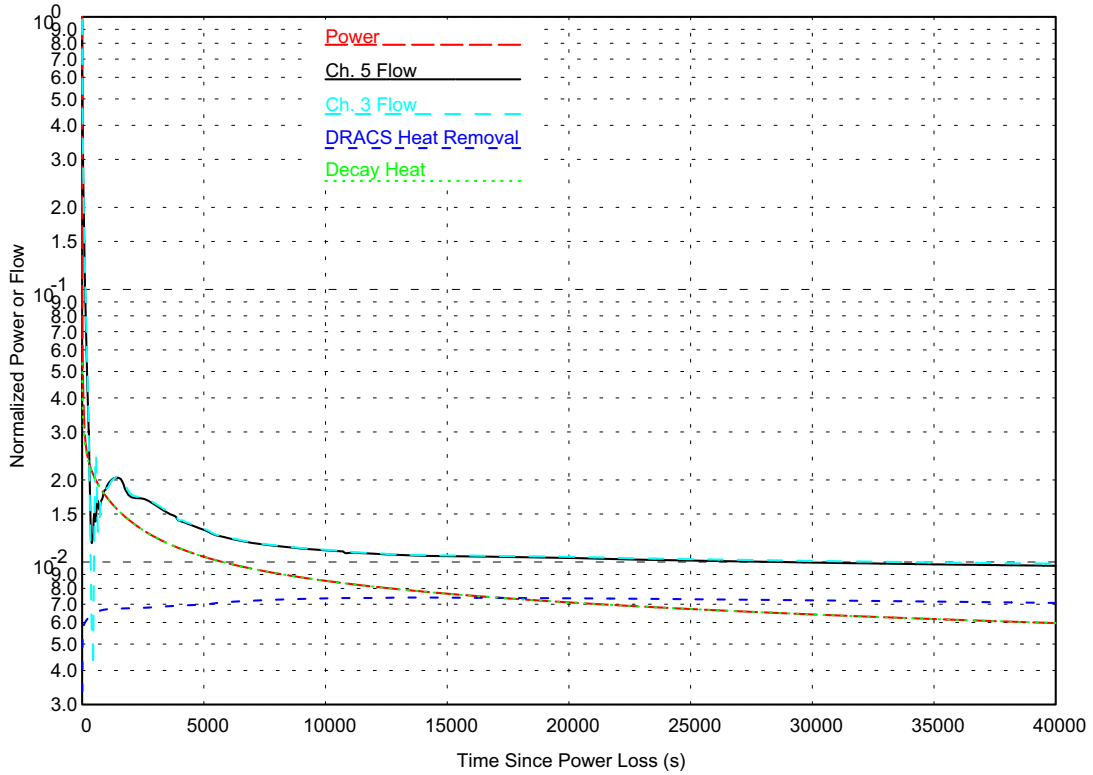


Figure III.7-10 PLOF Power and Flow History, Extended Times

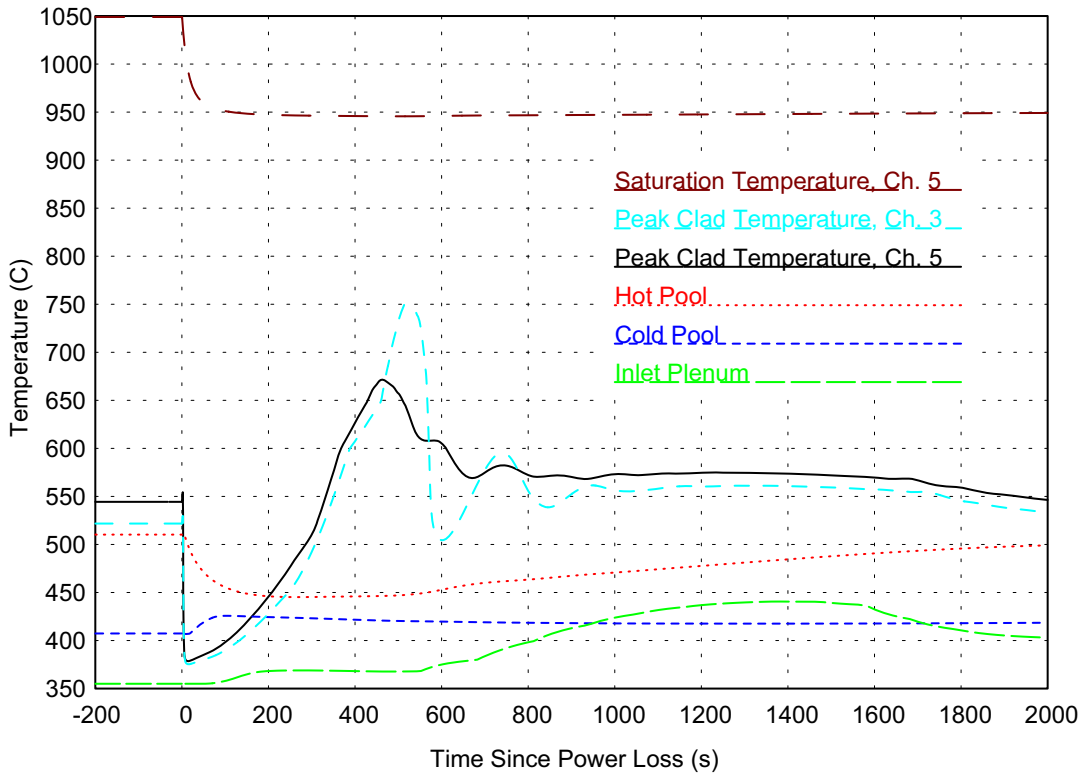


Figure III.7-11 PLOF Temperature History, Early Times

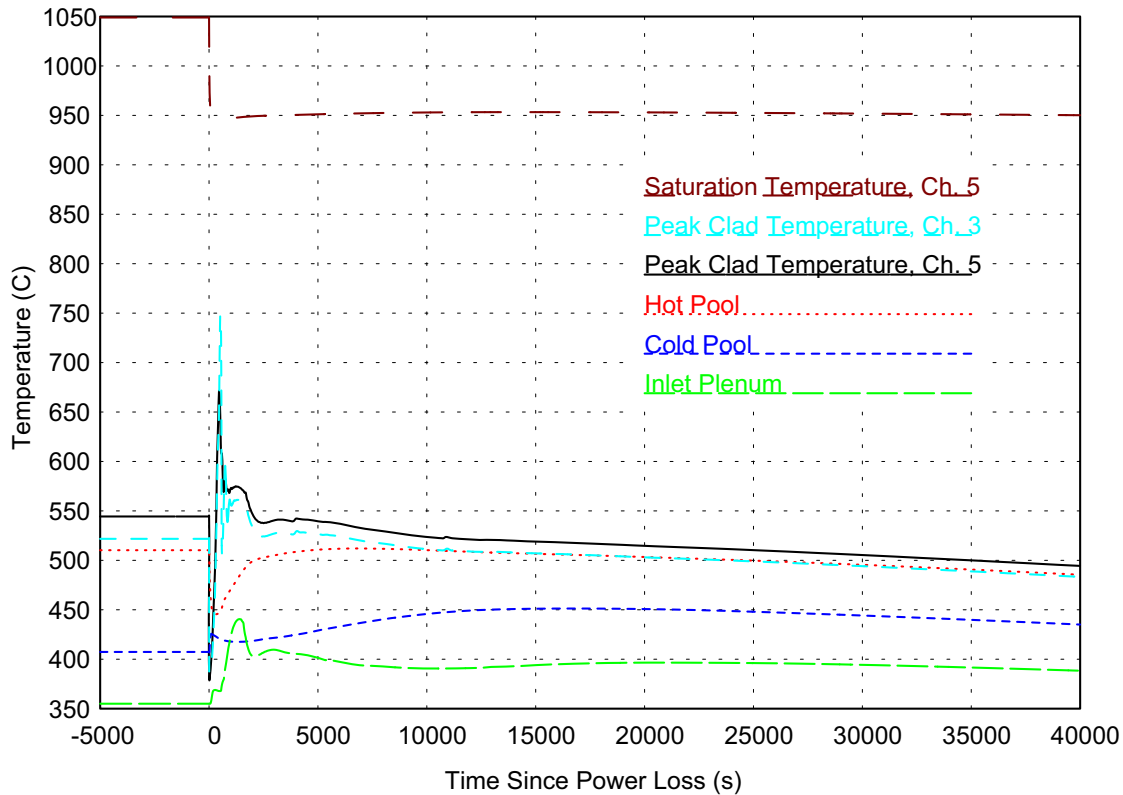


Figure III.7-12 PLOF Temperature History, Extended Times

Unprotected Loss-of-Flow (ULOF) Accident Sequence

The ULOF transient is initiated by the same set of failures as for the PLOF accident (loss of forced flow and loss of normal heat rejection). However, for the ULOF case, the reactor control system also fails to scram the reactor; so the accident proceeds from full power. All heat rejection is through the DRACS, with a design heat rejection of 0.5% of full power at nominal conditions. Results from the analysis of the ULOF accident sequence are shown in Figure III.7-13 through Figure III.7-15.

Figure III.7-13 shows the histories for the total reactor power, the decay heat production, and the coolant flow in channel 5 (the peak inner core assembly). The power-to-flow imbalance during the first 800 seconds results in significant transient reactor heating. Peak fuel, peak clad, and coolant outlet temperatures for channel 5 are shown in Figure III.7-14. Coolant and cladding temperatures increase to approximately 600°C within the first 30 seconds. This heating causes the reactivity feedbacks shown in Figure III.7-15. Axial and Radial expansion are the main contributors to the initial negative reactivity feedback, which causes power and fuel temperatures to decline. Reduced fuel temperatures provide a positive Doppler feedback, although the magnitude is modest due to the high thermal conductivity and relatively low operating temperatures of metallic fuel. Shortly after the onset of the transient, higher-temperature coolant begins

washing over and heating the control-rod drivelines. As the drivelines expand, an additional negative reactivity component is introduced, as shown in Figure III.7-15.

The flow coast-down provided by the inertia of the primary pumps ends at approximately 450 seconds. At this point, natural circulation has not yet been fully established, and fuel, cladding, and local coolant temperatures begin to rise to form a second temperature peak at approximately 480 seconds. The increased temperatures provide the necessary driving force to establish natural circulation flow and the coolant flow rate in channel 5 begins to increase. While the second temperature peak also causes considerable thermal expansion and negative reactivity feedback, fission power has already been significantly reduced, and residual heating is dominated by decay heat. Therefore, the dramatic changes in reactivity feedback (particularly radial expansion) have negligible impact on subsequent transient development.

As natural circulation is being established, the peak in the coolant temperature moves up through the core and to the subassembly outlet. While the delay in observing the temperature peak at the outlet is partly due to the low flow conditions, a bigger contributor to the delay is the large thermal inertia of the structural materials above the core, which must all be heated before the temperature peak reaches the outlet. Nevertheless, the development of natural circulation reduces peak fuel and cladding temperatures back to around 600°C. Beyond 800 seconds, the normalized power-to-flow falls below unity, and the temperature difference from inlet to outlet falls below that of normal operating conditions. In the long term, once the decay heat falls below the heat rejection capability of the DRACS, overall system temperatures will begin to decline.

The significance of the ULOF accident analysis results is captured in Figure III.7-14. As shown for channel 5, the peak fuel, cladding, and coolant temperatures remain well below the coolant saturation (boiling) temperature, with a minimum margin to coolant boiling of nearly 300°C. The analysis suggests that the core would survive an unprotected loss-of-flow accident without pin failures or fuel damage. This very favorable result comes about because of 1) the high thermal conductivity and relatively low operating temperature of metallic fuel, 2) the capability of a sodium-cooled reactor in a pool-type primary system to remove decay heat in natural circulation, and 3) the beneficial negative reactivity feedback coefficients and reactor physics performance of metallic fuel.

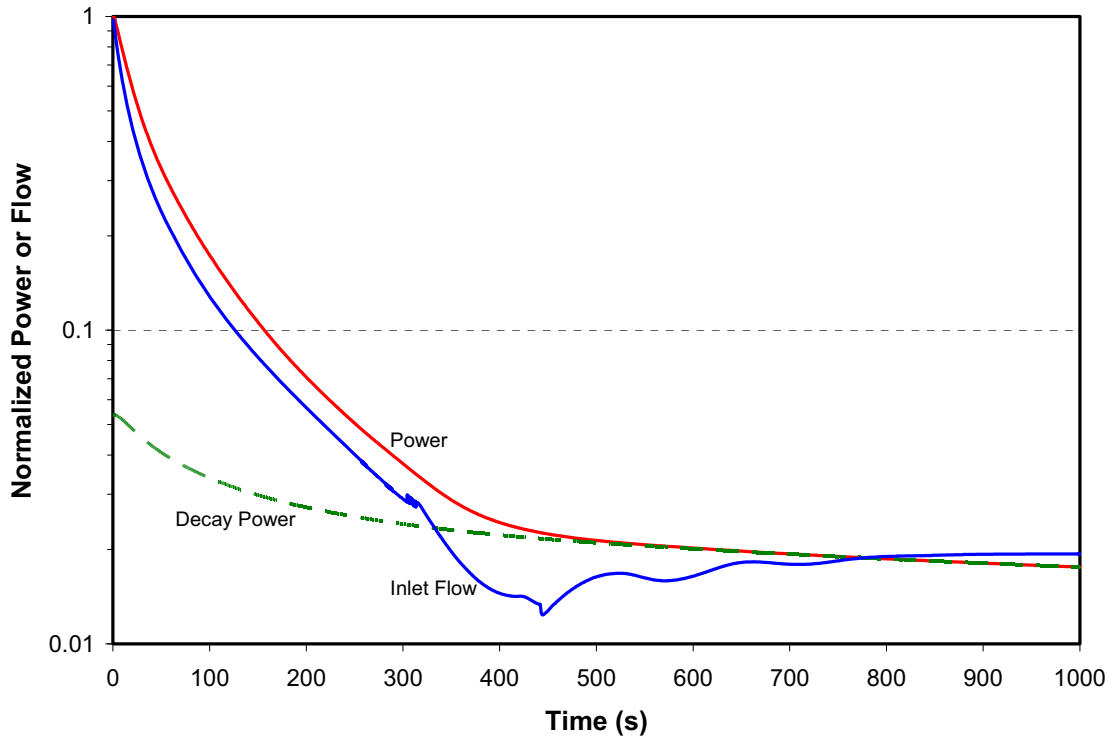


Figure III.7-13 ULOF Transient Total Power and Channel 5 Flow

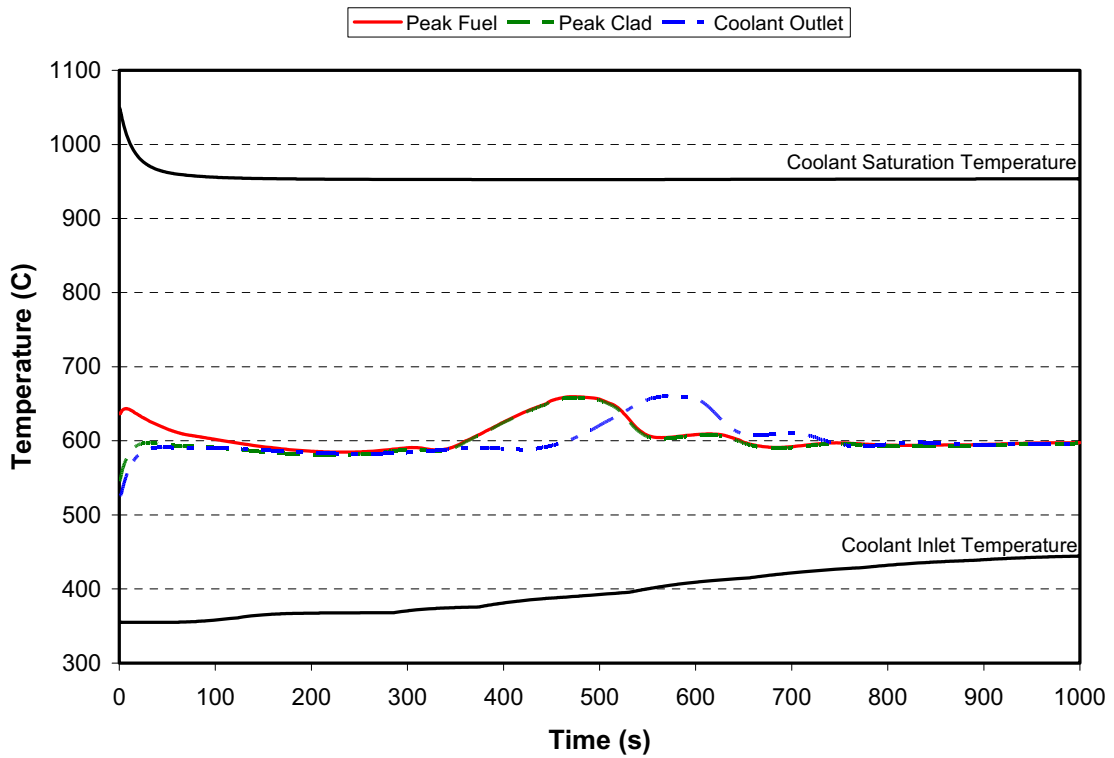


Figure III.7-14 ULOF Transient Temperatures for Channel 5

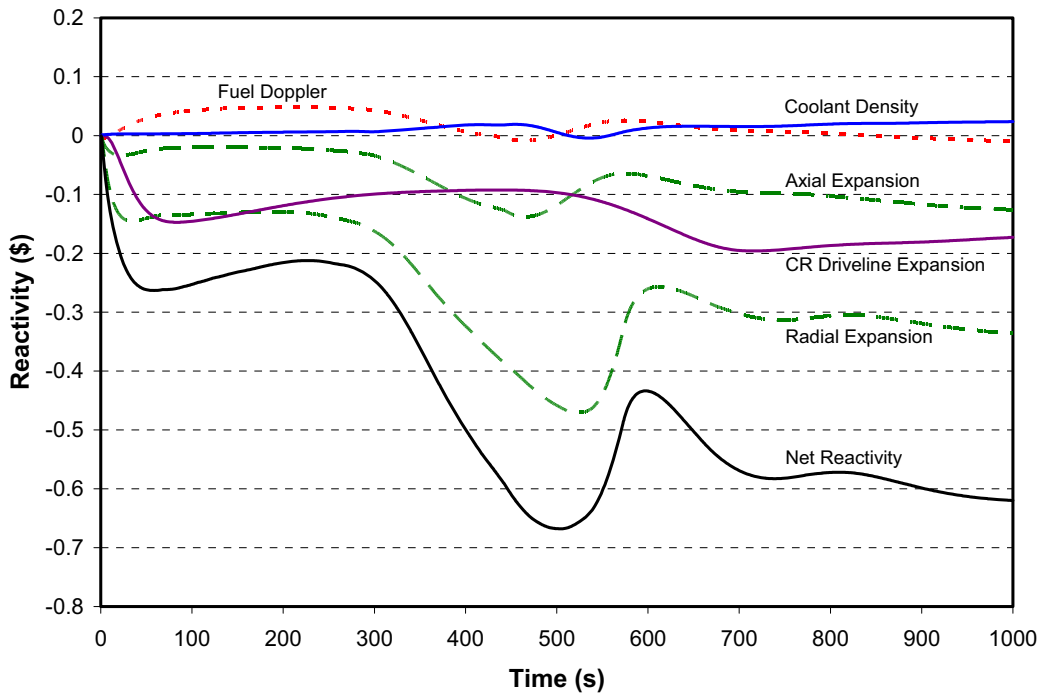


Figure III.7-15 ULOF Transient Reactivity Feedback

References

1. *American National Standard Decay Heat Power in Light Water Reactors*, ANSI/ANS-5.1-2005, American Nuclear Society, 2005.
2. J. E. Cahalan, A. M. Tentner, and E. E. Morris, "Advanced LMR Safety Analysis Capabilities in the SASSYS-1 and SAS4A Computer Codes," Proceedings of the International Topical Meeting on Advanced Reactors Safety, American Nuclear Society, Vol. 2, pp. 1038-1045, Pittsburgh, PA, April 17-21, 1994.
3. L. Leibowitz and R. A. Blomquist, "Thermal Conductivity and Thermal Expansion of Stainless Steels D9 and HT9," *International Journal of Thermophysics*, Vol. 9, No. 5, pp. 873-883, September, 1988.

III.8 System Response during LOF/LOHS Events

As noted in Section II.6, given the overall DRACS design, engineering calculations were performed to verify that the shutdown heat removal system is capable of maintaining system temperatures at acceptably low levels during a protected loss of flow/loss of heat sink (LOF/LOHS) event. This engineering analysis provided the basis to proceed with the detailed SASSYS safety-basis analyses described in Section III.7. The engineering model treats four coupled natural convection flow circuits. As shown previously in Figure II.6-1, the first flow circuit is within the reactor vessel. In this region, the natural convection flow path is from the core, through the redan, and then into the cold pool through the IHX flow paths. The sodium then flows from the cold pool through the EM pumps and back to the core inlet to complete the flow circuit. Assuming quasi-steady flow behavior, then Bernoulli's equation for the flow circuit can be written as:

$$\rho_p g \beta_p (T_c - T_{cp}) E_c - \frac{1}{2} \sum_p \left[(K_{loss} + fL/D)/A^2 \right] \frac{m_p^2}{\rho_p} = 0$$

where m denotes mass flow rate, g is the gravitational constant, β is the linear expansion coefficient, E denotes elevation difference, T denotes temperature, f denotes friction factor, K_{loss} denotes form loss coefficient, L is flow length, A is flow area, and subscripts c , hp , and cp denote the core, hot plenum and cold plenum regions within the reactor vessel, respectively. Similar equations apply to the three other flow circuits described below.

In addition to the overall natural convection flow pattern through the core, a second natural convection flow circuit will also develop in the cold pool around the DRACS, since these units are essentially isolated 'cold fingers' residing in the cold pool. The cold pool sodium enters each DRACS through window-type openings in the outer shroud just below the upper tube sheet. The sodium then flows down the shell side while depositing heat and returns to the cold pool at a reduced temperature through a second opening just above the lower tube sheet. For this particular case, the thermal centers separation distance is approximately equal to the DRACS tube length (~ 2.5 m).

Aside from the two flow fields inside the reactor vessel, a third natural convection flow field also develops in the piping system from the tube side of the DRACS to the tube side of the NDHX. Finally, the fourth natural convection flow field is through the NDHX which serves as the final heat sink for the system. For all the system flow paths, flow resistance to natural convection is modeled assuming one-dimensional flow behavior in which flow form and frictional losses are calculated using standard (i.e., $\Sigma K + fL/D$) engineering methods.

In addition to solving for flow rates throughout the system, the thermal response within the reactor vessel is determined by solving time-dependent equations for the core, redan, and cold plenum regions, respectively, using a lumped capacitance method in which each region is characterized by a mass and an effective specific heat. In particular, the temperatures of these regions are calculated from the following three coupled ordinary differential equations:

$$m_c^c c_c \frac{dT_c}{dt} = \dot{Q}_{dec} - \dot{m}_p c_p (T_{cp} - T_c)$$

$$m_{hp}^c c_{hp} \frac{dT_{hp}}{dt} = \dot{m}_p c_p (T_c - T_{hp})$$

$$m_{cp}^c c_{cp} \frac{dT_{cp}}{dt} = \dot{m}_p c_p (T_{hp} - T_{cp}) + \dot{m}_{dr} c_p (T_{dr}^{exit} - T_{cp})$$

where m denotes mass, \dot{Q}_{dec} is the core decay heat level, and T_{dr}^{exit} is the DRACS shell side sodium temperature at the HX exit. The core decay heat level is evaluated using the ANS standard decay heat curve assuming a uranium core. Heat transfer within the heat exchangers is evaluated using fairly detailed models that calculate the heat removal rates based on the current mass flowrates on the shell and tube sides of each unit. The heat transfer coefficients used on the shell and tube sides of the DRACS in the transient analysis are identical to those used in the IHX design calculations.

A summary of the model input data that has been assembled for this preliminary analysis is provided in Table III.8-1. Approximate masses for the redan and cold plenums were developed based on the overall system design provided in Section II.6 assuming sodium properties in these regions. Lumped capacitance property estimates for the core (density, specific heat) were developed based on the core configuration data provided in Section II.1.1. The initial core-average temperature was set at 520 °C, while the initial temperatures of the hot and cold plenum were set equal to the nominal core full power inlet and outlet operating temperatures of 510 °C and 355 °C, respectively.

The required data to calculate the flow pressure drop in the three regions inside the reactor vessel are also provided in Table III.8-1. For the purposes of this analysis, a total of four EM primary reactor coolant pumps are assumed. The DRACS and NDHX design parameters are taken from Tables II.6-1 and II.6-2, respectively. The diameter of the secondary piping is assumed to be 7.5 cm. The engineering data required to evaluate flow losses (i.e., pipe length of 10 m and total loss coefficient of 5.0) are design specific; representative values have been assumed here to move forward with the analysis.

Table III.8-1 Summary of model input parameters for transient system analysis

Component	Input parameters	Value
Core	Full power rating	250 MW
	Mass, specific heat, initial temperature	14,238 kg, 520 J/kg-K, 520 °C
	Flow area, length, D_h , ΣK_{loss}	0.32 m ² , 3.05 m, 3.36 mm, 1.5
Redan	Mass, specific heat, initial temperature	65,535 kg, 1272 J/kg-K, 510 °C
	Flow area, length, D_h , ΣK_{loss}	1.23 m ² , 4.0 m, 1.25 m, 1.0
Cold plenum	Mass, specific heat, initial temperature	41,346 kg, 1273 J/kg-K, 355 °C
EM pumps	Number, flow area, length, D_h , ΣK_{loss}	4, 0.028 m ² , 5.5 m, 9.7 cm, 3.0
Piping from pumps to core inlet	Length, D_h , ΣK_{loss}	15 cm, 0.30 m, 2.5
Sodium properties	Density, viscosity, conductivity, specific heat, expansion coefficient	849 kg/m ³ ; 2.65•10 ⁻⁴ kg/m-s; 69.4 W/m-K; 1272 J/kg-K; 2.80•10 ⁻⁴ K ⁻¹
Nak properties	Density, viscosity, conductivity, specific heat, expansion coefficient	827 kg/m ³ ; 3.54•10 ⁻⁴ kg/m-s; 24.7 W/m-K; 915 J/kg-K; 2.80•10 ⁻⁴ K ⁻¹
Air properties	Density, viscosity, conductivity, specific heat, expansion coefficient	1.0 kg/m ³ ; 2.22•10 ⁻⁵ kg/m-s; 0.035 W/m-K; 1012 J/kg-K; 2.1•10 ⁻³ K ⁻¹
DRACS	Number	1 or 2
	No. of tubes, tube pitch, ID, OD, length, thermal conductivity	25, 3.79 cm, 2.04 cm, 2.22 cm, 2.75 m, 28.0 W/m-K
	Primary (shell) and secondary (tube) side ΣK_{loss}	1.5, 1.5
IHX	Number	2
	No. of tubes, tube pitch, ID, OD, length, thermal conductivity	3300, 2.23 cm, 1.41 cm, 1.59 cm, 4.00 m, 28.0 W/m-K
	Primary (shell) and secondary (tube) side ΣK_{loss}	26.6, 1.5
Secondary piping	Pipe ID (D_h), length, ΣK_{loss}	0.075 m, 10.0 m, 4.0
Inlet duct to NDHX	Pipe id (D_h), length, ΣK_{loss}	2.0 m, 10.0 m, 4.0
Outlet duct to NDHX	Pipe id (D_h), length, ΣK_{loss}	2.0 m, 10.0 m, 4.0
Chimney	Pipe id (D_h), length, ΣK_{loss} , T_{air}	1.62 m, 5.0 m, 1.5, 15°C
ΔH driving natural convection	Primary system, DRACS, secondary, tertiary	1.0 m, 2.87 m, 5.0 m, 5.0 m

Given the above set of assumptions, the particular accident sequence selected for this preliminary evaluation of shutdown heat removal capability is a protected LOF/LOHS event. In particular, at time $t = 0$, the reactor is scrammed from the full-power operating point of 250 MWt. The primary system pumps are assumed to coast down with a 4 second halving time until the flow rate falls below that predicted under buoyancy-driven natural convection conditions. As soon as the reactor is scrammed, the dampers on the NDHXs open to bring the SHRS into operation. The EM pumps on the DRACS flow circuits are not assumed to active upon scram, and therefore system flowrates are calculated solely on the basis of natural convection flow response. For the base case, only one of the three DRACS systems is assumed to activate at time $t = 0$. To examine the effect of the number of operational DRACS on the peak core temperature, a second calculation was performed with two DRACS activated upon scram. The calculations

were carried out over a period of 1 day (24 hours). In both cases, the core had reached peak temperature within this time interval and started to decline.

Figure III.8-1 provides the core and plena temperature responses with either one or two operational DRACS, while Figure III.8-2 shows the DRACS heat removal rates for the same two cases. In addition, Figures III.8-3 through III.8-5 provide other calculated information for the case of a single operational DRACS. As shown in Figure III.8-1, with one DRACS operational the maximum (lumped capacitance) core temperature is predicted to reach $\sim 567^\circ\text{C}$ at ~ 14 hours following scram, but thereafter it steadily declines over the balance of the transient. For the case of two operational DRACS, the peak core temperature is reduced to $\sim 530^\circ\text{C}$, which occurs ~ 15.3 hours after scram.

As shown in Figure III.8-2, the DRACS heat removal for the base case rises to meet the decay heat input at ~ 15 hours into the transient. The heat removal rate at this time reaches ~ 1.4 MWt. This heat removal rate significantly exceeds the design removal rate of 625 kWt, which is based on limited mass flowrates of 3.1 to 4.4 kg/sec through the DRACS on the primary and secondary sides, respectively (see Table II.6-1). However, due to the relatively open flow path of this particular reactor design, the actual flowrates and temperature drops through the DRACS exceed those assumed in the DRACS HX design analysis, and therefore the heat removal rate is quite high (see Figures III.8-4 and III.8-5). In general, the results of these calculations indicate that the DRACS system is quite robust in terms of maintaining acceptably low temperatures inside the reactor vessel, even with only one unit operational.

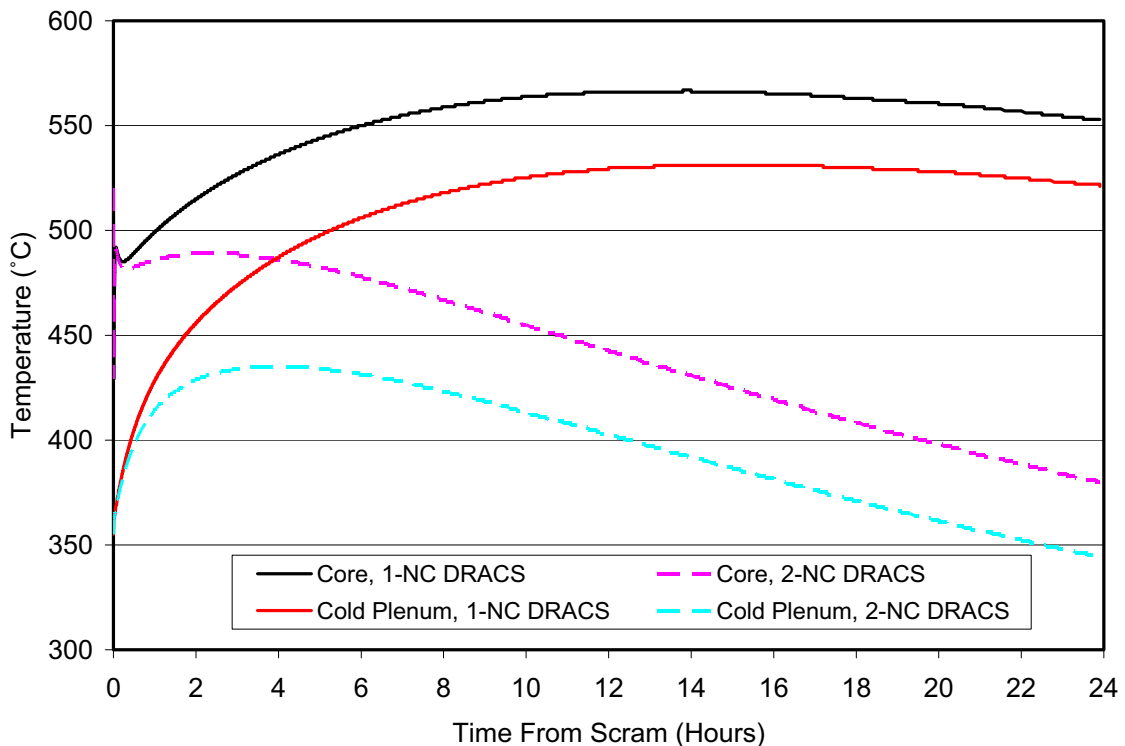


Figure III.8-1 Core and plena temperatures with one or two operational DRACS

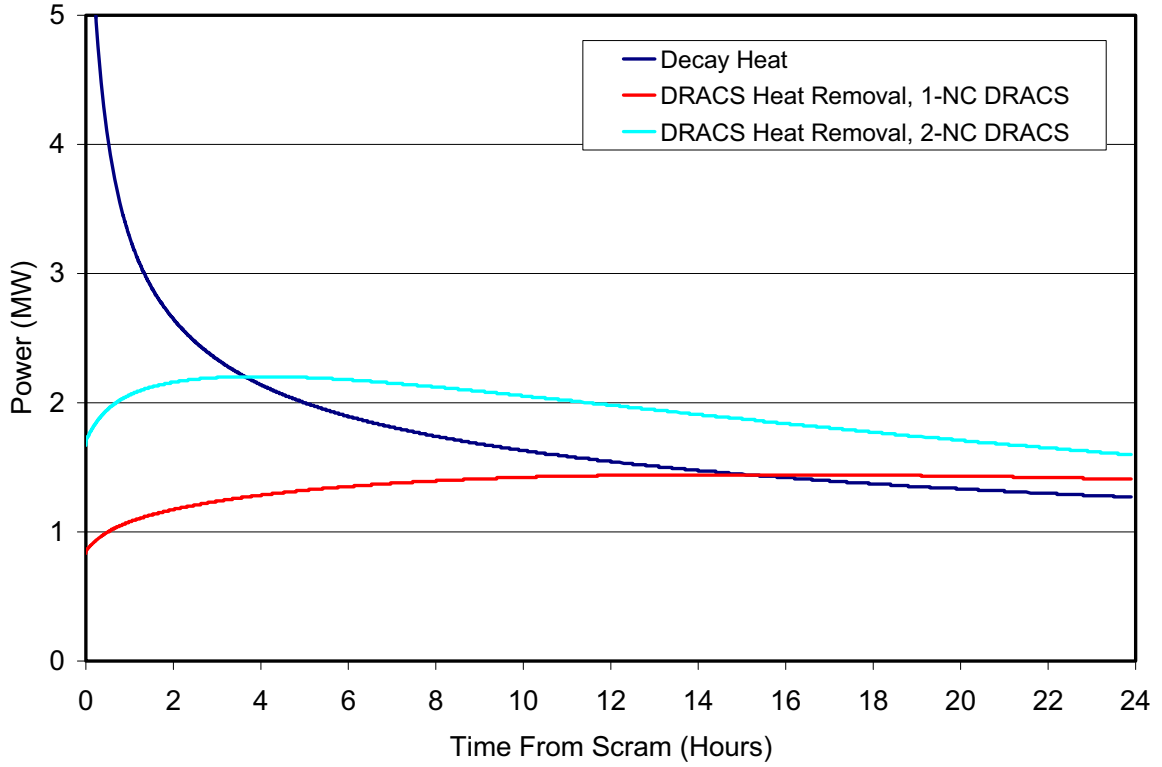


Figure III.8-2 Decay and DRACS heat rates with one or two operational DRACS

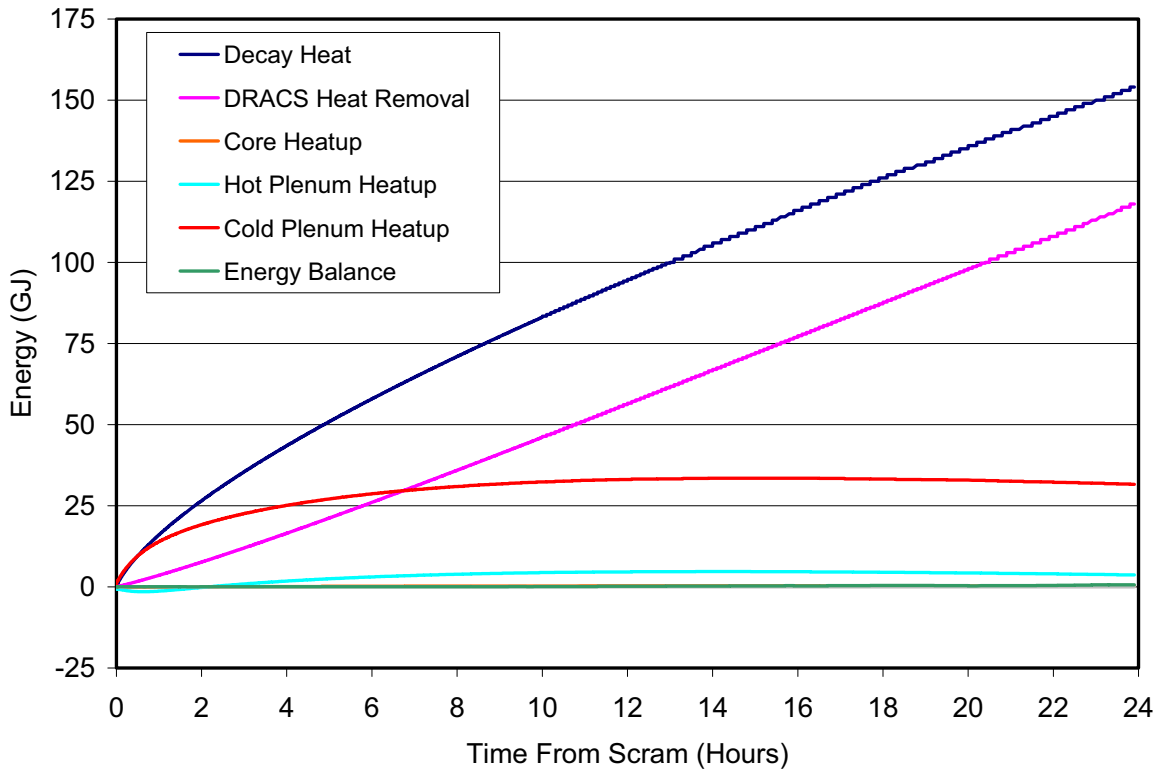


Figure III.8-3 Overall system energy balance with one operational DRACS

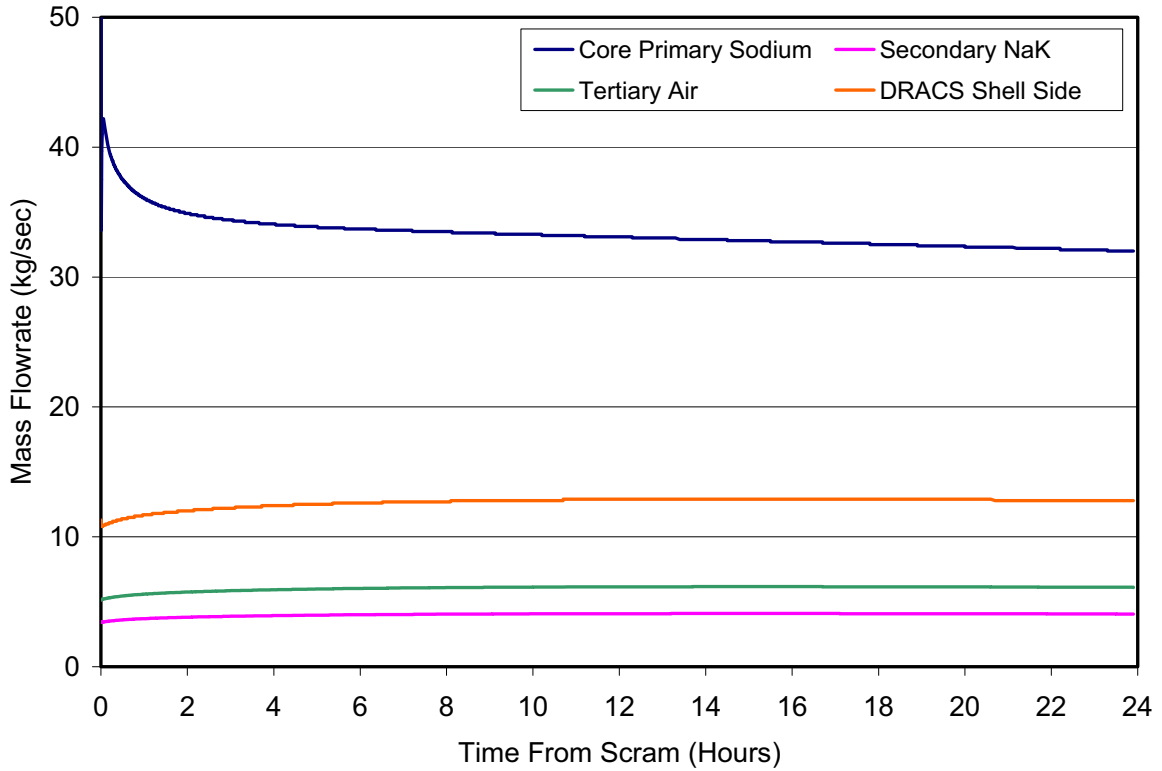


Figure III.8-4 System mass flowrates with one operational DRACS

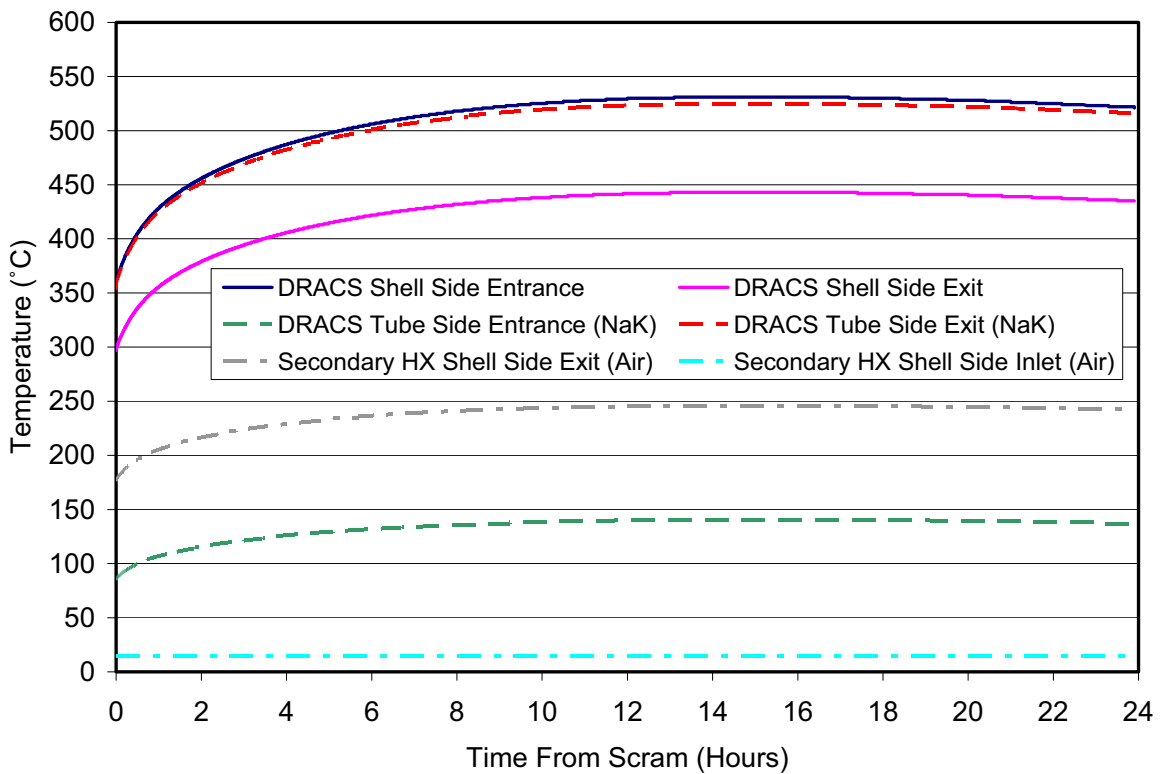


Figure III.8-5 HX inlet and exit temperatures with one operational DRACS

III.9 Spent Fuel Cooling Requirements for Transfer Operations

Fuel transfer operations where thermal loadings are a concern include not only the transfer of spent fuel from the vessel to the fuel cycle facility, but also the transfer of TRU-bearing fuel from the fuel facility into the reactor. Analyses of the assembly cooling requirements for these two cases are presented in this Section.

III.9.1 Spent Fuel Assembly Transfer

Spent fuels will be transported from the reactor vessel to the fuel cycle facility with an inter-building cask (IBC) with gas cooling. The decay heat level in the fuel at the time of the transfer operation will determine whether passive or active cooling is required. The ABTR design provides in-vessel storage positions for fresh as well as spent fuel. The cooling time in the reactor depends on not only the number of spent fuel assemblies, but also on the number of available storage positions. In the current ABTR design, a total of 36 in-vessel positions are provided. During each refueling operation, four driver assemblies and, most likely, at least one test assembly will be unloaded from the core. Thus, given the number in-vessel storage positions, then the assembly residence time in the vessel will be limited to 7 reactor cycles (28 months). In this case, the maximum decay heat level of the spent fuel is estimated to be 1.5 kW per assembly, as shown in Figure III.9-1.

To determine if active cooling is needed, an estimate of the capacity of natural convection cooling is required. The relationship between the required flow rate and decay heat level is shown in Figure III.9-2. There are four cases that parameterize on the gas coolant (air or argon), and the outside temperature of the wrapper tube (50 or 200 °C). The most realistic case is felt to be the 200°C argon gas case since the IBC will use argon and there is no air conditioning system at this pre-conceptual design stage. The parametric cases are provided for evaluating potential design changes to the IBC. The minimum required flow rate of 0.15 Nm³/min (normal m³/min) corresponds to the 50°C air case. The more realistic flow rate corresponds to the case of argon gas with a 200°C wrapper temperature, for which the required flow rate is 0.3 Nm³/min.

The natural circulation cooling capacity depends on the pressure drop inside the subassembly, as well as the circulation head caused by the temperature difference between the inside and outside of the subassembly. Pressure drops on the interior and exterior of the wrapper tube are described through the equation [1]:

$$\Delta P = f \times \frac{L}{D_e} \times \rho \times \frac{u^2}{2g}$$

where f = friction factor,

$$f = \frac{93}{\text{Re}} \text{ for laminar flow inside wrapper tube (Re} < 548),$$

$$f = \frac{0.17}{\text{Re}^{0.18}} \text{ for turbulent flow inside wrapper tube (Re} > 12820),$$

$$f = \frac{64}{\text{Re}} \text{ for laminar flow outside wrapper tube (re} < 2300),$$

$$f = \frac{0.3164}{\text{Re}^{0.25}} \text{ for turbulent flow outside wrapper tube,}$$

D_e = equivalent diameter,

L = channel length, and

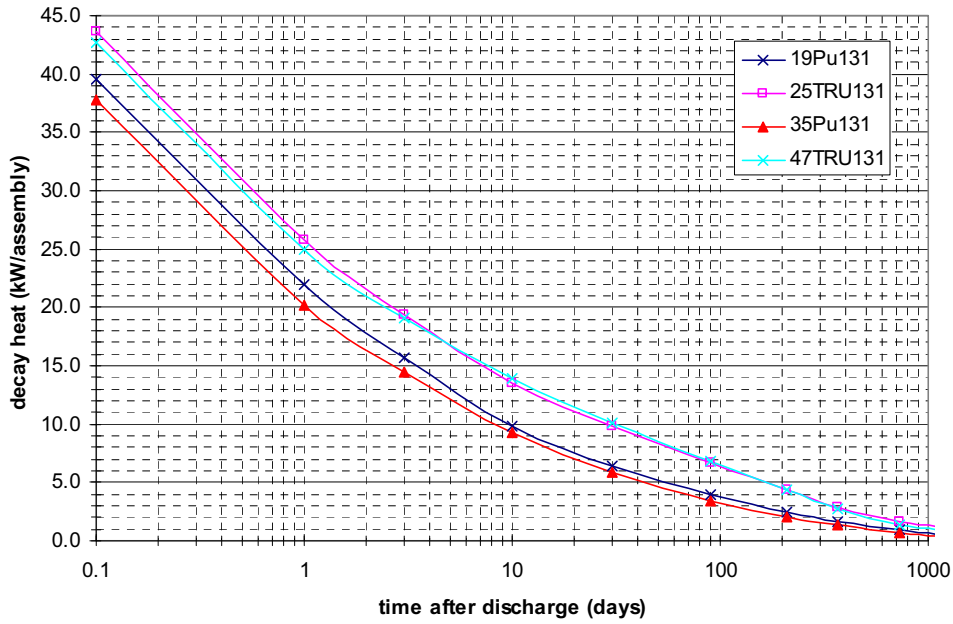
ρ = coolant density.

The calculated pressure drops inside and outside the subassembly wrapper are shown in Figures III.9-3 and III.9-4, respectively. These figures indicate that the pressure drop outside the wrapper is negligible compared to that on the interior of the wrapper. Natural circulation inside the wrapper is calculated to be in the laminar region since the Reynolds number lies in the range of 90 to 220. The relation between natural circulation head and the wrapper interior temperature is shown in Figure III.9-5. The maximum head is around 30 Pa when the outside temperature is 50 °C, and 15 Pa when the temperature is increased to 200 °C.

When the outside pressure drop is negligible and the flow is in the laminar region, the flow velocity can be expressed through the following simple equation:

$$u = \frac{2}{93\rho} \frac{D_e^2}{L} \Delta P \frac{1}{\nu}$$

where ν is the kinematic viscosity. The velocity and flow rate calculated from this equation are shown in Figures III.9-6 and III.9-7, respectively. The flow rates for outside temperatures of 50 and 200°C are ~0.005 and 0.002 Nm³/min, respectively. These results show that the natural convection flow rates are much smaller than the minimum required rate of 0.15 Nm³/min required to remove the decay heat without excessive heatup of the fuel. From Figure III.9-2, it is evident that the assembly can be kept adequately cool when the decay heat level is at or below 0.05 kW per subassembly when the heat removal is limited to natural circulation alone.



Case	19pu131	25tru131	35pu131	47tru131
TRU enrichment, %	18.81	24.83	34.86	46.70
Peak discharge burnup (MWD/kg)	130.84	130.55	130.83	130.45
Specific power density (kW/kg)	59.42	59.42	120.51	120.06
Resident time (EFPD)	2202	2197	1086	1087
Total HM mass in core (MT)	4.03	4.03	1.98	1.98
Total driver fuel (including test)	63	63	63	63
HM mass per assembly (kg)	70.6	70.6	34.54	34.54

Figure III.9-1 Decay heat of spent fuel

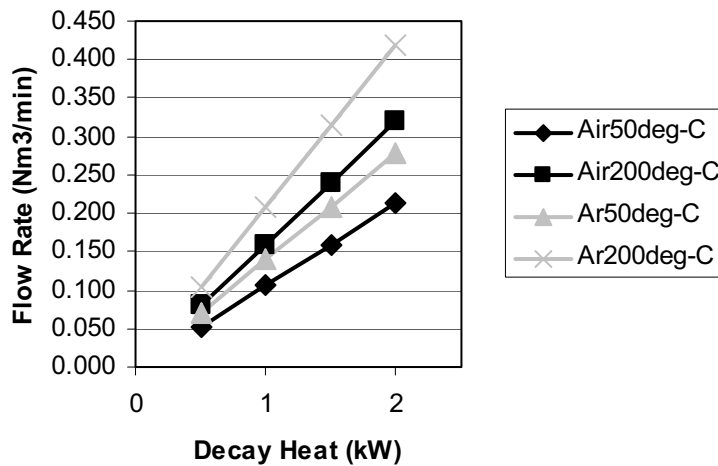


Figure III.9-2 Relationship between required gas flow rate and assembly decay heat level

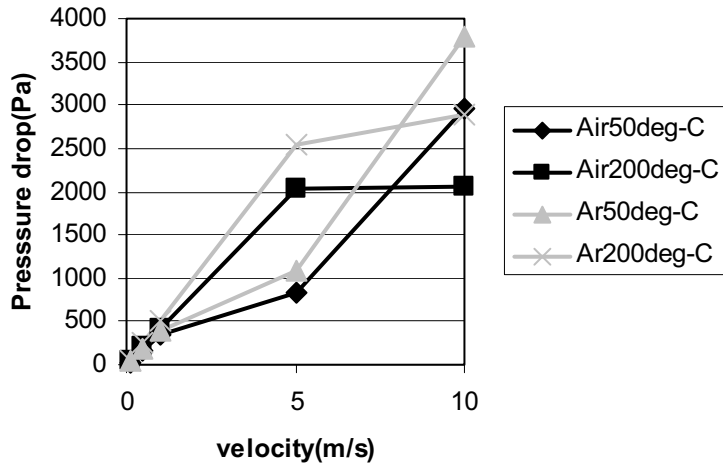


Figure III.9-3 Pressure drop inside the wrapper tube

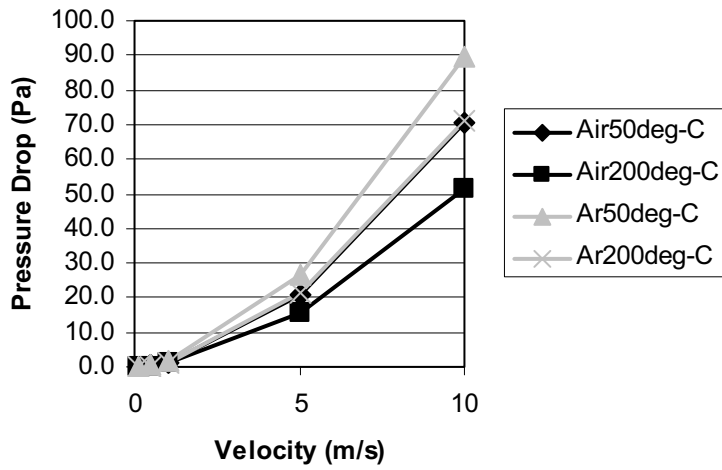


Figure III.9-4 Pressure drop outside the wrapper tube

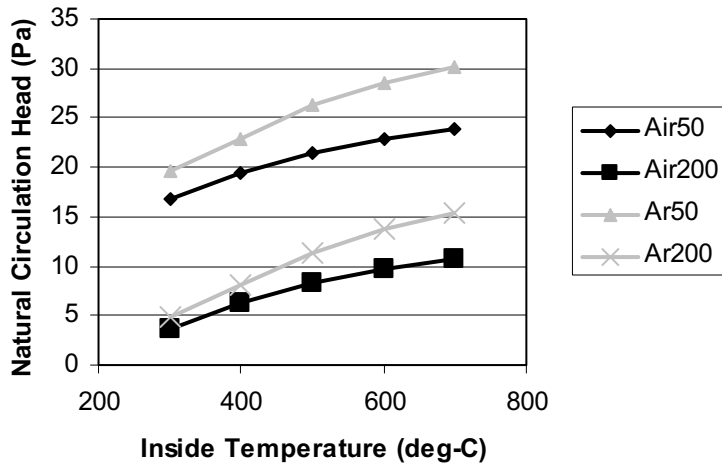


Figure III.9-5 Natural circulation head

Aside from natural convection, radiation heat transfer will also contribute to passive cooling of the assemblies. The potential contribution of this heat transfer mechanism is now considered. The simplified geometry assumed for the analysis is shown in Figure III.9-8. The radiant heat flux between surface 1 and 2 can be evaluated through the following well-known equation:

$$Q = \frac{1}{\frac{1}{\varepsilon_1} + \frac{1}{\varepsilon_2} - 1} \sigma (T_1^4 - T_2^4)$$

where

σ = Stefan-Boltzmann constant $4.88 \times 10^{-8} \text{ kcal/m}^2 \text{ hr-K}$,

ε_i = emissivity of surface i .

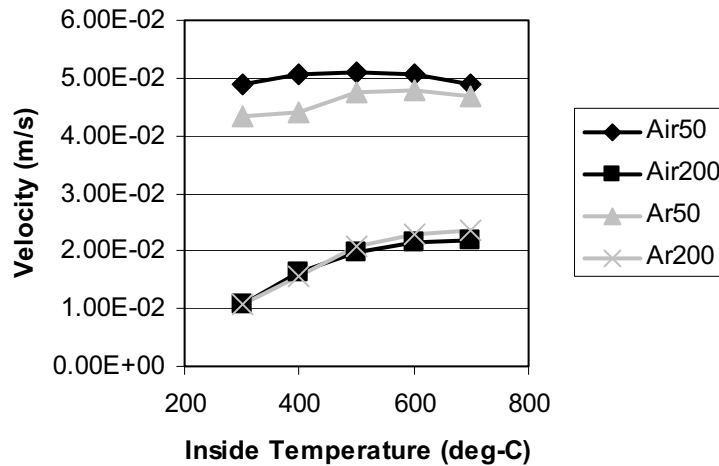


Figure III.9-6 Natural circulation coolant velocity

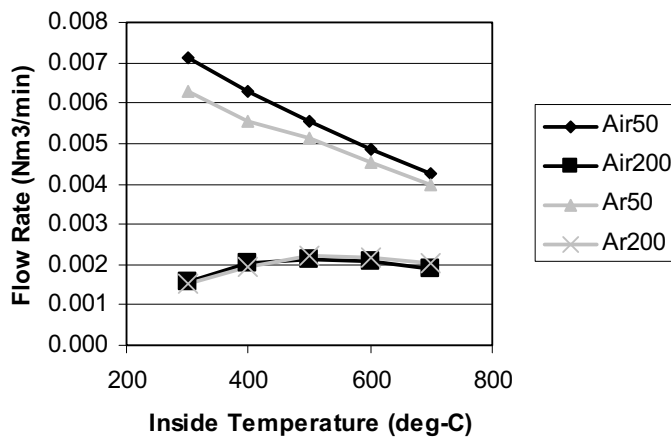


Figure III.9-7 Volumetric flow rate due to natural circulation

In this scoping analysis, gas circulation and heat conduction through the cladding on the interior of the wrapper are ignored. The effective height for radiation is assumed to be that of the active core height which is 0.8 meters. The radiation heat transfer depends on emissivity which varies widely with the material type, surface condition, and temperature. For example, pure iron has an emissivity of 0.08, unoxidized carbon steel has an emissivity of 0.1, and oxidized steel has an emissivity of 0.8 at 260°C. In this analysis, the emissivity is conservatively assumed to equal 0.1. The relation between wrapper temperature, which is treated parametrically between 50 and 200°C, and decay heat level is shown in Figure III.9-9. The wrapper temperature exceeds 600°C for decay heat levels above 0.6 kW. This result shows that radiation heat transfer is more efficient than natural circulation in reducing the assembly temperature, but the decay heat level is still below the 1.5 kW threshold required for passive cooling assuming a 28 month assembly residence time inside the vessel. This result is also in good agreement with reference [1], where it was found that the maximum passive cooling capacity of the EBR-II IBC was 0.8 kW when both radiation and conduction were considered.

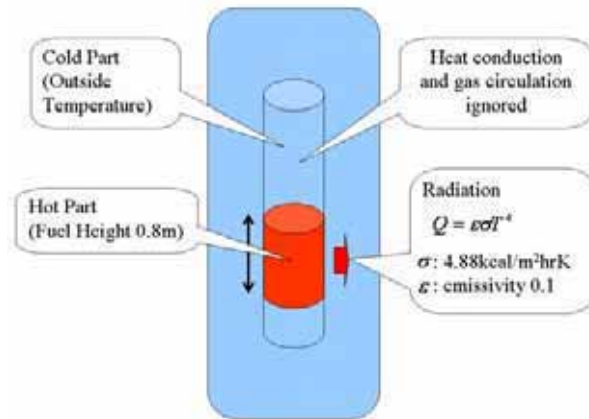


Figure III.9-8 Simplified geometry for radiation cooling evaluation

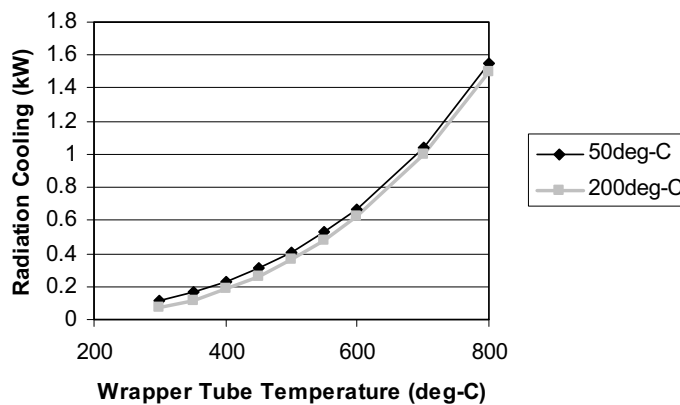


Figure III.9-9 Relation between radiation cooling and wrapper tube temperature

III.9.2 Fresh Fuel Assembly Transfer

ABTR may use plutonium fuel for the initial core, but will gradually transfer to TRU fuel with minor actinide content. The TRU fuels are expected to have a non-negligible decay heat level, as shown in Table III.9-1. As these data indicate, the decay heat of the fresh plutonium fuel is limited to 0.03 kW per assembly, but the maximum decay heat of the TRU fuel reaches 0.37 kW per assembly. Although this value is much smaller than that of spent fuel, the maximum cladding temperature of fresh TRU fuel during storage/refueling operations must be kept much lower than that of spent fuel, since no cladding damage can be tolerated prior to core loading. In reference [2], the maximum cladding temperature is limited to 375°C to stay well below the creep temperature of high chromium steel. The same criterion is adopted for ABTR since the same steel type (HT-9) will be utilized for the cladding. The previous spent fuel cooling analysis indicated that the maximum assembly decay heat level that can be passively cooled by natural circulation alone is 0.05 kW, and when radiation heat transfer is included, this limit is increased to approximately 0.2 kW. As shown in Figure III.9-9, radiation heat transfer is only capable of maintaining the subassembly wrapper temperature below 350°C when the subassembly decay heat level is at or below 0.2 kW. This implies that the new TRU fuels will also require forced gas cooling during ex-vessel fuel handling operations.

Table III.9-1 Decay heat level of various driver fuel compositions

Case	19Pu131	35Pu131	25TRU131	47TRU131
TRU enrichment, %	18.81	34.86	24.83	46.70
Peak discharge burnup (MWd/kg)	130.84	130.83	130.55	130.45
Specific power density (kW/kg)	59.42	120.51	59.42	120.06
Resident time (EFPD)	2202	1086	2197	1087
Total HM mass in core (MT)	4.03	1.98	4.03	1.98
Total driver fuel (including test)	63	63	63	63
HM mass per assembly (kg)	70.06	34.54	70.06	35.54
Decay heat (W/kg)	0.4	0.8	5.3	9.9
Decay heat (kW/assembly)	0.03	0.03	0.37	0.34

III.9.3 Intra-Building Cask Transient Analysis

The previous scoping calculations indicated that both spent and new TRU fuels will require forced cooling during ex-vessel fuel handling operations. However, these steady state calculations assumed that the inner temperature of the IBC was held constant at 200°C. In this section, a two-dimensional transient analysis is performed in order to estimate the time required for the IBC to reach this elevated temperature under passive cooling conditions. The radial temperature distribution is evaluated using the heat transfer model shown in Figure III.9-10. Heat conduction in the axial direction is also considered. Heat transfer from the fuel pins to the wrapper tube, and from the wrapper tube to the inner surface of the IBC, is assumed to occur by radiation. View-factor effects throughout the domain are neglected. In this case, the same radiation heat

transport equation that was used in the previous steady state calculations can be applied. As discussed earlier, radiation is strongly dependent on the emissivity of the surfaces. Spent fuel cladding will most likely have an emissivity larger than the value of ~ 0.1 expected for new fuel (indicative of polished steel) since dirty surfaces generally have higher emissivities. In this analysis, the conservative assumption is made that the emissivities of both new and spent fuel claddings are ~ 0.1 . Heat transport from the IBC surface to the air is assumed to be by natural convection assuming the heat transfer coefficient is $5 \text{ W/m}^2\text{-K}$ [1].

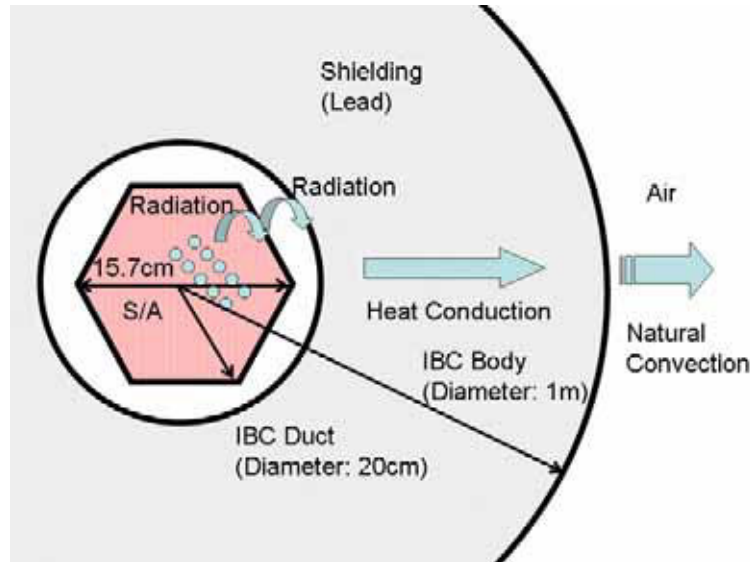


Figure III.9-10 Illustration of IBC transient calculational model

Table III.9-2 IBC transient analysis input parameters and results

Item	Case 1	Case 2
Fuel Type	Spent	New
Decay Heat	1.5 kW	0.37 kW
Emissivity from Fuel Pin to Wrapper Tube	0.1	0.1
Emissivity from Wrapper Tube to IBC	0.1	0.1
Density of Fuel	15.8 g/cm ³	15.8 g/cm ³
Density of Stainless Steel	7.9 g/cm ³	7.9 g/cm ³
Density of Lead	11.4 g/cm ³	11.4 g/cm ³
Specific Heat of Fuel	0.2 J/g-K	0.2 J/g-K
Specific Heat of Stainless Steel	0.5 J/g-K	0.5 J/g-K
Specific Heat of Lead	0.13 J/g-K	0.13 J/g-K
Conductivity of Stainless Steel	0.15 W/cm-K	0.15 W/cm-K
Conductivity of Lead	0.35 W/cm-K	0.353 W/cm-K
Heat Transfer Coefficient at the IBC Surface	0.0005 W/cm ² -K	0.0005 W/cm ² -K
Outside Temperature	50 °C	50 °C

Table III.9-2 shows the assumed input parameters. There are two cases. The first is the spent fuel case with an assumed assembly decay heat level of 1.5 kW, while the second case is for new TRU fuel with a decay heat level of 0.37 kW (see Table III.9-1). Figure III.9-11 shows the temperature transient in the case of spent fuel. The peak cladding temperature reaches 800°C after ~ 1 hour. This result is in good agreement with the previous rough estimate of the peak steady-state cladding temperature for spent fuel with passive cooling by radiation heat transfer alone (see Figure III.9-9). Figures III.9-12 and III.9-13 show the radial and axial temperature distribution at the end of the transient after the peak cladding temperature is reached. The temperature inside the IBC is evaluated as 163°C. This indicates that the assumption of a 200°C inner surface temperature for the IBC used in the previous steady state calculations was reasonable.

Figures III.9-14, III.9-15 and III.9-16 respectively provide the temperature transient, radial, and axial temperature profiles across the IBC after the peak clad temperature is reached for the case of new TRU fuel. Peak clad temperature for this case is reduced to 467°C. This result is in good agreement with the previous steady state analysis that indicated that the temperature can exceed the creep limit of 375°C [2]. As shown in Figure III.9-15, the inner surface temperature of the IBC eventually reaches 77°C. This indicates that the assumption of a 200°C IBC inner surface temperature in the steady state analysis was too conservative, but did not strongly affect the predicted cladding temperature. This is due to the fact that the radiation heat transfer is determined by the subtraction of the fourth power of temperatures, and so the effect of the lower boundary temperature is small.

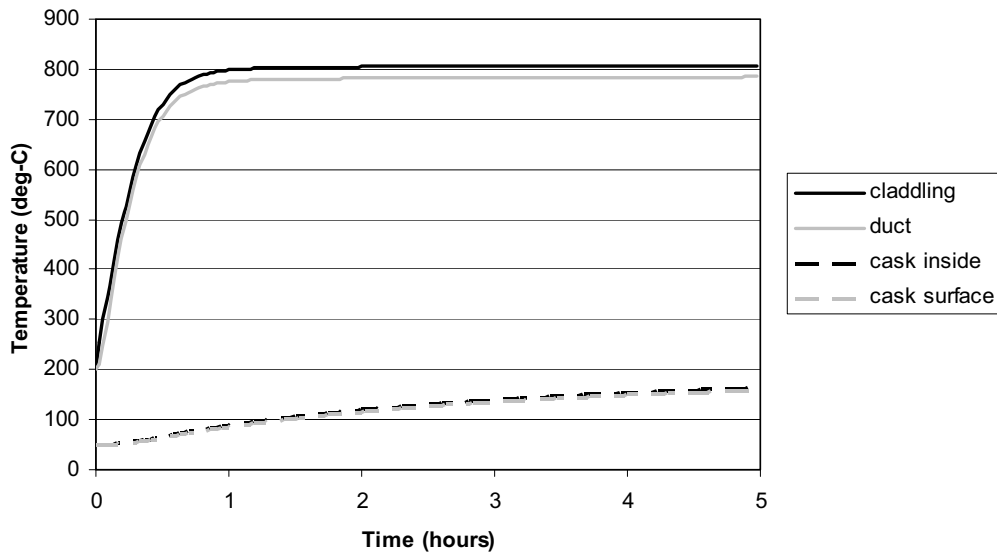


Figure III.9-11 Transient temperature (case 1: spent fuel)

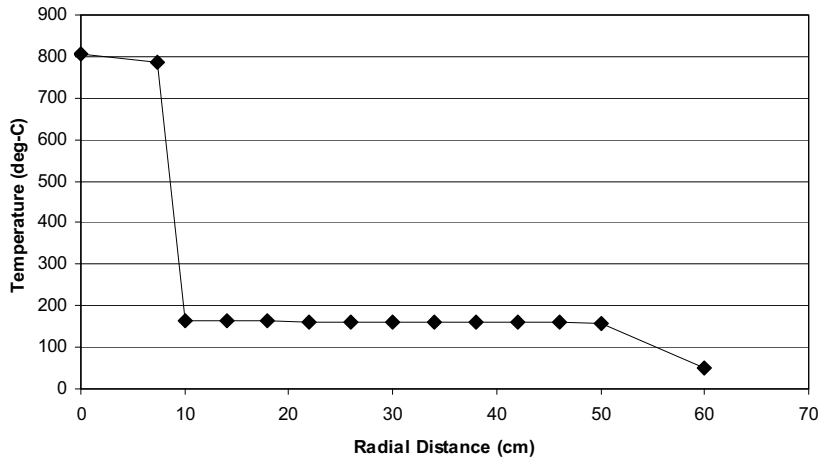


Figure III.9-12 Radial Temperature distribution in IBC (case 1: spent fuel)

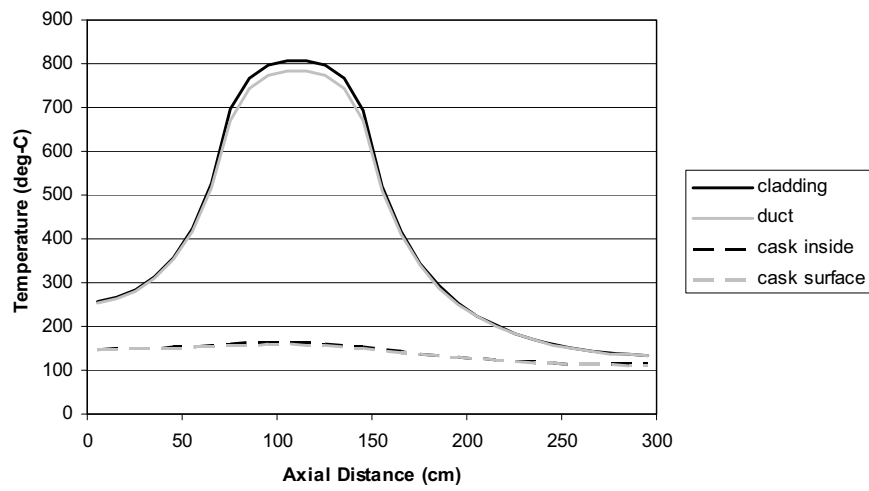


Figure III.9-13 Axial Temperature distribution in IBC (case 1: spent fuel)

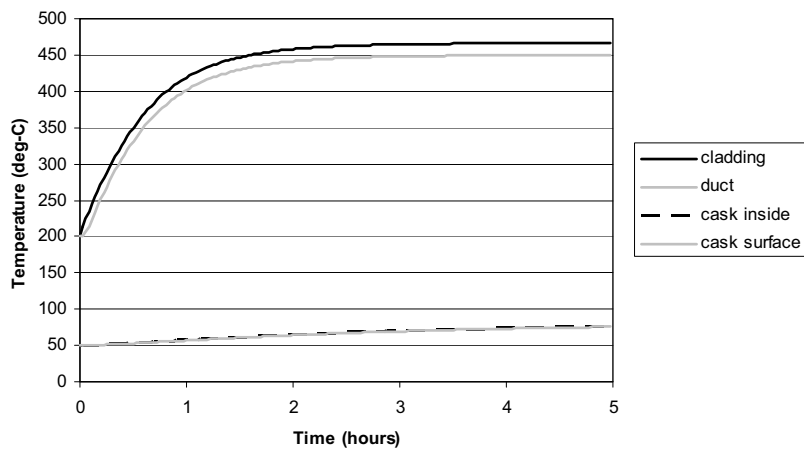


Figure III.9-14 Transient temperature (case 2: new TRU fuel)

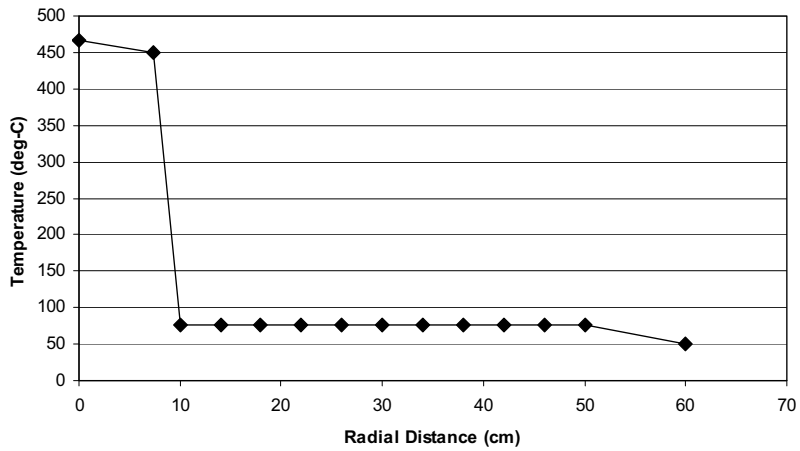


Figure III.9-15 Radial Temperature distribution in IBC (case 2: new TRU fuel)

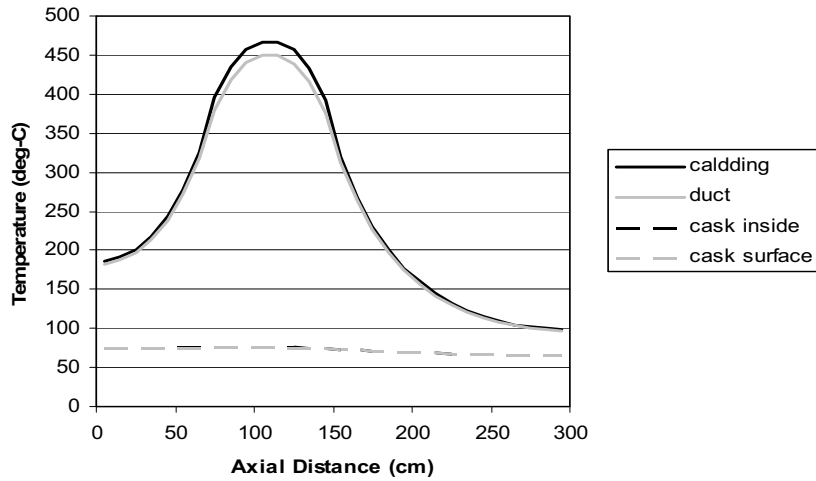


Figure III.9-16 Axial Temperature distribution in IBC (case 2: new TRU fuel)

References

1. R.T. Klann and B.A. Picker, Jr., "A conceptual redesign of an inter-building fuel transfer cask", Proc. of ICONE-2, San Francisco, California (1993).
2. Y. Chikazawa, S. Ushui, M. Konomura, H. Ikeda, "Design Study on a Fuel Handling System in a Sodium Cooled Reactor Study in FY2004 (joint study)," JAEA Research 2006-032 (2006).

LIST OF ACRONYMS

ANL	Argonne National Laboratory
ANS	American Nuclear Society
ANSI	American National Standards Institute
ASME	American Society of Mechanical Engineers
ATWS	Anticipated Transient Without Scram
BOC	Beginning of Cycle
B&PV	Boiler and Pressure Vessel
CEA	Commissariat a l'Energie Atomique
CFD	Computational Fluid Dynamics
DBE	Design Basis Events
DOE	Department of Energy
DRACS	Direct Reactor Auxiliary Cooling System
EBR-II	Experimental Breeder Reactor II
EM	Electromagnetic
EMAT	Electromagnetic Acoustic Transducer
EOC	End of Cycle
EPA	Environment Protection Agency
FFTF	Fast Flux Test Facility
HEPA	High Efficiency Particulate Air
HTR	High Temperature Recuperator
HVAC	Heating, Ventilation and Air Conditioning
HX	Heat Exchanger
IBC	International Building Code
IEEE	Institute of Electrical and Electronics Engineers
IHTS	Intermediate Heat Transport System
IHX	Intermediate Heat Exchanger
ISI	In-Service Inspection
IVIM	In-Vessel Inspection Machine
JAPC	Japan Atomic Power Company
JNC	Japan Nuclear Cycle Development Institute
LMR	Liquid Metal Reactor
LRB	Laminated Rubber Bearing
LTR	Low Temperature Recuperator
MOC	Middle of Cycle
MOX	Mixed Oxide
MWe	Megawatt Electric
NDE	Non-Destructive Examination
NDHX	Natural Draft Heat Exchanger
NPSH	Net Positive Suction Head
NRC	Nuclear Regulatory Commission
OBE	Operating Basis Earthquake
OSHA	Occupational Safety and Health Administration
PCHE	Printed Circuit Heat Exchanger

PHTS	Primary Heat Transport System
PLOF	Protected Loss of Flow
PLOHS	Protected Loss of Heat Sink
PRISM	Power Reactor Inherently Safe Module
RBCB	Run Beyond Cladding Breach
RCB	Remote Controlled Vehicle
SHRS	Shutdown Heat Removal System
ABTR	Small Modular Fast Reactor
SS	Stainless Steel
SSE	Safe Shutdown Earthquake
TREAT	Transient Reactor Test Facility
TRU	Transuranic
ULOF	Unprotected Loss of Flow
ULOHS	Unprotected Loss of Heat Sink
UTOP	Unprotected Transient Overpower

APPENDIX A Evaluation Of Safety Design Criteria

This Appendix provides a survey of safety design criteria applicable to sodium cooled fast reactors. Criteria selected for consideration include 1) generalized design criteria specified by Title 10, Part 50, Appendix A of the Code of Federal Regulations for application to light water nuclear power reactors, 2) American National Standard general safety design criteria for a liquid metal reactor nuclear power plant, and 3) U.S. Department of Energy nuclear reactor safety design criteria. Considerations of design criteria by U.S. Nuclear Regulatory Commission in licensing and safety evaluation of proposed liquid metal cooled nuclear power reactor designs are reviewed. Applicability of the selected set of design criteria to sodium cooled fast reactor design features and operational characteristics are discussed. Recommendations are also made for modifications to existing safety design criteria for relevance to sodium cooled fast reactor designs.

The safety philosophy guiding the design, construction, and operation of nuclear facilities in the U.S. is based on the principle of “defense in depth” [1]. The objectives of “defense in depth” are first to protect the health and safety of the public and plant operating personnel, and second to preserve the facility investment by assuring its operational readiness. In terms of physical elements, “defense in depth” is exemplified by multiple, successive barriers to guard against the escape of radioactivity from nuclear facilities. However, in the evolution of U.S. nuclear safety philosophy, the “defense in depth” principle has been extended and applied to all aspects of nuclear facility design, construction, and operation, so that all safety critical functions are achieved by multiple systems/procedures/processes that are diverse and independent.

In the nuclear facility design process, the “defense in depth” principle has fostered the development of guidelines for identifying those engineered systems that are important for safety. Safety class systems are designed to be very reliable. They are constructed using specifications and materials that will assure functionality. In addition, multiple systems of diverse design are provided so that failure of any single safety system will not put people or equipment at risk.

The system configurations and functional requirements for nuclear facilities are routinely documented early in the design process as a set of safety design criteria. Commercial water cooled nuclear power plants licensed by the U.S. Nuclear Regulatory Commission must comply with general design criteria documented in the Code of Federal Regulations [2]. Suggestions for modifications of these criteria for application to liquid metal cooled reactor designs have been supplied by representatives of the nuclear power industry [3]. Nuclear research reactors built by the U.S. Department of Energy must comply with safety design criteria documented in a DOE Order [4].

The purpose of this Appendix is to provide an evaluation of documented nuclear reactor safety design criteria, with the aim of identifying changes necessary for application to a sodium-cooled fast reactor design. Existing general design criteria

developed by the USNRC for light water reactors [2], by industry for liquid metal reactors [3], and by USDOE for research reactors [4] are examined for relevance. Recommendations are made for modifications to the existing safety design criteria for application to sodium-cooled system designs.

A.1 Safety Design Criteria Comparison

In the methodological framework built on the defense-in-depth foundation, the role of safety design criteria is to set requirements for design performance. During the formative stages of design development, safety design criteria specify the configuration and functional performance characteristics the design must have for it to receive construction and operation approvals from the regulatory agency. Once the design is developed, safety analyses are performed and documented to quantify the margins between the safety requirements and expected performance. After the design is constructed, safety tests are performed to verify design safety performance. Therefore, it is necessary to establish safety design criteria early in the design process, and the requirements set by the safety design criteria largely determine the plant configuration, equipment inventory, and equipment arrangement.

The U.S. Nuclear Regulatory Commission has developed a set of general safety design criteria for commercial light water-cooled nuclear power reactors [2]. These criteria are the base-line requirements for nuclear power reactors in the U.S. However, the 10CFR50 Appendix A requirements are intended for application to light water reactors, and so are only partly applicable to the sodium cooled reactor designs.

During the years of the U.S. sodium cooled fast reactor development program, industry representatives developed an American National Standards Institute standard [3] for safety design criteria applicable to liquid metal cooled reactors. This set of criteria followed the organization and intent of 10CFR50 Appendix A, but modified certain criteria details for applicability to the low pressure, chemically reactive liquid metal coolant.

The U.S. Department of Energy has developed a set of safety design criteria [4] to apply to USDOE reactors that are exempt from USNRC regulation. Such reactors include one-of-a-kind designs built for research, and other special purpose reactors. The USDOE criteria are similar in organization and intent to the 10CFR50 Appendix A criteria, with some variations to address generically the design variations of the USDOE reactors.

Table A-1 contains a listing of the design criteria from 10CFR50 Appendix A, and a cross reference to the criteria proposed in Refs. 3 and 4. These three sets of safety design criteria have been reviewed for applicability to the sodium cooled fast reactor design. The “Comments” column in Table A-1 references the list of comment statements that follow the Table and record the results of the review. The review takes into account the

technical safety evaluations performed by the USNRC for the PRISM [5] and SAFR [6] sodium cooled fast reactor designs.

Table A-1 Safety Design Criteria Cross Comparison

Criterion/Requirement	10CFR50, App. A	ANSI/ANS 54.1	DOE 5480.30	Comments
I. Overall Requirements				
Single Failure			8.c.1	1,2
Quality Standards and Records	GDC 1	3.1.1	8.c.2	1
Design Bases for Protection Against Natural Phenomena	GDC 2	3.1.2	8.c.3	1
Fire Protection	GDC 3	3.1.3	8.c.4	1
Protection Against Sodium and NaK Reactions		3.1.4		3
Environmental and Dynamics Effects Design Bases	GDC 4	3.1.5	8.c.5, 8.c.10	4
Sharing of Structures, Systems, and Components	GDC 5	3.1.6	8.c.6	1
Sodium Heating Systems		3.1.7		3
Siting			8.c.7	5
Human Factors Engineering			8.c.9	6
Safeguards and Security			8.c.11	6
Reactor Decontamination and Decommissioning			8.c.13	6
Support Systems			8.c.15	6
Non-Safety Class Structures, Systems, and Components			8.c.16	6
II. Protection by Multiple Fission Product Barriers				
Reactor Design	GDC 10	3.2.1	8.d.3.a	1
Reactor Inherent Protection	GDC 11	3.2.2	8.d.3.b	7
Suppression of Reactor Power Oscillations	GDC 12	3.2.3	8.d.3.c	1
Instrumentation and Control	GDC 13	3.2.4	8.d.5.a	1
Reactor Coolant Pressure Boundary	GDC 14	3.2.5	8.d.1.a	1
Reactor Coolant System Design	GDC 15	3.2.6	8.d.6.a	8
Containment Design	GDC 16	3.2.7	8.c.8	1
Electric Power Systems	GDC 17	3.2.8	8.d.2.a	1
Inspection and Testing of Electric Power Systems	GDC 18	3.2.9	8.d.2.b	1
Control Room	GDC 19	3.2.10	8.d.5.e	1
Remote Shutdown			8.d.5.f	9
Heating, Ventilation, and Air Conditioning (HVAC) Systems			8.d.7.a,b,c	10

Table A-1 Safety Design Criteria Cross Comparison (cont.)

Criterion/Requirement	10CFR50, App. A	ANSI/ANS 54.1	DOE 5480.30	Comm- ents
III. Protection and Reactivity Control Systems				
Protection System Functions	GDC 20	3.3.1	8.d.4.a	1
Protection System Reliability and Testing	GDC 21	3.3.2	8.d.4.a	1
Protection System Independence	GDC 22	3.3.3	8.d.4.b	1
Protection System Failure Modes	GDC 23	3.3.4	8.d.4.c	1
Separation of Protection and Control Systems	GDC 24	3.3.5	8.d.4.d	1
Protection System Requirements for Reactivity Control Malfunctions	GDC 25	3.3.6	8.d.4.e	1
Reactivity Control System Redundancy and Capability	GDC 26	3.3.7	8.d.5.b	11
Combined Reactivity Control Systems Capability	GDC 27	3.3.8	8.d.5.c	11
Reactivity Limits	GDC 28	3.3.9	8.d.5.d	11
Protection Against Anticipated Operational Occurrences	GDC 29	3.3.10	8.d.4.f	1
IV. Fluid Systems				
Assurance of Adequate Reactor Coolant Inventory		3.4.1		12
Quality of Reactor Coolant Pressure Boundary	GDC 30	3.4.2	8.d.1.b	1
Fracture Prevention of Reactor Coolant Pressure Boundary	GDC 31	3.4.13	8.d.1.c	4
Inspection of Reactor Coolant Pressure Boundary	GDC 32	3.4.3	8.d.1.d	1
Reactor Coolant Makeup	GDC 33		8.d.6.c	13
Reactor and Intermediate Coolant and Cover Gas Purity Control		3.4.4		14
Intermediate Coolant System		3.4.5		14
Inspection and Surveillance of Intermediate Coolant Boundary		3.4.6		14
Residual Heat Removal	GDC 34	3.4.7	8.d.6.b	1
Emergency Core Cooling	GDC 35		8.d.6.d	13
Inspection of Emergency Core Cooling System	GDC 36	3.4.8	8.d.6.d	15
Testing of Emergency Core Cooling System	GDC 37	3.4.9	8.d.6.d	15
Containment Heat Removal	GDC 38		8.c.8	16
Inspection of Containment Heat Removal System	GDC 39		8.c.8	16

Table A-1 Safety Design Criteria Cross Comparison (cont.)

Criterion/Requirement	10CFR50, App. A	ANSI/ANS 54.1	DOE 5480.30	Comments
Testing of Containment Heat Removal System	GDC 40		8.c.8	16
Containment Atmosphere Cleanup	GDC 41	3.5.11	8.c.8	16
Inspection of Containment Atmosphere Cleanup Systems	GDC 42	3.5.12	8.c.8	16
Testing of Containment Atmosphere Cleanup Systems	GDC 43	3.5.13	8.c.8	16
Cooling Water	GDC 44	3.4.10	8.d.6.e	1
Inspection of Cooling Water System	GDC 45	3.4.11	8.d.6.e	1
Testing of Cooling Water System	GDC 46	3.4.12	8.d.6.e	1
V. Reactor Containment				
Containment Design Basis	GDC 50	3.5.1, 3.5.2, 3.5.3	8.c.8	17
Fracture Prevention of Containment Pressure Boundary	GDC 51	3.5.4	8.c.8	1
Capability for Containment Leakage Rate Testing	GDC 52	3.5.5	8.c.8	1
Provisions for Containment Testing and Inspection	GDC 53	3.5.6	8.c.8	1
Piping Systems Penetrating Containment	GDC 54	3.5.7	8.c.8	1
Reactor Coolant Pressure Boundary Penetrating Containment	GDC 55	3.5.8	8.c.8	1
Primary Containment Isolation	GDC 56	3.5.9	8.c.8	1
Closed System Isolation Valves	GDC 57	3.5.10	8.c.8	1
VI. Fuel and Radioactivity Control				
Control of Releases of Radioactive Materials to the Environment	GDC 60	3.6.1	8.c.12.a, 8.c.14	1
Fuel Storage and Handling and Radioactivity Control	GDC 61	3.6.2	8.d.8.a, 8.d.8.d	1
Prevention of Criticality in Fuel Storage and Handling	GDC 62	3.6.3	8.d.8.b	1
Monitoring Fuel and Waste Storage	GDC 63	3.6.4	8.d.8.c	1
Monitoring Radioactivity Releases	GDC 64	3.6.5	8.c.12.b, 8.c.14	1

Comment 1. The relevant criteria from Refs. 2, 3, and 4 are essentially congruent in intent and are applicable to the liquid metal-cooled reactor design.

Comment 2. The single failure criterion for safety class structures, systems, and components is listed as a definition applied to specified criteria in Refs. 2 and 3. The single failure criterion is explicit in Ref. 4.

Comment 3. Explicit requirement for liquid metal coolant that considers the impact of chemical reactivity or thermophysical properties.

Comment 4. The 10CFR50 criterion addresses phenomena for a high pressure water system. The criteria should be revised to address phenomena relevant to low pressure, chemically reactive liquid metal coolant.

Comment 5. Siting criteria are considered in 10CFR100.

Comment 6. Explicit USDOE requirement beyond the scope of 10CFR50 Appendix A.

Comment 7. In LWR designs, the requirement for a prompt, negative power coefficient is met by the combination of the negative fuel Doppler coefficient and the negative moderator density coefficient. If the sodium cooled fast reactor coolant void coefficient is positive, the regulator may require additional design features to compensate, as noted in the PRISM [5] and SAFR [6] safety evaluation reports.

Comment 8. Systems cited should include the liquid metal heating system.

Comment 9. The USDOE separate requirement for a remote shutdown capability is included in GDC 19.

Comment 10. USDOE criterion for confinement superseded by containment criterion, GDC 16.

Comment 11. 10CFR50 Appendix A criteria contain references to LWR specific reactivity mechanisms (Xe, cold shutdown, ECCS boron injection, rod dropout, cold coolant shock) that are either irrelevant or require re-interpretation for fast spectrum LMR.

Comment 12. Liquid metal reactor criterion for maintaining core submersion in coolant is the equivalent of ECCS requirement for light water reactor (GDC 33, 35).

Comment 13. 10CFR50 Appendix A criterion is not applicable for liquid metal coolant.

Comment 14. Intermediate loop criteria for liquid metal cooled design.

Comment 15. The liquid metal reactor design does not include an ECCS, but inspection and testing requirements are applied to the residual heat removal system.

Comment 16. In the light water reactor design, the containment heat removal system is intended to reduce temperature and pressure following a loss-of-coolant accident.

Because such an accident sequence is not a design basis for the liquid metal cooled reactor, this criterion may not be relevant.

Comment 17. In the light water reactor design the containment design is based on loss of coolant accident consequences. For the low pressure liquid metal cooled reactor, in which a pipe break event is much less severe (leak before break), an alternative design basis accident must be specified.

A.2 Evaluation of Safety Design Criteria

The cross comparison of safety design criteria in Section A.1 shows that the sets of design criteria defined by the USNRC [2], the ANSI [3], and the USDOE [4] are generally and specifically convergent with regard to scope and content. The NRC design criteria are intended for application to light water cooled power reactors, and the ANSI criteria were proposed for sodium cooled reactors.

In its safety evaluation reports for the PRISM [5] and SAFR [6] designs, the USNRC has provided analyses of the applicability of the criteria in Ref. 2 to specific sodium cooled fast reactor designs, taking Ref. 3 into account. These analyses have been reviewed with a perspective of the general characteristics of a sodium cooled fast reactor system. From this review, the following general statements can be made with regard to the applicability of the design criteria in Ref. 2 to sodium cooled systems:

1. Many of the 10CFR50 Appendix A general design criteria are directly applicable to the sodium cooled fast reactor systems, without wording changes or modifications. The intent of the design criterion is clear, and the design implication for application to a sodium cooled system is apparent. Criteria included in this class are GDCs 1, 2, 3, 5, 10, 12, 13, 14, 16, 17, 18, 19, 20, 21, 22, 23, 24, 25, 29, 30, 32, 34, 44, 45, 46, 51, 52, 53, 56, 60, 61, 62, 63, 64.
2. Some of the 10CFR50 Appendix A general design criteria are worded with reference to specific light water reactor design features, performance characteristics, or regulatory requirements. These criteria must be reworded to preserve the original intent for sodium cooling. A listing of the criteria in this class and suggested changes are given in Table A-2.

**Table A-2 Suggested Changes to 10CFR50 Appendix A General Design Criteria
for Application to Sodium Cooled Systems**

GDC No.	Suggested Change
4	This criterion is written in reference to a high pressure, water coolant, and includes explicit references to loss-of-coolant accidents (LOCAs) and pipe ruptures. The words should be changed 1) to include dynamic and environmental phenomena relevant to low pressure sodium, e.g. the environmental effects of aerosols and oxidation products, 2) to delete references to dynamic and environmental accident phenomena specific to water coolant, and 3) to include references to generic design basis events, i.e. “anticipated operational occurrences.”
11	This criterion requires a prompt inherent nuclear feedback effect to compensate a rapid reactivity increase in the power operating range. NRC reviews of the PRISM and SAFR designs highlighted the positive coolant void reactivity worth as an area of significant concern for a beyond-design-basis loss-of-flow-without-scrum accident sequence. The criterion should be modified to specifically exclude or include coolant voiding effects, depending on the safety strategy dealing with severe accident.
15	This criterion is written to require that the reactor coolant pressure boundary is built to withstand design basis conditions. Reference 5 specifically requires inclusion of the sodium heating system in the listing of coolant systems subject to this requirement.
26	This criterion requires two independent reactivity control systems, one of which shall use control rods. Specific control reactivity requirements are listed in terms of LWR performance characteristics. The criterion should be rewritten in terms of equivalent sodium cooled fast reactor characteristics.
27	This criterion specifies combined control reactivity requirements including liquid poison injection. The criterion should be rewritten to eliminate the explicit mention of liquid poison addition.
28	This criterion requires that the reactivity control system be designed to limit the possible rate of reactivity addition to avoid damage to the reactor and its associated structures, systems, and components. Specific control reactivity requirements are listed in terms of LWR performance characteristics. The criterion should be rewritten in terms of equivalent sodium cooled fast reactor characteristics.
31	This criterion specifies conditions and phenomena to be considered in the design of the reactor coolant pressure boundary. For sodium coolant, Ref. 5 specifies addition of coolant chemistry and mechanical properties degradation to the list of considered phenomena, in recognition of the chemically active nature of sodium.

**Table A-2 Suggested Changes to 10CFR50 Appendix A General Design Criteria
for Application to Sodium Cooled Systems (cont.)**

GDC No.	Suggested Change
33	This criterion provides for a coolant supply system to assure reactor coolant inventory in the event of a small break in the coolant pressure boundary. As formulated, the criterion is not relevant to low pressure sodium coolant. Reference 3 specifies a replacement criterion dealing with assurance of adequate coolant inventory to maintain core cover and operation of the residual heat removal system in all cases.
35	This criterion provides for emergency core cooling in the event of a loss of coolant accident. Such an event is outside the design basis for the low pressure sodium coolant system. Coolant inventory, core covering, and residual heat removal are assured by GDC 33 and 34.
36	This criterion provides for inspection of the emergency core cooling system. Reference 5 recommends rewriting this criterion to provide for inspection of the residual heat removal system (GDC 34).
37	This criterion provides for testing of the emergency core cooling system. Reference 5 recommends rewriting this criterion to provide for testing of the residual heat removal system (GDC 34).
38	This criterion provides for the design of a containment heat removal system with the capability of rapidly reducing the temperature and pressure within the containment following a loss-of-coolant accident. The LOCA sequence is not relevant to the low pressure sodium coolant system. The criterion should be rewritten with wording to replace the LOCA reference with the appropriate design basis accident reference.
39	This criterion provides for inspection of the containment heat removal system, and includes specific reference to design features relevant to water cooled systems. The criterion should be rewritten to include design characteristics relevant to sodium cooled systems.
40	This criterion provides for testing of the containment heat removal system, and includes specific reference to design features relevant to water cooled systems. The criterion should be rewritten to include design characteristics relevant to sodium cooled systems.
41	This criterion provides for the design of a system to control fission gases and combustible gases in containment following a postulated accident. Reference 3 recommends modification of this criterion to include sodium aerosols and combustion products, and to identify sodium leakage and interaction with concrete as events in the accident sequence. The criterion should be rewritten to include design characteristics relevant to sodium cooled systems.
42	This criterion provides for inspection of the containment atmosphere cleanup system provided by GDC 41. The criterion should be rewritten to include design characteristics relevant to sodium cooled systems.

**Table A-2 Suggested Changes to 10CFR50 Appendix A General Design Criteria
for Application to Sodium Cooled Systems (cont.)**

GDC No.	Suggested Change
43	This criterion provides for testing of the containment atmosphere cleanup system provided by GDC 41. The criterion should be rewritten to include design characteristics relevant to sodium cooled systems.
50	This criterion stipulates design basis conditions and phenomena for the containment, and makes specific mention of loss-of-cooling accidents and metal-water interactions. The criterion should be rewritten to include design characteristics relevant to sodium cooled systems. Reference 5 recommends replacement of the LOCA sequence with the appropriate postulated accident, and replacement of metal-water interactions with phenomena relevant to sodium cooling.
55	This criterion provides for isolation design requirements for lines connected to the reactor coolant pressure boundary that penetrate the containment. In sodium cooled systems, this criterion also applies to lines connected to the reactor cover gas space.

Reference 5 identifies nine additional design criteria relevant to sodium cooled fast reactor designs that are not explicitly stated in 10CFR50 Appendix A. Six of these additional nine criteria are also cited in Ref. 3. These nine criteria are as follows:

1. Protection Against Sodium Reactions. (Cited in Ref. 3 as Criterion 3.1.4). This criterion explicitly provides for measures to protect against the consequences of chemical reactions resulting from sodium leaks. It calls for prevention, detection, and consequence mitigation design features, as well as measures to protect personnel and equipment from corrosive and potentially radioactive oxidation products.
2. Sodium Heating Systems. (Cited in Ref. 3 as Criterion 3.1.7). This criterion provides safety and performance requirements for systems intended to maintain as a liquid. Such systems are required to perform assuming a single failure.
3. Heat Transport System Design. (No corresponding Criterion in Ref. 3). This requirement ensures sufficient reactor cooling for normal operation and anticipated operational occurrences by providing two independent coolant flow paths between the reactor and the heat sinks, and stipulates that the integrity of the reactor coolant pressure boundary shall be maintained for postulated accidents. This criterion covers the same requirements as GDCs 34 (Residual Heat Removal), 35 (Emergency Core Cooling), and 44 (Cooling Water) in the original 10CFR50 Appendix A.
4. Assurance of Adequate Reactor Coolant Inventory. (Cited as Criterion 3.4.1 in Ref. 3). This criterion provides for sufficient coolant inventory to assure residual heat removal for normal operation, anticipated operational occurrences, and

- postulated accidents assuming a single failure. The criterion has the same intent as the original GDC 33 (Reactor Coolant Makeup).
5. Design of the Intermediate Coolant System. (Cited as Criteria 3.4.5 and 3.4.6 in Ref. 3). These criteria provide for the design, inspection, testing, and surveillance of the intermediate coolant system, and cover the intent of the original GDCs 44, 45, and 46 (Cooling Water).
 6. Reactor and Intermediate Coolant and Cover Gas Purity Control. (Cited as Criterion 3.4.4 in Ref. 3). This criterion requires systems to monitor and maintain the purity of reactor and intermediate coolants and cover gases within specified design limits.
 7. Inspection and Testing of Residual Heat Removal Systems. (Cited as Criteria 3.4.8 and 3.4.9 in Ref. 3). This criterion provides for inspection, testing, and surveillance of the residual heat removal system. The intent of these criteria is the same as that of the original GDCs 36 and 37, which provide for inspection and testing of the emergency core cooling system for water cooled reactor designs.
 8. Protection Against Fuel Rod Failure Propagation. (No corresponding Criterion in Ref. 3). This criterion was proposed for early sodium cooled fast reactor designs for which fuel irradiation experience was limited. As fuel irradiation experience was gained, confidence in fuel performance was assured, and this criterion was explicitly excluded in Ref. 5, which notes that fuel design limits and failure performance are included by GDCs 10, 27, and 35.
 9. Protection Against Coolant Flow Blockage. (No corresponding Criterion in Ref. 3). This criterion requires the fuel assembly design to include specific features to prevent and minimize the likelihood of coolant flow blockages, so that such events can be eliminated from the design basis. This consideration arises due to use of ducted fuel assemblies, for which inlet flow blockages or restrictions could lead to fuel damage or failure.

References

1. U.S. Atomic Energy Commission, *The Safety of Nuclear Power Reactors (Light Water-Cooled) and Related Facilities*, WASH-1250, July, 1973.
2. U.S. Nuclear Regulatory Commission, *Code of Federal Regulations*, Title 10, "Energy," Part 50, "Domestic Licensing of Production and Utilization Facilities," Appendix A, "General Design Criteria for Nuclear Power Plants."
3. American National Standards Institute/American Nuclear Society, *General Safety Design Criteria for a Liquid Metal Reactor Nuclear Power Plant*, ANSI/ANS-54.1-1989, American Nuclear Society, La Grange Park, Illinois.
4. U.S. Department of Energy, *Nuclear Reactor Safety Design Criteria*, Order DOE 5480.30, Chg. 1: 3-14-01.
5. U.S. Nuclear Regulatory Commission, *Preapplication Safety Evaluation Report for the Power Reactor Innovative Small Module (PRISM) Liquid Metal Reactor, Final Report*, NUREG-1368, February, 1994.
6. U.S. Nuclear Regulatory Commission, *Preapplication Safety Evaluation Report for the Sodium Advanced Fast Reactor (SAFR) Liquid-Metal Reactor*, NUREG-1369, December, 1991.

APPENDIX B Overall ABTR Design Requirements

B.1 Base Requirements

These requirements define functional and performance characteristics of the ABTR plant, and code and regulatory requirements which the plant design must satisfy. They also define features and characteristics of fabrication and construction which are utilized to effect a safe, reliable, and economical design of the ABTR plant.

- The ABTR plant design shall be capable of being licensed by the Nuclear Regulatory Commission (NRC).
- The ABTR plant shall be capable of being located on a remote site with minimal infrastructure support.
- The reference power plant size shall provide 250 MWt (~95 MWe).
- The ABTR plant shall utilize modular construction methods such that nuclear plant cost elements which have demonstrated significant instability in the past, specifically field labor and materials and field engineering and services, are minimized and maximum reliance is placed on the cost elements which have demonstrated stability, such as factory-produced equipment and replicated installation.
- The ABTR design shall have passive means of negative reactivity insertion and decay heat removal sufficient to place the reactor system in a safe stable state for specified anticipated transient without scram (ATWS) events without significant damage to the core or reactor system structure. (Note: A passive feature is one which relies only on the laws of nature and the integrity of structural members; requires no sensing, switching, motive power, or human interaction; and is not defeated or is difficult to defeat, by human action. Examples of passive features include naturally circulating fluid systems, thermal expansion, mechanical stops, and rupture discs or double-tube steam generator design.)
- The ABTR plant shall have features which minimize the probability of major sodium fires and minimize the damage from such fires.
- The ABTR reactor nuclear island and balance-of-plant design shall minimize operator demands during operation and shall provide ease of plant inspection and maintenance.
- The plant's safety, operational, maintenance and in-service inspection features shall be capable of demonstration and confirmation in an affordable full-scale prototype to provide a credible basis for NRC design certification and user acceptance of the ABTR.
- The ABTR plant shall be designed with emphasis on simplification as a prime consideration to enhance reliability, availability, and maintainability and shall integrate the following functional capabilities into the design:
 - Load following capability over the range of 25 to 100% power, including a 10% step load change.

- Rapid plant recovery following protection system actuation.
- Sustain load rejection from rated power without reactor scram.
- The reactor shall be designed to minimize the risk of sabotage or proliferation, either through design features, or by proven safeguards and security techniques, or a combination of the two.
- The design life of the ABTR plant shall be 30 years with the expectation of life extension.
- The design shall comply with all applicable codes and standards issued by the American National Standards Institute (ANSI), the American Nuclear Society (ANS), the American Society of Mechanical Engineers (ASME), and the Institute of Electrical and Electronics Engineers (IEEE).
- The ABTR shall be designed for significant margins of safety under all design basis events (DBE). These margins shall be such that:
 - No clad failure or structural failure shall result from the design basis events, including allowance for uncertainties.
 - The design allowable fatigue life cycles shall be at least twice the expected number of duty cycle transients.
- The ABTR plant design shall meet NRC and DOE release requirements and EPA protective action guidelines and shall incorporate sufficient passive and engineered safety features such that the emergency response is not required.
- As a minimum, the safety grade portions of the ABTR plant shall be designed to withstand a 0.2 to 0.3 g safe shutdown earthquake (SSE) seismic event without loss of function. The minimum operating basis earthquake (OBE) design value shall be $\sim 1/3$ of the SSE value.
- Nonsafety grade portions of the plant shall be designed to the International Building Code (IBC) requirements such that their intended function is not lost as a result of IBC seismic levels. Seismic Use Group III structures and systems shall ensure that the safety functions of all interfacing safety systems are not compromised at Design Basis Seismic accelerations.
- The ABTR shall transmute minor actinides and minimize the wastes that are generated during the reactor life cycle.
- The ABTR plant shall have the capability to achieve a capacity factor greater than 90%.

B.2 Technical Requirements

This section contains specific engineering, technical, and/or functional requirements necessary to achieve the desired performance of the ABTR nuclear power plant.

- Plant operating procedures and diagnostics shall be automated to the extent required to minimize operating and maintenance (O&M) cost, public risk, and operator exposure to radiation.
- Diagnostic systems shall be provided to detect incipient accident conditions and to aid identification of operator actions needed to return the plant conditions to normal. No operator action in the control room or remote shutdown locations shall prevent the reactor protection system from performing its safety function nor inhibit the function of the passive safety features.
- The plant design shall include reliable equipment for the balance of plant (or safety-system independence from balance of plant) to reduce the number of challenges to safety systems.
- The design shall minimize required maintenance and facilitate maintenance when needed. The design shall minimize the manpower required for maintenance and minimize the skills required to keep the plant maintained.
- All systems and components shall be designed so that routine maintenance activities may be performed during operations.
- The design shall allow for access, viewing, inspection, and testing of systems and components, working and laydown space for component repair or replacement, and facilitate plant cleanup. Remote maintenance shall be minimized; where remote maintenance/inspection is required, proven robotic methods shall be utilized.
- The maintenance plan shall ensure that all failures with a probability of occurrence greater than 10^{-4} per reactor year shall have a specified plan for corrective action. Failures with a probability of occurrence of less than 10^{-4} events per reactor year shall have a feasible means of corrective action.
- An In-service Inspection (ISI) program shall be developed which meets the intent of Division 3 of Section XI of the ASME B&PV Code. The ISI program shall ensure the nuclear safety-related structures, components, and systems maintain their integrity as necessary to perform their safety functions. The program shall be applied to safety-related components subject to the jurisdiction of Section III of the ASME B&PV Code. For areas not covered by Section III of the ASME B&PV Code, the design shall include inspection provisions consistent with the objective of maintaining safe operable conditions throughout the plant.
- The design of systems and components shall incorporate features to implement required surveillance and ISI with the plant on-line to the greatest degree practical.

- Radiation protection shall be provided to maintain radiation exposure to as low as reasonably achievable (ALARA), in conformance with radiation exposure requirements of this specification and DOE/NRC requirements.
- Provisions shall be made for handling and transporting new and spent cores.
- The normal system for forced convection transfer of reactor heat to the sodium/CO₂ heat exchanger shall be the heat transport system (consisting of primary and intermediate heat transport systems). The heat transport system shall provide sufficient capability to prevent exceeding acceptable fuel design limits, and to maintain ASME B&PV Section III Code Levels A and B design limits during conditions of normal operation. The heat transport system shall also be configured to ensure natural circulation coolant flow and to limit sodium coolant inventory loss in the event of a major pipe or vessel rupture.
- The shutdown heat removal system (SHRS) shall be safety grade and shall be designed with sufficient capability to prevent exceeding ASME B&PV Code Section III Level B and fuel design limits in the event that the normal heat sink is unavailable.
- The SHRS shall employ operating principles which assure passive, continuous decay heat removal without human intervention under all postulated accident conditions. It shall incorporate the necessary heat transfer means to prevent exceeding ASME B&PV Code Section III Level C design limits and fuel safety limits when normal decay heat removal means are unavailable.
- The containment system, including all access openings and penetrations, internal compartments, and structures, shall be designed with sufficient margin to accommodate the calculated pressure and temperature conditions under normal operating conditions, DBEs, and specified Anticipated Transients without Scram (ATWS) events without exceeding the design leakage rate. The design shall provide a barrier against uncontrolled release of radioactivity to the environment, and to ensure that site release limits are not exceeded.
- The containment system margin shall also account for: (1) the effects of potential energy sources, such as decay heat in fission products, potential spray or aerosol formation, and potential exothermic chemical reactions; (2) the limited experimental data available for defining accident phenomena and containment response; and (3) the conservatism and uncertainties of the models that are used.
- The containment system and equipment shall be designed to permit periodic leakage rate testing and surveillance of the containment boundaries.
- The containment system boundary gas leak rate shall not exceed 0.1% volume per day under design basis conditions.
- The containment system shall be capable of maintaining site release limits in the event there is a breach in the primary system boundary.

- A safety grade, Class 1E reactor protection system, which is separate and independent from the plant control system, shall be provided to prevent fuel damage, limit reactor structural challenges to less than ASME B&PV Code Section III Level C limits, and monitor reactor safety functions.
- The reactor protection system equipment for monitoring safe shutdown conditions shall be designed to monitor selected system parameters over their anticipated ranges of normal operation through Design Basis Earthquake (DBE), specified ATWS, and bounding event conditions, including those variables and systems that can affect the fission process, integrity of the reactor core, reactor coolant boundary, and containment and its associated systems.
- Instrumentation for monitoring safe shutdown conditions shall be designed to be highly reliable and fault tolerant.
- Two independent reactivity control systems employing different design principles shall be provided. Sufficient capability shall be provided in each system to ensure that the reactor can be maintained in a safe shutdown state under all operating and postulated accident conditions assuming failure of the other system.
- The IHX and supercritical CO₂ secondary system shall be designed such that any failure of the sodium/supercritical CO₂ boundary in the supercritical CO₂ heat exchanger and resulting sodium/CO₂ reactions will not result in a breach of the IHX to the primary sodium.



Nuclear Engineering Division
Argonne National Laboratory
9700 South Cass Avenue, Bldg. 208
Argonne, IL 60439-4842

www.anl.gov



A U.S. Department of Energy laboratory
managed by The University of Chicago